Copper (II) Catalyzed C-C and C-O Bond Formation in Organic Synthesis and Their Applications

A THESIS

submitted by

Krishna Mohan Das

for the award of the degree

of

DOCTOR OF PHILOSOPHY (SCIENCE)

Department of Chemistry

Jadavpur University

Kolkata-700032, India

May 2024

DECLARATION

I hereby declare that the research work embodied in this thesis entitled *"Copper (II) Catalyzed C-C and C-O Bond Formation in Organic Synthesis and Their Applications"* is the result of investigations carried out by me in the Department of Chemistry, Jadavpur University, Kolkata, under the supervision of Dr. Arunabha Thakur, Assistant Professor, Jadavpur University. This work is original and has not been submitted in part or in full, for any degree whatsoever.

Date: 15.05.2024

Krishna Mohan Das

Krishna Mohan Das

JADAVPUR UNIVERSITY
KOLKATA - 700 032

Dr. Arunabha Thakur
Assistant Professor
Department of Chemistry
Organic Chemistry Section

SUPERVISOR'S CERTIFICATE

This is to certify that the thesis entitled "*Copper (II) Catalyzed C-C and C-O Bond Formation in Organic Synthesis and Their Applications*" submitted by Sri **Krishna Mohan Das**, who has got his name registered on 18.03.2021 for the award of Ph.D (Science) degree of Jadavpur University, is absolutely based upon his own work under the supervision of **Dr. Arunabha Thakur** and that neither this thesis nor any part of it has been submitted for either any degree / diploma or any other academic award anywhere before.

Thakur 15|05|24

Dr. Arunabha Thakur

(Signature of the Supervisor(s) date with official seal)

Dr. Arunabha Thakur
Assistant Professor
Department of Chemistry
Jadavpur University
Kolkata-700032, India

v

Phone : 033 2457 2779 (O), E-mail : arunabha.thakur@jadavpuruniversity.in / babuiitm07@gmail.com
Mobile : 9937760940, Webpage : https://sites.google.com/site/arunabhathakur3221/

Dedicated to My Beloved Family

and

Respected Teachers…

ACKNOWLEDGEMENTS

It gives me immense pleasure to acknowledge the people who have directly or indirectly contributed to the thesis. This note of acknowledgements is a token respect, gratefulness and appreciation to all of them.

At the outset I express my sincere gratitude to my honorific supervisor Dr. Arunabha Thakur for facilitating me with lot of opportunities to accomplish my research work. I am extremely indebted to him for accepting me as his PhD student without any hesitation. This work would not have been possible without his valuable bits of advice, support, encouragement, relentless patience, constructive criticism and extensive discussion around my work. I am grateful to him for introducing me to the field of synthetic organic and organometallic chemistry. Under his guidance, I have successfully overcome many difficulties and learnt a lot. I would like to express my gratitude for his sincerity, dignity, and decency towards work. His truly scientific perception and logical ideas exceptionally inspire and enrich my growth as a student, a researcher and a scientist want to be. He has always been my great source of inspiration. My token of appreciation will be given to him through my future work.

I take this opportunity to sincerely acknowledge Prof. Kajal Krishna Rajak, Head of the Chemistry Department and former heads Prof. Subratanath Koner and Prof. Chittaranjan Sinha, Section-in-Charge, Organic Chemistry Section. I wish to express my gratitude to my coursework teachers and other faculty members of the Department of Chemistry, Jadavpur University. I remember my gratefulness to all the staff members of this department for their help in various appreciations. I would also like to convey my special thanks to Dr. Sumanta Jana (Micro Analyst), Mr. Raju Biswas and Baby di (NMR operator), Jadavpur University, for their kind support in my research career. I convey my special acknowledge to IACS and IICB for the instrumentation facilities.

I am indebted to all of my present and past lab mates for the invigorating and fun filled environment. My special appreciation goes to my seniors Dr. Sushil Ranjan Bhatta and Dr. Manisha Karmakar for allowing me to discuss various results pertaining to their research and thereby to educate myself. I do express my heartfelt thankfulness to all of my lab mates; Adwitiya Pal, Sayan Kumar Bag, Subham Sau, Subhendu Jana for their constant cooperation, help and kind

so boundless. At last, I thank almighty God for bestowing me with powers to complete this task up to my satisfaction.

Many others have helped me directly or indirectly throughout my research. I offer my humble thanks to them also.

Department of Chemistry

Jadavpur University

Kolkata- 700 032

India

Date: 15.05.2024

Krishna Mohan Das

Krishna Mohan Das

Preface

The research embodied in the present thesis entitled "Copper(II) Catalyzed C-C and C-O Bond Formation in Organic Synthesis and Their Applications" deals with the synthesis of various organic derivatives in presence of cheap transition copper catalyst *via* C-C and C-O bond formation under mild reaction conditions and their various applications.

Investigations described in this thesis have been carried out by the author in the Jadavpur University, Jadavpur, Kolkata-700032, India during the time of November, 2018 to April, 2024 under the supervision of Dr. Arunabha Thakur. The entire work has been described and summarized within the five chapters of this thesis.

Chapter 1 is the general introduction which provides the comprehensive literature survey on copper-catalyzed various organic transformations through C-H bond activation in comparatively mild reaction conditions. This chapter highlights the importance of copper metal in organic transformations compared to other 4d and 3d transition metals which are highly expensive and low abundant in earth crusts. At the end of this chapter, copper catalyzed 1,3-diyne synthesis *via* Glaser-Hay coupling are summarized and their applications in metal ion sensing have been surveyed briefly.

Chapter 2 describes the synthesis of allylic ester compound in presence of a copper complex catalyst by oxidative CDC mechanism. Using only 1 mol% of catalyst, high yields of products are achieved under mild reaction condition. The detailed study shows that HAT mediated radical formation is involved in presence of both catalyst and oxidant (TBHP). This is the first report where minimal amount of catalyst loading provides allylic ester in an overall product yield that is comparable to those reported in other literature.

Chapter 3 describes synthesis of enol/phenol carbamates from cyclic as well as acyclic formamides derivatives using a copper catalyst in oxidatitve CDC under mild condition. This method does not need pre-functionalized starting materials and wide range of functional group tolerance makes this protocol more advantageous. A plausible mechanism has been proposed based on various control experiments and characterization of generated radical intermediated during the course of reaction.

Chapter 4 describes the difunctionalization of vinyl arenes in presence of anhyd. CuCl$_2$ catalyst using unactivated cycloalkanes as coupling partner. We synthesized β-disubstituted ketones from various styrene derivatives which proceeds through a radical-mediated oxidative alkylation pathway. This robust synthetic strategy is compatible with diverse functional groups and scalable for gram-scale synthesis. Mechanistic studies and DFT analyses revealed the precise efficiency of Cu(II), TBHP, and 1-methylimidazole in the catalytic cycle involved. Product formation involved two HAT mechanisms in which the first one generating the cycloalkyl radical is the rate-determining step.

Chapter 5 presents, little different kind of work, which does not include any catalysis work rather, in this work we have developed a unique probe *via* Cu(II) catalyzed Glaser-Hay coupling. The designed probe is capable of detecting dual metal ions *via* different binding sites and different mechanisms within a single molecular scaffold and applied in molecular logic gates. Therefore, this chapter of thesis deals with the comparison of metal ion interaction with cyclic and acyclic molecules containing Hard and Soft centers towards different metal ions.

Each chapter (chapter 2 to 5) begins with a short 'Introduction' followed by 'Results and discussion', 'Conclusion' and 'Experimental Section'. For convenience, 'References' are given at the end of each chapter. Overall conclusions and outlook, list of publications, list of poster presentation has been appended at the end of the thesis.

Abstract

Index No: 12/21/Chem/27

Thesis Title: Copper (II) Catalyzed C-C and C-O Bond Formation in Organic Synthesis and Their Applications

The main aim of the research work is functionalization of C-H bond in presence of cheap and earth abundant copper catalyst under mild reaction conditions. Copper catalysts are indeed ubiquitous catalysts in organic transformations due to their versatile oxidation states and their ability to participate in a broad range of reactions *via* both radical and two-electron transfer mechanisms. Copper's ability to access a range of oxidation states, typically from 0 to +3, makes it highly adaptable in catalysis. The work presented in this study reports the C-H bond activation of various organic derivatives using copper as catalyst under an oxidative environment by CDC mechanism to construct complex organic molecules and their applications in various fields.

In **first work**, we report for the first time that the quinoline-based NNN-pincer Cu(II) complex acts as an air stable superior catalyst for the oxidative cross-coupling of the allyl $C(sp^3)$–H bond with an acid derivatives for the construction of C-O bond at ambient temperature in a homogeneous system. The synthesized catalyst **1**, showed excellent catalytic activity for the oxidative esterification of allylic $C(sp^3)$–H bonds at 40 °C within a very short time (1 h) using only 1 mol% of the catalyst. A wide variety of aromatic allylic esters were synthesized in moderate to good yields, which could be extended to aliphatic allyl esters as well.

Further, we have developed a methodology for C-O bond formation in **second work** at slightly elevated temperature. In this context, we have developed a novel benzothiazole appended 2,6-di picolinamide-based Cu(II) complex which acts as a catalyst for the formation of carbamates *via* the cross-coupling reaction of various 2-carbonyl substituted phenolic derivatives or 1,3-diketo derivatives with N,N-disubstituted formamides. A wide range of aromatic carbamates was synthesized using copper complex in good/excellent yield with decent functional group tolerance under mild conditions. Control experiments suggest that the reaction proceeds *via* the radical

mechanism, and the formation of radical-mediated intermediates was confirmed by the gas chromatography (GC), GCMS and HRMS. The use of low cost and environmentally benign catalysts in mild conditions along with the tolerance of a wide range of functional groups makes this an easy synthetic approach for the development of carbamates.

In **third work**, we report the Cu(II) catalyzed synthesis of β-disubstituted ketones from styrene *via* oxo-alkylation with unactivated cycloalkanes as the alkylating agent in presence of tert-butylhydroperoxide (TBHP) and 1-methylimidazole as oxidant and base respectively. β-disubstituted ketones are known to be synthesized by using either expensive Ru/Ir complexes, or low-cost metal complexes (e. g., Fe, Mn) with activated species like aldehyde, acid, alcohol, or phthalimide derivatives as the alkylating agent, however, use of unactivated cycloalkanes directly as the alkylating agent remains challenging. A wide range of aliphatic C–H substrates as well as various olefinic arenes and heteroarene are well-tolerated in this method. Furthermore, various controlled experiments such as kinetic isotope effect study, Hammett analysis and theoretical calculations (DFT) enable us to gain deeper insight of mechanistic intricacies of this new simple and atom-economic methodology.

The work in **Chapter 5** does not include any catalysis work rather, in this work we have developed a unique probe *via* Cu(II) catalyzed Glaser-Hay coupling. The designed probe is capable of detecting dual metal ions *via* different binding sites and different mechanisms within a single molecular scaffold. On account of this, two pyridine-derived scaffolds, **5** and **7**, containing identical molecular cores but different appendages, *viz*., terminal alkyne (**5**) and internally 1,3-conjugated alkyne units (**7**), are successfully synthesized. Alkyne is a versatile functional group in organic chemistry, and can undergo a wide variety of reactions and interactions. Both compounds are subjected to metal ion sensing at the molecular level and are found to bind Cu^{2+} and Hg^{2+} ions with different functionalities. Compounds **5** and **7** interact with Cu^{2+} by the pyridine N and the two adjacent amide N's in a tripodal fashion, whereas they interact with Hg^{2+} by their respective open-end and closed-end alkyne units. Both experimental studies and theoretical (DFT) calculations have converged on the result that terminal alkynes cannot function as a chemosensor for Hg^{2+} ions, although they can respond by functional group transformation, whereas cyclic internally

conjugated alkynes can perform as potential Hg^{2+} sensors. The combination of Cu^{2+} and Hg^{2+} ions has been used to generate a molecular system exhibiting the OR logic operation. This creates an avenue for differential recognition of multiple heavy metal ions simultaneously with similar molecular motifs.

Thakur 15|05|24

....

Signature of the Supervisor (date with official seal)

Dr. Arunabha Thakur
Assistant Professor
Department of Chemistry
Jadavpur University
Kolkata-700032, India

Krishna Mohan Das 15.05.2024

Signature of the candidate with date

CONTENTS

CHAPTER-1: Introduction

CHAPTER-2: A Novel Quinoline-Based NNN-Pincer Cu(II) Complex as a Superior Catalyst for Oxidative Esterification of Allylic C(sp³)-H Bonds

CHAPTER-3: Oxidative Cross Dehydrogenative Coupling Directed Carbamates Synthesis using Cu(II) Pincer Complex as Active Catalyst under Mild Reaction Condition

CHAPTER-4: Cu(II) Promoted C(sp^3)-H Activation in Unactivated Cycloalkanes: Oxo-Alkylation of Styrenes to Synthesize β-Disubstituted Ketones

CHAPTER-5: Strategic Design of a 2,6-Disubstituted Pyridine-Based Probe Having Hard-Soft centers: Responsive Divergence from One Core

LIST OF FIGURES

CHAPTER -1

CHAPTER-2

Figure 2.1. (a) ORTEP representation of complex **1** with thermal ellipsoids drawn at the 50% probability level (b) EPR spectra of complex **1** in $CHCl_3$ at room

CHAPTER-3

CHAPTER-4

CHAPTER-5

LIST OF SCHEMES

CHAPTER-1

LIST OF TABLES

Abbreviations

AU	Absorbance units
a.u.	Arbitrary units
α	alpha
β	Beta
Boc	Tertiary butyloxycarbonyl
Bz	Benzyl
Cp	Cyclopentadienyl ligand
CV	Cyclic voltammetry
CH_3CN	Acetonitrile
CCDC	Cambridge crystallographic data centre
$CDCl_3$	Deuterated chloroform
Calcd	Calculated
δ	Chemical shift
d	Doublet
dq	Doublet of quartet
deg	degree
DCM	Dichloromethane
DFT	Density functional theory
DG	Directing group
DMF	Dimethylformamide
DMSO	Dimethyl sulfoxide
EDG	Electron donating group
EWG	Electron withdrawing group
ESI	Electro spray ionization
ESI-MS	Electrospray ionization- mass spectrometry
EtOAc	Ethylacetate

equiv.	Equivalent
EDTA	Ethylenediaminetetraacetic acid
FL	Fluorescence
FT-IR	Fourier transform-Infra red
GOF	Goodness of fit
h	Hours
HOMO	Highest occupied molecular orbital
HRMS	High resolution mass spectrometry
IR	Infra-red
J	Coupling constant
k	Rate constant
K	Binding constant
LAS	Sodium L-ascorbate
LOD	Limit of detection
LUMO	Lowest unoccupied molecular orbital
M	Molar
m	Multiplate
Me	Methyl
MeOH	Methanol
m/z	Mass/charge
MHz	Megahertz
MS	Mass spectrometry
n-BuLi	*n*-butyl lithium
Nm	Nanometer
NMR	Nuclear magnetic resonance
Ppm	Parts per million
Ph	Phenyl
r. t.	Room temperature

s	Singlet (in NMR)
s	Seconds
t	Triplet
TD-DFT	Time-dependent Density Functional Theory
TBAP	Tetrabutylammonium perchlorate
TEMPO	2,2,6,6-Tetramethylpiperidin-1-yl)oxyl
TFA	Trifluoroacetic acid
THF	Tetrahydrofuran
TLC	Thin layer chromatography
TMS	Tetramethylsilane
UV/Vis	Ultraviolet/visible spectroscopy
V	Volt
XRD	X-ray diffraction

CHAPTER-1

General Introduction
and
Literature Survey

1.1 Introduction to catalysis

Swedish scientist Berzelius first introduced the word "catalysis" in 1835.[1,2] However, Wilhelm Ostwald (1909 Nobel prize) improved an appropriate description in 1894, realizing the importance of a catalyst on a reaction's rate. His statement about catalysis stated as: ''*Catalysis is the acceleration of a slow chemical process by the presence of a foreign material*''.[3] A chemical reaction might happen more quickly when a catalyst is used. Reactants, or starting chemicals, are converted into products, or other compounds with new properties, during a chemical reaction. Throughout the reaction, reactants are consumed and transformed into products.

A catalyst operates in a chemical reaction by facilitating the conversion of reactants into products while changing its own chemical structure which is ultimately reversible. Catalysts present in the system, increase the rate of a chemical reaction by reducing its activation energy needed without getting consumed in the reaction.[4a] This process can be understood in several key steps:

1. **Adsorption**: The reactant molecules (or sometimes intermediate species) are adsorbed onto the surface of the catalyst. This adsorption weakens certain chemical bonds within the reactant molecules, making them more prone to undergo reaction.

2. **Activation**: Once the reactant molecules are adsorbed on the catalyst surface, they undergo a change in their electronic structure or orientation that lowers the activation energy barrier for the desired chemical transformation. This step often involves the formation of temporary chemical bonds between the reactants and the catalyst.

3. **Chemical Transformation**: With the activation energy lowered, the reactant molecules can undergo chemical transformation to form products. This step may involve bond breaking, bond formation, rearrangement of atoms, or other chemical processes, depending on the specific reaction.

4. **Desorption**: After the reaction has occurred, the product molecules are desorbed from the catalyst surface. The catalyst itself is also released from the surface, potentially undergoing changes in its chemical structure as a result of the reaction.

5. **Regeneration**: In many cases, the catalyst can be regenerated by releasing any byproducts or other species that may have accumulated on its surface during the reaction. This allows the catalyst to continue participating in multiple reaction cycles.

A catalyst's overall impact is to offer a alternative reaction route with reduce activation energy of the preocesss than the uncatalyzed reaction. This results in a higher reaction rate and, often,

improved selectivity for desired products.[4b] Catalysts can be heterogeneous, where the catalyst is separated from both starting material and final products, or homogeneous, where starting material and products are present in the similar phase with catalyst. Catalysts play a critical role in numerous industrial processes, including petroleum refining, chemical synthesis, and environmental remediation. As an illustration, a catalyst may stabilize a transition state or bring two reactants closer together (Figure 1.1). The reaction rate increases as the activation energy is lowered because it permits the reaction to happen more frequently at a given temperature.
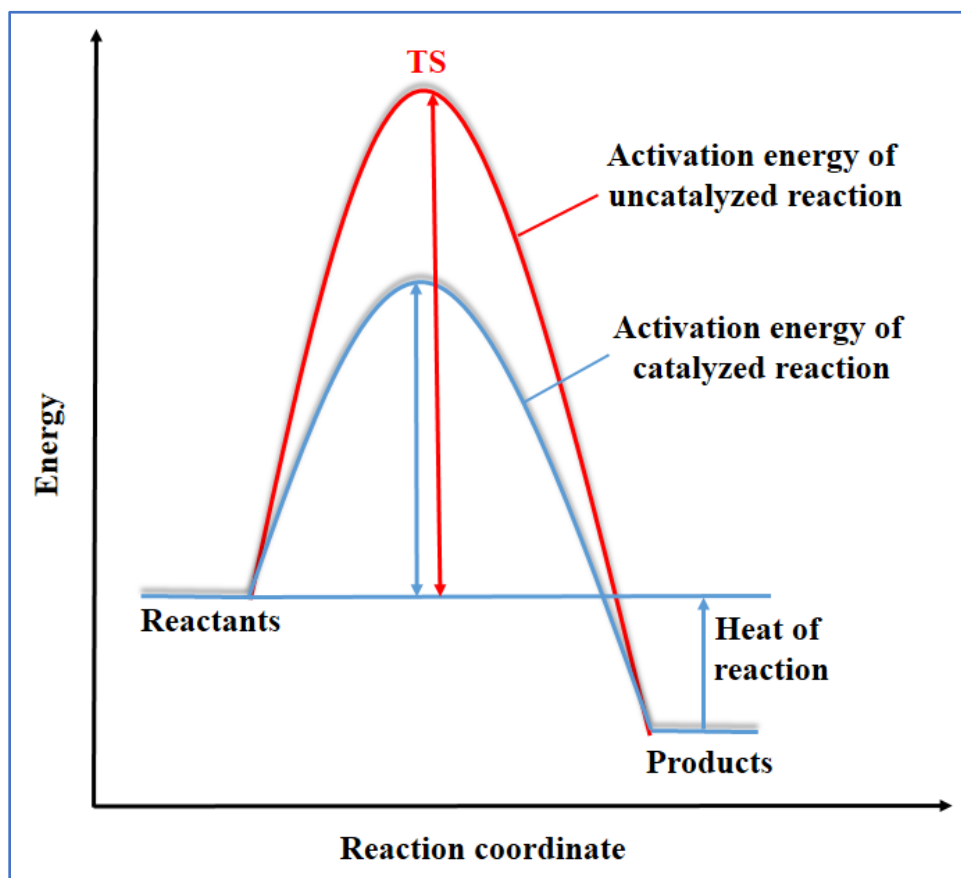
Figure 1.1. Role of a catalyst in a chemical reaction.

1.2 Classification of catalyst

There are two main categories of catalytic processes. One is homogeneous catalysis, where both catalyst and reagents are present in same phase. On the other hand, in case of heterogeneous catalyst both catalyst and the reactants are exist in different phase and the reactions occur at the

catalyst's surface where the two phases are interacted to each other. Heterogeneous catalysis has the major advantage in terms of practicality, which is the ability to generally achieve higher process temperatures and facilitates easier product separation from the reaction mixture after the reaction.

1.2.1 Heterogeneous catalyst

Catalyst that present in a different state from the starting materials are reffered as heterogeneous catalyst.[5] In this case, catalyst are present in mostly solid state whereas reactants and products are exist in gas or liquid phase (Figure 1.2). Heterogeneous catalysis plays a significant role in many industries such as petroleum refining, chemical synthesis, environmental remediation, and emission control. Common examples include catalytic converters in automobiles[6] (which use metals such as platinum, palladium, and rhodium supported on a ceramic substrate to catalyze the conversion of harmful pollutants into less harmful substances), the Haber-Bosch process for ammonia synthesis[7] (which employs iron catalysts supported on alumina), and various hydrogenation and oxidation reactions in the production of fine chemicals and pharmaceuticals. Overall, heterogeneous catalysis offers several advantages, including easy separation and recovery of the catalyst, scalability for industrial applications, and versatility in catalyzing a wide range of chemical transformations. These catalysts play a crucial role in modern chemical manufacturing and environmental protection.
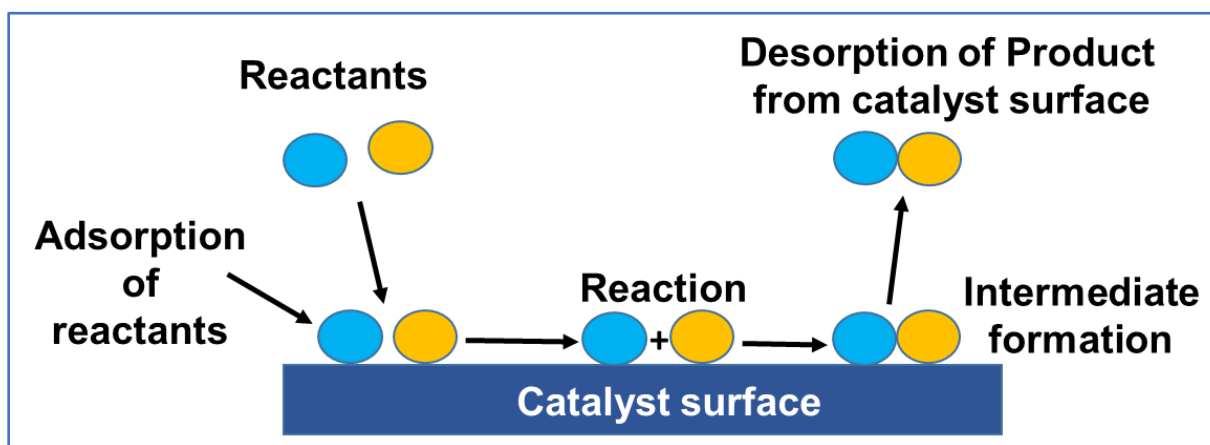
Figure 1.2: Heterogeneous catalyst and its activity.

However the heterogeneous catalyst has many disadvantages. The major drawbacks are listed below:

➢ **Complexity of Active Sites**: The active sites on heterogeneous catalysts can be complex and heterogeneous in nature. Understanding the structure-activity relationships and

optimizing catalyst performance often requires sophisticated characterization techniques and computational modeling.

➢ **Deactivation**: Heterogeneous catalysts can undergo deactivation over time due to various factors, such as fouling, poisoning, or sintering of active sites. Deactivation can reduce catalyst activity and selectivity, necessitating regeneration or replacement of the catalyst.

➢ **Difficult Catalyst Design**: Designing effective heterogeneous catalysts with optimal activity, selectivity, and stability can be challenging. It often requires careful selection of catalyst materials, support structures, and surface modifications, as well as thorough testing under relevant reaction conditions.

➢ **Environmental Impact**: Some heterogeneous catalysts may contain toxic or environmentally harmful components, such as heavy metals or metal oxides. Proper management of catalysts and byproducts is necessary to minimize environmental impact and ensure sustainability.

Despite these all challenges, heterogeneous catalysts remain essential tools in chemical synthesis, industrial processes, and environmental protection, offering unique advantages and enabling numerous technological advancements. Ongoing research efforts aim to address the limitations of heterogeneous catalysis and develop more efficient and sustainable catalytic systems.

1.2.2 Homogeneous catalyst

Homogeneous catalysts are present in the same phase (e.g., gas, liquid, or solution) with the reactants in a chemical reaction (Figure 1.3). Unlike heterogeneous catalysts, which are typically solid and exist in a different phase from the reactants, homogeneous catalysts are intimately mixed with the reactants throughout the entire reaction medium.[8] Here's a brief discussion about homogeneous catalysts, including their advantages, disadvantages, and applications:
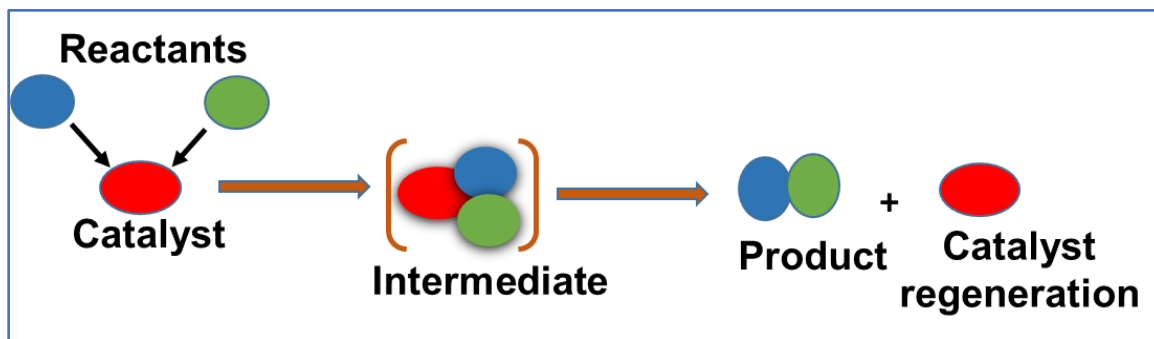
Figure 1.3: Mechanistic diagram for a homogeneous catalyst.

Advantages of Homogeneous Catalysts:

➢ **Uniform Reactant Interaction**: Since homogeneous catalysts are in the same phase as the reactants, they can interact with all reactant molecules uniformly. Compared to heterogeneous catalysis, this can lead to faster reaction rates and improved efficiency.

➢ **Precise Control of Catalytic Activity**: Homogeneous catalysts often offer precise control over reaction conditions and catalyst composition, enabling fine-tuning of catalytic activity, selectivity, and reaction kinetics. This level of control can be crucial in complex organic synthesis and fine chemical manufacturing.

➢ **High Catalytic Turnover Numbers**: High turnover number (TON) can be seen in homogeneous catalysts also they shows high turnover frequencies (TOF), which implies each catalyst molecule can facilitate multiple reaction cycles, leading to efficient use of the catalyst and potentially higher productivity.

➢ **Flexibility in Catalyst Design**: Designing homogeneous catalysts allows for flexibility in molecular structure and ligand environment, which can be tailored to optimize catalytic performance for specific reactions. Because of its versatility, new catalytic processes and novel reaction mechanisms can be explored and developed using homogeneous catalyst.

Even with all of its benefits, homogeneous catalysts have several disadvantages.[9] One of the main challenges is the separation of the catalyst as well as their recovery from the reaction mixture, particularly in large-scale industrial processes. Also, homogeneous catalysts promote various side reactions due to their intimate interaction with reactant molecules. Controlling side reactions and maintaining high selectivity can be challenging, especially in complex reaction systems. Some homogeneous catalysts contain toxic or environmentally harmful components, such as heavy metals or complex organic ligands. Proper catalyst design and waste treatment must be done properly to reduce possible negative effects on the environment.

Homogeneous catalysts find applications across various fields, including organic synthesis, polymerization, fine chemical manufacturing, and pharmaceuticals.[10] They are commonly used in various cross-coupling reactions,[11a] hydrogenation,[11b] oxidation, and metathesis[11c] reactions in presence of transition metals. Homogeneous catalysis also plays a crucial role in industrial processes, such as petrochemical refining and specialty chemical production. They offer unique advantages in terms of uniform reactant interaction, precise control over catalytic activity, and flexibility in catalyst design. However, challenges related to catalyst separation, stability, and

environmental impact must be carefully considered in their application and development. Ongoing research efforts aim to address these challenges and expand the homogeneous catalysis's utility in advanced chemical synthesis and process technology.

1.3 Homogeneous catalysis in organometallic chemistry for carbon-carbon (C-C) bond or carbon-heteroatom (C-X, X= O, N, S and halogen) bond formation

Over the last decades, the main goal of organic synthesis has been laid on the efficient and eco-friendly methodology.[12] Among many other transformations, the selective formation of C-C and C-X bonds (X = N, O, S, etc.) is crucial in order to build complex molecules in organic synthesis. These transformations allow researchers to stitch together smaller molecular building blocks into larger, more intricate structures with specific functionalities. For example, C-C bond formation enables the synthesis of carbon frameworks, which are the backbone of organic molecules. On the other hand, C-X bond formation introduces heteroatoms into the molecule, providing sites for further functionalization and enhancing the molecule's diversity and properties. Glaser created the first C–C bond-forming process mediated by transition metals over 150 years ago *via* oxidative dimerization of terminal acetylene.[13] Around the start of 20th century, Ullmann invented coupling between two aryl/alkyl groups from activated aryl/alkyl bromides to produce biaryl compounds using copper catalyst.[14] Later on, using this methodology carbon-heteroatom bond formation has been developed at elevated temperatures using stoichiometric amounts of copper. Frankland's method for producing diethylzinc[15a,b] and Grignard's organomagnesium reagents are the basis of modern organometallic chemistry.[15c,d] Indeed, a wide range of metals have been used in organic synthesis for various applications, owing to their ability to catalyze a wide range of reactions. Interestingly, both the reactivity and the selectivity of the organometallic reagent can be finely tuned by selecting different metal as central atom (Figure 1.4). This principle is a fundamental aspect of organometallic chemistry and plays a crucial role in synthetic chemistry, catalysis, and various industrial processes.

Among the various organometallic reagents organo lithium compounds react violently towards many electrophiles even at very low temperature because of their highly polarized carbon-metal bonds. However there are lot of drawbacks to using organolithium reagents including poor selectivity and lack of tolerance for sensitive functional groups. Other organometallic reagent such as organo zinc, organo boron or organotin reagents all are selectively reacts with suitable electrop-

Metal centre (M): • Charge
• Oxidation state and electronic configuration
• 18 electron rule
• Coordination number and geometry

Ligands (L, X): • Binding mode, number of donated electrons
• Electronic propertie (charge, donor strength)
• Steric propeties (cone angle)

Important ligands L= PR_3, CO, C=C, NR_3; X= $\overset{\ominus}{Cl}$, $\overset{\ominus}{H}$, $\overset{\ominus}{R}$, $\overset{\ominus}{cp}$
(R= alkyl, cp= cyclopentadienyl)
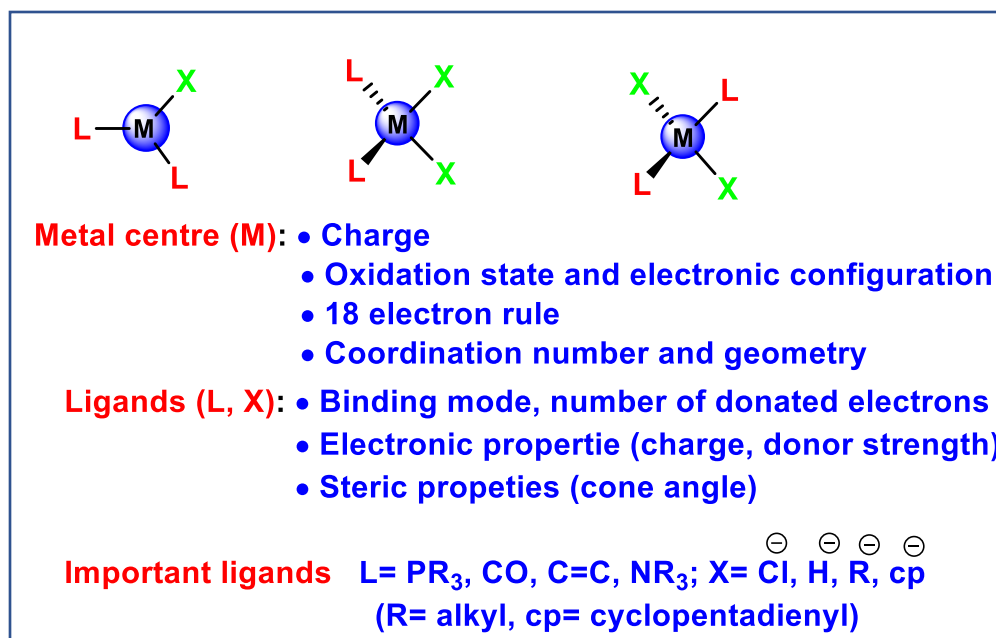
Figure 1.4: Characteristics of organometallic complexes.

-hile because of their high carbon-metal covalent bond character compared to organo lithium reagent. However, electrophiles have restricted applicability because of the comparatively poor reactivity of these chemicals. Transition metals like Pd, Cu, Ni, Co, Ru can be used to address this reactivity and selectivity issue.[16] The use of these transition metals to form C-C and C-X bonds through cross-coupling reactions has revolutionized chemistry in the last three decades. In 2010, Richard F. Heck, El-ichi Negishi, and Akira Suzuki, these three scientists were awarded Nobel Prize in Chemistry for their work on "palladium-catalyzed cross-couplings in organic synthesis". This protocol allows synthetic chemistry to open up new directions in organic synthesis field. Over the past few decades, numerous progress has been achieved toward the functionalization of C-H bonds to create C-C and C-Heteroatom bonds. However, precise role of metal in C-H bond activation step varies greatly based on the substrate nature, solvent, and additives in the active MLn species. Majority of C-H bond functionalization requires harsh reaction condition due to thier high bond dissociation energy. In general, higher temperatures (>120 °C) were required to functionalize the C-H bond. Many catalytic transformations required expensive and hazardous ligands, stoichiometric amounts of oxidants, and basic or acidic additives. Efforts have been undertaken in the last few years to address these drawbacks for C-H bond functionalization reaction comparatively mild reaction conditions. Novel methodology and greener protocols are

now privileged topics in modern synthetic chemistry for the formation of various C-C and C-Heteroatom bonds.

1.4 Transition metal catalyzed C-C bond formation

Significant advancements have been noted over the past few decades involving transition metal catalyzed C-C cross coupling reactions. Numerous research teams concentrated on this area to create new methods that covered a broad spectrum of substrates. Herein, we discuss C-C cross coupling reaction that catalyzed by transition metals.

1.4.1 Transition metal catalyzed classical cross-coupling reaction

Classical cross-coupling involves the reactions between aryl halides and organometallic reagents using a palladium catalyst that provides (hereto)biaryl as a product. Several methodologies have been established to prepare biaryl compounds in presence of various organometallic reagents. The terms Kumada, Negishi, Stille, Suzuki, and Hiyama coupling reactions refer to the coupling between aryl halides/pseudo halides and organometallic reagents containing Mg, Zn, Sn, B, and Si respectively.[17] Mechanistically at first aryl halides are inserted into the metal center and generate aryl-metal species through an oxidative addition process. Then transmetalation with the organometallic reagent provides crosscoupled biaryl product followed by reductive elimination (Scheme 1.1). Despite their great usefulness, traditional cross-coupling reactions have several drawbacks like organometallic compounds are moisture sensitive and the prefunctionalisation of starting materials are required for efficient transformations. Therefore, it is essential to develop an atom efficient methodology for C-C and C-X bond formation.
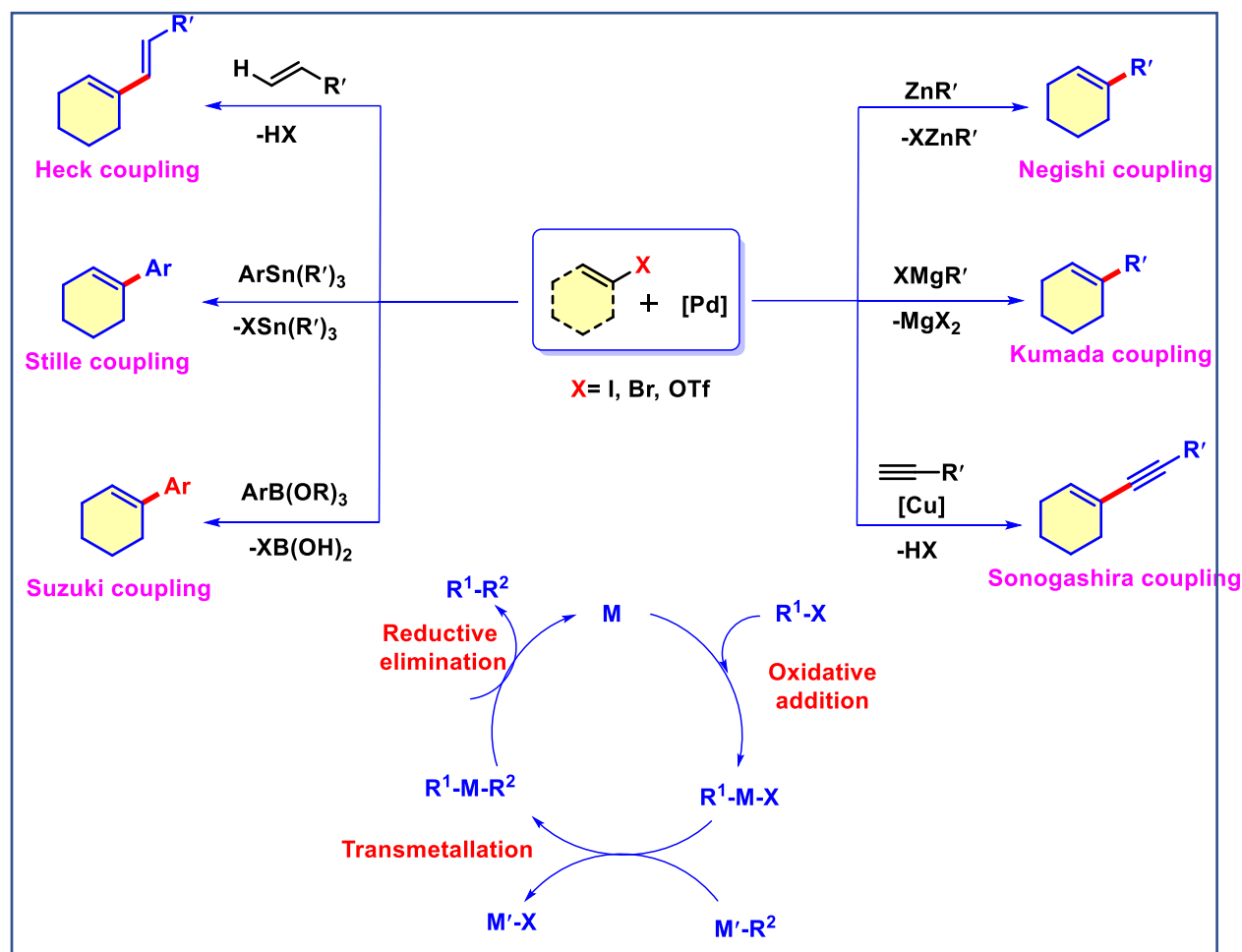
Scheme 1.1: Various classical cross-coupling reactions and its general mechanism.

1.4.2 DG directed C-C coupling using transition metal catalyst

Transition metal catalyzed DG directed C-C or C-Heteroatom bond formation *via* inert C-H bonds activation is known as contemporary technique introduce to the organic chemist's toolbox as a potent substitute to classical cross-coupling reactions. To build aryl-metal intermediates in a conventional cross coupling, pre-functionalized coupling partners such as aryl halides, triflates, etc. are necessary. Whereas, in C−H activation these undesired product and steps are minimized. An essential part of the region selective C-H bond modification of arenes is played by this chelating group. In coordination chemistry, metal salts are commonly the Lewis acid and the chelating group is the Lewis base in nature. Typically, the first step involves the metal salt or complex coordinating with the chelating group (heteroatom) of the organic molecule experience an agostic interation with metal and the σ-bond present in *ortho*-C-H bond. The prominent sites selectivity is observed

under DG control in the reaction site substrate because of this metal chelation and its location in close proximity to a single C-H bond. A metallacycle intermediate forms when a metal complex deprotonates the ortho C-H bond. Subsequently, the generated metallacycle undergoes reactions with various π-components or electrophiles to give the corresponding C-H functionalized product (Scheme 1.2).[18] *Ortho*-C−H activation is widely known to occur in presence of 4d block transition metals like Ru, Rh, Pd as well as 3d block transition metals like Fe, Ni, Co, Cu. However, compared to other metals palladium's reactivity, selectivity, and reliability also contributed to its prominence in this field of C-H activation.[19]
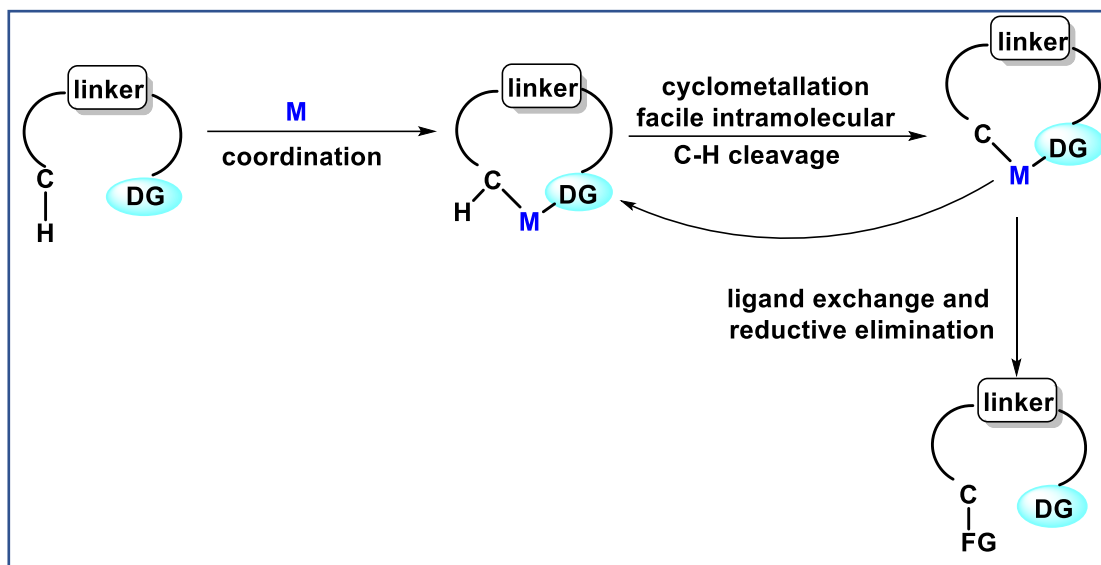
Scheme 1.2: C-H bond activation in presence of directing group.

1.4.3 Various examples for transition metal catalyzed C-C bond formations

The ability to synthesize C-C bonds efficiently and selectively is fundamental to the advancement of organic chemistry. In the last few decades, transition metal catalysts play a vital role in these transformations by facilitating the activation of C-H bonds and subsequent C-C bond formation. Various transition metals, including ruthenium, palladium, rhodium, iridium, and others, have been used extensively as catalysts for C-H activation reactions that are exemplified below (Scheme 1.3).[20]
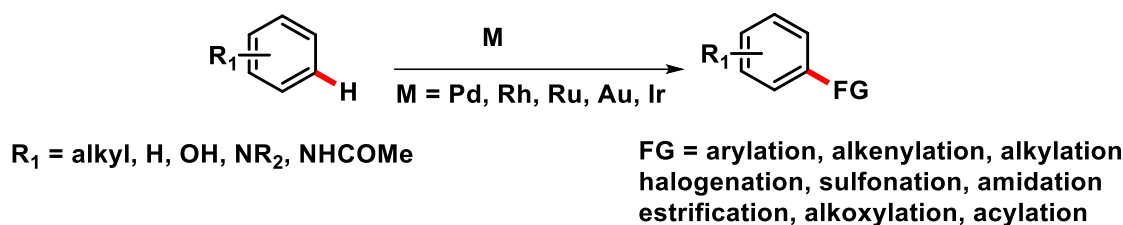
Scheme 1.3: C-H functionalization using transition metal catalysts.

1.4.3.1 Copper (Cu) catalyzed C-C bond formation

Copper catalysts are indeed ubiquitous catalysts in organic transformations due to their versatile oxidation states and their ability to participate in a broad range of reactions *via* both radical and two-electron transfer mechanisms. Copper's ability to access a range of oxidation states, typically from 0 to +3, makes it highly adaptable in catalysis.[21-23] In the past three decades copper chemistry has gained significant attention because of the element's low toxicity, high abundance and low cost in nature. Thus based on innovative findings by Ullmann and Goldberg,[24-27] a remarkable quantity of copper catalyzed organic transformations including cross-coupling reactions, oxidation reactions, addition and radical reactions have been documented for the synthesis of various carbon-carbon bonds (C–C) and C-X bonds (X = N, O, S, etc.).[28-30] Although previously reports show that copper mediated dimerization of various electron-rich arenes in oxidative conditions were proceeded *via* SET methods through C−H activation reactions but recent research on C-H activation have demonstrated that the process proceeds *via* organic C-Cu intermediates. [31-33] On the basis of those mechanistic discoveries copper complexes can be successfully utilized in C–H activation processes.[34-36]

> ➢ **C(sp^2)-H arylation**

Recent developments in copper catalyzed transformations have demonstrated the importance of copper catalysts as a substitute for expenive metals catalyzed C-H arylations with aryl halides. Even though stoichiometric C-H arylation has been known to be promoted by the copper complexes since 1968, the intriguing work involves copper-catalyzed C-H arylation of heterocyclic compounds with aryl iodides has significantly advanced the field of study, as described by Ackermann, Miura, and Daugulis. Daugulis reported the arylations heterocycle compounds using t-BuOLi as the base and 10 mol% CuI catalyst in DMF solvent at 140 °C (Scheme 1.4).[37]
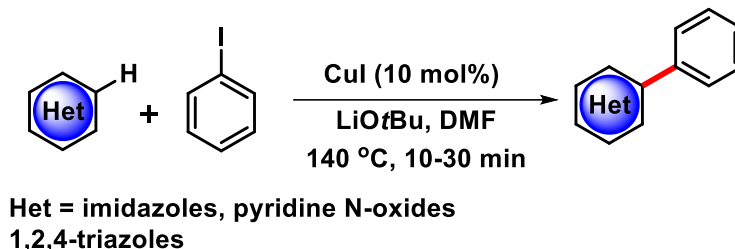
Scheme 1.4: C-H arylation of heteroarenes using Cu catalyst.

➢ **C(sp³)-H arylation**

Ge *et al*. revealed copper catalyzed C(sp³)−H arylation of amides in 2015. Coupling between polyfluorobenzenes and amides gives the arylated product. During this procedure, α-methyl (-CH₃) groups of aliphatic amides were preferentially functionalized compared to α-methylene (-CH₂) or *β*- and *γ*-methyl (-CH₃) groups present in amides (Scheme 1.5).[38]
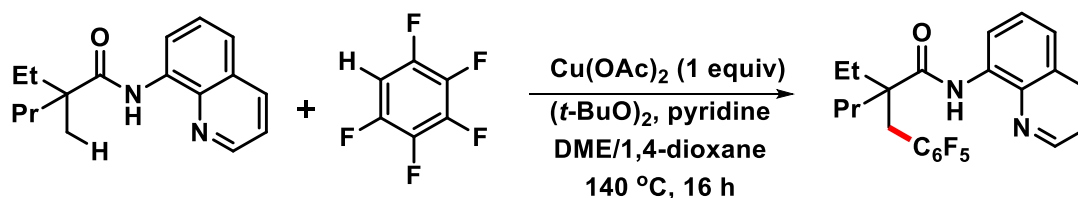
Scheme 1.5: Arylation of C(sp³)-H bonds using Cu(II) catalyst.

➢ **C(sp²)-H alkylation**

Belhomme *et al*. disclosed C(sp²)-H alkylation of electron rich aromatic compounds like anisole and aniline derivatives in presence of copper catalyst. Apart from the normal alkylations, copper catalysis was also used to produce 3,3-difluoro-2-oxindole derivatives through *ortho* C-H difluoroacetylation. At the end, intramolecular amidation from afforded the oxindole derivatives with good yield (Scheme 1.6).[39]
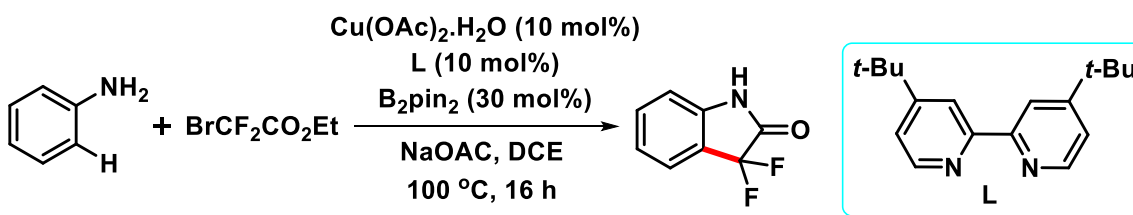
Scheme 1.6: Formation of oxindole derivatives using Cu(II) catalyst.

> ➢ **C(sp²)-H alkenylation**

Li *et al*. demonstrated the potential application of allyl halides in selective alkenylations in presence of copper(I) catalyst. Allyl bromide react with benzoxazole formed a selective C2-alkenylations product in LiO*t*Bu base in toluene. A probable mechanistic cycle was suggested in which allylic azoles are first formed and then they are isomerized to produce the internal alkene which is conjugated with benzoxazole ring (Scheme 1.7).[40]
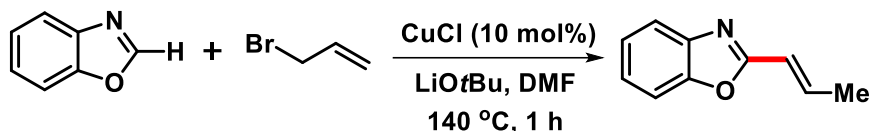
Scheme 1.7: Alkenylation of benzoxazole using Cu(I) catalyst.

> ➢ **Decarboxylative homo-coupling**

Lee's group disclosed a method for synthesizing 2,5-diaryl substituted furans in one pot using a decarboxylative homocoupling reaction of aryl alkynyl carboxylic acid derivatives (Scheme 1.8). This reaction furnished a high yield of products as CO_2 was produced as a sole byproduct. A broad range of substrates were screened, and good to exceptional yields of 2,5-diaryl substituted furans were obtained.[41]
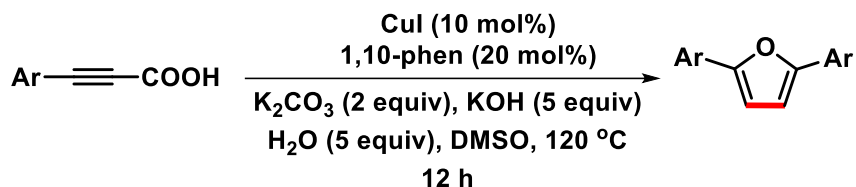
Scheme 1.8: Cu(I) catalyzed synthesis of 2,5-diaryl substituted furans.

> ➢ **C(sp²)-H alkynylation**

Miura *et al*. demonstrated alkynylations of azole compounds in presence of copper catalyst with terminal alkynes in 2010 (Scheme 1.9). Initially, copper(II) chloride reacted with terminal alkyne and formed an intermediate after ligands exchange to each other which subsequently undergoes coordination with oxadiazole and formed another intermediate. At the end, reductive elimination gives the alkynylated product from the catalytic cycle.[42]
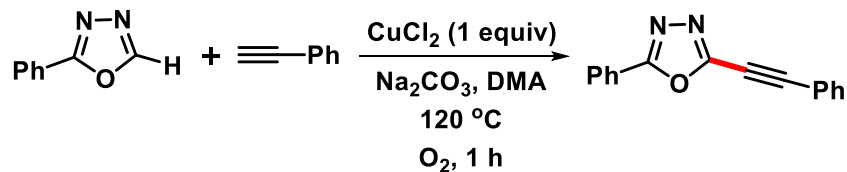
Scheme 1.9: Alkynylation of azoles using Cu(II) catalyst.

➤ **Alkynylation of aromatic halides**

In 2015, Gao and co-workers disclosed Sonogashira-type coupling reactions of aryl iodides with aromatic or aliphatic terminal alkynes accelerated by employing poly aromatic compounds or organophosphate as ligand. In presence of copper triflate catalyst, coupling compound was obtained in DMF. The desired products are produced with high to excellent yields when arylalkynes react with aryl iodides containing both electron-donating as well as electron-withdrawing groups (Scheme 1.10).[43]
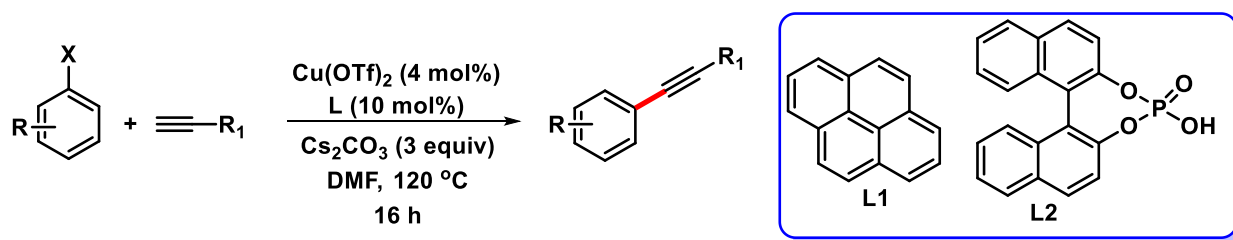
Scheme 1.10: Alkynylation of aromatic halides.

➤ **C(sp^2)-H annulation**

Formation of heterocyclic ring *via* C-H bond activation and annulation of internal alkyne using transition metal catalyst are most effective methods for gaining one-pot access to complex organic compounds. Jiang *et al*. applied this method to synthesize benzofurans through the intermolecular reaction between phenols and alkynes catalyzed by copper (Scheme 1.11). Reaction optimization showed that the reaction efficiency was greatly increased by the Lewis-acid additive ZnCl$_2$.[44]
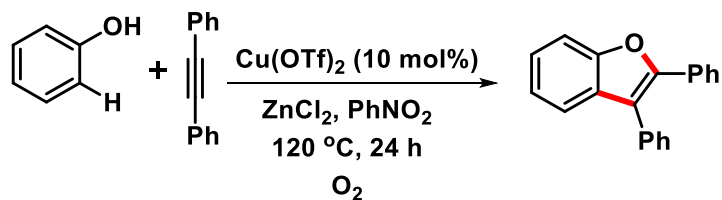
Scheme 1.11: Cu(II) catalyzed annulation of phenols.

1.4.4 Transition metal catalyzed cross-coupling reaction for C-X (X= O, N, S, halides) bond formation

The backbones of many organic compounds are emboided in C−C bonds. However, the functions of molecules are frequently derived from the existence of heteroatoms like oxygen, sulfur, and nitrogen, which are occupied in these molecules in terms of C−X (X= N, S, O, halides) bond formation. These methodology can be successfully utilised in the synthesis of useful compounds for the material sciences, important molecules for medicine, and agrochemicals. Almost all natural compounds contain ketone, ether or ester C-O bond linkage. Almost all natural products comprise ketone, ether or ester C-O bonds. Therefore, since years ago, C-O bond formation reactions have become a powerful tool in organic field.[45] In this section, we will discuss on C-O bond formation reaction using a copper (Cu) transition metal catalyst. Representative examples for construction of C-O bonds are exemplified below.

1.4.4.1 Copper (Cu) catalyzed C-O bond formation

The traditional approach for generating C-O bond between alcohols and aryl halide was Ullman coupling.[14] However, their large-scale uses are limited by their intrinsic limitations, such that in this reaction very low to moderate yield of product was formed using stoichiometric copper salt as catalyst. In most of the cases, reaction needs very high temperature to give moderate yield of product. During the last decade, *O*-arylation processes have been carried out using transition metals, primarily palladium and copper. Furthermore, the costly and hazardous palladium metal they employ makes them less desirable for industrial use. Therefore, for the C-O bond formation processes, less expensive and hazardous metals like copper have been employed extensively. As a result, formation of carbon-oxygen (C-O) bonds is another crucial aspect of organic synthesis. These methods offer chemists a versatile toolkit for synthesizing various organic molecules containing C-O bonds, which are prevalent in natural products, medicinal chemistry, polymers, and other important chemical substances.

➢ *O*-**Arylation of arenes**

In 2003, Ma *et al*. reported C-O bond formation reaction of acetanilide derivatives. Reaction between substituted phenols and aryl bromides or iodides gives *O*-arylated product in presence copper catalyst and *N,N*-dimethylglycine as ligand in dioxane. In this case, *ortho*

NHCOR group present in the ring facilitate the C-O bond formation at room temperature (Scheme 1.12).[46]
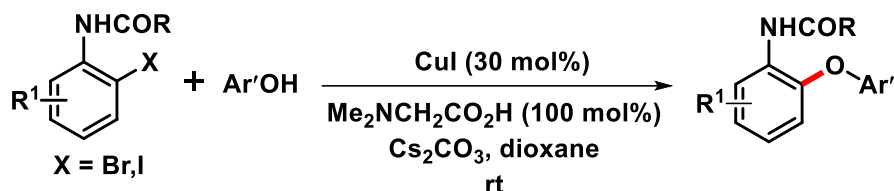
Scheme 1.12: Cu(I) catalyzed C-O bond formation of arenes.

➢ **Alkoxylation of C(sp^2)-H bond**

In 2013, Gooβen *et al*. reported Cu-catalyzed C–H bond activation of arenes to obtain alkoxylated products. The direct *ortho*-alkoxylated of benzoates with boron alkoxides in the presence of one equivalent of silver carbonate and a catalytic amount of copper acetate provided aryl ethers in satisfactory quantities. In this reaction, the decarboxylation and alkoxylation processes both depend on the presence of silver carbonate (Scheme 1.13).[47]
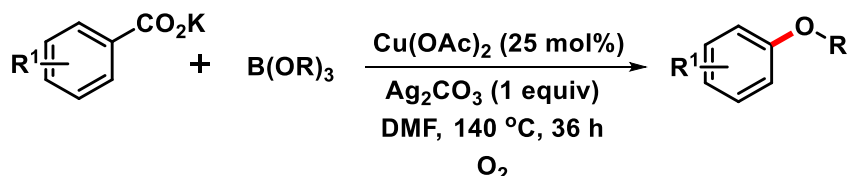
Scheme 1.13: Cu(II) catalyzed alkoxylation of benzoates.

➢ **Ligand directed alkoxylation**

Gooβen and coworkers reported C-H alkoxylation of arenes by copper catalyst. In presence of directing group aryl ethers are formed by Cu catalyzed alkoxylation of alcohols and arenes. Control experiment showed oxygen atmosphere is necessary for this reaction (Scheme 1.14).[48]
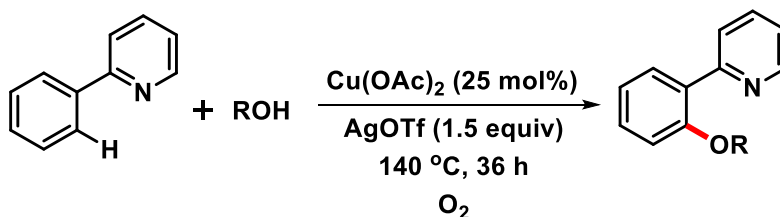
Scheme 1.14: Cu(II) catalyzed alkoxylation of arenes.

➢ **Hydroxylation of arenes**

In 2012, Lei *et al*. reported copper catalyzed C-H activation reaction of electron-poor arenes. In this case hydroxy arenes were formed in presence of atmopheric O_2 *via* oxygen-atom transfer (Scheme 1.15).[49] High yield of products were obtained at room temperature.
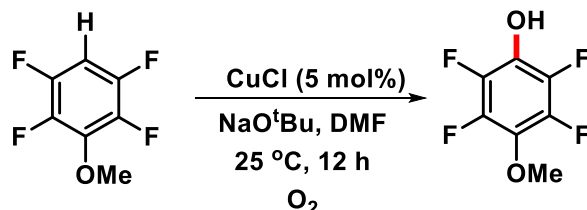
Scheme 1.15: Cu(I) catalyzed hydroxylation of arenes.

➢ **Acyloxylation of C(sp³)-H bond**

Ge and co-workers reported the acyloxylation of *α*-methyl group of aliphatic amides by employing a bidentate ligand in 2014 *via* C(sp³)-H bond activation. According to their mechanistic studies, Cu(OAc)$_2$ acts as both oxygenation source and as a promoter in this reaction (Scheme 1.16).[50]
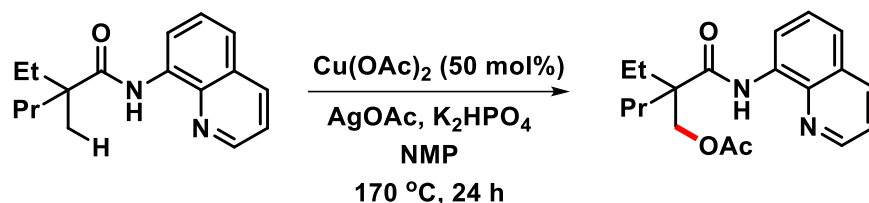
Scheme 1.16: Acetoxylation of amides using Cu(II) catalyst.

➢ **C(sp³)-O bond formation**

Recently, Maiti group reported copper catalyzed formation of dihydrooxazinones. They showed that in presence of Cu-catalyst, intramolecular dehydrogenetive coupling of salicylamides furnished the dihydrooxazinones products in good yields (Scheme 1.17). Interestingly, to predict the position for formation of C(sp³)-O bond in salicylamide compounds, electronic parameters of the *N*-substituents amides can be used.[51]
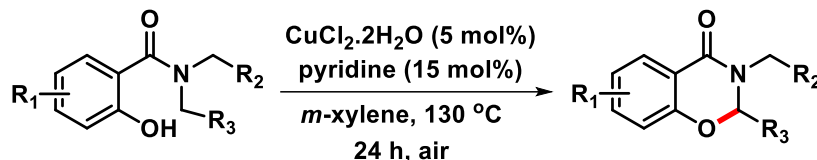
Scheme 1.17: C(sp^3)-O bond formation in presence of Cu(II) catalyst.

1.5 Oxidative cross-coupling

Following their discovery in the last century, cross-coupling reactions have become an effective methodology for the production of a wide range of chemical connections in the presence of transition metal catalysts.[52] Due to their exceptional ability to create many kinds of bonds, they have found extensively in various fields that includes food industries, agriculture, materials science, and pharmaceuticals.[53a] Typically, in those traditional cross-coupling processes, a transition metal catalyst facilitates the creation of bonds between an electrophile and a nucleophile without using any additional redox reagents desired products were formed.[53b] The typical method for obtaining electrophiles needs the prefunctionalization of the starting material. Also, the functionalization of the starting material provides organometallic nucleophiles from their corresponding R-Hs hydrocarbon (where R = C, O, N, S, etc.). However, due to their unavoidable disadvantages which include step economy and significant production of unwanted byproducts, classical cross-couplings face significant challenges in light of the advancement of current synthetic methods and urgent need for green and economical synthesis.[54a] As a consequence, an ideal substitute to replace classical cross-coupling methodology would be the coupling between two nucleophiles for the formation of a new bond, particularly between two hydrocarbons. As the coupling between two nucleophiles requires the introduction of an additional oxidant to facilitate the formation of bonds, these protocols are known as oxidative cross-coupling.[54b]

1.5.1 Importance of oxidative cross-coupling

Due to their significant benefits over conventional cross-couplings and tremendous potential, oxidative cross-couplings have developed extensively in recent decades particularly those combinations between two C–H nucleophiles in aspects of green and economical synthesis.[55] Nucleophiles can be ctegorized into different classes, such as MX, MC and XH or CH (where X = N, O, S, halides). Metal halides salts are used as reactants in the MX group to create carbon-halogen linkages. In presence of transition metal, C–M group of organometallic compounds acts

as nucleophiles (carbon) that participate in various coupling reactions. Notably, the most prevalent nucleophiles are C–H or X–H nucleophiles (where X = O, N, S, etc.) which are high abundant in nature. For several years, the study field focused on substituting organometallic reagents with different C–H or X–H nucleophiles as these chemicals must be synthesized from their corresponding hydrocarbons. As a result, in order to generate greener coupling protocols like R_1-H/R_1-M or R_1-H/R_2-H, many exceptional outcome have been documented in recent times.[56] Especially, the best method for bond formation is to use aerial O_2 as the oxidant in oxidative cross coupling reactions in the presence of a transition metal catalyst. In the case of traditional cross-coupling reactions, corresponding hydrocarbons are converted to organometallic nucleophiles and organohalides as electrophiles for the formation of C–C bond under catalytic conditions (Scheme 1.18). Additional waste and additional reaction steps are inevitable in this protocol. In addition to the growth of environmentally friendly chemical processes, there is a query regarding the possibility of directly forming C–C bonds from C–H substrates without any pre-functionalization of substrates. It will significantly cut down synthetic paths and waste formation. Since H_2 is the only byproduct formed in this process, atom economy is greatly enhanced which exhibiting significant potential in industrial and pharmaceutical applications. Since an oxidant is typically needed to take the hydrogen, it was given the term as a result of oxidative coupling. The hydrogen acceptor can be oxygen or organic peroxides and can be *N*-halosuccinimides (NBS or NCS).
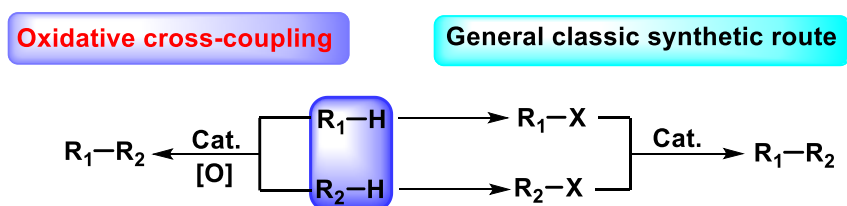
Scheme 1.18. Comparison between traditional coupling and oxidative cross coupling.

Numerous metal catalysts, including Cu, Fe, Pd, Rh and Ru have been demonstrated to work well with CDCs in order to activate the electrophilic coupling partner. Strong nucleophiles such organometallic reactants are avoided in favor of the substrates used in cross dehydrogenetive coupling (CDC), which does not need pre functionalized reagents like in "classical" cross-coupling methods (Sonogashira, Negishi, Suzuki–Miyaura, Stille and others). On the other hand, under oxidative conditions, only C–H containing nucleophiles or electrophiles are required to form the

requisite C–C or C-Hetero bonds.[57] Because of their high energetic barrier, C-H bonds are generally difficult to cleave homolytically. Breaking of C-H bond mostly determined by the stability of the corresponding radical intermediate formed during C-H bond breaking. The C-H bond's bond dissociation energy (BDE) falls along the following series in a diminishing fashion: (sp)C–H →(sp^2)C–H → (sp^3)C–H → allylic-(C-H) → (sp^3)C(α-to heteroatom)–H. The final class of C–H bond in the sequence includes most of the documented CDC reactions and is associated with sp^3 carbons that are in α -positions with respect to heteroatom (O, N, S, etc.) belongs to those carbons.[58] It's interesting to note that there are some examples of CDCs being effectively applied in water, hence increasing their environmental friendliness.

1.5.2 Typical examples of transition metal catalyzed C-C and C-O bond formation by CDC reactions

During the past several years, oxidative coupling between two unfunctionalized hydrocarbons has received a lot of interest in developing new protocols. It is still undergoing rapid development. But there are still a lot of challenges in this field. It is still difficult to achieve regioselective C-H functionalization since hydrocarbons often have various reactive C-H bonds. To achieve direct functionalization of an unreactive C–H bonds, both oxidants and transition metal catalysts are required in this process. Transition metal catalysts that are used the most include Pd, Cu, Ru, and Rh (Scheme 1.19).[59] In this discussion, we will focus solely on the copper-catalyzed CDC reaction.
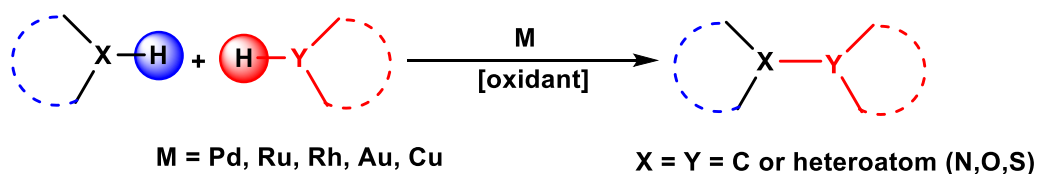
Scheme 1.19: Transition metal-catalyzed CDC reactions.

1.5.3 Representative example for copper (Cu) catalyzed CDC reactions

➢ **Alkynylation of C(sp^2)-H bond**

In 2013, Jiao *et al.* reported dehydrogenative annulation between a heterocyclic compound and terminal alkyne under aerobic condition. In this process, *N*-iminopyridinium ylide converted to various pyrazolo[1,5-a]pyridine derivatives in moderate to good yields. In presence of CuI

catalyst and oxygen (O_2) as oxidant pyrazole derivatives were formed succesfully. Ag_2CO_3 present in reaction medium acts as base to abstract the alkyne proton and promotes the reaction rate faster (Scheme 1.20).[60]
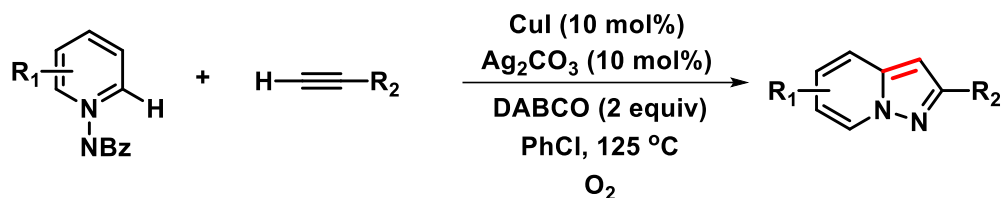
Scheme 1.20. Alkynylation of *N*-iminopyridinium ylide.

➢ **Alkynylation of C(sp³)-H bond**

Su *et al*. disclosed the alkynylation of isoquinoline derivatives by ball milling methodology in presence of copper catalyst. Terminal alkynes were used as alkyne source and DDQ used as oxidant. This reaction was carried out under solvent free condition (Scheme 1.21).[61]
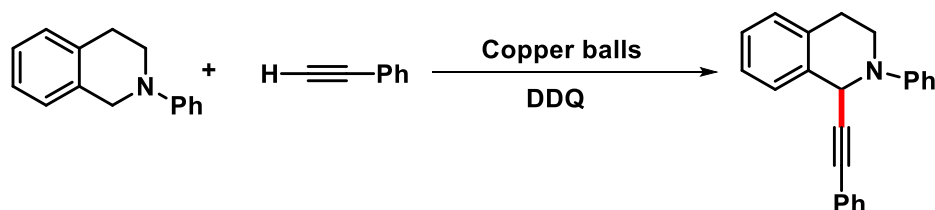
Scheme 1.21. Alkynylation of isoquinoline derivatives.

➢ **Alkylation of C(sp²)-H bond**

Wei's group revealed alkylation of styrene derivatives in presence of copper catalyst. With the aid of $Cu(OTf)_2$ as catalyst and DTBP oxidant, a wide variety of alkenes react with different cycloalkanes and produce the their alkenylation product (Scheme 1.22). Alkylated products were formed in good to excellent yields. Kinetic isotopic effects (KIE) experiment for cyclohexane with styrene suggested that C(sp³)-H bond breaking was rate-determining step in this transformations.[62]
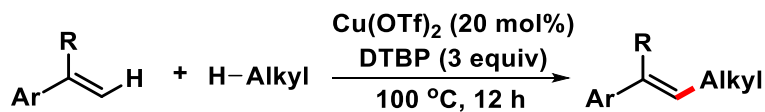
Scheme 1.22. Alkylation of C(sp²)-H bond.

➢ **Arylation of C(sp²)-H bond**

In 2011, Miura *et al*. reported biaryl coupling with out using any palladium catalysts. They showed that in presence of Cu catalyst reaction between arylazines and azoles provided the desired coupling product through dual C-H bond activation. By chossing right copper salt is essential in this process because the reactions performed flawlessly with $Cu(OAc)_2$ whereas using $CuCl_2$ and $Cu(OTf)_2$ reaction was failed. Although more than the stoichiometric amount copper salt was needed for full conversion, this report was one of the first to show that pricey palladium might be substituted for the arylation procedure (Scheme 1.23).[63]
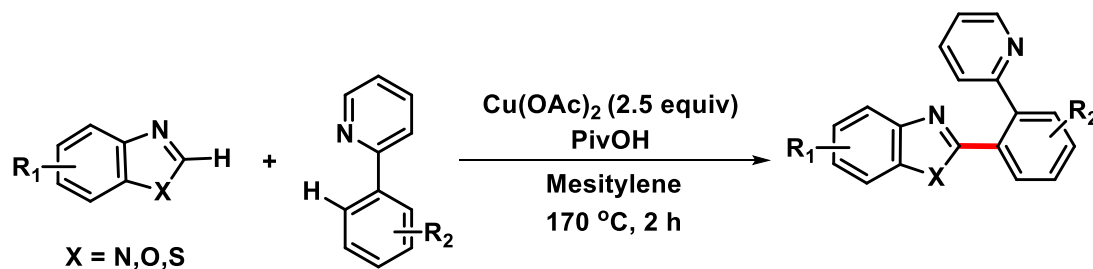
Scheme 1.23. Biaryl coupling using copper catalyst.

➢ **Arylation of C(sp³)-H bond**

In 2011, Zhang *et al*. disclosed *N,N*-dimethylanilines and heteroarenes can be oxidatively cross-coupled using a CuBr catalyst. Here molecular oxygen acts as oxidant and the reaction went efficiently in mild condition. This procedure outlined a straightforward way for arylating Csp³–H bonds with heteroarenes next to a nitrogen atom using copper salt catalysis (Scheme 1.24).[64]
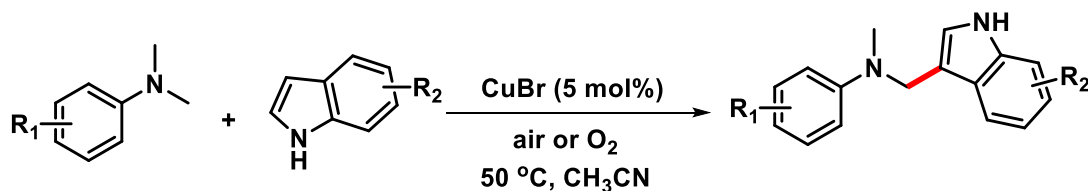
Scheme 1.24. Functionalization of C(sp³)-H bond.

➢ **C(sp²)-C(sp²) bond formation**

Lei *et al*. reported a novel methodology for the formation of α,β-unsaturated ketones in presence of copper catalyst. Coupling between between aldehydes and styrenes using organic peroxide (TBHP) as oxidant afforded unsaturated ketones in oxidative condition. Among the

various metal salts only CuCl$_2$ gives coupled product with high yield. Further radical trapping experiment conclude that reaction mechanism follows the radical pathway (Scheme 1.25).[65]
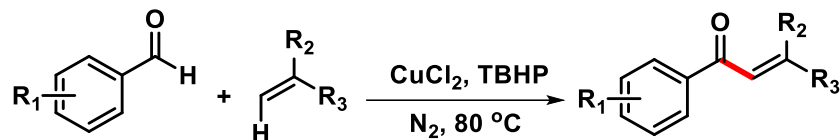
Scheme 1.25. Formation of unsaturated ketones using copper catalyst.

➢ **C(sp³)-C(sp²) coupling**

In 2014, Duan *et al.* reported oxidative CDC between cinnamamides and benzyl hydrocarbon starting material followed by cyclization for dihydroquinolinones synthesis using Cu-catalyst. Ethers, alcohols, and alkanes also utilized as coupling partner in place of benzyl hydrocarbons in this reaction. Control experiment suggested that both oxidant (TBPB) and catalyst (Cu$_2$O) are necessary for this reaction (Scheme 1.26).[66]
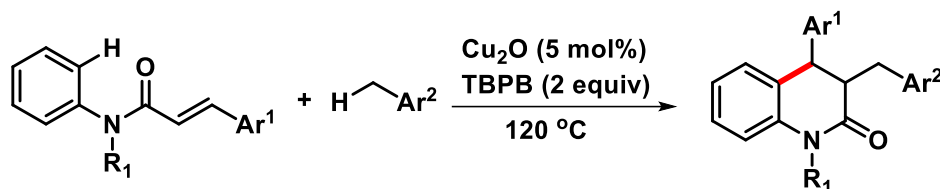
Scheme 1.26. Copper-catalyzed synthesis of dihydroquinolinones.

➢ **C(sp²)-O bond formation**

By employing copper catalysis to create oxidative C–O bonds toward synthesis of carbamates from formamides were disclosed by Reddy group. Enol carbamates were formed with high stereoselectivity and the current approach was expanded to include the oxidative esterification of phenols that have been substituted with carbonyls (Scheme 1.27).[67]
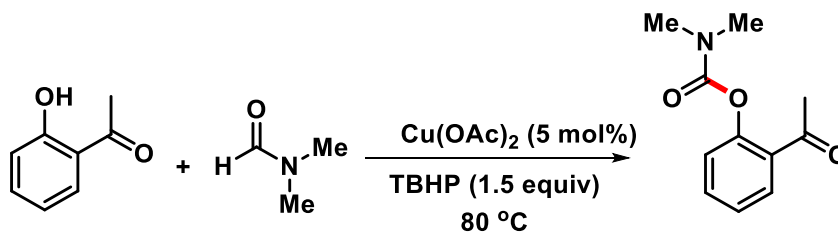
Scheme 1.27. Cu(II) catalyzed carbamates formation.

➢ **C(sp³)-O bond formation**

Pan's group revealed copper catalyzed dehydrogenetive olifination followed by esterification of aldehyde compounds in 2014. The reaction was carried out at 140 °C with the aid of stoichiometric oxidant TBHP. The reaction mechanism follows radical pathway (Scheme 1.28).[68]
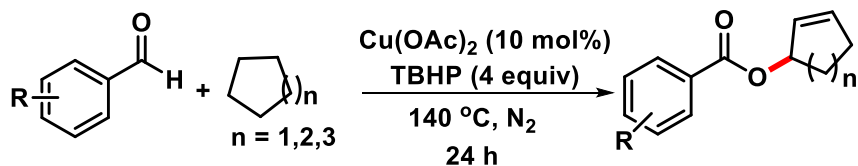
Scheme 1.28. Synthesis of ester using Cu(II) catalyst.

➢ **C(sp³)-O bond formation**

Guan *et al*. disclosed reaction between acetophenone oxime and THF using a copper catalyst in 2016. Here, allyl bromide serves as a propagator to improve product yield by generating a radical from THF (Scheme 1.29).[69]
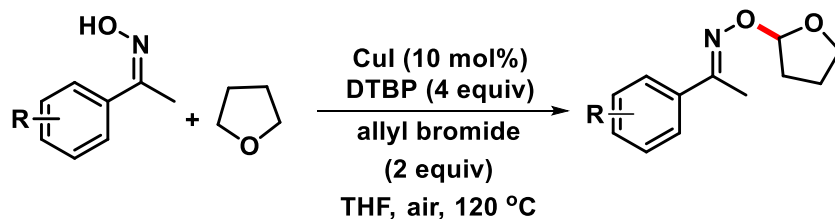
Scheme 1.29. Synthesis of oxime ethers using Cu(II) catalyst.

➢ **Alkoxylation of allylic compounds**

In 2020, Stahl group disclosed formation of benzyl ethers through cross coupling of alcohol and allylic arenes which is catalyzed by copper. Cu(I)-assisted *N*-fluorobenzenesulfonimide (NFSI) activation is the first step in this reaction. This forms an *N*-centered radical that can promote HAT from the benzylic C–H bond present in allylic arenes. Resultant Cu(II) then facilitates interaction between alcohol and benzylic radical to produce benzylic ethers (Scheme 1.30).[70]
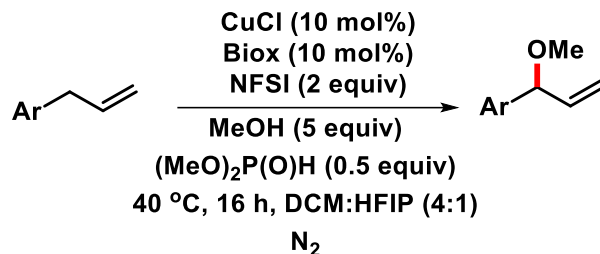
Scheme 1.30. Synthesis of ether using Cu(II) catalyst.

➢ **Esterification of aldehyde compounds**

In 2012, Patel's group reported oxidative esterification reaction between aldehydes and alkylbenzenes as a coupling partner in preence of copper catalyst. TBHP was used as the oxidant, and inexpensive Cu-catalyst was employed to stimulate the benzylic (sp³)C-H bond of alkylbenzenes. Based on various control experiment it was proposed that reaction proceed via coupling between aldehydes and benzyl alcohol (generated in situ from alkylbenzenes), which developed from the hemiacetal intermediate (Scheme 1.31).[71]
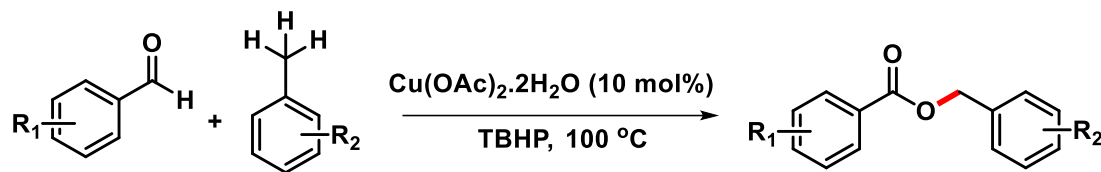
Scheme 1.31: Conversion of aldehydes to ester derivatives using copper catalyst.

➢ **Esterification of benzyl alcohol derivatives**

Yuan group has reported the formation of acyloxy ethers through C-O bond generation using Cu catalysts. in the presence of TBHP as the oxidant and. Unactivated ethers reacted with electron donating and electron withdrawing benzyl ethrts to give product in high yield which were the major advantages of this protocol. It was suggested that the reaction would occur *via* the cross-coupling of alkyl or oxonium species with acyloxy radicals (Scheme 1.32).[72]
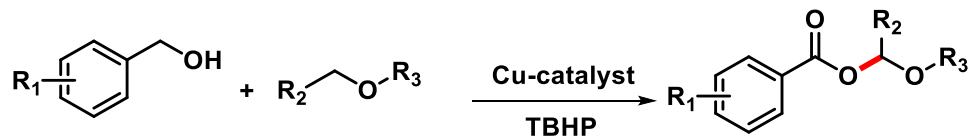
Scheme 1.32: Cu- catalyzed synthesis of *α*-acyloxy ethers.

1.6 Copper (Cu) catalyzed synthesis of acyclic and cyclic compounds using Glaser-Hay coupling and their application

The history of acetylenic coupling reactions in presence of copper catalyst is established approximately 150 years back. The reaction was first reported by Glaser in 1869. He noticed that noticed that cu(I)phenyl acetylide oxidized in the air produced diphenyldiacetylene by dimerization.[13] The process of alkyne dimerization in oxidative condition with oxygen and a copper catalyst is known as Glaser coupling. This process garnered significant interest in the production of C-C bonds in organic synthesis (Scheme 1.33).

$$2\ R\!-\!\!\!\equiv\!\!\!-H \xrightarrow[\text{NH}_4\text{OH, EtOH}]{\text{CuCl}} 2\ R\!-\!\!\!\equiv\!\!\!-Cu \xrightarrow[\text{NH}_4\text{OH, EtOH}]{\text{O}_2} R\!-\!\!\!\equiv\!\!\!-\!\!\!\equiv\!\!\!-R$$
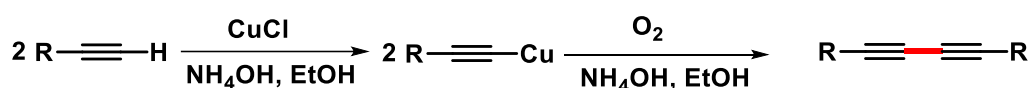
Scheme 1.33: Copper promoted Glaser coupling reaction.

Hay further modified the Glaser coupling in 1962 by solubilizing copper(I) halides with a catalytic quantity chelating ligand in presence of aerial O_2.[73] He used *N,N,N′,N′*-tetramethylethylenediamine (TMEDA) as chelating ligand. Hay coupling reaction, also known as Glaser-Hay coupling (Scheme 1.34). Due to the wide solubility of copper–chelating complex in various solvents, Hay coupling reactions become more valuable in organic synthetic perspectives.

$$2\ R\!-\!\!\!\equiv\!\!\!-H \xrightarrow[\text{O}_2,\ \text{solvent}]{\text{CuCl/TMEDA}} R\!-\!\!\!\equiv\!\!\!-\!\!\!\equiv\!\!\!-R$$

Scheme 1.34: Copper catalyzed Glaser-Hay coupling reaction.

Various diynes derivatives were synthesized using Glaser-Hay coupling reaction in organic synthesis methodology. The conjugated triple bonded diynes compounds were synthesized by using copper catalyst *via* homocoupling reaction between two terminal alkynes. Since conjugated diynes are extensively used in a wide range of polymers, supramolecular materials and physiologically active compounds, herein we will discuss about synthesis of some acyclic and cyclic 1,3-diynes-containing compounds which is synthesized by Glaser-Hay coupling in presence of copper as catalyst.

Homocoupling reaction of acetylenic hydrocarbons while producing aryl acetylenic Mannich bases that are biologically active. was reported by Chibale and coworkers. Using 0.5

equiv. of Cu(OAc)$_2$ catalyst (normally, Glaser reactions needs stoichiometric amount (10 eq.) of Cu catalyst without dioxygen) and 1.0 equiv. of triethylamine, acetylenic hydrocarbons were efficiently dimerized in dioxane with high yields (Scheme 1.35).[74]
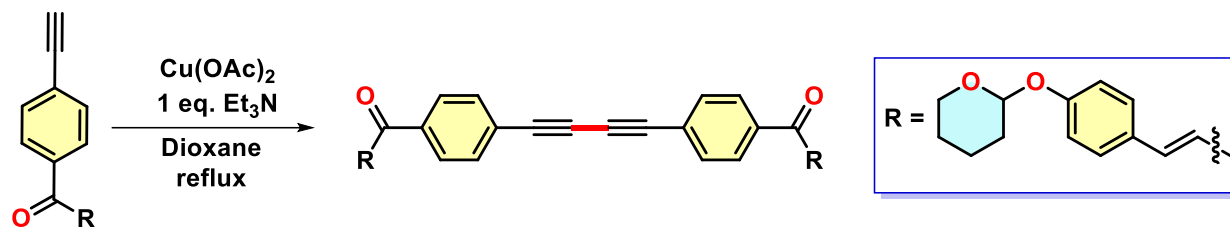
Scheme 1.35: Homocoupling of acetylenic hydrocarbons.

To create per-(2-thienyl)pyridine compounds which is symmetrical in nature from readily accessible substituted pyridines, Glaser coupling was employed as the essential process. 2,4,5,6-Penta(2-thienyl)pyridine substituted with alkynes formed butadiyne derivatives in good yields using Glaser coupling that had intriguing photophysical and electrochemical properties (Scheme 1.36).[75]
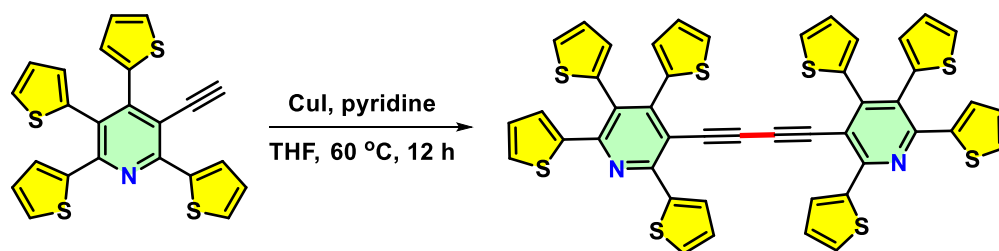
Scheme 1.36: Homocoupling of thienyl pyridine derivatives.

Tykwinski *et al.* reported oxidative acetylenic coupling protocols to synthesize completely a macrocyclic compound from 3,5-diethynylpyridyl subunits (Scheme 1.37). Concerning the macrocyclic core, the pyridyl moiety was oriented both endocyclically and exocyclically, and in the solid state, it took on a virtually planar shape devoid of ring strain.[76]
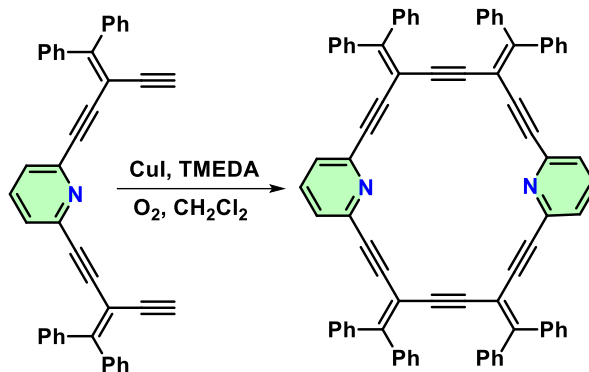
Scheme 1.37: Synthesis of macrocyclic compounds using copper catalyst.

Another cyclization approach was reported by Babu *et al*. in presence of Cu(II) as efficient catalyst in DMSO solvent. The optimal temperature was 110 °C for this reaction under air to give 50% yield of macrocyclic compound (Scheme 1.38).[77]
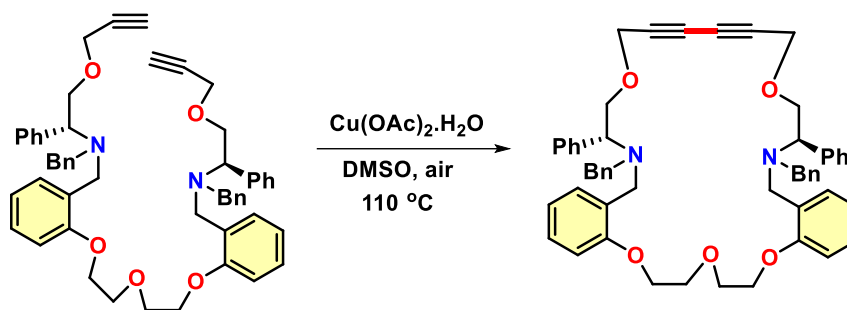
Scheme 1.38: Synthesis of macrocycle compounds *via* Glaser-Hay coupling.

1,3-Diynes, compounds with two triple bonds separated by a single carbon-carbon bond, have a variety of utilisation in organic methodology, materials science, and pharmaceuticals because of their unique structural linkages and reactivity.[78] 1,3-Diynes are valuable building blocks for the development of complex natural compounds. Also, conjugated diynes have been employed in synthesizing porous materials like MOFs. The rigid and conjugated structure of 1,3-diynes makes them useful in developing functional materials such as organic semiconductors, liquid crystals, and conducting polymers.[79] Additionally, 1,3-diynes and their derivatives have shown promising pharmacological activities, including anticancer, antimicrobial, and anti-inflammatory properties. Due to their π-conjugated structures, they are mostly used in optoelectronic instruments like organic field-effect transistors (OFETs), organic light-emitting diodes (OLEDs), and organic photovoltaics (OPVs), 1,3-diynes and their derivatives have been

studied.[80] 1,3-diynes have garnered attention as potential ligands for metal ion detection due to their unique optical and structural properties. These compounds can form complexes with metal ions, leading to changes in their absorption, fluorescence, or other spectroscopic properties, which can be exploited for sensing purposes. Herein, we will discuss metal ion detection in presence of some cyclic and acyclic molecules.

1.6.1 Synthesis of acyclic and cyclic molecules for metal ion (Cu^{2+}/Hg^{2+}) detection

The detection of biologically significant species or environmental contaminants has garnered significant interest since precise and quantitative assessment of these contaminated components offers crucial signals for the appropriate disposal of contaminated environmental and biomedical materials.[81] Heavy and transition metal (HTM) ions are involved in a multitude of processes and phenomena that take place in the environment or within biological organisms. Inadequate supply of these micronutrients causes many deficiency diseases or syndromes. As a result of the widespread use and processing of heavy metals in numerous activities to meet the demands of the fast expanding population, heavy metal contamination is now a serious issue throughout the world. An element with a high atomic weight and molecular density is referred to as a heavy metal.[82] Natural water is typically the source of heavy metals, many of them are toxic even at extremely low amounts. Even at low quantities, metals like Ni, Pb, Hg, Cu, Cd, As, Cr, Zn, Co, and Se are quite toxic and harmful. Copper is a necessary nutrient needed for a variety of physiological and biochemical processes which is a 3d block transition metal in periodic table. Alzheimer's, prion diseases, Wilson's disease, and amyotrophic lateral sclerosis are all brought on by an imbalance of copper levels in the human body.[83] Overconsumption of copper, sometimes referred to as copper poisoning, causes malignancies, the formation of new blood vessels, damage to the kidneys and liver, digestive problems. On the other hand, mercury metal has been utilized for numerous economic uses and as a poison and medication for ages.[84,85] Recently, because of environmental exposure this metal refocused its attention. Mercury is primarily found in three forms: organic compounds, inorganic salts, and metallic elements which shows different toxicity and bioavailability. These mercury forms are extensively distributed in water resources like lakes, rivers, seas and absorbed by microbes and eventually change into methyl mercury within the microorganism, which undergoes biomagnification and seriously disrupts aquatic life. By consuming this tainted aquatic species, humans are mostly exposed to methyl mercury. In addition,

it finds application in the pulp and paper sectors, as well as in battery manufacturing and dental amalgam preparations. Methylmercury is a neurotoxic substance that damages mitochondria, breaks down microtubules, causes lipid peroxidation, and accumulates neurotoxic substances like glutamate, aspartate, and serotonin.[86,87] It has the potential to interfere with intracellular calcium homeostasis and disturb the membrane potential. Mercury attaches itself to readily available thiols because of their high stability constants. When mercury binds with selenohydryl and sulfhydryl functional groups, it readily reacts with methyl mercury to cause structural disruption in cells. Cellular function is altered by this process, which also affects the protein structures present in human body.

Therefore, the development of sensors using small organic molecules has shown promising interest in this regard because of their easy to synthesize, ease of manipulation and broad applicability. To determine a broad range of significant environmental and biological target components such as heavy metal ions (Cu^{2+}/ Hg^{2+}) and anions present in the environment or the bacteria and viruses present in biological species, several numbers of sensors have been developed that can detect analytes with high-performance.[88-90] Due to their selective ability to bind with a specific metal ion, cyclic and acyclic molecules have significant applications in metal ion sensing and produce detectable signals. From this view point, the development of sensors with good stabilities, high reproducibility and excellent tolerance of complex detection environments is of significant current interest. Here a brief review has been made based on literature survey on cyclic and acyclic compounds which are mainly behaving as metal ion sensors to detect copper and mercury simultaneously. Here few acyclic derivatives have been shown in Figure 1.5 that are developed by various research group as copper ion sensors. Some molecules also can recognize mercury ion (Hg^{2+}) simultaneously (Figure 1.5). Sie *et al*. developed a 1,10-phenanthroline based colorimetric probe (**A**) for dual sensing of Cu^{2+} and Hg^{2+} ions in water.[91] Li *et al*. reported an imine compound (**B**) that selectively detects mercury ion (Hg^{2+}). The reported compound can detect mercury in living cell organisms as well as it can recognize metal ion in aqueous medium.[92] Wu *et al*. developed a fluorescent chemosensor containing a picolinylhydrazide receptor and pyrene component (**C**) for recognizing copper ion (Cu^{2+}) from aqueous medium.[93] Wu and co-workers reported an imine linked thiourea sensor (**D**) that selectively recognize copper and mercury ions.[94] Duan and co-workers developed rhodamine based colorimetric chemosensor (**E**) for dual ion detection (Cu^{2+} and Hg^{2+}) ions in aqueous media.[95] Sivalingam *et al*. described an imine linked

thiophene compound (**F**) for selective detection of copper ion (Cu^{2+}) in living cells by fluorescence turn-on process.[96] Ghosh *et al.* reported rhodamine based optical chemosensors (**G**) for the selective recognition of copper and mercury ions.[97]
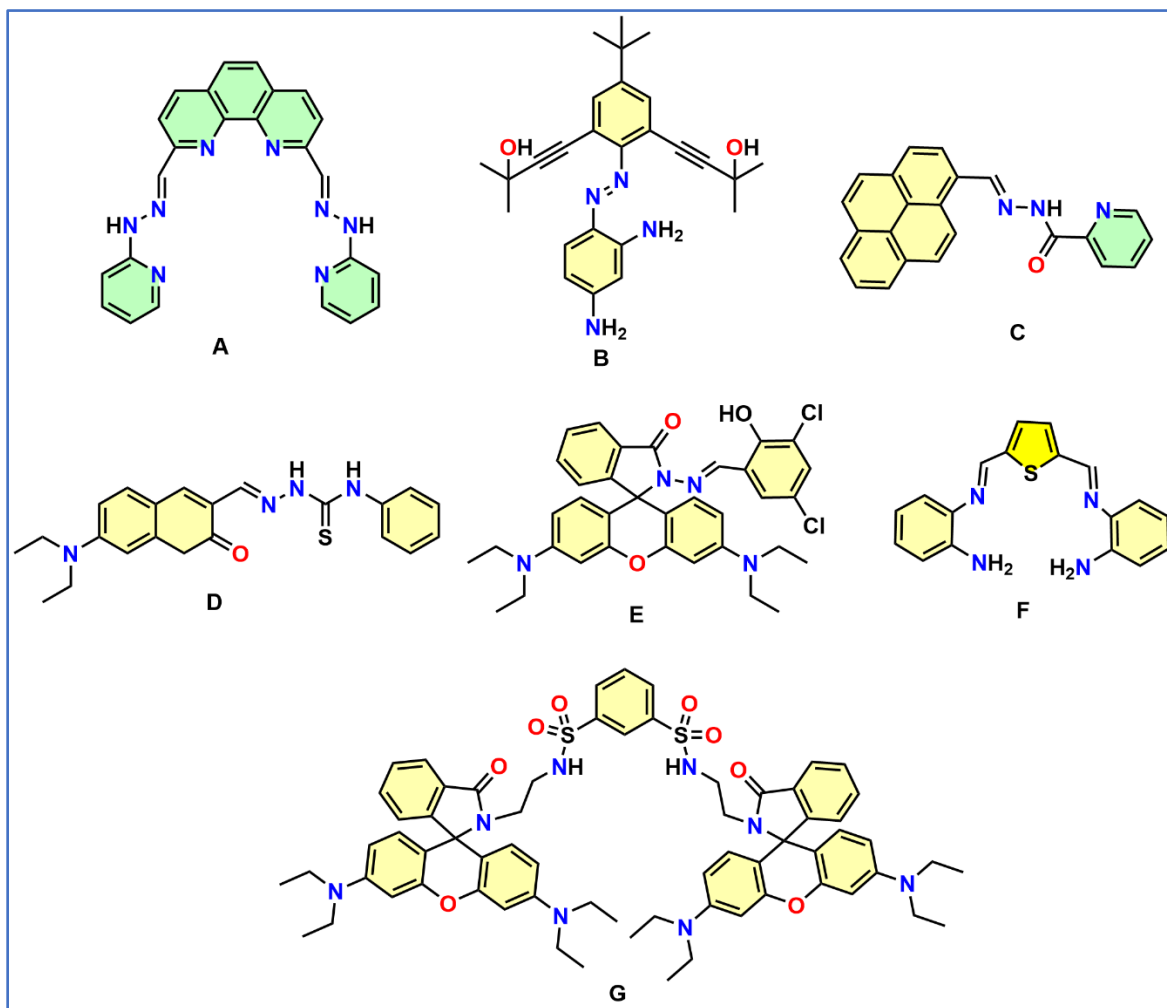
Figure 1.5. Examples of acyclic compounds for Cu^{2+} and Hg^{2+} ion detection.

Schematic diagram of some cyclic ligands are listed below that have been used by various research groups in field of the coordination chemistry to detect Copper and mercury metal ions (Figure 1.6). Paul and co-workers synthesized a cyclic fluorescent chemosensor (**H**) where bipyridine was connected with a crown nitrogen atom. This calixarene-based chemosensor shows fluorescent turn-on upon metal ion binding with the host molecule. This molecule detects both Hg^{2+} and Cu^{2+} ions.[98] Xie *et al.* reported carbohydrate-based BODIPY-functionalized fluorescent macrocycles (**I**) for selective recognition of copper ion.[99] Parra and co-workers synthesized a 2,4,6-

triphenylthiopyrylium (**J**) functionalized chemosensors for selective Hg^{2+} and Cu^{2+} ions detection.[100] Jiang *et al*. reported a porphyrin containing chromophore (**K**) as a fluorescent sensors for Cu^{2+} detection.[101] Chen *et al*. reported tritptycene derived heeteracalixarenes (**L**) for selective Hg^{2+} ion recognition.[102]
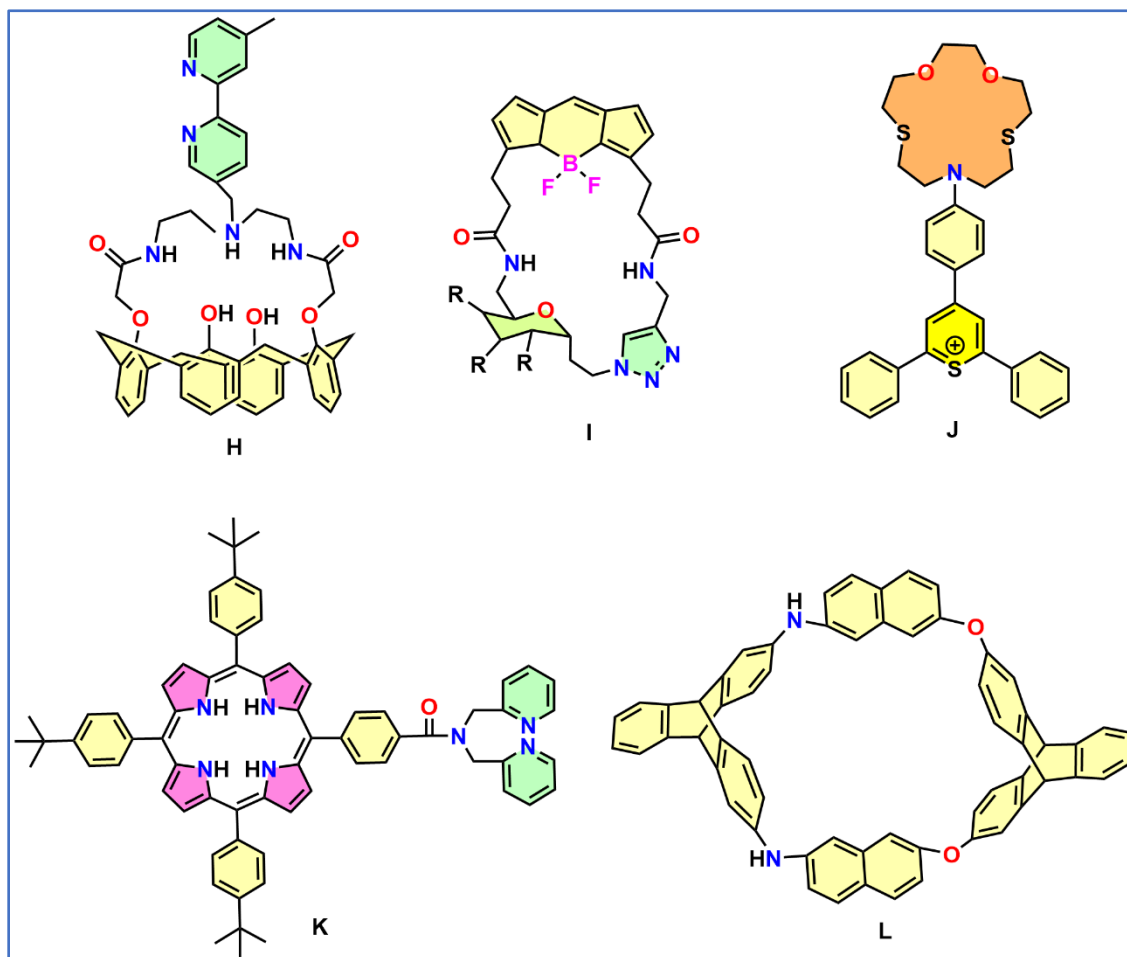
Figure 1.6. Examples of cyclic compounds for Cu^{2+} and Hg^{2+} ion detection.

1.7 References

1 S. Green, Industrial Catalysis, Macmillan Company, New York, 1928.

2 J. J Berzelius, The annual report on progress in physics and chemistry, Royal Swedish Academy of Sciences, 1835.

3 G. Ertl, *Angew. Chem., Int. Ed*., 2009, **48**, 6600–6606.

4 (a) S. H. Taylor, *J. Am. Chem. Soc*., 1931, **53**, 578-597; (b) R. Chinchilla and C. Nμjera, *Chem. Rev*., 2007, **107**, 874.

5 R. Schlögl, *Angew. Chem. Int. Ed.,* 2015, **54**, 3465 – 3520.

6 (a) R. M Heck and R.J. Farrauto, Catalytic Pollution Control, second ed., Wiley Interscience, New York, 2002; (b) P. Papaefthimiou, T. Ioannides and X. E. Verykios, *Appl. Catal. B*, 1997, **13**, 175; (c) P. Marécot, A. Fakche, B. Kellali, G. Mabilon, P. Prigent and J. Barbier, *Appl. Catal. B,* 1994, **3**, 283.

7 M. Appl, "Ammonia", Ullmann's Encyclopedia of Industrial Chemistry, Weinheim, Wiley-VCH, 2006, DOI: 10.1002/ 14356007.a02_143.pub2.

8 B. Cornils and W. A. Herrmann, *Journal of Catalysis*, 2003, **216**, 23-31.

9 M. Ramos, A. P. S. Dias, J. F. Puna, J. Gomes and J. C. Bordado, *Energies,* 2019, **12**, 4408.

10 T.A. Bender, J.A. Dabrowski and M.R. Gagné, *Nat. Rev. Chem.,* 2018, **2**, 35–46.

11 (a) R. Jana, T. P. Pathak and M. S. Sigman, *Chem. Rev.,* 2011, **111**, 3, 1417–1492; (b) J. H. Xie, S.-F. Zhu and Q.-L. Zhou, *Chem. Rev.* 2011, **111**, 3, 1713–1760. (c) R. H. Grubbs and C. R. Hoppin, *J. Am. Chem. Soc.,* 1979, **101**, 6, 1499–1508.

12 B. M. Trost, *Angew. Chem. Int. Ed*., 1995, **34**, 259.

13 C. Glaser, *Ber. Dtsch. Chem. Ges*., 1869, **2**, 422-424.

14 F. Ullmann and J. Bielecki, *Ber. Dtsch. Chem. Ges*., 1901, **34**, 2174-2185.

15 (a) E. Frankland, *Liebigs Ann. Chem*., 1848, 71, 171; (b) E. Frankland, *J. Chem. Soc.,* 1848, 2, 263; (c) V. Grignard, *Compt. Rend. Acad. Sci. Paris*, 1900, **130**, 1322; (d) V. Grignard, *Ann. Chim*., 1901, 24, 433.

16 (a) A. de. Meijere and F. Diederich, Metal-Catalyzed Cross-Coupling Reactions 2nd ed., Wiley-VCH, Weinheim, 2004; (b) J. Tsuji, Transition Metal Reagents and Catalysts: Innovations in Organic Synthesis, Wiley, Chichester, 1995.

17 F. Diederich and P. J. Stang, Metal-catalyzed cross-coupling reactions, John Wiley & Sons, 2008.

18 M. Zhang, Y. Zhang, X. Jie, H. Zhao, G. Li and W. Su, *Org. Chem. Front.*, 2014, **1**, 843-895.

19 T. W. Lyons and M. S. Sanford, *Chem. Rev.*, 2010, **110**, 1147-1169.

20 (a) C.-H. Jun, *Chem. Soc. Rev.*, 2004, **33**, 610–618; (b) T.-Y. Luh, M.-kit Leung and K.-T. Wong. *Chem. Rev.,* 2000, **100**, 3187–3204. (c) F. Chen, T. Wang and N. Jiao, *Chem. Rev.*, 2014, **114**, 8613–8661.

21 G. Evano and N. Blanchard, Copper-Mediated Cross-Coupling Reactions; Wiley: Hoboken, New Jersey, 2014.

22 N. Krause, Modern Organocopper Chemistry; Ed.; Wiley-VCH: Weinheim, Germany, 2002.

23 A. Alexakis, N. Krause and S. Woodward, Copper-Catalyzed Asymmetric Synthesis; Wiley-VCH: Weinheim, Germany, 2014.

24 J. Hassan, M. Sévignon, C. Gozzi, E. Schulz and M. Lemaire, *Chem. Rev.*, 2002, **102**, 1359−1470.

25 P. E. Fanta, *Chem. Rev.*, 1964, **64**, 613−632.

26 I. Goldberg, *Ber. Dtsch. Chem. Ges*. 1906, **39**, 1691−1692.

27 F. Ullmann and J. Bielecki, *Ber. Dtsch. Chem. Ges*. 1901, *34*, 2174−2185.

28 X. Zhu and S. Chiba, *Chem. Soc. Rev.*, 2016, **45**, 4504−4523.

29 M. T. Pirnot, Y.-M. Wang and S. L. Buchwald, *Angew. Chem. Int. Ed.*, 2016, **55**, 48−57.

30 C. Sambiagio, S. P. Marsden, A. J. Blacker and P. C. McGowan, *Chem. Soc. Rev.*, 2014, **43**, 3525−3550.

31 X. Ribas, D. A. Jackson, B. Donnadieu, J. Mahía, T. Parella, R. Xifra, B. Hedman, K. O. Hodgson, A. Llobet and T. D. P. Stack, *Angew. Chem., Int. Ed.*, 2002, **41**, 2991−2994.

32 L. M. Huffman and S. S. Stahl, *J. Am. Chem. Soc*. 2008, **130**, 9196−9197.

33 R. Xifra, X. Ribas, A. Llobet, A. Poater, M. Duran, M. Solà, T. D. P. Stack, J. Benet-Buchholz, B. Donnadieu, J. Mahía and T. Parella, *Chem. - Eur. J.*, 2005, **11**, 5146−5156.

34 O. Daugulis, H.-Q. Do and D. Shabashov, *Acc. Chem. Res.*, 2009, **42**, 1074−1086.

35 X.-X. Guo, D.-W. Gu, Z. Wu and W. Zhang, *Chem. Rev.*, 2015, **115**, 1622−1651.

36 A. E. Wendlandt, A. M. Suess and S. S. Stahl, *Angew. Chem., Int. Ed.*, 2011, **50**, 11062−11087.

37 H.-Q. Do and O. Daugulis, *J. Am. Chem. Soc.*, 2007, **129**, 12404−12405.

38 X. Wu, Y. Zhao and H. Ge, *Chem. Sci.*, 2015, **6**, 5978−5983.

39 M. Ke and Q. Song, *Chem. Commun.*, 2017, **53**, 2222−2225.

40 D. Li, X.-X. Wu, T. Gao, B. Li and S. Chen, *Org. Biomol. Chem.*, 2017, **15**, 7282−7285.

41 F. M. Irudayanathan, G. C. E. Raja and S. Lee, *Tetrahedron*, 2015, **71**, 4418-4425.

42 M. Kitahara, K. Hirano, H. Tsurugi, T. Satoh and M. Miura, *Chem. - Eur. J.*, 2010, **16**, 1772−1775.

43 W. Xu, B. Yu, H. Sun, G. Zhang, W. Zhang and Z. Gao. *Appl. Organometal. Chem.*, 2015, **29**, 301–304.

44 W. Zeng, W. Wu, H. Jiang, L. Huang, Y. Sun, Z. Chen and X. Li, *Chem. Commun.*, 2013, **49**, 6611−6613.

45 O. Soltani and J. K. De Brabander, *Angew. Chem. Int. Ed.*, 2005, **44**, 1696-1699.

46 Q. Cai, B. Zou and D. Ma, *Angew Chem Int Ed.*, 2006, **45**, 1276-1279.

47 S. Bhadra, W. Dzik, and L. J. Gooβen, *Angew. Chem. Int. Ed.*, 2013, **52**, 2959–2962.

48 S. Bhadra, C. Matheis, D. Katayev and L. J. Gooβen, *Angew. Chem. Int. Ed.*, 2013, **52**, 9279–9283.

49 Q. Liu, P. Wu, Y. Yang, Z. Zeng, J. Liu, H. Yi and A. Lei, *Angew. Chem., Int. Ed.*, 2012, **51**, 4666−4670.

50 X. Wu, Y. Zhao and H. Ge, *Chem. - Asian J.*, 2014, **9**, 2736−2739.

51 A. Modak, U. Dutta, R. Kancherla, S. Maity, M. Bhadra, S. M. Mobin and D. Maiti, *Org. Lett.*, 2014, **16**, 2602.

52 A. de Meijere and F. Diederich, Metal-Catalyzed Cross-Coupling Reactions, 2nd, completely rev. and enl. ed.; Wiley-VCH, Weinheim, 2004.

53 (a) M. Beller, and C. Bolm, Transition Metals for Organic Synthesis: Building Blocks and Fine Chemicals; 2nd rev. and enl. ed.; Wiley-VCH, Weinheim, 2004; (b) C. Liu, H. Zhang, W. Shi and A. Lei, *Chem. Rev.*, 2011, **111**, 1780–1824.

54 (a) E.-i. Negishi and A. de Meijere, Handbook of Organopalladium Chemistry for Organic Synthesis, Wiley-Interscience, New York. 2002; (b) C. Liu, J. Yuan, M. Gao, S. Tang, W. Li, R. Shi, and A. Lei, *Chem. Rev.*, 2015, **115**, 12138–12204.

55 (a) J. Le Bras and J. Muzart, *Chem. Rev.*, 2011, **111**, 1170–1214; (b) C. S. Yeung and V. M. Dong, *Chem. Rev.*, 2011, **111**, 1215–1292.

56 W. Shi, C. Liu, and A. Lei, *Chem. Soc. Rev.*, 2011, **40**, 2761–2776.

57 (a) C.-J. Li, *Acc. Chem. Res*. 2009, **42**, 335; (b) S. A. Girard, T. Knauber and C.-J. Li, *Angew. Chem. Int. Ed*., 2014, **53**, 74.

58 A. Gini, T. Brandhofer and O. G. Mancheño, *Org. Biomol. Chem*., 2017, **15**, 1294.

59 Recent reviews on CDC in general: (a) B. V. Varun, J. Dhineshkumar, K. R. Bettadapur, Y. Siddaraju, K. Alagiri and K. R. Prabhu, *Tetrahedron Lett*., 2017, **58**, 803–824; (b) C.-J. Li, *Acc. Chem. Res*.2009, **42**, 335–344.

60 S. Ding, Y. Yan and N. Jiao, *Chem. Commun*., 2013, **49**, 4250.

61 W. Su, J. Yu, Z. Li, and Z. Jiang, *J. Org. Chem*., 2011, **76**, 9144−9150.

62 Y. Zhu and Y. Wei, *Chem. Sci*., 2014, **5**, 2379−2382.

63 M. Kitahara, N. Umeda, K. Hirano, T. Satoh and M. Miura, *J. Am. Chem. Soc*., 2011, **133**, 2160–2162.

64 L. Huang, T. Niu, J. Wu and Y. Zhang, *J. Org. Chem*., 2011, **76**, 1759–1766.

65 J. Wang, C. Liu, J. Yuan and A. Lei, *Angew. Chem. Int. Ed*., 2013, **52**, 2256 –2259.

66 S. L. Zhou, L. N. Guo, S. Wang, and X.-H. Duan, *Chem. Commun*., 2014, **50**, 3589—3591.

67 G. S. Kumar, C. U. Maheswari, R. A. Kumar, M. L. Kantam, K. R. Reddy, *Angew. Chem.,* 2011,**123**, 11952 –11955.

68 J. Zhao, H. Fang, J. Han and Y. Pan, *Org. Lett*., 2014, **16**, 2530−2533.

69 Z.-H. Ren, M. N. Zhao and Z.-H. Guan, *RSC Adv*., 2016, **6**, 16516-16519.

70 H. Hu, S.-J. Chen,M. Mandal, S. Md Pratik, J. A. Buss, S. W. Krsk, C. J. Cramer and S. S. Stahl. *Nat. Catal.,* 2020, **3**, 358–367.

71 S. K. Rout, S. Guin, K. K. Ghara, A. Banerjee and B. K. Patel, *Org. Lett*., 2012, **14**, 3982-3985.

72   Q. Wang, H. Zheng, W. Chai, D. Chen, X. Zeng, R. Fu, R. Yuan, *Org. Biomol. Chem*., 2014, **12**, 6549-6553.

73 A. S. Hay, *J. Org. Chem*., 1962, **27**, 3320–3321.

74 V. Kumar, A. Chipeleme and K. Chibale, *Eur. J. Org. Chem*., 2008, **2008**, 43–46.

75 S. L. Gholap, P. Hommes, K. Neuthe and H.-U. Reissig, *Org. Lett*., 2013, **15**, 318–321.

76 K. Campbell, N. M. Tiemstra, N. S. Prepas-Strobeck, R. McDonald, M. J. Ferguson and R. R. Tykwinski, *Synlett*, 2004, 182–186.

77 N. S. Babu, *Synlett*, 2016, **28**, 253–259.

78 C. Zhang and C.-F. Chen, *J. Org. Chem*., 2007, **72**, 9339–9341.

79 (a) P. Kuhn, A. Alix, M. Kumarraja, B. Louis, P. Pale and J. Sommer, *Eur. J. Org. Chem.*, 2009, **2009**, 423–429; (b) W. J. Youngblood, D. T. Gryko, R. K. Lammi, D. F. Bocian, D. Holten and J. S. Lindsey, *J. Org. Chem.*, 2002, **67**, 2111–2117.

80 (a) A. R. Murphy and J. M. J. Fr´echet, *Chem. Rev.*, 2007, **107**, 1066–1096; (b) B. S. Ong, Y. Wu, Y. Li, P. Liu and H. Pan, *Chem.–Eur. J.*, 2008, **14**, 4766–4778.

81 (a) E. M. Nolan and S. J. Lippard, *Acc. Chem. Res.*, 2009, **42**, 193−203; (b) T. Ueno and T. Nagano, *Nat. Methods*, 2011, **8**, 642−645.

82 G. Banfalvi, Cellular effects of heavy metals. Netherlands, London, NewYork: Springer; 2011.

83 I. Bremner, *Am. J. Clin. Nutr.*, 1998, **67**, 1069S–1073S.

84 A. Bhan and N. N. Sarkar, *Rev. Environ. Health,* 2005, **20**, 39–56.

85 R. A. Bernhoft, *J. Environ. Public Health*, 2011, **2012**, 1–10.

86 I. Onyido, A. R. Norris and E. Buncel, *Chem. Rev.*, 2004, **104**, 5911–5929.

87 T. W. Clarkson and L. Magos, *Crit. Rev. Toxicol.*, 2006, **36**, 609–662.

88 G. E. M. Maguire and K. R. A. S. Sandanayake*, Chem. Soc. Rev.*, 1992, **21**, 187−195.

89 E. Galbraith and T. D. James, *Chem. Soc. Rev.*, 2010, **39**, 3831−3842.

90 P. Jiang and Z. Guo, *Coord. Chem. Rev.*, 2004, **248**, 205−229.

91 Y.-W. Sie, C.-L. Li, C.-F. Wan, J.-H. Chen, C.-H. Hu, H. Yan, A-T. Wua, *Inorganica Chimica Acta*, 2017, **467**, 325–329.

92 M. Tian, L. Liu, Y. Li, R. Hu, T. Liu, H. Liu, S. Wanga and Y. Li, *Chem. Commun.*, 2014, **50**, 2055—2057.

93 S.-P. Wu, Z.-M. Huang, S.-R. Liu and P. K. Chung, *J. Fluoresc.*, 2012, **22**, 253–259.

94 Y.-W. Sie, C.-F. Wan and A-T. Wu, *RSC Adv.*, 2017, **7**, 2460–2465.

95 Y. Yang, C. Gao, B. Li, L. Xu and L. Duan, *Sensors and Actuators B*, 2014, **199**, 121–126.

96 S. Suganya, S. Velmathi, D. M. Ali, *Dyes and Pigments,* 2014, **104**, 116e122.

97 K. Ghosh, T. Sarkar, A. Samadder and A. R. K. Bukhshb, *New J. Chem.*, 2012, **36**, 2121–2127.

98 S. Patra, V. P. Boricha and P. Paul, *Eur. J. Inorg. Chem.*, 2019, **2019**, 199–205.

99 Y. Yu, N. Bogliotti, J. Tang and J. Xie, *Eur. J. Org. Chem.*, 2013, **2013**, 7749–7760.

100 T. Ábalos, D. Jiménez, R. M.-Máñez, J. V. Ros-Lis, S. Royo, F. Sancenón, J. Soto, A. M. Costero, S. Gil and M. Parra, *Tetrahedron Lett.*, 2009, 50, 3885–3888.

101 Y. Chena and J. Jiang, *Org. Biomol. Chem.*, 2012, **10**, 4782–4787.

102 S.-Z. Hu and C.-F. Chen, *Org. Biomol. Chem.*, 2011, **9**, 5838–5844.

Chapter-2

A Novel Quinoline-Based NNN-Pincer Cu(II) Complex as a Superior Catalyst for Oxidative Esterification of Allylic C(sp^3)-H Bonds
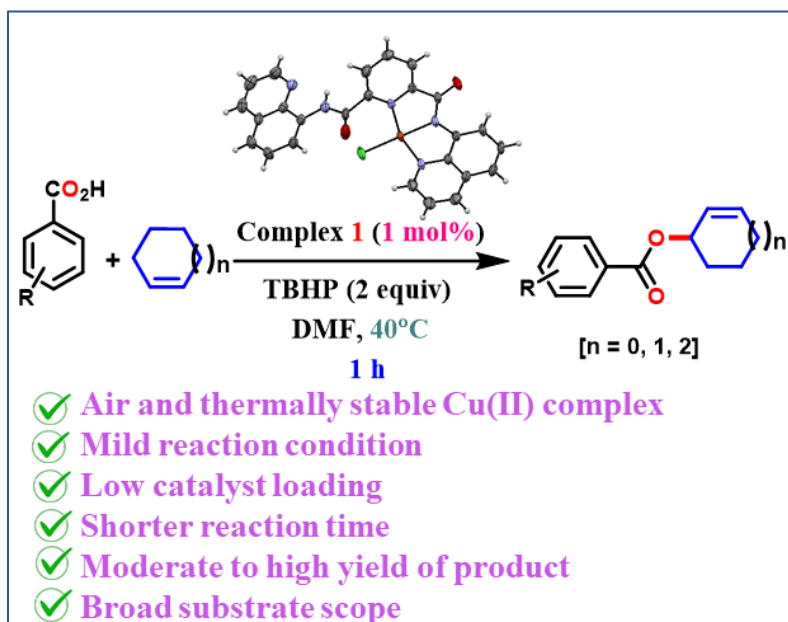
Representative publication

2.1 Introduction

The C-H functionalization is one of the most straightforward methods to carry out a synthetic strategy in a sustainable and atom-economic way.[1] This can lead to formation of either C-X (X = N, O, S, P etc.) or C-C bond. However, the direct functionalization of C-H bond (C(sp^3/sp^2/sp)-H) for generating C-X or C-C bonds needs to be catalysed by transition metals or their chiral/achiral complexes in most of the cases.[2-9] Among the three kinds of C-H functionalization, the C(sp^3)-H bonds possess a lot more challenge to functionalize, owing to the low polarity of the bond, giving low reactivity, and absence of π-cloud, which is responsible for metal-coordination.[10] Despite these challenges, expensive transition-metal catalysts such as palladium,[11] ruthenium[12] or rhodium,[13] are able to functionalize C(sp^3)-H bonds effectively. This has turned the interest of the scientific community towards the exploration of cheap earth-abundant metals and their noble complexes as catalysts in direct C-H functionalization and is one of the emerging fields in catalysis. Among the C-C and C-X bond formation by C-H activation, the former is a widely explored, while the latter, particularly C-O, has comparatively a limited number of literature reports.[14-22] Among the various transition metals capable of catalysing direct C-H activation, Cu is cheap and earth-abundant and has the huge potential to replace the expensive and scarcely abundant metals used widely in catalysis. A classic example of utilization of Cu in catalysing the generation of C-O bond involves the allylic oxidation of olefins[23] giving ester functionality by oxidative cross dehydrogenative coupling (CDC). Ester is one of the broadly embodied structural motifs in organic chemistry, which finds its place in a large number of natural products, pharmaceuticals or fine chemicals.[24-26] The traditional esterification process, involving reaction between a carboxylic acid or acid derivative (acyl chlorides or anhydrides) and an alcohol in presence of catalytic amount of acid or base, is known for centuries.[27-29] However, the use of alcohol is limited due to their high expenses and commercial unavailability in some cases.[30] Advancement in research have paved the way for direct esterification by oxidative cross dehydrogenative coupling (CDC) using C-H activation from C(sp^3)–H bond.[31]

Recently, a few oxidative CDC based synthetic methodologies have been reported for the construction of C-O bonds for direct esterification, by using earth abundant transition-metal catalysts in combination with various oxidants[32] (Scheme 2.1a-e). As shown in Scheme 2.1, all these previously reported Fe, Co, Cu catalysed reactions mostly required a high temperature ranging 80 ˚C-120 ˚C along with long reaction time (18-24 h) and high catalyst loading. CDC

reactions with cyclohexene as one of the components also required high temperature. Even though in some cases the catalyst loading is low, a longer reaction time and a high temperature are required. Taken together, all these factors create an avenue for further research on reactions that can be carried out under milder reaction conditions and with low catalyst loadings. We have developed a quinoline-based NNN-pincer Cu(II) catalyst, which worked at only 1 mol% loading for the smooth esterification of allylic C(sp3)–H bonds. This particular catalyst completed the reaction within 1 h at ambient temperature (40 °C). This is the first report in the literature that states that the allylic esterification by the oxidative CDC mechanism can be conducted in such a fast manner under mild reaction conditions with moderate to good product yields.
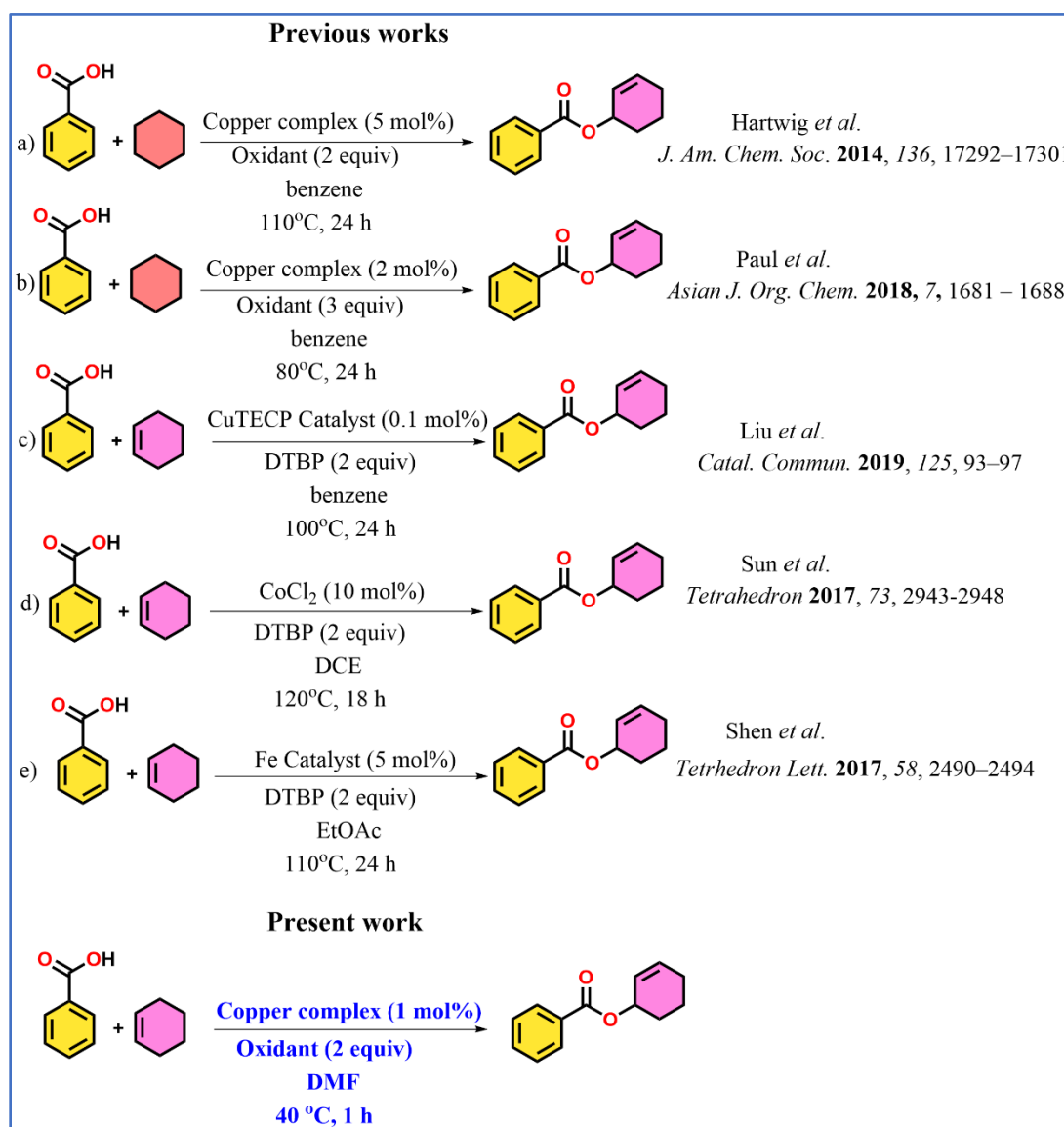
Scheme 2.1. Representative examples of ester synthesis by CDC mechanism.

Herein, we report the synthesis, characterization and catalytic activity of an air stable Cu(II) complex, 1, featuring a pyridine and quinoline-based tridentate scaffold, N,N-di(quinolin-8-yl)pyridine-2,6-dicarboxamide (**L**), in the cross-coupling of acids with alkenes to form allylic esters. The complex 1 showed excellent catalytic activity in the cross coupling of a wide variety of acids and alkenes to form the corresponding allylic esters. The reaction proceeds very fast (1 h) at ambient temperature (40 ˚C), with 100% conversion and moderate yield, which is so far, not reported in the literature. Several control experiments demonstrate the plausible mechanism.

2.2. Results and Discussion

2.2.1. Synthesis of the quinoline-based NNN-pincer-Cu(II) catalyst

The ligand (**L**) was synthesised according to literature reported procedure by amidation reaction between pyridine-2,6-dicarbonyl dichloride and 8-aminoquinoline (2 equiv) in dry THF solvent with triethyl amine as base at 0 ˚C-room temperature for 30 min.[33] The white-colored ligand (**L**), when reacted with equimolar ratio of $CuCl_2 \cdot 2H_2O$ in chloroform at room temperature for 8 h, produced an air stable neutral complex CuLCl (**1**) as green precipitate in nearly 75% yield (Scheme 2). The synthesized complex is well-characterized by HRMS and single crystal X-ray diffraction. In addition to these, the spectral fingerprints of the complex with respect to UV-vis absorption, EPR spectra and cyclic voltammetry have been investigated.
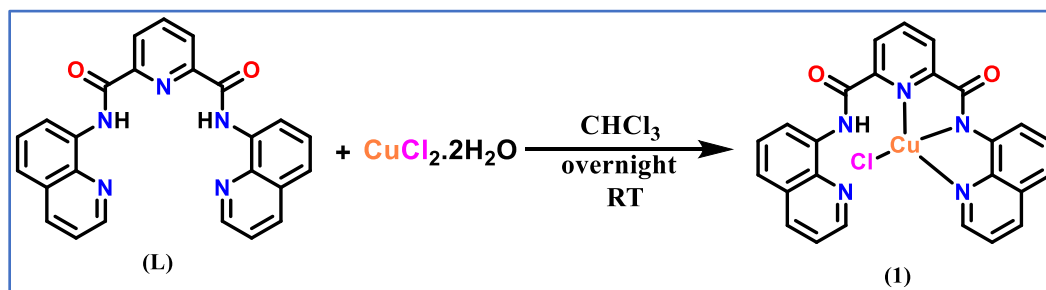
Scheme 2.2. Synthesis of the complex **1**

2.2.2. Characterization of the quinoline-based NNN-pincer-Cu(II) catalyst (X-ray Crystallography, Cyclic voltammetry (CV), electron paramagnetic resonance (EPR) and UV-vis spectra of complex 1)

X-ray-quality single crystals of complex **1** were grown by slow evaporation of DMF solution at room temperature. The molecular structure of complex **1** is shown in Figure 2.1a with

some selected bond angles and bond lengths. From X-ray diffraction study, the structure of the complex is found to be NNN-pincer type, where the N atoms of pyridine, one of the quinoline moieties and its neighbouring amide are the chelating sites arranged in a distorted square planar geometry around the coordination site. The deprotonation from the amide N and the attachment of a Cl atom has restored the oxidation state of the metal (Cu) as dipositive (Cu(II)) in the air, moisture and thermally stable complex **1**.

Furthermore, the oxidation state of the metal centre was confirmed by the EPR spectral analysis. Since the Cu(II) has d^9 system, hence it is paramagnetic and EPR active. The $CHCl_3$ solution of the metal complex at room temperature gave the EPR signal as shown in Figure 2.1b. Here, the $g_\parallel$ (2.22) > $g_\perp$ (2.05), which is the typical for Cu(II) oxidation state.[34] Furthermore, due to hyperfine splitting (2nI+1) of d^9 system, (I = 3/2), the number of peaks were expected to be 4,[35] however, here, only three peaks are visible owing to slight broadening of the peaks. This may occur due to the absence of the complex in neat solid condition or at low temperature.[36]

To investigate the electrochemical behaviour of the complex, cyclic voltammetry (CV) was conducted in acetonitrile solvent with TBAP as the supporting electrolyte at scan rate 0.02 Vs^{-1} within the potential window -1.6 to 1.8 V at 25°C against saturated Ag/AgCl reference electrode. The CV shows reversible one electron reduction and oxidation waves with ΔE = 0.491 V and $E_{1/2}$ = -0.87 V corresponding to the Cu(II)/Cu(I) redox couple (Figure 2.1c).[32b] This signifies the feasibility of one electron transfer in the Cu(II) core of the catalyst.

The UV-vis spectrum of complex **1** in CH_3CN solvent (3.12×10-5 M) gives four peaks at 270 nm, 319 nm, 370 nm and 679 nm. The free ligand **L** (3.12×10-5 M, CH_3CN) displays an absorption band at 323 nm, which gets shifted to 319 nm in the complex, and a shoulder peak at 270 nm, which is also present in the complex. These peaks may generate due to π-π* transition of the quinoline ring.[37] The other peak at 370 nm is newly generated in the complex and it may be assigned to the ligand-to-metal charge transfer.[38] The peak at 679 nm, possessed by the complex can be assigned to the d-d transition of the Cu(II) centre[16] (Figure 2.1d).
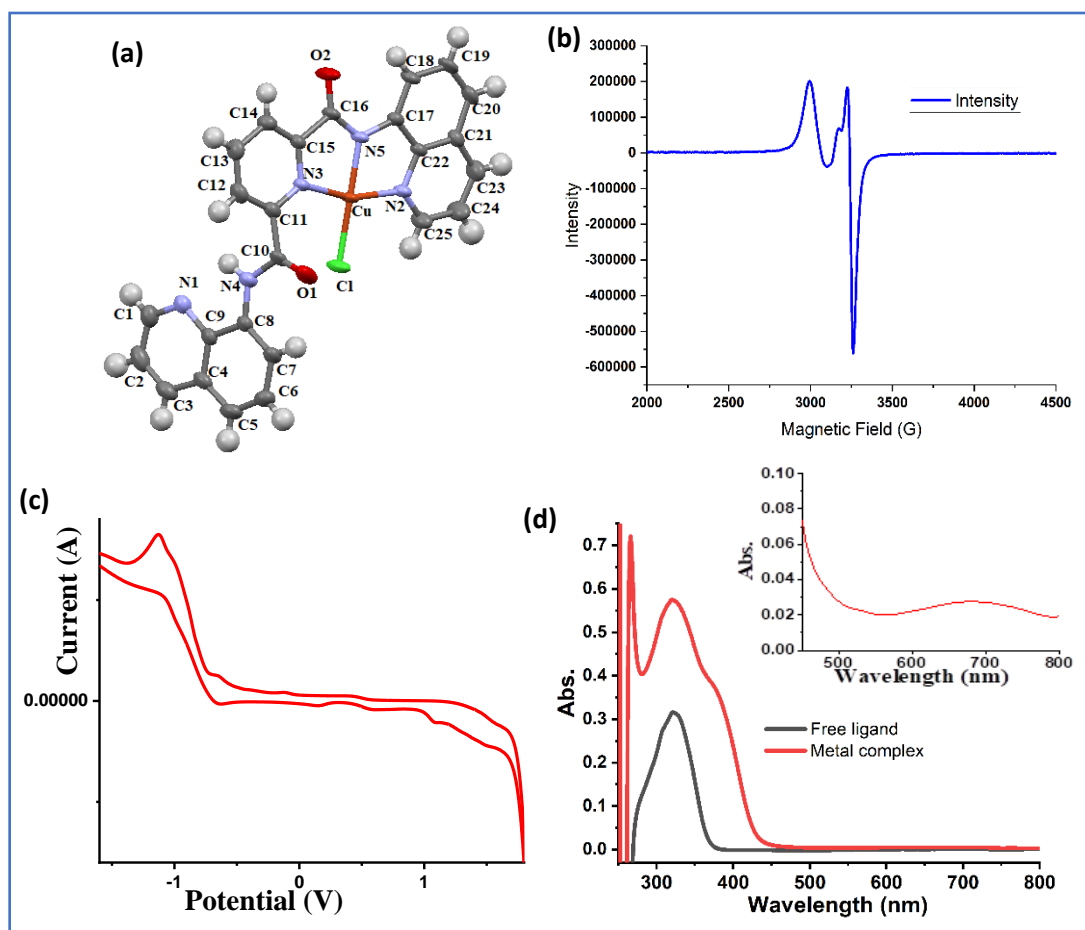
Figure 2.1 (a) ORTEP representation of complex **1** with thermal ellipsoids drawn at the 50% probability level. Some selected bond lengths (Å) and bond angles (deg) for **1**: N3-Cu 2.100, N5-Cu 1.923, N2-Cu 2.021, Cu-Cl 2.198; N3-Cu-N5 80.661, N5-Cu-N2 81.38, N3-Cu-Cl 101.70, N2-Cu-Cl 96.42. (b) EPR spectra of complex **1** in CHCl₃ at room temperature. (c) CV of complex **1** (1×10⁻³ M) in acetonitrile with TBAP as supporting electrolyte at scan rate 0.02 Vs⁻¹ at 25˚C. (d) Absorption spectra of copper complex **1** and free ligand (3.12×10⁻⁵ M) (inset: d-d transition present in copper complex **1**).

2.2.3. Catalytic activity

The cross-coupling reaction of aromatic and aliphatic acids and alkenes reported so far required high temperature, high catalyst loading and a considerably longer reaction time.[32] Herein, we have synthesized the NNN-pincer type complex of Cu(II) and investigated its utility in the oxidative cross-coupling reactions between acids and alkene. Several aromatic as well as aliphatic

acids have been used as the substrates with alkenes of varying ring size (cyclohexene, cycloheptene, cyclooctene *etc.*) as the alkene counterpart to form allylic esters using the complex **1** as a catalyst.

2.2.4. Oxidative cross-coupling reaction between aromatic acids and cyclohexene

Optimization of the intermolecular oxidative coupling reaction conditions between aromatic acids and cyclohexene (**3a**) was done taking benzoic acid (**2a**) as the model aromatic acid component (Table 2.1). An oxidizing agent is required in addition to the catalyst for the reaction to happen and changes in these components bring about the optimal conditions for the reaction. Initial experiment with the catalyst **1** and TBHP as the oxidant was screened in different solvent systems, like THF, CH_3OH, DMSO, dichloromethane and CH_3CN, among polar and benzene, toluene, and xylene among non-polar solvents (Table 2.1, entries 1-12). Except the DMF solvent, none of them gave any good result in terms of product yield, even with varying temperature and/or reaction time, rather no reaction was witnessed for some conditions (Table 2.1, entries 1, 4, 5, 7-10). In DMF solvent, the reaction went to completion in 8 hours at room temperature with 30% yield of product. After several trials with different reaction conditions, the reaction was found to proceed efficiently in DMF solvent at 40 ˚C, using 2 equiv TBHP and 1 mol% of catalyst loading, within one hour giving 70% product yield. Replacement of TBHP with other oxidants like H_2O_2, O_2 yielded no product (Table 2.1, entries 13, 14). Even upon increasing the amount of TBHP or reaction temperature from 40 to 80 ˚C or reaction time gave no significant improvement in the product yield (Table 2.1, entries 15, 16). Upon using other Cu(II) sources like $Cu(OAc)_2 \cdot H_2O$ and $CuCl_2 \cdot 2H_2O$ instead of catalyst **1**, the desired allylic ester was obtained with even lower yield (Table 2.1, entries 17, 18). Furthermore, no reaction occurred in absence of either of TBHP and catalyst **1** (Table 2.1, entries 19, 20), keeping other parameters same, which signifies the participation of both of them in the formation of the desired product. Our optimized reaction condition uses an ambient temperature (40 ˚C) for a short span of time (1 h), for the first time in literature, to obtain the desired allylic ester in 70-72% yield. A slight amount of cross-coupling with DMF gives N,N-dimethyl benzamide as the trace side product.[39]

Table 2.1. Optimisation of the reaction conditions.[a]
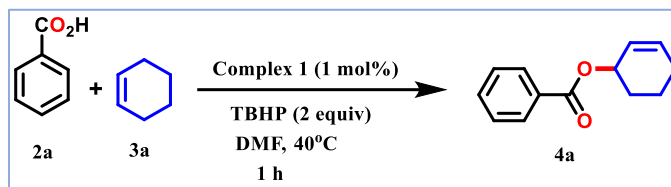
Entry	Catalyst (mol %)[a]	Oxidant (equiv)	Solvent	Temperature (˚C)	Time (h)	% Yield[b]
1	Catalyst **1** (1)	TBHP (2)	DMSO	40	4	NR
2	Catalyst **1** (1)	TBHP (2)	DMSO	80	4	40
3	Catalyst **1** (1)	TBHP (2)	CH_3CN	80	4	30
4	Catalyst **1** (1)	TBHP (2)	DCM	RT	24	NR
5	Catalyst **1** (1)	TBHP (2)	THF	RT	24	NR
6	Catalyst **1** (1)	TBHP (2)	Benzene	80	4	40
7	Catalyst **1** (1)	TBHP (2)	CH_3OH	40	4	NR
8	Catalyst **1** (1)	TBHP (2)	CH_3COCH_3	40	4	NR
9	Catalyst **1** (1)	TBHP (2)	Xylene	40	4	NR
10	Catalyst **1** (1)	TBHP (2)	Toluene	40	4	NR
11	**Catalyst 1 (1)**	**TBHP (2)**	**DMF**	**RT**	**8**	**30**
12	**Catalyst 1 (1)**	**TBHP (2)**	**DMF**	**40**	**1**	**70**
13	Catalyst **1** (1)	H_2O_2 (2)	DMF	40	1	NR
14	Catalyst **1** (1)	O_2 (2)	DMF	40	1	NR
15	Catalyst **1** (2)	TBHP (2)	DMF	80	1	70
16	Catalyst **1** (2)	TBHP (3)	DMF	80	1	70
17	$Cu(OAc)_2.H_2O$	TBHP (2)	DMF	40	1	40
18	$CuCl_2.2H_2O$	TBHP (2)	DMF	40	1	40
19	-	TBHP (2)	DMF	40	1	NR
20	Catalyst **1** (1)	-	DMF	40	1	NR

[a]Catalytic conditions: benzoic acid (1 mmol), cyclohexene (10 mmol), Cu catalyst (1 mol%), TBHP (2 equiv), 40 ˚C, 1h. [b]Isolated yield based on column chromatography. NR: No Reaction.

The optimized reaction condition, as described above, have been applied in the reaction between different substituted aromatic acids (**2a-r**) and cyclohexene (**3a**) to investigate the domain of applicability of the catalyst. The subsequent results thus obtained are enlisted in Table 2.2. The change in nature of substitution of the aromatic acids from unsubstituted to electron-withdrawing/electron donating does not have a significant influence on the yield of the product formed, hence all of them give moderate to good yield (67-72%) of the corresponding allylic esters (**4a-r**). X-ray quality single crystals were obtained for **4f** (DCM/hexane medium) from which the structural elucidation of the molecules was confirmed. Gram-scale synthesis of the desired esters can be achieved by applying this optimized reaction condition, which was confirmed by the reaction of benzoic acid and 4-hydroxybenzoic acid with cyclohexene. In addition, to test the generality of the reaction in terms of the allylic part, other homologues like cycloheptene and cyclooctene were reacted with benzoic acid under the optimized condition. In both the cases, the desired products **4s** and **4t** were obtained in low yields even after prolonged reaction time (8 h), which may be due to the instability of the generated allyl radicals in the strained 7 and 8-membered cycloalkene systems.[40] The optimized reaction condition was also implied on acylic alkenes such as α–methylstyrene, 1-hexene, 2-octene, however, the corresponding desired allylic esters were not obtained for any of the acyclic alkene system.

Table 2.2. Substrate scope of the cross-coupling reaction catalysed by **1**[a,b]

4a (70%) 4b (68%) 4c (67%) 4d (69%)

4e (71%) 4f (72%) 4g (68%) 4h (70%)

4i (68%) 4j (68%) 4k (69%) 4l (70%)

4m (68%) 4n (67%) 4o (67%) 4p (69%)

4q (68%) 4r (68%) **4f**

4s (30%) 4t (20%)
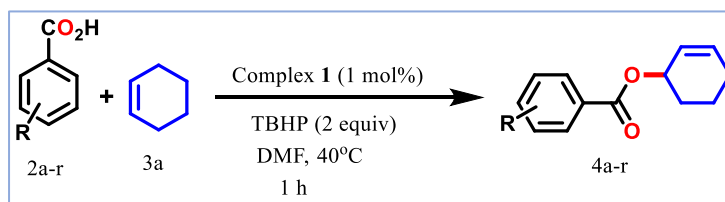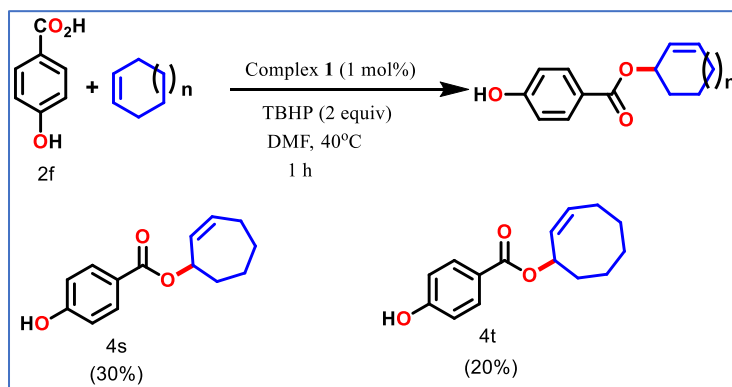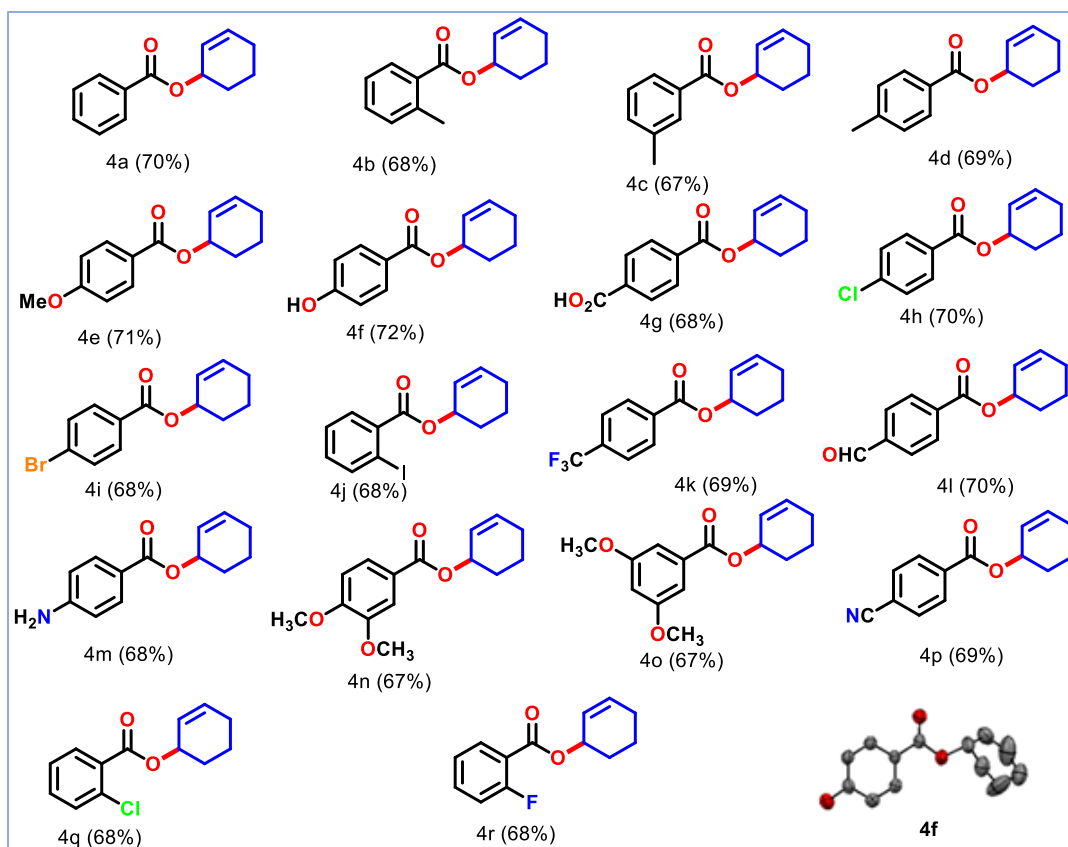
[a]Reaction conditions: **2a-r** (1 mmol), **3a** (10 mmol), copper catalyst (1 mol%), 40 °C, 1h. [b]Isolated yield after column chromatography.

2.2.5. Oxidative cross-coupling reaction between aliphatic acids and cyclohexene

The successful applicability of the catalytic reaction with aromatic acids induced us to widen the substrate scope with some aliphatic carboxylic acids to synthesize their corresponding allylic esters, under the optimised reaction conditions. Several aliphatic acids, such as 2-

bromoacetic acid (**5a**), 2-(2-bromophenyl) acetic acid (**5b**), 2-(2-formyl phenyl) acetic acid (**5c**), diphenyl acetic acid (**5d**) were reacted with cyclohexene to form the corresponding allylic esters. For 2-bromoacetic acid (5a), the corresponding allylic ester (**6a**) was formed in trace amount, however, in case of **5c** and **5d**, the corresponding allylic esters (**6c** and **6d**) were obtained in 48% and 52% yield respectively (Table 2.3).

Table 2.3. Coupling reaction with some aliphatic acids
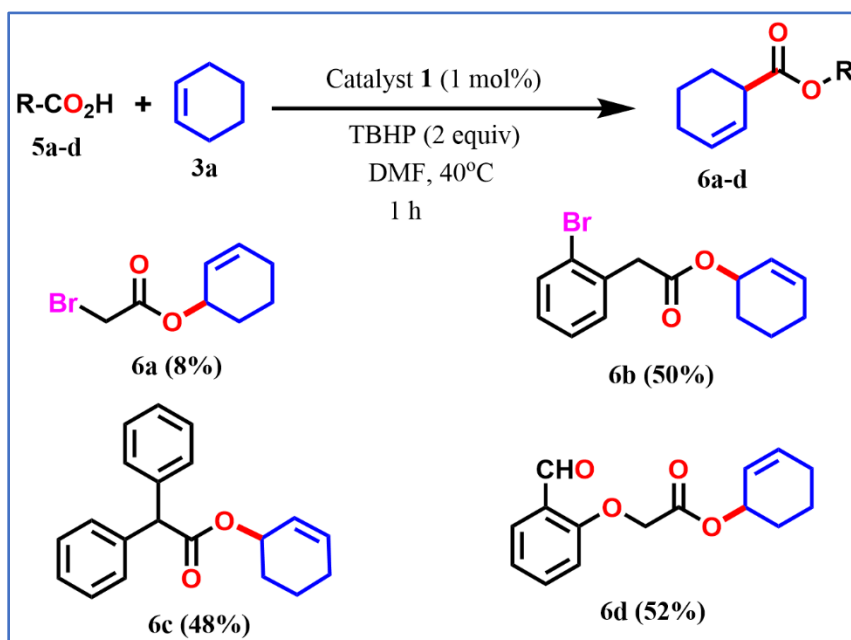
[a]Reaction conditions: **5a-d** (1 mmol), **3a** (10 mmol), copper catalyst (1 mol%), 40 ˚C, 1h. [b]Isolated yield after column chromatography.

2.2.6. Mechanistic investigation and plausible catalytic cycle

Determination of the catalytic cycle must be preceded by the investigation of the mechanism involved for this Cu(II) catalyzed oxidative esterification. Anticipating the reaction to undergo through a radical pathway, TEMPO (2,2,6,6-tetramethylpiperidin-1-yl)oxyloroxidanyl), a radical scavenger, was added to the reaction mixture. Notably, the desired esterification product was not formed, whereas, the TEMPO-based alkoxyamine product, 1-(cyclohex-2-en-1-yloxy)-2,2,6,6-tetramethylpiperidine, formed by the reaction of the generated allyl radical from the cyclohexene part with TEMPO was observed (Figure 2.32). This validates the anticipation of a radical mediated pathway. Thus, in the reaction pathway, the generated allylic radical, in presence

of the catalyst, attaches itself to the O atom of the acid counterpart, yielding the ester. On the basis of above obtained experimental results and reported literature,[41] a plausible reaction mechanism for allylic esterification of aromatic esters and cyclohexene is depicted in Scheme 2.3. At first TBHP is converted to its tert butoxy radical and hydroxyl radical by homolytic bond cleavage and then the tert butoxy radical, generated through hydrogen atom transfer (HAT), got inserted into the catalyst **1**, changing the oxidation state of metal center from +2 to +3. After that benzoic acid got inserted into catalytic system followed by removal of tert butanol as a leaving group. The cyclohexene radical, generated simultaneously from cyclohexene by the action of tert butoxy radical, got attached to the benzoate part and by reductive elimination; the desired allylic ester got separated from the catalytic cycle.
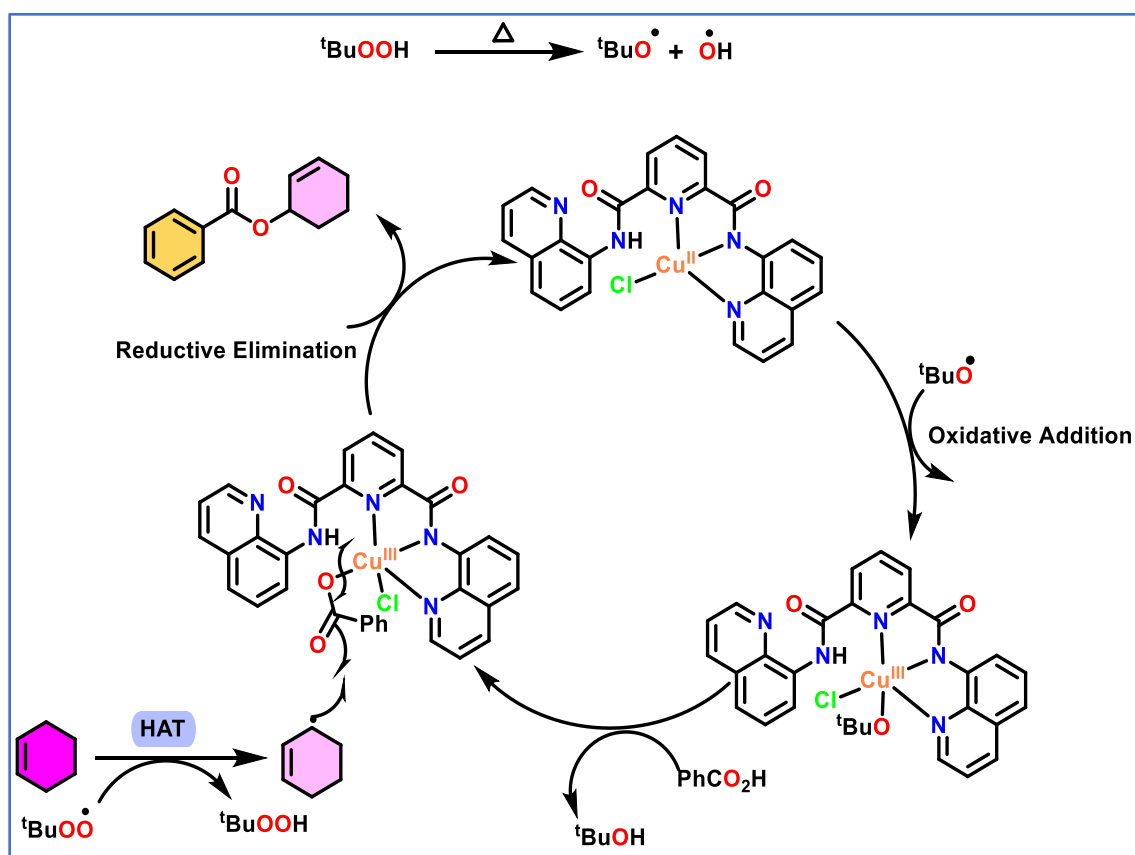
Scheme 2.3. Plausible mechanism for the catalytic cycle.

2.3. Conclusion

The allylic esterification by oxidative CDC, with a broad domain of acid and alkene counterparts was achieved in good to moderate yields by using only 1 mol% of the Cu(II) catalyst **1**. The reactions do not require any extreme condition (high temperature or high catalyst loading) and proceeds well in ambient temperature (40 °C). To the best of our knowledge, this is the first report where such a minimal amount of catalyst works very fast at ambient temperature to give the allylic ester with an overall product yield comparable to other literatures. The mechanistic pathway of the reaction involves the generation of the allylic radical by TBHP through HAT mechanism and the oxidation of Cu(II) to Cu(III) within the catalytic cycle. Such $C(sp^3)$-H activation mechanisms by using least amount of earth-abundant metal catalysts can proliferate the synthetic research towards a more sustainable future.

2.4. Experimental section

2.4.1. Materials and reagents

8-amino quinoline was purchased from TCI India. 2,6- di picolinic acid was purchased from Sigma–Aldrich. Different substituted carboxylic acids were purchased from Sigma–Aldrich and TCI Chemicals. All other reagents and chemicals were obtained from commercial sources and used without further purification. N,N-di(quinolin-8-yl)pyridine-2,6-dicarboxamide (**L**) was synthesised by literature reported procedure.[33] Chromatography was carried out using 60-120 mesh silica gel in a column.

2.4.2. Instrumentation

^{1}H and ^{13}C NMR spectra were obtained with BRUKER 300 MHzFT-NMR spectrometers and the chemical shifts are reported in ppm, using tetramethylsilane as an internal standard and were referenced to the residual solvent as follows: $CDCl_3$ = 7.26 (^{1}H), 76.16 (^{13}C) ppm at room temperature. For ^{1}H NMR, coupling constants *J* are given in Hz and the resonance multiplicity is described as s (singlet), d (doublet), t (triplet), m (multiplet).

2.4.3. X-ray Crystallographic Analysis

X-ray-quality crystal of complex **1** was grown by slow evaporation of DMF solution at room temperature and that of **4f** was obtained by layering dichloromethane with hexane at room temperature. The intensity data were collected on a CCD area-detector, MoK/a diffractometer. With OLEX2,[42] the structure was solved with the Superflip[43] structure solution program using

charge flipping and refined with the SHELXL[44] refinement package and least-squares minimization. The hydrogen atoms were refined isotropically at calculated positions using a riding model. CCDC 2141873 (**1**) and 2143447 (**4f**) contain the supplementary crystallographic data for this paper. These data can be obtained free of charge from the Cambridge Crystallographic Data Centre *via* www.ccdc.cam.ac.uk/data_request/cif.

2.4.4. Synthesis

2.4.4.1. Synthesis of complex 1

In a 100 mL round-bottom flask, ligand **L** (100 mg, 0.406 mmol) was dissolved in chloroform (10 mL). $CuCl_2 \cdot 2H_2O$ (54.5 mg, 0.406 mmol) was then added to the ligand solution. The colourless ligand solution becomes green upon addition of $CuCl_2 \cdot 2H_2O$. The reaction mixture was allowed to stir at room temperature overnight. A dark-green precipitate was formed, which was collected by filtration of the reaction mixture. The complex [CuLCl] (**1**) was crystalized by slow evaporation of DMF solution. Its yield and characterization data are as follows: yield: 60%. ESI-MS: calcd. for $C_{25}H_{16}CuN_5O_2Cl$ $[M-Cl]^+ = 481.0599$, found 481.0589.

2.4.4.2. General procedure for the catalytic reaction: A Schlenk tube equipped with a stir bar was charged with carboxylic acid (1.0 mmol, 20 mg) and catalyst (0.01 mmol, 1.5 mg). The Schlenk tube was then evacuated and back filled with nitrogen. The process was repeated three times. Under nitrogen atmosphere, the Schlenk was charged with cyclohexene (0.14 mL, 10 mmol), TBHP (0.04 mL, 2 mmol), and DMF (3 mL) by syringe. The Schlenk tube was then placed in an oil bath preheated at 40 °C. After 1 h, the reaction mixture was cooled to room temperature and extracted with EtOAc and water. Organic phase was dried under reduced pressure. The crude product was purified by column chromatography on silica gel (5% EtOAc/pet ether) to afford corresponding product.

2.4.4.3. General Procedure for gram-scale reaction

Benzoic acid (**A**) and 4-hydroxybenzoic acid (**B**) have been used for exploring the gram-scale reaction.

A Schlenk flask equipped with a stir bar was charged with carboxylic acid derivative (1 g, 8.2 mmol (**A**)/ 7.2 mmol (**B**)) and catalyst (0.08 mmol, 85 mg (**A**)/ 0.07 mmol, 75 mg (**B**)). The Schlenk flask was then evacuated and back-filled with nitrogen. The process was repeated three

times. Under nitrogen atmosphere, the Schlenk was charged with cyclohexene (8.2 mL, 82 mmol (**A**)/ 7.2 ml, 72 mmol (**B**)), TBHP (2.36 mL, 24.6 mmol (**A**)/ 2.07 ml, 21.6 mmol (**B**)), and DMF (10 mL) by syringe. The Schlenk flask was then placed in an oil bath preheated at 40 $^{\circ}$C. After 1 h, the reaction mixture was cooled to room temperature and extracted with EtOAc and water. Organic phase was dried under reduced pressure. The crude product was purified by column chromatography on silica gel (5% EtOAc/pet ether) to afford the corresponding products **4a** and **4f** in 72% (1.2 g, 5.9 mmol) and 73% (1.14 g, 5.25 mmol) yields respectively.

2.4.4.4. Compound characterization Table

Known		Unknown
Compound name	**Reference**	
4a-4e, 4i	45	
4n	46	
4h, 4p, 4q	47	**4g, 4l, 4m, 4o, 4s, 4t, 6b, 6d**
4k, 4r, 4f	48	
4j	49	
6a	50	
6c	51	

2.4.4.5. Spectral data of all synthesized compounds

Cyclohex-2-en-1-yl-benzoate (**4a**): Colourless oil (yield 70%). ^{1}H NMR (300 MHz, CDCl$_3$): δ = 8.05 (d, 2H, J = 9 Hz), 7.54 (t, 1H), 7.43 (t, 2H), 6.02 (t, 1H), 5.83 (d, 1H, J = 9 Hz), 5.51 (s, 1H), 2.19-1.72 (m, 6H). ^{13}C NMR (75 MHz, CDCl$_3$): 166.2, 132.8, 132.7, 130.8, 129.6, 128.3, 125.7, 68.6, 28.4, 24.9, 18.9.

Cyclohex-2-en-1-yl-2-methyl benzoate (**4b**): Colourless oil (yield 68%). ^{1}H NMR (300 MHz, CDCl$_3$): δ = 7.91 (d, 1H, J = 6 Hz), 7.38 (t, 1H), 7.25-7.22 (m, 2H), 6.02-5.98 (m, 1H), 5.87-5.83 (m, 1H), 5.50 (d, 1H, J = 3 Hz), 2.60 (s, 3H), 2.17-1.69 (m, 6H). ^{13}C NMR (75 MHz, CDCl$_3$): 167.5, 139.9, 132.9, 131.8, 131.7, 130.7, 130.4, 125.9, 125.8, 68.5, 28.5, 25.1, 21.9, 19.3.

Cyclohex-2-en-1-yl-3-methyl benzoate (**4c**): Colourless oil (yield 67%). ^{1}H NMR (300 MHz, CDCl$_3$): δ = 7.85 (d, 2H, J = 6 Hz), 7.36-7.29 (m, 2H), 6.03-5.98 (m, 1H), 5.86-5.81 (m, 1H), 5.51 (d, 1H, J = 6 Hz), 2.40 (s, 3H), 2.18-1.67 (m, 6H). ^{13}C NMR (75 MHz, CDCl$_3$): 166.5, 138.1, 133.6, 132.9, 130.8, 130.2, 128.3, 126.8, 125.9, 68.6, 28.5, 25.1, 21.3, 19.3.

Cyclohex-2-en-1-yl-4-methyl benzoate (**4d**): Colourless oil (yield 69%). ^{1}H NMR (300 MHz, CDCl$_3$): δ = 7.94 (d, 2H, J = 6 Hz), 7.22 (d, 2H, J = 6 Hz), 5.99 (d, 1H, J = 9 Hz), 5.82 (d, 1H, J = 9 Hz), 5.50 (s, 1H), 2.40 (s, 3H), 2.18-1.72 (m, 6H). ^{13}C NMR (75 MHz, CDCl$_3$): 166.2, 143.3, 132.6, 129.6, 128.9, 128.1, 125.9, 68.3, 28.4, 26.5, 24.9, 21.6, 18.9.

Cyclohex-2-en-1-yl-4-methoxy benzoate (**4e**): Colourless oil (yield 71%). ^{1}H NMR (300 MHz, CDCl$_3$): δ = 8 (d, 2H, J = 12 Hz), 6.90 (d, 2H, J = 6 Hz), 5.98 (d, 1H, J = 9 Hz), 5.81 (d, 1H, J = 9 Hz), 5.46 (s, 1H), 3.84 (s, 3H), 2.16-1.71 (m, 6H).^{13}C NMR (75 MHz, CDCl$_3$): 165.9, 163.2, 132.6, 131.6, 125.9, 123.2, 113.5, 68.2, 55.4, 28.5, 24.9, 19.0.

Cyclohex-2-en-1-yl-4-hydroxy benzoate (**4f**): Colourless solid (yield 72%). ^{1}H NMR (300 MHz, CDCl$_3$): δ = 7.96 (d, 2H, J = 6 Hz), 6.87 (d, 2H, J = 6 Hz), 6.26 (s, 1H), 6.02-5.98 (m, 1H), 5.84-5.80 (m, 1H), 5.48 (d, 1H, J = 6 Hz), 2.16-1.68 (m, 6H). ^{13}C NMR (75 MHz, CDCl$_3$): 166.8, 160.5, 133.1, 132.2, 125.9, 123.1, 115.4, 68.8, 28.6, 25.2, 19.2.

Cyclohex-2-en-1-yl-4-carboxy benzoate (**4g**): Colourless solid (yield 68%). ^{1}H NMR (300 MHz, CDCl$_3$): δ = 8.15 (s, 4H), 6.06-6.01 (m, 1H), 5.86-5.83 (m, 1H), 5.54 (d, 1H, J = 3 Hz), 2.17-1.71 (m, 6H). ^{13}C NMR (75 MHz, CDCl$_3$): 171.3, 165.5, 135.5, 133.5, 133, 130.2, 129.8, 125.4, 69.5, 28.5, 25.1, 19.0. HRMS (TOF MS EI$^+$): m/z calcd for [C$_{14}$H$_{14}$O$_4$] 246.0892, found 246.0894 [M]$^+$. Elemental analysis: Anal. Calcd for C$_{14}$H$_{14}$O$_4$: C, 68.28; H, 5.73. Found: C, 68.25; H, 5.78.

Cyclohex-2-en-1-yl-4-chloro benzoate (**4h**): Colourless oil (yield 70%). ^{1}H NMR (300 MHz, CDCl$_3$): δ = 7.97 (d, 2H, J = 9 Hz), 7.39 (d, 2H, J = 9 Hz), 6.02-5.98 (m, 1H), 5.82 (d, 1H, J = 9 Hz), 5.49 (s, 1H), 2.17-1.68 (m, 6H). ^{13}C NMR (75 MHz, CDCl$_3$): 165.5, 139.3, 133.2, 131.1, 129.4, 128.7, 125.6, 69.1, 28.5, 25.1, 19.0.

Cyclohex-2-en-1-yl-4-bromo benzoate (**4i**): Colourless oil (yield 68%). ^{1}H NMR (300 MHz, CDCl$_3$): δ = ^{1}H NMR (300 MHz, CDCl$_3$): δ = 7.91 (d, 2H, J = 9 Hz), 7.57 (d, 2H, J = 9 Hz), 6.01 (d, 1H, J = 12 Hz), 5.81 (d, 1H, J = 6 Hz), 5.49 (s, 1H), 2.17-1.61 (m, 6H). ^{13}C NMR (75 MHz, CDCl$_3$): 165.6, 133.2, 131.7, 131.3, 129.8, 127.9, 125.6, 69.1, 28.5, 25.1, 19.0.

Cyclohex-2-en-1-yl-2-iodo benzoate (**4j**): Colourless oil (yield 68%). ^{1}H NMR (300 MHz, CDCl$_3$): δ = 7.92 (t, 1H), 7.49 (d, 1H, J = 6 Hz), 7.21-7.08 (m, 2H), 6.01 (d, 1H, J = 12 Hz), 5.85 (d, 1H, J = 9 Hz), 5.51 (s, 1H), 2.10-1.69 (m, 6H). ^{13}C NMR (75 MHz, CDCl$_3$): 166.5, 141.3, 135.9, 133.3, 132.5, 130.9, 127.9, 125.4, 94.1, 69.8, 28.3, 25.0, 18.9.

Cyclohex-2-en-1-yl-4-trifluoro methyl benzoate (**4k**): Colourless oil (yield 69%). ^{1}H NMR (300 MHz, CDCl$_3$): δ = 8.16 (d, 2H, J = 6 Hz), 7.69 (d, 2H, J = 6 Hz), 6.04-6.01 (m, 1H), 5.84 (t, 1H), 5.52 (d, 1H, J = 3 Hz), 2.14-1.70 (m, 6H). ^{13}C NMR (75 MHz, CDCl$_3$): 165.1, 134.6, 134.2, 133.5, 130.1, 125.6, 122.0, 69.5, 28.5, 25.1, 18.9.

Cyclohex-2-en-1-yl-4-formyl benzoate (**4l**): Colourless solid (yield 70%). ^{1}H NMR (300 MHz, CDCl$_3$): δ = 10.09 (s, 1H), 8.20 (d, 2H, J = 6 Hz), 7.94 (d, 2H, J = 9 Hz), 6.03 (d, 1H, J = 12 Hz), 5.84 (d, 1H, J = 9 Hz), 5.52 (s, 1H), 2.18-1.72 (m, 6H). ^{13}C NMR (75 MHz, CDCl$_3$): 191.8, 165.4, 139.1, 135.9, 133.5, 130.3, 129.6, 125.3, 69.5, 28.3, 25.0, 18.9. HRMS (TOF MS EI$^+$): m/z calcd for [C$_{14}$H$_{14}$O$_3$] 230.0942, found 230.0940 [M]$^+$. Elemental analysis: Anal. Calcd for C$_{14}$H$_{14}$O$_3$: C, 73.03; H, 6.13. Found: C, 73.13; H, 6.10.

Cyclohex-2-en-1-yl-4-amino benzoate (**4m**): Colourless solid (yield 68%). ^{1}H NMR (300 MHz, CDCl$_3$): δ = 7.86 (d, 2H, J = 9 Hz), 6.63 (d, 2H, J = 9 Hz), 6.00-5.95 (m, 1H), 5.83-5.79 (m, 1H), 5.46 (d, 1H, J = 3 Hz), 4.04 (s, 1H), 2.17-1.66 (m, 6H). ^{13}C NMR (75 MHz, CDCl$_3$): 166.4, 150.8, 132.5, 131.7, 126.4, 120.7, 113.9, 68.1, 28.7, 25.1, 19.2. HRMS (TOF MS EI$^+$): m/z calcd for [C$_{13}$H$_{15}$NO$_2$Na] 240.1000, found 240.1049 [M+Na$^+$]. Elemental analysis: Anal. Calcd for C$_{13}$H$_{15}$NO$_2$: C, 74.67; H, 6.27; N, 5.81. Found: C, 74.56; H, 5.94.

Cyclohex-2-en-1-yl-3,4-di methoxy benzoate (**4n**): Colourless oil (yield 67%). ^{1}H NMR (300 MHz, CDCl$_3$): δ = 7.69 (d, 1H, J = 6 Hz), 7.55 (s, 1H), 6.87 (d, 1H, J = 6 Hz), 6.02-5.97 (m, 1H), 5.83 (d, 1H, J = 6 Hz), 5.49 (s, 1H), 3.93 (s, 6H), 2.13-1.70 (m, 6H). ^{13}C NMR (75 MHz, CDCl$_3$): 165.9, 152.8, 148.5, 132.5, 125.9, 123.4, 123.2, 111.9, 110.1, 68.4, 55.9, 28.4, 24.9, 19.2.

Cyclohex-2-en-1-yl-3,5-di methoxy benzoate (**4o**): Colourless oil (yield 67%). ^{1}H NMR (300 MHz, CDCl$_3$): δ = 7.19 (d, 2H, J = 3 Hz), 6.63 (t, 1H), 6.00 (d, 1H, J = 12 Hz), 5.82 (d, 1H, J = 9 Hz), 5.48 (d, 1H, J = 6 Hz), 3.82 (s, 6H), 2.16-1.69 (m, 6H). ^{13}C NMR (75 MHz, CDCl$_3$): 166.1, 160.7, 132.8, 125.8, 107.4, 105.5, 68.9, 55.7, 28.5, 25.1, 19.1. HRMS (TOF MS EI$^+$): m/z calcd for [C$_{15}$H$_{18}$O$_4$Na] 285.1102, found 285.1104 [M+Na$^+$]. Elemental analysis: Anal. Calcd for C$_{15}$H$_{18}$O$_4$: C, 68.68; H, 6.92. Found: C, 68.59; H, 6.85.

Cyclohex-2-en-1-yl-4-cyano benzoate (**4p**): Colourless solid (yield 69%). ^{1}H NMR (300 MHz, CDCl$_3$): δ = 8.14 (d, 2H, J = 6 Hz), 7.72 (d, 2H, J = 9 Hz), 6.03 (t, 1H), 5.81 (d, 1H, J = 9 Hz),

5.52 (s, 1H), 2.18-1.69 (m, 6H). ^{13}C NMR (75 MHz, CDCl$_3$): 164.6, 134.7, 133.6, 132.2, 130.2, 125.1, 118.1, 116.3, 69.7, 28.4, 24.9, 19.1.

Cyclohex-2-en-1-yl-2-chloro benzoate (**4q**): Colourless oil (yield 68%). ^{1}H NMR (300 MHz, CDCl$_3$): δ = 7.78 (d, 1H, *J* = 9 Hz), 7.41 (t, 2H), 7.31 (t, 1H), 6.01 (d, 1H, J = 9 Hz), 5.85 (d, 1H, *J* = 6 Hz), 5.52 (s, 1H), 2.15-1.69 (m, 6H). ^{13}C NMR (75 MHz, CDCl$_3$): 165.6, 133.6, 133.3, 132.4, 131.4, 130.9, 126.6, 125.4, 69.5, 28.4, 25.0, 18.9.

Cyclohex-2-en-1-yl-2-fluoro benzoate (**4r**): Colourless oil (yield 68%). ^{1}H NMR (300 MHz, CDCl$_3$): δ = 7.92 (t, 1H), 7.51 (t, 1H), 7.21-7.08 (m, 2H), 6.01 (d, 1H, J = 12 Hz), 5.84 (d, 1H, J = 9 Hz), 5.51 (s, 1H), 2.18-1.71 (m, 6H). ^{13}C NMR (75 MHz, CDCl$_3$): 163.8, 160.3, 134.4, 134.3, 133.3, 132.1, 125.5, 123.9, 123.9, 117.2, 116.9, 69.1, 28.5, 25.1, 18.9.

Cyclohept-2-en-1-yl 4-hydroxybenzoate (**4s**): White solid (yield 30%). ^{1}H NMR (300 MHz, CDCl$_3$): δ = 7.97 (d, 2H, *J* = 6 Hz), 6.86 (d, 2H, *J* = 6 Hz), 5.90-5.84 (m, 1H), 5.77 (d, 1H, *J* = 9 Hz), 5.62 (d, 1H, *J* = 6 Hz), 2.27-1.25 (m, 8H). ^{13}C NMR (75 MHz, CDCl$_3$): 166.4, 161.2, 133.6, 131.9, 131.9, 122.2, 115.4, 74.6, 32.9, 28.6, 26.7, 26.6. Elemental analysis: Anal. Calcd for C$_{14}$H$_{16}$O$_3$: C, 72.39; H, 6.94. Found: C, 72.33; H, 6.88.

Cyclooct-2-en-1-yl 4-hydroxybenzoate (**4t**): White solid (yield 20%). ^{1}H NMR (300 MHz, CDCl$_3$): δ = 7.96 (d, 2H, *J* = 9 Hz), 6.85 (d, 2H, *J* = 6 Hz), 5.88-5.84 (m, 1H), 5.74-5.67 (m, 1H), 5.62-5.58 (m, 1H), 2.35-1.25 (m, 10H). ^{13}C NMR (75 MHz, CDCl$_3$): 166.5, 160.4, 132.0, 130.8, 130.0, 122.8, 115.4, 73.1, 35.3, 28.9, 26.5, 26.0, 23.5. HRMS (TOF MS EI$^+$): m/z calcd for [C$_{15}$H$_{18}$O$_3$Na] 269.1153, found 269.1151 [M+Na]$^+$. Elemental analysis: Anal. Calcd for C$_{15}$H$_{18}$O$_3$: C, 73.15; H, 7.37. Found: C, 73.13; H, 7.42.

Cyclohex-2-en-1-yl 2-(2-bromophenyl) acetate (**6b**): Colourless oil (yield 50%). ^{1}H NMR (300 MHz, CDCl$_3$): δ = 7.55 (d, 1H, *J* = 6 Hz), 7.29-7.24 (m, 2H), 7.14-7.10 (m, 1H), 5.96-5.92 (m, 1H), 5.73-5.69 (m, 1H), 5.30 (t, 1H), 3.77 (s, 2H), 2.10-1.59 (m, 6H). ^{13}C NMR (75 MHz, CDCl$_3$): 170.4, 134.7, 132.9, 132.9, 131.6, 128.9, 127.6, 125.6, 125.2, 68.9, 42.2, 29.8, 28.4, 24.9, 18.9. Elemental analysis: Anal. Calcd for C$_{14}$H$_{15}$BrO$_2$: C, 56.96; H, 5.12. Found: C, 56.83; H, 5.09.

Cyclohex-2-en-1-yl 2, 2-diphenylacetate (**6c**): Colourless oil (yield 50%). ^{1}H NMR (300 MHz, CDCl$_3$): δ = 7.35-7.26 (m, 10H), 5.99-5.93 (m, 1H), 5.75-5.71 (m, 1H), 5.37 (d, 1H, J = 3 Hz),

5.04 (s, 1H), 2.06-1.61 (m, 6H). ^{13}C NMR (75 MHz, CDCl$_3$): 172.1, 138.9, 133.0, 128.7, 128.6, 128.6, 128.5, 127.2, 125.4, 69.0, 57.3, 28.2, 24.9, 18.8.

Cyclohex-2-en-1-yl (2-formylphenyl) carbonate (**6d**): Colourless oil (yield 50%). ^{1}H NMR (300 MHz, CDCl$_3$): δ = 10.57 (s, 1H), 7.87 (d, 1H, J = 9Hz), 7.56-7.50 (m, 1H), 7.08 (t, 1H), 6.86 (d, 1H, J = 6Hz), 6.02-5.97 (m, 1H),5.71 (d, 1H, *J* = 12 Hz), 5.3 (d, 1H, *J* = 3 Hz), 4.75 (s, 2H), 2.07-1.64 (m, 6H). ^{13}C NMR (75 MHz, CDCl$_3$): 189.8, 160.3, 135.8, 133.9, 128.7, 124.7, 121.9, 112.7, 69.8, 65.9, 28.3, 24.9, 18.7. HRMS (TOF MS EI$^+$): m/z calcd for [C$_{15}$H$_{16}$O$_4$Na] 283.0946, found 283.0938 [M+Na]$^+$. Elemental analysis: Anal. Calcd for C$_{15}$H$_{16}$O$_4$: C, 69.22; H, 6.20. Found: C, 69.15; H, 6.14.

2.5. References

1. C. -L. Sun, B. -J. Li and Z. -J. Shi, *Chem. Rev.,* 2011, **111**, 1293–1314.

2. X, Chen, K. M. Eagle, D. H. Wang and J. Q. Yu, *Angew. Chem. Int. Ed*., 2009, **48**, 5094−5115.

3. O. Daugulis, H. Q. Do and D. Shabashov, *Acc. Chem. Res*. 2009, **42**, 1074−1086.

4. C. J. Li, *Acc. Chem. Res*., 2009, **42**, 335−344.

5. C. Coperet, *Chem. Rev*., 2010, **110**, 656−680.

6. H. Werner, *Angew. Chem. Int. Ed*., 2010, **49**, 4714−4728.

7. C. L. Sun, B. J. Li and Z. J. Shi, *Chem. Rev.* 2011, **111**, 1293−1314.

8. A. N. Campbell and S. S. Stahl, *Acc. Chem. Res*., 2012, **45**, 851−863.

9. S. I. Kozhushkov and L. Ackermann, *Chem. Sci*., 2013, **4**, 886−896.

10. J. Zhao, H. Fang, W. Zhou, J. Han and Y. Pan, *J. Org. Chem.* 2014, **79**, 3847-3855.

11. (a) B. Mariampillai, J. Alliot, M. Li and M. Lautens, *J. Am. Chem. Soc*., 2007, **129**, 15372-15379; (b) G. He, B. Wang, W. A. Nack and G. Chen, *Acc. Chem. Res*., 2016, **49**, 635-645; (c) S. R. Neufeldt and M. S. Sanford, *Acc. Chem. Res.* 2012, **45**, 936-946; (d) S. Bag, R. Jayarajan, U. Dutta, R. Chowdhury, R. Mondal and D. Maiti, *Angew. Chem. Int. Ed*., 2017, **56**, 12538-12542; (e) A. Deb, A. Hazra, Q. Peng, R. S. Paton and D. Maiti, *J. Am. Chem. Soc*., 2017, **139**, 763-775; (f) M. Utsunomiya, M. Kawatsura and J. F. Hartwig, *Angew. Chem. Int. Ed*., 2003, **47**, 6045-6048.

12. (a) D. A. Colby, A. S. Tsai, R. G. Bergmann and J. A. Ellman, *Acc. Chem. Res.* 2012, **45**, 814-825; (b) X. Qi, Y. Li, R. Bai and Y. Lan, *Acc. Chem. Res*., 2017, **50**, 2799-2808; (c) A. Seoane,

N. Casanova, N. QuiÇones, J. L. MascareÇas and M. Gul, *J. Am. Chem. Soc.,* 2014, **136**, 834-837; (d) G. Song and X. Li, *Acc. Chem.Res.*, 2015, **48**, 1007-1020; (e) Y. Lian, R. G. Bergman, L. D. Lavis and J. A. Ellman, *J. Am. Chem. Soc.*, 2013, **135**, 7122-7125; (f) M. Bera, S. Agasti, R. Chowdhury, R. Mondal, D. Pal and D. Maiti, *Angew. Chem. Int. Ed.*, 2017, **56**, 5272-5276.

13. (a) P. Nareddy, F. Jordan and M. Szostak, *ACS Catal.*, 2017, **7**, 5721-5745; (b) J. Hubrich, T. Himmler, L. Rodefeld and L. Ackermann, *ACS Catal.*, 2015, **5**, 4089-4093; (c) K. Murakami, S. Yamada, T. Kaneda and K. Itami, *Chem. Rev.*, 2017, **117**, 9302-9332; (d) B. Ramesh and M. Jeganmohan, *Org. Lett.*, 2017, **19**, 6000-6003; e) L. Ackermann, *Acc. Chem. Res.*, 2014, **47**, 281-295.

14. S. Guin, S. K. Rout, A. Banerjee, S. Nandi and B. K. Patel, *Org. Lett.,* 2012, **14**, 5294-5297.

15. (a) S. K. Rout, S. Guin, K. K. Ghara, A. Banerjee and B. K. Patel, *Org. Lett.*, 2012, **14**, 3982-3985; (b) G. Majji, S. Guin, A. Gogoi, S. K. Rout and B. K. Patel, *Chem. Commun.*, 2013, **49**, 3031-3033.

16. J. Zhao, H. Fang, J. Han and Y. Pan, *Org. Lett.*, 2014, **16**, 2530-2533.

17. (a) Z. Q. Liu, L. Zhao, X. Shang and Z. Cui, *Org. Lett.*, 2012, **14**, 3218-3221; (b) Z. Li, Y. Zhang, L. Zhang and Z. Q. Liu, *Org. Lett.*, 2014, **16**, 382-385.

18. L. Liu, L. Yun, Z. Wang, X. Fu and C. H. Yan, *Tetrahedron Lett.*, 2013, **54**, 5383-5386.

19. J. Huang, L. T. Li, H. Y. Li, E. Husan, P. Wang and B. Wang, *Chem. Commun.*, 2012, **48**, 10204-10206.

20. W. Wei, C. Zhang, Y. Xu and X. Wan, *Chem. Commun.,* 2011, **47**, 10827-10829.

21. H. Liu, G. Shi, S. Pan, Y. Jiang and Y. Zhang, *Org. Lett.*, 2013, **15**, 4098-4101.

22. (a) J. Eames and M. Watkinson, *Angew. Chem. Int. Ed.*, 2001, **40**, 3567-3571; (b) M. S. Chen, N. Prabagaran, N. A. Labenz and M. C. White, *J. Am. Chem. Soc.*, 2005, **127**, 6970-6971; (c) E. M. Stang and M. C. White, *Nat. Chem.* 2009, **1**, 547-551; (d) B. Mondal, S. C. Sahoo and S. C. Pan, *Eur. J. Org. Chem.*, 2015, 3135-3140; (e) C. Li, T. Jin, X. Zhang, C. Li, X. Jia and J. Li, *Org. Lett.*, 2016, **18**, 1916-1919; (f) Y. Zheng, J. Mao, G. Ronga and X. Xu, *Chem. Commun.*, 2015, **51**, 8837-8840.

23. (a) M. Kharasch and G. Sosnovsky, *J. Am. Chem. Soc.,* 1958, **80**, 756. (b) M. Kharasch, G. Sosnovsky and N. Yang, *J. Am. Chem. Soc.* 1959, **81**, 5819-5824.

24. A. G. A. Sa, A. C. de Meneses, P. H. H. de Araujo and D. de Oliveira, *Trends Food Sci. Technol.*, 2017, **69**, 95–105.

25.   A. Das and P. Theato, *Chem. Rev.*, 2016, **116**, 1434-1495.

26.   M. J. O'Donnell, *Acc. Chem. Res.*, 2004, **37**, 506–517.

27.   M. Curini, O. Rosati and E. Pisani, *Tetrahedron Lett.*, 1997, **38**, 1239.

28.   C.-T. Chen and Y. S. Munot, *J. Org. Chem.*, 2005, **70**, 8625.

29.   S. S. Weng, C. S. Ke, F. K. Chen, Y. F. Lyu and G. Y. Lin, *Tetrahedron*, 2011, **67**, 1640-1648.

30.   H. -H. Wang, W. -H. Wen, H. -B. Zou, F. Cheng, A. Ali, L. Shi, H. -Y. Liu and C. -K. Chang, *New J. Chem.*, 2017, **41**, 3508-3514.

31.   (a) Z. Li, D. S. Bohle and C. J. Li, *Proc. Natl. Acad. Sci. USA*, 2006, **103**, 8928-8933; (b) G. Majji, S. K. Rout, S. Rajamanickam, S. Guin and B. K. Patel, *Org. Biomol. Chem.*, 2016, **14**, 8178-8211; (c) A. Batra, P. Singh and K. N. Singh, *Eur. J. Org. Chem.*, 2016, 4927-4947; (d) S. A. Girard, T. Knauber and C. J. Li, *Angew. Chem. Int. Ed.*, 2014, **53**, 74-100; (e) M. W. Marnell, B. Li, T. Zhou, K. Krogh-Jespersen, W. W. Brennessel, T. J. Emge, A. S. Goldman and W. D. Jones, *J. Am. Chem. Soc.*, 2017, **139**, 8977-8989; (f) C. Liu, D. Liu and A. Lei, *Acc. Chem. Res.*, 2014, **47**, 3459-3470.

32.   (a) B. L. Tran, M. Driess and J. F. Hartwig, *J. Am. Chem. Soc.* 2014, **136**, 17292–17301; (b) U. Jash, G. Chakraborty, S. Sinha, R. Sikari, R. Mondal and N. D. Paul, *Asian J. Org. Chem.*, 2018, **7**, 1681-1688; (c) M. F. Xiong, A. Ali, W. Akram, H. Zhang, L. P.Si and H. Y. Liu, *Catal. Commun.*, 2019, **125**, 93–97. (d) T. L. Ren, B. H. Xu, S. Mahmood, M. X. Sun and S. J. Zhang, *Tetrahedron*, 2017, **73**, 2943-2948; (e) B. Lu, F. Zhu, D. Wang, H. Sun, Q. Shen, *Tetrahedron Lett.*, 2017, **58**, 2490–2494.

33.   K. Majee, J. Patel, S. Rai, B. Das, B. Panda and S. Kumar Padhi, *Phys.Chem.Chem.Phys.*, 2016, **18**, 21640-21650.

34.   B. Show, Sk. F. Ahmed, A. Mondal and N. Mukherjee,*J. Environ. Chem. Eng.*, 2021, **9**, 104748.

35.   W. Froncisz, *J. Chem. Phys.*, 1980, **73**, 3123.

36.   (a) B. L. Bales Inhomogeneously Broadened Spin-Label Spectra. In: Berliner L.J., Reuben J. (eds) Spin Labeling. Biological Magnetic Resonance, vol 8. Springer, Boston, MA, 1989. https://doi.org/10.1007/978-1-4613-0743-3_2 (b) B. L. Bales, K. L. Schumacher and F. L. Harris, *J. Phys. Chem.*, 1987, **97**, 1701-1702.

37.   Y. Hitomi, Y. Iwamoto and M. Kodera, *Dalton Trans.*, 2014, **43**, 2161–2167.

38.   K. Majee, J. Patel, B. Das and S. K. Padhi, *Dalton Trans.*, 2017, **46**, 14869–14879.

39.   S. Priyadarshini, P. J. Amal Joseph and M. Lakshmi Kantam, *RSC Adv.,* 2013, **3**, 18283−18287.

40.   S. K. Rout, S. Guin, W. Ali, A. Gogoi and B. K. Patel, *Org. Lett.,* 2014, **16**, 3086–3089.

41. (a) M. B. Andrus and Z. Zhou, *J. Am. Chem. Soc*., 2002, **124**, 8806-8807; (b) R. Mondal, G. Chakraborty, K. M. van Vliet, N. P. van Leest, B. de Bruin and N. D. Paul, *Inorganica Chimica Acta,* 2020, **500**, 119190; (c) S. Yang, M. F. Xiong, W. Q. Tian, H. Zhang, X. Y Xiao, H. Y. Liu and C. K. Chang, *Tetrahedron*, 2020, **76**, 131569.

42. O.V. Dolomanov, L. J. Bourhis, R. J. Gildea, J. A. K. Howard and H. Puschmann, *J. Appl. Cryst.*, 2009, **42**, 339–341.

43.   L. Palatinus and G. Chapuis, *J. Appl. Cryst*., 2007, **40**, 786-790.

44. G. M. Sheldrick, *Acta Cryst.,* 2008, **A64**, 112–122.

45. S. K. Rout, S. Guin, W. Ali, A. Gogoi and B. K. Patel, *Org. Lett.,* 2014, **16**, 3086–3089.

46. J. Zhao, H. Fang, J. Han and Y. Pan, *Org. Lett*., 2014, **16**, 2530-2533.

47. T. L. Ren, B. H. Xu, S. Mahmood, M. X. Sun and S. J. Zhang, *Tetrahedron*, 2017, **73**, 2943-2948.

48. X. -Y. Chena, S. Yang, B. -P. Ren, L. Shi, D. -Z. Lin, H. Zhang and H. -Y. Liu, *Tetrahedron*, 2021, **96**, 132377.

49. S. Samadi, A. Ashouri and M. Samadi, *ACS Omega*, 2020, **5**, 22367−22378.

50. É. Balaux and R. Ruel*, Tetrahedron Lett.*, 1996, **37**, 801-804.

51. R. E. McKinney Brooner and R. A. Widenhoefer, *Chem. Eur. J.*, 2011, **17**, 6170-6178.

Spectroscopic Details
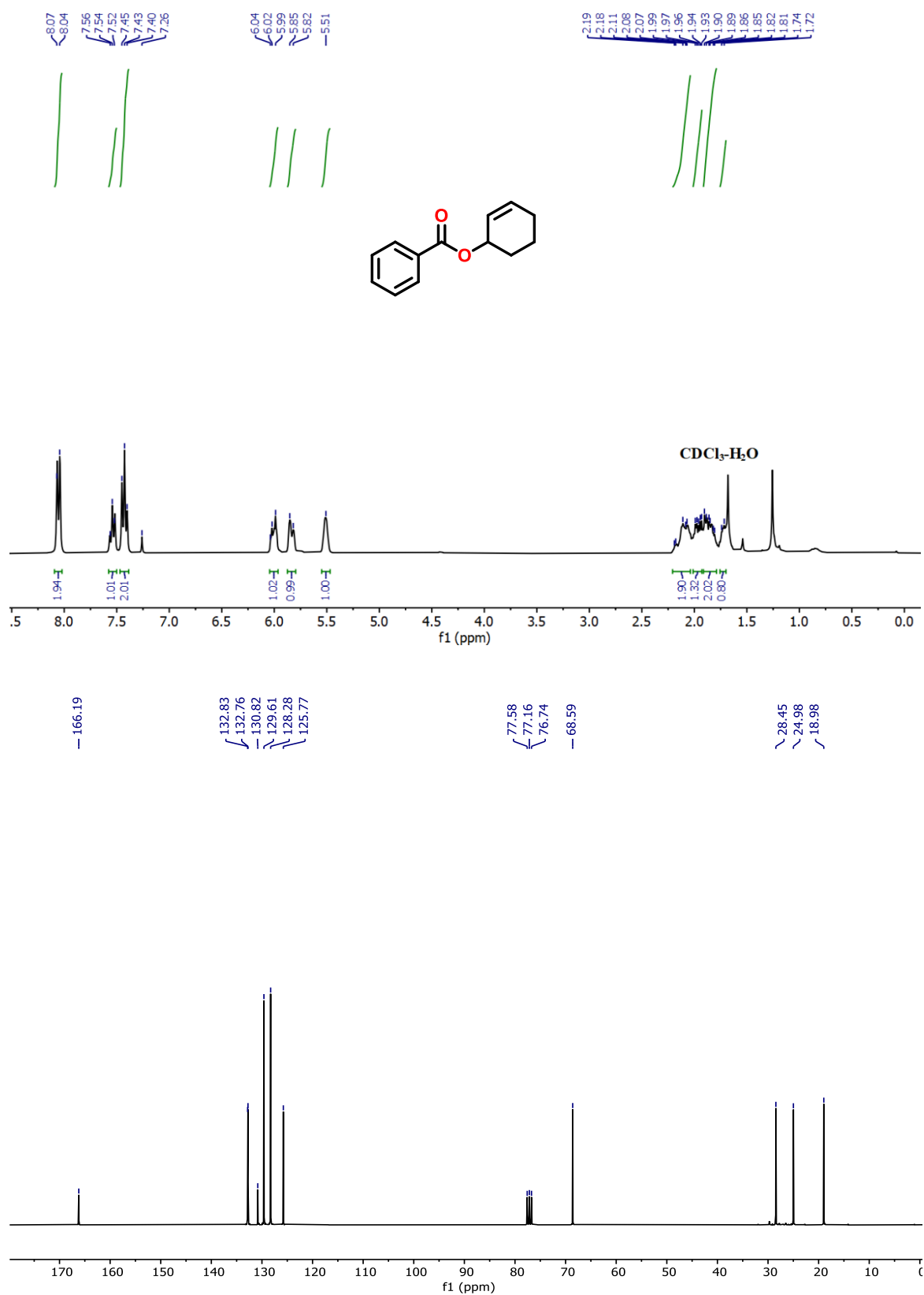
Figure 2.2. ¹H and ¹³C NMR spectra of compound **4a**
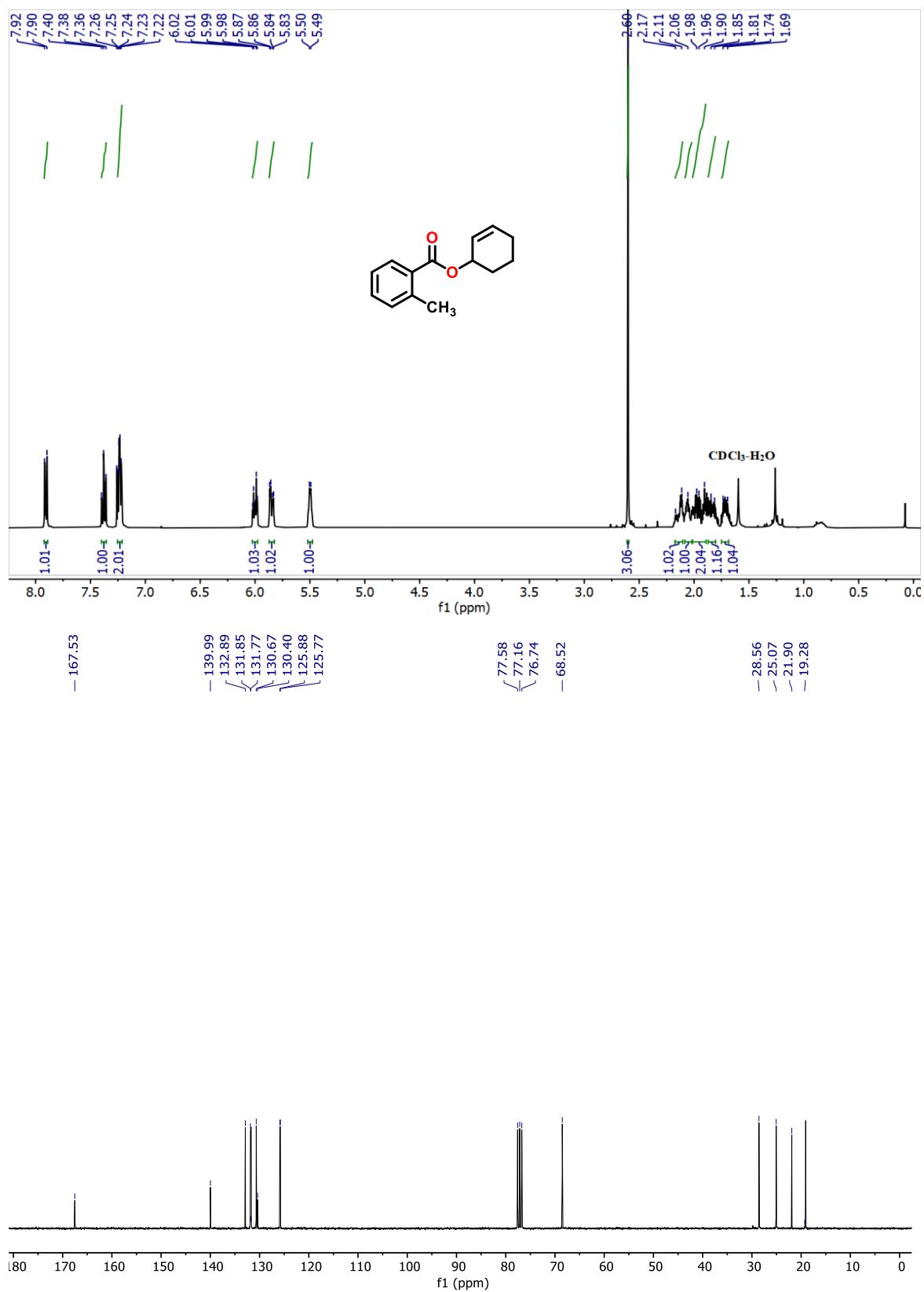
Figure 2.3. ^1H and ^{13}C NMR spectra of compound **4b**
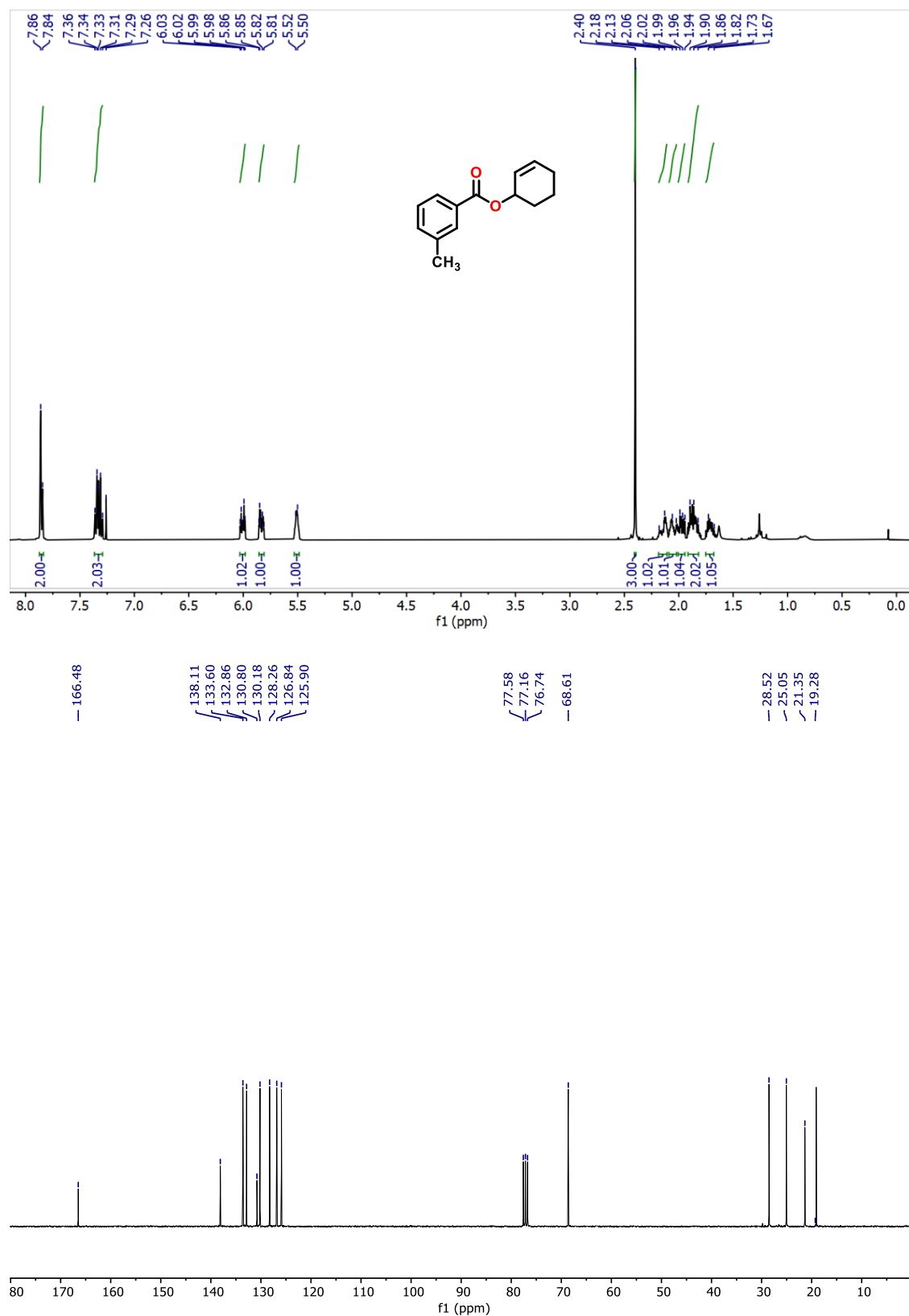
Figure 2.4. ^{1}H and ^{13}C NMR spectra of compound **4c**
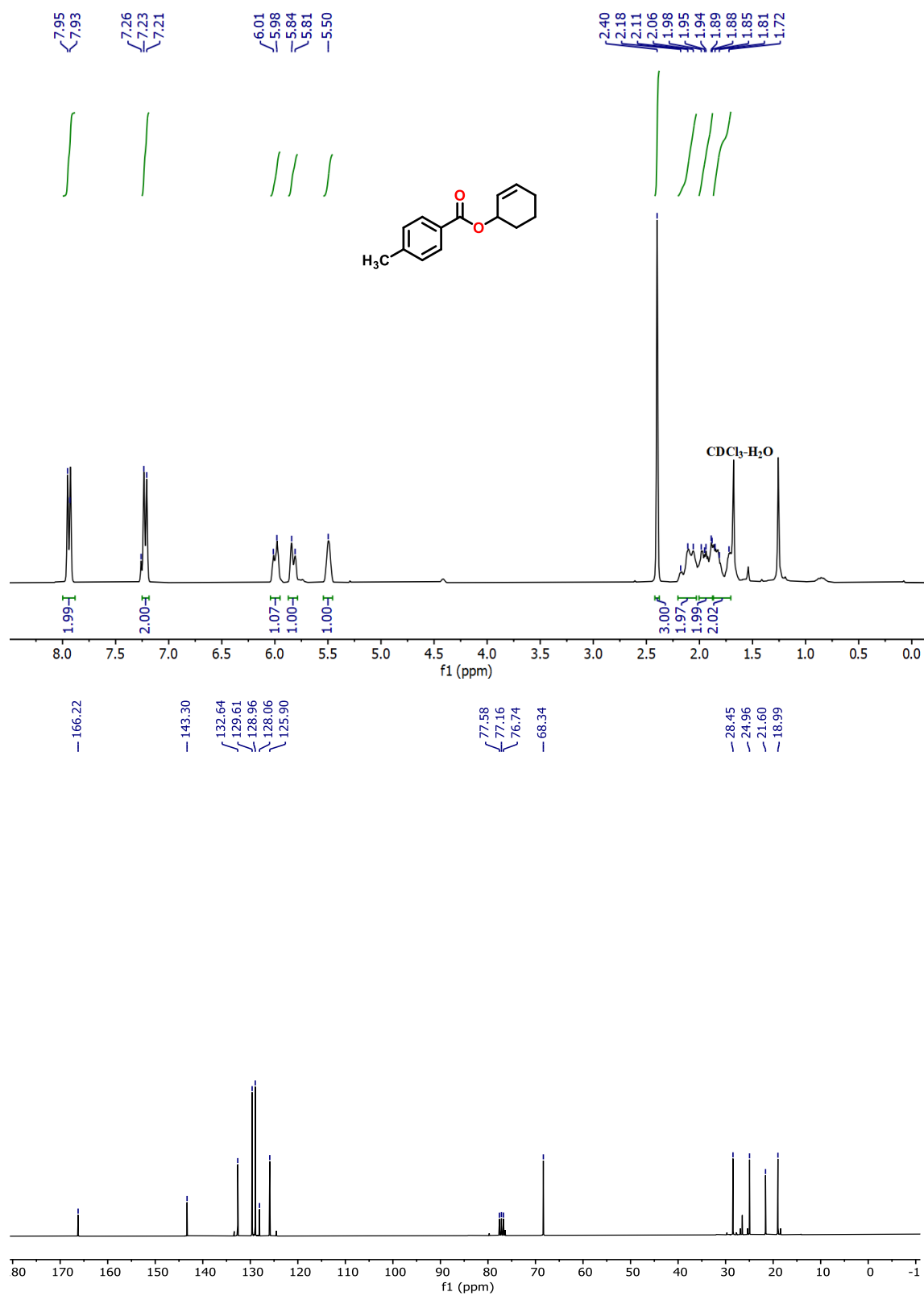
Figure 2.5. ^{1}H and ^{13}C NMR spectra of compound **4d**
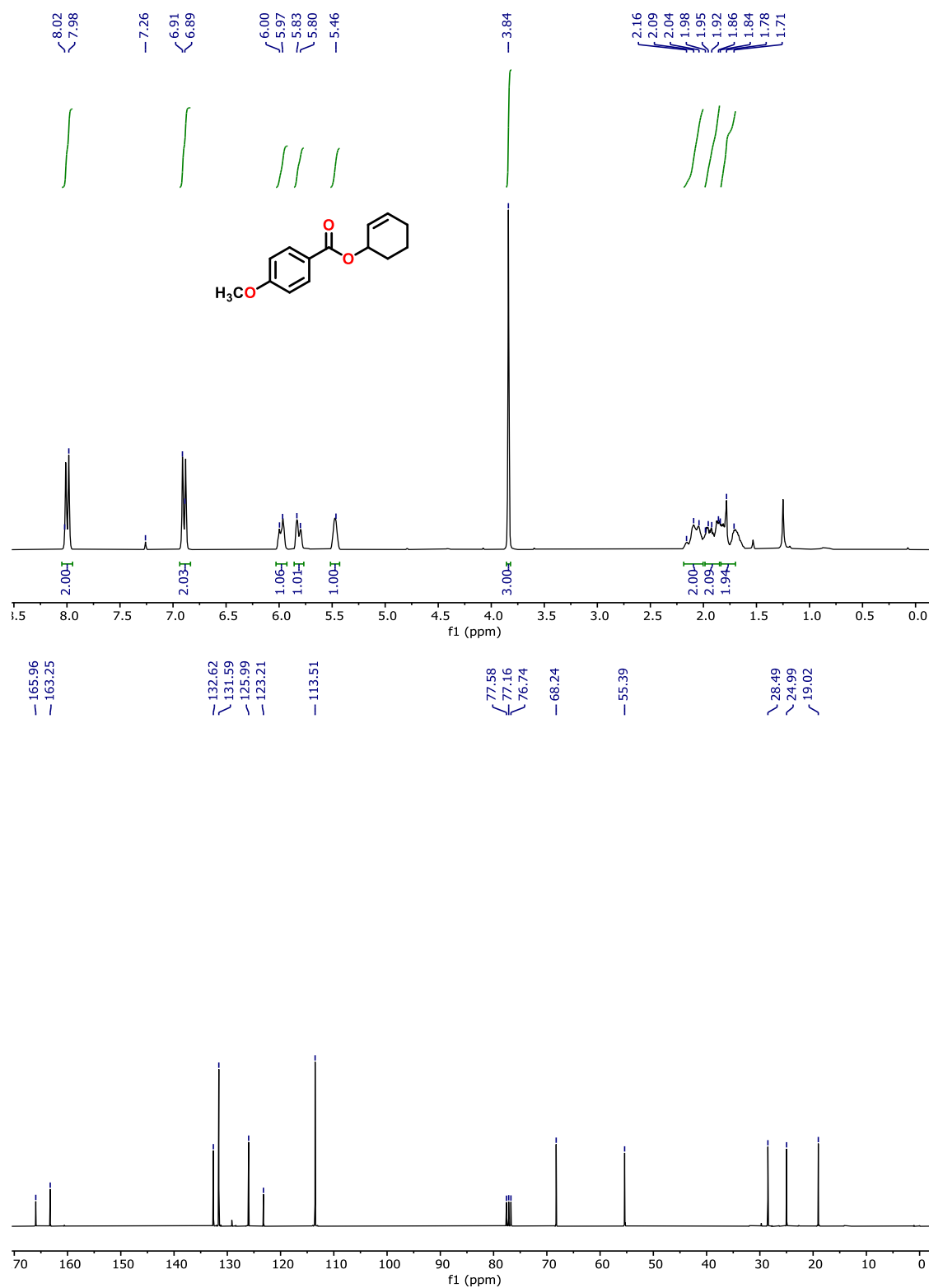
Figure 2.6. ^{1}H and ^{13}C NMR spectra of compound **4e**

Figure 2.7. ^{1}H and ^{13}C NMR spectra of compound **4f**
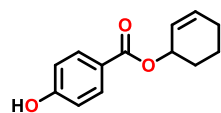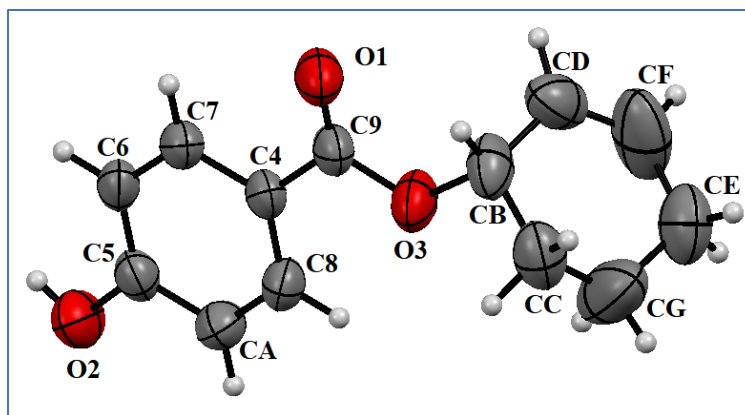
Figure 2.8. ORTEP representation of the molecular structure of **4f** with thermal ellipsoids drawn at the 50% probability level. Selected bond lengths (Å) and angles (deg) for **4f**: O3-CB 1.481(4), C9-O3 1.334(4), CB-CD 1.488(5), CD-CF 1.339(8), CF-CE 1.44(1), CE-CG 1.464(7), CG-CC 1.396(9), CC-CB 1.498(7); C9-O3-CB 118.8(3), O3-CB-CD 108.4(3), O3-CB-CC 106.1(3), O3-C9-C4 111.6(2), CB-CD-CF 120.4(5), CB-CC-CG 115.0(4), CG-CE-CF 111.0(5).

Table 2.4: Crystallographic details of compound **4f**

Empirical formula	$C_{13}H_{14}O_3$
Formula weight	218.24
Crystal size (mm)	0.32 X 0.22 X 0.12
Crystal system	monoclinic
Space group	*P21/c*
a [Å]	a=10.8811(2)
b [Å]	b=10.233(2)
c [Å]	c=11.017(2)
α [°]	90
β [°]	108.43(3)
γ [°]	90
volume [Å³]	1163.7(4)
Z	4
F(000)	464
μ MoK$_\alpha$ [mm^{-1}]	0.088
Temperature [K]	293(2)
R_{int}	0.4013
Range of h, k, l	−13/13, −13/13, −14/14
θ$_{min/max}$ (°)	1.973/27.290
GOF on F^2	1.048
Final R indices [I > 2σ(I)]	R1 = 0.0565 wR2 = 0.1555
R indices [all data]	R1 = 0.0776 wR2 = 0.1735
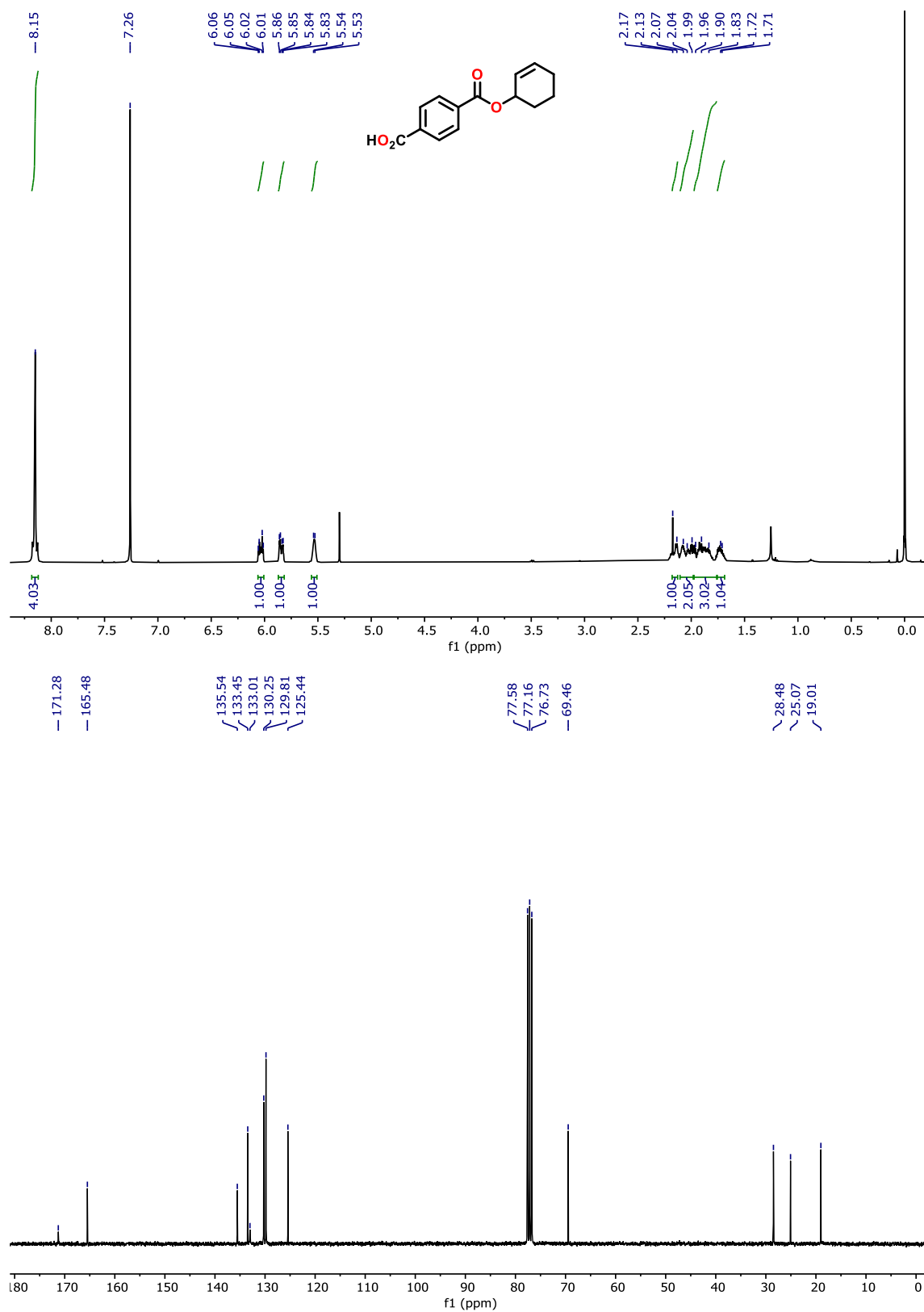
Figure 2.9. ^{1}H and ^{13}C NMR spectra of compound **4g**
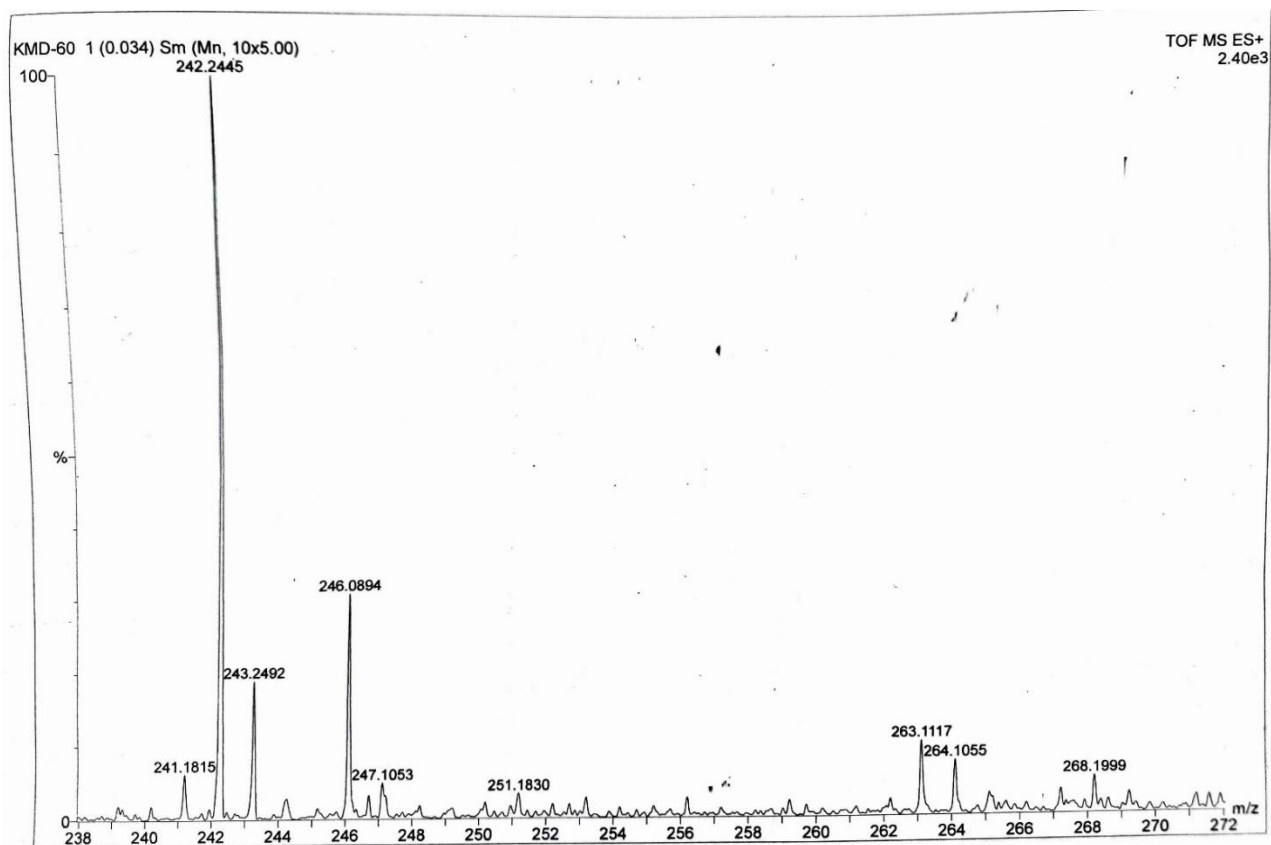
Figure 2.10. HRMS of compound **4g**
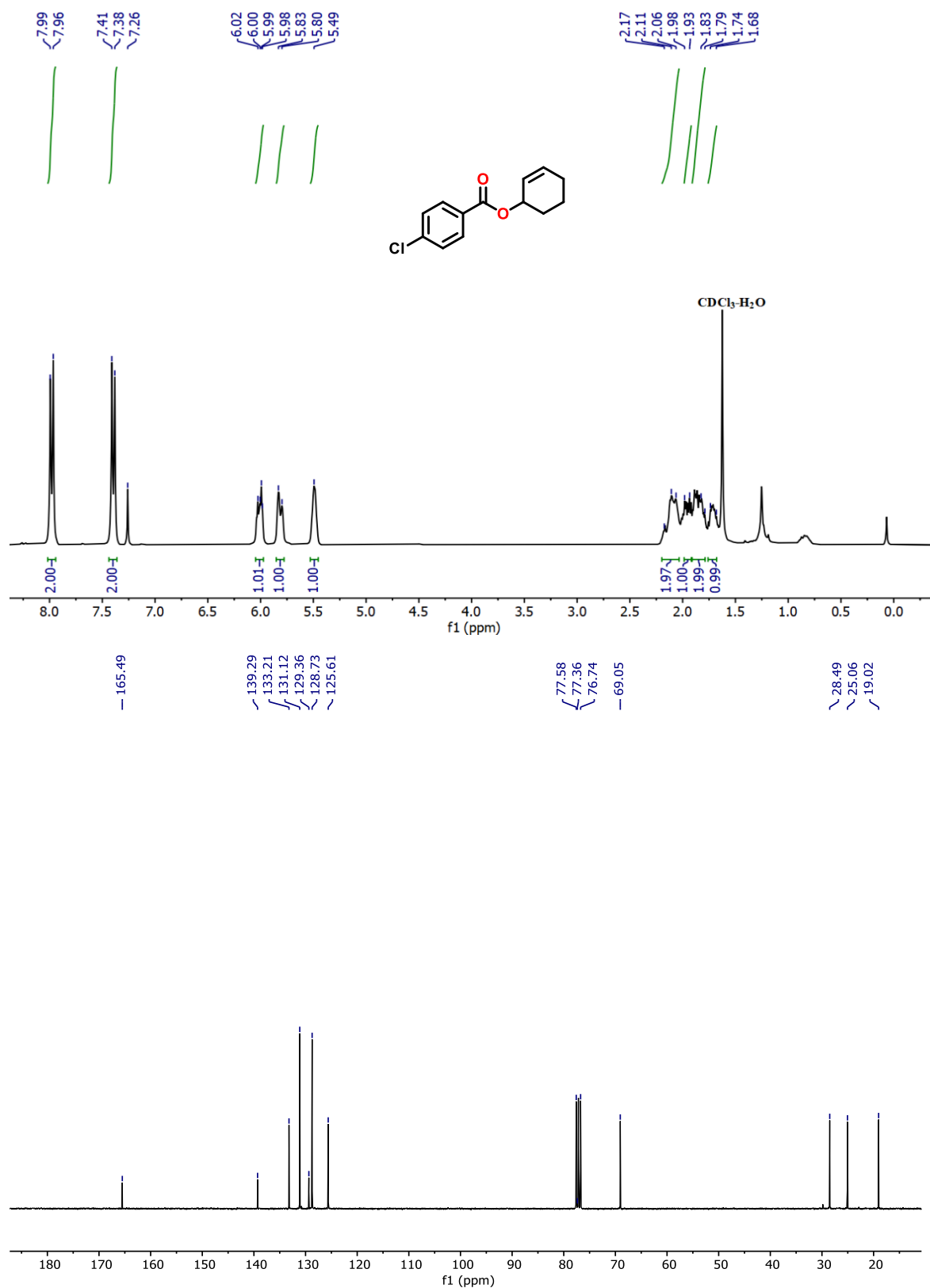
Figure 2.11. ¹H and ¹³C NMR spectra of compound **4h**
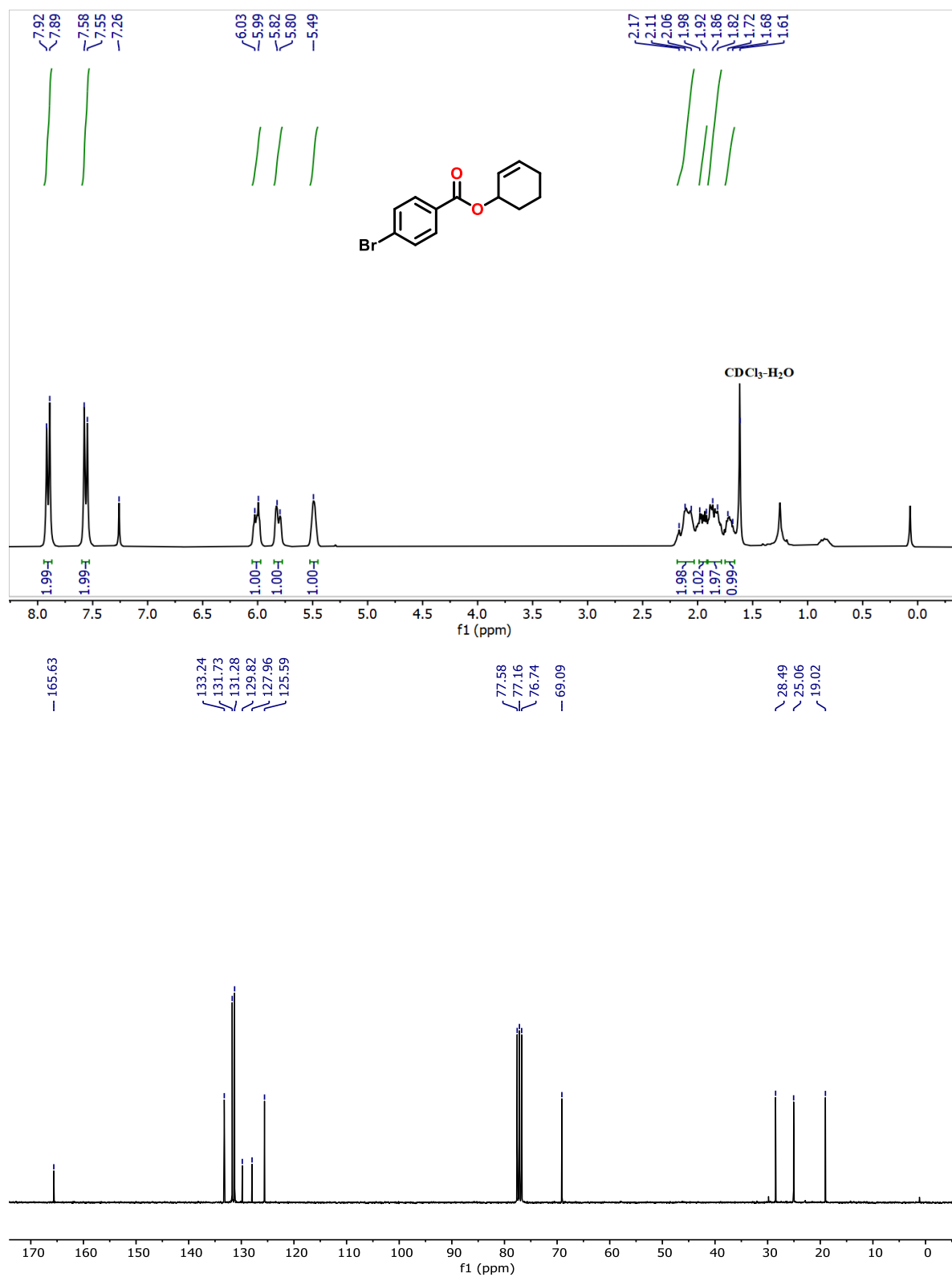
Figure 2.12. ^{1}H and ^{13}C NMR spectra of compound **4i**
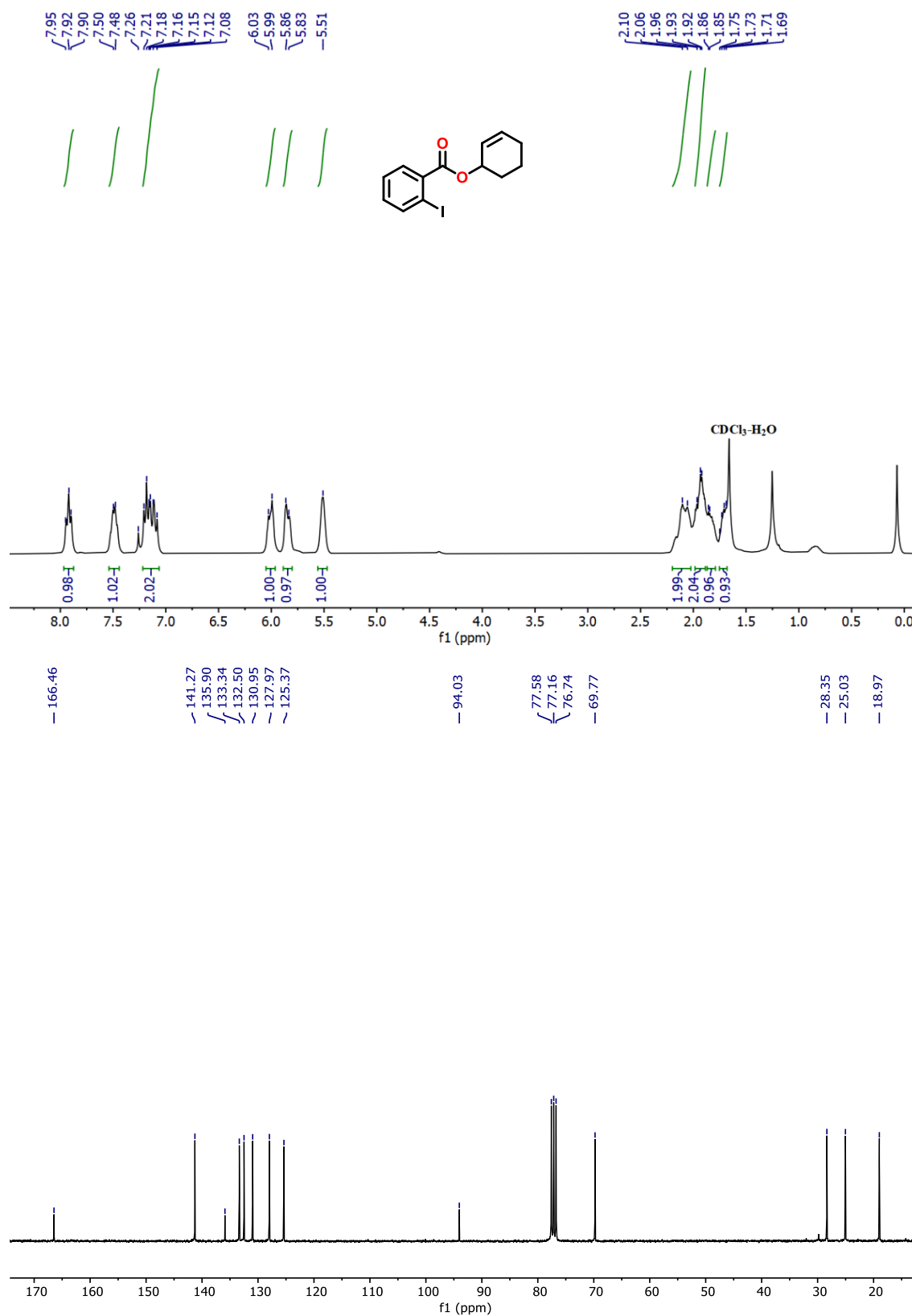
Figure 2.13. ^{1}H and ^{13}C NMR spectra of compound **4j**
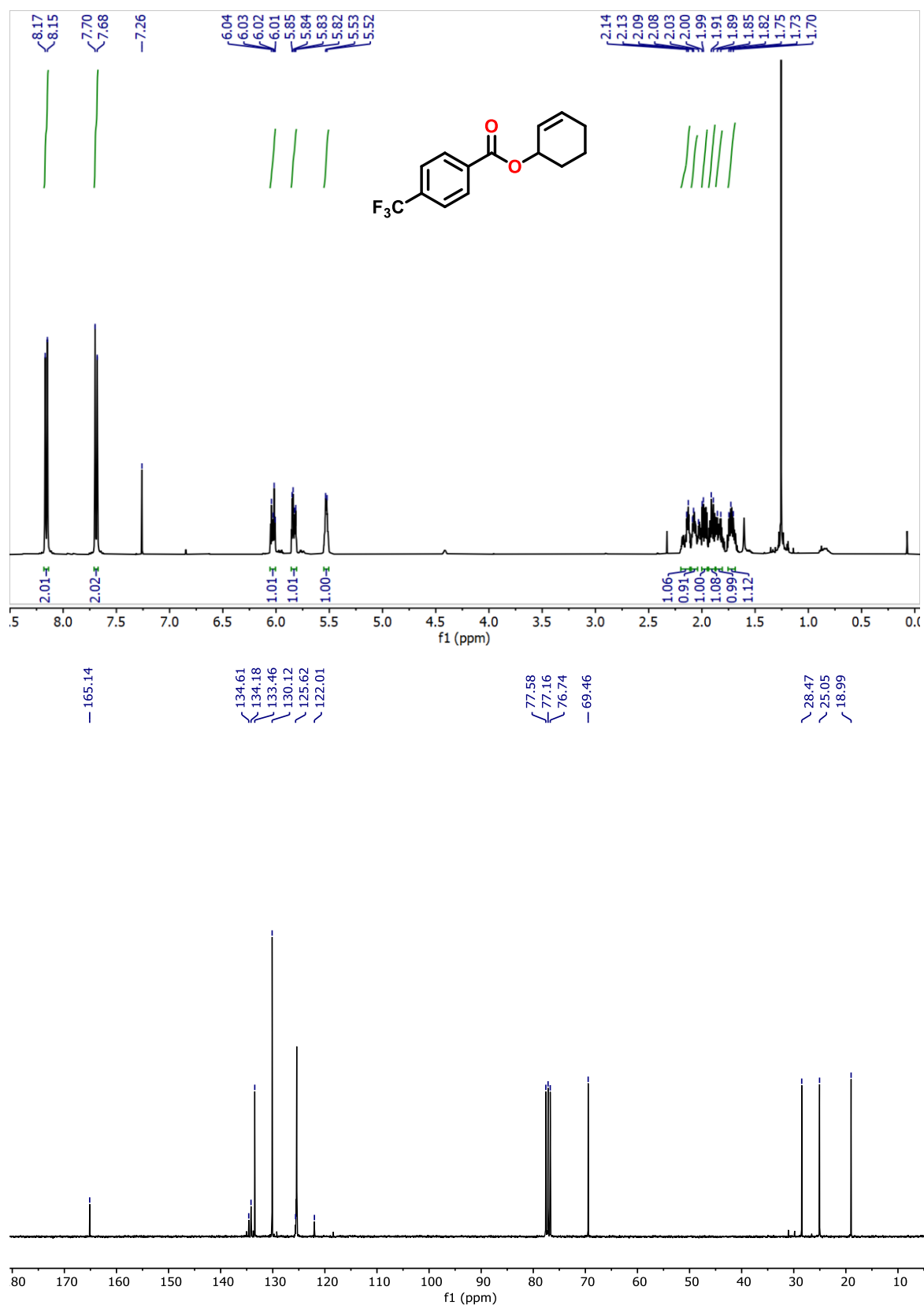
Figure 2.14. ^{1}H and ^{13}C NMR spectra of compound **4k**
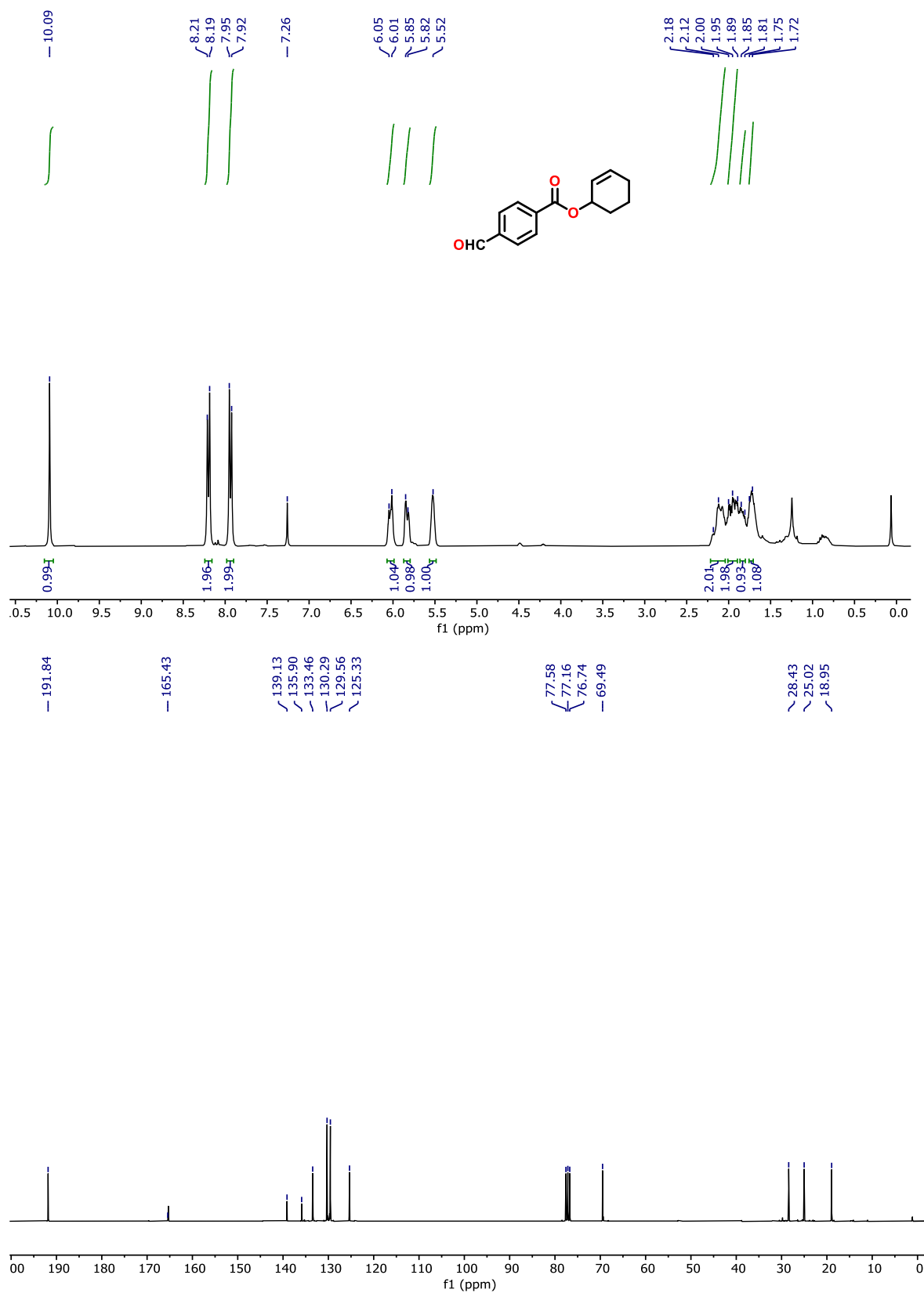
Figure 2.15. ^{1}H and ^{13}C NMR spectra of compound **4l**
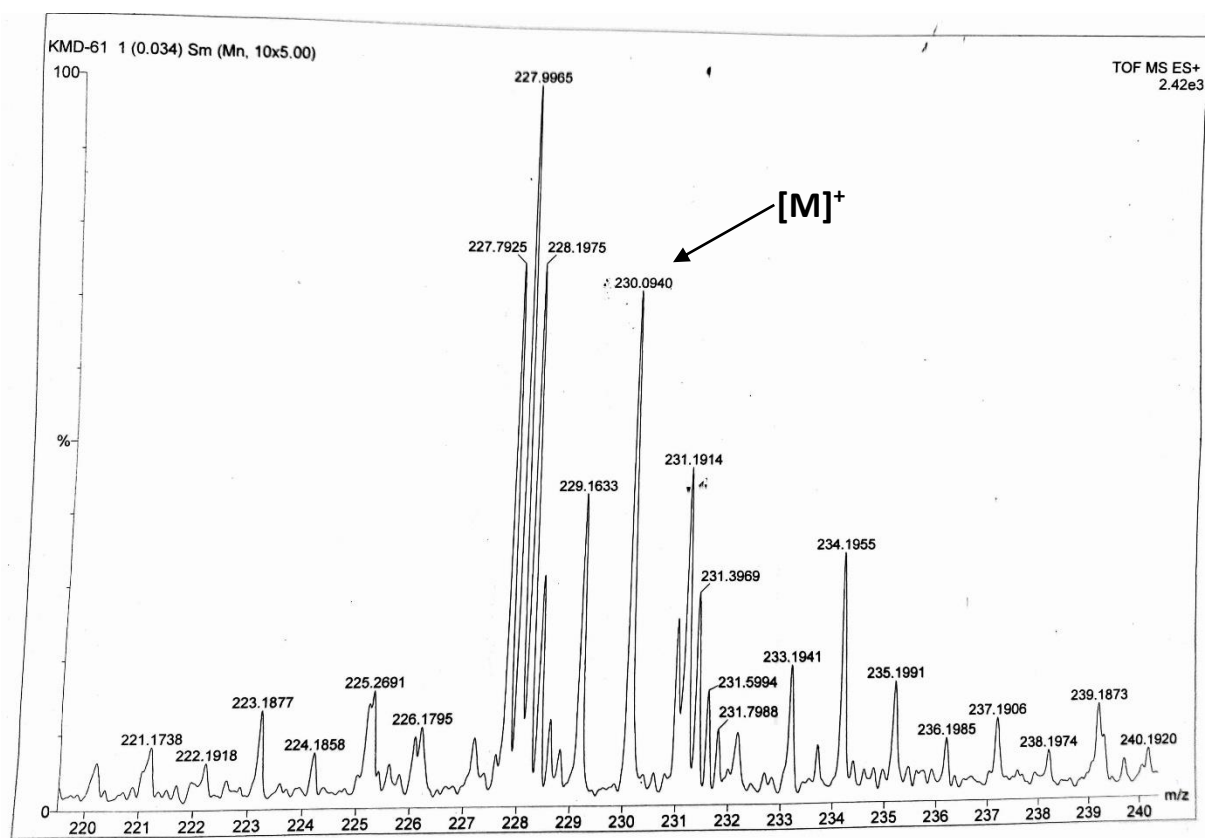
Figure 2.16. HRMS of compound **4l**
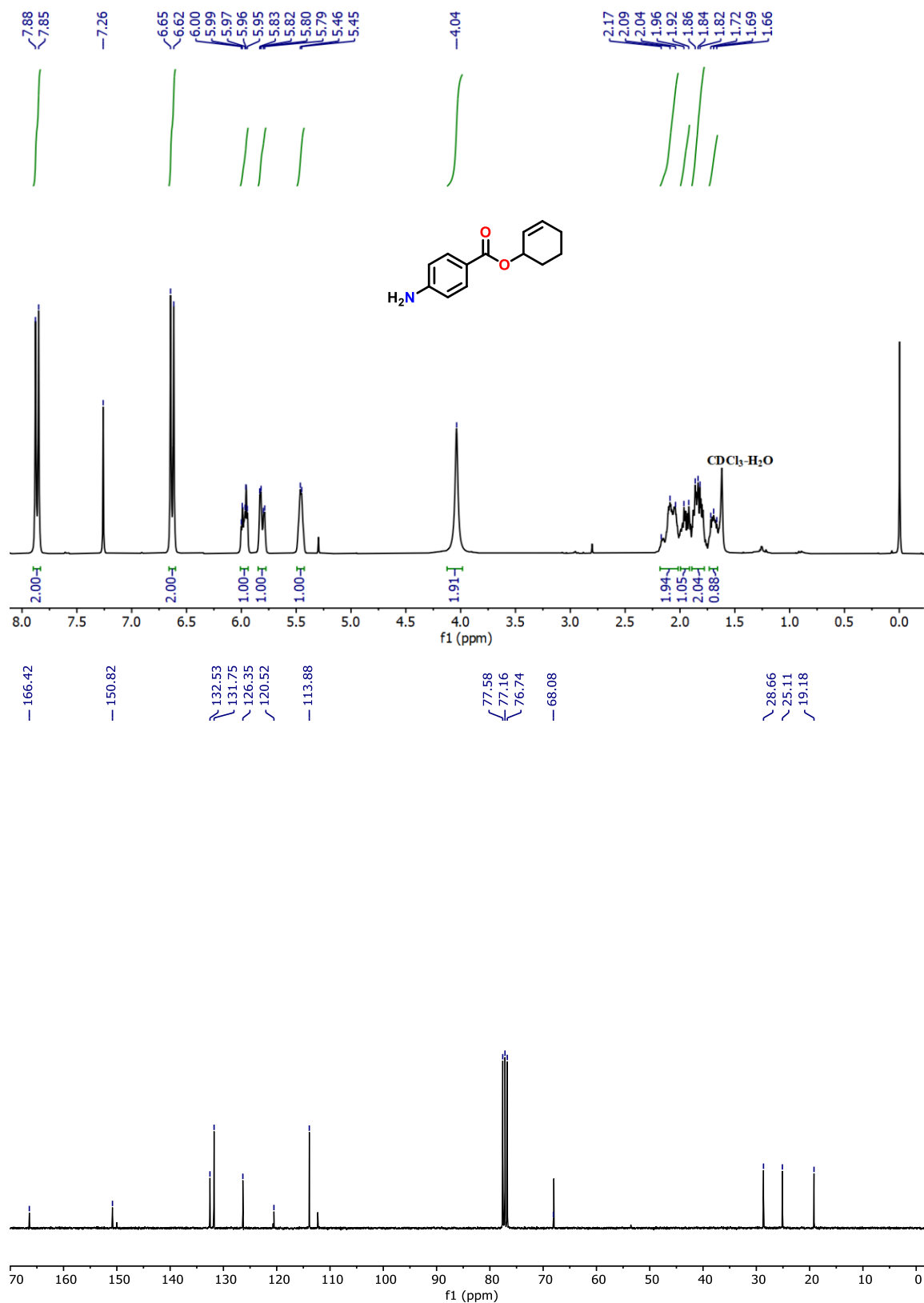
Figure 2.17. ^{1}H and ^{13}C NMR spectra of compound **4m**
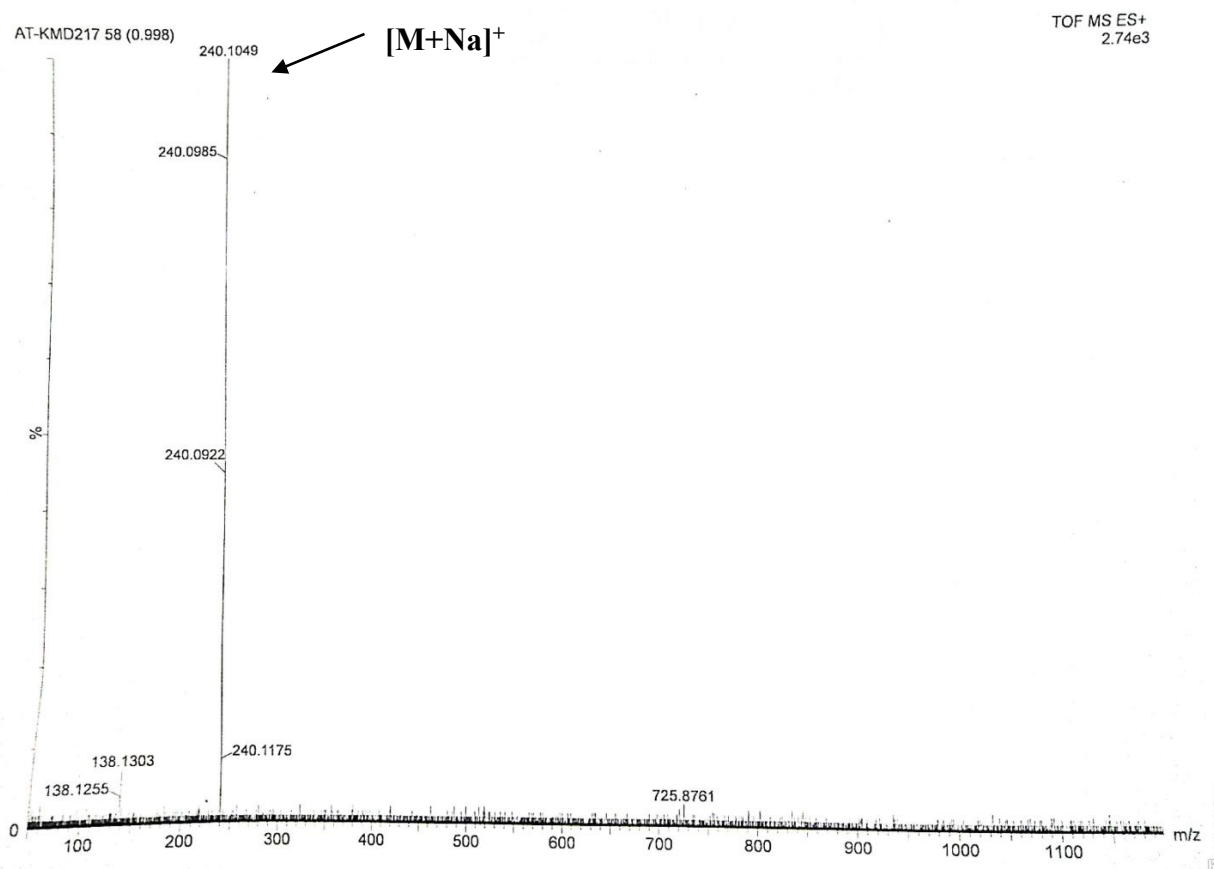
Figure 2.18. HRMS of compound **4m**
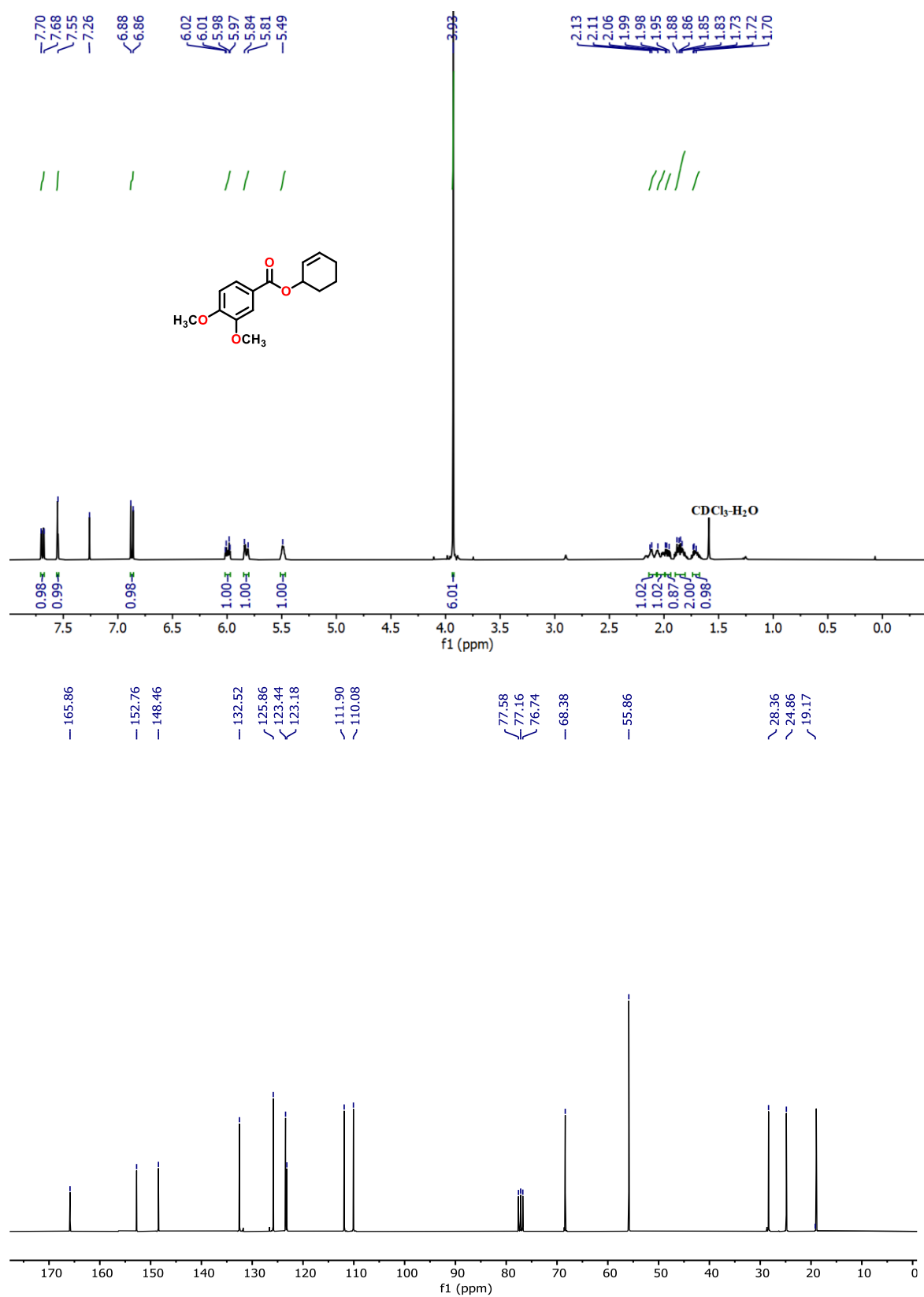
Figure 2.19. ^{1}H and ^{13}C NMR spectra of compound **4n**
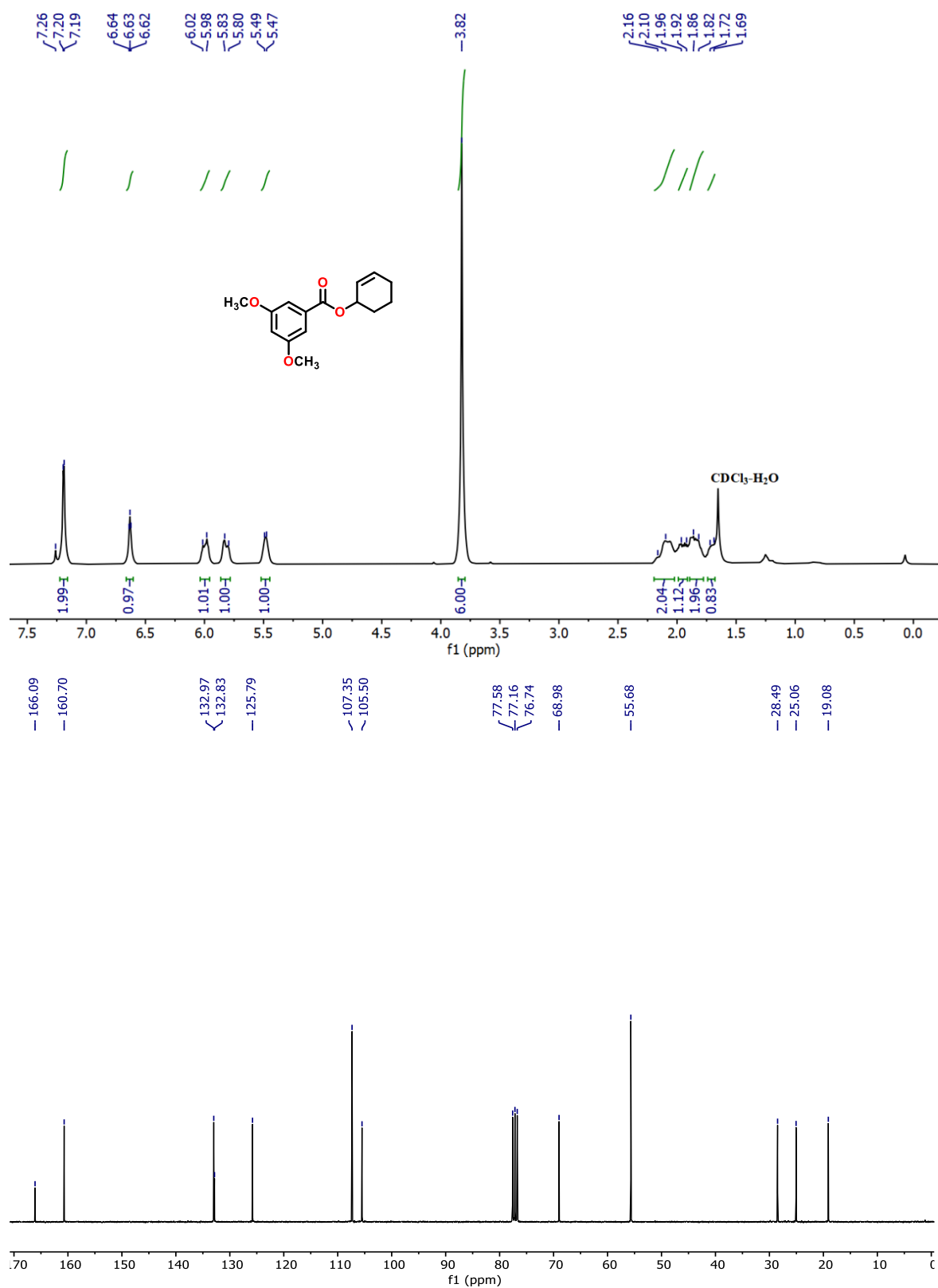
Figure 2.20. ¹H and ¹³C NMR spectra of compound **4o**
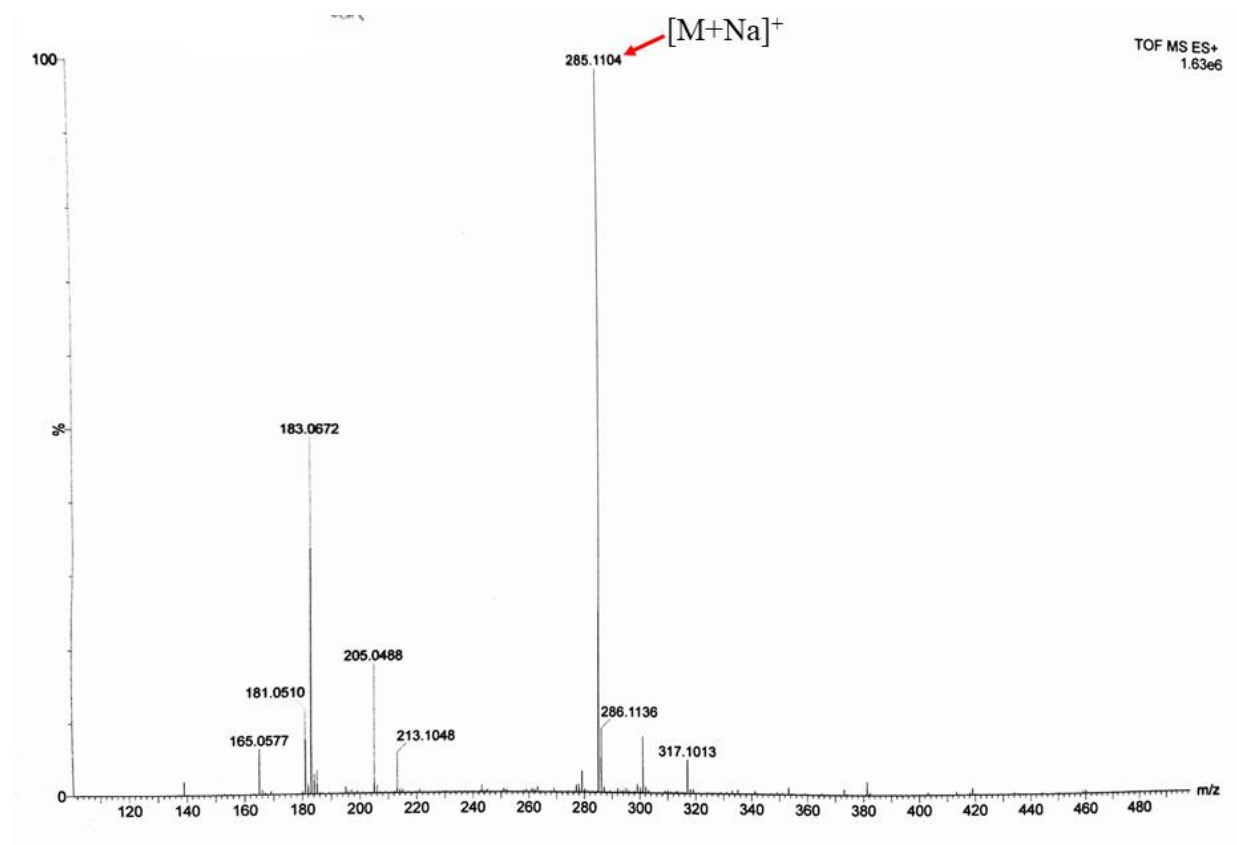
Figure 2.21. HRMS of compound **4o**
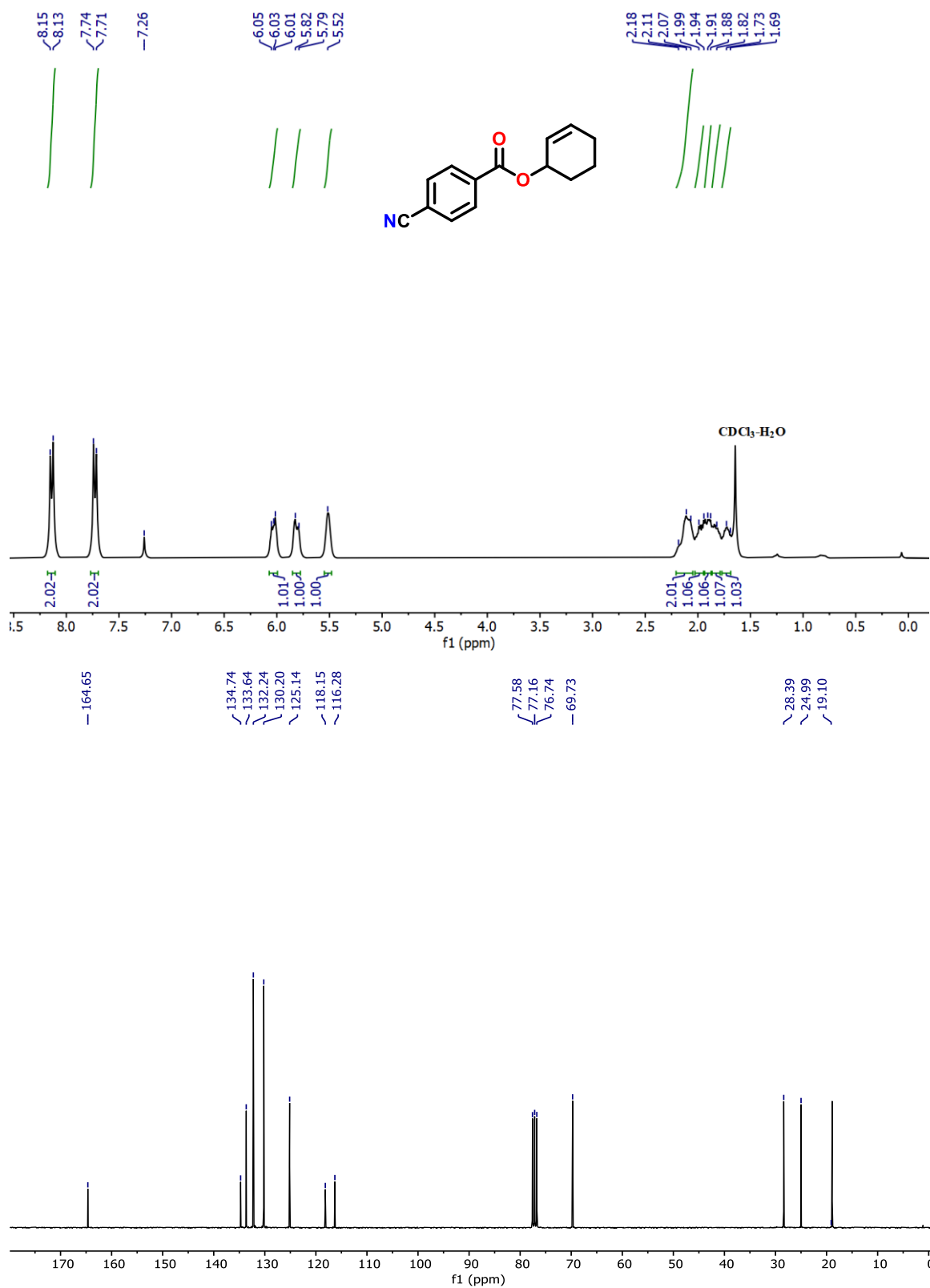
Figure 2.22. ^{1}H and ^{13}C NMR spectra of compound **4p**
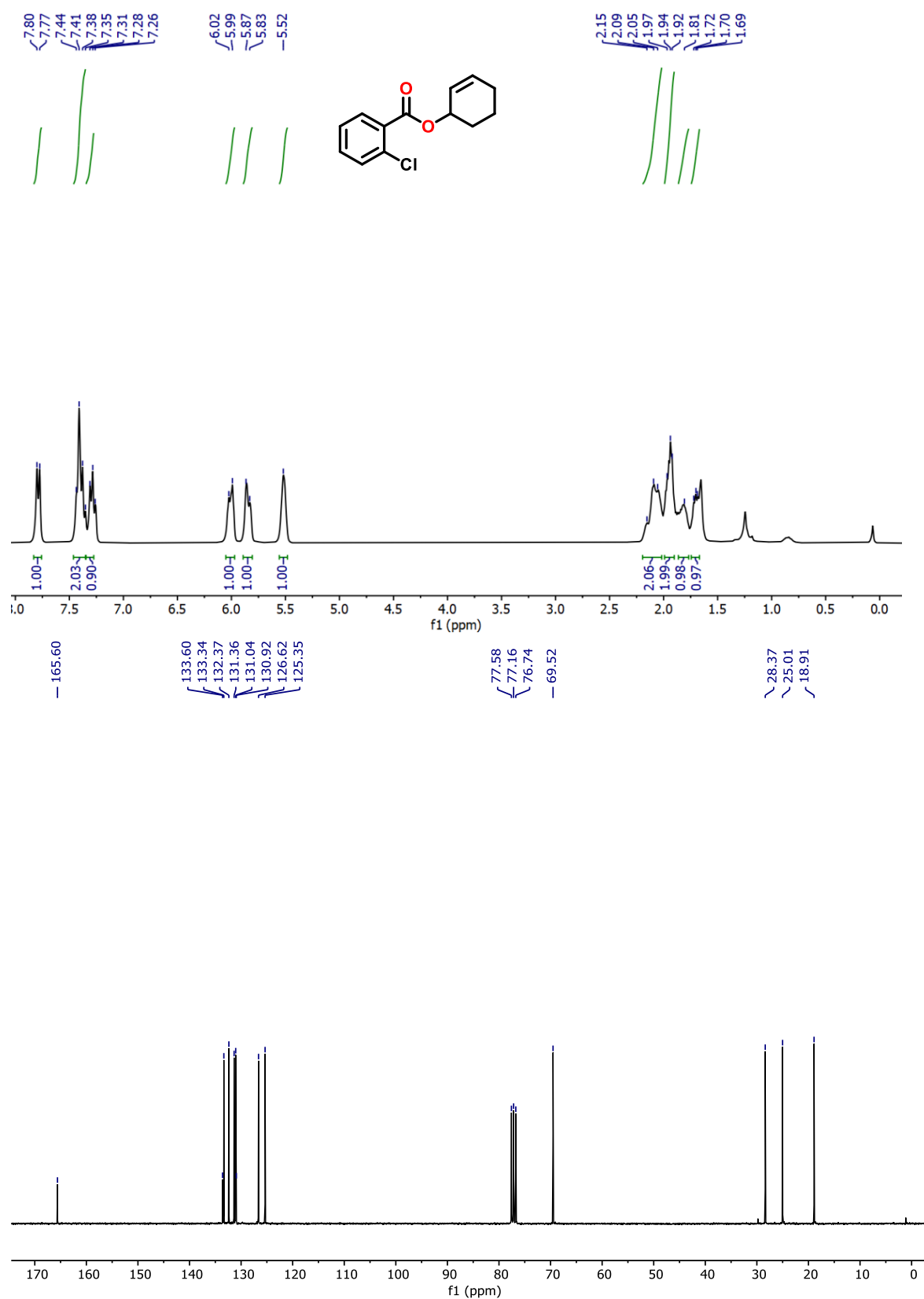
Figure 2.23. ¹H and ¹³C NMR spectra of compound **4q**
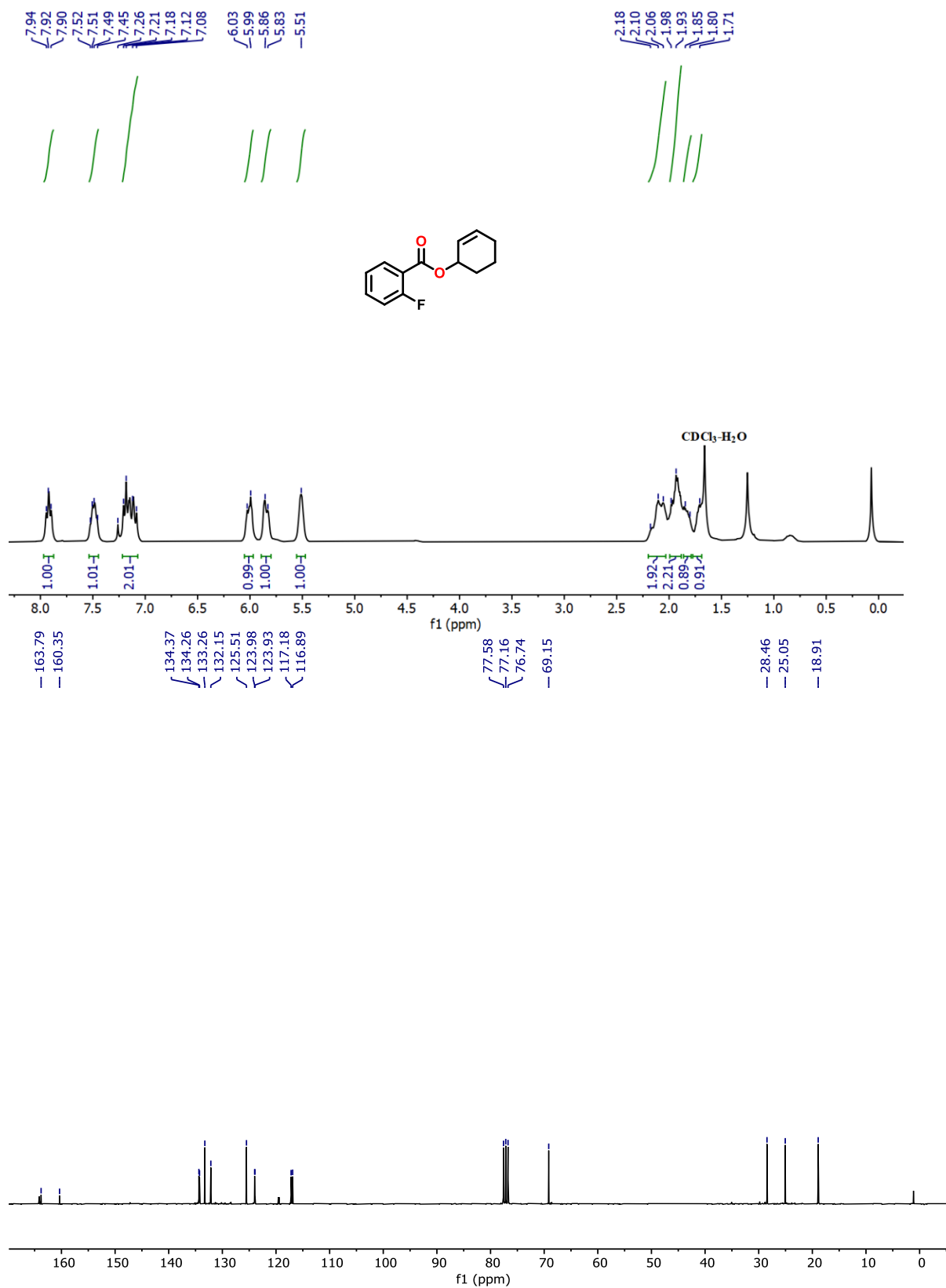
Figure 2.24. ^1H and ^{13}C NMR spectra of compound **4r**
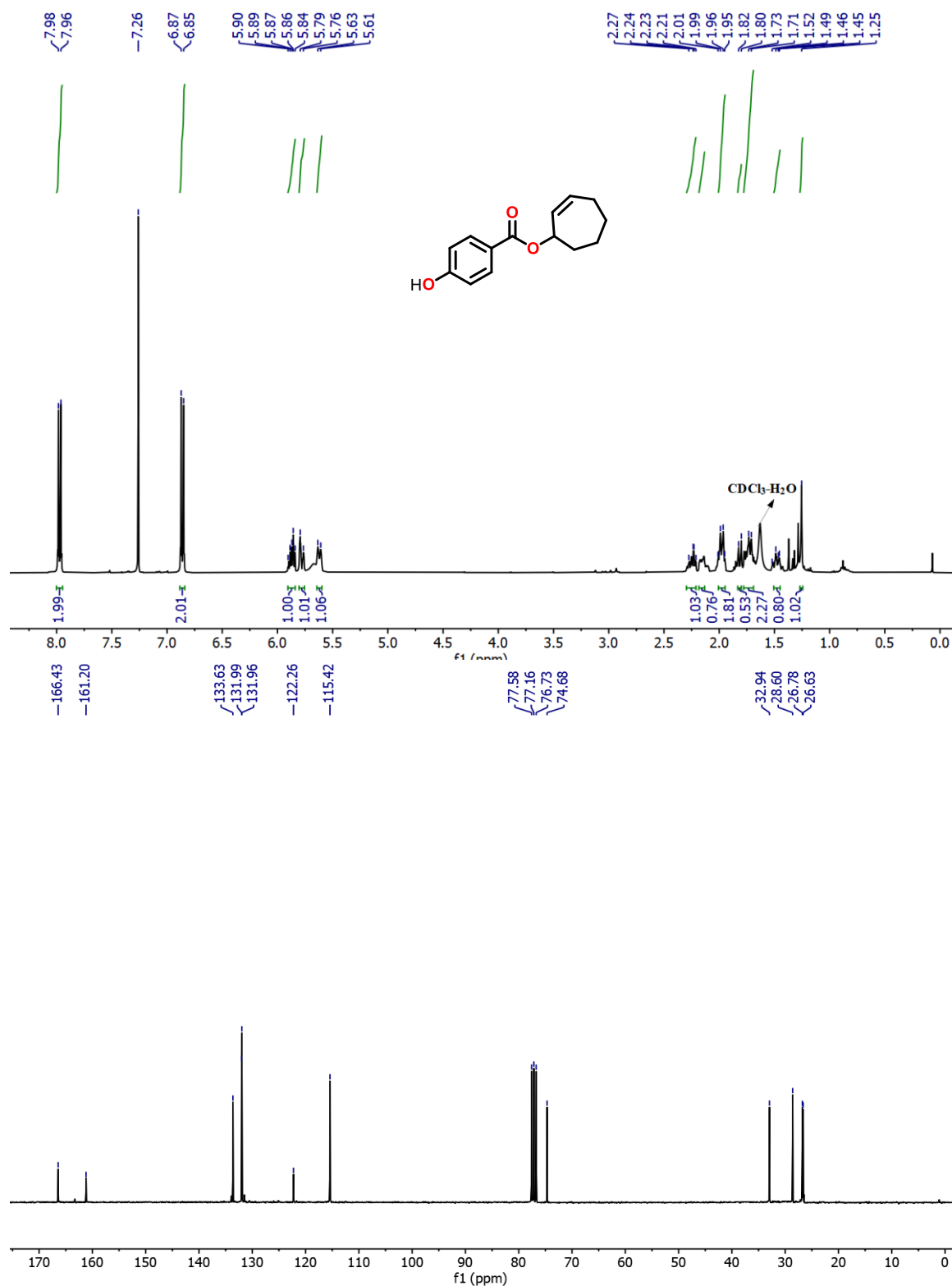
Figure 2.25. ^{1}H and ^{13}C NMR spectra of compound **4s**

Figure 2.26. ^{1}H and ^{13}C NMR spectra of compound **4t**
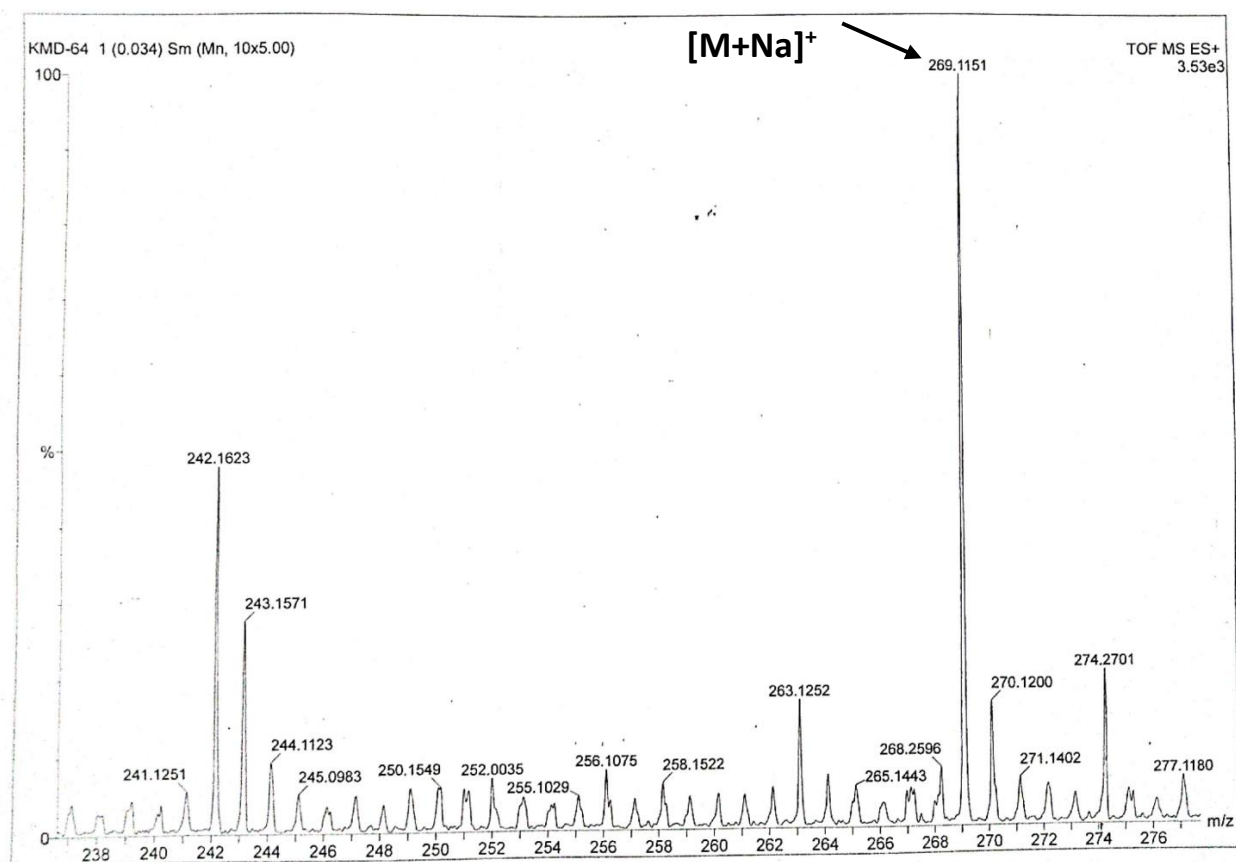
Figure 2.27. HRMS of compound **4t**
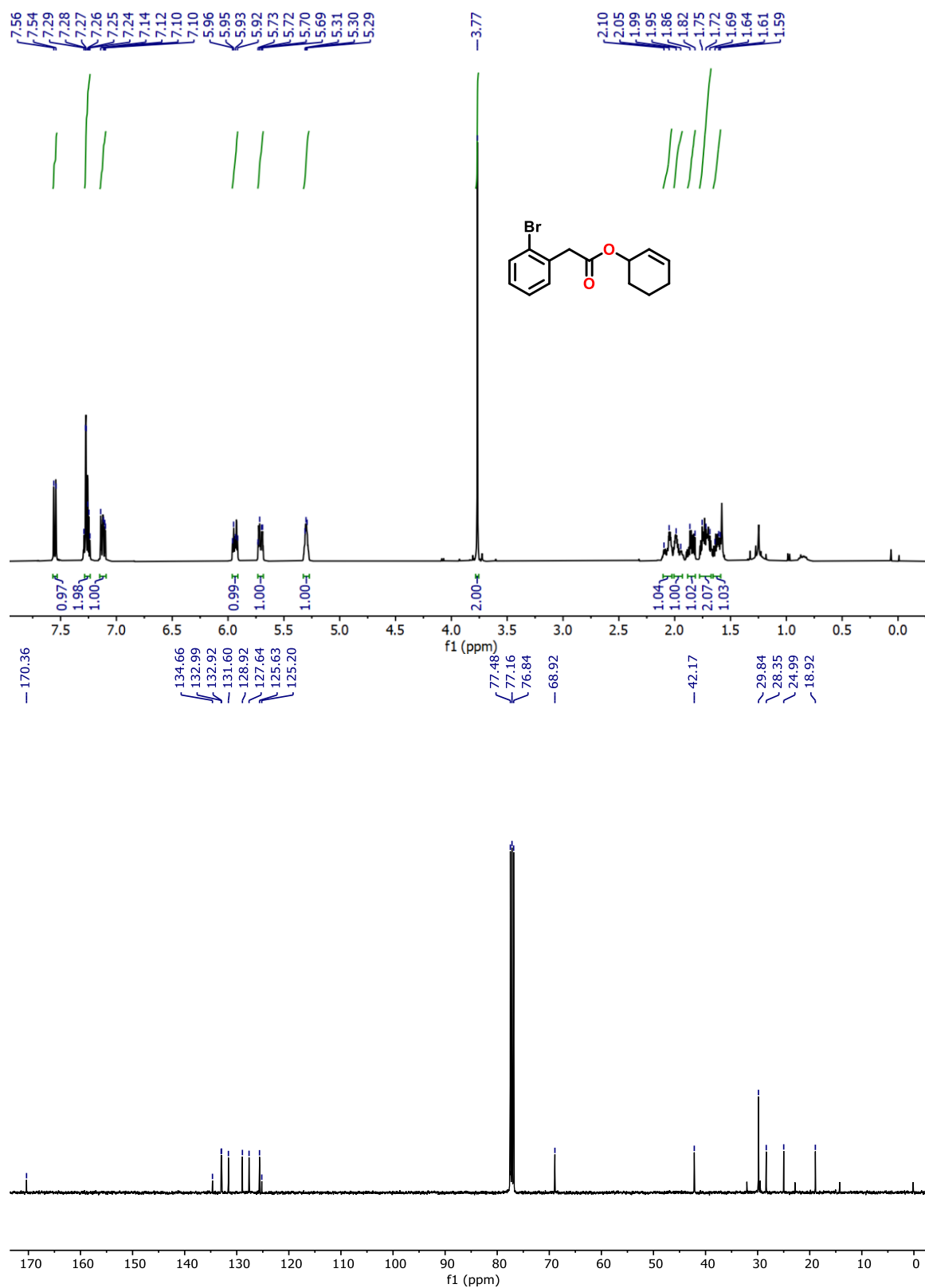
Figure 2.28. ^{1}H and ^{13}C NMR spectra of compound **6b**
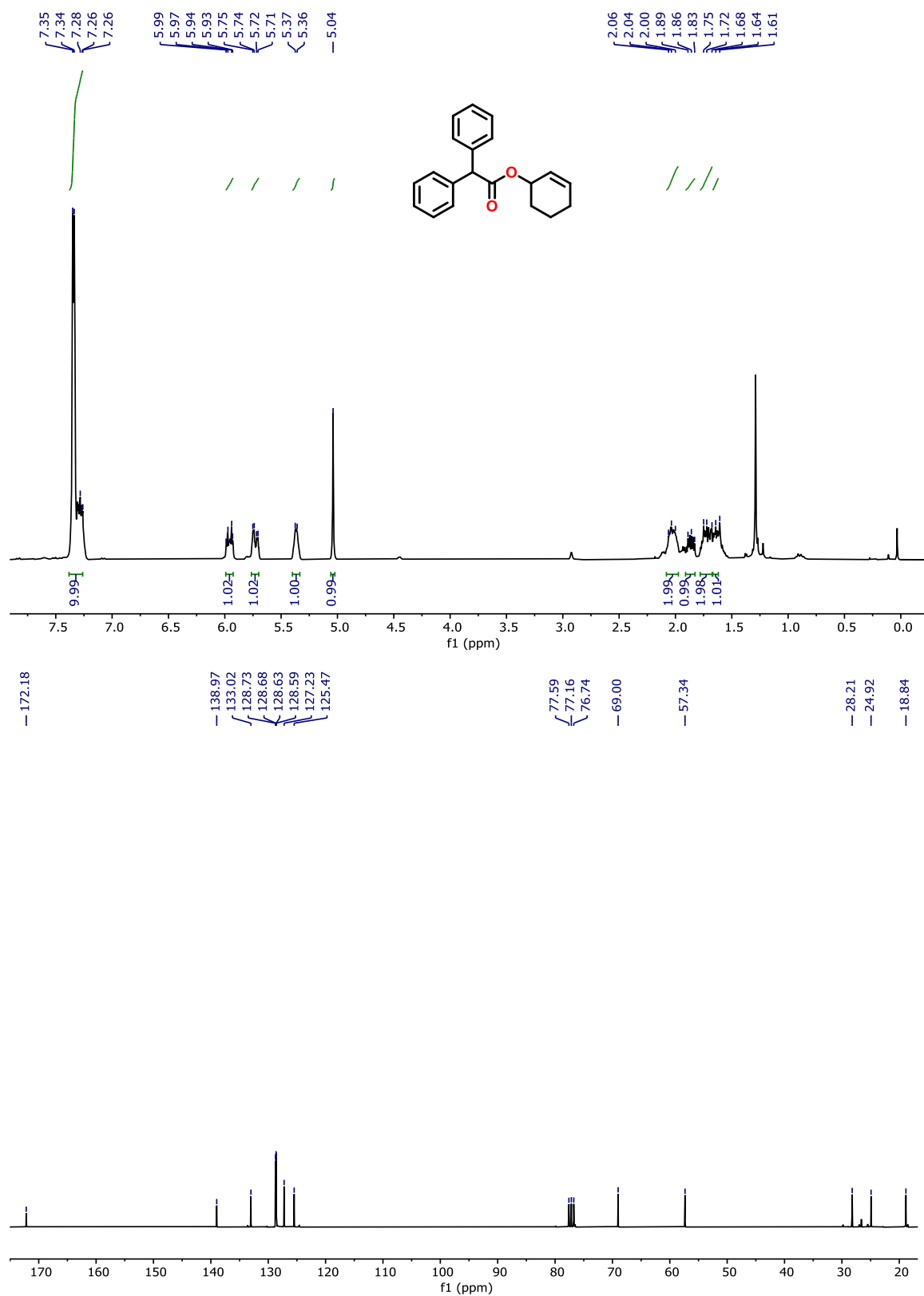
Figure 2.29. ¹H and ¹³C NMR spectra of compound **6c**
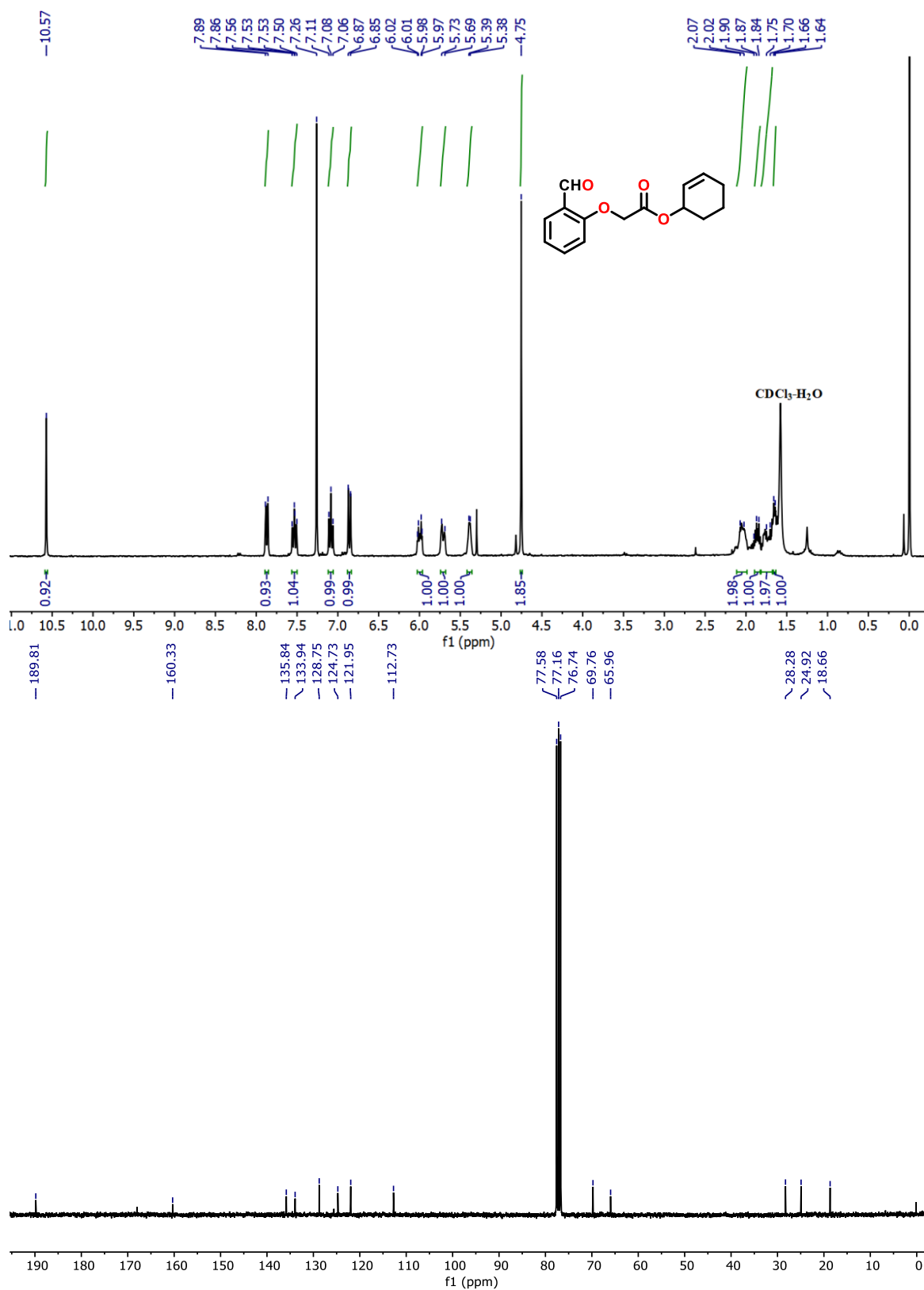
Figure 2.30. ¹H and ¹³C NMR spectra of compound **6d**
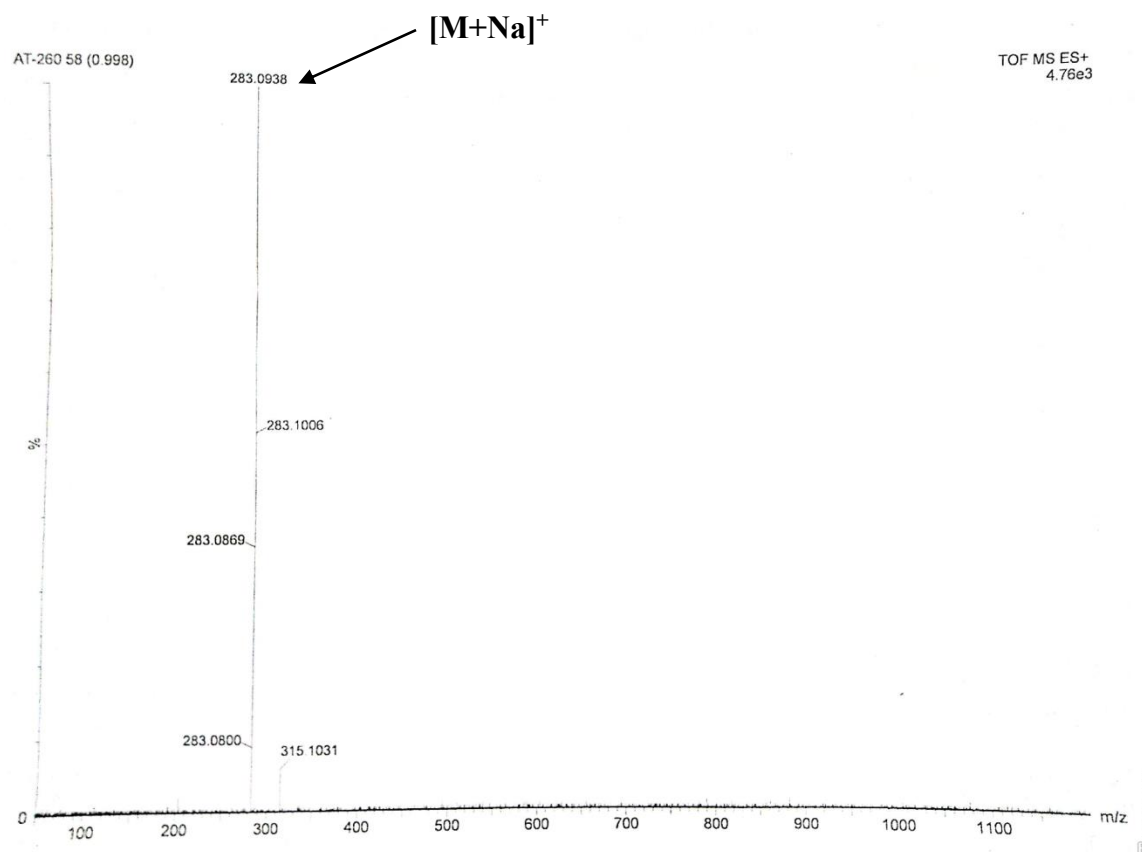
Figure 2.31. HRMS spectra of compound **6d**
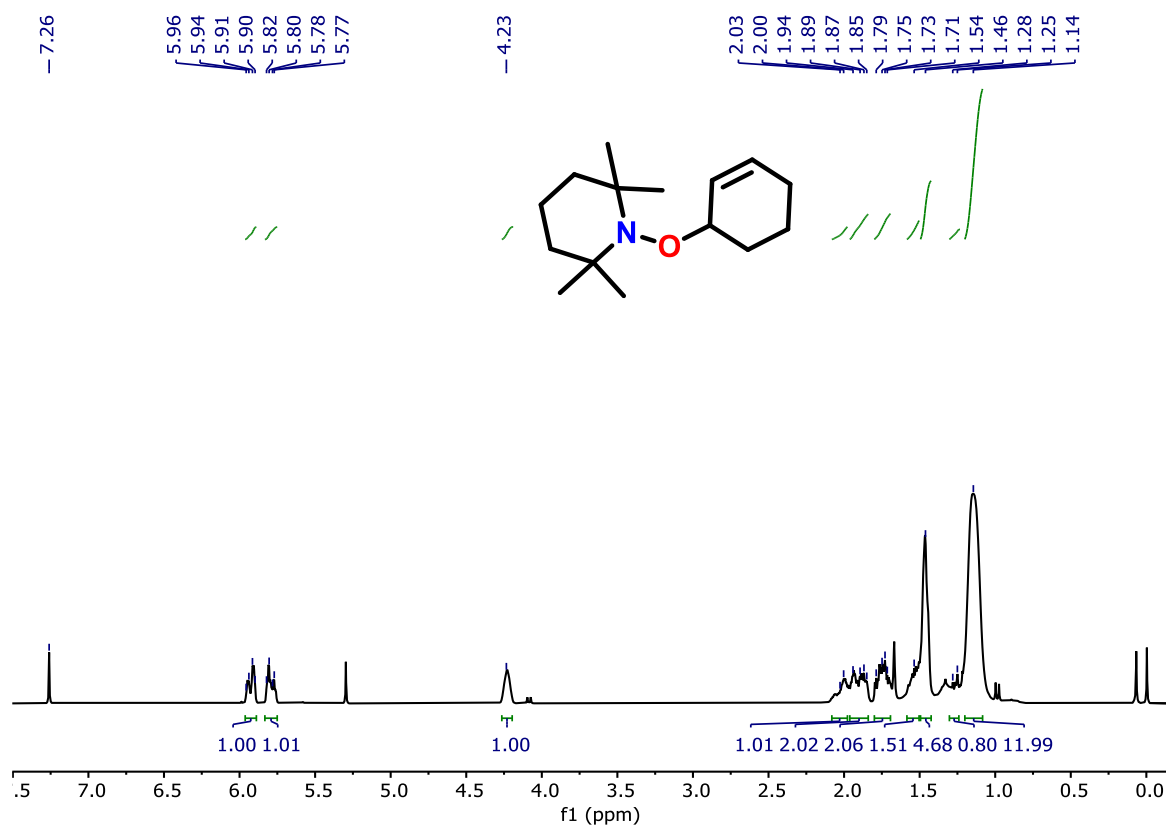
Figure 2.32. ^{1}H NMR spectra of the TEMPO-based alkoxyamine compound 1-(cyclohex-2-en-1-yloxy)-2,2,6,6-tetramethylpiperidine.
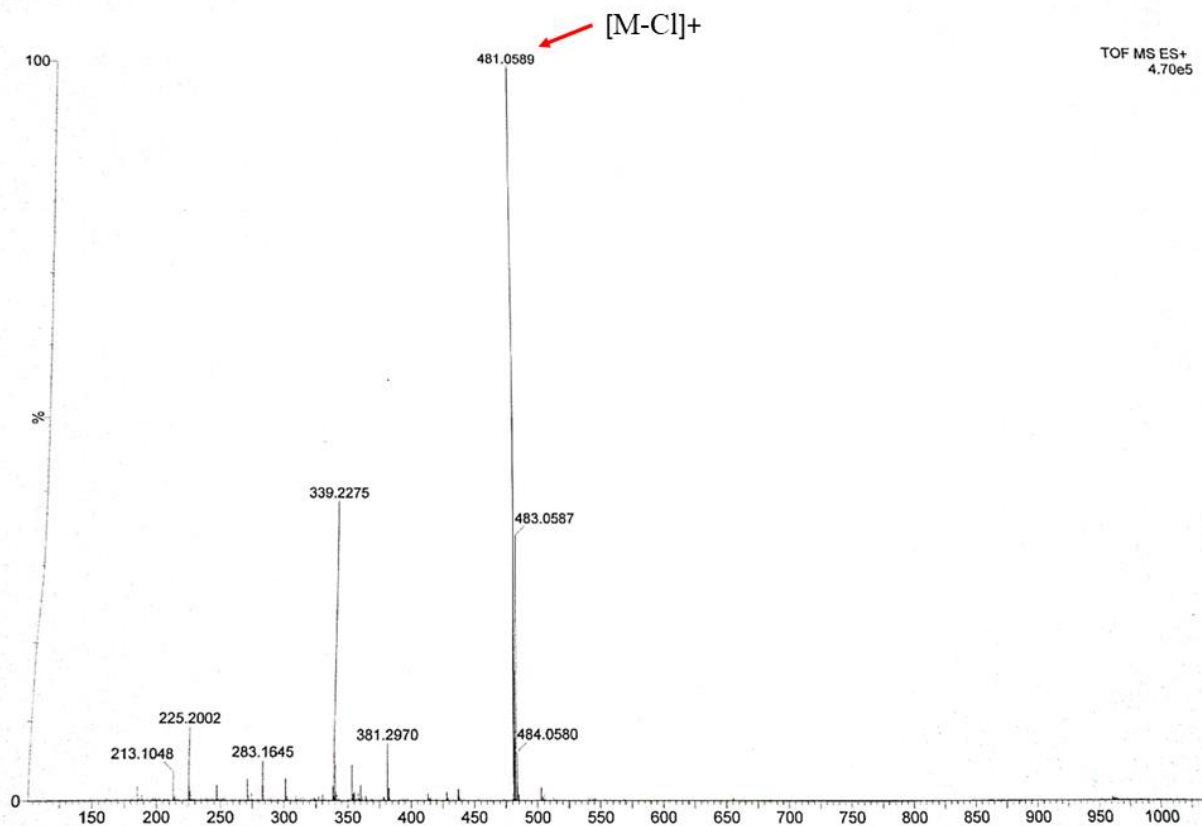
Figure 2.33. HRMS of copper complex **1**

Table 2.5 Crystallographic details of complex **1**

Empirical formula	$C_{25}H_{13}ClN_5O_2$
Formula weight	517.42
Crystal size (mm)	0.2 X 0.2 X 0.1
Crystal system	triclinic
Space group	P -1
a [Å]	a=8.1305(7)
b [Å]	b=9.2545(8)
c [Å]	c=14.7289(13)
α [°]	96.831(3)
β [°]	98.583(3)
γ [°]	104.865(3)
volume [Å^3]	1044.74(16)
Z	2
F(000)	526.0
μ MoK$_\alpha$ [mm^{-1}]	1.21
Temperature [K]	273(2)
R_{int}	0.0589
Range of h, k, l	−10/10, −12/12, −19/14
$\theta_{min/max}$ (°)	2.308/28.358
GOF on F^2	1.133
Final R indices [I > 2σ(I)]	$R1 = 0.0785$ $wR2 = 0.2316$
R indices [all data]	$R1 = 0.0828$ $wR2 = 0.2338$

Chapter-3

Oxidative Cross Dehydrogenative Coupling Directed Carbamates Synthesis using Cu(II) Pincer Complex as Active Catalyst Under Mild Reaction Condition

33 examples; Yield upto 55%-85%

- ✓ **Air stable Cu(II) complex**
- ✓ **Mild reaction condition**
- ✓ **Low catalyst loading**
- ✓ **Shorter reaction time**
- ✓ **Good to excellent yield of product**
- ✓ **Functional group tolerance**
- ✓ **Broad substrate scope**
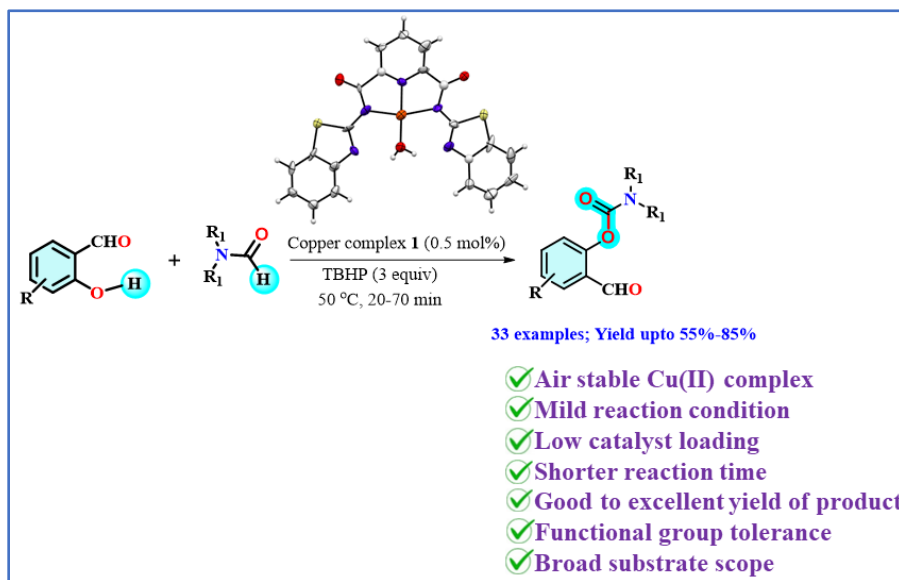
Representative publication

J. Heterocycl. Chem., 2023, **60**, 1165-1178

3.1 Introduction

Over the past few decades, the coupling reactions especially cross-coupling reactions catalyzed by transition metals have become a paramount important synthetic strategy in both industry and academia for the formation of a C-C and C-X (X = N, O, S) bonds.[1] However, the requirement of pre-functionalized hydrocarbons as starting materials and stoichiometric organometallic reagents such as Grignard and organolithium reagents, provides an opportunity to the scientist for further development. To circumvent these issues, the direct C-H bond functionalization has come up as an alternative pathway as this process is atom economic and environmentally friendly synthetic strategy.[2] Inert C-H bond can be functionalized by two pathways: (a) metal chelate assisted functionalisation [3] and (b) the cross dehydrogenative coupling (CDC).[4] Among them, CDC reaction is widely employed mainly for C-C[4a-d,5], C-N[6] and C-O[7] bond formation reactions. Noteworthy, CDC protocols are mostly investigated for C-O bond formation leading to the synthesis of various esters, whereas, C-O bond formation leading to the synthesis of carbamates are very few so far.[8]

Organic carbamates have found widespread applications in pharmaceutical, polymer and agrochemical industries due to their pesticides, fungicides, and herbicides nature.[9,10] They are also usually considered as protecting groups, synthetic intermediates and directed metalating groups.[11] Traditionally, carbamates are prepared by reaction of amines with phosgene or its derivatives like chloroformate, dialkyl carbonates or *via* the reaction of alcohol with isocyanate.[12] High toxicity of all these reagents provide a room for further development for the generation of carbamates in more greener approach such as (i) oxidative and reductive carbonylation of amines and nitro aromatics [11a,c,9a] (ii) reaction of amines with CO_2[11e] and many others.[12] Lately, the cross dehydrogenative coupling protocol has enhanced the efficiency of the reaction methods for the generation of C-O bonds.[9a]

Apart from the oxidative C-C and C-N bond formation, N-N dialkylformamides can also act as an aminocarbonyl surrogate for the synthesis of carbamates *via* C-O bond formation.[13a-b] Recently, a few oxidative cross coupling reactions (CDC) have been reported for the formation of carbamates by using copper salt in combination with oxidants and all those reported reaction conditions need high catalyst loading, high temperature (80-120 °C) and anhydrous metal salt and

sensitive Cu(I) salt.[8] Together, all these factors create an opportunity for further development of an expedient and safe milder reaction condition with a well-defined air stable catalyst.

Herein, we have designed and synthesized a benzothiazole-appended picolinamide-based Cu(II) complex which can catalyze the reaction of various substituted salicylaldehyde or 1,3-di keto derivatives with differently substitute formamide to generate carbamates with only 0.5 mol% catalyst loading at slightly elevated temperature (50 °C). Using this air-stable copper complex, the oxidative CDC reaction is completed within 20 min with good yield. The complex **2** showed excellent catalytic activity in the cross-coupling of a wide variety of phenol derivatives and N,N di-alkyl formamides to form the corresponding carbamates. To the best of our knowledge, this is the first time in literature where the organic carbamates can be prepared with very low catalyst loading, a shorter reaction time with a well-defined cheap transition metal catalyst.

3.2 Results and Discussions

3.2.1 Synthesis and characterization of the 2,6-picolinamide-based Cu(II) complex

The ligand (**L**) was synthesized according to a literature-reported procedure.[14] Ligand **L** was taken in a 100 mL round bottom flask and dissolved in chloroform. $CuCl_2.2H_2O$ was dissolved in methanol and the resulting mixture was added dropwise to the ligand solution. The reaction mixture was kept at room temperature overnight, producing a green colour complex as a precipitate in nearly 70% yield (Scheme 3.1). X-ray quality single crystals were grown by slow evaporation of DMF solvent at room temperature. From the molecular structure (Figure 3.1), it is evident that complex **2** crystallizes in distorted square planar geometry where the N_1 atom of the pyridine ring and adjacent two amidic nitrogen atoms (N_2,N_3) of benzothiazole moieties take part in chelation with the Cu metal ion and one water molecule got attached with metal centre to make it tetra-coordinated complex.
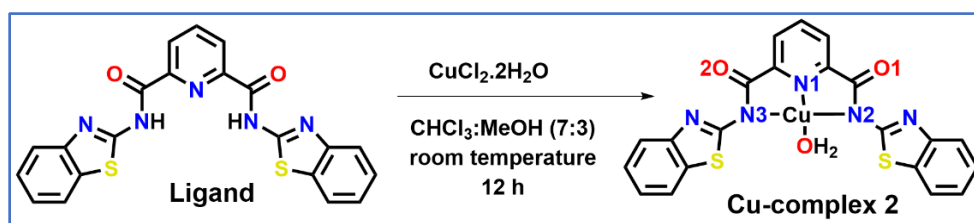
Scheme 3.1: Synthesis of complex **2**.
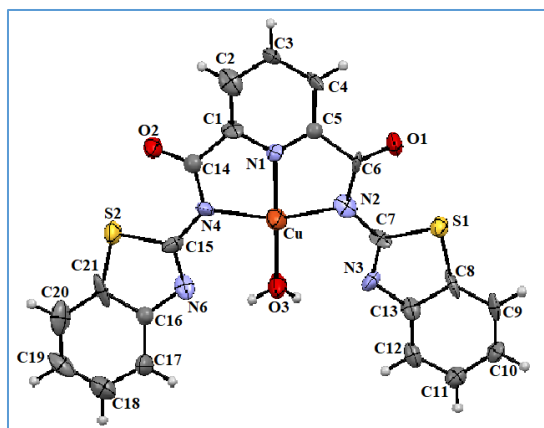
**Figure 3.1.** ORTEP representation of complex **2** with thermal ellipsoids drawn at the 50% probability level. Some selected bond lengths (Å) and bond angles (deg) of complex **1** are N4-Cu 2.044, N1-Cu 1.9136, N2-Cu 2.016, Cu-O3 1.868; N4-Cu-N1 81.41, N1-Cu-N2 80.58, N2-Cu-O3 99.71, N4-Cu-O3 98.24.

3.2.2 UV-vis, cyclic voltammetry, electron paramagnetic resonance (EPR) and IR spectra of complex 2
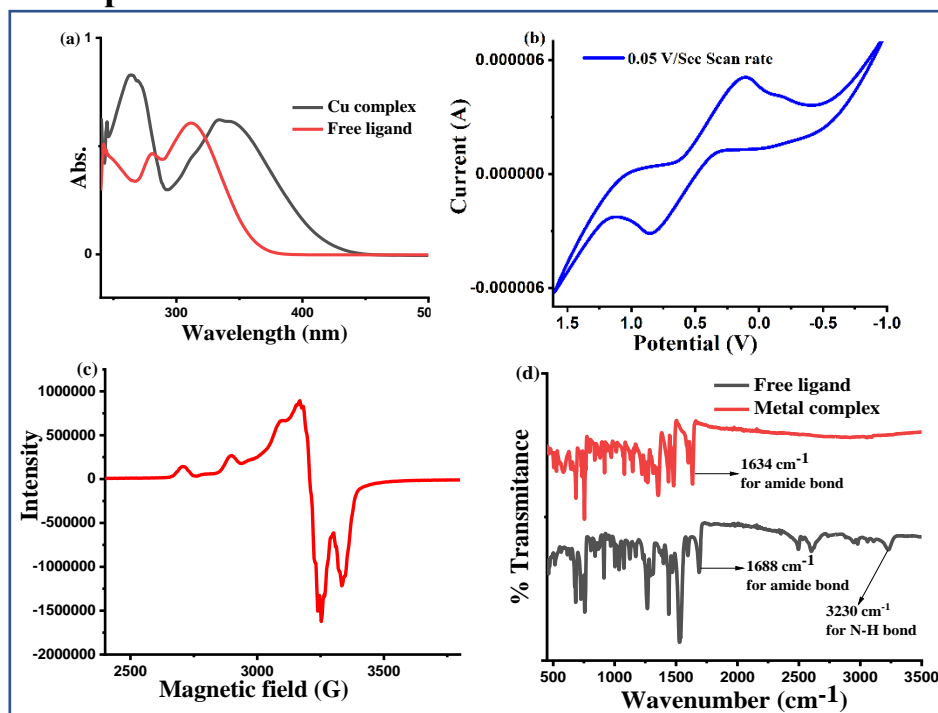
Figure 3.2. (a) UV-vis spectra of free ligand and copper complex **2** in THF solvent (1.25×10^{-4} M), at 293 K (b) cyclic voltammetry plot of copper complex **2** in THF solvent (7.5×10^{-3} M) at scan rate 0.05V/sec against Pt as a working electrode and carbon as counter electrode using 0.1 M [(n-

Bu)$_4$N]ClO$_4$ as a supporting electrolyte (c) electron paramagnetic spectra of complex **2** in THF at temperature 100 K and (d) IR spectra of free ligand and copper complex **2** at 295 K.

UV-vis absorption study is one of the unique studies for a molecule to get an idea about its mechanistic change when a molecule reacts with a metal to form a metal complex. UV-vis spectrum of complex **2** and free ligand was done in THF solvent (1.25×10^{-4} M) at 295 K (Figure 3.2a). From UV-vis spectra it was shown that free ligand gives two peaks at 311 nm and 280 nm which may be due to π-π* and n- π* transition resulting from the aromatic delocalization of benzothiazole ring respectively.[15a,b] Whereas in case of metal complex **2** two peaks at 337 nm and 264 nm were observed respectively. Upon chelation with the metal, a new peak 337 nm was appeared which may be attributed ligand to metal charge transfer (LMCT) transition[15c,d] involving the transfer of lone pairs of electron from nitrogen atom to metal (Cu) centre. The original π-π* transition of benzothiazole unit at 311 remained as a shoulder peak after forming the complex with metal as well; however the major transition peak is LMCT for the metal complex at 337 nm.

The electrochemical behaviour of complex **2** was explored by cyclic voltammetry using TBAP (tetrabutylammonium perchlorate) as a supporting electrolyte at a scan rate 0.05 V/sec within the potential range 1.6 to 1.0 V at 295 K against saturated Ag/AgCl electrode as reference electrode (Figure 3.2b). Cyclic voltammetry plot shows reversible one-electron reduction and oxidation with ΔE = 0.75 V and $E_{1/2}$ = 0.485 V corresponding to the Cu(III)/Cu(II) redox couple.[16a,b]

The oxidation state of coordinated metal centre was confirmed by EPR spectroscopy. EPR spectrum of copper complex **2** was shown in Figure 3.2c and it was recorded in THF solvent at 100 K. According to hyperfine splitting (2nI+1) four line is expected from EPR spectrum as I = 3/2 for Cu metal ion. The EPR spectra of the complex **2** displayed the corresponding g$_∥$ and g$_⊥$ values as 2.295 and 2.052 respectively which indicated the presence of tetra coordinated distorted square-planar-based geometry around the Cu(II) centre.[17] The spectra of complex **2** consists of four well-defined hyperfine lines which can also confirm that the metal oxidation state is +2.

IR spectra was further recorded in order to understand the binding nature of copper metal with the ligand. As shown in Figure 3.2d, the free ligand shows characteristic peaks of amide at 1688 cm^{-1} and the N-H bond stretching at 3230 cm^{-1} whereas after metal chelation the corresponding N-H bond stretching is absent and the amide stretching is shifted to 1634 cm^{-1}.

Based on this observation it can be confirmed that Cu^{2+} ion is bound with amidic nitrogen atom of benzothiazole in tripodal fashion.

3.2.3 Synthesis of carbamates using cross coupling reaction

The success of using copper catalysts in the preparation of phenol carbamates has encouraged us to investigate our catalyst systems in our current study. Initially, we have chosen salicylaldehyde (**1a**) and DMF (**2a**) as model substrates for optimization of the reaction (Table 3.1). At first the reaction was carried out in presence of 2 mol% of copper catalyst **2** and in presence of 3 equivalent of various oxidants like manganese dioxide (MnO_2), iodine (I_2), hydrogen peroxide (H_2O_2), meta-chloroperbenzoic acid (m-CPBA), 2,3-dichloro-5,6-dicyano-1,4-benzoquinone (DDQ) and *tert*-butyl hydroperoxide (TBHP) at temperature 80 °C for 12 h and it shows that only TBHP was found to be a superior oxidant compared to the other oxidants and the product was formed in 85% yield (Table 3.1, entry 1-6). Then the reaction temperature was reduced to 60 °C along with the reduction of reaction time from 12 h to 6 h (Table 3.1, entry 7). Interestingly, yield of the product remained unaltered. In our attempt to optimize the reaction condition, we have further reduced the catalyst loading and temperature, and reaction time sequentially (Table 3.1, entry 8-12). Surprisingly, we have observed that the reaction can be completed within 20 min in the presence of only 0.5 mol% copper catalyst and 3 equivalents of TBHP at 40 °C with 85% product yield (Table 3.1, entry 13). But unfortunately, when we performed the substrate scope reaction, we observed that in every case the conversion of starting material to product is somewhat less at 40 °C temperature. Using this observation, we perform all the reaction at 50 °C and it shows that at 50 °C all the starting material is consumed and yield of the product is increased. For this reason, we optimized our reaction condition at 50 °C (Table 3.1, entry 14). After getting the optimized reaction condition in hand we have performed the reaction in presence of different solvents like THF, CH_3CN, DMSO and MeOH and it shows that the desired phenol carbamates are not formed substantially (Table 3.1, entry 15-18). In the presence of other copper sources like $CuCl_2.2H_2O$, $Cu(OAc)_2.H_2O$ and CuI the expected product is formed but in low yield in our optimized reaction condition (Table 3.1, entry 22-24). It may be due to the fact that many copper salts are insoluble in organic solvents, thus higher temperatures are required to obtain the desired product in good yields. No significant change in product yield was observed with the increase of oxidant equivalent and loading of copper complex (Table 3.1, entry 12). From the optimized table, it is also evident that both copper complex and oxidant are essential for this reaction (Table 3.1, entry 20-21).

Table 3.1: Optimisation of reaction conditions.[a]
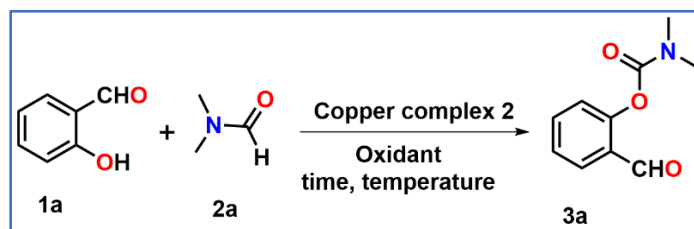
Entry	Catalyst (mol %)[a]	Oxidant (equiv)	Solvent	Temperature (°C)	Time (h)	% Yield[b]
1	Catalyst **2** (2)	MnO$_2$ (3)	DMF	80	12	NR
2	Catalyst **2** (2)	I$_2$ (3)	DMF	80	12	NR
3	Catalyst **2** (2)	H$_2$O$_2$ (3)	DMF	80	12	NR
4	Catalyst **2** (2)	m-CPBA (3)	DMF	80	12	60
5	Catalyst **2** (2)	DDQ (3)	DMF	80	12	NR
6	Catalyst **2** (2)	TBHP (3)	DMF	80	12	85
7	Catalyst **2** (2)	TBHP (3)	DMF	80	6	85
8	Catalyst **2** (1)	TBHP (3)	DMF	80	6	85
9	Catalyst **2** (1)	TBHP (3)	DMF	80	1	85
10	Catalyst **2** (1)	TBHP (3)	DMF	60	1	85
11	Catalyst **2** (1)	TBHP (3)	DMF	50	1	85
12	Catalyst **2** (1)	TBHP (4)	DMF	50	20 min	85
13	Catalyst 2 (0.5)	TBHP (3)	DMF	40	20 min	85
14	**Catalyst 2 (0.5)**	**TBHP (3)**	**DMF**	**50**	**20 min**	**85**
15	Catalyst 2 (0.5)	TBHP (3)	THF	50	30 min	NR
16	Catalyst 2 (0.5)	TBHP (3)	ACN	50	30 min	NR
17	Catalyst 2 (0.5)	TBHP (3)	DMSO	50	30 min	NR
18	Catalyst 2 (0.5)	TBHP (3)	CH$_3$OH	50	30 min	NR
19	Catalyst 2 (0.5)	TBHP (2)	DMF	50	30 min	55
20	Catalyst 2 (0.5)	-	DMF	50	30 min	NR
21	-	TBHP (3)	DMF	50	30 min	NR
22	CuCl$_2$.2H$_2$O	TBHP (3)	DMF	50	30 min	60
23	Cu(OAc)$_2$.H$_2$O	TBHP (3)	DMF	50	30 min	58
24	CuI	TBHP (3)	DMF	50	30 min	50

Having the optimized reaction condition in hand, we have performed the cross-coupling reaction with different combinations of substituted salicylaldehyde derivatives with different formamides using complex **2** as a catalyst. As shown in Table 3.2, both the cyclic and acyclic formamides gave the corresponding carbamates in moderate to good yields, however, in case of cyclic formamides, the yield is lower compared to their acyclic analogues (Table 3.2, **3i** and **3l**). Salicylaldehyde derivatives having the electron-donating groups as well as electron-withdrawing groups provided the corresponding carbamates in excellent to good yields. Salicylaldehyde derivatives, having the methoxy group at different positions of aromatic moiety led to the product in moderate to good yield (Table 3.2, **3c**, **3m-3p**) whereas salicylaldehyde with an electron-withdrawing group like bromo, chloro and fluoro (Table 3.2, **3f-h**, **3j**) also react with formamides producing the corresponding carbamates comparatively in lesser yield. Phenol derivatives, having *ortho*-substituted ester (Table 3.2, **3d-3e**) or *ortho*-acetyl group (Table 3.2, **3q-3r**) also led to the corresponding carbamates in good yield. Interestingly, moderate to good yield of products can be obtained with N,N-di methyl amino-substituted salicylaldehyde (Table 3.2, **3k**, **3l**) or heterocyclic aromatic compounds like 8-hydroxy quinoline and 4-hydroxy coumarin (Table 3.2, **3s-3u**) as substrates. Remarkably, in all of the conversions, the sensitive and versatile aldehyde group remained intact in the presence of oxidant and transition-metal catalyst, which creates scope of further functionalization of the aldehyde group.

Table 3.2: Substrate scope of the coupling reaction catalyzed by complex **2**
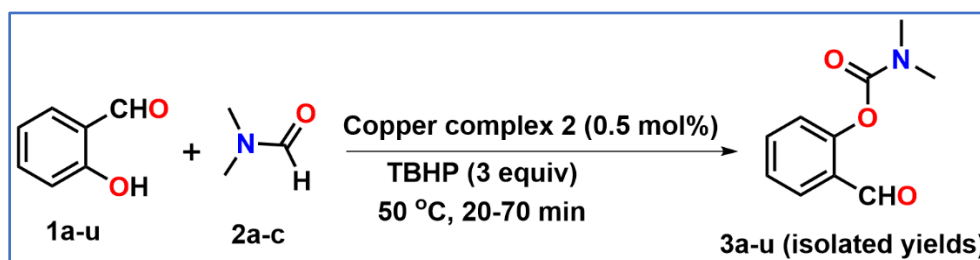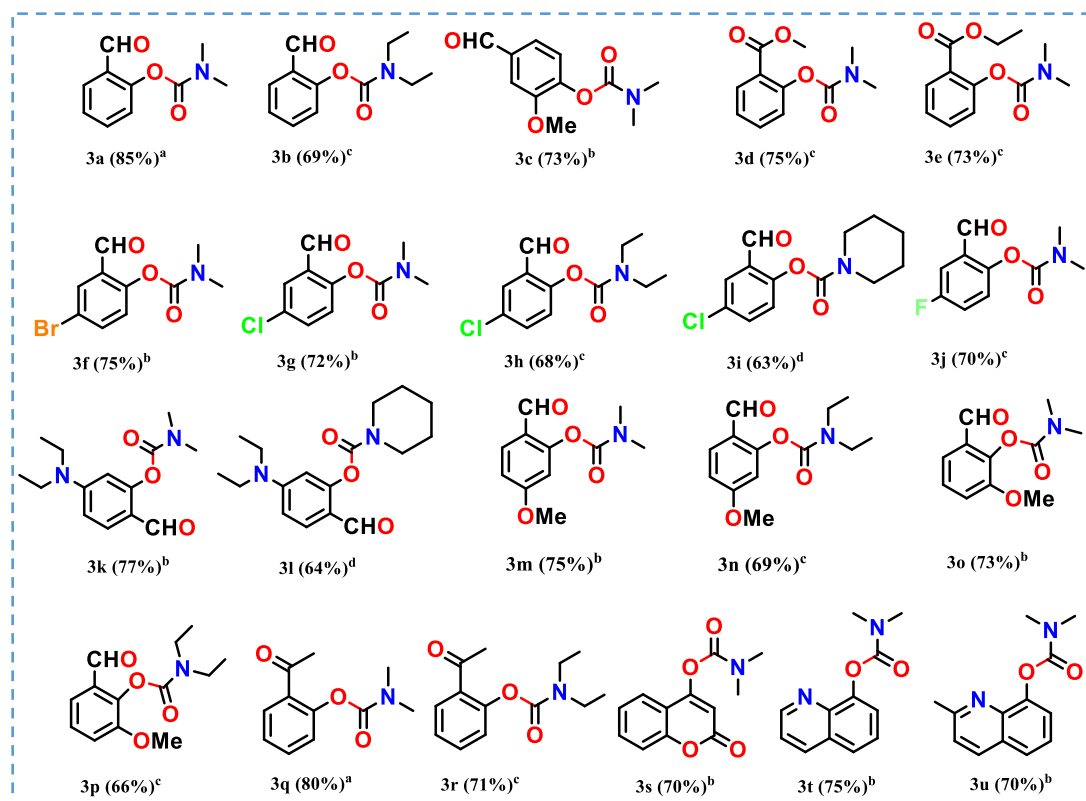
3a (85%)[a] 3b (69%)[c] 3c (73%)[b] 3d (75%)[c] 3e (73%)[c]

3f (75%)[b] 3g (72%)[b] 3h (68%)[c] 3i (63%)[d] 3j (70%)[c]

3k (77%)[b] 3l (64%)[d] 3m (75%)[b] 3n (69%)[c] 3o (73%)[b]

3p (66%)[c] 3q (80%)[a] 3r (71%)[c] 3s (70%)[b] 3t (75%)[b] 3u (70%)[b]

Reaction conditions: **1a-u** (1 mmol), TBHP (70 wt % in water, 3 equiv.), copper catalyst **2** (0.5 mol%), 50 °C temperature. [a] Reaction time 20 min, [b] reaction time 35 min and [c,d] reaction time 50 and 70 min respectively.

The practicality of the method has been demonstrated by performing the reaction on a multi-gram scale in case of salicylaldehyde and 2-hydroxy acetophenone. In both the cases, the target carbamates were formed in 80% and 75% yields respectively (Scheme 3.2).
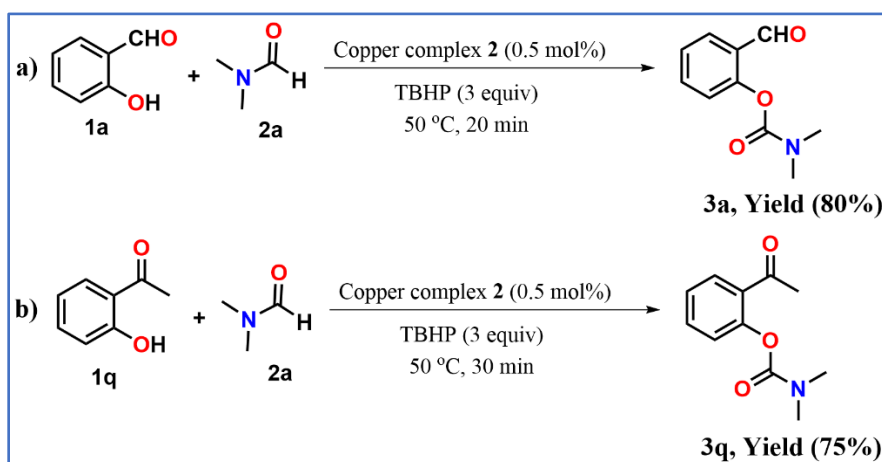
Scheme 3.2: Synthesis of carbamates in gram scale.

From Table 3.2 it can be concluded that both the formyl (-CHO) and acetyl (-COCH$_3$) groups are effective ortho directing group for the formation of phenol carbamates. After that we thought that the same reaction can be achieved in presence of carboxylic group (-COOH) as a directing group in salicylic acid. We have performed the reaction of salicylic acid with DMF in the optimised condition. However, in this case the corresponding amide product was formed instead of corresponding phenol carbamates (Table 3.3, **5a-5b**). In case of acid derivatives decarboxylation occurred and the liberation of CO$_2$ gas from reaction mixture was further confirmed by GC and GC-MS experiments (Figure 3.27). Even in presence of electron withdrawing chloro group acid derivatives yielded amide as the major product (Table 3.3, **5c**).

Table 3.3: Substrate scope of aromatic acid cross coupling reaction catalyzed by complex **2**
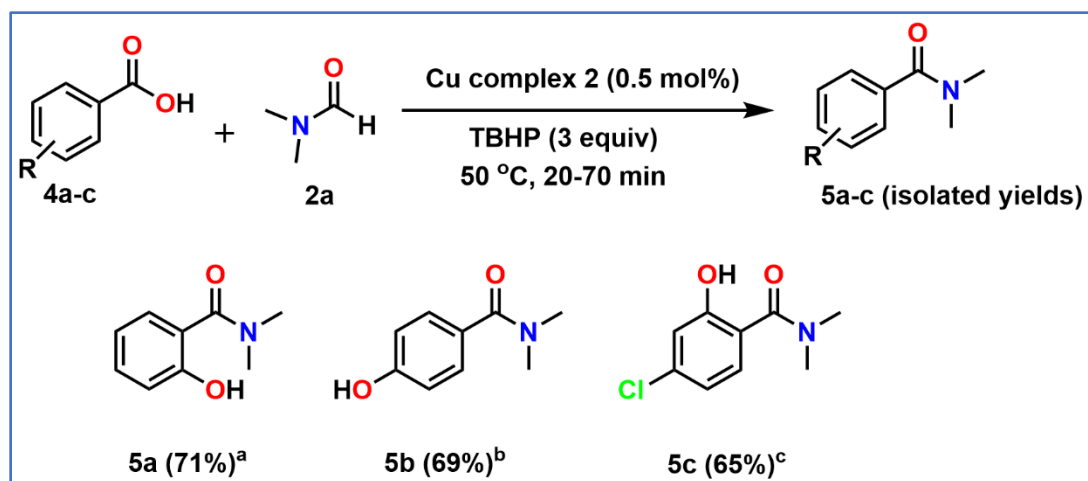
Reaction conditions: **4a-c** (1 mmol), TBHP (70 wt % in water, 3 equiv.), copper catalyst **2** (0.5 mol%), 50 °C temperature. [a,b] Reaction time 40 and 70 min respectively.

Due to the structural similarity with that of salicylaldehyde, enol tautomer of the 1,3-dicarbonyl moiety exhibits a similar attitude toward transition metals, forming the coordination complex.[18] Therefore, using the optimised reaction condition we have carried out the same reaction with 1,3-di ketone derivatives. In case of acetyl acetone and ethyl acetoacetate corresponding product was formed in good yield (Table 3.4, **7a-7e**).

Table 3.4: Cross coupling reaction of aliphatic di ketone catalyzed complex **2**
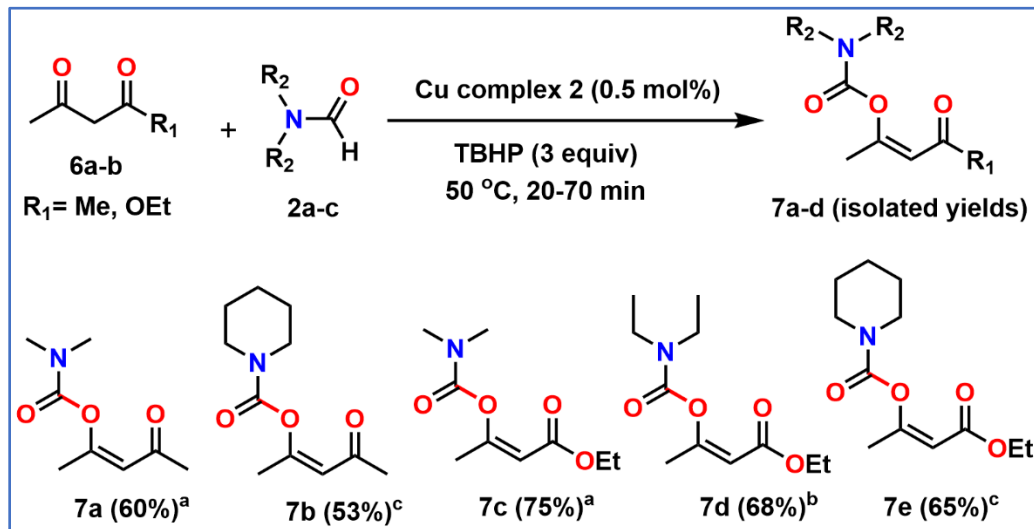
Reaction conditions: **6a-b** (1 mmol), TBHP (70 wt % in water, 3 equiv.), copper catalyst **1** (0.5 mol%), 50 °C temperature. [a] Reaction time 30 min and [b,c] reaction time 45 min and 70 min respectively.

We have also performed the same reaction in case of phenol derivatives using our optimised reaction condition and it shows that in presence of alcohol group also corresponding carbamate products were formed in moderate to good yields. In case of catechol, resorcinol and quinol, corresponding mono carbamates were formed in good yields (Table 3.5, **9a-b**). Trace amount of di-carbamate may also formed but isolation and characterization of the corresponding di-carbamates were not successful. Noteworthy, in presence of more than two –OH groups in the benzene ring (in case of phluroglucinol and pyrogallol) carbamates formations were unsuccessful.

Table 3.5: Substrate scope of phenols cross coupling reaction catalyzed by complex **2**
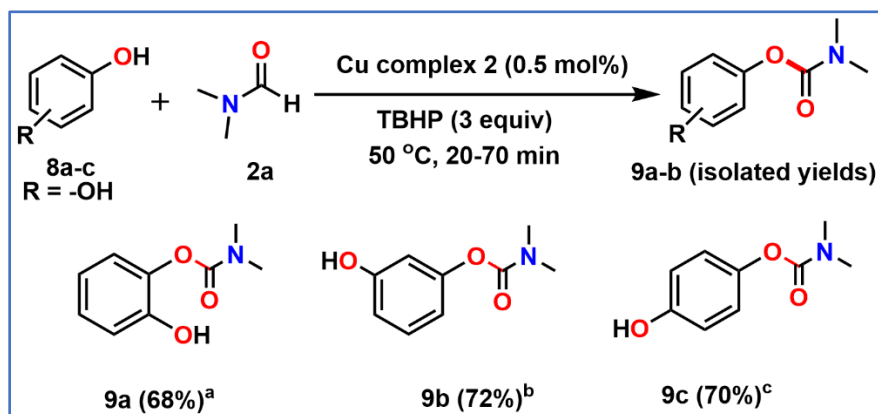
Reaction conditions: **8a-c** (1 mmol), TBHP (70 wt % in water, 3 equiv.), copper catalyst **2** (0.5 mol%), 50 °C temperature. [a,b] Reaction time 40 min and 60 min respectively.

3.2.4 Plausible catalytic cycle

To further investigate the reaction mechanism whether the reaction follows radical pathway or not, we did the reaction in presence of radical scavenger like TEMPO. It shows that in presence of radical scavenger TEMPO, the reaction was shut down. Both the radical formed in presence of TBHP (2-formyl phenoxy radical from salicylaldehyde and amino acyl radical from DMF) get coupled with radical scavenger and it gives 2-((2,2,6,6-tetramethylpiperidin-1-yl)peroxy) benzaldehyde and TEMPO-DMF adduct (Scheme 3.3) as products which are further confirmed by ^{1}H NMR spectroscopy and ESI-MS (Figure 3.37, 3.38). As a result, the corresponding carbamate formation is failed and the reaction is completely stopped. This observation can strongly suggest that the reaction mechanism follows the radical pathway.
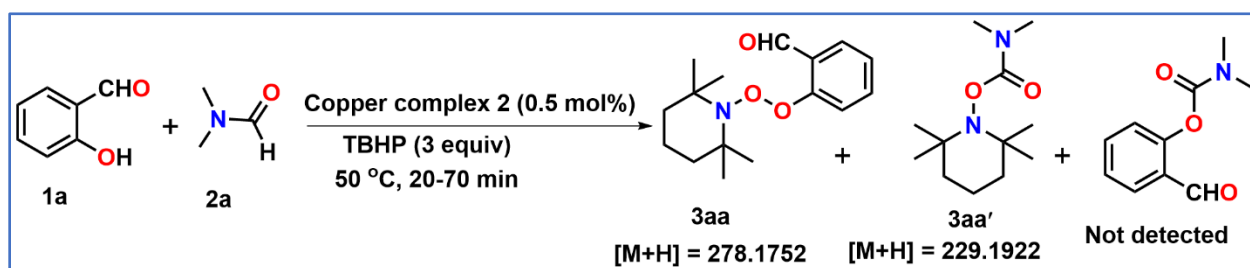
Scheme 3.3 Radical inhibition experiment.

On the basis of the above experimental result and reported literature a plausible catalytic cycle was shown in Scheme 3.4. Here radical initiator TBHP is converted to its tert-butoxy radical by homolytic bond cleavage [19], which can abstract a proton from salicylaldehyde to form a 2-formyl phenoxy radical. Then the tert-butoxy radical inserted into catalyst **2**, changing the oxidation state of Cu centre from +2 to +3. After that phenoxy radical get attached into the catalytic system. Simultaneously tert-butoxy radical abstracts a proton from DMF to produce an aminoacyl radical which make a coupling with the 2-formyl phenoxy radical. After that desired carbamate eliminated from the catalytic cycle as a product and the Cu(II) catalyst is regenerated.
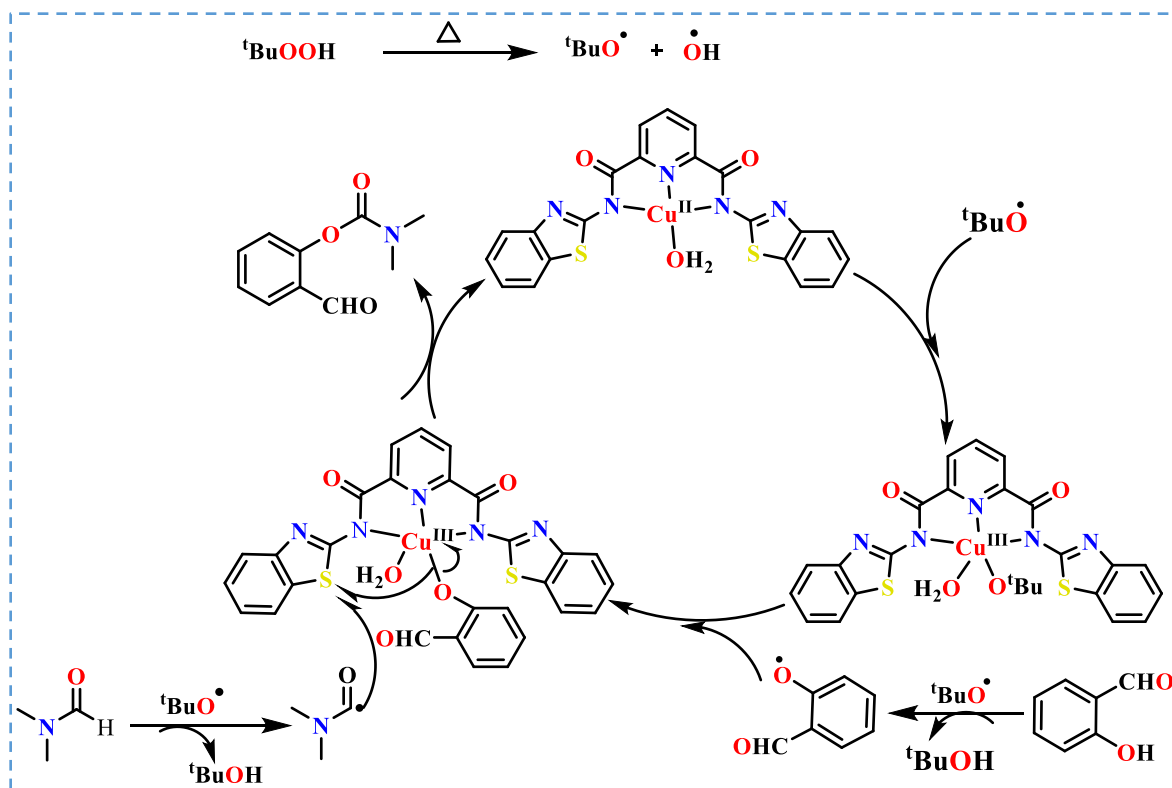
Scheme 3.4. Plausible mechanism for catalytic cycle.

3.3. Conclusion

In conclusion, we have developed a new and easy to synthesize copper catalyst for the synthesis of enol/phenol carbamates and cyclic as well as acyclic derivatives of formamides involving the oxidative cross-dehydrogenative coupling (CDC) under mild condition. This method is atom economic and does not need any prefunctionalised starting material and the broad range of functional group tolerance makes this protocol more advantageous. This reaction does not demand harsh condition and proceeds under mild reaction conditions (50 °C and very low catalyst loading) to achieve the products in high yield. A probable mechanistic pathway has been proposed following the several control reactions and characterization of radical intermediates generated during the course of the reaction. The use of minimum amount earth-abundant copper catalyst to efficiently synthesize the enol/phenol carbamates by C-H activation mechanism under mild condition directed the use of developed catalyst for a more sustainable future.

3.4. Experimental section

3.4.1. Materials and reagents

2-amino benzothiazole and 2,6-dipicolinic acid were purchased from Sigma-Aldrich. Different substituted salicylaldehyde derivatives were purchased from Sigma-Aldrich and TCI Chemicals. All other reagents and chemicals were obtained from commercial sources and used without further purification. N^2,N^6-bis(benzothiazol-2-yl)pyridine-2,6-dicarboxamide (**L**) was synthesized by literature reported procedure.[14] Chromatography was carried out using 60-120 and 100-200 mesh silica gel in a column.

3.4.2. Instrumentation

^1H and ^{13}C NMR spectra were obtained with BRUKER 300 MHz, FT-NMR spectrometers and the chemical shifts are reported in ppm, using tetramethylsilane as an internal standard and were referenced to the residual solvent as follows: $CDCl_3$ = 7.26 (^1H), 76.16 (^{13}C) ppm at 295 K. The absorption spectra were recorded with a SHIMADZU-2450 UV-vis spectrophotometer at 295 K. Cyclic voltammetry was performed on a CH instruments electrochemical workstation at 295 K. X-band EPR spectra were recorded using a Bruker Biospin EMX^{micro} spectrometer at 100 K. IR spectral studies were done on Perkin Elmer LX-1 FTIR spectrophotometer at 295 K. Diffraction data of copper complex **1** was measured with MoK$_\alpha$ radiation (a graded multilayer mirror monochromator, λ = 0.71073 Å) at 273 K on a micro focus Single Crystal X-ray Diffraction instrument (Make: Bruker, Model: D8 Quest). For ^1H NMR, coupling constants *J* are given in Hz and the resonance multiplicity is described as s (singlet), d (doublet), t (triplet), m (multiplet).

3.4.3. X-ray Crystallographic Analysis

X-ray-quality crystal of complex **2** was grown by slow evaporation of DMF solution at room temperature. The intensity data were collected on a CCD area detector, MoKα diffractometer. With OLEX2 [20] the structure was solved with the superflip [21] structure solution program using charge flipping and refined with the SHELXL [22] refinement package and least-squares minimization. The hydrogen atoms were refined isotropically at calculated positions using a riding model. CCDC 2179149 (**1**) contains the supplementary crystallographic data for this paper. These data can be obtained free of charge from the Cambridge Crystallographic Data Centre *via* www.ccdc.cam.ac.uk/data_request/cif.

3.4.4. Synthesis

3.4.4.1. Synthesis of complex 2

In a 100 mL round-bottom flask, ligand **L** (100 mg, 0.231 mmol) was dissolved in chloroform (10 mL). In another round bottom flask, $CuCl_2 \cdot 2H_2O$ (54.5 mg, 0.406 mmol) was dissolved in methanol (3 mL) and the solution was added dropwise to the ligand solution. Colourless ligand solution becomes greenish. The reaction mixture was allowed to stir at room temperature overnight. A dark-green precipitate was formed, which was collected by evaporation of the solvent under reduced pressure. The complex [$CuLOH_2$] (**2**) was crystallized by slow evaporation of DMF solution at room temperature giving 70% yield. ESI-MS calcd. for $C_{21}H_{15}CuN_5O_3S_2$ $[M + H]^+$ = 512.9990, found 512.9773.

3.4.4.2. General procedure for the catalytic reaction: Preparation of 3a as

representative example: An oven dried round bottom flask equipped with a stir bar was charged with **1a** (1.0 mmol, 0.17 mL) and catalyst (0.005 mmol, 1.5 mg). TBHP (0.04 mL, 3 mmol) and DMF (3 mL) were added to it by syringe. The round bottom flask was then placed in an oil bath preheated at 50 °C. After 20 min, the reaction mixture was cooled to room temperature and extracted with EtOAc and water. The organic phase was dried under reduced pressure. The crude product was purified by column chromatography on silica gel (5% EtOAc/pet ether) to afford the corresponding product (yield 85%).

3.4.4.3. General Procedure for gram-scale reaction

Salicylaldehyde (**A**) and 2-hydroxy acetophenone (**B**) were used for multigram scale reaction. An oven dried round bottom flask equipped with a stir bar was charged with salicylaldehyde ((1 g, 8.2 mmol (**A**)/ 7.2 mmol (**B**)) and catalyst ((0.08 mmol, 23 mg (**A**)/ 0.036 mmol, 20 mg (**B**)). Then DMF (15 mL) was added to it by syringe. After that TBHP ((2.23 mL, 24.6 mmol (**A**)/ 2.2 ml, 21.9 mmol (**B**)) was added to it. The round bottom flask was then placed in an oil bath preheated at 50 °C. After 20 min, the reaction mixture was cooled to room temperature and extracted with EtOAc and water. Organic phase was dried under reduced pressure. The crude product was purified by column chromatography on silica gel (5% EtOAc/pet ether) to afford the corresponding product (yield 80% and 75% respectively).

3.4.4.4. Spectral data of all synthesized compounds

Dimethylcarbamic acid 2-formylphenyl ester (**3a**):[8c] Colourless oil (yield 85%). ^{1}H NMR (300 MHz, CDCl$_3$): δ = 10.19 (s, 1H), 7.89 (dd, J_1 = 3 Hz, J_2 = 7.5 Hz, 1H), 7.60 (td, J_1 = 3 Hz, J_2 = 7.5 Hz, 1H), 7.33 (t, J = 7.5 Hz, 1H), 7.23 (dd, J_1 = 3 Hz, J_2 = 7.5 Hz, 1H), 3.16 (s, 3H), 3.04 (s, 3H). ^{13}C NMR (75 MHz, CDCl$_3$): δ = 188.9, 154.3, 153.1, 135.3, 129.9, 128.6, 125.9, 123.7, 36.9, 36.7.

Diethylcarbamic acid 2-formylphenyl ester (**3b**): [8c] Colourless oil (yield 69%). ^{1}H NMR (300 MHz, CDCl$_3$): δ = 10.20 (s, 1H), 7.88 (dd, J_1 = 3 Hz, J_2 = 7.5 Hz, 1H), 7.61 (t, J = 7.5 Hz, 1H), 7.33 (t, J = 7.5 Hz, 1H), 7.23 (d, J = 9 Hz, 1H), 3.50 (q, J = 6.9 Hz, 2H), 3.40 (q, J = 6.9 Hz, 2H), 1.29 (t, J = 7.5 Hz, 3H), 1.22 (t, J = 7.5 Hz, 3H). ^{13}C NMR (75 MHz, CDCl$_3$): δ = 188.8, 153.6, 153.2, 135.2, 129.6, 128.7, 125.7, 123.7, 42.6, 42.2, 14.4, 13.4.

Dimethylcarbamic acid 2-methoxy-4-formylphenyl ester (**3c**):[23a] White solid (yield 73%). ^{1}H NMR (300 MHz, CDCl$_3$): δ = 9.71 (s, 1H), 7.23 (d, J = 1.8 Hz, 2H), 7.06-7.03 (m, 1H), 3.68 (s, 3H), 2.91 (s, 3H), 2.80 (s, 3H). ^{13}C NMR (75 MHz, CDCl$_3$): δ = 191.3, 153.9, 152.6, 146.0, 134.8, 124.9, 123.9, 110.8, 56.3, 36.9, 36.8.

Benzoic acid, 2-[[(dimethylamino)carbonyl]oxy]-methyl ester (**3d**):[8e] Colourless oil (yield 75%). ^{1}H NMR (300 MHz, CDCl$_3$): δ = 7.97 (dd, J_1 = 1.2 Hz, J_2 = 4.8 Hz, 1H), 7.52 (td, J_1 = 0.9 Hz, J_2 = 4.5 Hz, 1H), 7.24 (d, J = 9.9 Hz, 1H), 7.14 (d, J = 4.8 Hz, 1H), 3.85 (s, 3H), 3.13 (s, 3H), 3.01 (s, 3H). ^{13}C NMR (75 MHz, CDCl$_3$): δ = 164.7, 154.2, 151.0, 133.2, 131.0, 124.9, 123.8, 123.3, 51.5, 36.2, 36.0.

Benzoic acid, 2-[[(dimethylamino)carbonyl]oxy]-ethyl ester (**3e**):[23b] Colourless oil (yield 73%). ^{1}H NMR (300 MHz, CDCl$_3$): δ = 7.96 (dd, J_1 = 3 Hz, J_2 = 4.5 Hz, 1H), 7.49 (td, J_1 = 3 Hz, J_2 = 4.5 Hz, 1H), 7.24 (t, J = 4.5 Hz, 1H), 7.12 (d, J = 6 Hz, 1H), 4.29 (q, J = 3.9 Hz, 2H), 3.11 (s, 3H), 2.99 (s, 3H), 1.32 (t, J = 3 Hz, 3H). ^{13}C NMR (75 MHz, CDCl$_3$): δ = 164.9, 154.6, 151.1, 133.3, 131.4, 125.3, 124.1, 124.0, 60.9, 36.6, 36.4, 14.2.

Dimethylcarbamic acid 2-formyl-4-bromophenyl ester (**3f**):[8c] White solid (yield 75%). ^{1}H NMR (300 MHz, CDCl$_3$): δ = 10.13 (s, 1H), 7.98 (d, J = 3 Hz, 1H), 7.70 (dd, 1H, J_1 = 3 Hz, J_2 = 9 Hz), 7.16 (d, J = 9 Hz, 1H), 3.16 (s, 3H), 3.04 (s, 3H). ^{13}C NMR (75 MHz, CDCl$_3$): δ = 187.4, 153.8, 152.2, 137.9, 132.2, 129.8, 125.6, 119.1, 37.1, 36.7.

Dimethylcarbamic acid 2-formyl-4-chlorophenyl ester (**3g**):[23c] White solid (yield 72%). ^{1}H NMR (300 MHz, CDCl$_3$): δ = 10.20 (s, 1H), 7.89 (d, *J* = 3 Hz, 1H), 7.61 (dd, *J$_1$* = 2.1 Hz, *J$_2$* = 6.6 Hz, 1H), 7.27 (d, *J* = 6.3 Hz, 1H), 3.22 (s, 3H), 3.10 (s, 3H). ^{13}C NMR (75 MHz, CDCl$_3$): 187.5, 153.9, 151.6, 134.9, 131.8, 129.5, 129.1, 125.3, 37.0, 36.7.

Diethylcarbamic acid 2-formyl-4-chlorophenyl ester (**3h**):[23c] Colourless oil (yield 68%). ^{1}H NMR (300 MHz, CDCl$_3$): δ = 10.13 (s, 1H), 7.83 (d, *J* = 3 Hz, 1H), 7.54 (dd, *J$_1$* = 3 Hz, *J$_2$* = 9 Hz, 1H), 7.21 (d, *J* = 9 Hz, 1H), 3.49 (q, *J* = 7.9 Hz, 2H), 3.39 (q, *J* = 6.9 Hz, 2H), 1.28 (t, *J* = 6 Hz, 3H), 1.22 (t, *J* = 7.5 Hz, 3H). ^{13}C NMR (75 MHz, CDCl$_3$): 187.4, 153.3, 151.7, 134.9, 131.5, 129.6, 128.9, 125.2, 42.7, 42.2, 41.9, 14.4, 13.3.

Piperidine-1-carboxylic acid 2-formyl-4-chlorophenyl Ester (**3i**): Colourless oil (Yield 63%). ^{1}H NMR (300 MHz, CDCl$_3$): δ = 10.17 (s, 1H), 7.86 (d, *J* = 3 Hz, 1H,), 7.59 (dd, *J$_1$* = 3 Hz, *J$_2$* = 9 Hz, 1H), 7.24 (d, *J* = 9 Hz, 1H), 3.70 (s, 2H), 3.56 (s, 2H), 1.68 (s, 5H). ^{13}C NMR (75 MHz, CDCl$_3$): 187.5,152.7, 151.8, 134.9, 131.7, 129.6, 129.1, 125.4, 45.9, 45.6, 26.1, 25.6, 24.3. Elemental analysis: anal. calcd for C$_{13}$H$_{14}$ClNO$_3$: C, 58.32; H, 5.27; N, 5.23. Found: C, 58.26; H, 5.20; N, 5.19.

Dimethylcarbamic acid 2-formyl-4-fluorophenyl ester (**3j**): White solid (yield 70%):^{1}H NMR (300 MHz, CDCl$_3$): δ = 10.12 (d, *J* = 3 Hz, 1H,, 7.53 (dd, *J$_1$* = 3 Hz, *J$_2$* = 6 Hz, 1H), 7.31-7.26 (m, 1H), 7.23-7.19 (m, 1H), 3.15 (s, 3H), 3.02 (s, 3H).^{13}C NMR (75 MHz, CDCl$_3$): δ = 187.5, 161.6, 158.3, 154.2, 149.3, 149.2, 129.7, 129.6, 125.6, 125.5, 122.3, 121.9, 115.2, 114.9, 37.0, 36.6. Elemental analysis: anal. calcd for C$_{10}$H$_{10}$FNO$_3$: C, 56.87; H, 4.77; N, 6.63. Found: C, 56.79; H, 4.70; N, 6.59.

Dimethylcarbamic acid 2-formyl-5-(diethylamino)phenyl ester (**3k**):[8c] Brown oil (yield 77%): ^{1}H NMR (300 MHz, CDCl$_3$): δ = 9.84 (s, 1H), 7.68 (d, *J* = 9 Hz, 1H), 6.51 (dd, *J$_1$* = 2.7 Hz, *J$_2$* = 8.8 Hz, 1H), 6.34 (d, *J* = 2.7 Hz, 1H), 3.40 (q, *J* = 6.9 Hz, 4H), 3.15 (s, 3H), 3.03 (s, 3H), 1.19 (t, *J* = 7.5 Hz, 6H). ^{13}C NMR (75 MHz, CDCl$_3$): δ = 186.7, 155.2, 154.5, 153.2, 132.4, 116.9, 108.3, 104.7, 44.8, 36.9, 36.7, 12.6.

Piperidine-1-carboxylic acid 2-formyl-5-(diethylamino)phenyl ester (**3l**): Yellow oil (yield 64%): ^{1}H NMR (300 MHz, CDCl$_3$): δ = 10.87 (s, 1H), 7.11 (d, *J* = 6 Hz, 1H), 6.19 (s, 1H), 6.13 (d, *J* = 9 Hz, 1H), 3.63 (t, *J* = 4.5 Hz, 4H), 3.35 (q, *J* = 6.9 Hz, 4H), 1.70-1.60 (m, 6H), 1.17 (t, *J* = 7.5 Hz,

6H). ^{13}C NMR (75 MHz, CDCl$_3$): δ = 192.6, 172.5, 162.5, 151.4, 130.3, 103.8, 102.2, 98.7, 47.5, 44.5, 29.8, 26.3, 24.9, 12.8. Elemental analysis: anal. calcd for C$_{17}$H$_{24}$N$_2$O$_3$: C, 67.08; H, 7.95; N, 9.20. Found: C, 67.02; H, 7.89; N, 9.10.

Dimethylcarbamic acid 2-formyl-5-methoxyphenyl ester (3m):[8c] White solid (yield 75%). ^{1}H NMR (300 MHz, CDCl$_3$): δ = 10.03 (s, 1H), 7.80 (d, *J* = 9 Hz, 1H), 6.84 (dd, *J$_1$* = 2.7 Hz, *J$_2$* = 9 Hz, 1H), 7.74 (d, *J* = 3 Hz, 1H), 3.86 (s, 3H), 3.15 (s, 3H), 3.03 (s, 3H). ^{13}C NMR (75 MHz, CDCl$_3$): δ = 187.6, 165.3, 154.9, 154.1, 131.8, 122.3, 112.3, 108.7, 55.9, 36.9, 36.7.

Diethylcarbamic acid 2-formyl-5-methoxyphenyl ester (3n):[8c] Colourless oil (yield 69%). ^{1}H NMR (300 MHz, CDCl$_3$): δ = 10.03 (s, 1H), 7.82 (d, *J* = 9 Hz, 1H), 6.83 (d, *J$_1$* = 3 Hz, *J$_2$* = 9 Hz, 1H), 6.73 (d, *J* = 9 Hz, 1H), 3.86 (s, 3H), 3.35 (q, *J* = 6.9 Hz, 2H), 3.26 (q, *J* = 6.9 Hz, 2H), 1.18 (t, *J* = 7.5 Hz, 3H), 1.12 (t, *J* = 7.5 Hz, 3H). ^{13}C NMR (75 MHz, CDCl$_3$): δ = 187.3, 165.1, 162.1, 154.9, 153.3, 131.2, 122.1, 111.9, 108.4, 55.7, 41.7, 36.4, 14.7, 12.6.

Dimethylcarbamic acid 2-formyl-6-methoxyphenyl ester (3o):[8c] White solid (yield 73%). ^{1}H NMR (300 MHz, CDCl$_3$): δ = 10.20 (s, 1H), 7.46 (d, *J* = 9 Hz, 1H), 7.29 (d, *J* = 9 Hz, 1H), 7.19 (d, *J* = 9 Hz, 1H), 3.87 (s, 3H), 3.18 (s, 3H), 3.04 (s, 3H). ^{13}C NMR (75 MHz, CDCl$_3$): δ = 189.1, 154.1, 152.5, 143.1, 130.0, 126.3, 120.4, 117.9, 56.5, 37.1, 36.8.

Diethylcarbamic acid 2-formyl-6-methoxyphenyl ester (3p):[8c] Colourless oil (yield 66%). ^{1}H NMR (300 MHz, CDCl$_3$): δ = 10.20 (s, 1H), 7.45 (dd, *J$_1$* = 1.2 Hz, *J$_2$* = 5.7 Hz, 1H), 7.26 (d, *J* = 12 Hz, 1H), 7.17 (dd, *J$_1$* = 1.2 Hz, *J$_2$* = 6 Hz, 1H), 3.86 (s, 3H), 3.35 (q, *J* = 5.4 Hz, 2H), 3.26 (q, *J* = 5.4 Hz, 2H), 1.18 (t, *J* = 5.4 Hz, 3H), 1.12 (t, *J* = 5.4 Hz, 3H). ^{13}C NMR (75 MHz, CDCl$_3$): δ = 189.1, 162.3, 153.5, 152.4, 143.4, 130.0, 126.2, 119.9, 117.8, 56.4, 41.9, 36.7, 14.9, 12.8.

Dimethyl carbamic acid 2-acetylphenyl ester (3q):[8e] Yellow oil (yield 80%): ^{1}H NMR (300 MHz, CDCl$_3$): δ = 7.75 (d, *J* = 6 Hz, 1H), 7.49 (t, *J* = 9 Hz, 1H), 7.27 (d, *J* = 9 Hz, 1H), 7.13 (d, *J* = 9 Hz, 1H) 3.13 (s, 3H), 3.01 (s, 3H), 2.54 (s, 3H). ^{13}C NMR (75 MHz, CDCl$_3$): δ = 198.1, 154.4, 149.9, 133.1, 131.5, 129.8, 125.4, 123.9, 36.7, 36.5, 29.6.

Diethyl carbamic acid 2-acetylphenyl ester (3r):[23d] Yellow oil (yield 71%): ^{1}H NMR (300 MHz, CDCl$_3$): δ = 7.73 (d, *J* = 9 Hz, 1H), 7.49 (t, *J* = 6 Hz, 1H), 7.25 (d, *J* = 6 Hz, 1H), 7.12 (d, *J* = 9 Hz, 1H), 3.48 (q, *J* = 6.9 Hz, 2H), 3.37 (q, *J* = 6.9 Hz, 2H), 2.54 (s, 3H) 1.28 (t, *J* = 6 Hz, 3H),

1.20 (t, J = 6 Hz, 3H). ^{13}C NMR (75 MHz, CDCl$_3$): δ = 198.4, 153.8, 149.9, 133.1, 132.1, 129.7, 125.4, 123.9, 42.4, 42.0, 29.6, 14.2, 13.4.

2-Oxo-2H-1-benzopyran-4-yl N,N-dimethyl carbamate (**3s**):[23e] White solid (yield 70%): ^{1}H NMR (300 MHz, CDCl$_3$): δ = 7.66 (dd, J_1 = 3 Hz, J_2 = 9 Hz, 1H), 7.57 (td, J_1 = 3 Hz, J_2 = 8.7 Hz, J_3 = 7.8 Hz, 1H), 7.37-7.29 (m, 2H), 6.53 (s, 1H), 3.20 (s, 3H), 3.08 (s, 3H). ^{13}C NMR (75 MHz, CDCl$_3$): δ = 161.9, 159.0, 153.7, 151.4, 132.6, 124.3, 122.7, 117.1, 115.9, 103.3, 37.2, 36.9.

N,N-dimethyl carbamic acid-8-quinolinyl ester (**3t**):[8e] Brown solid (yield 75%). ^{1}H NMR (300 MHz, CDCl$_3$): δ = 8.93 (d, J = 6 Hz, 1H), 8.13 (d, J = 6 Hz, 1H), 7.66 (d, J_1 = 3 Hz, J_2 = 6 Hz, 1H), 7.49 (q, J = 7.9 Hz, 2H), 7.40-7.36 (m, 1H), 3.28 (s, 3H), 3.06 (s, 3H). ^{13}C NMR (75 MHz, CDCl$_3$): δ = 155.3, 150.5, 148.1, 142.0, 135.9, 129.5, 126.3, 125.4, 121.8, 121.6, 36.9.

N,N-dimethyl carbamic acid-2-methyl-8-quinolinyl ester (**3u**):[23f] Brown oil (yield 70%). ^{1}H NMR (300 MHz, CDCl$_3$): δ = 8.02 (d, J = 9 Hz, 1H), 7.61 (t, J = 4.5 Hz, 1H), 7.44 (d, J = 3 Hz, 2H), 7.27 (d, J = 9 Hz, 1H), 3.30 (s, 3H), 3.07 (s, 3H), 2.71 (s, 3H). ^{13}C NMR (75 MHz, CDCl$_3$): δ = 155.7, 147.8, 135.9, 127.8, 125.3, 124.9, 122.5, 121.5, 36.9, 25.8.

2-hydroxy-N,N-dimethylbenzamide (**5a**):[23c] White solid (yield 71%). ^{1}H NMR (300 MHz, CDCl$_3$): δ = 7.32 (d, J = 9 Hz, 1H), 7.01 (d, J = 9 Hz, 1H), 6.85 (td, J_1 = 3 Hz, J_2 = 7.5 Hz, 1H), 3.17 (s, 6H). ^{13}C NMR (75 MHz, CDCl$_3$): δ = 171.6, 135.6, 132.0, 130.7, 128.4, 119.1, 118.9, 117.3, 117.3, 37.9, 29.7.

4-hydroxy-N,N-dimethylbenzamide (**5b**):[8c] White solid (yield 69%). ^{1}H NMR (300 MHz, CDCl$_3$): δ = 7.25 (d, J = 9 Hz, 2H), 6.71 (d, J = 6 Hz, 2H), 3.07 (d, J = 12 Hz, 6H). ^{13}C NMR (75 MHz, CDCl$_3$): 172.7, 158.7, 129.1, 126.4, 115.1, 39.9, 35.6.

4-Chloro-2-hydroxy-N,N-dimethylbenzamide (**5c**):[23g] White solid (yield 65%): ^{1}H NMR (300 MHz, CDCl$_3$): δ = 7.24 (d, J = 6 Hz, 1H), 6.99 (d, J = 3 Hz, 1H), 6.83 (d, J = 9 Hz, 1H), 3.15 (s, 6H). ^{13}C NMR (75 MHz, CDCl$_3$): δ = 171.3, 160.2, 138.1, 129.6, 118.8, 118.3, 115.8, 38.5.

1-Methyl-3-oxo-1-buten-1-yl N,N-dimethylcarbamate (**7a**):[24a] Colourless liquid (yield 60%): ^{1}H NMR (300 MHz, CDCl$_3$): δ = 5.76 (s, 1H), 3.03 (s, 3H), 2.98 (s, 3H), 2.20 (s, 3H), 2.06 (s, 3H). ^{13}C NMR (75 MHz, CDCl$_3$): δ = 203.8, 196.2, 159.0, 116.7, 64.9, 36.8, 31.1, 22.0.

1-Methyl-3-oxo-1-buten-1-yl-piperidine-1-carboxylate (**7b**): Colourless liquid (yield 53%): ^{1}H NMR (300 MHz, CDCl$_3$): δ = 5.75 (s, 1H), 3.49 (s, 4H), 2.22 (s, 3H), 2.06 (s, 3H), 1.63 (s, 6H). HRMS (ESI): m/z [M + Na][+] calcd. for C$_{11}$H$_{17}$NO$_3$Na 272.1106, found 272.1104.

Ethyl 3-[[(dimethylamino)carbonyl]oxy]-2-butenoate (**7c**):[23d] Greenish oil (yield 75%): ^{1}H NMR (300 MHz, CDCl$_3$): δ = 5.53 (s, 1H), 4.11 (q, *J* = 6.9 Hz, 2H), 3.02 (s, 3H), 2.96 (s, 3H), 2.03 (s, 3H), 1.23 (t, *J* = 7.5 Hz, 3H). ^{13}C NMR (75 MHz, CDCl$_3$): δ = 164.1, 160.8, 153.1, 108.0, 59.9, 36.6, 22.2, 14.2.

Ethyl 3-[[(diethylamino)carbonyl]oxy]-2-butenoate (**7d**):[23d] Colourless oil (yield 68%): ^{1}H NMR (300 MHz, CDCl$_3$): δ = 5.52 (s, 1H), 4.11 (q, *J* = 6.9 Hz, 2H), 3.34 (quint, *J* = 9 Hz, 4H), 2.04 (s, 3H), 1.25-1.14 (m, 12H). ^{13}C NMR (75 MHz, CDCl$_3$): δ = 164.1, 160.4, 152.4, 108.1, 59.8, 42.2, 41.9, 22.1, 14.3, 14.0, 13.4.

3-Ethoxy-1-methyl-3-oxo-1-propen-1-yl 1-piperidinecarboxylate (**7e**):[24b] Colourless oil (yield 65%): ^{1}H NMR (300 MHz, CDCl$_3$): δ = 5.52 (s, 1H), 4.11 (q, *J* = 6.9 Hz, 2H), 3.47 (s, 4H), 2.03 (s, 3H), 1.60 (s, 6H), 1.23 (t, *J* = 7.5 Hz, 3H). ^{13}C NMR (75 MHz, CDCl$_3$): δ = 164.1, 160.7, 15.9, 108.0, 59.8, 45.7, 45.1, 25.6, 24.3, 22.2, 14.3.

N,N-dimethyl carbamic acid-2-hydroxyphenyl ester (**9a**):[24c] Grey solid (yield 68%): ^{1}H NMR (300 MHz, CDCl$_3$): δ = 7.10 (t, *J* = 7.5 Hz, 1H), 7.02 (d, *J* = 6 Hz, 1H), 6.88 (t, *J* = 7.5 Hz, 1H), 3.15 (s, 3H), 3.04 (s, 3H). ^{13}C NMR (75 MHz, CDCl$_3$): δ = 155.4, 147.9, 140.2, 126.8, 122.3, 120.9, 119.2, 37.0, 36.9.

N,N-dimethyl carbamic acid-3-hydroxyphenyl ester (**9b**):[24d] Red oil (yield 72%). ^{1}H NMR (300 MHz, CDCl$_3$): δ = 7.96 (s, 1H), 7.02 (t, *J* = 9 Hz 1H), 6.40 (d, *J* = 6 Hz, 3H), 2.93 (s, 3H), 2.87 (s, 3H). ^{13}C NMR (75 MHz, CDCl$_3$): δ = 163.5, 157.5, 130.3, 107.6, 103.1, 36.9, 31.9.

N,N-dimethyl carbamic acid-4-hydroxyphenyl ester (**9c**):[24e] Yellow solid (yield 70%). ^{1}H NMR (300 MHz, CDCl$_3$): δ = 6.81 (s, 2H), 6.74 (s, 1H), 3.08 (s, 3H), 2.90 (s, 3H). ^{13}C NMR (75 MHz, CDCl$_3$): δ = 186.7, 184.5, 164.0, 136.8, 136.2, 132.6, 122.6, 116.1, 38.4, 34.8.

2-((2,2,6,6-tetramethylpiperidin-1-yl)peroxy)benzaldehyde (**3aa**): Red oil (Yield 50%). ^{1}H NMR (300 MHz, CDCl$_3$): δ = 10.57 (s, 1H), 8.45 (s, 2H), 8.10 (s, 2H), 20.05 (m, 20H). HRMS (TOF MS EI[+]): m/z calcd for [C$_{16}$H$_{24}$NO$_3$] 278.1756, found 278.1752 [M + H][+].

3.5. References

1. (a) S. V. Ley and A. W. Thomas, *Angew. Chem. Int. Ed.,* 2003, **42**, 5400-5449. (b) F. Monnier and M. Taillefer, *Angew. Chem. Int. Ed.,* 2009, **48**, 6954. (c) G. Evano, N. Blanchard and M. Toumi, *Chem. Rev.,* 2008, **108**, 3054-3031. (d) J. P. Corbet and G. Mignani, *Chem. Rev.,* 2006, **106**, 2651-2710. (e) A. Correa, O. Mancheno and C. Bolm, *Chem. Soc. Rev.,* 2008, **37**, 1108-1117. (f) S. Wurtz and F. Glorius, *Acc. Chem. Res.,* 2008, **41**, 1523-1533.

2. (a) G. Dyker, Handbook of C-H transformations: Applications in organic synthesis, Wiley-VCH, Weinheim, 2005. (b) J.-Q. Yu and Z.-J. Shi, C-H activation, Springer, Berlin, 2010. (c) K. I. Goldberg and A. S. Goldman, Activation and functionalization of C-H bond, ACS symposium series 885, American Chemical Society, Washington, DC, 2004. (d) J. C. Lewis, R. G. Bergman and J. A. Ellman, *Acc. Chem. Res*., 2008, **41**, 1013-1025. (e) X. Chen, K. M. Engle, D. H. Wang and J.-Q. Yu, *Angew. Chem. Int. Ed.,* 2009, **48**, 5094-5115. (f) C.-L. Sun, B.-J. Li and Z.-J. Shi, *Chem. Commun.,* 2010, **46**, 677-685. (g) A. Gunay and K. H. Theopold, *Chem. Rev.,* 2010, **110**, 1060-1081. (h) T. W. Lyons and M. S. Sanford, *Chem. Rev.,* 2010, **110**, 1147-1169. (i) C.-L. Sun, B.-J. Li and Z.-J. Shi, *Chem. Rev.,* 2011, **111**, 1293-1314. (j) L. Ackermann, *Chem. Rev.,* 2011, **111**, 1315-1345.

3. (a) N. Chatani, Directed metallation, Springer, Berlin, 2008. (b) O. Daugulis, H. Q. Do and D. Shabashov, *Acc. Chem. Res,.* 2009, **42**, 1074-1086. (c) D. A. Colby, R. G. Bergman and J. A. Ellman, *Chem. Rev.,* 2010, **110**, 624-655.

4. (a) C.-J. Li, *Acc. Chem. Res.,* 2009, **42**, 335-344. (b) S. A. Girard, T. Knauber and C.-J. Li, *Angew. Chem. Int. Ed.,* 2014, **53**, 74-100. (c) J. A. Ashenhurst, *Chem. Soc. Rev*., 2010, **39**, 540-548. (d) C. J. Scheuermann, *Chem. Asian J.,* 2010, **5**, 436-451.

5. (a) W. Han, P. Mayer and A. R. Ofial, *Angew. Chem. Int. Ed.,* 2011, **50**, 2178-2182. (b) K. M. Engle, D. H. Wang and J. Q. Yu, *Angew. Chem. Int. Ed*., 2010, **49**, 6169-6173. (c) G. Deng, L. Zhao and C. J. Li, *Angew. Chem. Int. Ed*., 2008, **47**, 6278-6282. (d) T. W. Lyons, K. L. Hull and M. S. Sanford, *J. Am. Chem. Soc.,* 2011, **133**, 6541-6544. (e) Z. Li and C. J. Li, *J. Am. Chem. Soc*., 2006, **128**, 56-57. (f) M. Kitahara, N. Umeda, K. Hirano, T. Satoh and M. Miura, *J. Am. Chem. Soc.,* 2011, **133**, 2160-2162. (g) N. Borduas and D. A. Powell, *J. Org. Chem*., 2008, **73**, 7822-7825.

6. For reviews on direct C-H bond amination/amidation, see: (a) H. M. L. Davies and M. S. Long, *Angew. Chem. Int. Ed.,* 2005, **44**, 3518-3520. (b) H. M. L. Davies and J. R. Manning, *Nature* 2008, **451**, 417-424. (c) F. Collet, R. H. Dodd and P. Dauban, *Chem. Commun.*, 2009, 5061-5074. (d) A. Armstrong and J. C. Collins, *Angew. Chem. Int. Ed.*, 2010, **49**, 2282-2285.

7. (a) W.-P. Mai, H.-H. Wang, Z.-C. Li, W. Yuan, Y.-M. Xiao, L.-R. Yang, P. Mao and L.-B. Qu, *Chem. Commun.*, 2012, **48**, 10117-10119. (b) M. Uyanik, H. Okamoto, T. Yasui and K. Ishihara, *Science* 2010, **328**, 1376-1379. (c) J. Jin, Y. Li, Z.-J. Wang, W.-X. Qian and W.-L. Bao, *Eur. J. Org. Chem.,* 2010, 1235-1238. (d) T. Dohi, A. Maruyama, M. Yoshimura, K. Morimoto, H. Tohma and Y. Kita, *Angew. Chem. Int. Ed.,* 2005, **44**, 6193-6196. (e) M. Uyanik and K. Ishihara, *ChemCatChem,* 2012, **4**, 177-185. (f) S. K. Rout, S. Guin, K. K. Ghara, A. Banerjee and B. K. Patel, *Org. Lett.,* 2012, **14**, 3982-3985. (g) S. Guin, S. K. Rout, S. Nandi, A. Banerjee and B. K. Patel, *Org. Lett.,* 2012, **14**, 5294-5297. (h) G. Majji, S. Guin, A. Gogoi, S. K. Rout and B. K. Patel, *Chem. Commun.,* 2013, **49**, 3031-3033. (i) S. K. Rout, S. Guin, A. Banerjee, N. Khatun, A. Gogoi and B. K. Patel, *Org. Lett.*, 2013, **15**, 4106-4109. (j) S. K. Rout, S. Guin, W. Ali, A. Gogoi and B. K. Patel, *Org. Lett.,* 2014, **16**, 3086-3089. (k) Das, K. M.; A. Pal, N. N. Adarsh and A. Thakur, *Org. Biomol. Chem.*, 2022, **20**, 3540–3549.

8. (a) C. K. Nguyen, N. N. Nguyen, K. N. Tran, V. D. Nguyen, T. T. Nguyen, D. T. Le and N. T. S. Phan, *Tetrahedron Lett.,* 2017, **58**, 3370–3373. (b) W. Ali, S. K. Rout, S. Guin, A. Modi, A. Banerjee and B. K. Patel, *Adv. Synth. Catal*., 2015, **357**, 515 – 522. (c) B. D. Barve, Y. C. Wu, M. E. Shazly, D. W. Chuang, Y. B. Cheng, J. J. Wang and F. R. Chang, *J. Org. Chem.,* 2014, **79**, 3206−3214. (d) Y. Zheng, W. B. Song and L. J. Xuan, *Tetrahedron Lett.,* 2015, **56**, 4569–4573. (e) S. Yang, X. Y. Chen, M. F. Xiong, H. Zhang, L. Shi, D. Z. Lin and H. Y. Liu, *J. Chin Chem Soc.,* 2021, **68**, 1541–1548. (f) S. Yang, M. F. Xiong, W. Q. Tian, H. Zhang, X. Y. Xiao, H. Y. Liu and C. K. Chang. *Tetrahedron* 2020, **76**, 131569.

9.   (a) D. Chaturvedi, *Tetrahedron* 2012, **68**, 15-45. (b) R. J. Kuhr and H. W. Dorough, Carbamate insecticides: chemistry, biochemistry and toxicology; CRC Press: Cleveland, 1976.

10. (a) N. Hen, M. Bialer and B. Yagen, *J. Med. Chem.,* 2012, **55**, 2835-2845. (b) M. J. Niphakis, D. S. Johnson, T. E. Ballard, C. Stiff and B. F. Cravatt, *ACS Chem. Neurosci*., 2012, **3**, 418-

426. (c) J. W. Chang, D. K. Nomura and B. F. Cravatt, *Chem. Biol*., 2011, **18**, 476-484. (d) M. Fuchs, D. Koszelewski, K. Tauber, W. Kroutila and K. Faber, *Chem. Commun*., 2010, **46**, 5500-5502. (e) M. Wienstock, C. Bejar, R. H. T. Wang, A. Poltyrev, J. P. M. Gross, M. Finberg and B. H. Youdim, *J. Neural Transm. Suppl*., 2000, **60**, 157.

11.   (a) J. Li, C. Kornhaab and L. Ackermann, *Chem. Commun.,* 2012, **48**, 11343-11345. (b) K. W. Quasdorf, A. A. Finch, P. Liu, A. L. Silberstein, A. Komaromi, T. Blackburn, S. D. Ramgren, K. N. Houk, V. Snieckus and N. K. Garg, *J. Am. Chem. Soc.,* 2011, **13***3*, 6352-6363. (c) J. C. Riggs, K. J. Singh, M. Yun and D. B. Collum, *J. Am. Chem. Soc*., 2008, **130**, 13709-13717. (d) T. W. Greene and P. G. M Wuts, Protective groups in organic synthesis, 4th ed.; Wiley: New York. 2007, Page-419. (e) V. Snieckus, *Chem. Rev.,* 1990, **90**, 879-933.

12.   (a) F. Shi and Y. Deng, *Chem. Commun*., 2001, 443-444. (b) T. W. Leung and B. D. Dombek, *J. Chem. Soc., Chem. Commun.,* 1992, 205-206. (c) H. Alper and F. W. Hartstock, *J. Chem. Soc. Chem. Commun.,* 1985, 1141-1142. (d) S. Fukuoka, M. Chono and M. Kohno, *J. Chem. Soc. Chem. Commun*., 1984, 399-400. (e) D. B. D. Amico, F. Calderazzo, L. Labella, F. Marchetti and G. Pampaloni, *Chem. Rev.,* 2003, **103**, 3857-3898. (f) M. Rohr, C. Geyer, R. Wandeler, M. Schneider, S. E. F. Murphy and A. Baiker, *Green Chem.,* 2001, **3,** 123-125. (g) R. N. Salvatore, S. I. Shin, A. S. Nagle and K. W. Jung *J. Org. Chem*., 2001, **66**, 1035-1037. (h) P. Tascedda and E. Dunach, *Chem. Commun*., 2000, 449-450. (i) M. A. Casadei, F. M. Moracci, G. Zappia, A. Inesi and L. Rossi, *J. Org. Chem*., 1997, **62**, 6754-6759. (j) T. Toda and Y. Kitagawa, *Angew. Chem. Int. Ed*., 1987, **26**, 334-335. (k) Y. Yoshida and S. Inoue, *J. Chem. Soc., Perkin Trans.,* 1979, 3146-3150.

13.   (a) G. S. Kumar, C. U. Maheswari, R. A. Kumar, M. L. Kantam and K. R. Reddy, *Angew. Chem. Int. Ed*., 2011, **50,** 11748-11751. (b) B. D. Barve, Y.-C. Wu, M. E. Shazly, D.-W. Chuang, Y.-M. Chung, Y.-H. Tsai, S.-F. Wu, M. Korinek, Y.-C. Du, C.-T. Hsieh, J.-J. Wang and F.-R. Chang, *Eur. J. Org. Chem*., 2012, 6760-6766.

14.   D. Bansal, G. Kumar, G. Hundal and R. Gupta, *Dalton Trans*., 2014, **43**, 14865-14875.

15.   (a) E. Ermis and K. Durmus. *J. Mol. Struct*., 2020, **1217**, 128354-128369. (b) J. Joseph and G. B. Janaki, *J. Mol. Struct.,* 2014, **1063**, 160–169. (c) K. K. Bania, G. V. Karunakar, K. Goutham and C. R. Deka, *Inorg. Chem.,* 2013, **52**, 8017−8029. (d) S. Godlewska, J. Jezierska, K. Baranowska, E. Augustin and A. Dołega, Polyhedron 2013, **65**, 288-297.

16.   (a) F. Chen, N. Wang, H. Lei, D. Guo, H. Liu, Z. Zhang, W. Zhang, W. Lai and R. Cao, *Inorg. Chem.,* 2017, **56**, 13368−13375. (b) J. K. Bower, A. D. Cypcar, B. Henriquez, S. Chantal, E. Stieber and S. Zhang, *J. Am. Chem. Soc.,* 2020, **142**, 18, 8514–8521.

17.   S. Muthuramalingam, K. Anandababu, M. Velusamy and R. Mayilmurugan, *Inorg. Chem.,* 2020, **59**, 5918−5928.

18.   (a) X. Huang and T. Zhang, *J. Org. Chem.,* 2010, **75**, 506-509. (b) C. He, G. Zhang, J. Ke, H. Zhang, J. T. Miller, A. J. Kropf and A. Lei, *J. Am. Chem. Soc.,* 2013, **135**, 488-493.

19.   (a) B. L. Tran, M. Driess and J. F. Hartwig, *J. Am. Chem. Soc.,* 2014, **136**, 17292-17301. (b) J. Zhao, H. Fang, J. Han and Y. Pan, *Org. Lett.*, 2014, **16**, 2530−2533.

20.   O. V. Dolomanov, L. J. Bourhis, R. J. Gildea, J. A. K. Howard and H. Puschmamn, *J. Appl. Crystallogr.,* 2009, **42**, 339-341.

21.   L. Palatimus and G. Chapuis, *J. Appl. Crystallogr.,* 2007, **40**, 786-790.

22.   G. M. Sheldrick, *Acta Crystallogr. Sect. A.: Found. Crystallogr.,* 2008, **64**, 112-122.

23.   (a) M. Gayke, N. Hirapara, H. Narode, S. D. Bhosle, R. S. Bhosale and J. S. Yadav. *ACS Omega* 2022, **7**, 36017−36027. (b) X. Sun, X. Yao, C. Zhang and Y. Rao, *Chem. Commun.,* 2015, 51, 10014-10017. (c) W. Ali, S. K. Rout, S. Guin, A. Modi, A. Banerjee and B. K. Patel. *Adv. synth. catal*., 2015, **357**, 515-522. (d) G. S. Kumar, C. U. Maheswari, R. A. Kumar, M. L. Kantam and K. R. Reddy. *Angew. Chem. Int. Ed*., 2011, **50**, 11748 –11751. (e) Z. Chen and C. M. So, *Org. Lett.,* 2020, **22**, 3879−3883. (f) A. F. Yepes, C. A. Ramírez, M. S. Rada, W. Cardona-G, K. Sierra, E. Osorio, L. A. G. Molina and R. P. Duque, *Med. Chem. Res.,* 2022, **31**, 867–885. (g) J. Kim, S. Kang, S. Hong, S. Yum, Y. M. Kim and Y. Jung, *Eur. J. Med. Chem.,* 2012, **48**, 36-44.

24.   (a) D. Saberi and A. Heydari. *Tetrahedron Lett.,* 2013, **54**, 4178–4180. (b) B. D. Barve, Y. C. Wu, M. E. Shazly, D. W. Chuang, Y. M. Chung, Y. H. Tsai, S. F. Wu, M. Korinek, Y. C. Du, C. T. Hsieh, J. J. Wang and F. R. Chang, *Eur. J. Org. Chem*., 2012, 6760–6766. (c) X. Yang, Y. Sun, Z. Chen and Y. Rao. *Adv. Synth. Catal*., 2014, **356**, 1625–1630. (d) A. Liu, L. Dong, X. L.Wei, X. H. Yang, J. H. Xiao and Z. Q. Liu. *Eur. J. Pharm. Sci.,* 2016, **88**, 50–58. (e) S. S. Bera and M. S.Maji, *Org. Lett.,* 2020, **22**, 2615−2620.

Spectroscopic Details
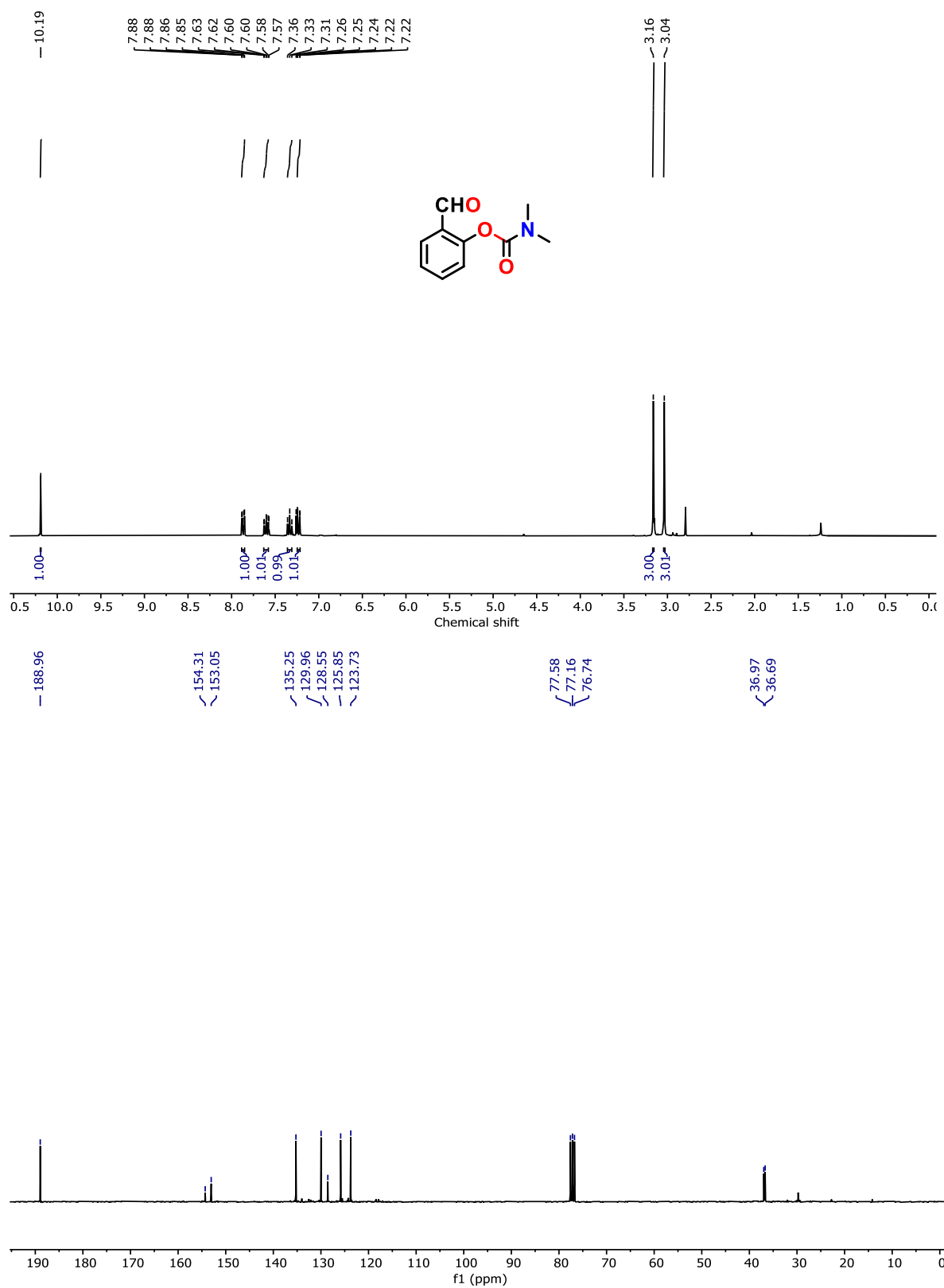
Figure 3.3. ¹H and ¹³C NMR spectra of **3a** in CDCl₃.
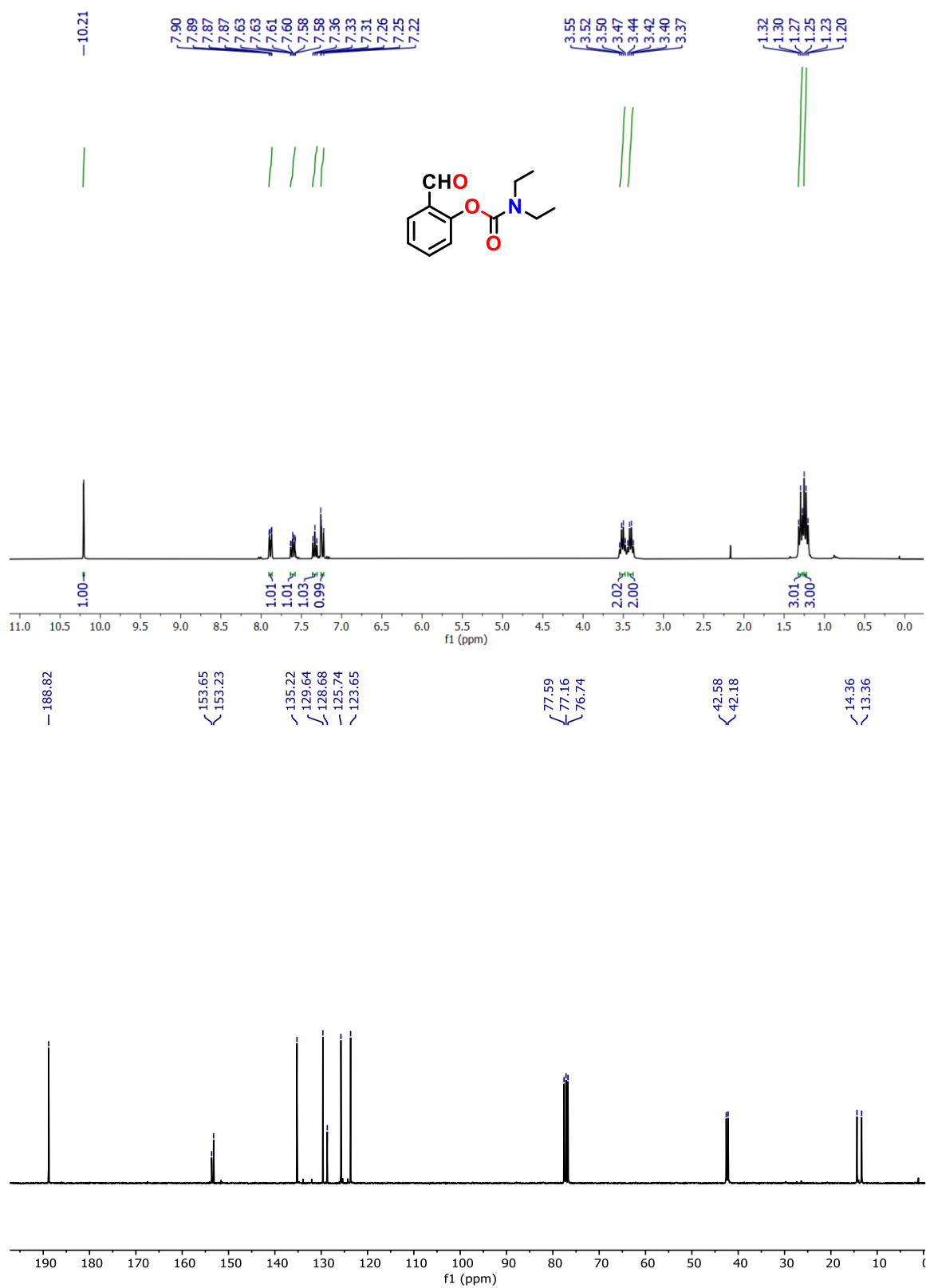
Figure 3.4. ¹H and ¹³C NMR spectra of **3b** in CDCl₃.
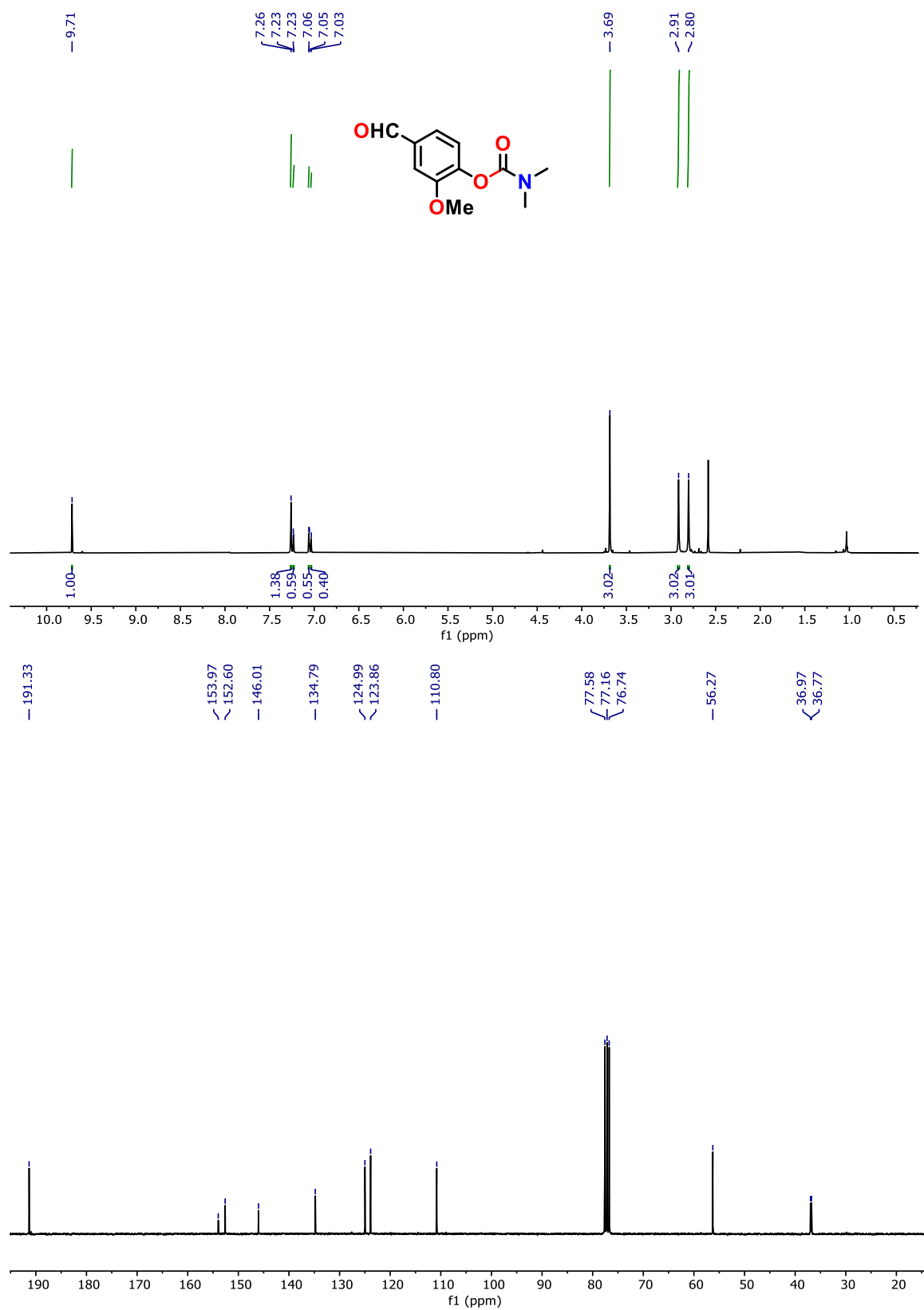
Figure 3.5. ^{1}H and ^{13}C NMR spectra of **3c** in CDCl$_3$**.**

7.973
7.970
7.958
7.954
7.535
7.532
7.520
7.516
7.504
7.501
7.272
7.257
7.239
7.156
7.140

—3.848

3.136
3.015

1.00

0.98
0.46
0.52
0.99

3.02

3.00
3.00

8.5 8.0 7.5 7.0 6.5 6.0 5.5 5.0 4.5 4.0 3.5 3.0 2.5 2.0 1.5 1.0 0.5 0.0
Chemical shift

—164.77

154.23
151.02

133.15
131.03

124.94
123.76
123.30

77.59
77.16
76.74

—51.52

36.21
36.03

170 165 160 155 150 145 140 135 130 125 120 115 110 105 100 95 90 85 80 75 70 65 60 55 50 45 40 35
f1 (ppm)
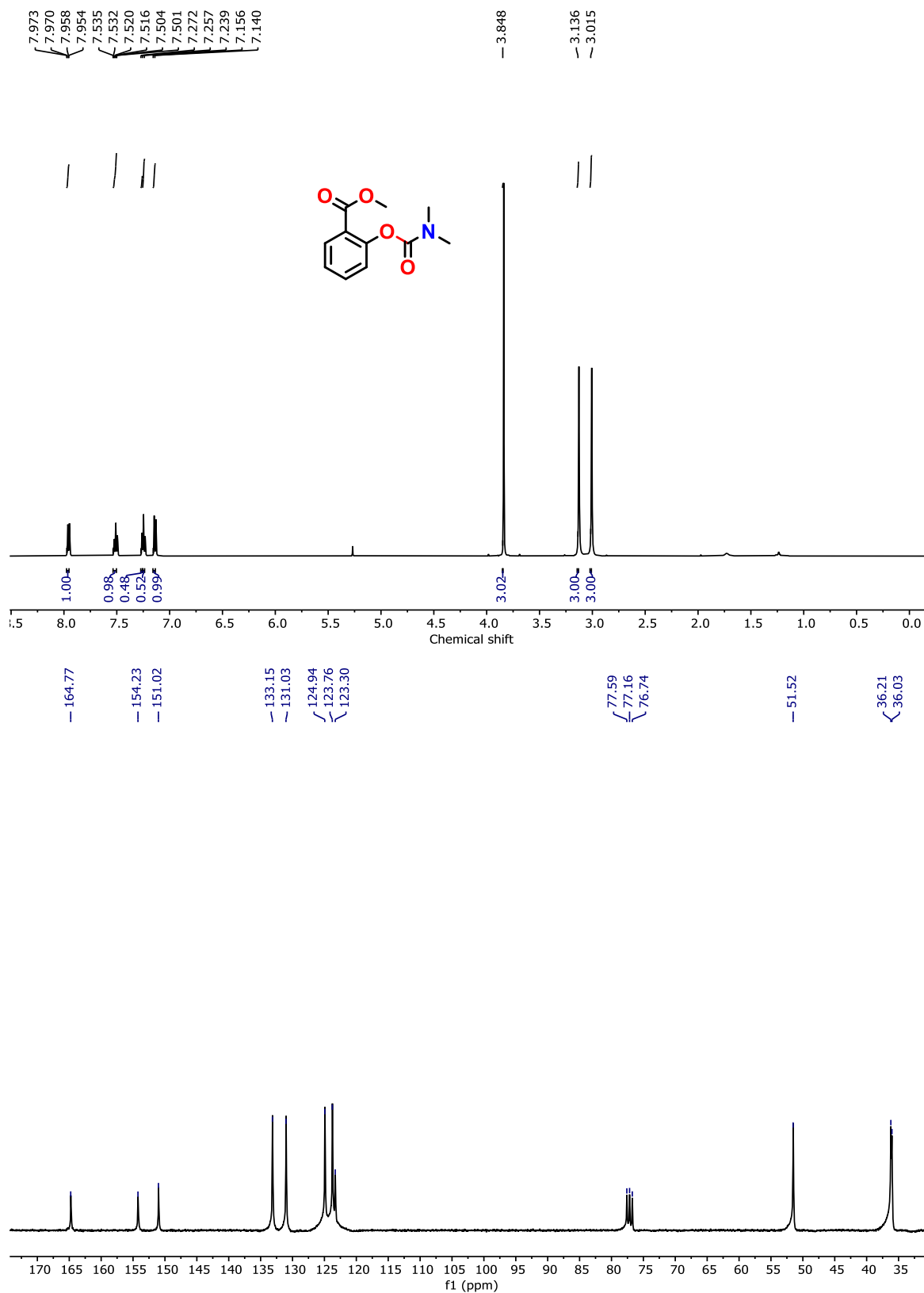
Figure 3.6. ^{1}H and ^{13}C NMR spectra of **3d** in CDCl$_3$**.**
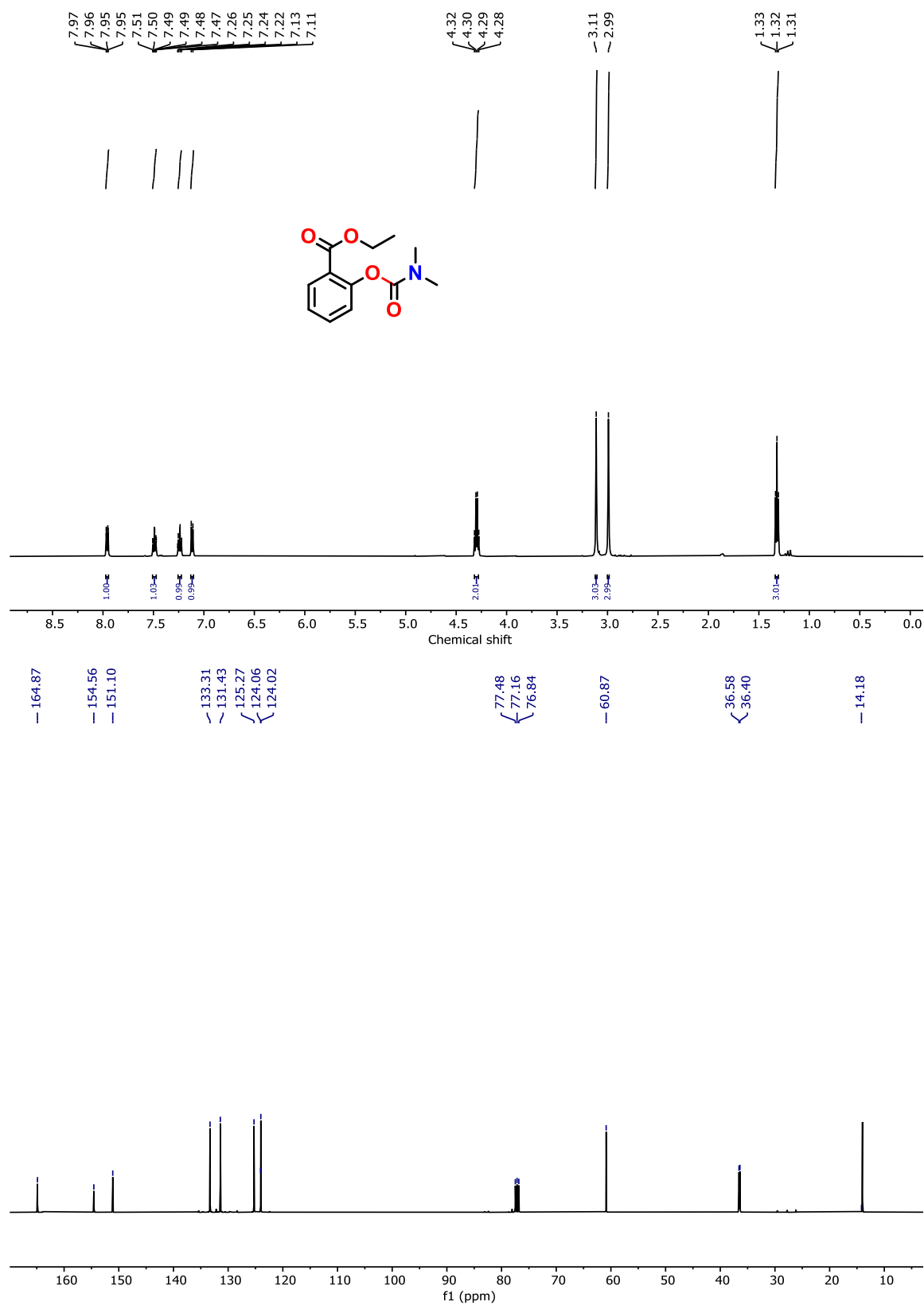
Figure 3.7. ^{1}H and ^{13}C NMR spectra of **3e** in CDCl$_3$**.**
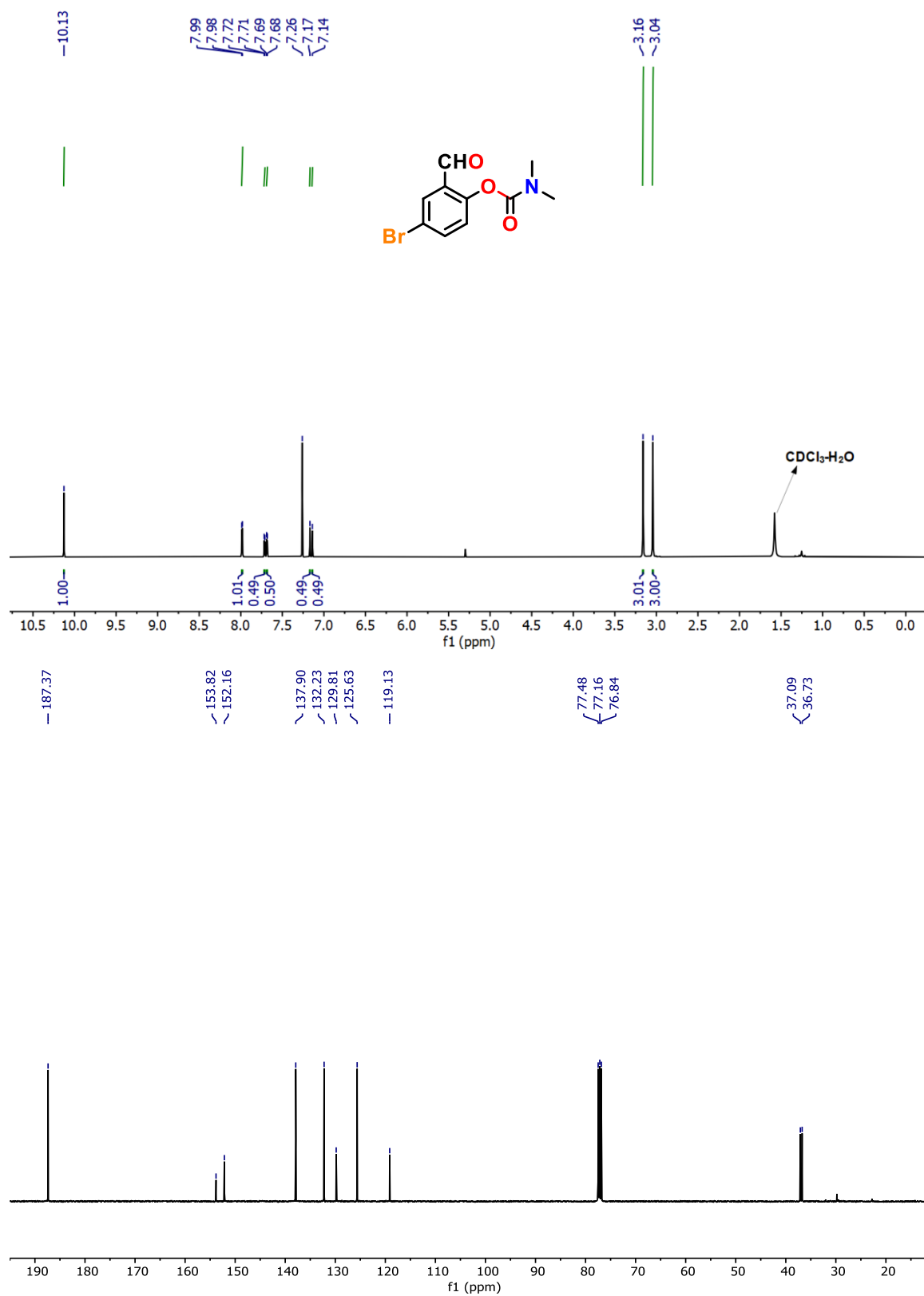
Figure 3.8. ^{1}H and ^{13}C NMR spectra of **3f** in CDCl$_3$.
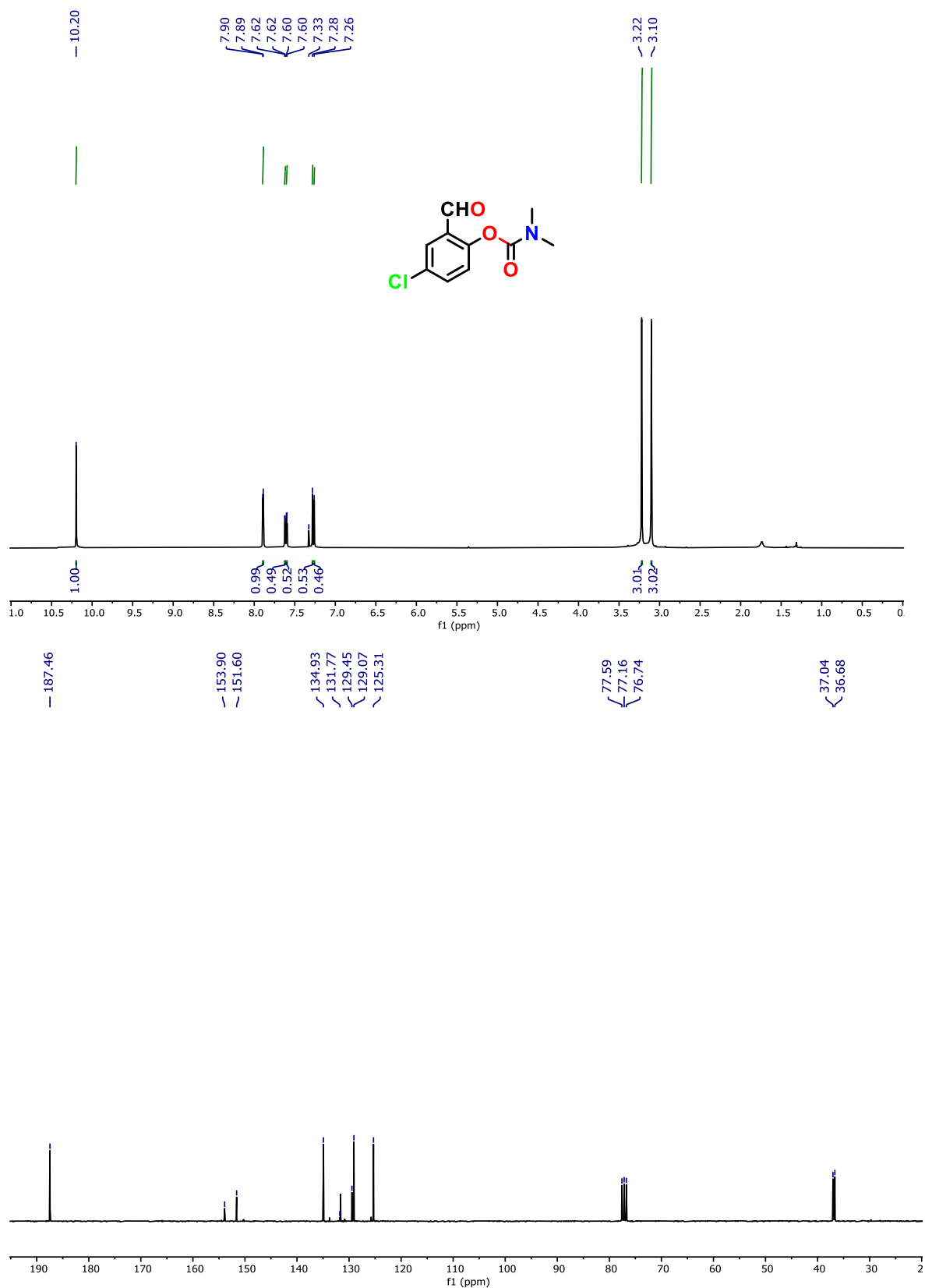
Figure 3.9. ¹H and ¹³C NMR spectra of **3g** in CDCl₃**.**
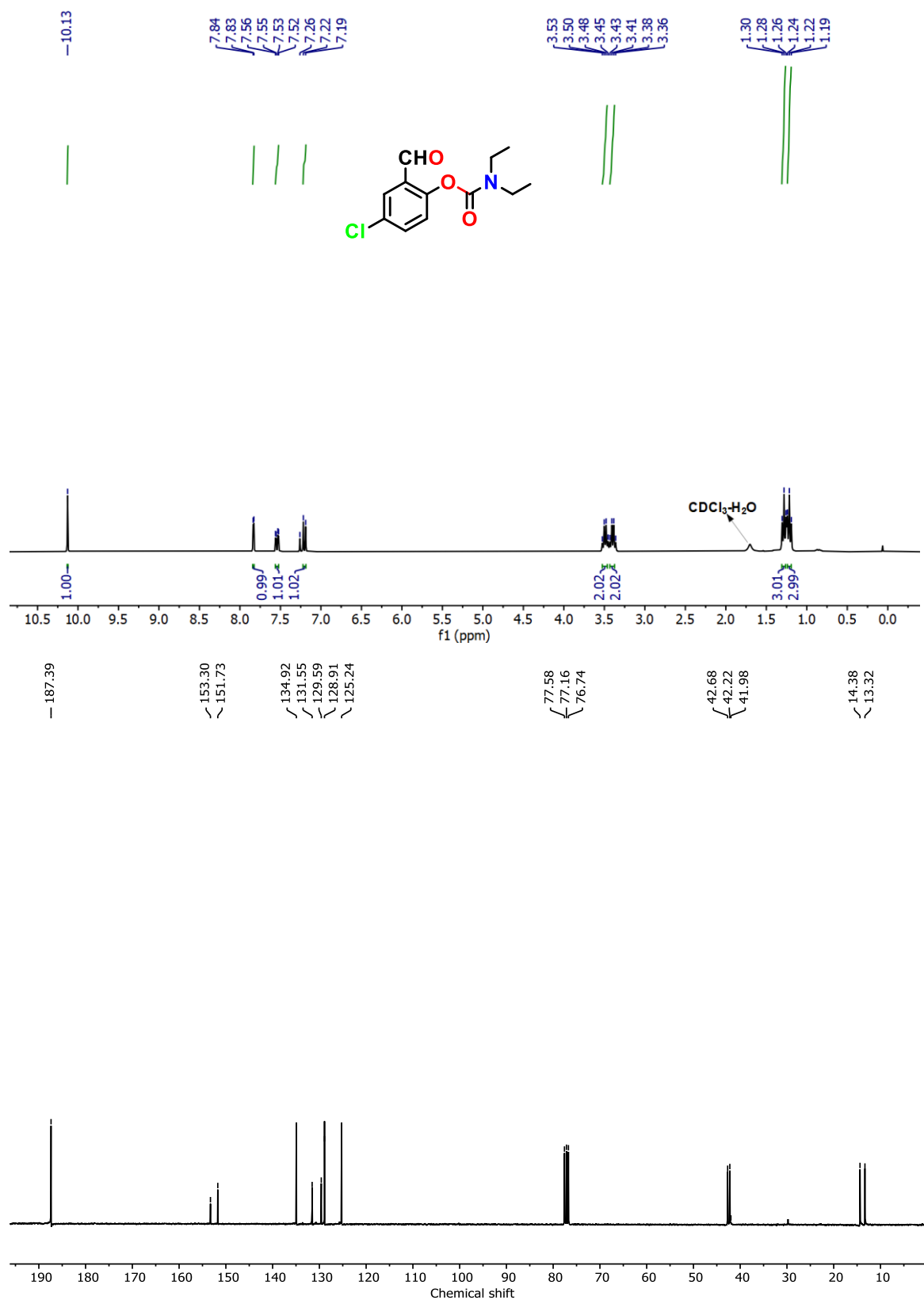
Figure 3.10. ^{1}H and ^{13}C NMR spectra of **3h** in CDCl$_3$.
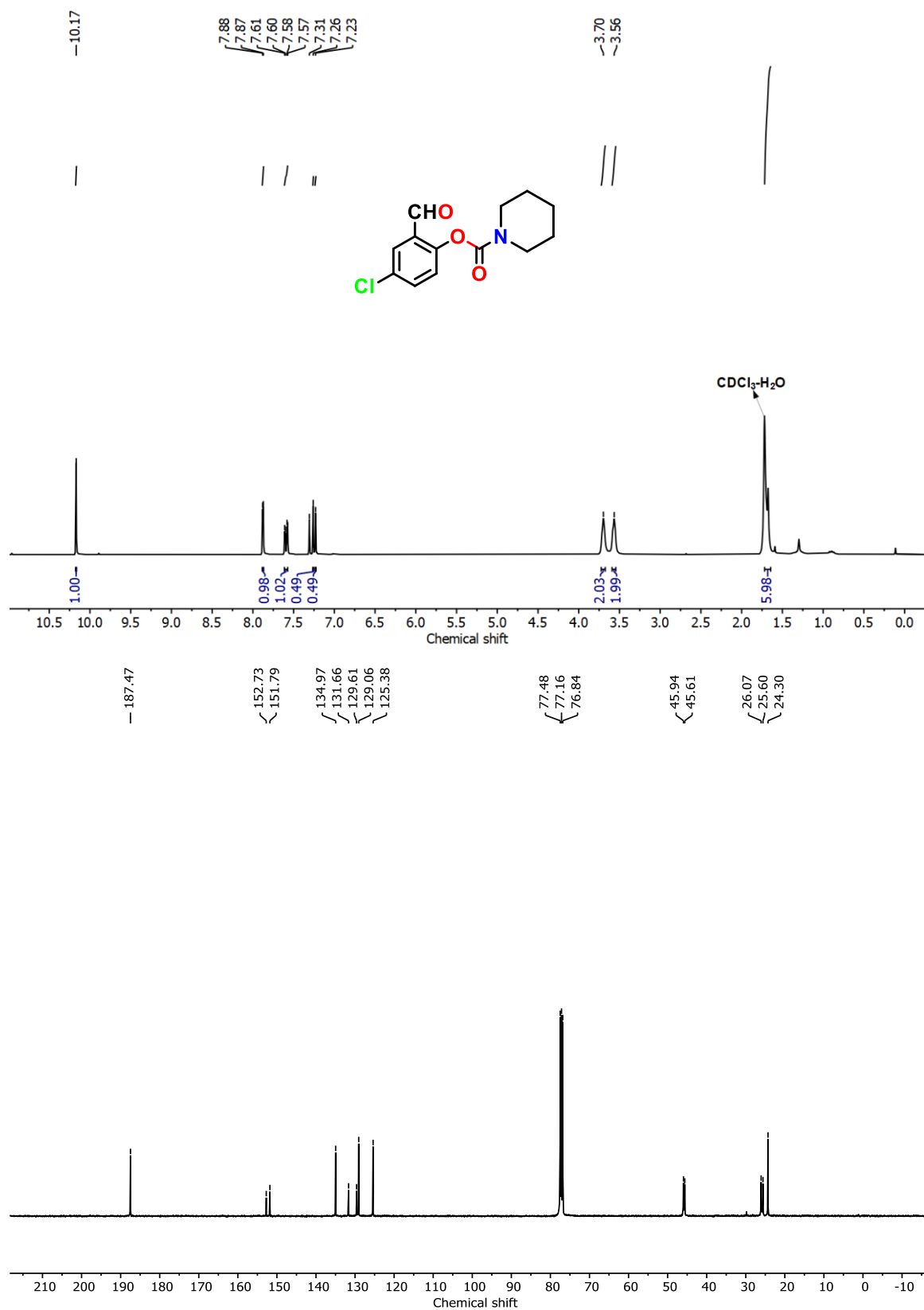
Figure 3.11. ^{1}H and ^{13}C NMR spectra of **3i** in CDCl$_3$.
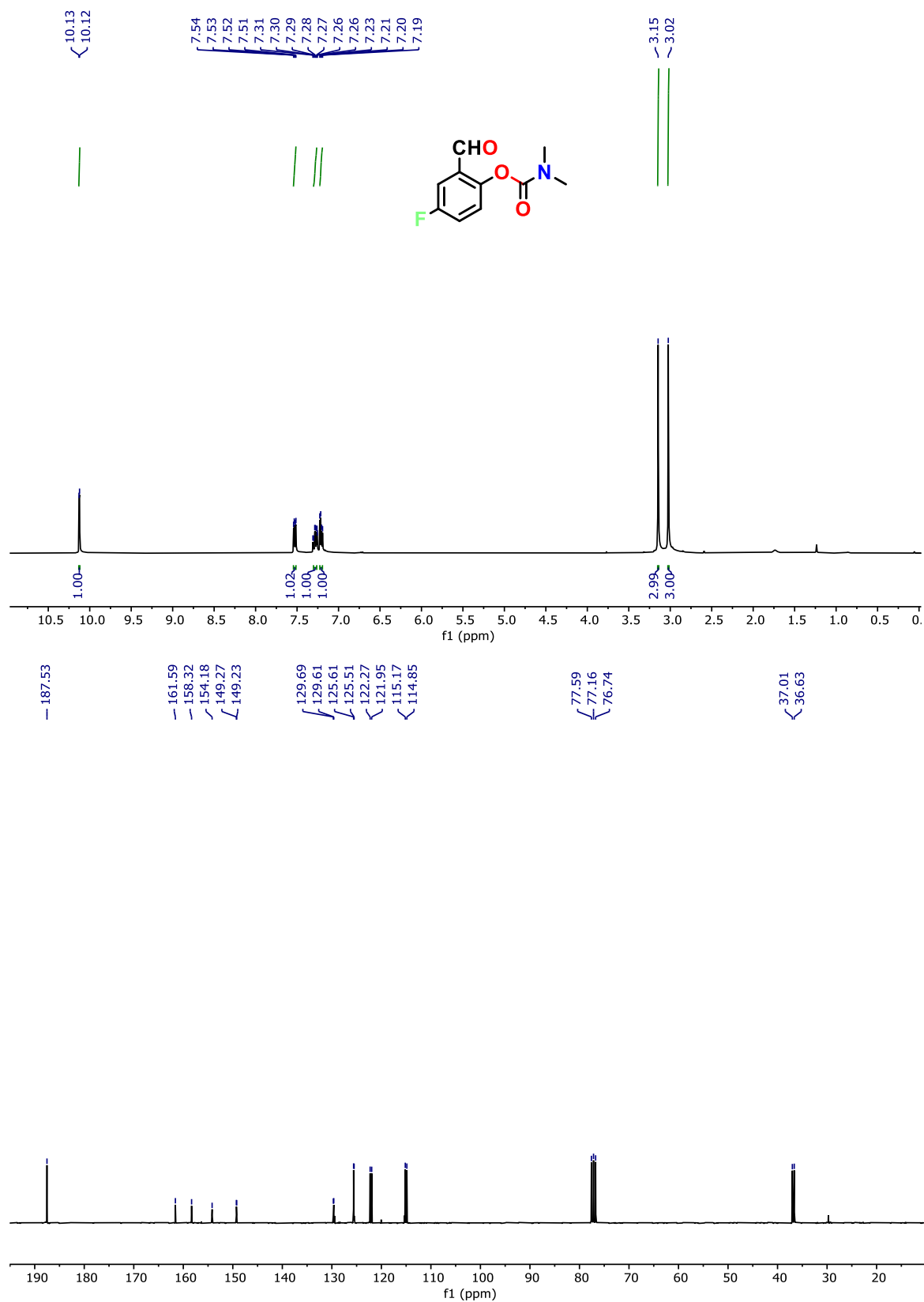
Figure 3.12. ^{1}H and ^{13}C NMR spectra of **3j** in CDCl$_3$.
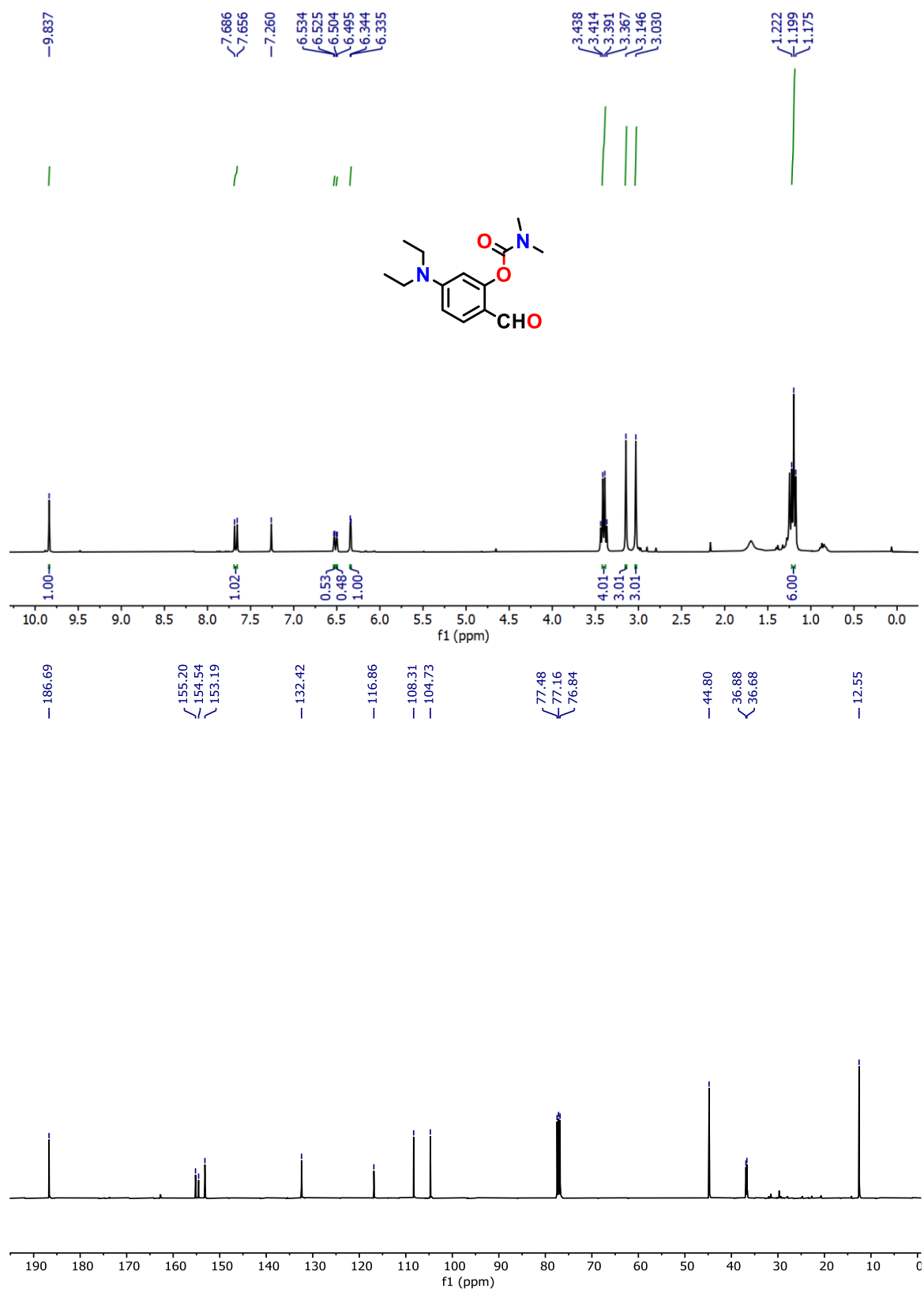
Figure 3.13. ^1H and ^{13}C NMR spectra of **3k** in CDCl$_3$.
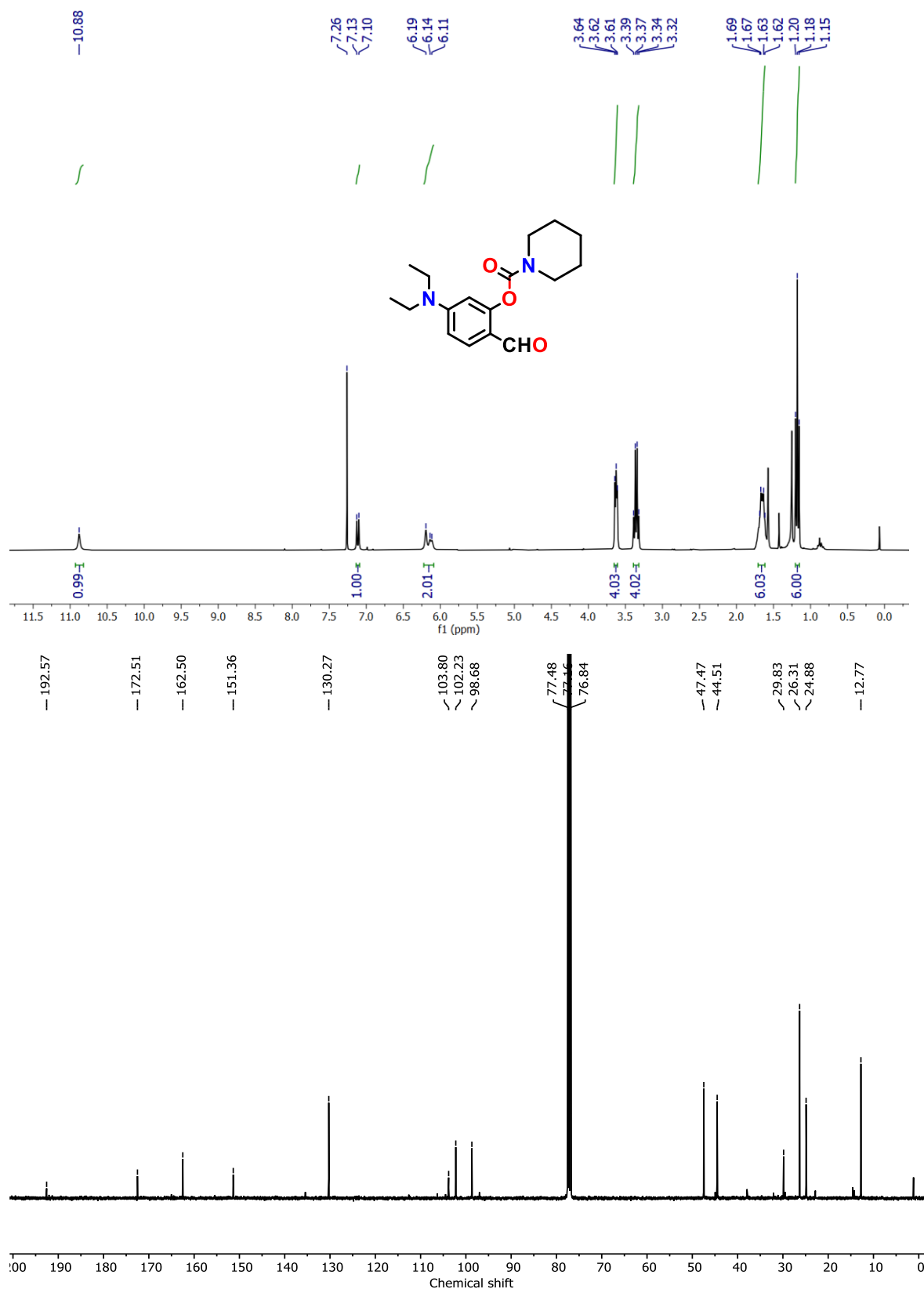
Figure 3.15. ^{1}H and ^{13}C NMR spectra of **3l** in CDCl$_3$.
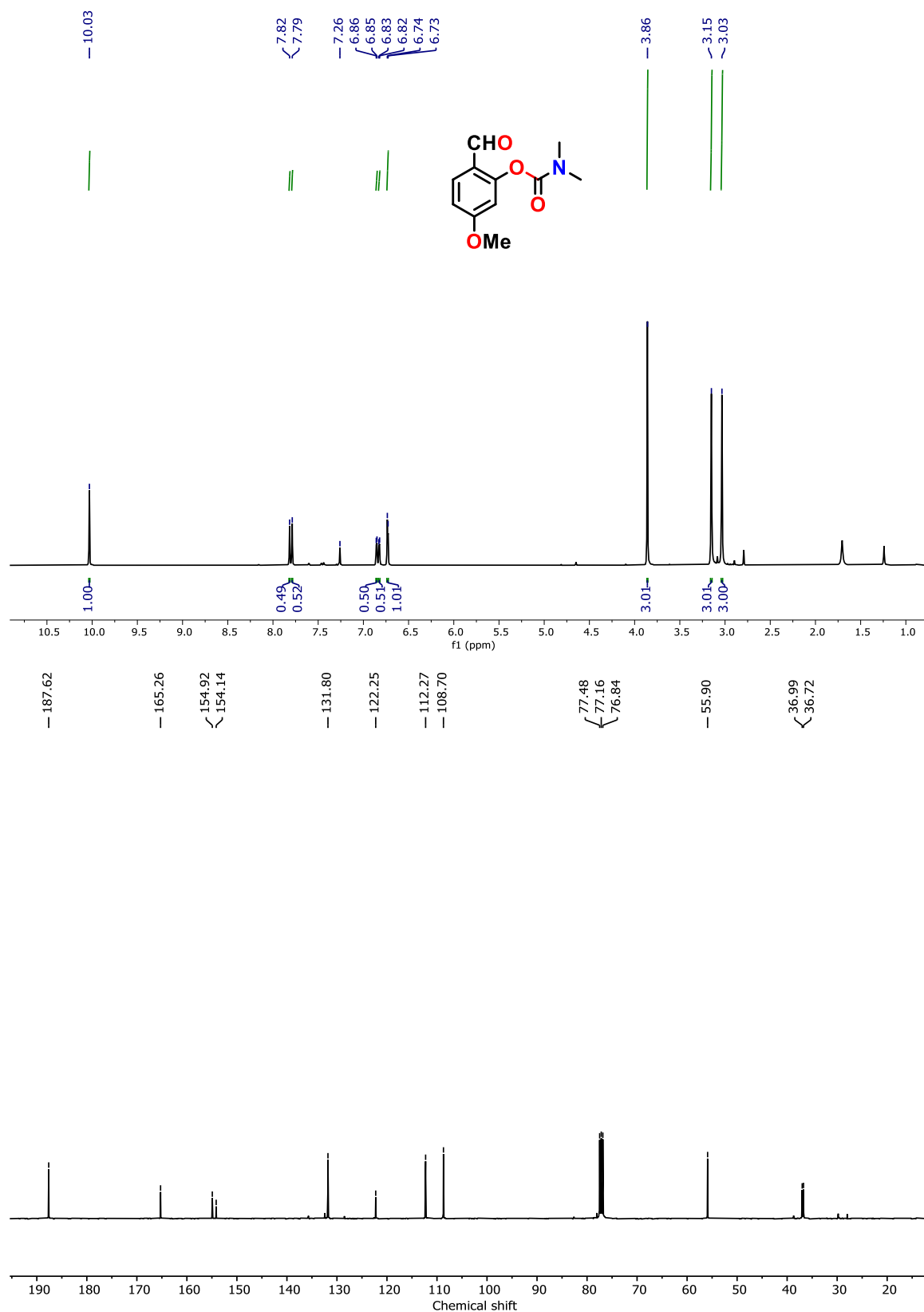
Figure 3.16. ¹H and ¹³C NMR spectra of **3m** in CDCl₃**.**
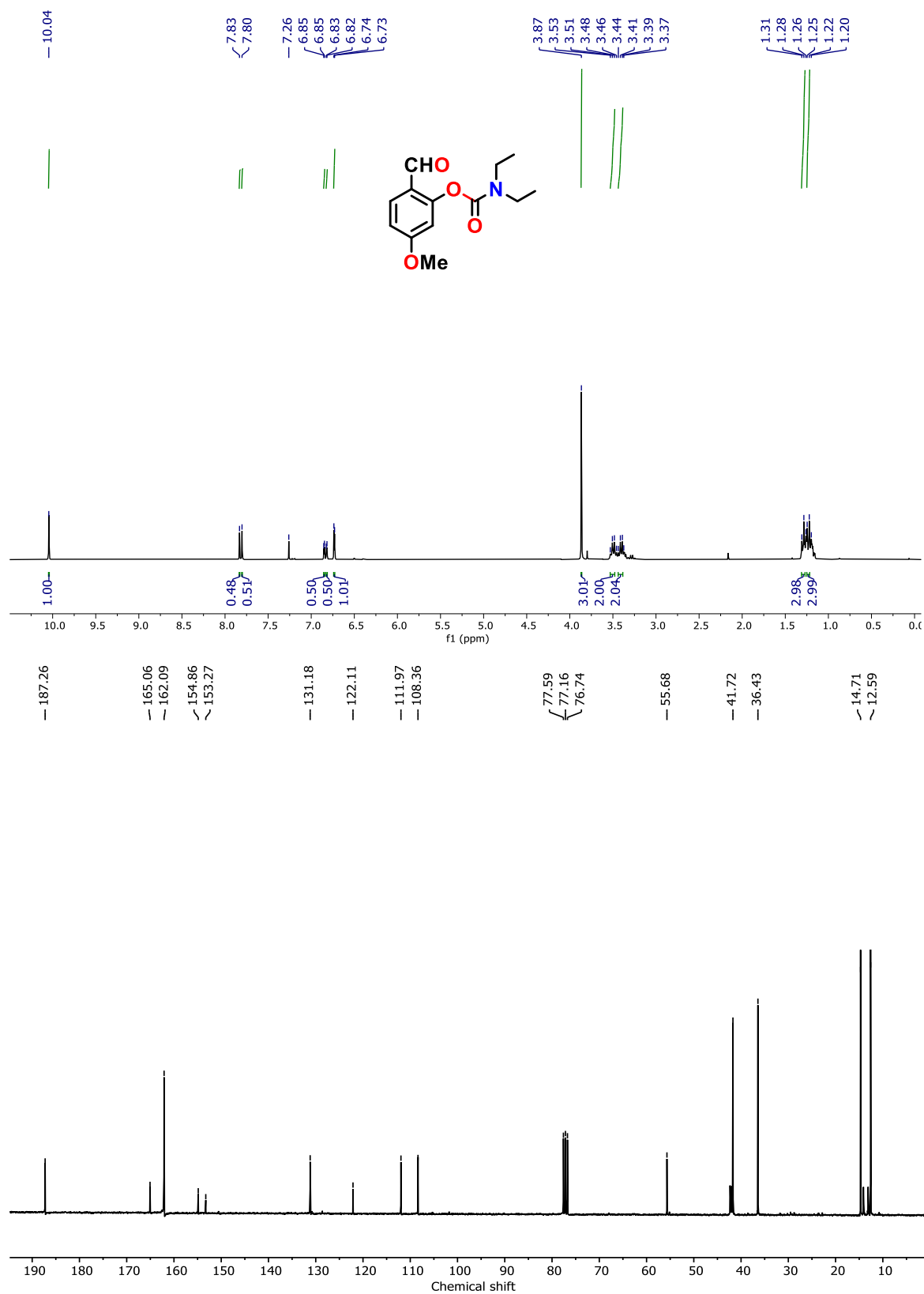
Figure 3.17. ¹H and ¹³C NMR spectra of **3n** in CDCl₃**.**
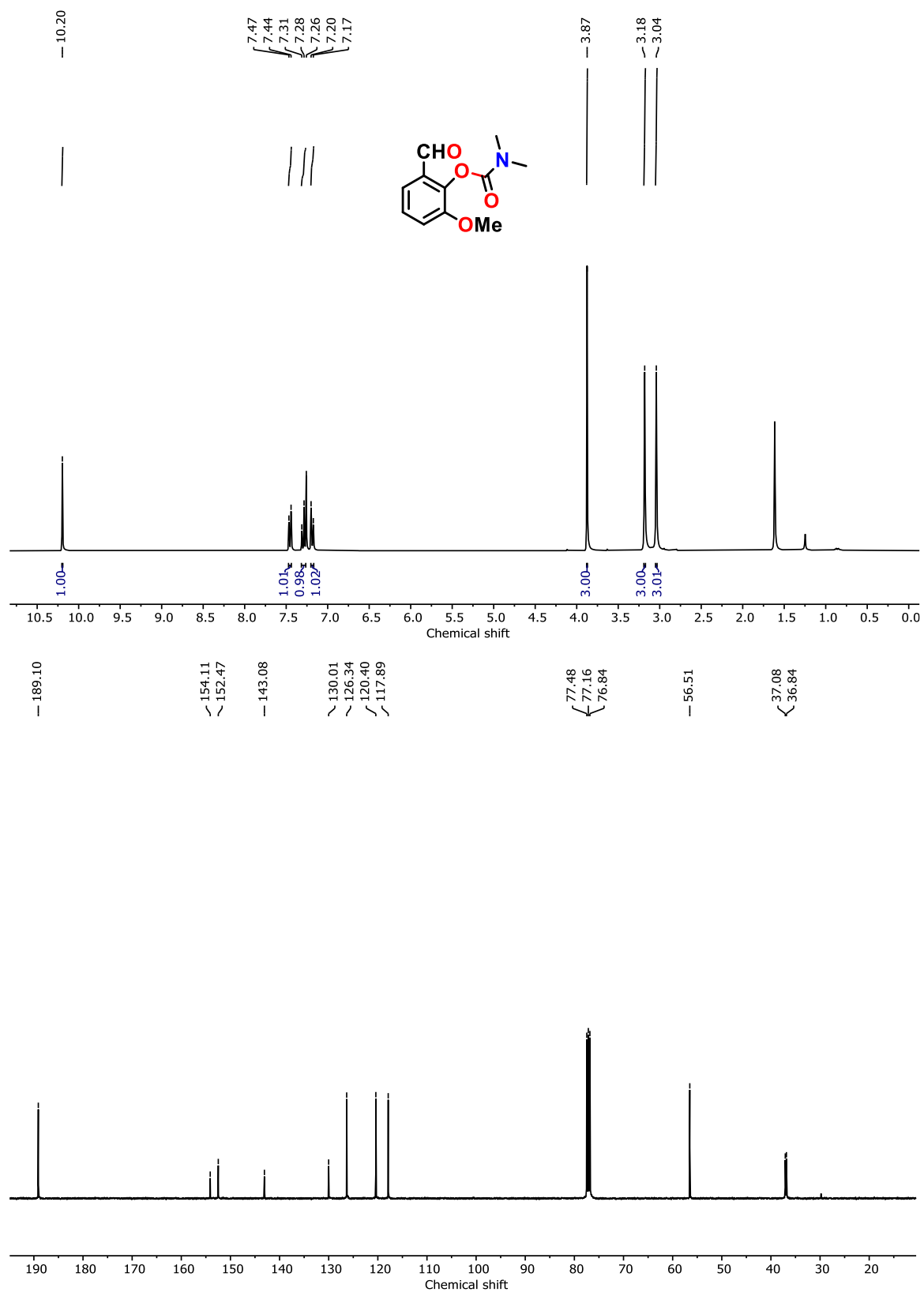
Figure 3.18. ^{1}H and ^{13}C NMR spectra of **3o** in CDCl$_3$.
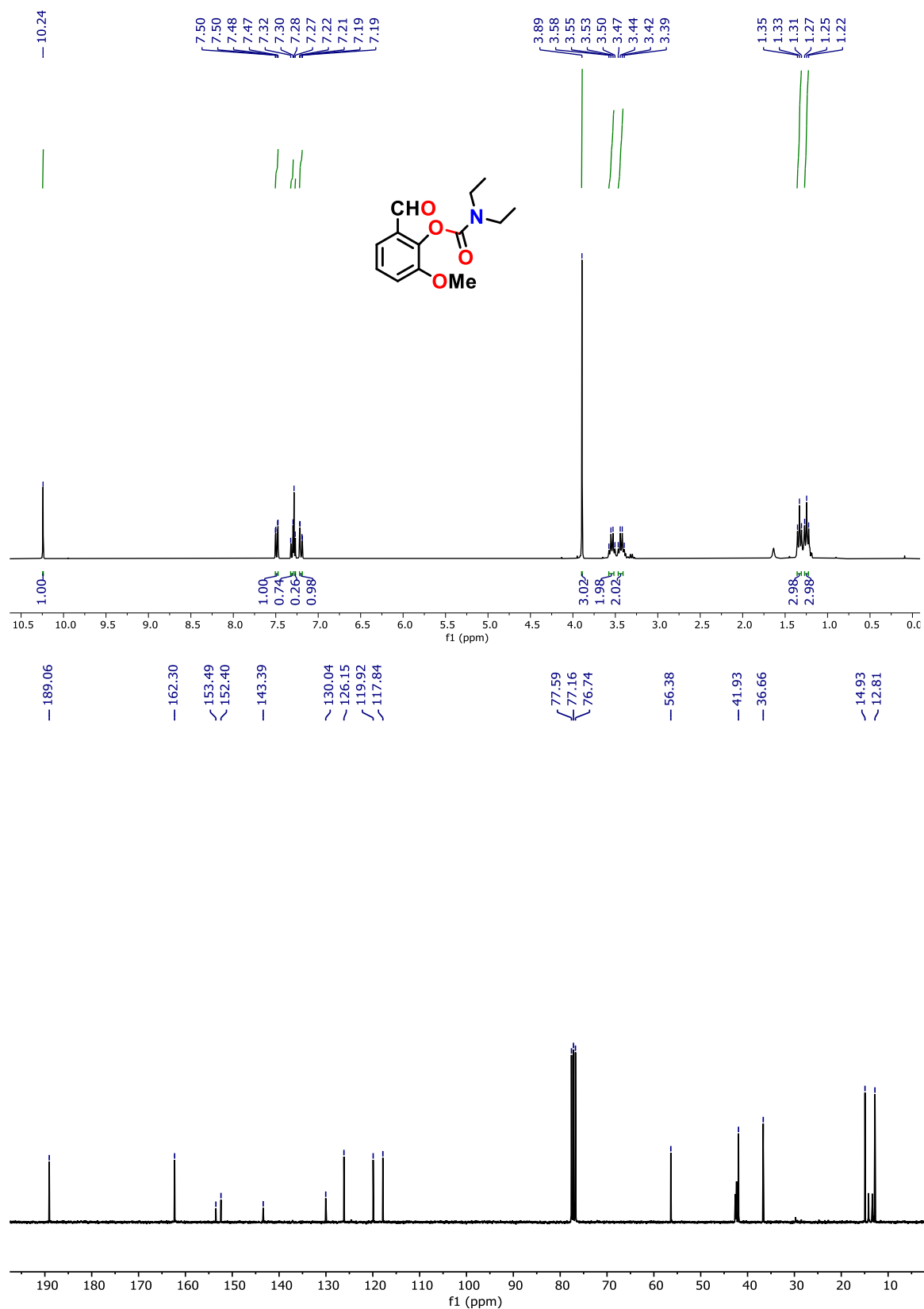
Figure 3.19. ^{1}H and ^{13}C NMR spectra of **3p** in CDCl$_3$.
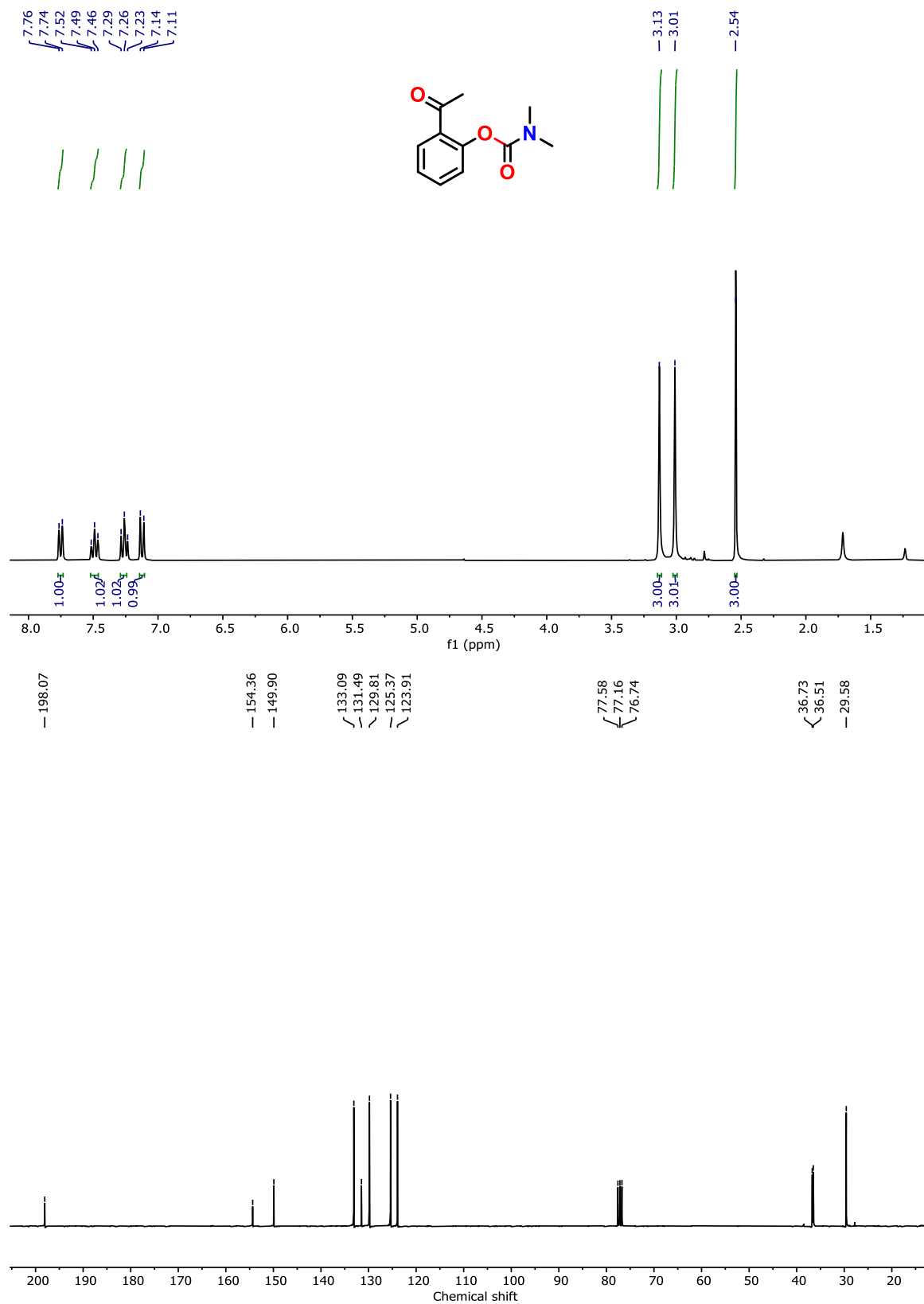
Figure 3.20. ^{1}H and ^{13}C NMR spectra of **3q** in CDCl$_3$.
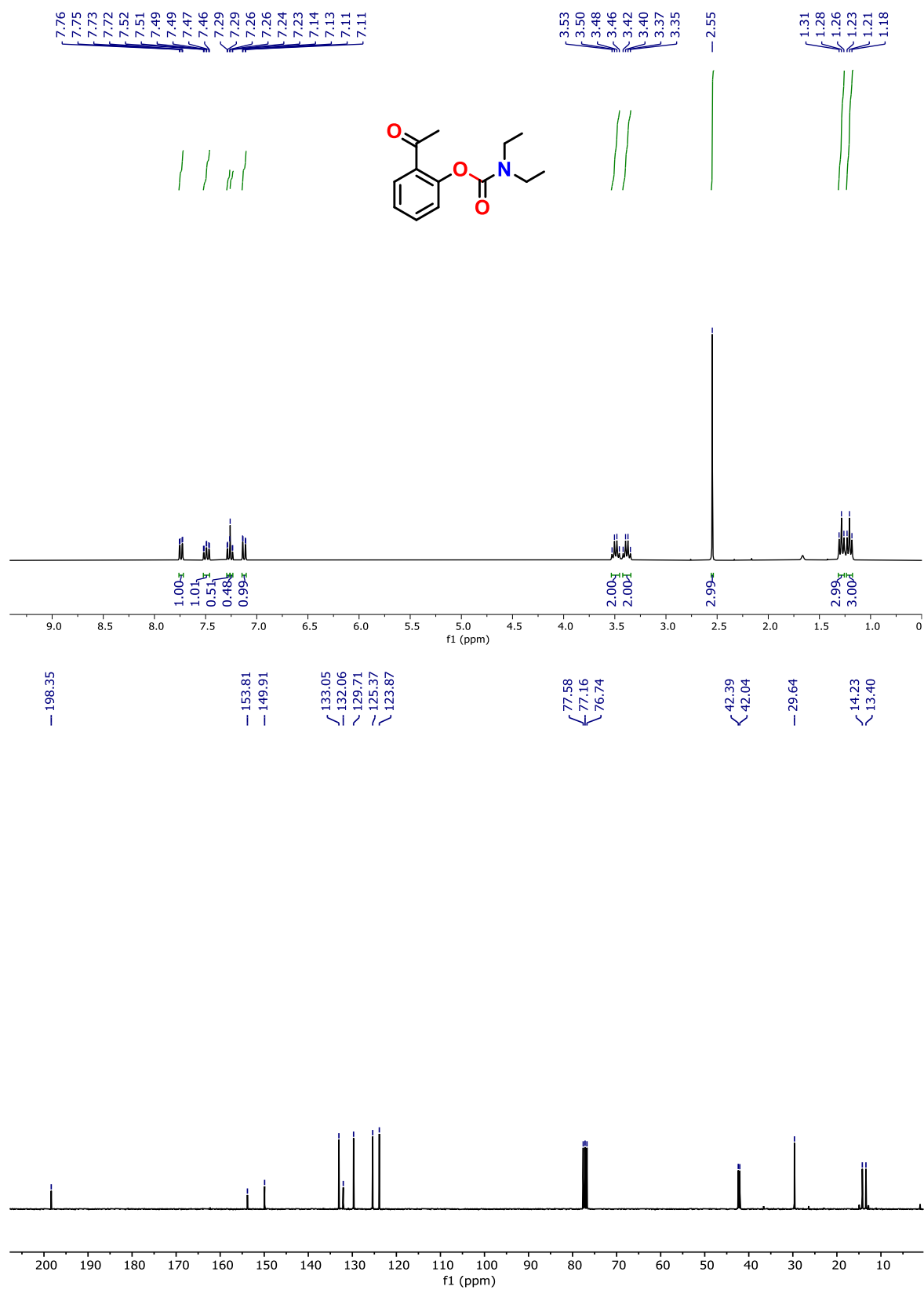
Figure 3.21. ¹H and ¹³C NMR spectra of **3r** in CDCl₃**.**
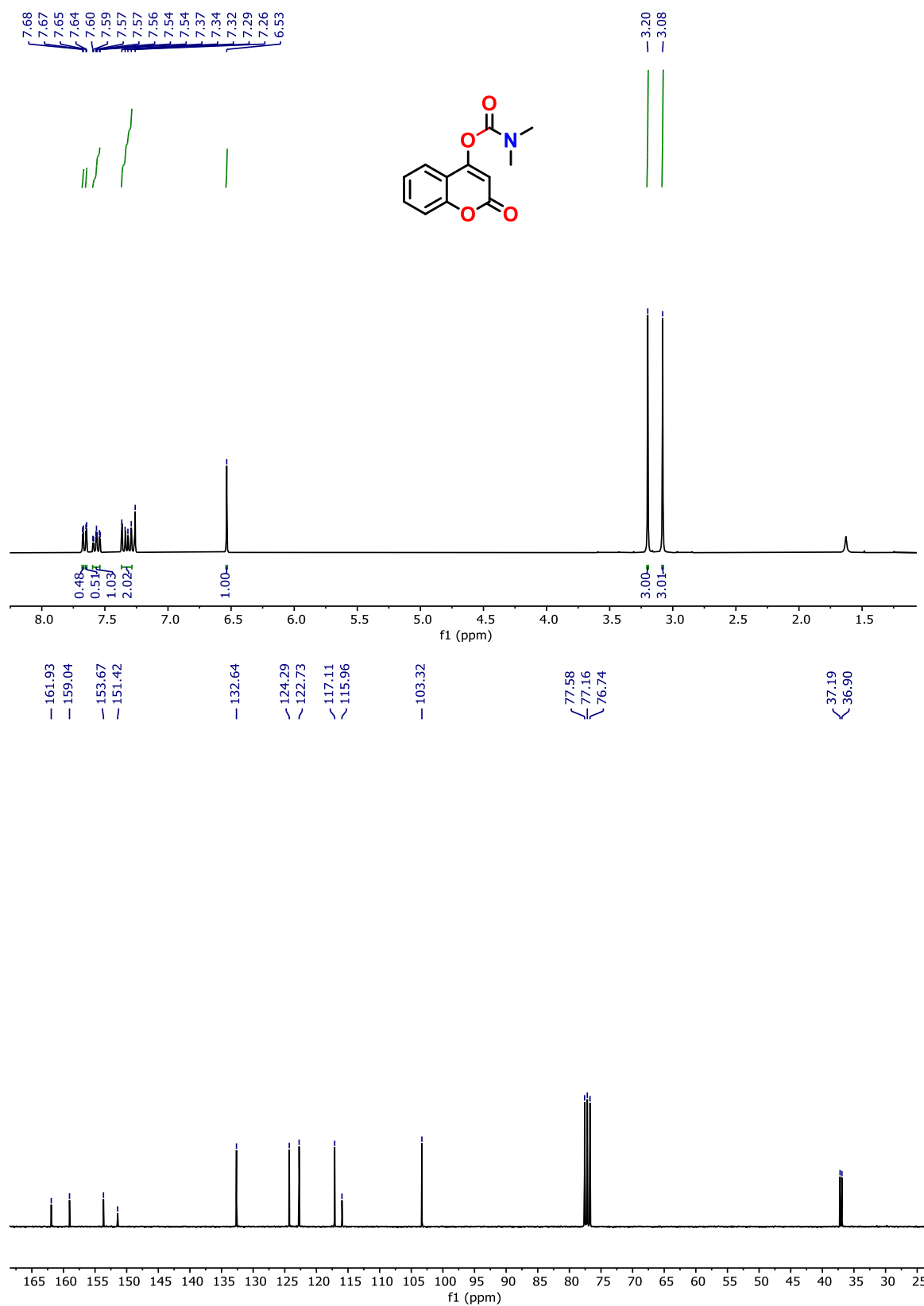
Figure 3.22. ¹H and ¹³C NMR spectra of **3s** in CDCl₃.
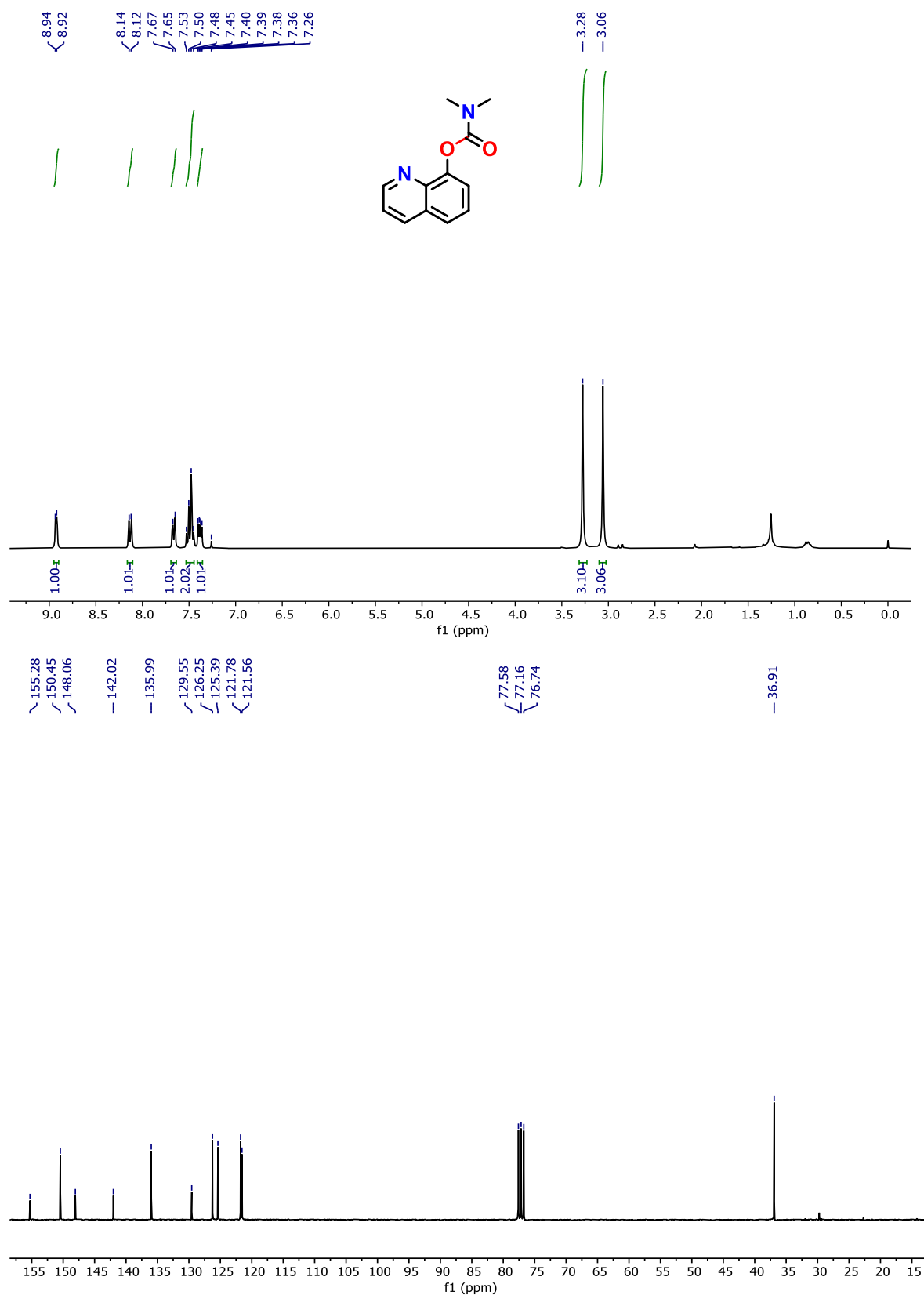
Figure 3.23. ¹H and ¹³C NMR spectra of **3t** in CDCl₃.
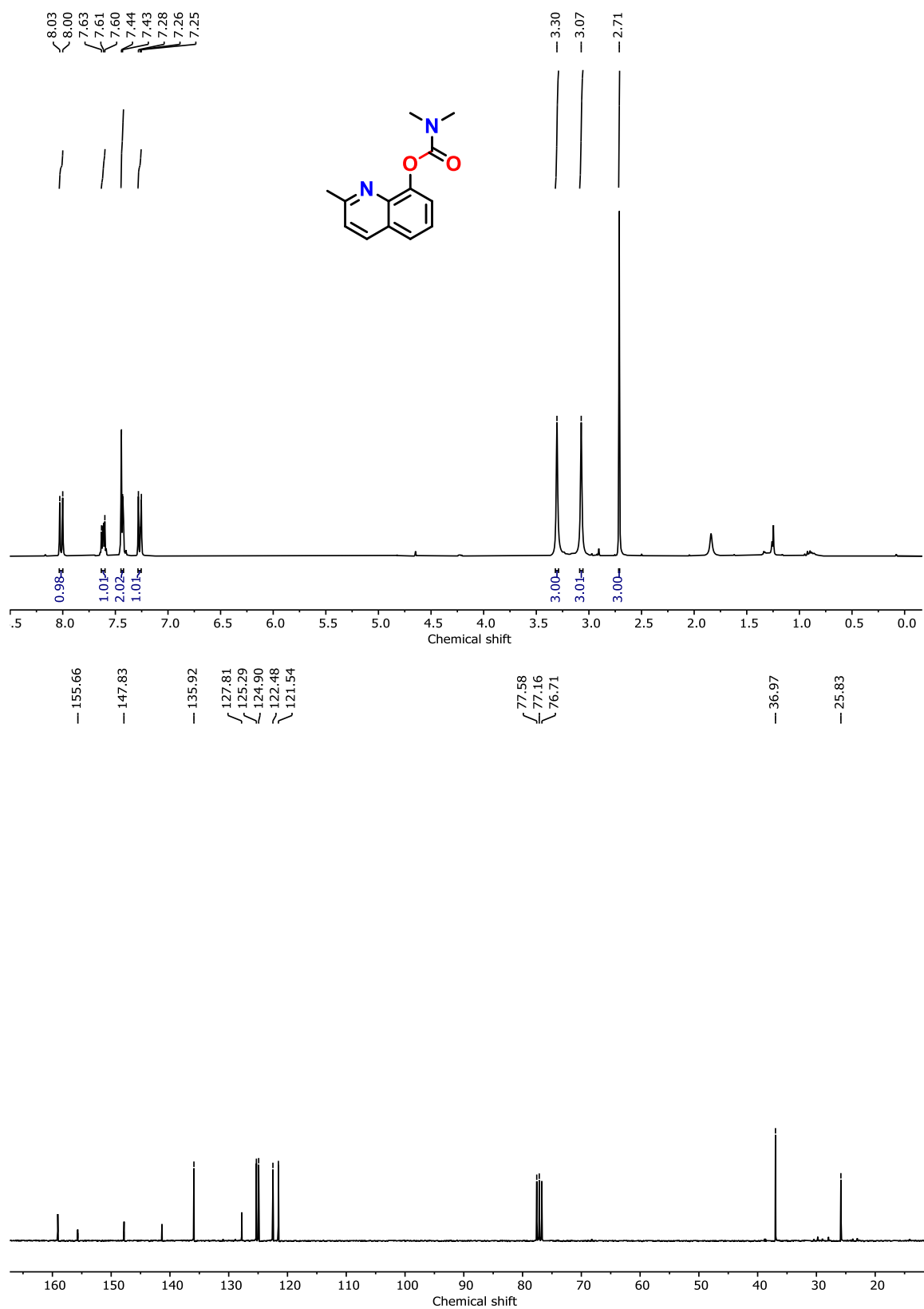
Figure 3.24. ^{1}H and ^{13}C NMR spectra of **3u** in CDCl₃.
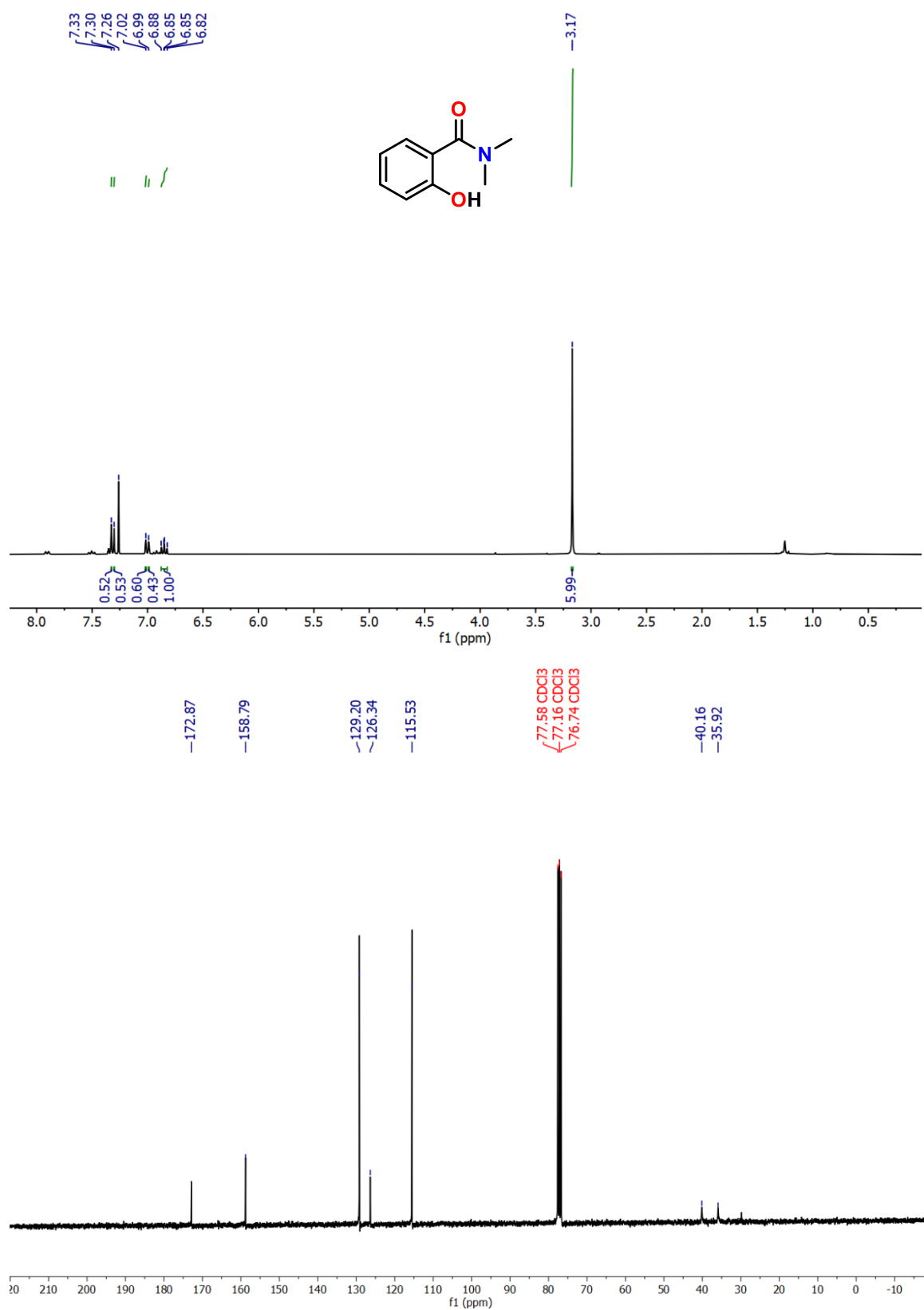
Figure 3.25. ^{1}H and ^{13}C NMR spectra of **5a** in CDCl$_3$.
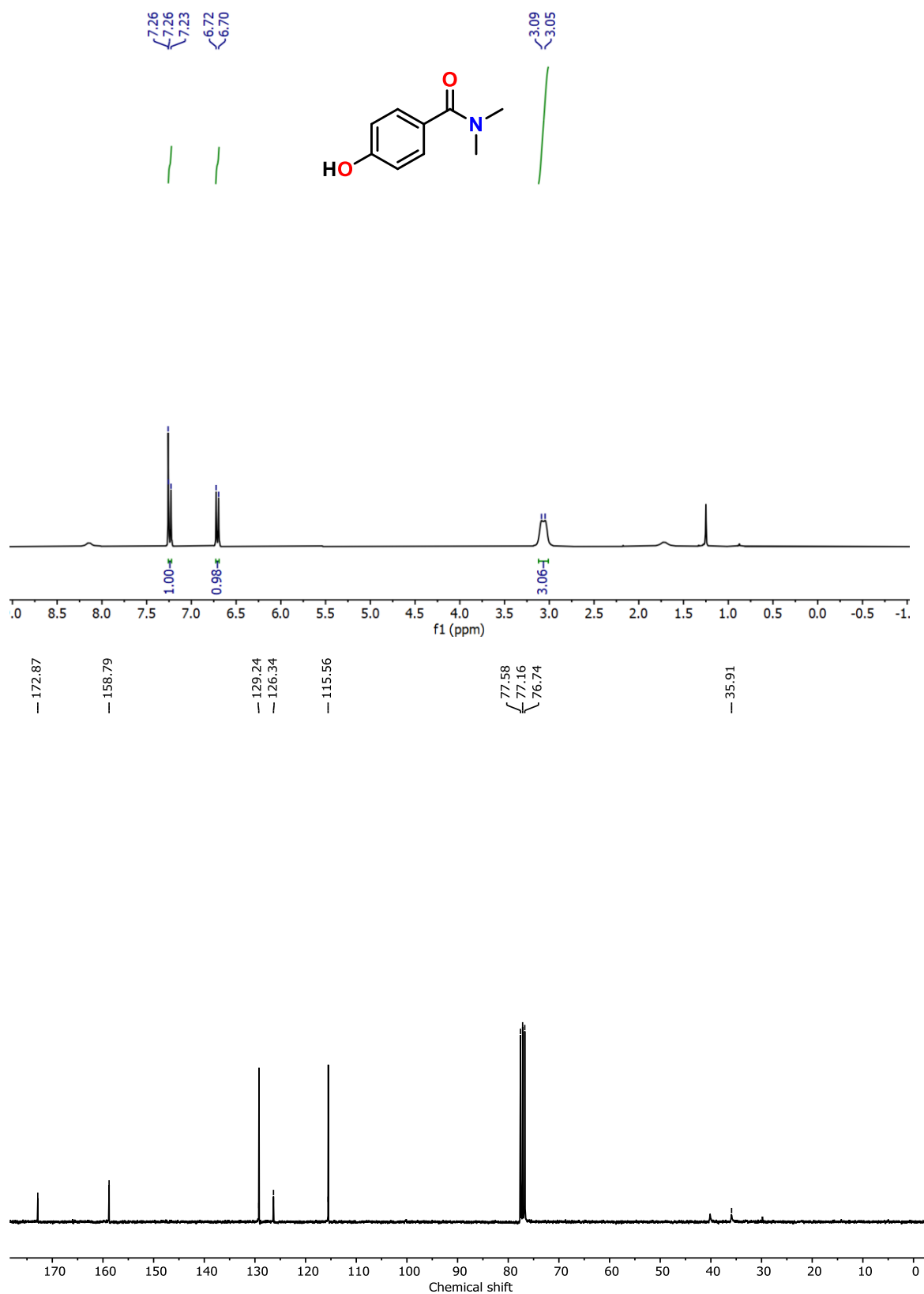
Figure 3.26. ^{1}H and ^{13}C NMR spectra of **5b** in CDCl$_3$.
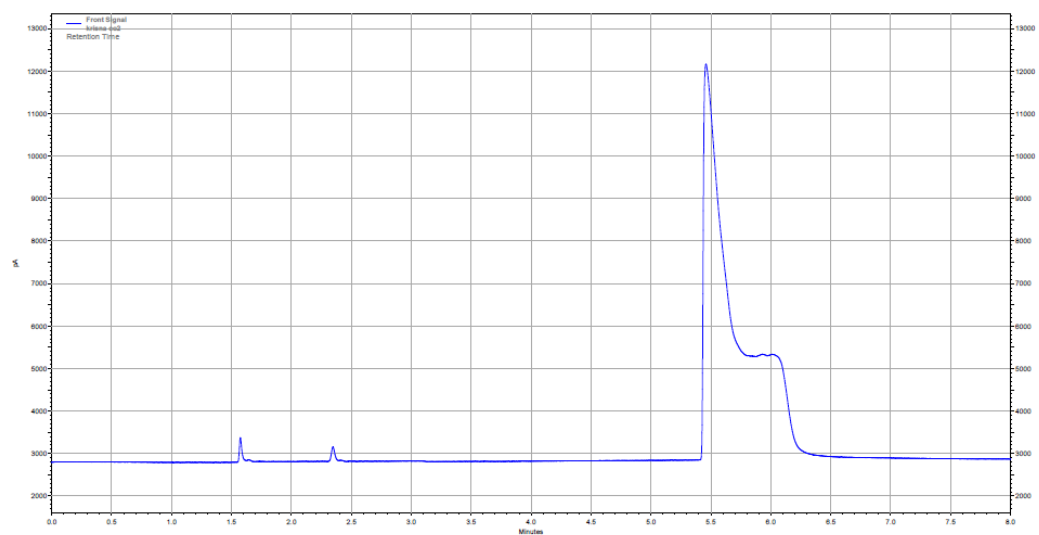
KMD1 425 (2.124) Cm (402:458-(1:364+522:621))   Scan EI+
                                                                                                        1.60e9
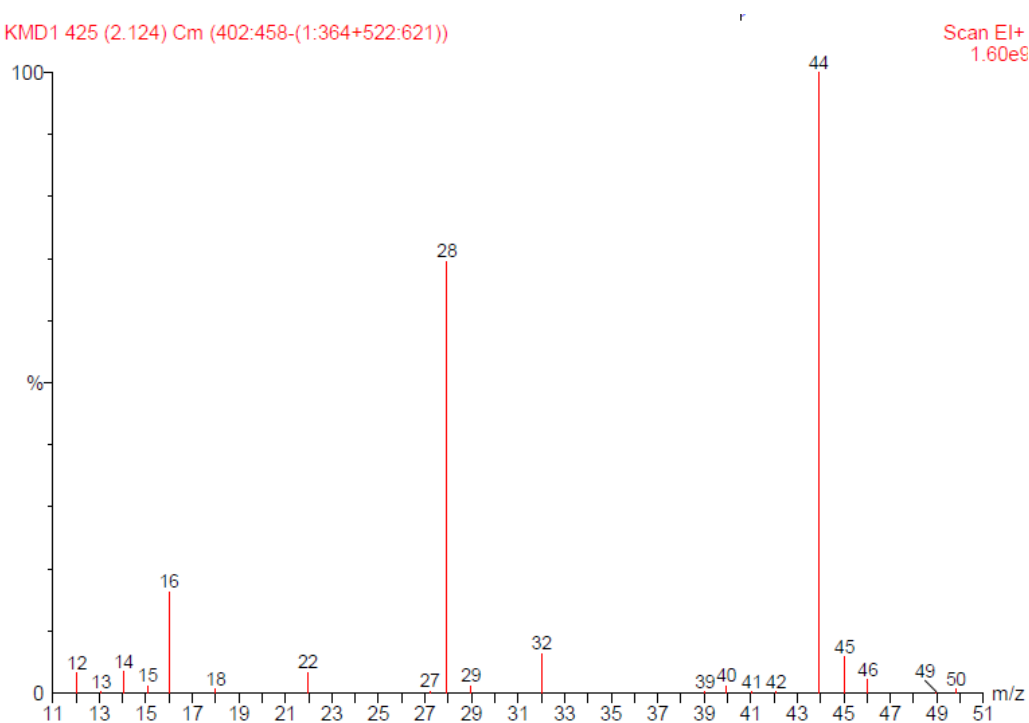
Figure 3.27. GC and GC-MS for confirmation of CO_2 gas liberation during salicylic acid and DMF reaction.
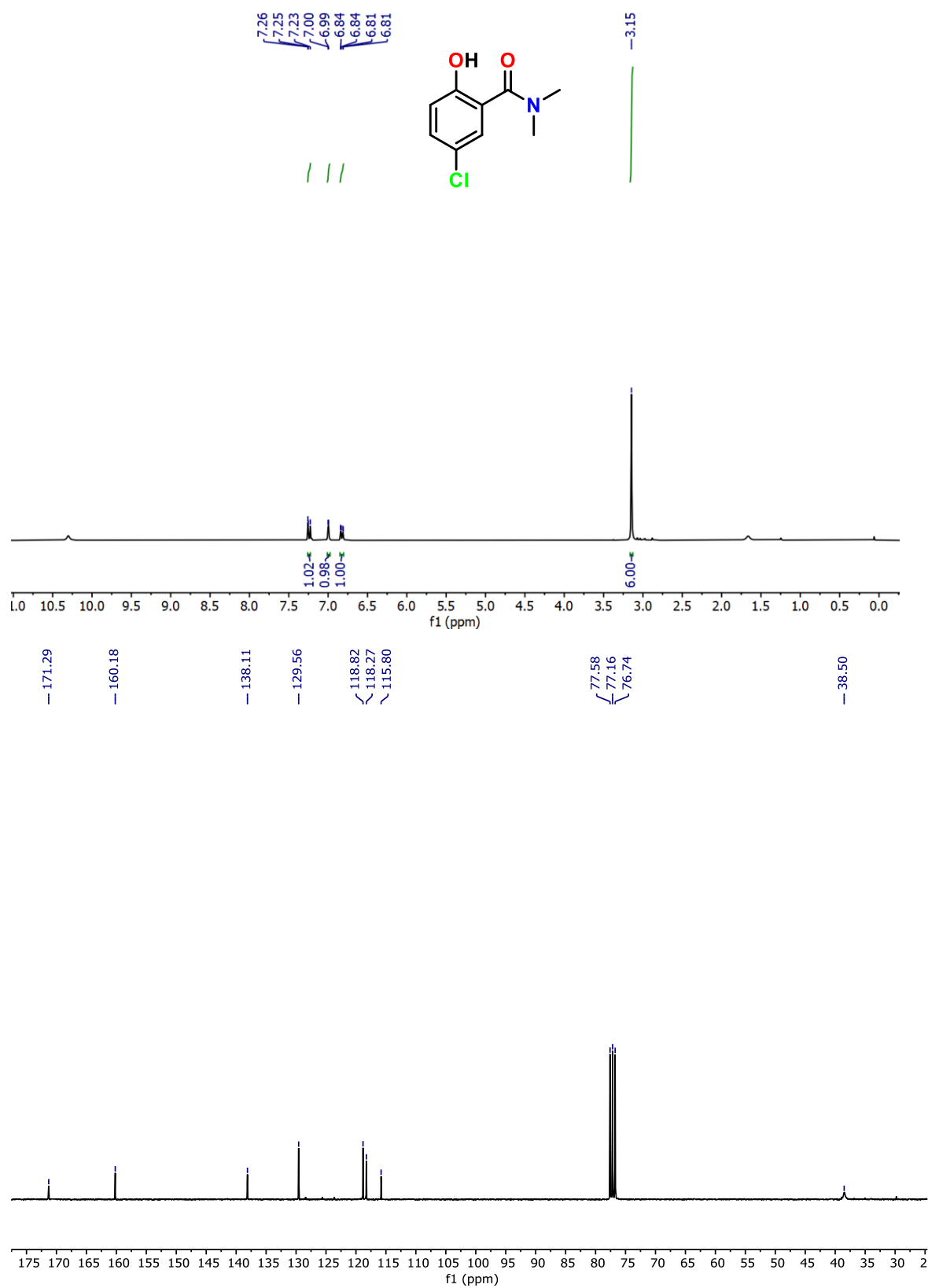
Figure 3.28. ¹H and ¹³C NMR spectra of **5c** in CDCl₃.
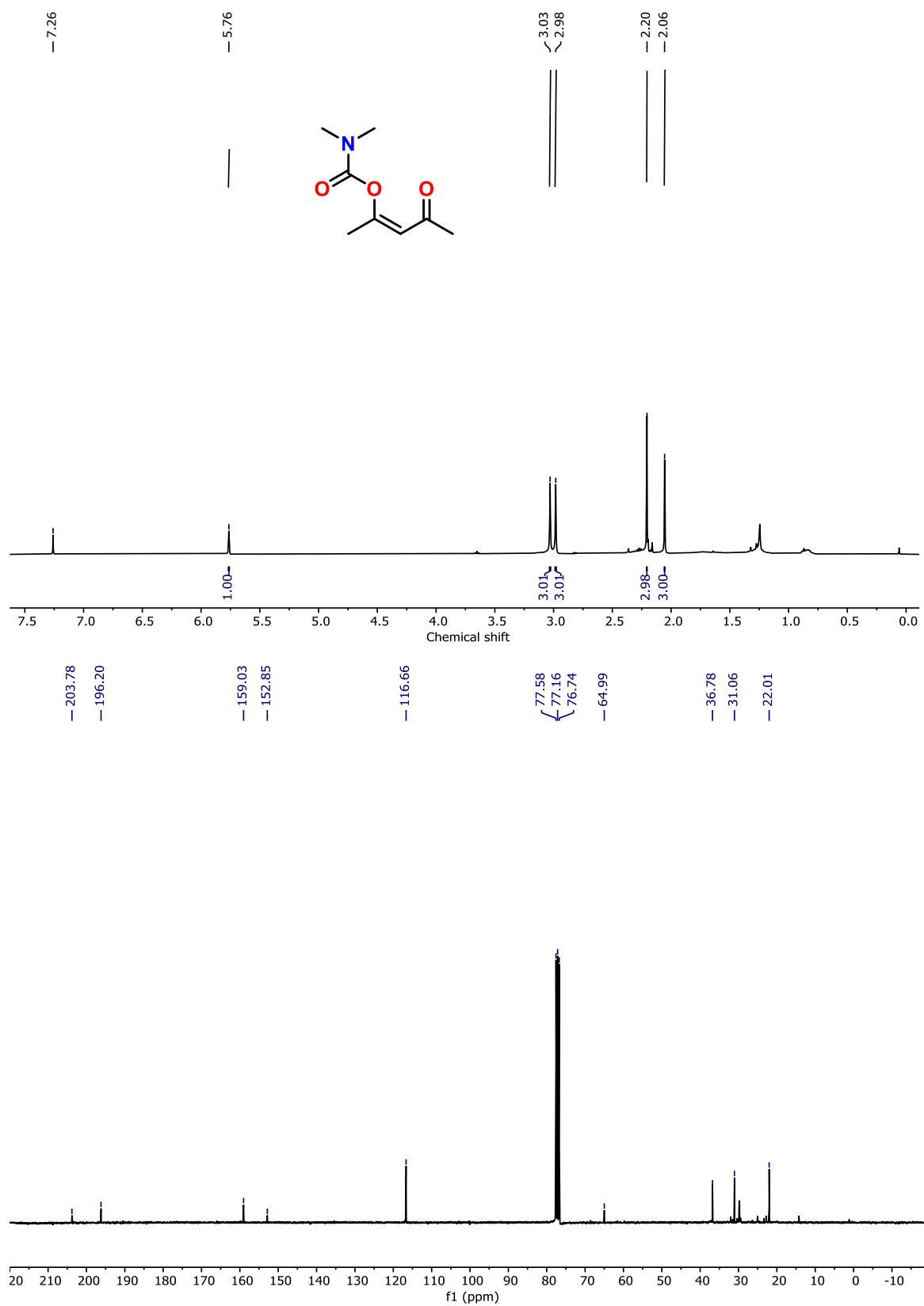
Figure 3.29. ^{1}H and ^{13}C NMR spectra of 7**a** in CDCl$_3$**.**
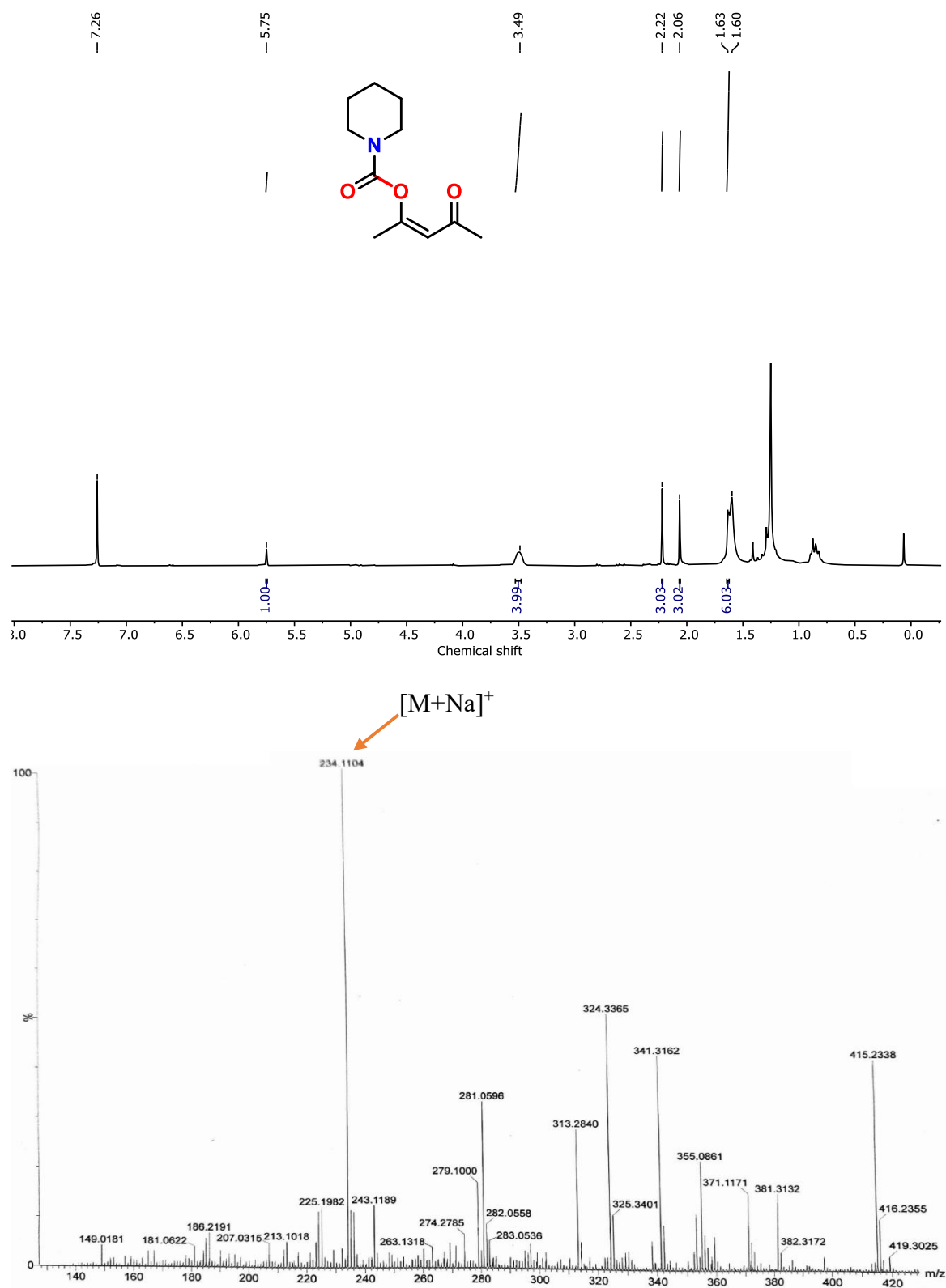
Figure 3.30. ¹H and HRMS spectra of 7**b.**
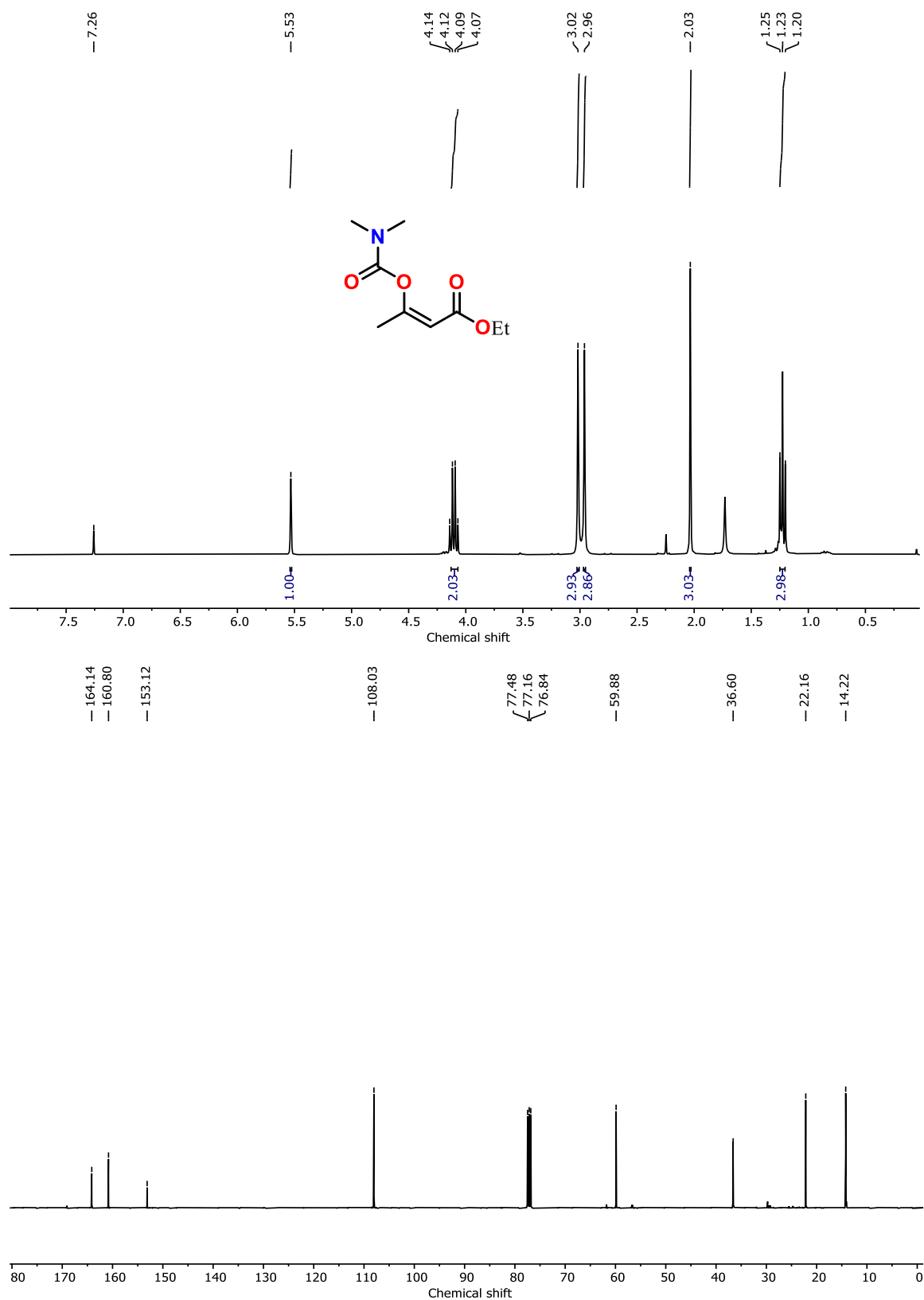
Figure 3.31. ^{1}H and ^{13}C NMR spectra of **7c** in CDCl$_3$.
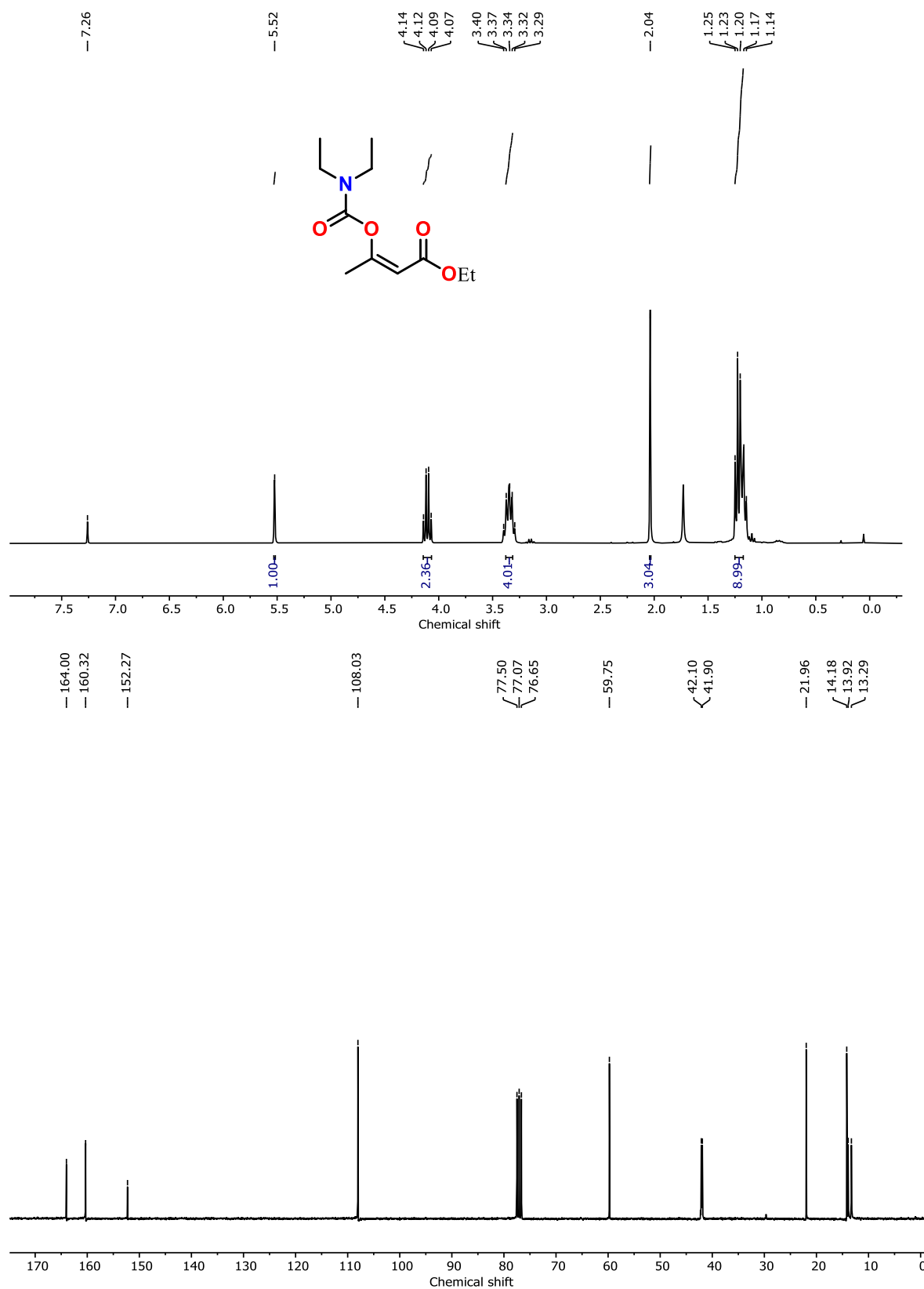
Figure 3.32. ^{1}H and ^{13}C NMR spectra of **7d** in CDCl$_3$.
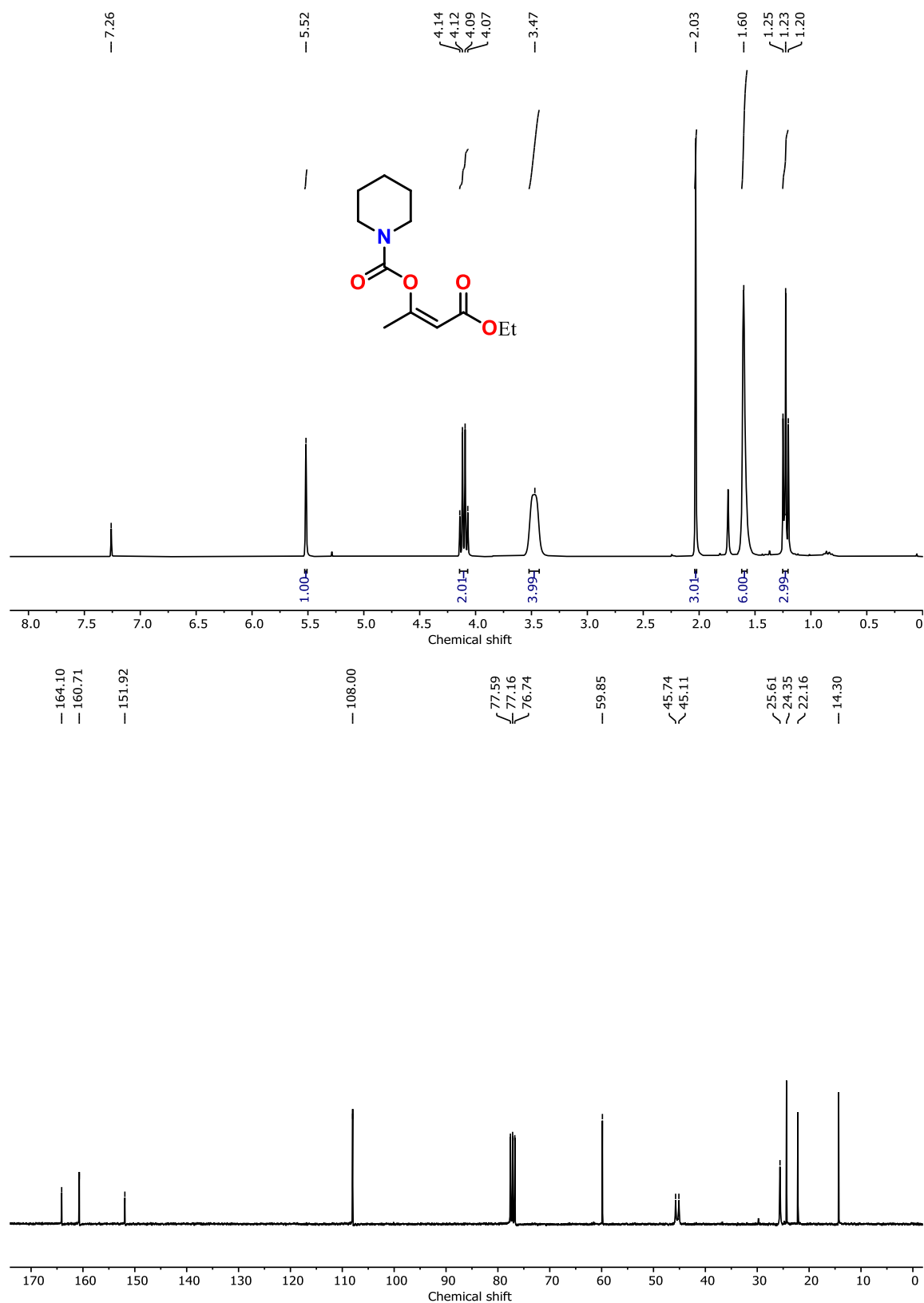
Figure 3.33. ^{1}H and ^{13}C NMR spectra of **7e** in CDCl$_3$.
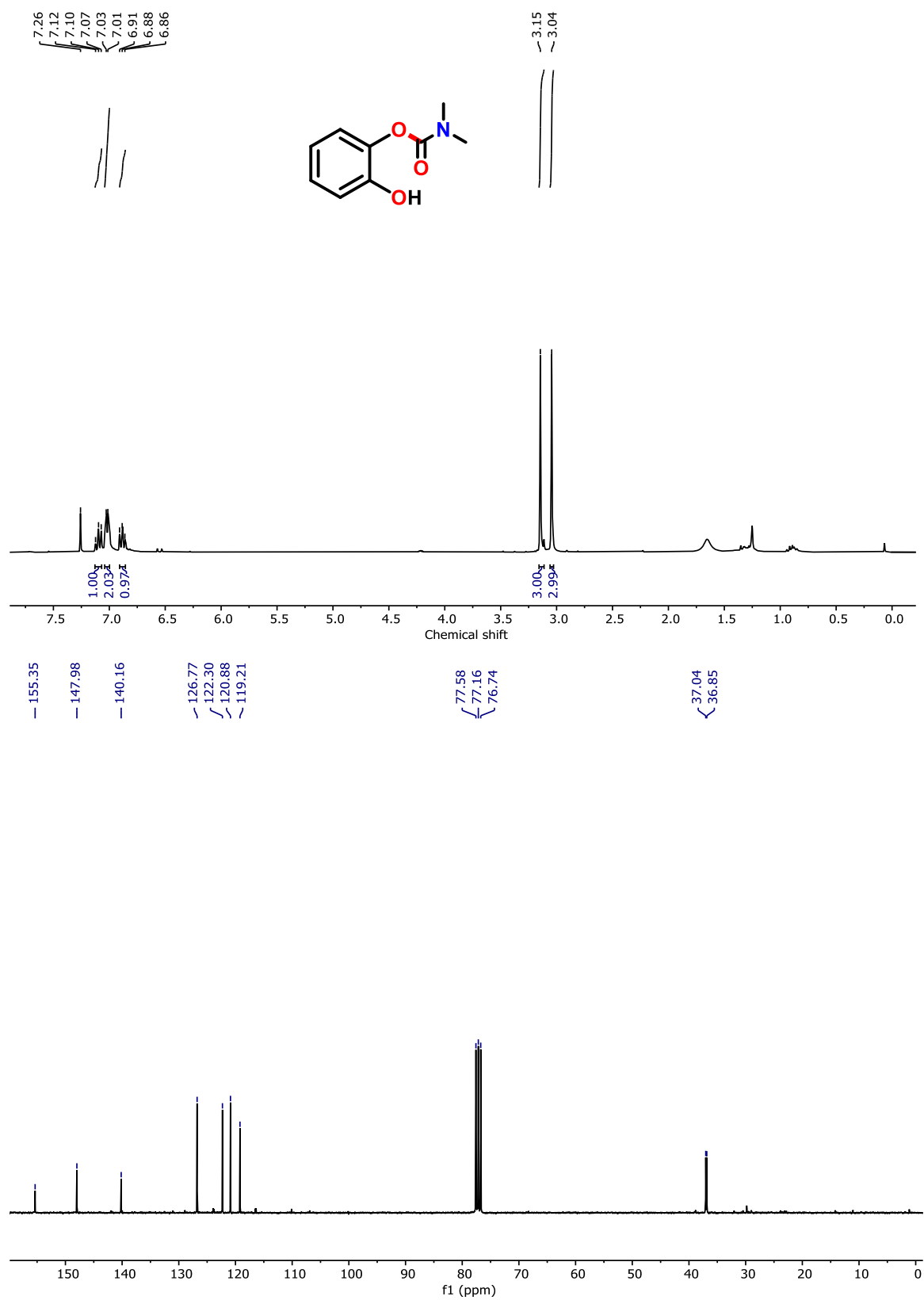
Figure 3.34. ¹H and ¹³C NMR spectra of **9a** in CDCl₃.
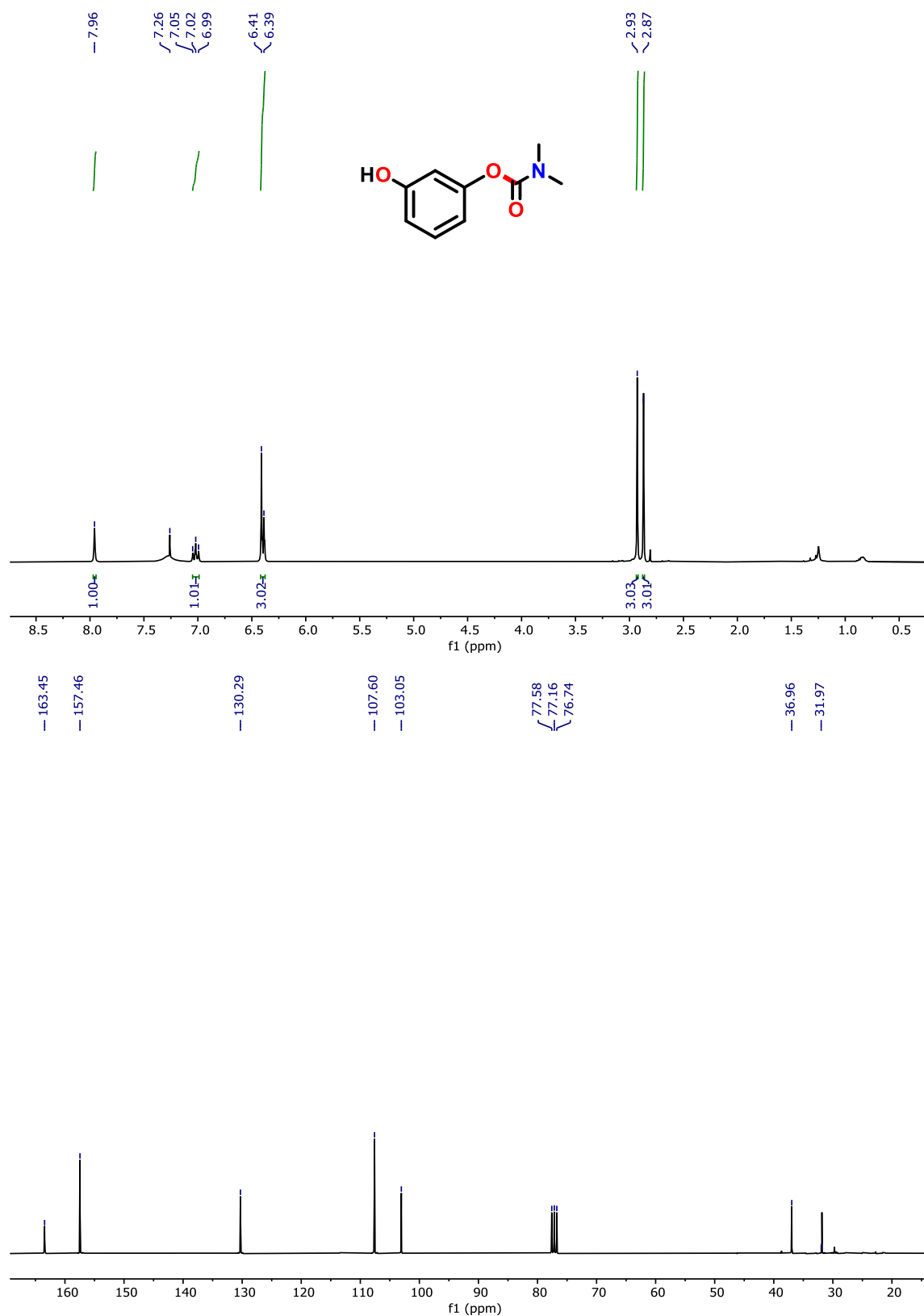
Figure 3.35. ^{1}H and ^{13}C NMR spectra of **9b** in CDCl$_3$.
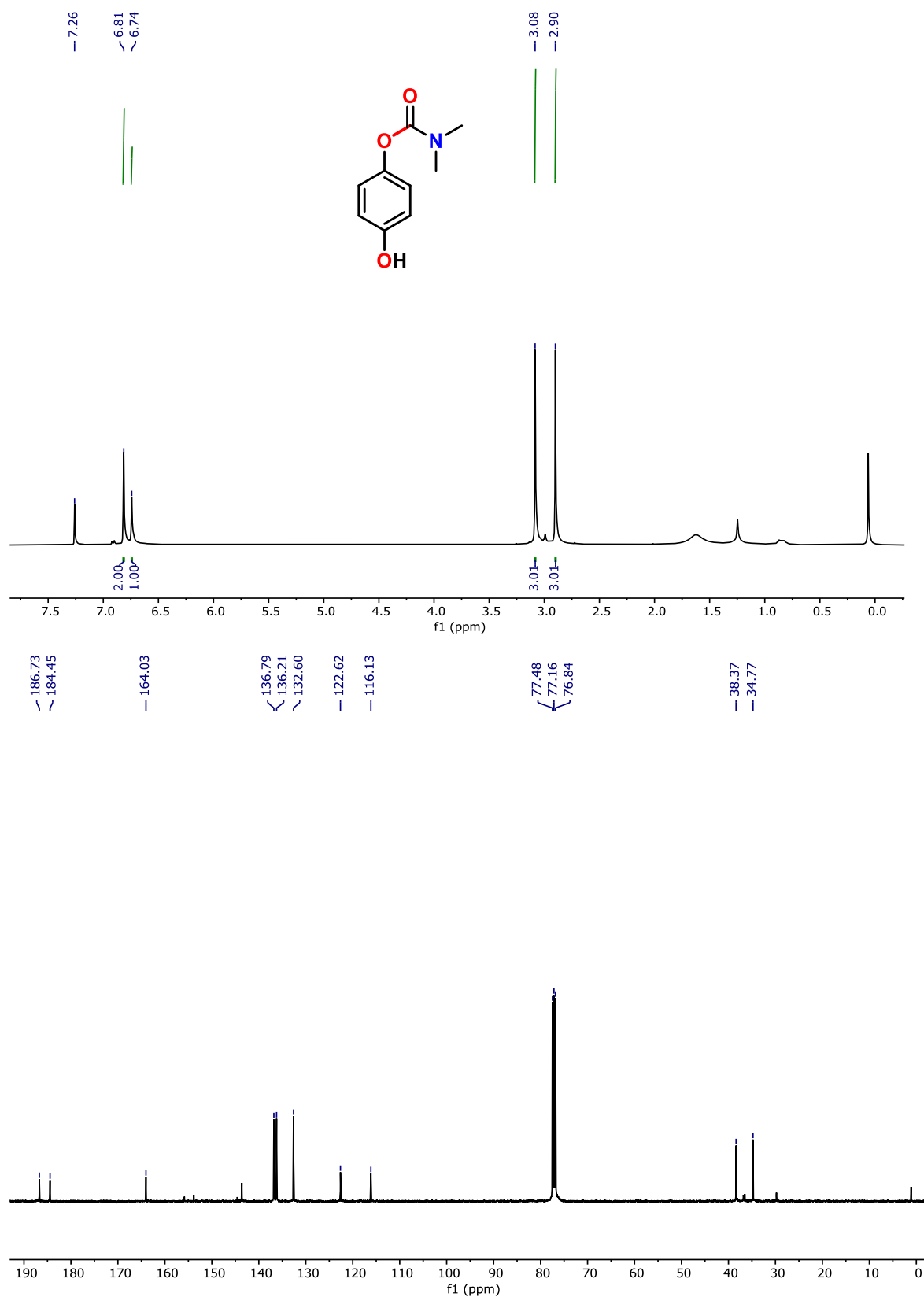
Figure 3.36. ^1H and ^{13}C NMR spectra of **9c** in CDCl$_3$.
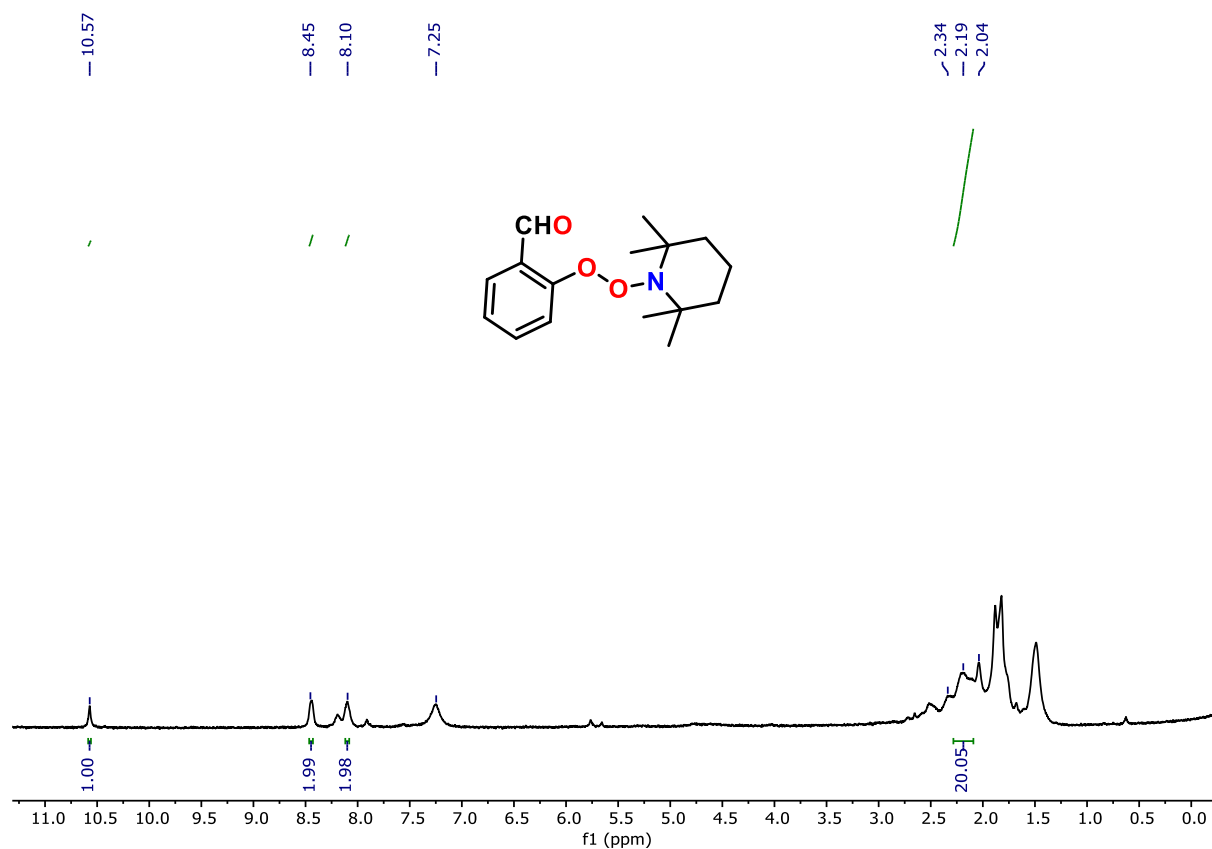
Figure 3.37. ^{1}H NMR spectra of compound **3aa** in CDCl$_3$.
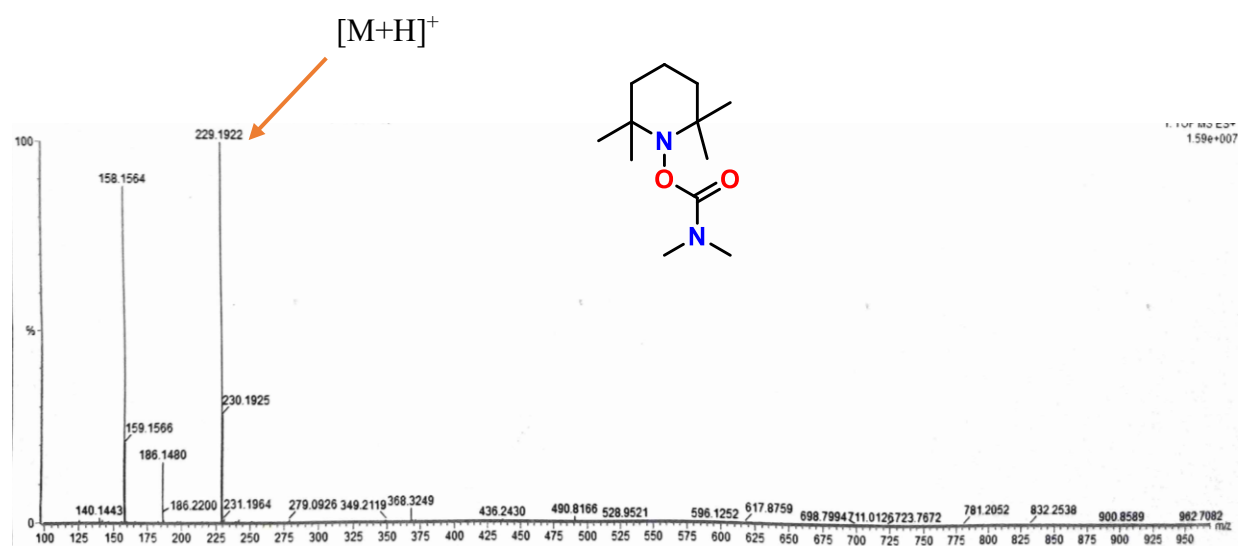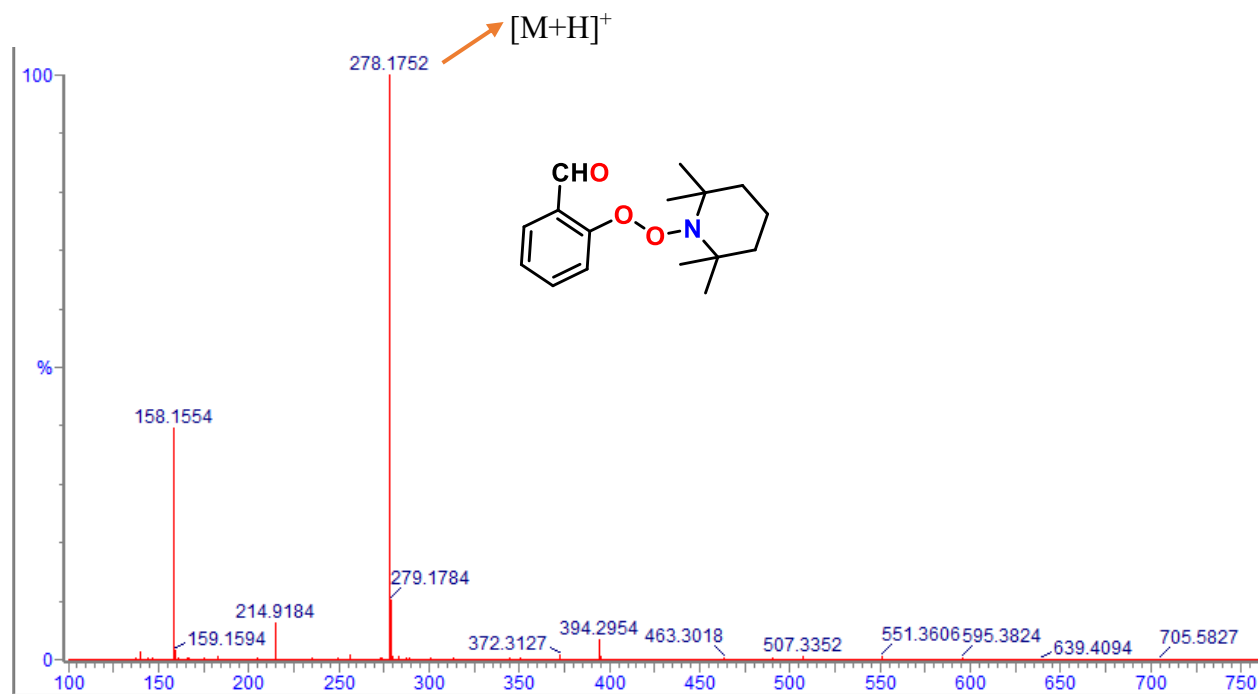
Figure 3.38. HRMS spectra of **3aa** and **3aa'** compounds.
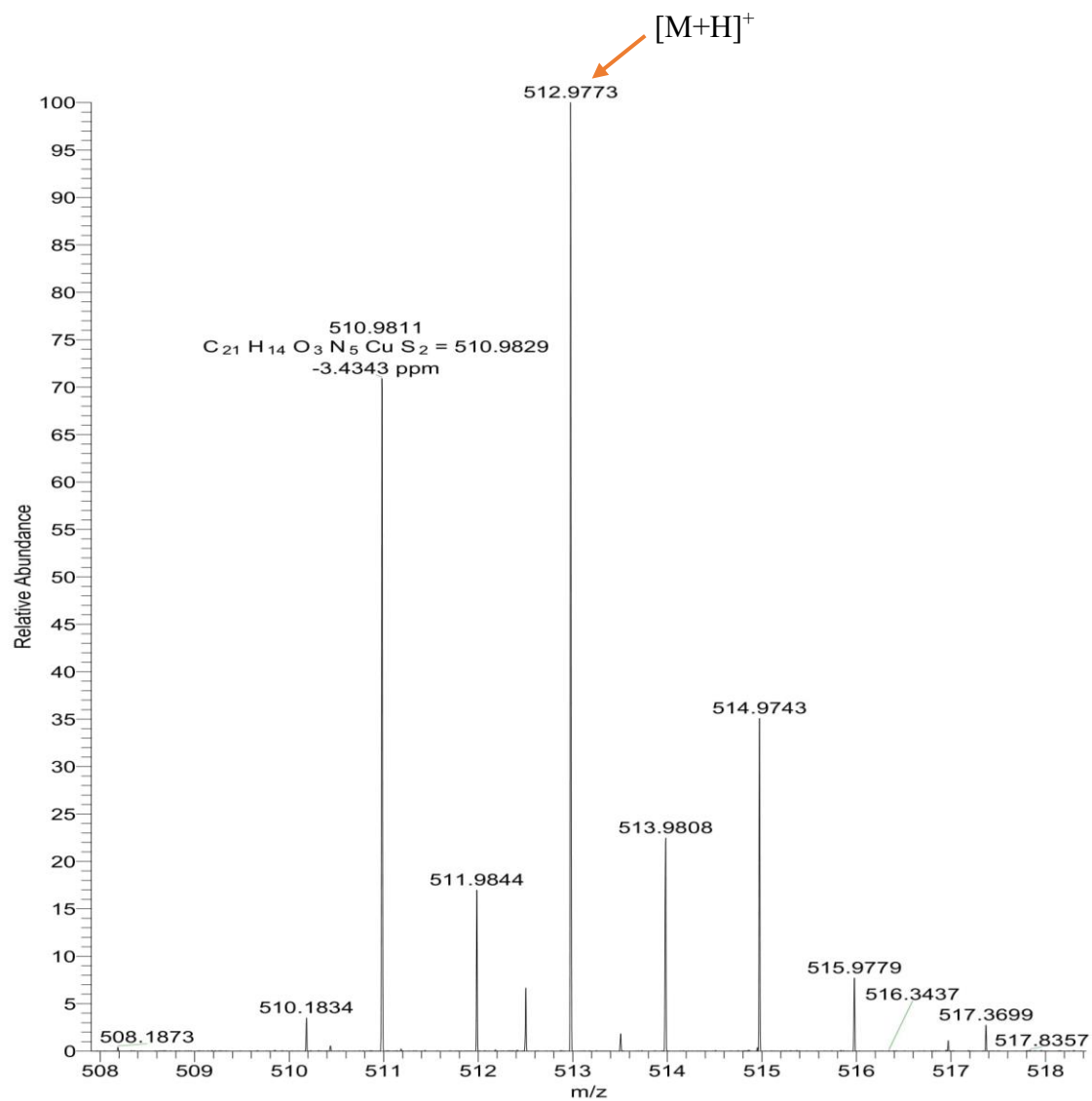
Figure 3.39. HRMS spectra of copper complex **1.**

Table 3.6 Crystallographic details of copper complex **1**

Empirical formula	$C_{21} H_{13} Cu N_5 O_3 S_2$
Formula weight	511.02
Crystal size (mm)	0.18 X 0.12 X 0.08
Crystal system	orthorhombic
Space group	*P 21 21 21*
a [Å]	6.0731(9)
b [Å]	12.067(2)
c [Å]	26.874(4)
α [°]	90
β [°]	90
γ [°]	90
volume [Å³]	1969.5(5)
Z	4
F (000)	1036
μ MoK_α [mm^{-1}]	1.359
Temperature [K]	273.15
R_{int}	0.0684
Range of h, k, l	–6/6, –12/12, –27/27
$\theta_{min/max}$ (°)	1.850/21.144
Reflections collected/Unique/observed [I > 2σ(I)]	14308/ 2154/1894
Data/restraints/parameters	2154/1/277
GOF on F^2	1.051
Final R indices [I > 2σ(I)]	$R1 = 0.0862$ $wR2 = 0.2250$
R indices [all data]	$R1 = 0.0978$ $wR2 = 0.2372$

Chapter-4

Cu(II) Promoted C(sp^3)-H Activation in Unactivated Cycloalkanes: Oxo-Alkylation of Styrenes to Synthesize β-Disubstituted Ketones

- Synthesis of β-disubstituted ketones
- Unactivated cycloalkanes as alkylating agent
- DFT studies
- Wide substrate scope
- Gram scale synthesis
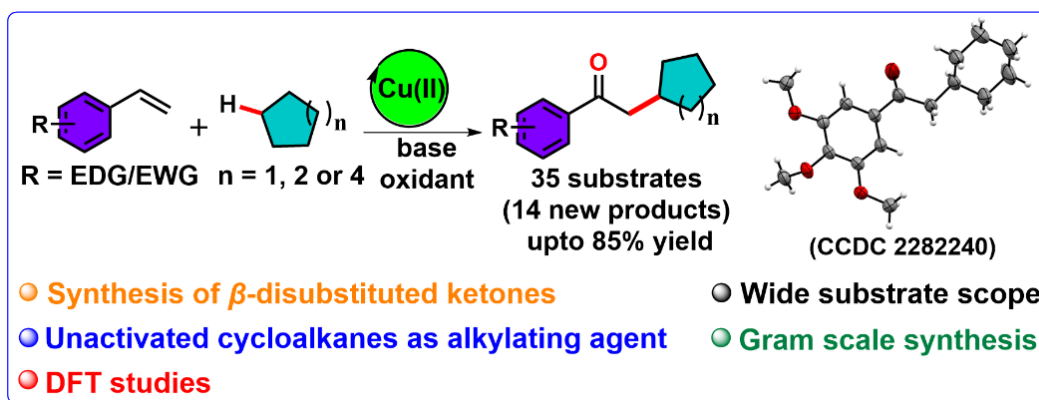
Representative publication

4.1 Introduction

The catalytic functionalization of unactivated secondary C(sp^3)−H bonds in simple alkanes has been a long-standing challenge in synthetic organic chemistry owing to the inert and non-polarized nature of C(sp^3)−H bonds.[1] Intermolecular hydrogen atom transfer (HAT) has evolved as a synthetically viable mechanism targeting the selective C−H functionalization in alkanes.[2] The generated alkyl radical after the C(sp^3)−H abstraction by HAT provides a reactive intermediate poised for bond formation with a variety of coupling partners,[3] which can lead to the production of various building blocks of high significance.

A synthetically important building block in chemistry is *β*–disubstituted ketone, which is used widely as industrial solvent, and for the construction of pharmaceuticals, polymers, biologically active compounds, and natural products[4] like taxol, phomactin *etc*.[5] Such *α/β*-substituted ketones can be traditionally synthesized by reaction of strong bases like *n*-BuLi or LDA with carbonyl compounds maintaining cryogenic conditions, followed by addition of haloalkanes.[6] This conventional enolate alkylation approach has serious drawbacks, like over-alkylation of ketones, generation of chemical wastes like metal halides and non- availability of the ketone substrates readily.[7] Owing to the wide utility and demand of *α/β*-substituted ketones as valuable synthetic building blocks, development of efficient, sustainable and atom-economical methodologies for their synthesis has received enormous attention. In contrast to *α*-branched ketones, formation of *β*-disubstituted ketone products is more challenging and less explored.

Among several alternative methodologies developed so far, transition-metal-based C-C bond formation leading to *α/β*-substituted ketones is pivotal with various starting materials and mechanistic approaches.[8-19] This includes *α*-alkylation of ketones (often hindered ketones) by secondary alcohols using Mn,[9a] Co[9b], Fe[9c] or Ru complexes[10] (Scheme 4.1 entry 1), or by borrowing hydrogen strategy using Ir catalyst,[11] oxyalkylation of alkynes using Fe(OTf)$_3$ as catalyst,[12] self-coupling[13] or cross- coupling of secondary alcohols by dehydrogenative coupling using Ru-complexes as catalyst (Scheme 4.1 entry 1),[14,15] oxidative decarbonylative alkylation-peroxidation-elimination cascade reaction with FeCl$_2$ as catalyst and DBU as base.[16] Apart from these methods, there is Grignard cross-coupling reaction using transition metals like Cu and Zn as catalyst[17] and oxo-alkylation of styrene derivatives by *N*-Hydroxyphthalimide esters as alkylating agent using photocatalysis by Ir-complex (Scheme 4.1, entry 2). [18,19] All of these methodologies,

although well-explored, are either dealt with the use of expensive Ru/Ir catalysts, which require prior preparation of their ligands and complexes, or the use of an activated species, like secondary/primary alcohol, aldehyde, acid or phthalimide ester as alkylating agent. Furthermore, the methodology involving borrowing hydrogen strategy also encounterted drawback of limited substrate scope of only sterically hindered ketones.[9a,11] However, the use of unactivated alkanes as alkylating agent for generation of β-disubstituted ketones virtually remained unexplored. The ready availability, low-cost and unpolarized nature of alkanes render them to be a demanding yet challenging candidate to be used as alkylating agent for the synthesis of β-disubstituted ketones. The fact that electron-rich $C(sp^3)$-H bond of alkanes can be functionalized into its corresponding alkyl radicals when activated by a suitable catalyst,[20] motivated us to explore the direct coupling of alkanes and alkenes in a novel oxidative alkylation reaction in presence of alkaline oxidizing environment and appropriate metal catalyst. In the advent of the high demand to utilize low-cost earth-abundant metals as catalysts in important organic transformations, we have developed our methodology with low-cost transition metal salt ($CuCl_2$) for the efficient, sustainable and one-step atom economical synthesis of β-disubstituted ketones *via* oxidative alkylation of styrene derivatives using unactivated cycloalkanes as alkylating agents. In this regard, a similar study on the $Cu(OTf)_2$ (20 mol%) and TBP at 100 ˚C for 12 h have obtained internal alkenes without employing any base.[21] Ours is altogether a new approach towards the synthesis of substituted ketones, where TBHP acts as both the radical source and oxidizing agent, 1-methylimidazole as the base and $CuCl_2$ as catalyst. The Cu(II) catalyst initiates the radical reaction, which carries on to give two hydrogen atom transfer (HAT) processes to yield the desired keto product *via* oxidative alkylation. Here the base plays a crucial role in carrying out the second HAT mechanism. This proposed mechanism is well supported by controlled experiments (including radical scavengers), Hammett analysis, kinetic isotope effect experiments as well as computational analysis. The use of simple alkanes as the alkylating agent and earth-abundant low-cost Cu(II) salt as a catalyst have added a green aspect towards the synthesis of industrially important β–disubstituted ketones considering the sustainability in incorporation of low-cost hydrocarbons directly into complex organic compounds without the need for pre-functionalization.
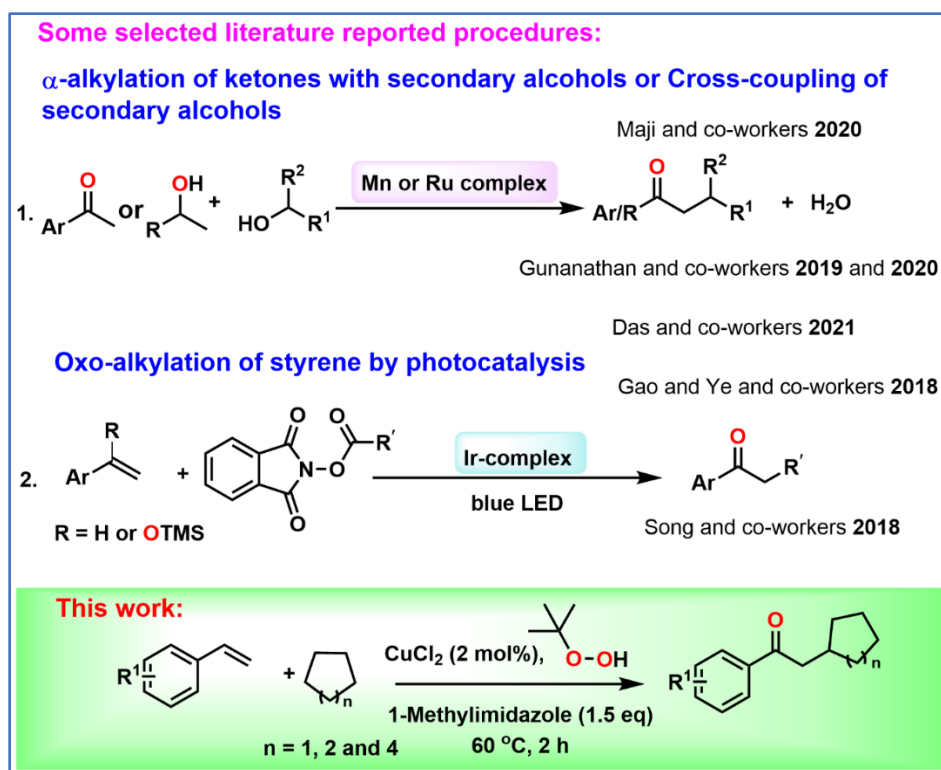
Scheme 4.1 Comparison of literature reported procedures for synthesis of β-disubstituted ketones with our synthetic strategy

4.2 Results and Discussion

To test the hypothesis, we initiated our investigation from the reaction of 4-methoxystyrene (**1a**) as the model alkene substrate and cyclohexane (**2a**) as the source of symmetrical β–disubstituted alkyl group. In our very first attempt of the reaction with earth-abundant metal salt $CuCl_2$ as the catalyst, the desired oxidative alkylated styrene derivative **3a** was observed in 40% yield upon employing 10 mol% of the catalyst, 3 equiv *tert*–butyl hydroperoxide (TBHP) and 2 equiv imidazole at 80 ˚C for 12 h (Table 4.1, entry 1), where, TBHP and imidazole act as oxidant and base respectively. Surprisingly, with another *N*-heterocyclic base oxazole, the desired product was not obtained at all (Table 4.1, entry 2). This rendered us to examine further the action of base in this reaction. Reactions with benzoxazole, 1,2,4-triazole and piperidine gave similar results as oxazole (Table 4.1, entries 3-5), however with DBU, the desired product was obtained in low yield (30 %) (Table 4.1, entry 6). The yield of desired product was found to improve (55%) with 1,2-dimethylimidazole as the base (Table 4.1, entry 7). Interestingly, the highest yield of product

(80%) was obtained employing 1-methylimidazole (minimum 1.5 equiv) as the base (Table 4.1, entry 9). Further reduction of base loading affected the yield of the product drastically and in absence of base, desired product formation did not occur at all (Table 4.1, entries 10,11). DFT calculations show that the TS-activation barrier for the HAT mechanism (*vide infra*) with 1-methylimidazole is comparatively lower (16.4 kcal/mol) than other bases like oxazole, benzoxazole, imidazole *etc.* (Table 4.5 and 4.6). Although TS-activation barrier of 1,2-dimethylimidazole is slightly lower than that of 1-methylimidazole, experimentally lesser yield was obtained with 1,2-dimethylimidazole.

Table 4.1. Optimisation of base for the reaction between 4-methoxystyrene and cyclohexane.[a,b]
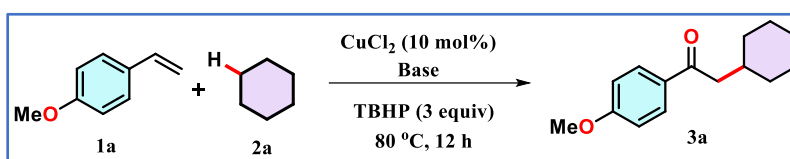
Entry	Cat. (mol%)	Base (equiv)	Solvent	% Yield[b]
1	CuCl$_2$ (10)	Imidazole (2)	Cy	40
2	CuCl$_2$ (10)	Oxazole (2)	Cy	ND
3	CuCl$_2$ (10)	Benzoxazole (2)	Cy	ND
4	CuCl$_2$ (10)	1,2,4-triazole (2)	Cy	ND
5	CuCl$_2$ (10)	Piperidine (2)	Cy	ND
6	CuCl$_2$ (10)	DBU (2)	Cy	30
7	CuCl$_2$ (10)	1,2-dimethylimidazole (2)	Cy	55
8	CuCl$_2$ (10)	1-methylimidazole (2)	Cy	80
9	**CuCl$_2$ (10)**	**1-methylimidazole (1.5)**	**Cy**	**80**
10	CuCl$_2$ (10)	1-methylimidazole (1)	Cy	45
11	CuCl$_2$ (10)	-	Cy	ND
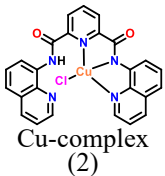
[a]Catalytic conditions: 4-methoxy styrene (1 mmol), TBHP (70 wt % in water, 3 equiv), catalyst (10 mol %), cyclohexane (3 mL), 80 °C temperature, 12 h; Cy = Cyclohexane (3 mL). [b]Isolated yield based on column chromatography. ND: Not detected.

With this preliminary success, other parameters like catalyst loading, oxidant, temperature, and time have been screened to find out the simplest and most effective version of our methodology. Among the various oxidants screened, only TBHP displays maximum efficiency for this catalytic

reaction (Table 4.2, entries 1-6). Reducing the time and temperature of the reaction (Table 4.2, entries 7-10) resulted in maximum 80% yield at 60 °C for 2 h (Table 4.2, entry 9). Finally, we have reduced the catalyst loading gradually from 5 to 1 mol% (Table 4.2, entries 11-13) and observed the maximum yield of 80% with a minimum of 2 mol% of catalyst (Table 4.2, entry 12). Further reduction in catalyst loading from 2 mol% to 1 mol% reduced the product yield to 50% (Table 4.2, entry 13). We have also screened the reaction in presence of a copper (II) complex, (as shown in Table 4.2 entry 14), which was developed in our lab previously[22] and was found to efficiently catalyze the reaction providing the product in 80% yield (Table 4.2, entry 14). However, the ease of reaction with a commercially available metal salt with comparable yield makes it predominant over metal complexes, where presynthesis of ligands and the complex needs to be done along with their purification. With hydrated copper(II) salts as catalysts, the yields were poor (Table 4.2 entries 15-17). Further, to ascertain whether the oxidation state of the metal catalyst has a role to play in this methodology or not, reactions with Cu(I) salts were monitored and it was found that they gave much lesser yield of product (Table 4.2 entries 18, 19). Hence, it can be predicted that the +2 oxidation state was more favorable in this reaction mechanism than the +1 oxidation state. We have also monitored the reaction in presence of several other metal salts such as $FeCl_2.4H_2O$ and $CoCl_2$ and product was formed in both the cases with lesser yield (Table 2, entries 20, 21). Hence the reaction was best suited with anhydrous $CuCl_2$ as catalyst. Increasing the oxidant loading did not alter the yield of the product (Table 4.2, entry 22), however its decrease impacted the yield (Table 4.2, entry 23). Noteworthy to mention that in all the above reactions, cyclohexane is used as both the coupling partner and solvent. Repeating the reaction with stoichiometric amount of cyclohexane in benzene afforded the desired product, however in low yield (55%) (Table 4.2, entry 24). Finally, reactions without $CuCl_2$ and without TBHP separately concluded that both $CuCl_2$ and TBHP along with 1- methylimidazole are all necessary to get the desired product for this catalytic reaction (Table 2, entries 25, 26). Screening all the various parameters, it was found that the use of styrene derivative (1 equiv), tert-butyl hydroperoxide (3 equiv), 1-methylimidazole (1.5 equiv) and $CuCl_2$ (2 mol%) in cyclohexane (**2a**) (3 mL) at 60 °C for 2 h is the optimal reaction condition to achieve desired *β*-disubstituted ketone (Table 4.2, entry 12) in 80% yield.

Table 4.2: Optimisation of reaction conditions [a,b]
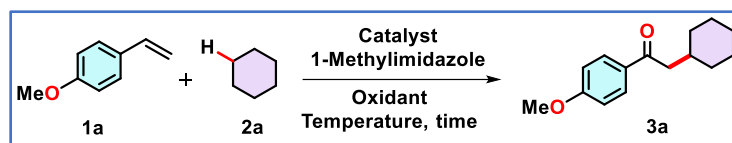
Entry	Cat. (mol %)	Oxidant (equiv)	Solvent	T (°C)/t (h)	% Yield[b]
1	CuCl$_2$ (10)	TBHP (3)	Cy	80/12	80
2	CuCl$_2$ (10)	DTBP (3)	Cy	80/12	40
3	CuCl$_2$ (10)	BPO (3)	Cy	80/12	25
4	CuCl$_2$ (10)	TBPB (3)	Cy	80/12	20
5	CuCl$_2$ (10)	DCP (3)	Cy	80/12	20
6	CuCl$_2$ (10)	TBHP[C] (3)	Cy	80/12	ND
7	CuCl$_2$ (10)	TBHP (3)	Cy	60/12	80
8	CuCl$_2$ (10)	TBHP (3)	Cy	60/6	80
9	CuCl$_2$ (10)	TBHP (3)	Cy	60/2	80
10	CuCl$_2$ (10)	TBHP (3)	Cy	40/2	25
11	CuCl$_2$ (5)	TBHP (3)	Cy	60/2	80
12	**CuCl$_2$ (2)**	**TBHP (3)**	**Cy**	**60/2**	**80**
13	CuCl$_2$ (1)	TBHP (3)	Cy	60/2	50
14	Cu-complex (2)	TBHP (3)	Cy	60/2	80
15	CuCl$_2$.2H$_2$O (2)	TBHP (3)	Cy	60/2	10
16	CuSO$_4$.5H$_2$O (2)	TBHP (3)	Cy	60/2	10
17	Cu(OAc)$_2$.H$_2$O (2)	TBHP (3)	Cy	60/2	15
18	CuI (2)	TBHP (3)	Cy	60/2	10
19	CuCl (2)	TBHP (3)	Cy	60/2	50
20	FeCl$_2$.4H$_2$O (2)	TBHP (3)	Cy	60/2	40
21	CoCl$_2$ (2)	TBHP (3)	Cy	60/2	30
22	CuCl$_2$ (2)	TBHP (4)	Cy	60/2	80
23	CuCl$_2$ (2)	TBHP (2)	Cy	60/2	60
24	CuCl$_2$ (2)	TBHP (3)	Cy/Benzene (0.5 /2.5)	60/2	55
25	-	TBHP (3)	Cy	60/2	ND
26	CuCl$_2$ (2)	-	Cy	60/2	ND

[a]Reaction scale: 4-methoxy styrene (1 mmol); Cy = Cyclohexane (3 mL). [b]isolated yield based on column chromatography. ND: Not detected.[C] TBHP in decane. DTBP = *tert*-butyl peroxide, TBPB = *tert*-butyl perbenzoate, BPO = benzoyl peroxide, DCP = dicumyl peroxide.

The optimized reaction condition was explored for generality in the alkene and alkane counterparts by initiating with various styrene derivatives keeping the alkane part fixed at cyclohexane (Table 4.3). Styrenes having electron-donating as well as electron-withdrawing groups provided their corresponding *β*–disubstituted ketone products in moderate to good yield (70-85%). Styrene derivatives possessing $-CH_3/-OCH_3$ at various positions (**3a-3i**) afforded the product in good yields (72-85%). All the synthesised products were characterized by ^1H and ^{13}C NMR spectroscopy. Additionally, compound **3h** was characterized by single crystal X-ray diffraction analysis. This methodology also works well in presence of electron-withdrawing halogen groups like fluoro, bromo and chloro at benzene ring (**3k-3p**). On the other hand, in presence of strong electron-withdrawing groups like *p/m*–NO_2, *p*—CF_3 and *m*-CN the corresponding products (**3q-3t**) are formed in moderate yield (69-72%). When 1-naphthylstyrene was subjected to react with cyclohexane, the yield of the corresponding product (**3u**) was decreased (63%), may be due to steric crowding at the adjacent benzene ring.[23] Notably, this strategy can be expanded to heterocyclic arenes containing terminal alkenes (**3v**).

Table 4.3: Substrate scope with different styrene derivatives and cyclohexane [a,b]
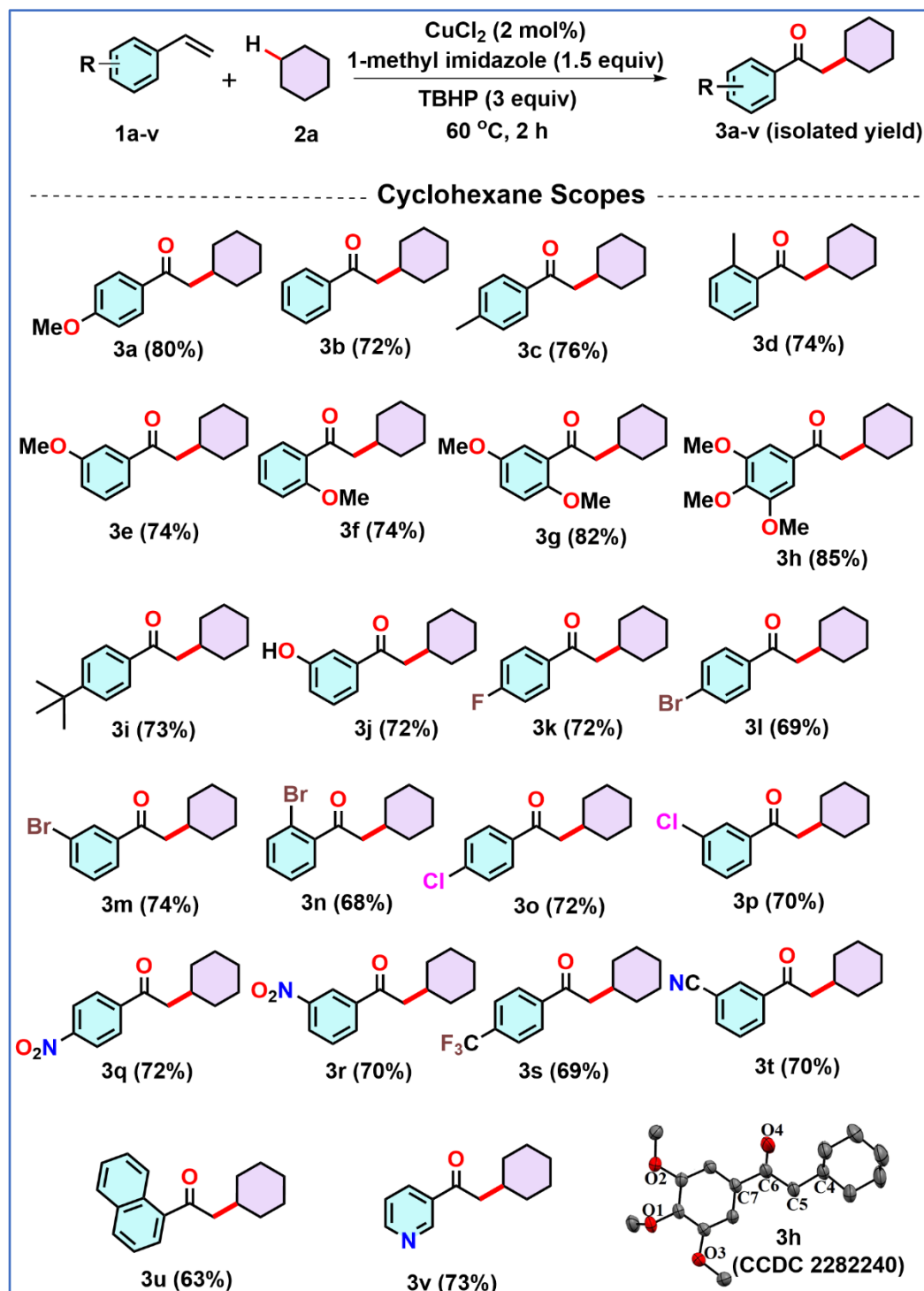
[a]Reaction conditions: **1a-u** (1 mmol), TBHP (70 wt % in water, 3 equiv.), CuCl$_2$ (2 mol%), 60 °C temperature, 2 h. [b]Isolated yield after column chromatography

To gain more insight into the substituent effect on the reaction mechanism, we extended our study towards Hammett analysis by taking some electron-donating and electron-withdrawing substituents on the styrene ring (Figure 4.1). The   Hammett analysis was done by a competitive study between styrene and substituted styrene derivatives and the consumption was monitored by ^{1}H NMR spectroscopy. A linear relationship was observed when relative rates of styrene consumption log (k_X/k_H) were plotted against the substituent constant (Figure 4.1). Hammett studies revealed a negative slope of ρ = -0.6356 (R^2 = 0.9328). This indicates the transition state involved in the reaction mechanism probably will have lower charge density than starting materials for both electron-withdrawing and electron-donating substituents.[24]
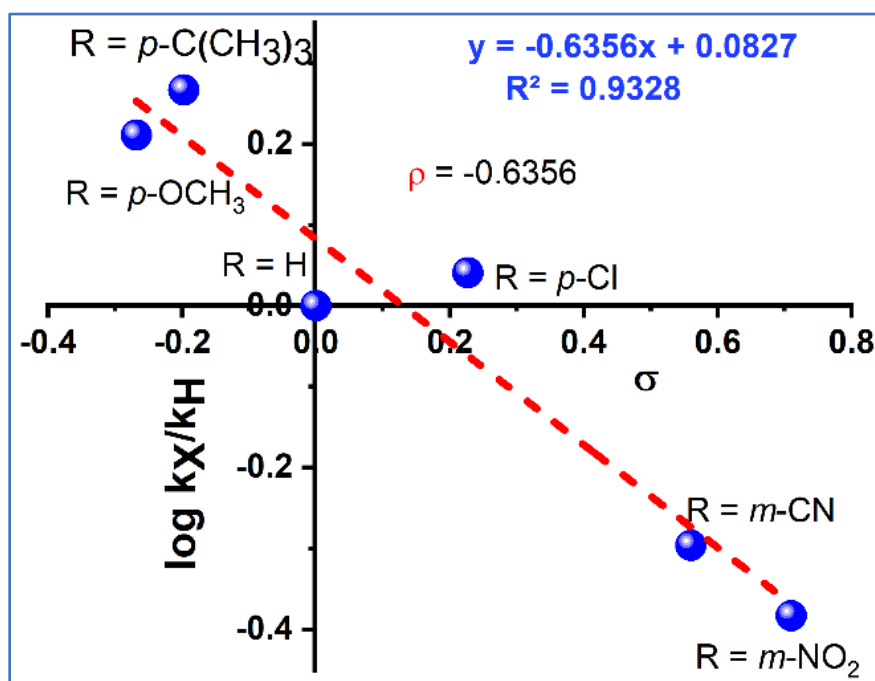
Figure 4.1 Hammett plot of the reaction between substituted styrene derivatives and cyclohexane under optimized reaction condition.

In an endeavor to expand the scope of the methodology, the alkylating part was varied from cyclohexane to cyclopentane and cyclooctane (Table 4.4). It was observed that both cyclopentane and cyclooctane provided their corresponding coupling products with electron-donating and electron-withdrawing styrenes (**3aa-3af** and **3aa'-3ag'**) in a comparatively lesser yield than the products with cyclohexane. This may point towards the stability of the generated species from the cycloalkane part being stable in six-membered ring structure rather than five or eight-membered

ring structure.[25] Acyclic alkanes like *n*-hexane and *n*-pentane as well as aliphatic alkenes were also subjected to react in identical reaction conditions but for both cases, reaction was unsuccessful.

Table 4.4: Substrate scope with different styrene derivatives and cyclopentane and cyclooctane [a,b]
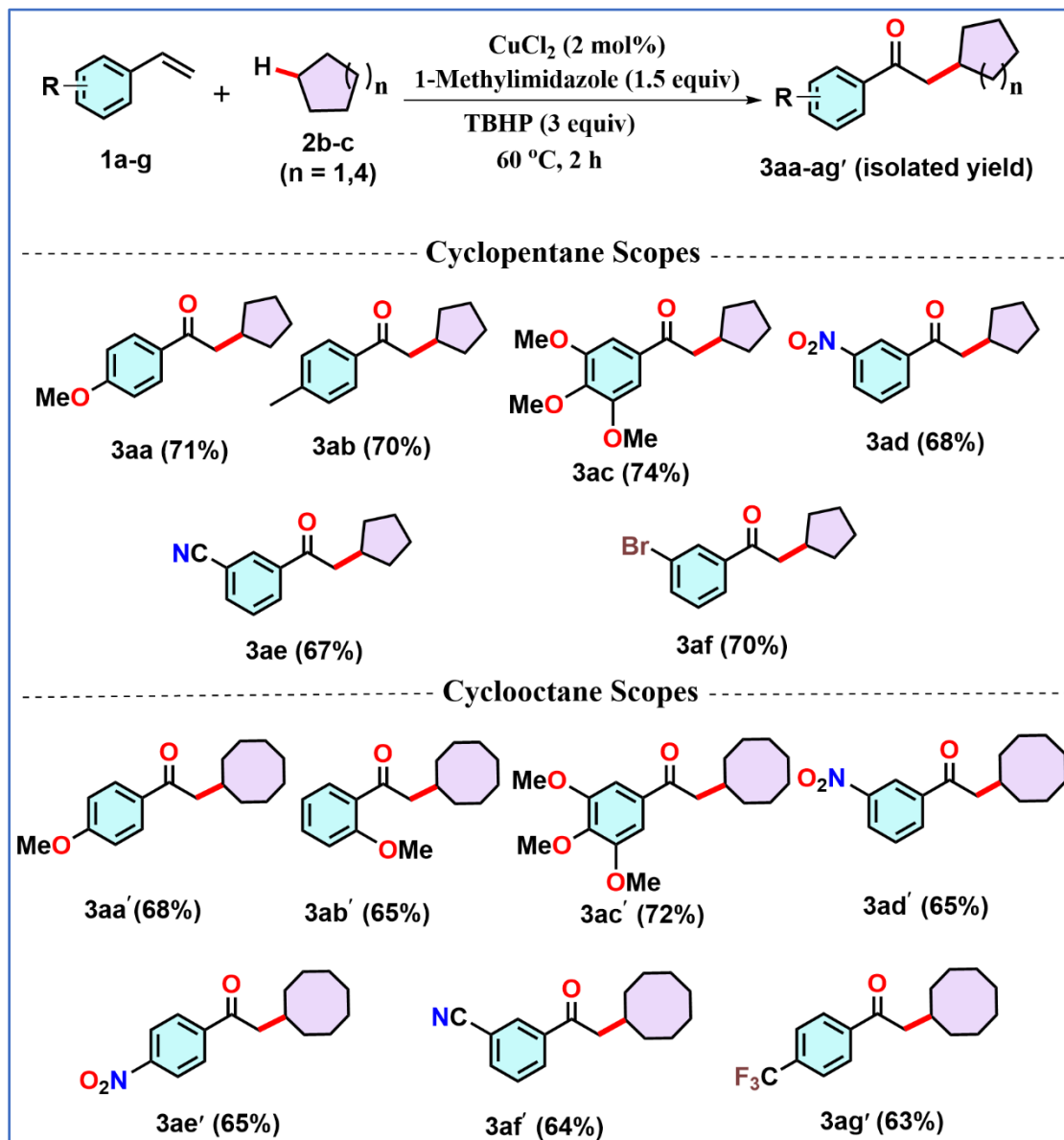
ᵃReaction conditions: **1a-g** (1 mmol), TBHP (70 wt % in water, 3 equiv.), CuCl$_2$ (2 mol%), 60 ˚C temperature, 2 h. ᵇIsolated yield after column chromatography.

To check the scalability of this protocol we have performed gram-scale reactions with styrene (**1b**) and cyclopentane (**2b**), cyclohexane (**2a**) and cyclooctane (**2c**) in our optimized condition. In all the cases, corresponding ketone products were obtained with 60%, 68%, and 58%

yields of products respectively (Scheme 4.2a). Further a variety of organic transformations were conducted to functionalize the ketone moiety of *β*-disubstituted compounds, which briefly explores its utility as a synthetic core. The carbonyl group present in compounds **3b** and **3o** can be converted easily to their corresponding oxime derivatives, giving **4a** and **4b** in 70% and 60% yields respectively (Scheme 4.2b). The oxime derivative **4a** was further reacted with polyphosphoric acid (PPA), wherein, it undergoes Beckmann rearrangement to give the corresponding rearranged amide derivative **5**. The compound **3b** was also subjected to react with organometallic reagents *n*-BuLi and *n*-butyl magnesium chloride in THF and diethyl ether solvents respectively to obtain the corresponding butylated alcohol derivative **6** in moderate yield (50%).
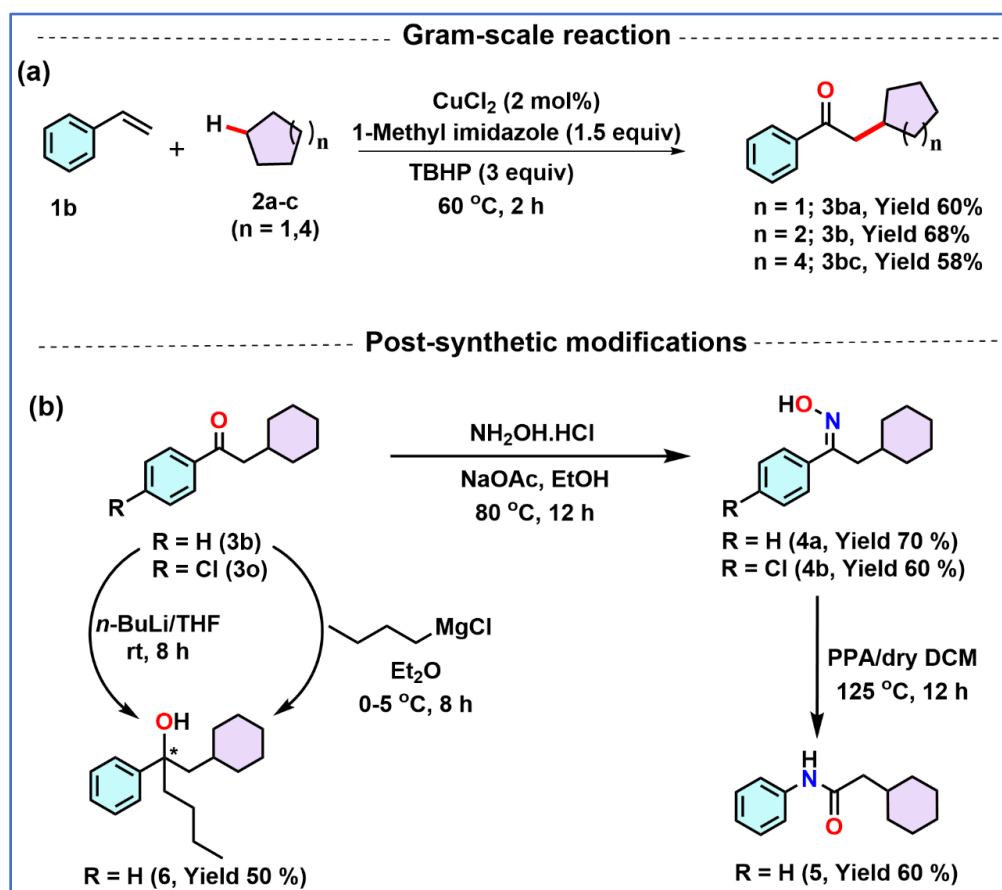
Scheme 2: (a) Gram-scale reactions and (b) post-synthetic modifications

Various control experiments were performed to get detailed mechanistic pathway of this reaction. In this regard, we have performed the reaction in presence of radical scavenger 2,2,6,6-tetramethylpiperidine-1-oxyl (TEMPO) and butylated hydroxy toluene (BHT) under optimized reaction conditions. Expectedly, the reaction between 4-methoxystyrene (**1a**) and cyclohexane

(2a) was quenched and a minute quantity of desired ketone **(3a)** product was obtained (Scheme 4.3). The radical adducts formed by coupling between cyclohexyl radical and TEMPO/BHT were detected by ^{1}H NMR and HRMS (Figure 4.53 and Figure 4.54) which suggests that the reaction proceeds through a radical intermediate.
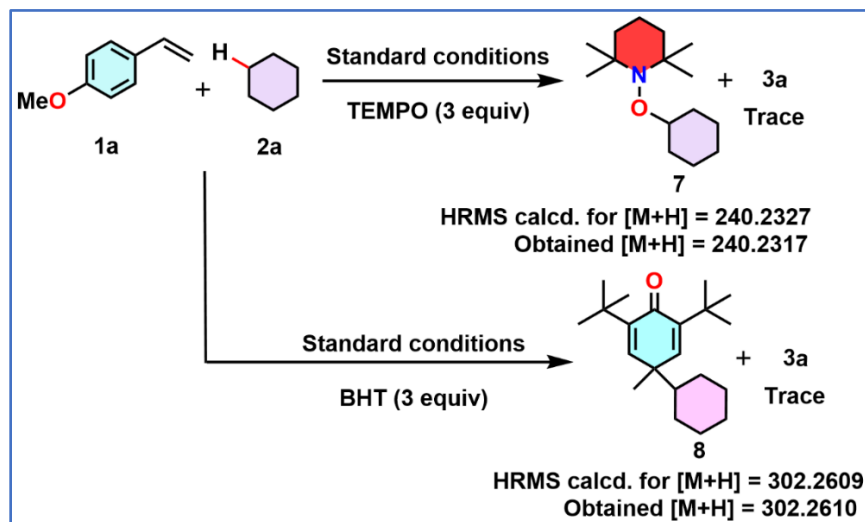
Scheme 4.3: Radical trapping experiment.

For a majority of radical reactions, the radical initiation step is the rate-determining step.[26] With a view to further get mechanistic insights about the rate-determining step of the reaction, the kinetic isotope effect (Scheme 4.4) was investigated by both competitive and parallel reactions between cyclohexane (C_6H_{12}) and deuterated cyclohexane (C_6D_{12}) with styrene (**1b**) under standard reaction conditions. K_H/K_D value was found to be ~5.67 (Figure 4.55) and ~5.15 (Figure 4.56) for competitive and parallel reactions respectively. This result signifies that the $C(sp^3)$-H bond cleavage from cycloalkane is the rate-determining step.
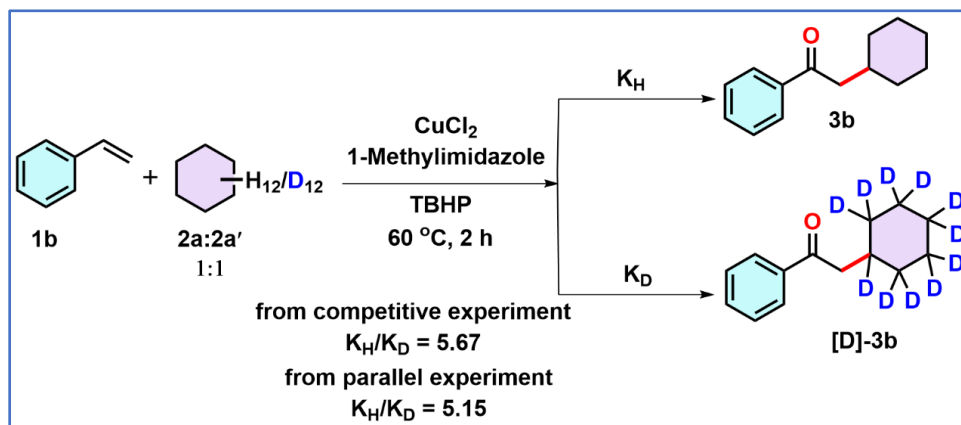
Scheme 4.4: Kinetic Isotope Effect (KIE) experiment.

On the basis of the aforementioned experimental findings (controlled and kinetic experiments), a plausible mechanism *via* radical pathway has been proposed as presented in Scheme 4.5. The Cu(II) species induces the formation of ^{t}BuOO$^\bullet$ from ^{t}BuOOH and itself gets reduced to Cu(I).[25] This Cu(I) under oxidizing environment of the reaction mixture can get oxidized back to the Cu(II) species for another catalytic cycle.[26] Meanwhile, the generated ^{t}BuOO$^\bullet$ takes up one hydrogen atom (HAT) from cyclohexane to produce cyclohexyl radical, which adds up on the styrene molecule to generate the most stable radical **A**. The ^{t}BuOO$^\bullet$ radical present in the reaction mixture makes an addition reaction with **A** to generate **B**, wherefrom a hydrogen atom transfer (HAT) by base gives our desired ketone product along with side product **C**. The side-product 2-(*tert*-butoxy)-1-methyl-2,3-dihydro-1*H*-imidazole (**C**) formed as a result of this concerted mechanism was detected by LCMS analysis (Figure 4.57).
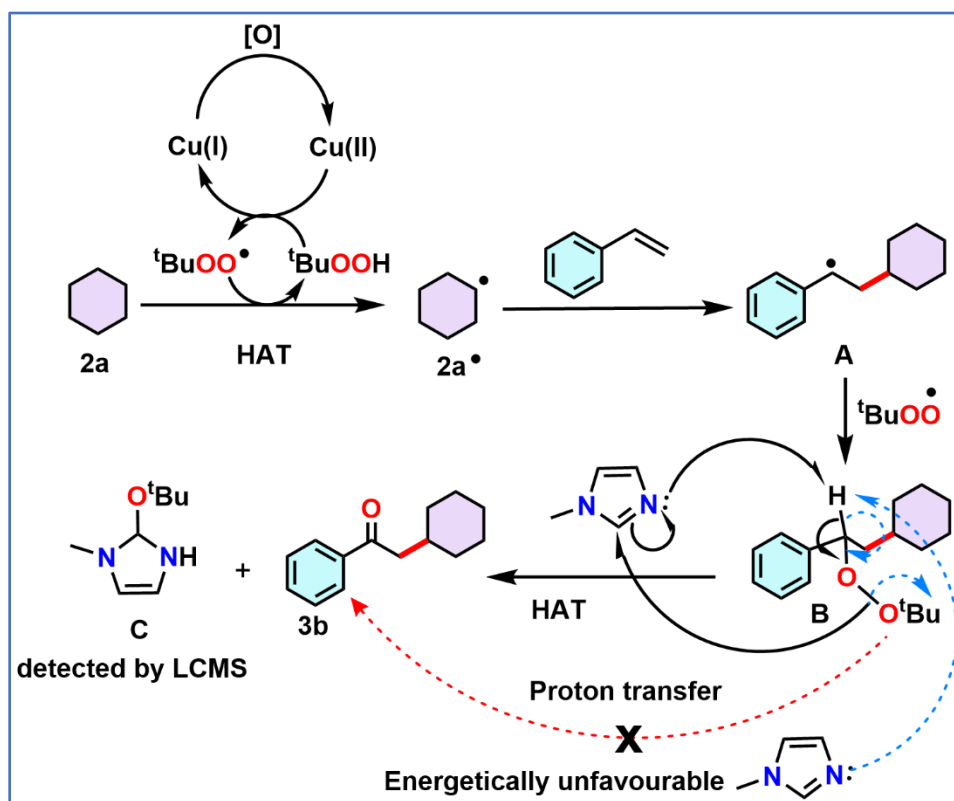
Scheme 4.5. Plausible catalytic cycle.

Further, to get more insight about the feasibility of our proposed reaction mechanism energetically, theoretical calculations were performed using density functional theory (Figure 4.2). We hypothesize that ^{t}BuOO$^\bullet$ radical resulting from oxidation of *tert*-butyl hydroperoxide (TBHP)

in presence of Cu(II) initiates hydrogen atom transfer (HAT) mechanism from the cyclohexyl substrate, **2a** *via* **TS1** at a calculated barrier of $\Delta G^{\ddagger}$ = 20.0 kcal/mol (at UB3LYP-D3(BJ)/6-311+G(d,p)/CPCM (Cyclohexane).[27] Simultaneously, Cu(II) is converted to Cu(I) species in the reaction medium. **TS1** is followed by an intermediate constituting of the newly generated TBHP and the cyclohexyl radical, **2a•** at ΔG = 16.4 kcal/mol. Notably, a new equilibrium is established when the generated TBHP goes out to the bulk medium. Therefore, starting from here we hypothesize a separate reaction energy profile in Figure 2.[28] This cyclohexyl radical then makes a coupling reaction with styrene and forms benzylic radical intermediate (**A**), overcoming a paltry barrier of 6.4 kcal/mol through **TS2**. The formation of **A** is highly exoergic with respect to **2a•** (ΔG = -22.5 kcal/mol). Notably, intermediate **A** is more stable than the other possible addition product 2-phenyl-2-cyclohexyl methyl radical. After that, ^{t}BuOO• radical couples with intermediate **A** and forms peroxide product **B** at ΔG = -61.6 kcal/mol. C_α-H activation of **B** by 1-methylimidazole (**1-MeImd**) occurs at a predominantly high barrier of 26.3 kcal/mol (**TS3(PT)**) through proton transfer (PT) mechanism. However, ^{t}BuO• mediated HAT by (**1-MeImd**) coupled to a concerted mechanism of peroxide bond cleavage has a significantly reduced kinetic expense though **TS3**, $\Delta G^{\ddagger}$ = 16.4 kcal/mol. Hence, we hypothesize that the HAT mechanism should predominate over
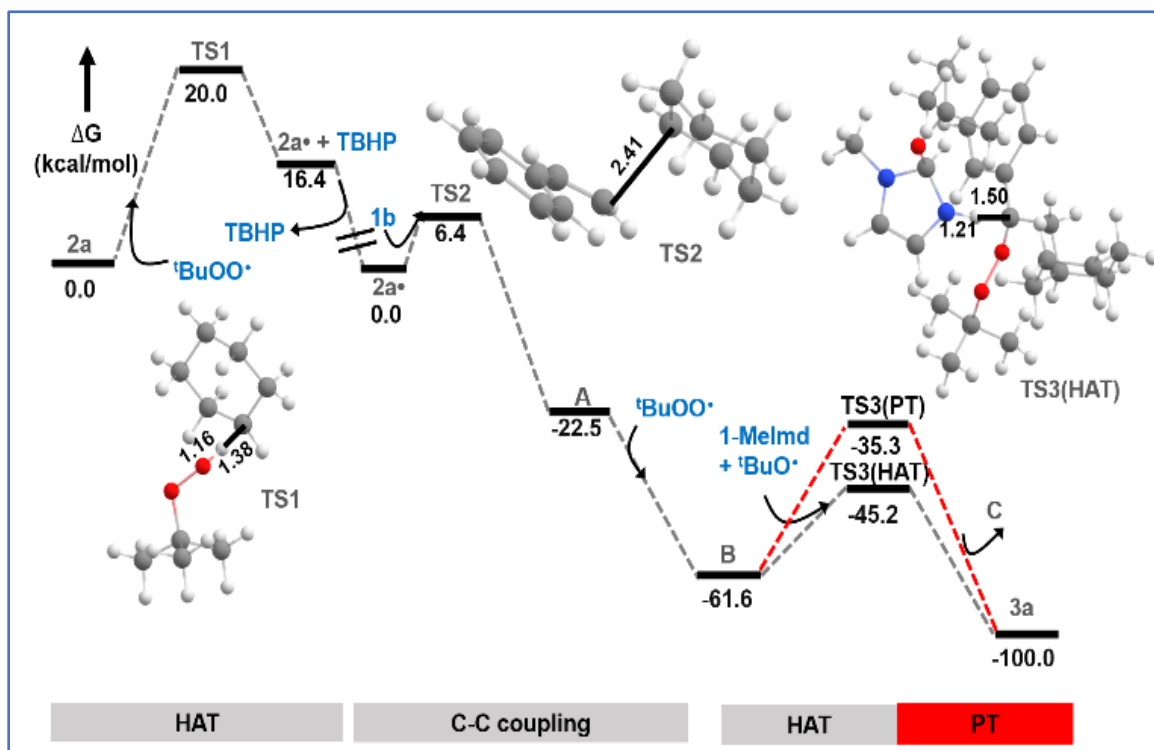
Figure 4.2. Energy profile diagram at UB3LYP-D3(BJ)/6-311+G(d,p)/CPCM(Cyclohexane)

the PT mechanism to generate the *β*-disubstituted ketone as the eliminated product at ΔG= -100.0 kcal/mol. To summarize, from DFT calculations, the HAT mechanism conducted with *tert*-butyl peroxide radical to dissect the strong (sp^3)C-H bond of cyclohexane *via* **TS1**, featuring the largest activation free energy of all the three steps predicted, appears to be the rate determining step (RDS). This is agreement to experimental deuterium labelling studies indicating a C-H activation step as rate limiting (*vide supra*).

4.3. Conclusion

In conclusion, we have developed an unprecedented protocol, for the synthesis of *β*-disubstituted ketone from styrene derivatives, which proceeds through a radical-mediated oxidative alkylation pathway, using earth-abundant Cu(II) salt as catalyst. This method employs commercially available unactivated cycloalkanes as alkylating agents directly without any functionalization. This robust synthetic strategy is compatible with diverse functional groups and scalable for gram-scale synthesis. Mechanistic studies and DFT analyses revealed the precise efficiency of Cu(II), TBHP, and 1-methylimidazole in the catalytic cycle involved. Two HAT mechanisms come into play to generate the product, among which, the first one generating the cycloalkyl radical is the rate-determining step. The synthetic versatility of the *β*-disubstituted ketone products has been examined by their transformation into appealing derivatives which have potential use as synthetic building blocks. Given the significant medicinal value of *β*-branched ketones, the pharmaceutical sector may find our protocol valuable and more affordable.

4.4. Experimental Section

4.4.1. Materials and reagents: All styrene derivatives are synthesized by literature-reported procedures.[29] *n*-BuLi (1.6 M in hexane) and anhydrous CuCl$_2$ were purchased from Spectrochem chemicals. THF is distilled using Na and benzophenone under N$_2$ conditions and used for reaction purposes. Commercially available hydroxylaminehydrochloride and *n*-butylmagnesium chloride (2.0 M in diethyl ether, Sigma-Aldrich) were used. Analytical thin layer chromatography (TLC) was performed on pre-coated silica gel 60 F254. Visualization on TLC was achieved with UV light (254 nm). Column chromatography was carried out using activated neutral alumina as the stationary phase and EtOAc/Hexane as the mobile phase.

4.4.2. Instrumentation: ^{1}H and ^{13}C NMR spectra were obtained with BRUKER 300 MHz FT-NMR spectrometers and the chemical shifts are reported in ppm, using tetramethylsilane as an

internal standard and were referenced to the residual solvent as follows: $CDCl_3 = 7.26$ (1H), 76.16 (^{13}C) ppm at room temperature. For ^{1}H NMR, coupling constants J are given in Hz and the resonance multiplicity is described as s (singlet), d (doublet), t (triplet), m (multiplet), dd (doublet of doublet), dt (doublet of triplet), td (triplet of doublet), tt (triplet of triplet), q (quartet). ^{13}C NMR spectra were fully decoupled by broadband proton decoupling. High resolution mass spectra (HRMS) were obtained from Waters (Xevo G2 Q-TOF) mass spectrometer in electrospray ionization mode (ESI^{+}).

4.4.3. X-ray Crystallographic Analysis: The compound **3h** was dissolved in minimum amount of THF solvent and layered with n-hexane. The resulting solution kept at 0 ˚C for 2-days to give the block shaped crystal. The intensity data were collected on a CCD area detector, MoK$_\alpha$ diffractometer. With OLEX2[30] the structure was solved with the superflip[31] structure solution program using charge flipping and refined with the SHELXL[32] refinement package and least-squares minimization. The hydrogen atoms were refined isotropically at calculated positions using a riding model. CCDC 2282240 (**3h**) contains the supplementary crystallographic data for this paper. These data can be obtained free of charge from the Cambridge Crystallographic Data Centre *via* www.ccdc.cam.ac.uk/data request/cif.

4.4.3.1. Crystallographic data for 3h

Empirical Formula $C_{17}H_{24}O_4$, crystal system, monolinic; space group, *P 1 21/c 1*; unit cell dimensions, $a = 24.0141(14)$ Å, $b = 5.3480(3)$ Å, $c = 12.5183(7)$ Å, $\alpha = 90$˚, $\beta = 92180(2)$˚, $\gamma = 90$˚ ; $V = 1606.53(16)$ Å^3; $Z = 4$; $\rho = 1.209$ g cm^{-3}, T (K) 298, θmin/max: 3.257/27.209, reflections: 51921 collected, Goodness-of-Fit (GOF) on F^2 1.078, $R_{int} = 0.0220$, R_1(all) = 0.0545, wR_2(all) = 0.1415. Final R indices [I>2σ(I)]: $R_1 = 0.0474$, $wR_2 = 0.1355$.

4.4.4. Computational details: All density functional theory (DFT) calculations were performed within the Gaussian 09 quantum chemical package.[33] All the geometries of stationary points were optimized in the solvent phase with the B3LYP functional, overlaid with Grimme's empirical dispersion D3(BJ) correction term, employing the IoP(3/124=40) keyword, in conjugation with Pople's 6-31G(d,p) basis set.[34] Solvent effect was introduced by utilizing the conductor-like polarized continuum model (CPCM) with dielectric constant of cyclohexane (ε=2.0165). Harmonic vibrational frequencies were computed at the same level of theory, to distinguish transition states (with one negative Hessian index) from minima (with all positive Hessian index).

The non-thermal zero-point energy (ZPE) correction and the thermal corrections to enthalpy and Gibbs free energy were obtained from frequency calculations, employing the experimental temperature (333.15 K) and 1 atm pressure. Moreover, the electronic energies were refined by single point calculations with the larger triple-ζ basis set at B3LYP-D3(BJ)/6-311+G (d, p)/CPCM(cyclohexane). Relative Gibbs free energies reported in the main text are evaluated by adding thermal corrections obtained from vibrational analyses to the solvent-phase electronic energies. Notably, we have performed all the geometry optimizations in the CPCM solvent model. However, the entropy of each solute was obtained through the Sakur−Tetrode equation, which essentially treats the molecules as an ideal gas. Since in the ideal gas model the damping of translational and rotational degrees of freedom in solvent phase gets ignored, the entropy is overestimated. This is in line with earlier observations.[35] Hence, we have computed the solution phase entropy of each solute species scaled by an empirical factor of 0.5 times the entropy obtained from the rigid-rotor model which is a standard practice.

4.4.5. General procedure for the catalytic reaction: Preparation of 3a as representative example: An oven-dried round-bottomed flask equipped with a stir bar was charged with anhydrous $CuCl_2$ (0.02 mmol, 2.69 mg) and 1-methylimidazole (1.5 mmol, 0.2 mL). After that, cyclohexane (3 mL) was added to the reaction mixture followed by **1a** (1.0 mmol, 0.12 mL) and TBHP (3 mmol, 0.29 mL) by syringe. The round bottom flask was then placed in an oil bath preheated at 60 ˚C. After 2 h the reaction mixture was cooled to room temperature and extracted with dichloromethane (3×20 mL) and water. The organic phase was washed with brine, dried with Na_2SO_4 and evaporated under reduced pressure. The crude product was purified by column chromatography on silica gel (2% EtOAc/pet ether) to afford the corresponding product **3a** (185 mg, yield 80%).

4.4.6. Gram-Scale reaction: Styrene (**1b**) was used for multigram scale reaction. An oven dried round-bottomed flask equipped with a stir bar was charged with $CuCl_2$ catalyst (0.19 mmol, 25.8 mg) and 1-methylimidazole (14.4 mmol, 1.98 mL). Then **1b** (9.6 mmol, 1 g) and TBHP (28.8 mmol, 2.76 mL) were added to it by syringe. After that cyclohexane (**2a**) cyclopentane (**2b**) and cyclooctane (**2c**) is added to the three different reaction mixture individually. The Schlenk tubes was then placed in an oil bath preheated at 60 ˚C. After 2 h the reaction mixture was cooled to room temperature and extracted with dichloromethane (3×50 mL) and water. Organic phase was

washed with brine, dried with Na_2SO_4 and evaporated under reduced pressure. The crude product was purified by column chromatography on silica gel (2% EtOAc/pet ether) to afford the desired products **3ba** (1.09 g, yield 60%), **3b** (1.32 g, yield 68%) and **3bc** (1.3 g, yield 58%) respectively.

4.4.7. General procedures for the post-synthetic modifications:

4.4.7.1. Synthesis of compounds 4a and 4b: In a round bottomed flask, compound **3a** (0.84 mmol, 170 mg) was dissolved in ethanol (5 mL). Then anhydrous NaOAc (1.26 mmol, 103.4 mg) and $NH_2OH.HCl$ (1.126 mmol, 131.3 mg) were added to the reaction mixture. Resulting reaction mixture was kept at 80 ˚C for 12 h. Then the reaction mixture was cooled to room temperature and extracted with dichloromethane (3×20 mL). The combined organic layer was washed with brine, dried with Na_2SO_4 and evaporated under reduced pressure. Crude product was purified by column chromatography on silica gel (1% EtOAc/pet ether) to give the desired product **4a** (129.15 mg, 70% yield).

Similar experiment was done also for compound **3o** (0.21 mmol, 50 mg) and the corresponding desired product **4b** formed in moderated yield (32 mg, 60% yield).

4.4.7.2. Synthesis of compound 5: Compound **5** was synthesized according to literature reported procedure.[36] In an oven-dried sealed tube, compound **4a** (0.276 mmol, 60 mg) was taken and dissolved in dry dichloromethane (5 mL) at N_2 atmosphere. Then polyphosphoric acid (1.52 mmol, 513 mg) was added to the reaction mix and the resulting solution was kept at 120 ˚C in a pre-heated oil bath for 12 h. Then the reaction mixture was cooled to room temperature and extracted with dichloromethane (3×10 mL). The combined organic layer was washed with brine, dried with Na_2SO_4 and evaporated under reduced pressure. Crude product was purified by column chromatography on silica gel (1% EtOAc/pet ether) to give the desired product **5** (36 mg, 60% yield).

4.4.7.3. Synthesis of compound 6: Two Schlenk flasks were charged with nitrogen. Diethyl ether (5 mL) and *n*-butylmagnesium chloride (1.5 equiv, 0.370 mmol, 0.185 mL) were added in one Schlenk flask and THF (5 mL) and *n*-butyllithium (1.5 equiv, 0.370 mmol, 0.23 mL) were added in another and the flasks were cooled to 0 ˚C. Compound **3b** (0.247 mmol, 50 mg) was dissolved in THF/ Et_2O (2 mL) separately, and the solution was added dropwise in the Schlenk flasks for 15 minutes. The reaction mixtures were allowed to stir for 8 h where temperature was maintained at 0-5 ˚C for n-butylmagnesium chloride and room temperature for *n*-butyllithium. Then the reaction

mixture was diluted with sat. aqueous NH_4Cl (5 mL) and extracted with ethyl acetate (3×10 mL). The combined organic layer was washed with brine, dried with Na_2SO_4 and evaporated under reduced pressure. Crude product was purified by column chromatography on silica gel (1% EtOAc/pet ether) to give the desired product **6** (32 mg, 50% yield).

4.4.8. Radical trapping experiment: In a Schlenk tube, 4-methoxy styrene **1a** (1 mmol), 1-methylimidazole (1.5 mmol), and anhydrous $CuCl_2$ (0.02 mmol) were mixed in cyclohexane (3 ml) at room temperature. Then TBHP (3 mmol) was added to it by syringe. Finally, TEMPO and BHT (3 mmol) were added separately to this reaction mixture and the resulting reaction mixture was kept at 60 ˚C in a pre-heated oil bath and stirred for 6 h. Then the reaction mixture was cooled to room temperature and a portion of crude reaction mixture was analysed directly by HRMS. After cooling down to room temperature reaction mixture was extracted with dichloromethane and water. The organic phase was washed with brine, dried with Na_2SO_4 and evaporated under reduced pressure. The crude product was purified by column chromatography on silica gel (pet ether) to give the pure product **7** in 40% yield.

4.4.9. Kinetic isotope effect (KIE) studies:

(a) By competitive reaction. An oven-dried round-bottomed flask equipped with a stir bar was charged with anhydrous $CuCl_2$ (0.014 mmol, 1.93 mg) and 1-methylimidazole (1.08 mmol, 0.15 mL). After that, cyclohexane (1.44 mmol, 0.16 mL) and D_{12}-cyclohexane (1.44 mmol, 0.15 mL) were added to the reaction mixture followed by **1b** (0.75 mmol, 0.082 mL) and TBHP (2.16 mmol, 0.21 mL) by syringe. The round bottom flask was then placed in an oil bath preheated at 60 ˚C. After 2 h the reaction mixture was cooled to room temperature and extracted with dichloromethane (3×10 mL) and water. The organic phase was washed with brine, dried with Na_2SO_4 and evaporated under reduced pressure. The crude product was purified by column chromatography on silica gel (2% EtOAc/pet ether) to afford the corresponding product **3b** and **[D]-3b** in 30% yield (43 mg). The KIE value calculated from ^1H NMR was found to be 5.67.

(b) By parallel reactions. An oven-dried round-bottomed flask equipped with a stir bar was charged with anhydrous $CuCl_2$ (0.02 mmol, 2.69 mg) and 1-methylimidazole (1.5 mmol, 0.2 mL). After that, cyclohexane (1.8 mmol, 0.2 mL) was added to the reaction mixture. Benzene (1.8 mL) was added to the reaction mixture as co-solvent followed by **1b** (1.0 mmol, 0.12 mL) and TBHP

(3 mmol, 0.29 mL) by syringe. The round bottom flask was then placed in an oil bath preheated at 60 °C. For 2 hours, an aliquot of 0.5 mL was taken by syringe every 30 min and analysed directly by ^{1}H NMR using 3,4,5-trimethyl benzene as internal standard.

Similar experiment was performed using D_{12}-cyclohexane (1.8 mmol, 0.19 mL). Data collected from these kinetic studies are plotted and the KIE value was found to be k_H/k_D 5.15.

4.4.10. Hammett analysis of styrene derivatives: An oven-dried round-bottomed flask equipped with a stir bar was charged with anhydrous $CuCl_2$ (0.01 mmol) and 1-methylimidazole (0.75 mmol). After that, cyclohexane (1 mL) was added to the reaction mixture. Then styrene (0.5 mmol) and styrene derivatives (($3-NO_2$, 3-CN, 4-Cl, $4-OCH_3$, $4-C(CH_3)$)) (0.5 mmol) were added to the reaction mixture followed by TBHP (1.5 mmol) by syringe. The round bottom flask was then placed in an oil bath preheated at 60 °C. After 2 h the reaction mixture was cooled down to room temperature and analysed directly for Hammett study by ^{1}H NMR spectroscopy.

4.4.11. Analytical data of final products:

2-cyclohexyl-1-(4-methoxyphenyl) ethanone (**3a**): Colourless oil (Yield 80%, 185 mg). ^{1}H NMR (300 MHz, CDCl$_3$): δ = 7.94 (d, J = 9 Hz, 2H), 6.93 (d, J = 9 Hz, 2H), 3.87 (s, 3H), 2.77 (d, J = 9 Hz, 2H), 1.97-1.91 (m, 1H), 1.76-1.68 (m, 5H), 1.21-0.98 (m, 5H). ^{13}C{^{1}H} NMR (75 MHz, CDCl$_3$): δ = 199.1, 163.4, 130.8, 130.6, 113.8, 55.6, 46.1, 34.9, 33.6, 26.4, 26.3.

2-cyclohexyl-1-phenylethanone (**3b**): Colourless oil (Yield 72%, 145 mg). ^{1}H NMR (300 MHz, CDCl$_3$): δ = 7.95 (dd, J_1 = 3 Hz, J_2 = 6 Hz, 2H), 7.58-7.52 (m, 1H), 7.48-7.43 (m, 2H), 2.83 (d, J = 9 Hz, 2H), 2.03-1.93 (m, 1H), 1.78-1.67 (m, 5H), 1.35-0.99 (m, 5H). ^{13}C{^{1}H} NMR (75 MHz, CDCl$_3$): δ = 200.4, 137.6, 132.9, 128.6, 128.3, 46.4, 34.7, 33.6, 26.4, 26.3.

2-cyclohexyl-1-(4-methyl phenyl) ethanone (**3c**): Colourless oil (Yield 76%, 164 mg). ^{1}H NMR (300 MHz, CDCl$_3$): δ = 7.87 (d, J = 9 Hz, 2H), 7.25 (d, J = 9 Hz, 2H), 2.79 (d, J = 6 Hz, 2H), 2.41 (s, 3H), 2.00-1.94 (s, 1H), 1.77-1.67 (m, 5H), 1.30-0.98 (m, 5H). ^{13}C{^{1}H} NMR (75 MHz, CDCl$_3$): δ = 200.2, 143.7, 135.2, 129.3, 128.4, 46.3, 34.8, 33.6, 26.3.

2-cyclohexyl-1-(2-methyl phenyl) ethanone (**3d**): Colourless oil (Yield 74%, 159 mg). ^{1}H NMR (300 MHz, CDCl$_3$): δ = 7.58 (dd, J_1 = 3 Hz, J = 6 Hz, 1H), 7.35 (td, J_1 = 9 Hz, J_2 = 6 Hz, 1H), 7.24-7.18 (m, 2H), 2.75 (d, J = 6 Hz, 2H), 2.48 (s, 3H), 1.97-1.91 (m, 1H), 1.76-1.67 (m, 5H),

1.32-0.97 (m, 5H). ^{13}C{^{1}H} NMR (75 MHz, CDCl$_3$): δ = 204.4, 142.4, 133.8, 131.4, 128.4, 127.5, 118.7, 50.5, 34.3, 33.4, 29.8, 26.3, 26.2.

2-cyclohexyl-1-(3-methoxyphenyl) ethanone (**3e**): Colourless solid (Yield 74%, 171 mg). ^{1}H NMR (300 MHz, CDCl$_3$): δ = 7.51 (t, *J* = 9 Hz, 2H), 7.36 (t, *J* = 9 Hz, 1H), 7.09 (dd, *J$_1$* = 3 Hz, *J$_2$* = 6 Hz, 1H), 3.86 (s, 3H), 2.80 (d, *J* = 6 Hz, 2H), 2.01-1.95 (m, 1H), 1.77-1.67 (m, 5H), 1.31-0.99 (m, 5H). ^{13}C{^{1}H} NMR (75 MHz, CDCl$_3$): δ = 197.9, 148.6, 138.7, 133.8, 129.9, 127.3, 123.1, 46.4, 34.4, 33.5, 26.2.

2-cyclohexyl-1-(2-methoxyphenyl) ethanone (**3f**): Colourless solid (Yield 74%, 172 mg). ^{1}H NMR (300 MHz, CDCl$_3$): δ = 7.60 (dd, *J$_1$* = 3 Hz, *J$_2$* = 6 Hz, 1H), 7.43 (td, *J$_1$* = 7.5 Hz, *J$_2$* = 15 Hz, 1H), 7.01-6.93 (m, 2H), 3.89 (s, 3H), 2.84 (d, *J* = 9 Hz, 2H), 1.95-1.89 (m, 1H), 1.74-1.65 (m, 5H), 1.30-0.95 (m, 5H). ^{13}C{^{1}H} NMR (75 MHz, CDCl$_3$): δ = 203.3, 158.3, 133.1, 130.1, 129.5, 120.8, 111.6, 55.6, 51.5, 34.5, 33.5, 29.8, 26.5, 26.4.

2-cyclohexyl-1-(2,5-dimethoxyphenyl) ethanone (**3g**): Colourless solid (Yield 82%, 215 mg). ^{1}H NMR (300 MHz, CDCl$_3$): δ = 7.17 (d, *J* = 3 Hz, 1H), 6.99 (dd, *J$_1$* = 3 Hz, *J$_2$* = 9 Hz, 1H), 6.89 (d, *J* = 9 Hz, 1H), 3.85 (s, 3H), 3.79 (s, 3H), 2.84 (d, *J* = 6 Hz, 2H), 1.93-1.87 (m, 1H), 1.74-1.65 (m, 5H), 1.20-0.85 (m, 5H). ^{13}C{^{1}H} NMR (75 MHz, CDCl$_3$): δ = 202.8, 153.6, 152.8, 129.6, 119.5, 114.1, 113.3, 56.2, 55.9, 51.5, 34.5, 33.5, 26.5, 26.4. HRMS (ESI): m/z [M+Na]$^+$ calcd. for C$_{16}$H$_{22}$O$_3$Na 285.1466, found 285.1468.

2-cyclohexyl-1-(3,4,5-trimethoxyphenyl) ethanone (**3h**): Colourless solid (Yield 85%, 248 mg). ^{1}H NMR (300 MHz, CDCl$_3$): δ = 7.20 (s, 2H), 3.91 (s, 9H), 2.77 (d, *J* = 6 Hz, 2H), 1.99-1.93 (m, 1H), 1.78-1.73 (m, 3H), 1.39-1.27 (m, 3H), 1.17-0.89 (m, 4H). ^{13}C{^{1}H} NMR (75 MHz, CDCl$_3$): δ = 199.2, 153.2, 142.6, 132.9, 105.8, 61.1, 56.4, 46.0, 34.9, 33.6, 26.4, 26.3.

1-(4-(*tert*-butyl) phenyl)-2-cyclohexyl ethanone (**3i**): Colourless oil (Yield 73%, 188 mg). ^{1}H NMR (300 MHz, CDCl$_3$): δ = 7.89 (d, *J* = 6 Hz, 2H), 7.47 (d, *J* = 9 Hz, 2H), 2.80 (d, *J* = 6 Hz, 2H), 2.00-1.94 (m, 1H), 1.78-1.67 (m, 5H), 1.34 (s, 12H), 1.23-0.99 (m, 4H). ^{13}C{^{1}H} NMR (75 MHz, CDCl$_3$): δ = 200.1, 156.7, 135.2, 128.3, 125.6, 46.3, 33.6, 31.3, 26.5, 26.3.

2-cyclohexyl-1-(3-hydroxyphenyl) ethanone (**3j**): Colourless solid (Yield 72%, 157 mg). ^{1}H NMR (300 MHz, CDCl$_3$): δ = 7.51-7.48 (m, 2H), 7.33 (t, *J* = 7.5 Hz, 1H), 7.06 (dd, *J$_1$* = 3 Hz, *J$_2$* = 7.5 Hz, 1H), 2.80 (d, *J* = 6 Hz, 2H), 1.98-1.91 (m, 1H), 1.76-1.67 (m, 5H), 1.34-0.88 (m, 5H). ^{13}C{^{1}H}

NMR (75 MHz, CDCl$_3$): δ = 200.9, 156.3, 129.9, 120.9, 120.4, 114.7, 46.5, 34.8, 33.5, 26.2. HRMS (ESI): m/z [M+Na]$^+$ calcd. for C$_{14}$H$_{18}$O$_2$Na 241.1204, found 241.1206.

2-cyclohexyl-1-(4-fluorophenyl) ethanone (**3k**): Colourless oil (Yield 72%, 158 mg). ^{1}H NMR (300 MHz, CDCl$_3$): δ = 7.97 (dd, J_1 = 9 Hz, J_2 = 12 Hz, 2H), 7.12 (t, J = 9 Hz, 2H), 2.79 (d, J = 6 Hz, 2H), 1.98-1.92 (m, 1H), 1.78-1.64 (m, 6H), 1.31-0.98 (m, 4H). ^{13}C{^{1}H} NMR (75 MHz, CDCl$_3$): δ = 198.8, 130.9, 130.8, 115.8, 115.6, 46.3, 34.7, 33.6, 26.4, 26.3.

2-cyclohexyl 1-(4-bromophenyl) ethanone (**3l**): Colourless oil (Yield 69%, 194 mg). ^{1}H NMR (300 MHz, CDCl$_3$): δ = 7.80 (d, J = 9 Hz, 2H), 7.59 (d, J = 9 Hz, 2H), 2.78 (d, J = 6 Hz, 2H), 1.97-1.91 (m, 1H), 1.76-1.67 (m, 5H), 1.22-0.83 (m, 5H). ^{13}C{^{1}H} NMR (75 MHz, CDCl$_3$): δ = 199.4, 136.3, 132.0, 129.8, 128.1, 46.3, 34.7, 33.6, 29.8, 26.4, 26.3.

2-cyclohexyl 1-(3-bromophenyl) ethanone (**3m**): Colourless oil (Yield 74%, 208 mg). ^{1}H NMR (300 MHz, CDCl$_3$): δ = 8.06 (s, 1H), 7.86 (d, J = 6 Hz, 1H), 7.67 (d, J = 6 Hz, 1H), 7.33 (t, J = 7.5 Hz, 1H), 2.79 (d, J = 6 Hz, 2H), 2.00-1.92 (m, 1H), 1.76-1.682 (m, 5H), 1.31-0.99 (m, 5H). ^{13}C{^{1}H} NMR (75 MHz, CDCl$_3$): δ = 198.9, 139.4, 135.8, 131.3, 130.3, 126.8, 123.1, 46.4, 34.6, 33.5, 26.4, 26.3.

2-cyclohexyl 1-(2-bromophenyl) ethanone (**3n**): Colourless oil (Yield 68%, 191 mg). ^{1}H NMR (300 MHz, CDCl$_3$): δ = 7.59 (d, J = 9 Hz, 1H), 7.34 (d, J = 3 Hz, 2H), 7.30-7.27 (m, 1H), 2.80 (d, J = 6 Hz, 2H), 1.99-1.90 (m, 1H), 1.80-1.67 (m, 5H), 1.22-0.85 (m, 5H). ^{13}C{^{1}H} NMR (75 MHz, CDCl$_3$): δ = 204.4, 142.4, 133.8, 131.4, 128.4, 127.5, 118.7, 50.6, 34.3, 33.4, 29.8, 26.3, 26.2.

2-cyclohexyl 1-(4-chlorophenyl) ethanone (**3o**): Colourless oil (Yield 72%, 170 mg). ^{1}H NMR (300 MHz, CDCl$_3$): δ = 7.88 (d, J = 6 Hz, 2H), 7.43 (d, J = 9 Hz, 2H), 2.79 (d, J = 6 Hz, 2H), 1.98-1.91 (m, 1H), 1.77-1.64 (m, 6H), 1.30-0.97 (m, 4H). ^{13}C{^{1}H} NMR (75 MHz, CDCl$_3$): δ = 199.1, 139.4, 135.9, 129.7, 128.9, 46.3, 34.7, 33.5, 26.4, 26.3.

2-cyclohexyl 1-(3-chlorophenyl) ethanone (**3p**): Colourless oil (Yield 70%, 165 mg). ^{1}H NMR (300 MHz, CDCl$_3$): δ = 7.90 (d, J = 3 Hz, 1H), 7.81 (d, J = 6 Hz, 1H), 7.52 (d, J = 6 Hz, 1H), 7.40 (t, J = 6 Hz, 1H), 2.79 (d, J = 3 Hz, 2H), 1.98-1.94 (m, 1H), 1.77-1.68 (m, 5H), 1.34-0.97 (m, 5H). ^{13}C{^{1}H} NMR (75 MHz, CDCl$_3$): δ = 199.0, 139.2, 135.1, 132.9, 130.0, 128.4, 126.3, 46.4, 34.6, 33.5, 26.4, 26.3.

2-cyclohexyl-1-(4-nitrophenyl) ethanone (**3q**): Yellow Solid (Yield 72%, 178 mg). ^{1}H NMR (300 MHz, CDCl$_3$): δ = 8.30 (d, *J* = 9 Hz, 2H), 8.09 (d, *J* = 9 Hz, 2H), 2.87 (d, *J* = 9 Hz, 2H), 2.01-1.94 (m, 1H), 1.78-1.68 (m, 5H), 1.32-0.97 (m, 5H). ^{13}C{^{1}H} NMR (75 MHz, CDCl$_3$): δ = 198.7, 150.3, 141.9, 129.2, 123.9, 46.8, 34.5, 33.5, 26.3, 26.2.

2-cyclohexyl-1-(3-nitrophenyl) ethanone (**3r**): Yellow Solid (Yield 70%, 173 mg). ^{1}H NMR (300 MHz, CDCl$_3$): δ = 8.75 (s, 1H), 8.41 (d, *J* = 9 Hz, 1H), 8.27 (d, *J* = 9 Hz, 1H), 7.67 (t, *J* = 9 Hz, 1H), 2.88 (d, *J* = 9 Hz, 2H), 2.02-1.95 (m, 1H), 1.78-1.65 (m, 4H), 1.32-1.00 (m, 6H). ^{13}C NMR (75 MHz, CDCl$_3$): δ = 197.9, 148.6, 138.8, 129.9, 127.3, 123.1, 46.4, 34.4, 33.5, 26.2. HRMS (ESI): m/z [M]$^+$ calcd. for C$_{14}$H$_{17}$NO$_3$ 247.1208, found 247.1207.

2-cyclohexyl-1-(4-(trifluoromethyl) phenyl) ethanone (**3s**): Colourless oil (Yield 69%, 186 mg). %). ^{1}H NMR (300 MHz, CDCl$_3$): δ = 8.04 (d, *J* = 6 Hz, 2H), 7.73 (d, *J* = 9 Hz, 2H), 2.84 (*J* = 6 Hz, 2H), 2.01-1.94 (m, 1H), 1.77-1.68 (m, 5H), 1.36-0.96 (m, 5H). ^{13}C{^{1}H} NMR (75 MHz, CDCl$_3$): δ = 199.3, 140.3, 134.5, 134.2, 128.6, 125.8, 46.6, 34.6, 33.5, 26.3, 26.2.

3-(2-cyclohexylacetyl) benzonitrile (**3t**): Colourless solid (Yield 70%, 159 mg). ^{1}H NMR (300 MHz, CDCl$_3$): δ = 8.24 (t, *J* = 3 Hz, 1H), 8.20 (t, *J* = 3 Hz, 1H), 8.17 (dt, *J* = 3 Hz, 1H), 2.85 (d, *J* = 6 Hz, 2H), 2.02-1.95 (m, 1H), 1.81-1.71 (m, 5H), 1.15-1.02 (m, 5H). ^{13}C{^{1}H} NMR (75 MHz, CDCl$_3$): δ = 198.1, 138.3, 135.8, 132.2, 132.0, 129.8, 118.1, 113.3, 46.4, 34.5, 33.5, 26.3, 26.2. Elemental analysis: anal. calcd for C$_{15}$H$_{17}$NO: C, 79.26; H, 7.54; N, 6.16. Found: C, 79.16; H, 7.45; N, 6.10.

2-cyclohexyl-1-(naphthalen-1-yl) ethanone (**3u**): Colourless oil (Yield 63%, 158 mg). ^{1}H NMR (300 MHz, CDCl$_3$): δ = 8.54 (d, *J* = 9 Hz, 1H), 7.97 (d, *J* = 9 Hz, 1H), 7.89-7.81 (m, 2H), 7.61-7.47 (m, 3H), 2.92 (d, *J* = 9 Hz, 2H), 2.07-2.00 (m, 1H), 1.84-1.62 (m, 7H), 1.10-0.83 (m, 3H). ^{13}C{^{1}H} NMR (75 MHz, CDCl$_3$): δ = 205.1, 136.9, 134.1, 132.4, 130.2, 128.5, 127.9, 127.4, 126.5, 125.9, 12.5, 50.2, 30.0, 33.5, 26.4, 26.3.

2-cyclohexyl-1-(pyridin-3-yl) ethanone (**3v**): Colourless oil (Yield 73%, 148 mg). ^{1}H NMR (300 MHz, CDCl$_3$): δ = 9.14 (d, *J* = 3 Hz, 1H), 8.76 (d, *J* = 6 Hz, 1H), 8.21 (dt, *J$_1$* = 3 Hz, *J$_2$* = 9 Hz, 1H), 7.43-7.39 (m, 1H), 2.83 (d, *J* = 6 Hz, 2H), 2.02-1.94 (m, 1H), 1.77-1.63 (m, 5H), 1.31-0.99 (m, 5H). ^{13}C{^{1}H} NMR (75 MHz, CDCl$_3$): δ = 199.1, 153.4, 149.9, 135.5, 132.8, 123.7, 46.6, 34.5, 33.5, 26.3, 26.2.

2-cyclopentyl-1-(4-methoxyphenyl) ethanone (**3aa**): Colourless oil (Yield 71%, 154 mg). ^{1}H NMR (300 MHz, CDCl$_3$): δ = 7.94 (d, J = 9 Hz, 2H), 6.93 (d, J = 9 Hz, 2H), 3.87 (s, 3H), 2.93 (d, J = 6 Hz, 2H), 2.42-2.32 (m, 2H), 1.91-1.82 (m, 2H), 1.66-1.53 (m, 3H), 1.25-1.15 (m, 3H). ^{13}C{^{1}H} NMR (75 MHz, CDCl$_3$): δ = 199.2, 163.4, 130.5, 113.8, 55.6, 44.6, 36.5, 32.9, 25.1.

2-cyclopentyl-1-(4-methyl phenyl) ethanone (**3ab**): Colourless oil (Yield 70%, 141 mg). ^{1}H NMR (300 MHz, CDCl$_3$): δ = 7.86 (d, J = 6 Hz, 2H), 7.25 (d, J = 9 Hz, 2H), 2.96 (d, J = 9 Hz, 2H), 2.41 (s, 3H), 2.35-2.31 (m, 4H), 1.90-1.82 (m, 2H), 1.66-1.60 (m, 4H). ^{13}C{^{1}H} NMR (75 MHz, CDCl$_3$): δ = 200.3, 143.7, 135.0, 129.3, 128.4, 44.9, 36.4, 32.9, 25.1, 21.7.

2-cyclopentyl-1-(3,4,5-trimethoxyphenyl) ethanone (**3ac**): Colourless solid (Yield 74%, 205 mg). ^{1}H NMR (400 MHz, CDCl$_3$): δ = 7.21 (s, 2H), 3.92 (s, 9H), 2.94 (d, J = 8 Hz, 2H), 2.42-2.35 (m, 1H), 1.92-1.86 (m, 2H), 1.67-1.55 (m, 3H), 1.23-0.98 (m, 3H). ^{13}C{^{1}H} NMR (100 MHz, CDCl$_3$): δ = 199.2, 153.2, 142.8, 132.8, 106.0, 61.1, 56.5, 44.7, 36.4, 32.9, 25.2. HRMS (ESI): m/z [M+Na]$^+$ calcd. for 301.1415, found 301.1414.

2-cyclopentyl-1-(3-nitrophenyl) ethanone (**3ad**): Colourless oil (Yield 68%, 158 mg). ^{1}H NMR (400 MHz, CDCl$_3$): δ = 8.77 (t, J = 4 Hz, 1H), 8.43-8.39 (m, 1H), 8.29 (dt, J_1 = 4 Hz, J_2 = 12 Hz, 1H), 7.67 (t, J = 10 Hz, 1H), 3.05 (d, J = 8 Hz, 2H), 2.45-2.35 (m, 1H), 1.96-1.17 (m, 8H). ^{13}C{^{1}H} NMR (100 MHz, CDCl$_3$): δ = 198.1, 138.5, 133.8, 129.9, 127.3, 123.1, 45.1, 35.9, 32.8, 29.8, 25.1. HRMS (ESI): m/z [M+Na]$^+$ calcd. for C$_{13}$H$_{15}$NO$_3$K 272.0689, found 272.0689.

3-(2-cyclopentylacetyl) benzonitrile (**3ae**): Colourless oil (Yield 67%, 142 mg). ^{1}H NMR (400 MHz, CDCl$_3$): δ = 8.22 (t, J = 4 Hz, 1H), 8.17 (dt, J_1 = 4 Hz, J_2 = 12 Hz, 1H), 7.83 (dt, J_1 = 4 Hz, J_2 = 12 Hz, 1H), 7.60 (t, J = 10 Hz, 1H), 2.99 (d, J = 8 Hz, 2H), 2.43-2.32 (m, 1H), 1.93-1.86 (m, 2H), 1.69-1.63 (m, 3H), 1.21-1.14 (m, 2H). ^{13}C{^{1}H} NMR (75 MHz, CDCl$_3$): δ = 198.2, 138.1, 135.9, 132.2, 131.9, 129.8, 118.1, 113.3, 45.1, 35.9, 32.9, 25.1. Elemental analysis: anal. calcd for C$_{14}$H$_{15}$NO: C, 78.84; H, 7.09; N, 6.57. Found: C, 78.72; H, 7.01; N, 6.48.

1-(3-bromophenyl)-2-cyclopentyl ethanone (**3af**): Colourless oil (Yield 70%, 187 mg). ^{1}H NMR (300 MHz, CDCl$_3$): δ = 8.07 (t, J = 4 Hz, 1H), 7.87 (dt, J_1 = 4 Hz, J_2 = 8 Hz, 1H), 7.68 (dt, J_1 = 4 Hz, J_2 = 12 Hz, 1H), 7.34 (t, J = 10 Hz, 1H), 2.96 (d, J = 12 Hz, 2H), 2.42-2.32 (m, 1H), 1.91-1.86 (m, 2H), 1.68-1.61 (m, 3H), 1.20-1.14 (m, 3H). ^{13}C{^{1}H} NMR (75 MHz, CDCl$_3$): δ = 199.1, 139.2,

135.8, 131.4, 130.3, 126.7, 123.1, 45.1, 36.1, 32.9, 29.8, 25.1. HRMS (ESI): m/z [M+Na]$^+$ calcd. for $C_{13}H_{15}BrONa$ 289.0204, found 289.0204.

2-cyclooctyl-1-(4-methoxyphenyl) ethanone (3aa'): Colourless oil (Yield 68%, 177 mg). ^{1}H NMR (300 MHz, CDCl$_3$): δ = 7.94 (d, *J* = 9 Hz, 2H), 6.93 (d, *J* = 9 Hz, 2H), 3.86 (s, 3H), 2.80 (d, *J* = 6 Hz, 2H), 2.28-2.24 (m, 1H), 1.67-1.31 (m, 7H). ^{13}C{^{1}H} NMR (75 MHz, CDCl$_3$): δ = 199.3, 163.4, 130.8, 130.5, 113.8, 46.7, 34.5, 32.6, 27.3, 26.3, 25.4.

2-cyclooctyl-1-(2-methoxyphenyl) ethanone (3ab'): Colourless solid (Yield 65%, 169 mg). ^{1}H NMR (300 MHz, CDCl$_3$): δ = 7.59 (dd, *J$_1$* = 3 Hz, *J$_2$* = 6 Hz, 1H), 7.43 (td, *J$_1$* = 6 Hz, *J$_2$* = 9 Hz, 1H), 7.01-6.93 (m, 2H), 3.89 (s, 3H), 2.86 (d, *J* = 9 Hz, 2H), 2.21-2.17 (m, 1H), 1.64-1.30 (m, 13H). ^{13}C{^{1}H} NMR (75 MHz, CDCl$_3$): δ = 203.5, 158.3, 133.0, 130.2, 120.8, 111.6, 55.6, 52.3, 34.0, 32.7, 29.8, 27.3, 26.4, 25.5. HRMS (ESI): m/z [M+H]$^+$ calcd. for $C_{17}H_{25}O_2$ 261.1854, found 261.1854.

2-cyclooctyl-1-(3,4,5-(trimethoxy) phenyl) ethanone (3ac'): Colourless oil (Yield 72%, 230 mg). ^{1}H NMR (300 MHz, CDCl$_3$): δ = 7.21 (s, 2H), 3.92 (s, 9H), 2.82 (d, *J* = 6 Hz, 2H), 2.31-2.26 (m, 1H), 1.67-1.34 (m, 14H). ^{13}C{^{1}H} NMR (75 MHz, CDCl$_3$): δ = 199.3, 153.2, 142.7, 132.9, 105.9, 61.1, 56.5, 46.8, 34.4, 32.8, 26.4, 25.5. HRMS (ESI): m/z [M+Na]$^+$ calcd. for $C_{19}H_{28}O_4Na$ 343.1885, found 343.1884.

2-cyclooctyl-1-(3-nitro phenyl) ethanone (3ad'): Colourless oil (Yield 65%, 178 mg). ^{1}H NMR (300 MHz, CDCl$_3$): δ = 8.76 (s, 1H), 8.41 (d, *J* = 9 Hz, 1H), 8.27 (d, *J* = 6 Hz, 1H), 7.67 (t, *J* = 6 Hz, 1H), 2.92 (d, *J* = 6 Hz, 2H), 2.32-2.29 (m, 1H), 1.68-1.36 (m, 14H). ^{13}C{^{1}H} NMR (75 MHz, CDCl$_3$): δ = 198.1, 138.9, 133.7, 129.9, 127.3, 123.1, 47.3, 34.1, 32.7, 29.8, 27.2, 26.4, 25.4. HRMS (ESI): m/z [M+Na]$^+$ calcd. for $C_{16}H_{21}NO_3K$ 314.1158, found 314.1157.

2-cyclooctyl-1-(4-nitro phenyl) ethanone (3ae'): Colourless oil (Yield 65%, 178 mg). ^{1}H NMR (300 MHz, CDCl$_3$): δ = 8.31 (d, *J* = 9 Hz, 2H), 8.09 (d, *J* = 9 Hz, 2H), 2.91 (d, *J* = 3 Hz, 2H), 2.30-2.26 (m, 1H), 1.67-1.37 (m, 14H). ^{13}C{^{1}H} NMR (75 MHz, CDCl$_3$): δ = 198.9, 150.4, 142.1, 129.2, 123.9, 47.6, 34.1, 32.7, 27.2, 26.3, 25.4. Elemental analysis: anal. calcd for $C_{16}H_{21}NO_3$: C, 69.79; H, 7.69; N, 5.09. Found: C, 67.71; H, 7.63; N, 5.01.

2-cyclooctyl-1-(3-cyano phenyl) ethanone (3af'): Colourless oil (Yield 64%, 163 mg). ^{1}H NMR (300 MHz, CDCl$_3$): δ = 8.21 (t, *J* = 3 Hz, 1H), 8.16 (dt, *J$_1$* = 3 Hz, *J$_2$* = 9 Hz, 1H), 7.83 (dt, *J$_1$* = 3

Hz, J_2 = 9 Hz, 1H), 7.60 (t, J = 7.5 Hz, 1H), 2.86 (d, J = 9 Hz, 2H), 2.30-2.25 (m, 1H), 1.67-1.33 (m, 13H). ^{13}C{^{1}H} NMR (75 MHz, CDCl$_3$): δ = 198.3, 138.4, 135.9, 132.1, 131.9, 129.8, 118.1, 113.3, 47.1, 34.1, 32.7, 27.2, 26.3, 25.4. HRMS (ESI): m/z [M+H]$^+$ calcd. for C$_{17}$H$_{22}$NO 256.1701, found 256.1701.

2-cyclooctyl-1-(4-trifluoromethyl phenyl) ethanone (**3ag'**): Colourless oil (Yield 63%, 187 mg). ^{1}H NMR (300 MHz, CDCl$_3$): δ = 8.04 (d, J = 6 Hz, 2H), 7.73 (d, J = 9 Hz, 2H), 2.89 (d, J = 6 Hz, 2H), 2.31-2.24 (m, 1H), 1.68-1.37 (m, 14H). ^{13}C{^{1}H} NMR (75 MHz, CDCl$_3$): 199.6, 140.2, 128.5, 125.7, 47.3, 34.1, 32.6, 27.2, 26.3, 25.4. HRMS (ESI): m/z [M+Na]$^+$ calcd. for C$_{17}$H$_{21}$F$_3$OK 337.1181, found 337.1182.

2-cyclohexyl-1-phenylethan-1-one oxime (**4a**): White solid (Yield 70%, 152 mg). ^{1}H NMR (300 MHz, CDCl$_3$): δ = 7.64 (dd, J_1 = 3 Hz, J_2 = 6 Hz, 2H), 7.42-7.40 (m, 3H), 2.81 (d, J = 6 Hz, 2H), 1.76-1.16 (m, 11H). ^{13}C{^{1}H} NMR (100 MHz, CDCl$_3$): 159.1, 136.4, 129.1, 128.6, 126.5, 35.8, 33.5, 29.9, 26.4, 26.3.

(4-chlorophenyl)-2-cyclohexylethan-1-one oxime (**4b**): White solid (Yield 60%, 151 mg). ^{1}H NMR (300 MHz, CDCl$_3$): δ = 9.06 (s, 1H), 7.53 (d, J = 9 Hz, 2H), 7.35 (d, J = 9 Hz, 2H), 2.71 (d, J = 9 Hz, 2H), 1.82-0.99 (m, 10H). ^{13}C{^{1}H} NMR (100 MHz, CDCl$_3$): 158.4, 135.2, 134.8, 128.9, 127.9, 35.9, 33.5, 33.3, 26.3, 26.2. Elemental analysis: anal. calcd for C$_{14}$H$_{18}$ClNO: C, 66.79; H, 7.21; N, 5.56. Found: C, 66.71; H, 7.13; N, 5.48.

2-cyclohexyl-N-phenylacetamide (**5**): White solid (Yield 60%, 36 mg). ^{1}H NMR (300 MHz, CDCl$_3$): δ = 7.51 (d, J = 9 Hz, 2H), 7.31 (t, J = 9 Hz, 2H), 7.20 (s, 1H), 7.09 (t, J = 7.5 Hz, 2H), 2.21 (d, J = 6 Hz, 2H), 1.94-1.78 (m, 1H), 1.83-1.69 (m, 5H), 1.31-0.98 (m, 5H). ^{13}C{^{1}H} NMR (100 MHz, CDCl$_3$): 170.8, 138.1, 129.1, 124.3, 119.9, 46.1, 35.7, 33.4, 26.4, 26.2.

1-cyclohexyl-2-phenylhexan-2-ol (**6**): Colourless oil (Yield 50%, 38.6 mg). ^{1}H NMR (300 MHz, CDCl$_3$): δ = 7.40-7.35 (m, 2H), 7.32-7.23 (m, 2H), 7.22-7.19 (m, 1H), 7.10 (s, 1H), 1.81-1.66 (m, 5H), 1.54-1.29 (m, 5H), 1.24-1.17 (m, 3H), 1.09-0.98 (m, 6H), 0.83 (t, J = 7.5 Hz, 3H). 2.21 (d, J = 6 Hz, 2H), 1.94-1.78 (m, 1H), 1.83-1.69 (m, 5H), 1.31-0.98 (m, 5H). ^{13}C{^{1}H} NMR (75 MHz, CDCl$_3$): 146.9, 128.0, 126.2, 125.4, 77.7, 50.8, 43.9, 35.3, 35.1, 33.5, 26.5, 26.4, 26.4, 25.6, 23.2, 14.2. Elemental analysis: anal. calcd for C$_{18}$H$_{28}$O: C, 83.02; H, 10.84. Found: C, 82.95; H, 10.77.

1-(cyclohexyloxy)-2,2,6,6-tetramethylpiperidine (**7**): Colourless oil (Yield 50%, 20 mg). ^{1}H NMR (300 MHz, CDCl$_3$): δ = 3.63-3.54 (m, 1H), 2.07-2.03 (m, 2H), 1.74-1.68 (m, 3H), 1.54-1.43 (m, 6H), 1.25-1.18 (m, 6H), 1.12 (s, 12H).

4.5. References

1. (a) J. F. Hartwig and M. A. Larsen, *ACS Cent. Sci.*, 2016, **2** (5), 281−292. (b) R. G. Bergman, *Nature*, 2007, **446**, 391. (c) T. Newhouse and P. S. Baran, *Angew. Chem., Int. Ed.*, 2011, **50**, 3362. (c) J. C. K. Chu and T. Rovis, *Angew. Chem., Int. Ed.*, 2018, **57**, 62. (d) J. W. Delord and F. Glorius, *Nat. Chem.*, 2013, **5**, 369 –37. (e) F. Kakiuchi and N. Chatani, *Adv. Synth. Catal.*, 2003, **345**, 1077 –1101. (f) J. Yamaguchi, A. D. Yamaguchi and K. Itami, *Angew. Chem. Int. Ed.*, 2012, **51**, 8960–9009. (g) D.Y.-K. Chen and S. W. Youn, *Chem. Eur. J.*, 2012, **18**, 9452 –947. (h) T. Cernak, K. D. Dykstra, S. Tyagarajan, P. Vachael and S. W. Krska, *Chem. Soc. Rev.*, 2016, **45**, 546 –576.

2. (a) R. Ludwig, *ChemPhysChem,* 2007, **8**, 2539−2539. (b) A. Hu, J. J. Guo, H. Pan and Z. Zuo, *Science,* 2018, **36**1, 668−672. (c) I. B. Perry, T. F. Brewer, P. J. Sarver, D. M. Schultz, D. A DiRocco and D. W. C. MacMillan, *Nature,* 2018, **56**0, 70−75. (d) G. Laudadio, Y. Deng, K. van der Wal, D. Ravelli, M. Nuño, M. Fagnoni, D. Guthrie, Y. Sun and T. Noël, *Science,* 2020, **369**, 92−96. (e) H. Yi, G. Zhang, H. Wang, Z. Huang, J. Wang, A. K. Singh and A. Lei, *Chem. Rev.*, 2017, **117** (13), 9016−9085. (f) M. H. Shaw, V. W. Shurtlef, J. A. Terrett, J. D. Cuthbertson and D. W. C. MacMillan, *Science,* 2016, **352**, 1304–1308. (g) X. Zhang and D. W. C. MacMillan, *J. Am. Chem. Soc.,* 2017, **139**, 11353–11356. (h) D. R. Heitz, J. C. Tellis and G. A. Molander, *J. Am. Chem. Soc.,* 2016, **138**, 12715–12718. (i) B. J. Shields and A. G. Doyle, *J. Am. Chem. Soc.*, 2016, **138**, 12719–12722.

3. (a) J. Twilton, C. Le, P. Zhang, M. H. Shaw, R. W. Evans and D. W. C. MacMillan, *Nature Reviews Chemistry* 2017, **1**, 52. (b) M. De Abreu, P. Belmont and E. Brachet, *Eur. J. Org. Chem.*, 2020, **2020**, 1327−1378. (c) S. Biswas and D. J. Weix, *J. Am. Chem. Soc.,* 2013, **135**, 16192−16197. (d) J. C. Tellis, D. N. Primer and G. A. Molander, *Science,* 2014, **345**, 433−436. (e) Z. Zuo, D. T. Ahneman, L. Chu, J. A. Terrett, A. G. Doyle and D. W. C. MacMillan, *Science,* 2014, **345**, 437−440. (f) J. W. Lockner, D. D. Dixon, R. Risgaard and P. S. Baran, *Org. Lett.*, 2011, **13**, 5628–5631. (g) G. A. Molander, V.

Colombel and V. A. Braz, *Org. Lett.*, 2011, **13**, 1852–1855. (h) Q. Huang and S. Z. Zard, *Org. Lett.*, 2018, **20**, 1413−1416.

4. (a) J. Otera, *Molecules,* 2000, **5**, 981-982. (b) S. K. Vooturi, C. M. Cheung, M. J. Rybak and S. M. Firestine, *J. Med. Chem.*, 2009, **52**, 5020. (c) M. W. Walter, *Nat. Prod. Rep.* 2002, **19**, 278.

5. (a) J. Liu, X. Liu, J. Wu and C. -C. Li, *Chem,* 2020, **6**, 579–615. (b) T. F. Molinski, *Org. Lett.*, 2014, **16**, 3849–3855. (c) K.C. Nicolaou, V. Dionisios, W. Nicolas and P.S. Baran, *Angew. Chem. Int. Ed.*, 2000, **39**, 44–122. (d) K.C. Nicolaou, C. R. H. Hale, C. Nilewski and H. A. Ioannidou, *Chem. Soc. Rev.*, 2012, **41**, 5185–5238. (e) M. B. Smith and J. March, March's Advanced Organic Chemistry: Reactions, Mechanisms, and Structure, 6th ed; Wiley-Interscience: Hoboken, 2007.

6. (a) M. T. Reetz, *Angew. Chem., Int. Ed.,* 1982, **21**, 96−108. (b) D. Caine, Comprehensive Organic Synthesis, Vol. 3; B. M. Trost, I. Fleming, Eds.; Pergamon: Oxford, 1991; pp *1−63*.

7. (a) G. H. Posner and C. M. Lentz, *J. Am. Chem. Soc.*, 1979, **101**, 934-946. (b) E. Negishi, M. J. Idacavage, F. Dipasguale and A. Silveira, *Tetrahedron Lett.*, 1979, **20**, 845-848. (c) J. F. Jenck, F. Agterberg and M. J. Droescher, *Green Chem.*, 2004, **6**, 544.

8. (a) W. Deng, C. Ye, Y. Li, D. Li and H. Bao, *Org. Lett.,* 2019, **21**, 261−265. (b) J. Ji, P. Liu and P. Sun, *Chem. Commun.*, 2015, **51**, 7546-7549. (c) J. Lai, L. Tian, X. Huo, Y. Zhang, X. Xie and S. Tang, *J. Org. Chem.*, 2015, **8**0, 5894–5899. (d) C. Liu, N. Shen and R. Shang, *Org. Chem. Front.*, 2021, **8**, 4166-4170. (e) A. Banerjee, S. K. Santra, A. Mishra, N. Khatun and B. K. Patel, *Org. Biomol. Chem.*, 2015, **13**, 1307-1312. (f) Y. Li, Z. Ma, X. Liu, Z. Li, F. Zhao and J. Wu, *Org. Chem. Front.*, 2023, **10**, 1710-1714. (g) R. Arias-Ugarte, F. S. Wekesa and M. Findlater, *Tetrahedron Lett.*, 2015, **56**, 2406–2411. (h) A. A. Zemtsov, S. S. Ashirbaev, V. V. Levin, V. A. Kokorekin, A. A. Korlyukov and A. D. Dilman, *J. Org. Chem.*, 2019, **84**, 15745−15753. (i) Y. Kita, M. Kuwabara, K. Kamata and M. Hara, *ACS Catal.,* 2022, **12**, 11767−11775. (j) B. Zhao, R. Shang, G.-Z. Wang, S. Wang, H. Chen and Y. Fu, *ACS Catal.*, 2020, **10**, 1334−1343. (k) X. Zhou, L. Guo, H. Zhang, R. Y. Xia, C. Yang and W. Xia, *Adv. Synth. Catal.,* 2022, **364**, 1526–1531. (l) F. Sun, J. Huang, Z. Wei, C. Tang and W. Liu, *Angew. Chem. Int. Ed.,* 2023, **62**, e202303433. (m) E. de Pedro Beato, D. Spinnato, W. Zhou and P. Melchiorre, *J. Am. Chem. Soc.,* 2021, **143**, 12304−12314. (n) J.Y. Lee, K. -C. Lim, X. Meng

and S. Kim, *Synlett,* 2010, **11**, 1647–1650. (o) M. -C. Fu, R. Shang, B. Zhao, B. Wang and Y. Fu, *Science*, 2019, **363**, 1429–1434.

9. (a) S. Waiba, S. K. Jana, A. Jati, A. Jana and B. Maji, *Chem. Commun.,* 2020, **56**, 8376-8379. (b) P. Chakraborty, M. K. Gangwar, B. Emayavaramban, E. Manoury, R. Poli and B. Sundararaju, *ChemSusChem*, 2019, **12**, 3463-3467. (c) L. Bettoni, S. Gaillard and J. -L. Renaud, *Org. Lett.,* 2020, **22**, 2064−2069.

10. S. Thiyagarajan, R. V. Sankar and C. Gunanathan, *Org. Lett.,* 2020, **22**, 7879−7884.

11. W. M. Akhtar, C. B. Cheong, J. R. Frost, K. E. Christensen, N. G. Stevenson and T. J. Donohoe, *J. Am. Chem. Soc*., 2017, **139**, 2577−2580.

12. X. Zhu, C. Ye, Y. Li and H. Bao, *Chem. Eur. J*., 2017, **23**, 10254 – 10258.

13. (a) C. Chaudhari, S. M. A. H. Siddiki and K. Shimizu, *Top. Catal*., 2014, **57**, 1042−1048. (b) I. S. Makarov and R. Madsen, *J. Org. Chem.*, 2013, **78**, 6593−6598.

14. D. Bhattacharyya, B. K. Sarmah, S. Nandi, H. K. Srivastava and A. Das, *Org. Lett*., 2021, **23**, 869−875.

15. (a) S. Thiyagarajan and C. Gunanathan, *J. Am. Chem. Soc*., 2019, **141**, 3822−3827. (b) S. Thiyagarajan and C. Gunanathan, *Synlett*, 2019, **30**, 2027−2034.

16. C. -S. Wu, Rong Li, Q. -Q. Wang and L. Yang, *Green Chem*., 2019, **21**, 269-274.

17. J. Rey, H. Hu, J. P. Snyder and A. G. M. Barrett, *Tetrahedron*, 2012, **68**, 9211.

18. Z. -H. Xia, C. -L. Zhang, Z. -H. Gao and S. Ye, *Org. Lett*., 2018, **20**, 3496–3499.

19. W. Kong, C. Yu, H. An and Q. Song, *Org. Lett*., 2018, **20**, 349–352.

20. (a) S. M. Treacy and T. Rovis, *J. Am. Chem. Soc*., 2021, **143**, 2729−2735. (b) X. Qi, L. Zhu, R. Bai and Y. Lan, *Sci Rep*., 2017, **7**, 43579.

21. Y. Zhu and Y. Wei, *Chem. Sci*., 2014, **5**, 2379–2382.

22. K. M. Das, A. Pal, N. N. Adarsh and A. Thakur, *Org. Biomol. Chem*., 2022, **20**, 3540–3549.

23. J. Shen, B. Xiao, Y. Hou, X. Wang, G. -Z. Li, J. -C. Chen, W. -L. Wang, J. -B. Cheng, B. Yang and S. -D. Yang, *Adv. Synth. Catal*., 2019, **361**, 5198–5209.

24. (a) J. Ren, K. Liu, N. Wang, X. Kong, J. Li and K. Li, *ACS Catal*., 2023, **13**, 11001−11011 (b) N. Yadav, J. Khan, A. Tyagi, S. Singh and C. K. Hazra, *J. Org. Chem.,* 2022, **87**, 6886−6901.

25. (a) S. K. Rout, S. Guin, W. Ali, A. Gogoi and B. K. Patel, *Org. Lett*., 2014, **16**, 3086–3089. (b) J. Zhao, H. Fang, J. Han and Y. Pan, *Org. Lett*., 2014, **16**, 2530–2533.

26. (a) H. Peng, J. T. Yu, Y. Jiang, H. Yang and J. Cheng, *J. Org. Chem*., 2014, **79***, 9847−9853. (b) C. Pan, B. Huang, W. Hu, X. Feng and J. T. Yu, J. *Org. Chem*., 2016, **81**, 2087−2093. (c) Q. Q. Wang, Z. X. Wang, X. Y. Zhang and X. S. Fan, *Asian J. Org. Chem*., 2017, **6**, 1445 – 1450.

27. R. Gujjarappa, N. Vodnala, A. Kandpal, L. Roy, S. Gupta and C. C. Malakar, *Org. Chem. Front*., 2021, **8**, 5389-5396.

28. L. Roy, P. M. Zimmerman and A. Paul, *Chem. Eur. J*., 2011, **17**, 435-439.

29. (a) J. Nguyen, A. Chong and G. Lalic, *Chem. Sci*., 2019, **10**, 3231–3236. (b) A. J. Perkowski, W. You and D. A. Nicewicz, *J. Am. Chem. Soc*., 2015, **137**, 24, 7580–7583. (c) W. Liu, L. Li, Z. Chen and C.-J. Li, *Org. Biomol. Chem*., 2015, **13**, 6170-6174. (d) A. Seoane, N. Casanova, N. Quiñones, J. L. Mascareñas and M. Gulías, *J. Am. Chem. Soc*., 2014, **136**, 3, 834–837.

30. O. V. Dolomanov, L. J. Bourhis, R. J. Gildea, J. A. K. Howard and H. Puschmamn, *J. Appl. Crystallogr*., 2009, **42**, 339-341.

31. L. Palatimus and G. Chapuis, J. *Appl. Crystallogr*., 2007, **40**, 786-790.

32. G. M. Sheldrick, *Acta Crystallogr. Sect. A.: Found. Crystallogr*. 2008, **64,** 112-122.

33. Gaussian 09 (Revision A.02), M. J. Frisch, G. W. Trucks, H. B. Schlegel, G. E. Scuseria, M. A. Robb, J. R. Cheeseman, G. Scalmani, V. Barone, B. Mennucci and G. A. Petersson, Gaussian, Inc., Wallingford CT, 2009.

34. S. Grimme, J. Antony, S. Ehrlich and H. A. Krieg, *J. Chem. Phys.,* 2010, **132**, 154104.

35. S. Bhunya, L. Roy and A. Paul, *ACS Catal.,* 2016, **6***,* 4068-4080.

36. X. Su, Y. Sun, J. Yao, H. Chen and C. Chen, *Chem. Commun*., 2016, **52***,* 4537-4540.

Spectroscopic Details

and

Computational Details
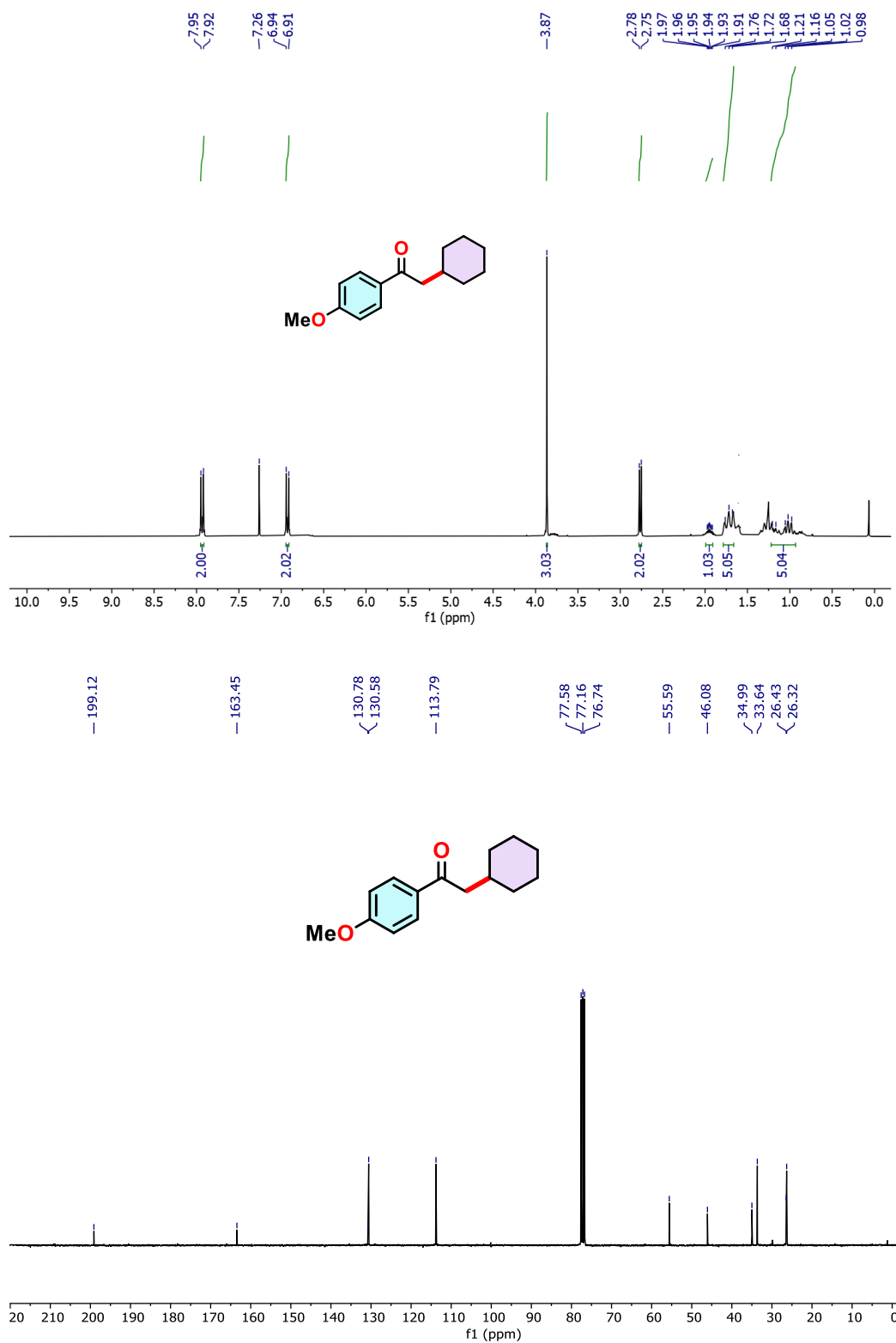
Figure 4.3. ^{1}H NMR (300 MHz) and ^{13}C NMR (75 MHz) spectra of compound **3a** in CDCl$_3$..
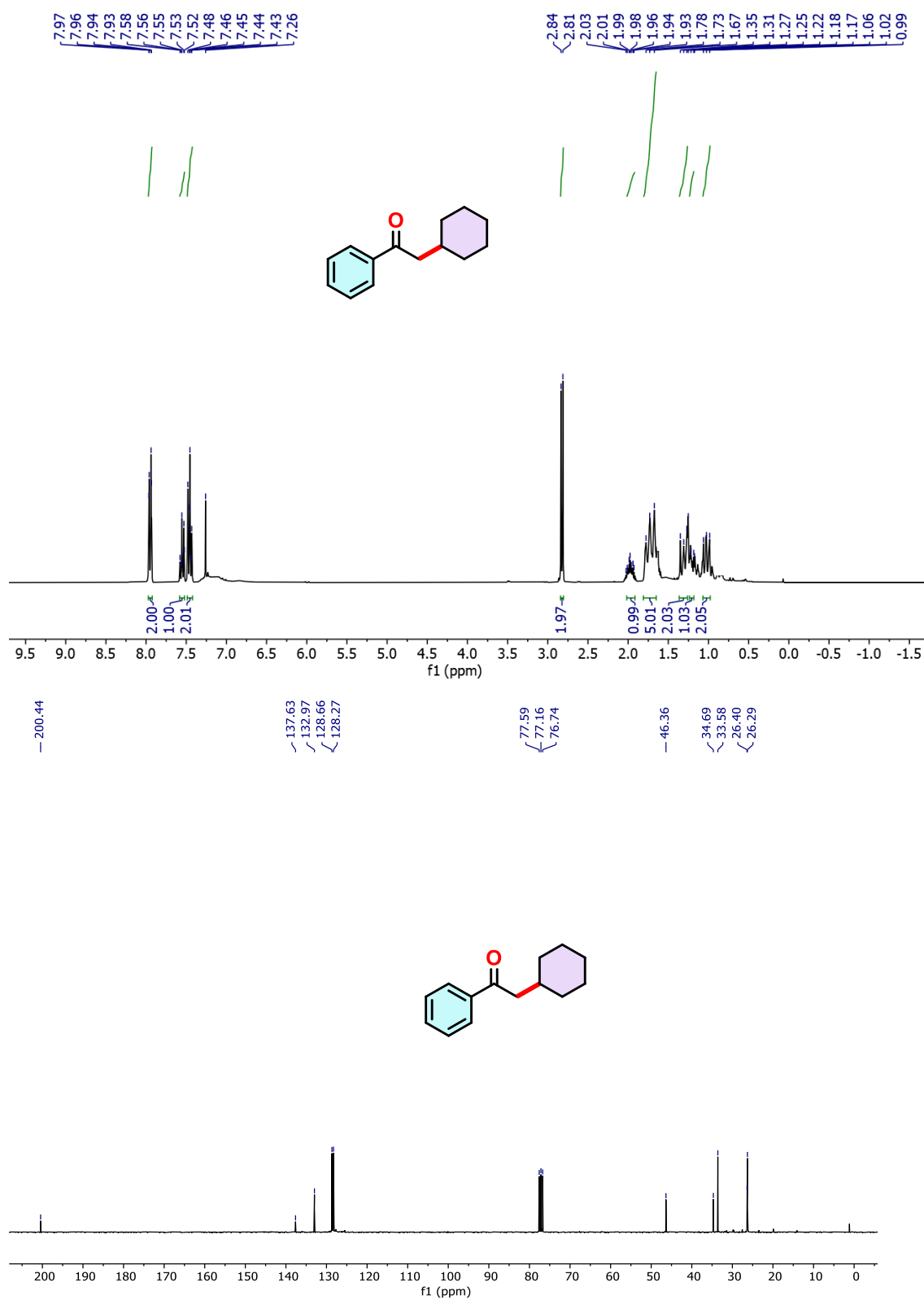
Figure 4.4. ¹H NMR (300 MHz) and ¹³C NMR (75 MHz) spectra of compound **3b** in CDCl₃..
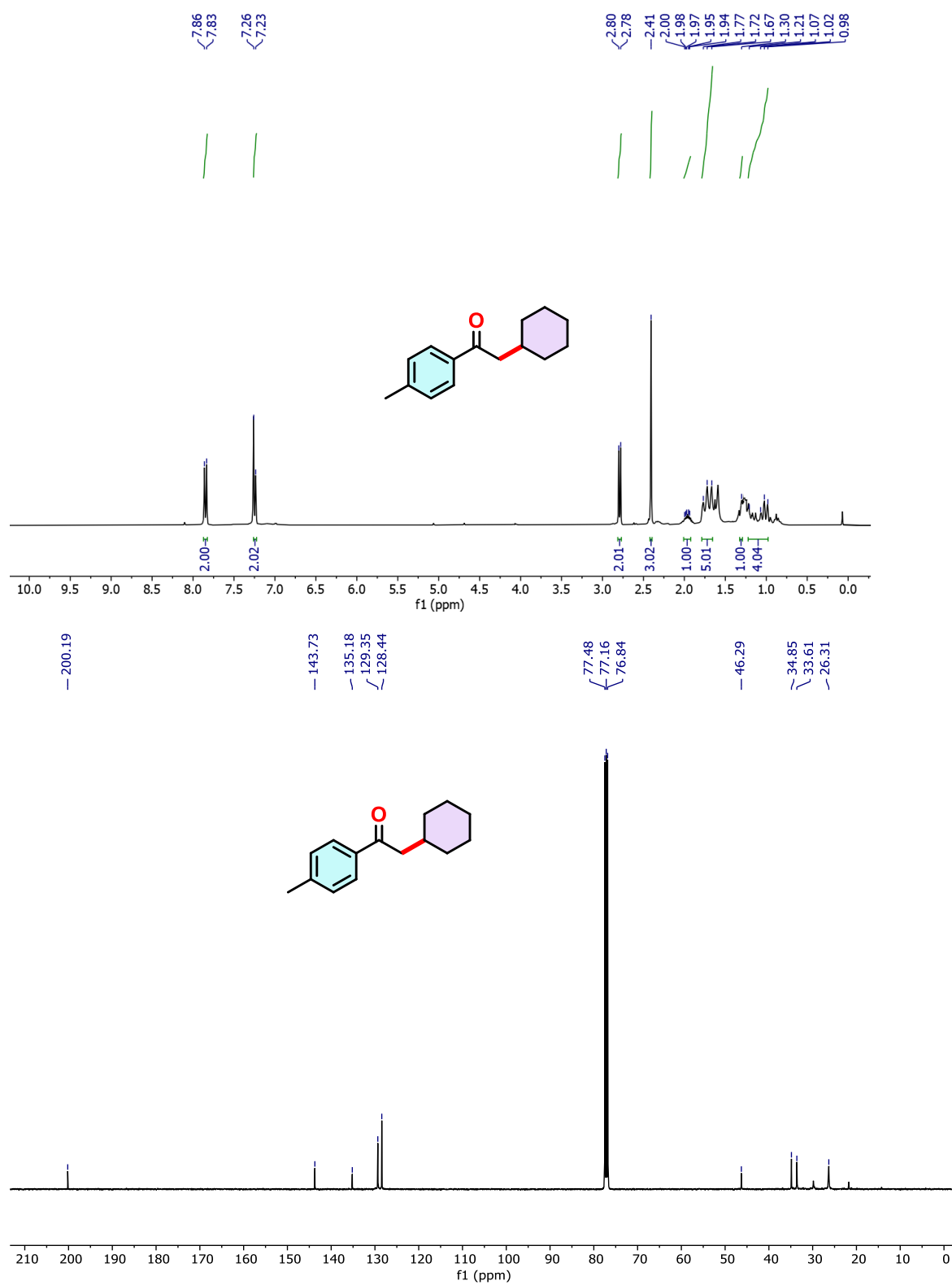
Figure 4.5. ^{1}H NMR (300 MHz) and ^{13}C NMR (75 MHz) spectra of compound **3c** in CDCl$_3$.
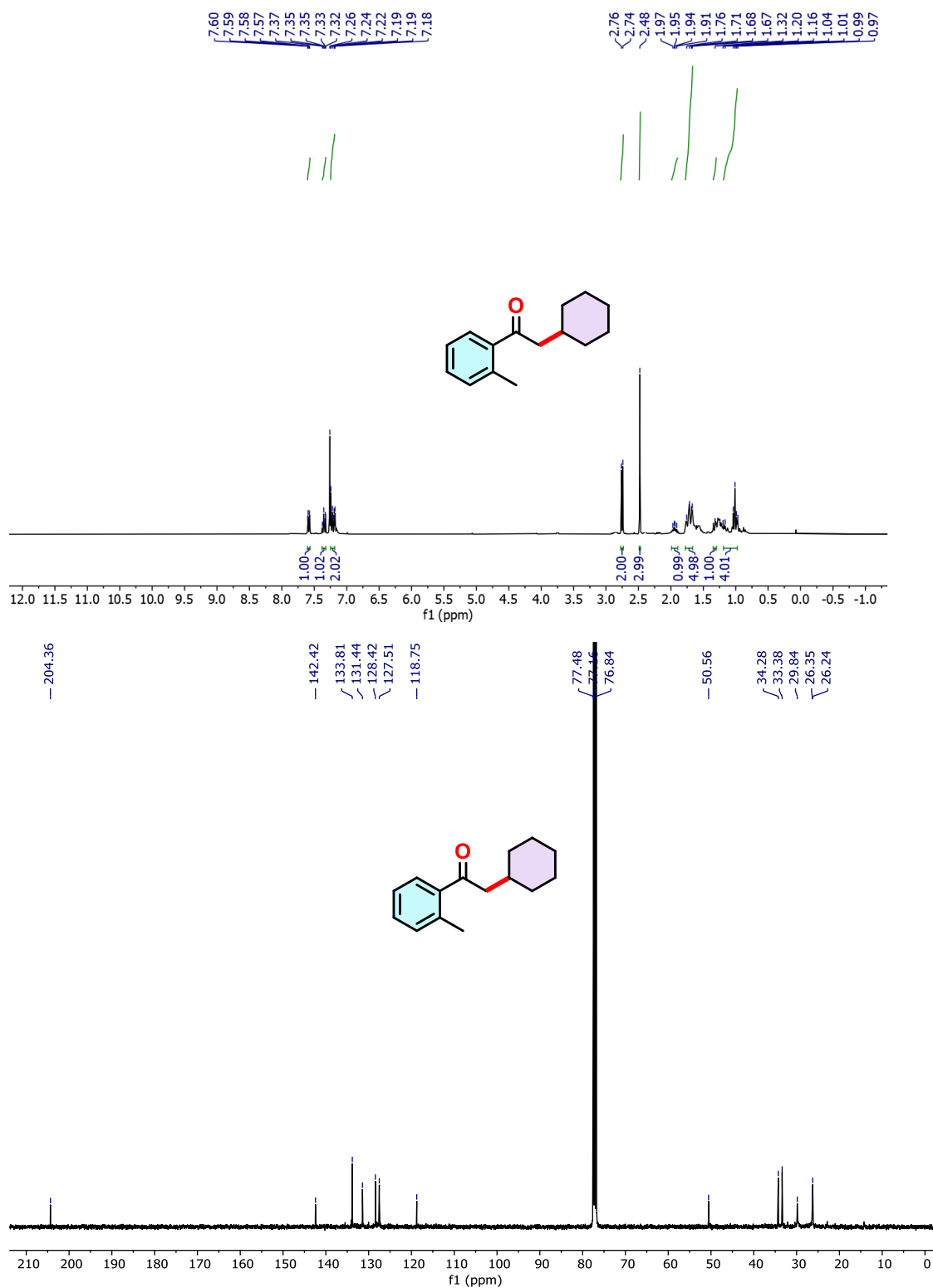
Figure 4.6. ¹H NMR (300 MHz) and ¹³C NMR (75 MHz) spectra of compound **3d** in CDCl₃.

Figure 4.7. ¹H NMR (300 MHz) and ¹³C NMR (75 MHz) spectra of compound **3e** in CDCl₃.
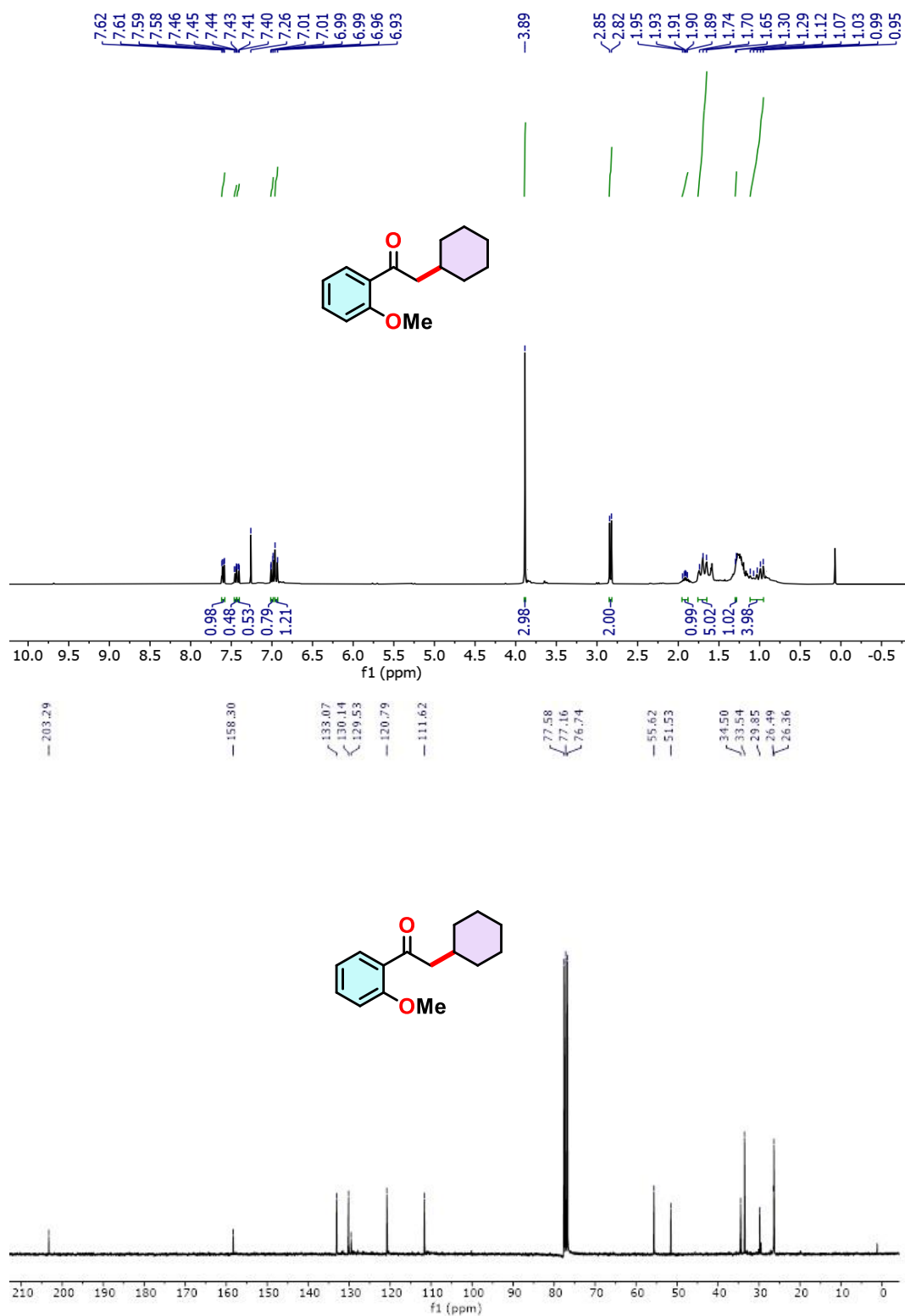
Figure 4.8. ¹H NMR (300 MHz) and ¹³C NMR (75 MHz) spectra of compound **3f** in CDCl₃.
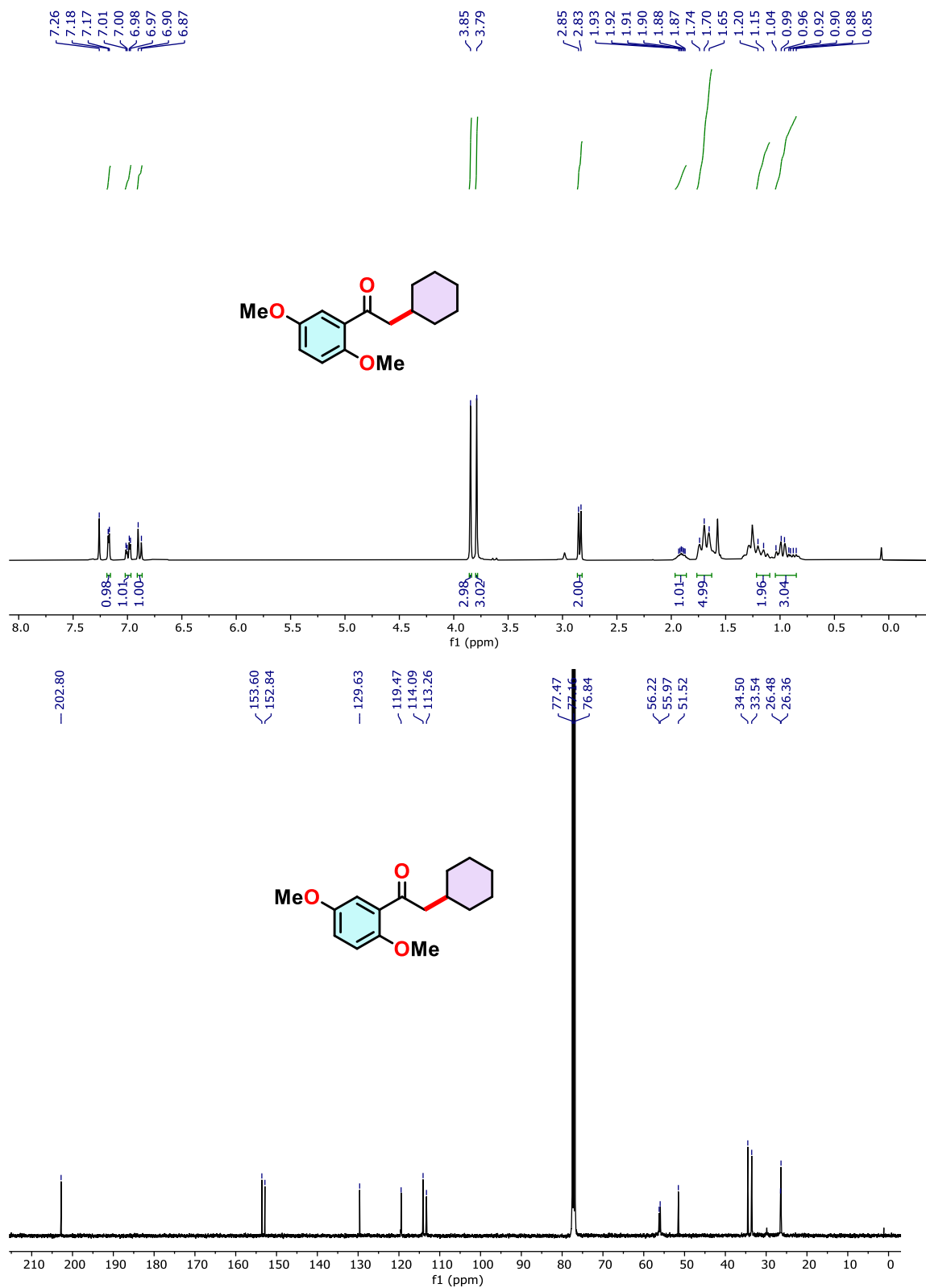
Figure 4.9. ¹H NMR (300 MHz) and ¹³C NMR (75 MHz) spectra of compound **3g** in CDCl₃.
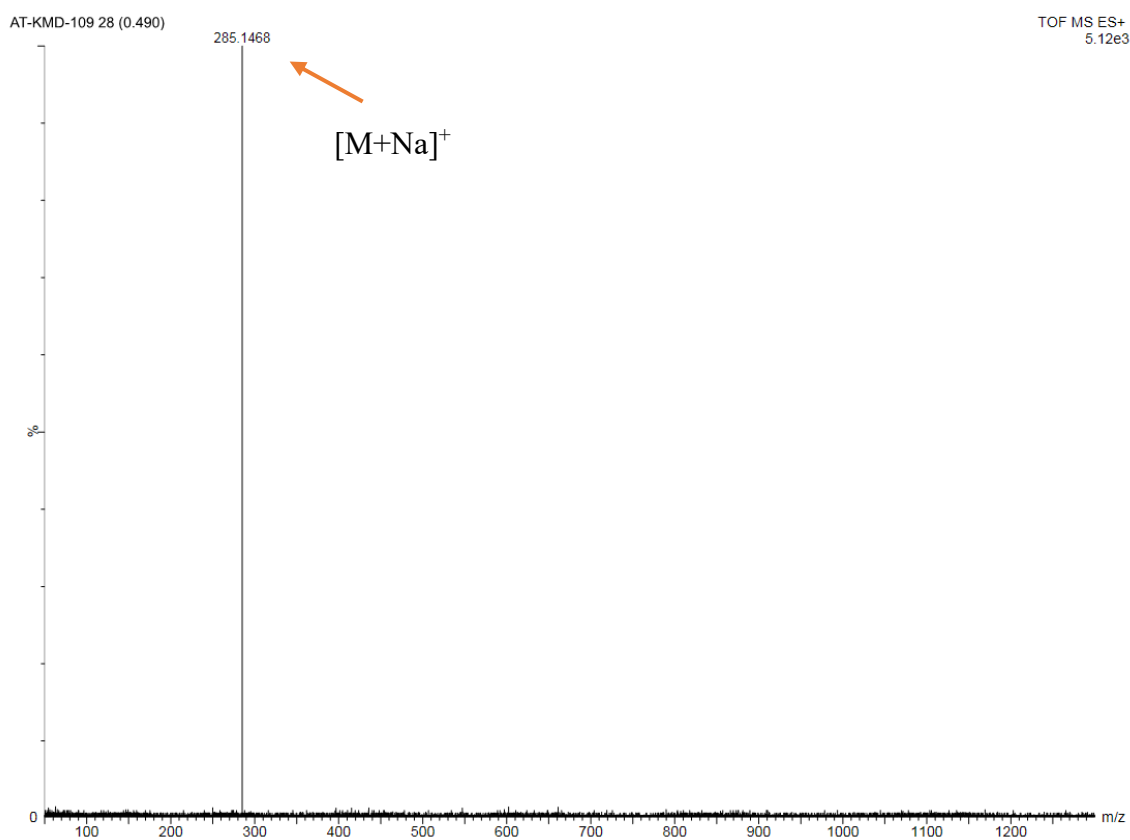
Figure 4.10. HRMS of compound **3g**.
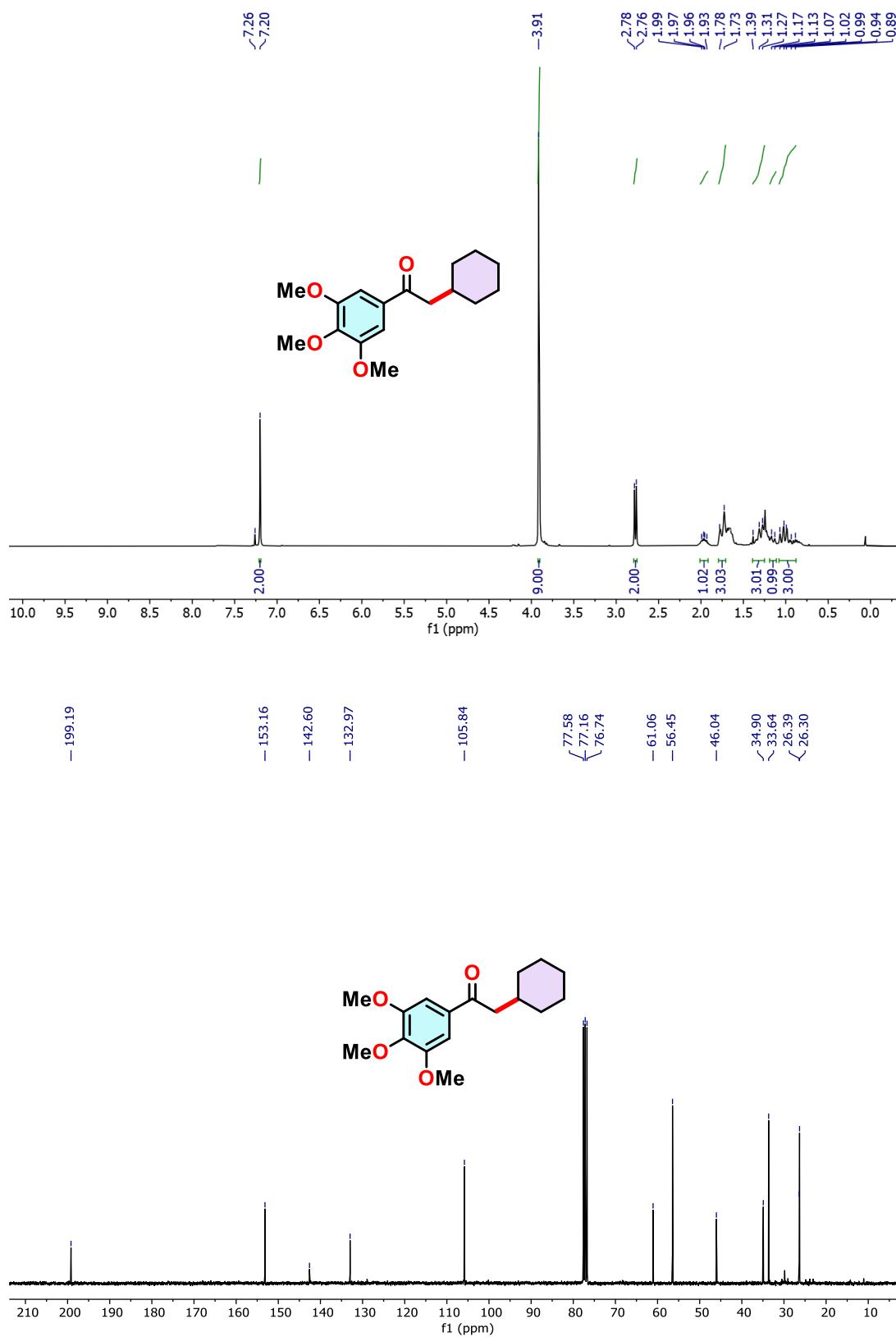
Figure 4.11. ¹H NMR (300 MHz) and ¹³C NMR (75 MHz) spectra of compound **3h** in CDCl₃.
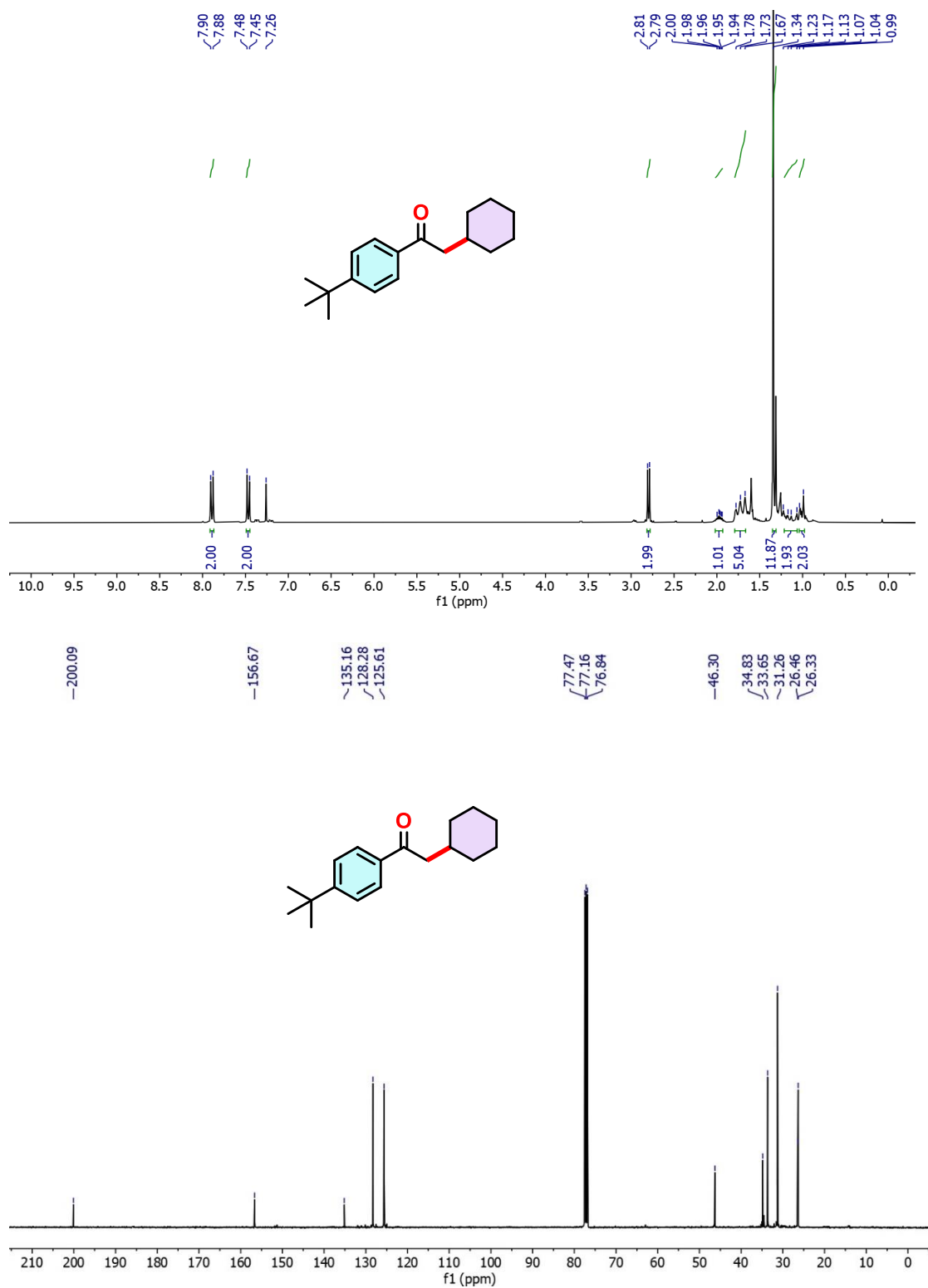
Figure 4.12. ¹H NMR (300 MHz) and ¹³C NMR (75 MHz) spectra of compound **3i** in CDCl₃.
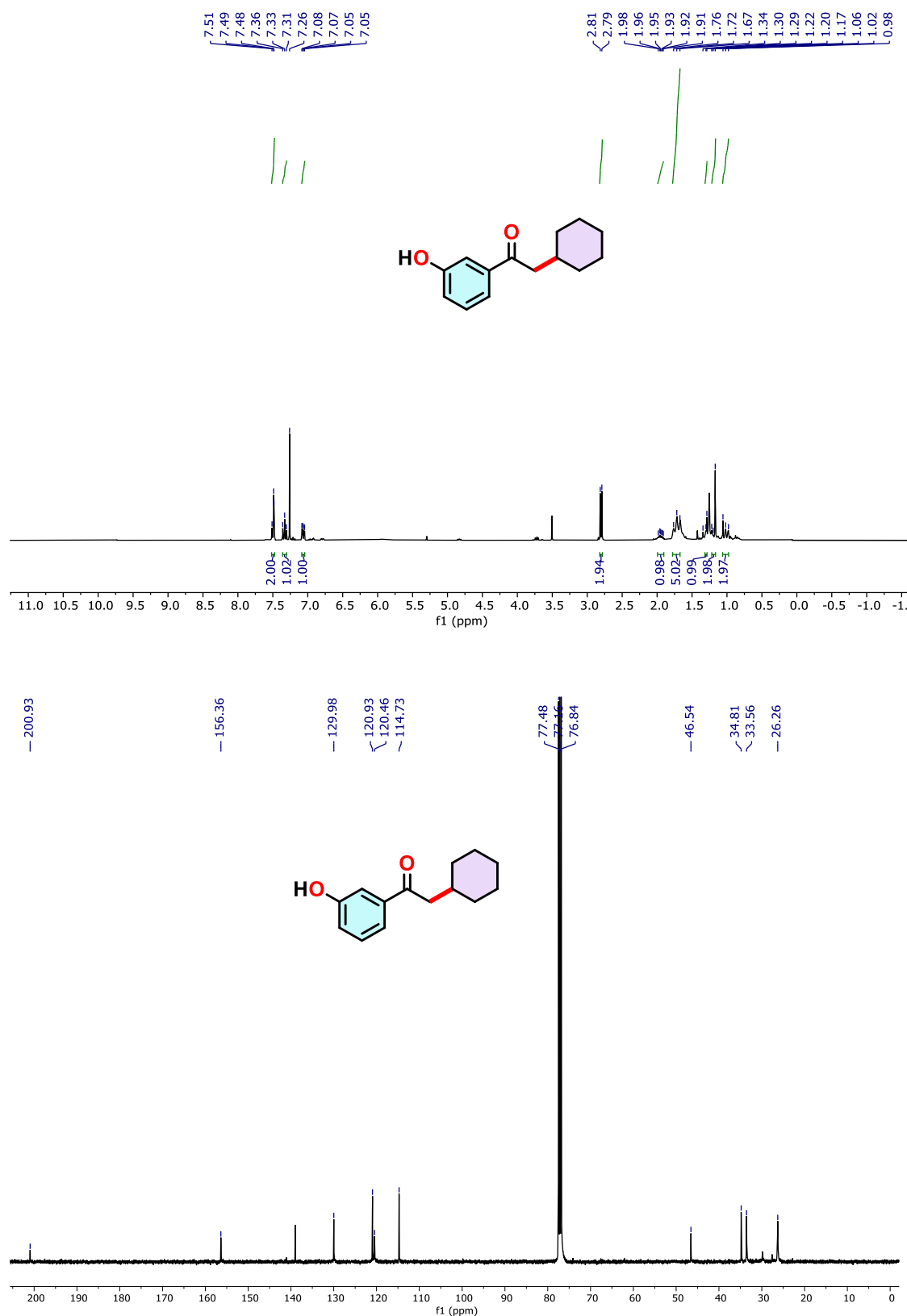
Figure 4.13. ^{1}H NMR (300 MHz) and ^{13}C NMR (75 MHz) spectra of compound **3j** in CDCl$_3$.
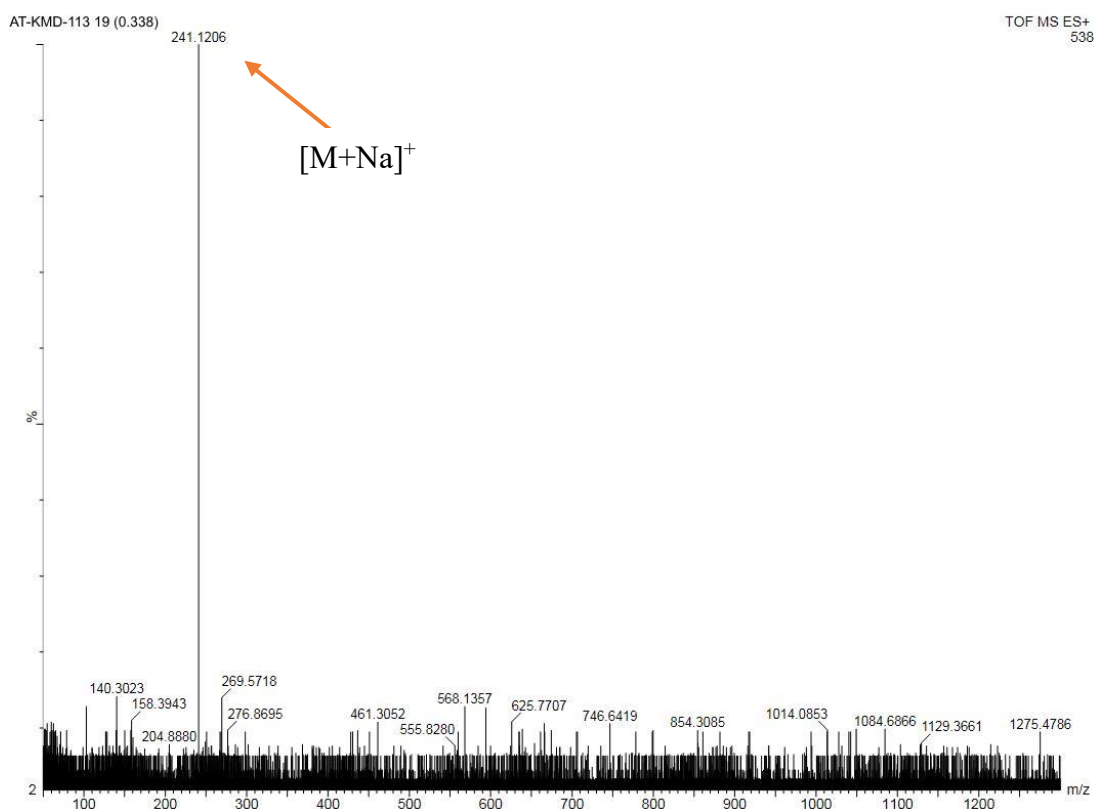
Figure 4.14. HRMS of compound **3j**.
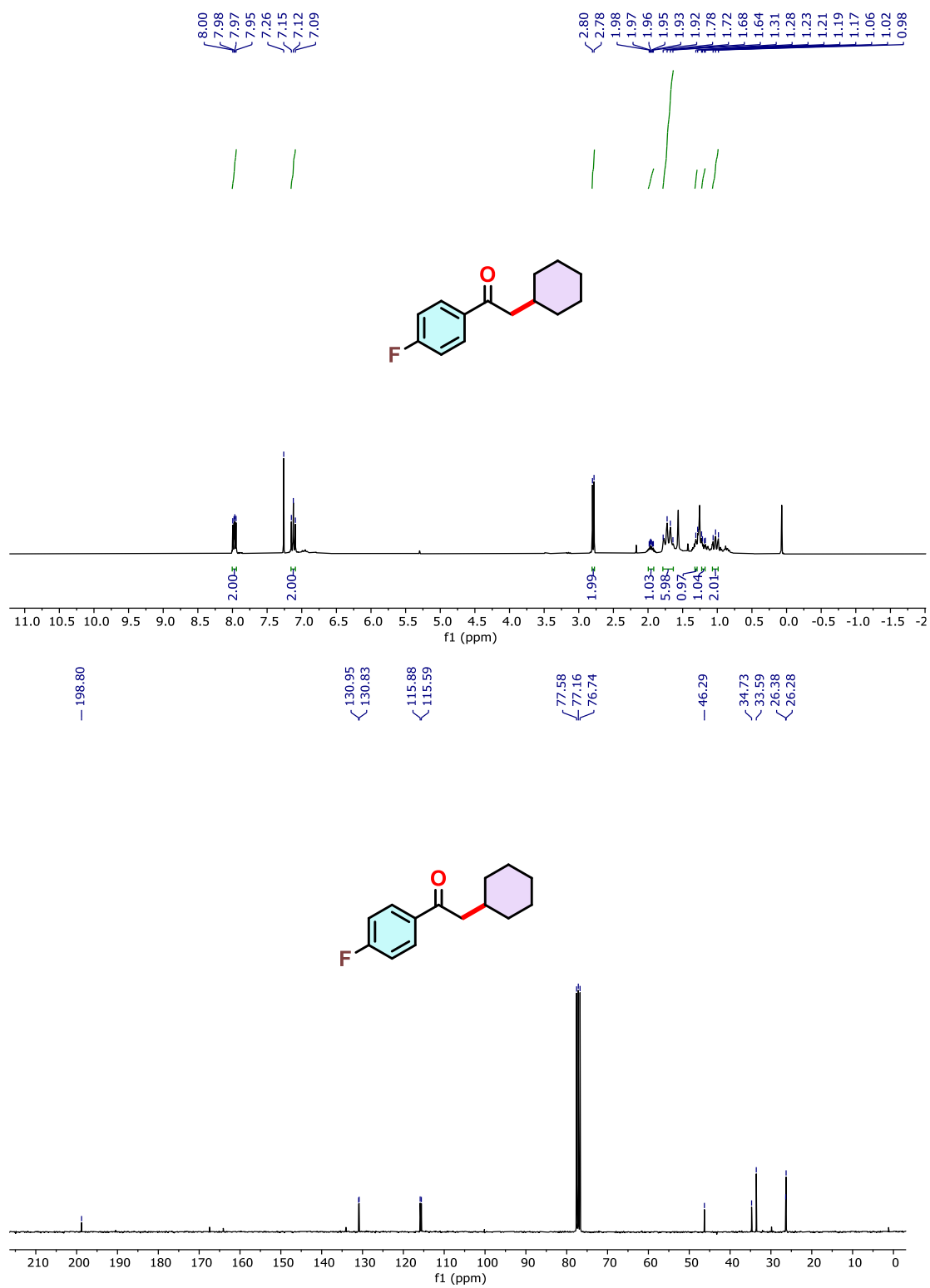
Figure 4.15. ^{1}H NMR (300 MHz) and ^{13}C NMR (75 MHz) spectra of compound **3k** in CDCl$_3$.
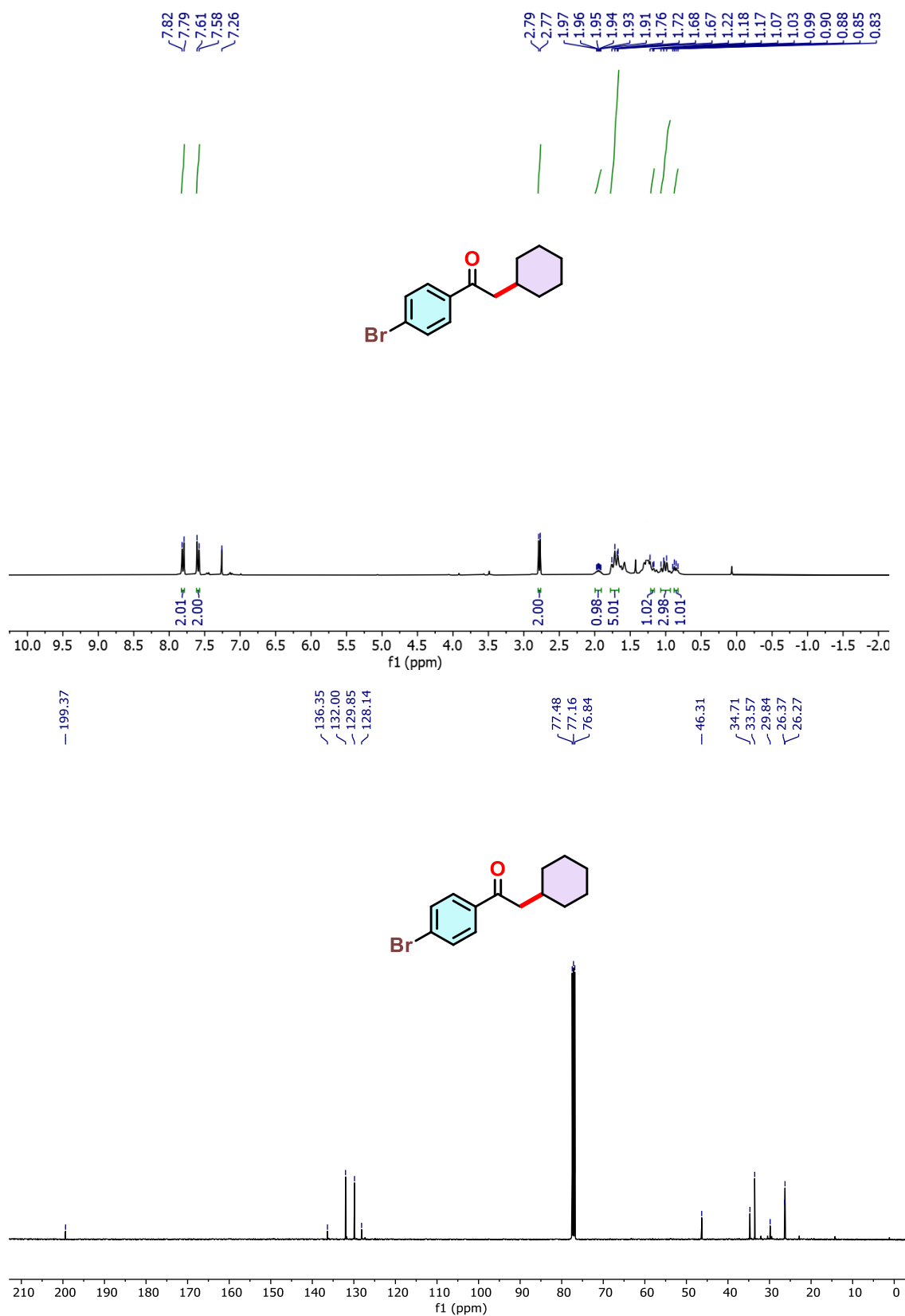
Figure 4.16. ¹H NMR (300 MHz) and ¹³C NMR (75 MHz) spectra of compound **3l** in CDCl₃.
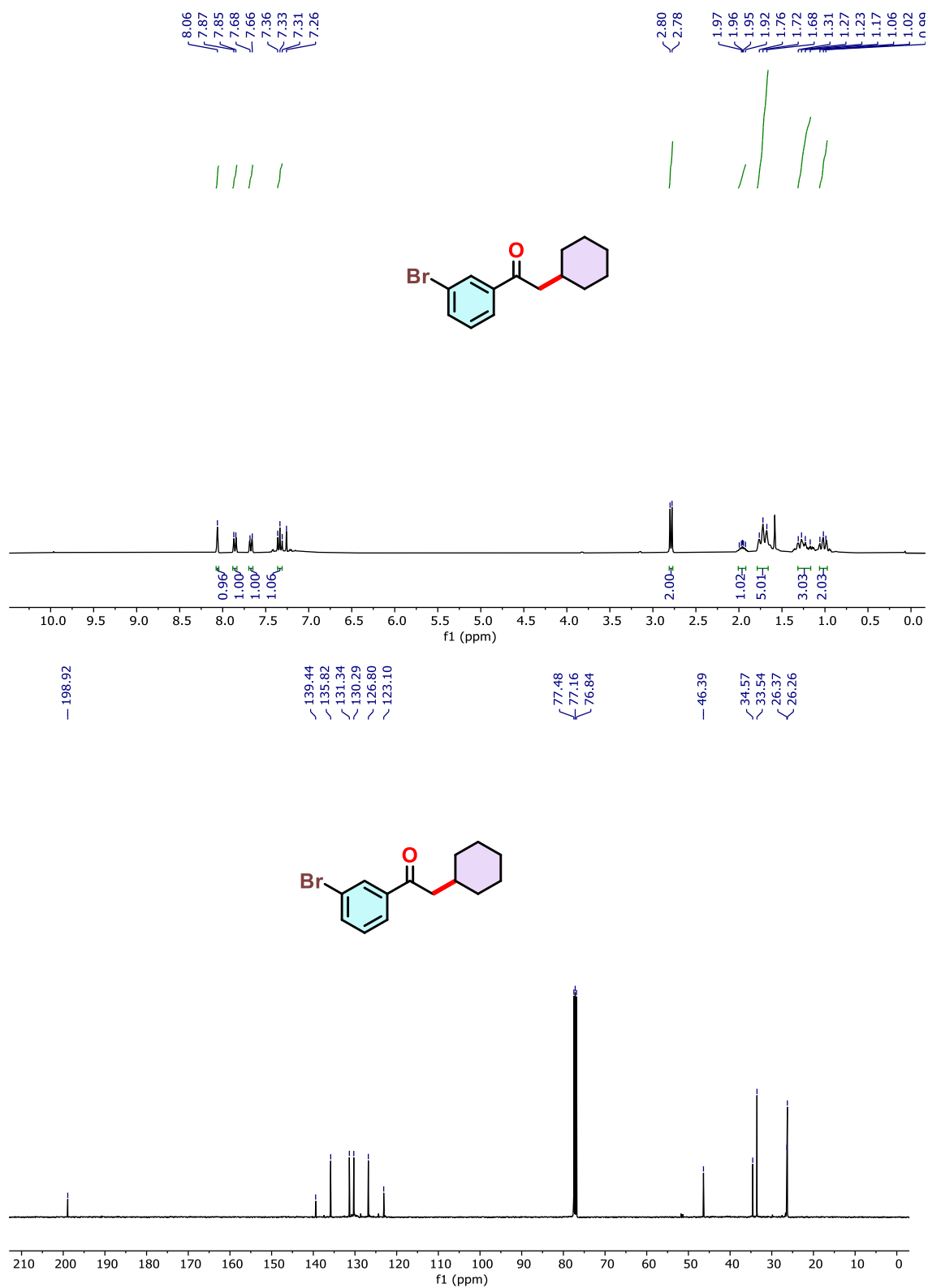
Figure 4.17. ^{1}H NMR (300 MHz) and ^{13}C NMR (75 MHz) spectra of compound **3m** in CDCl$_3$.
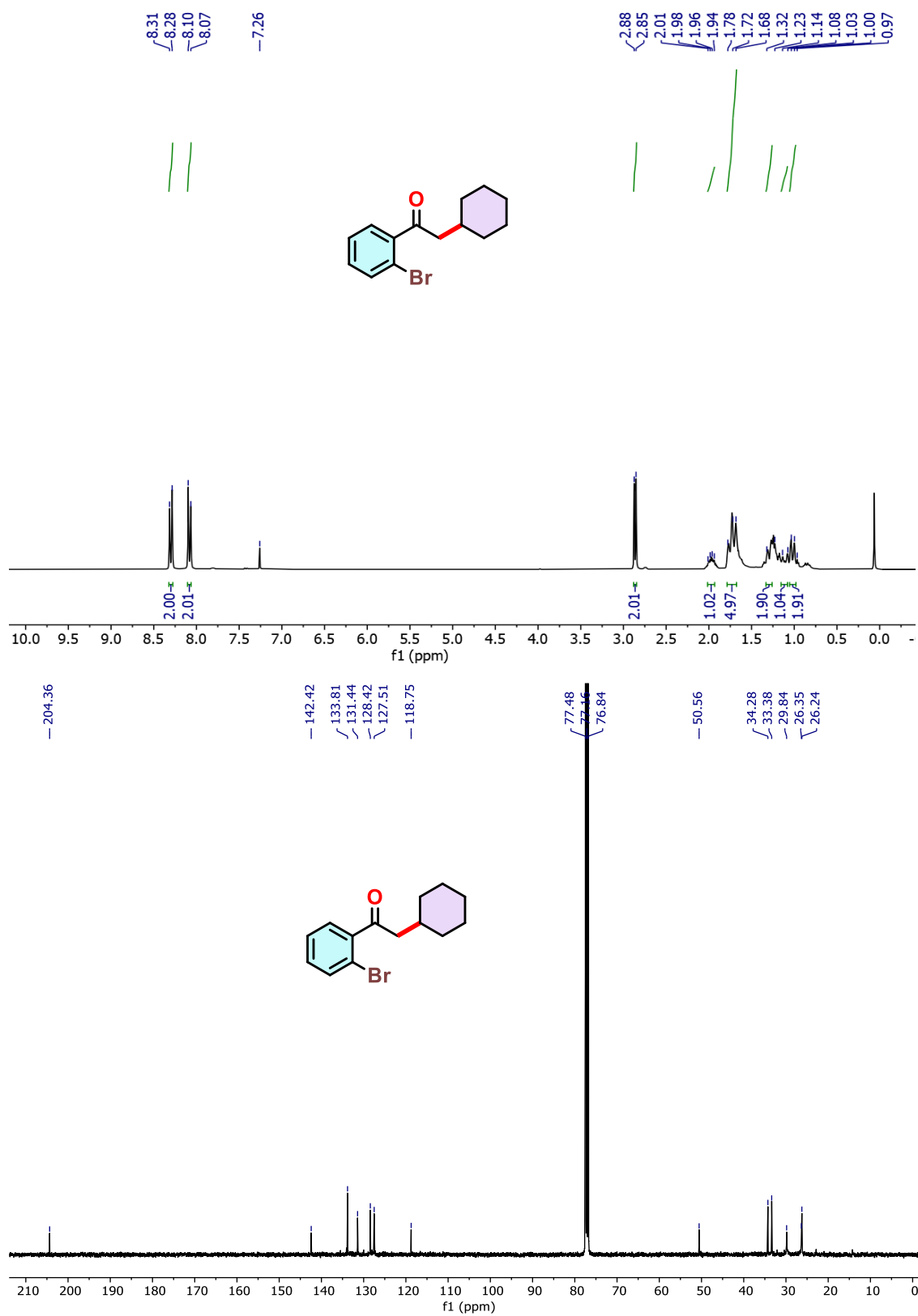
Figure 4.18. ¹H NMR (300 MHz) and ¹³C NMR (75 MHz) spectra of compound **3n** in CDCl₃.
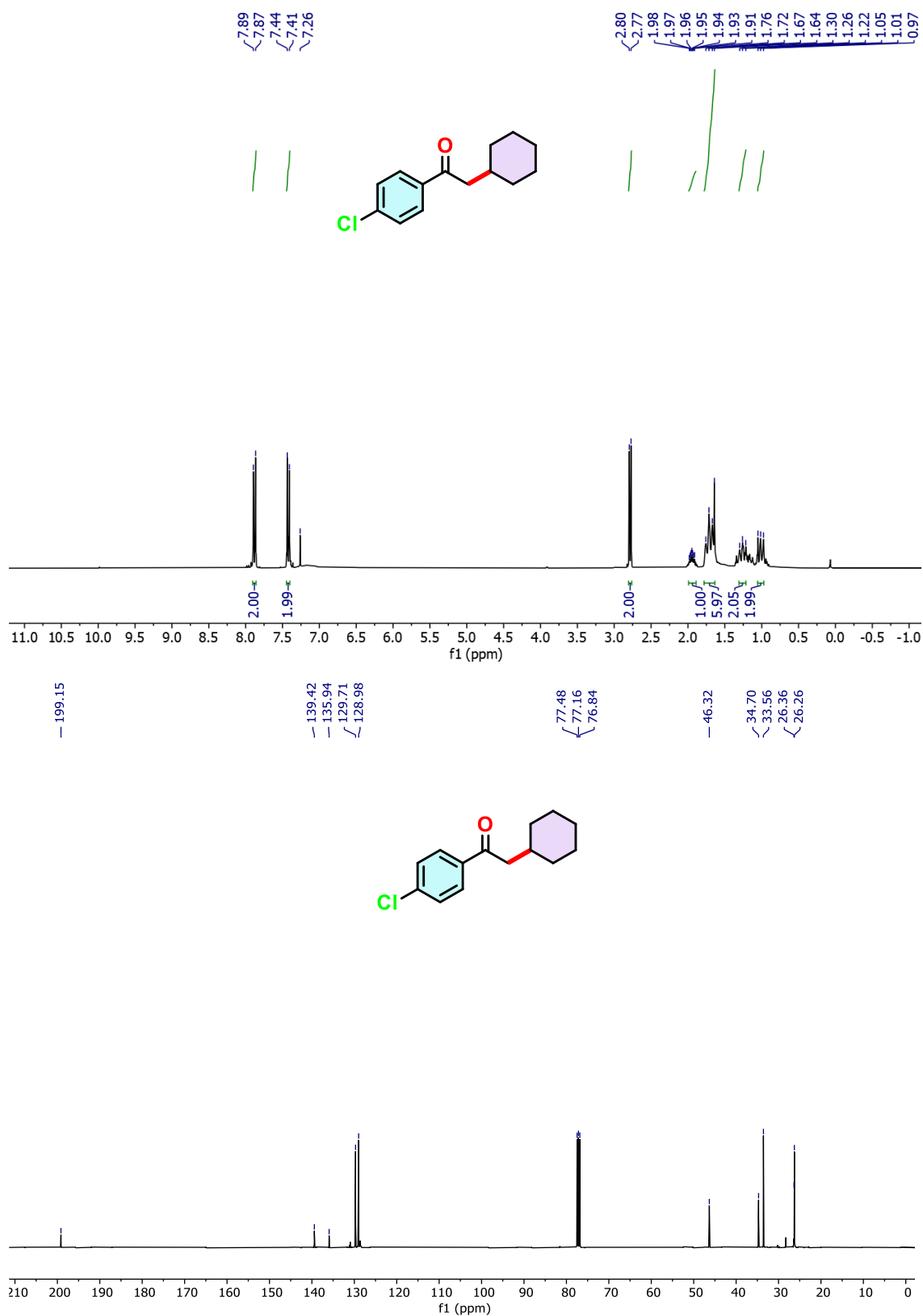
Figure 4.19. ^{1}H NMR (300 MHz) and ^{13}C NMR (75 MHz) spectra of compound **3o** in CDCl$_3$.
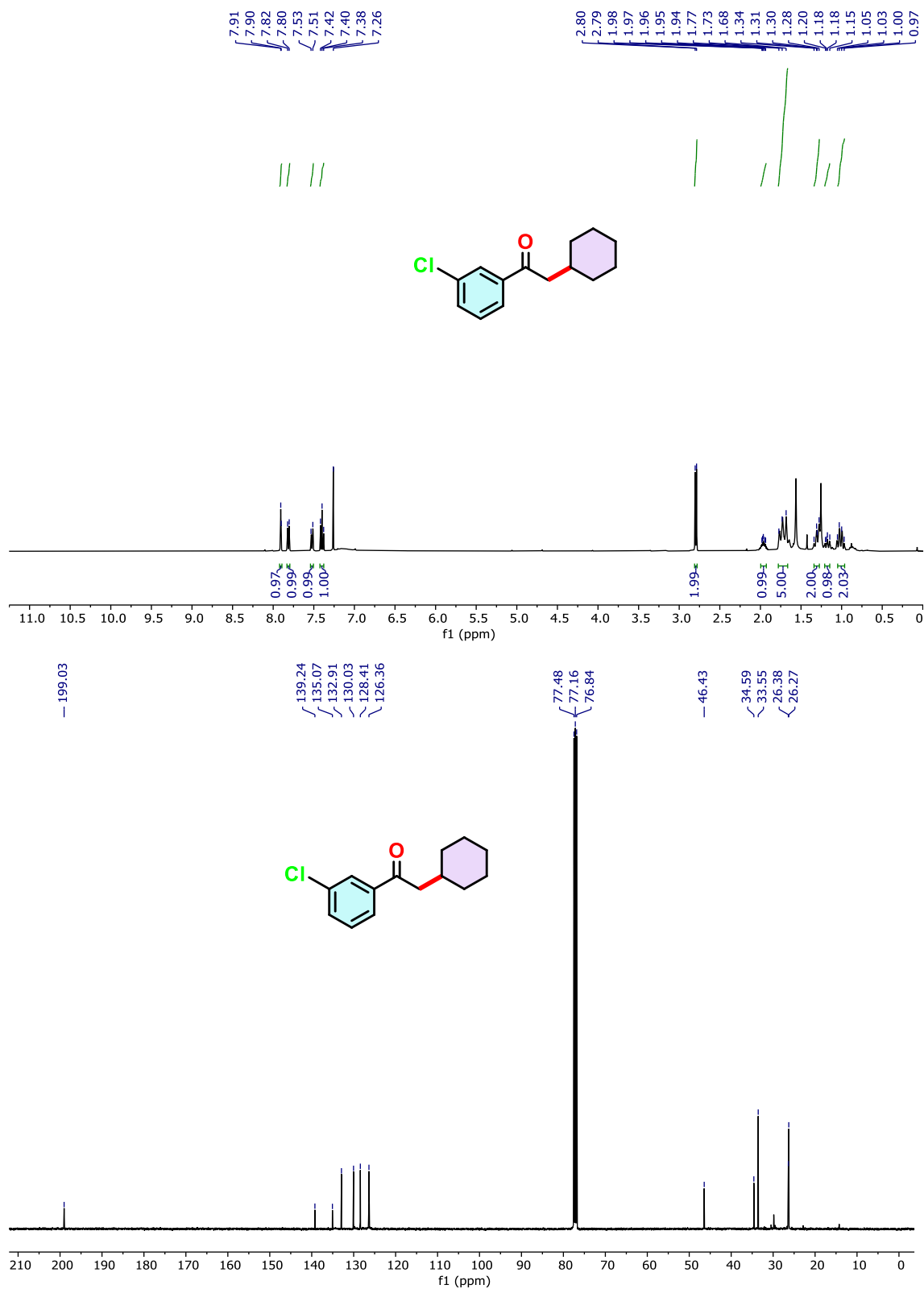
Figure 4.20. ¹H NMR (300 MHz) and ¹³C NMR (75 MHz) spectra of compound **3o** in CDCl₃.
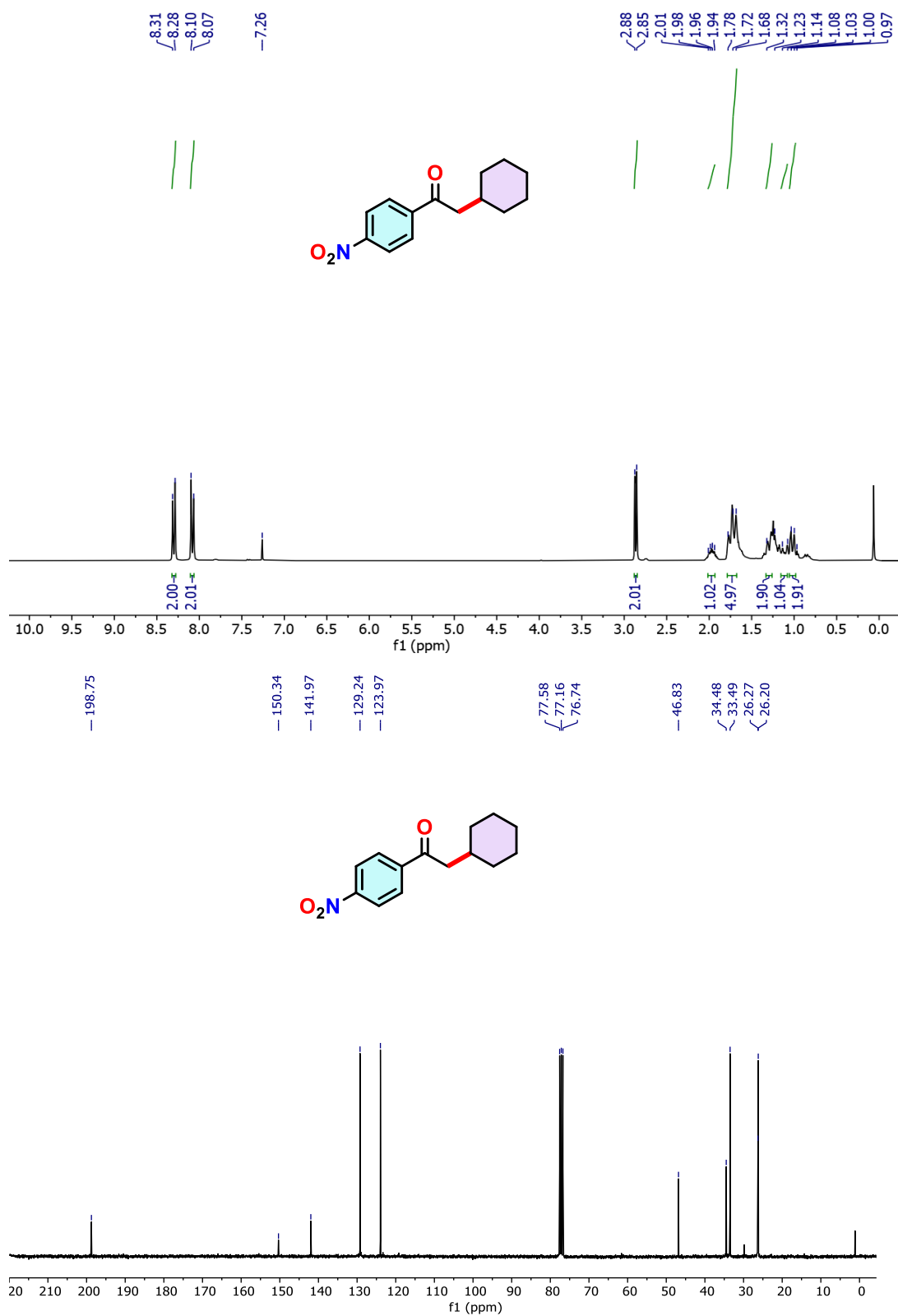
Figure 4.21. ¹H NMR (300 MHz) and ¹³C NMR (75 MHz) spectra of compound **3q** in CDCl₃.
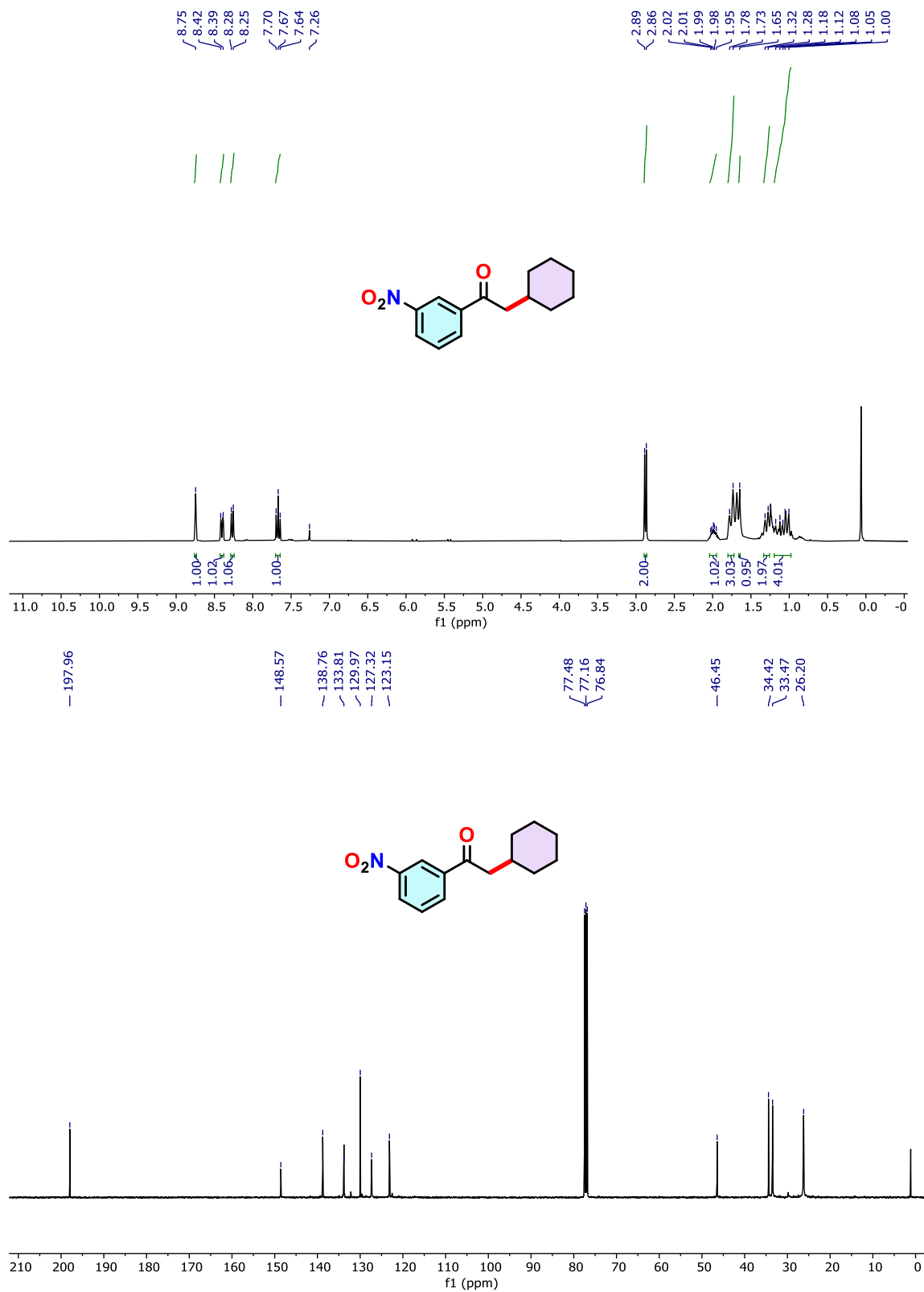
Figure 4.22. ^{1}H NMR (300 MHz) and ^{13}C NMR (75 MHz) spectra of compound **3r** in CDCl$_3$.
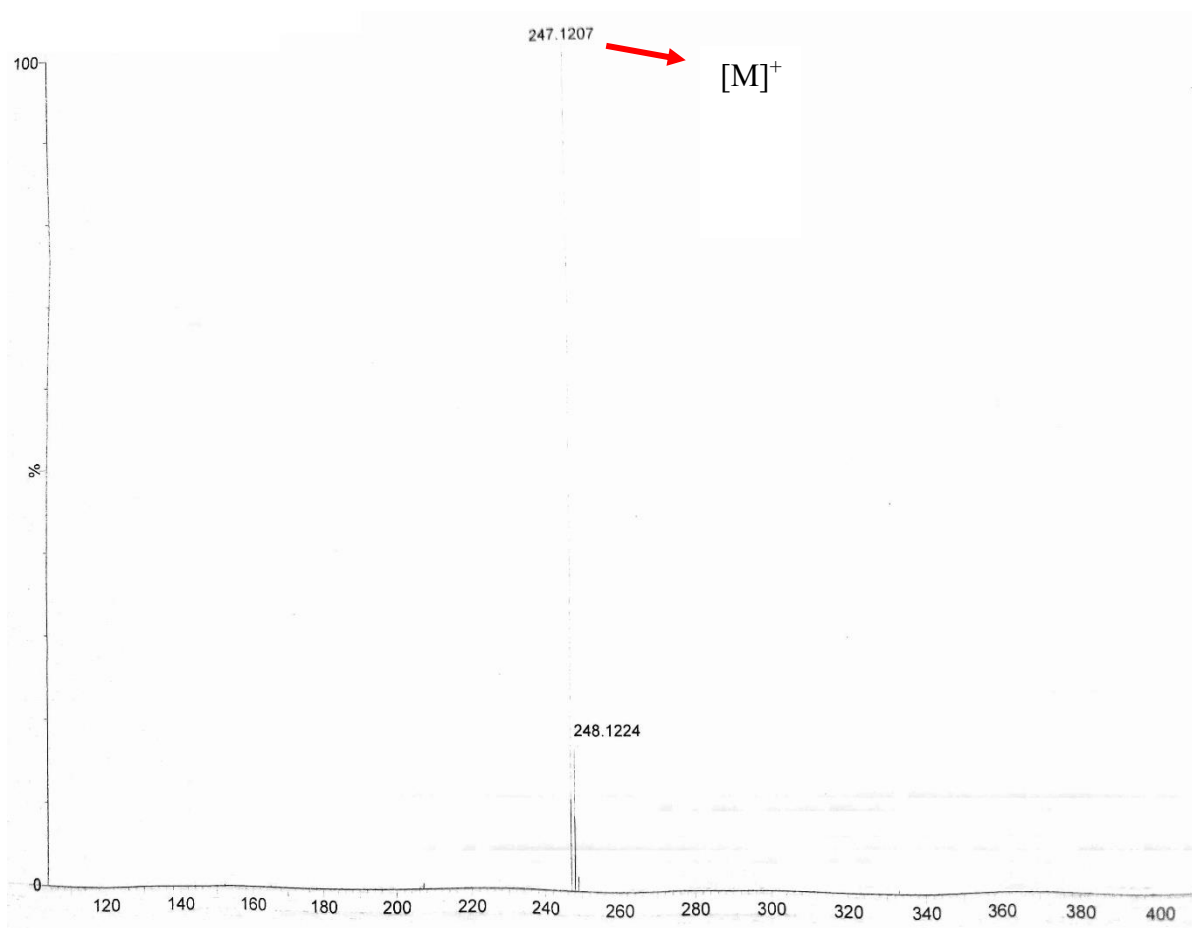
Figure 4.23. HRMS of compound **3r**.
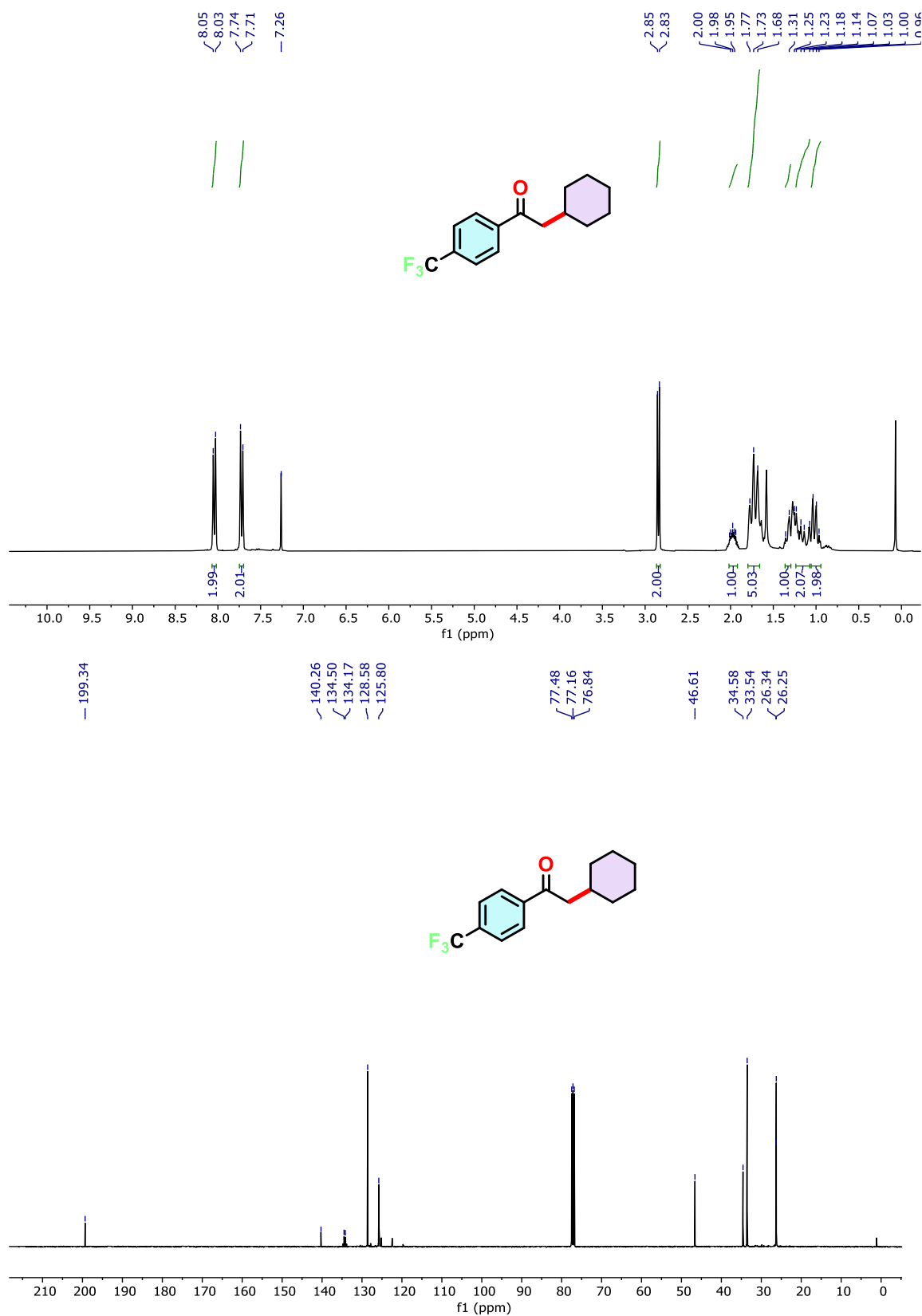
Figure 4.24. ¹H NMR (300 MHz) and ¹³C NMR (75 MHz) spectra of compound **3s** in CDCl₃.
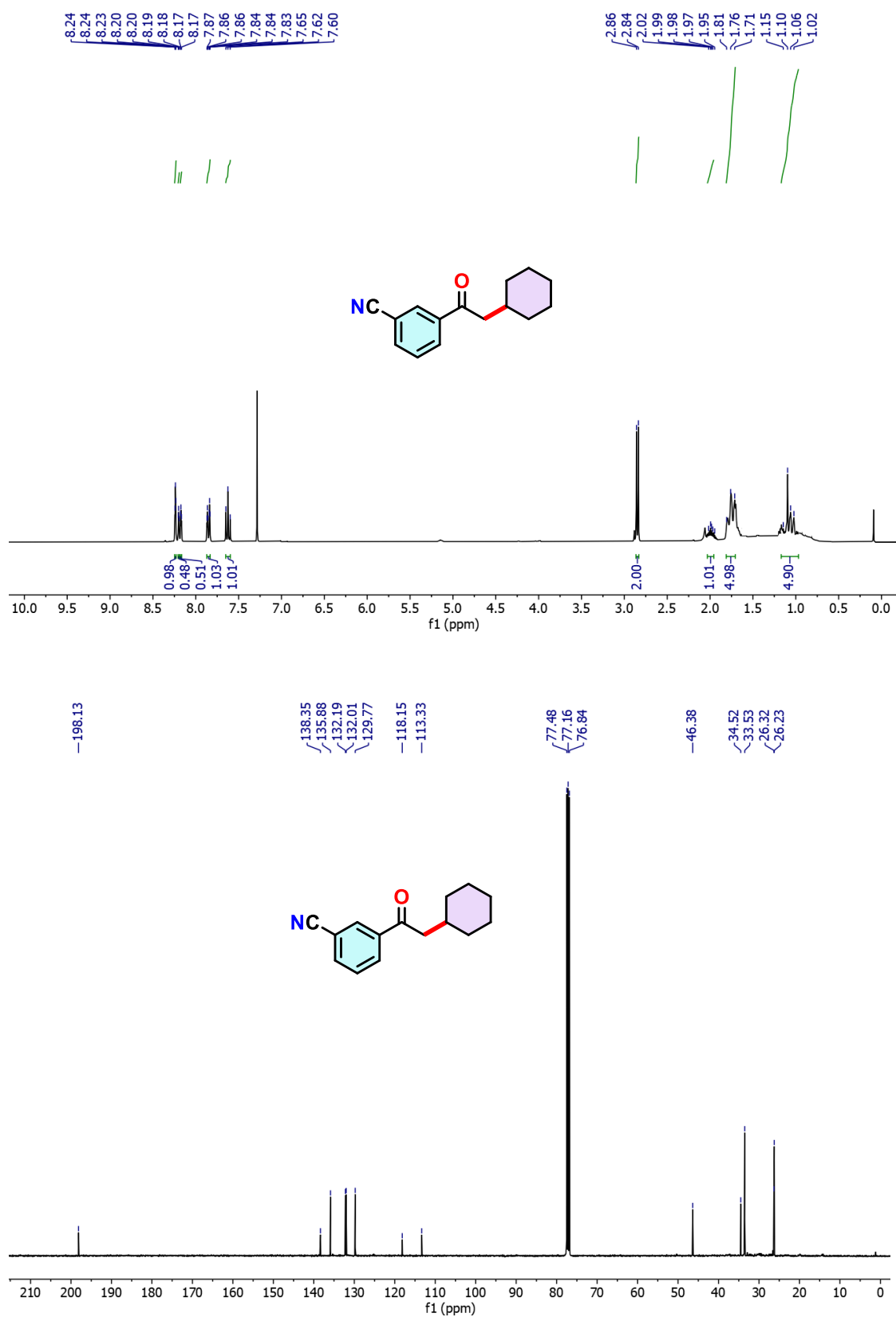
Figure 4.25. ^{1}H NMR (300 MHz) and ^{13}C NMR (75 MHz) spectra of compound **3t** in CDCl$_3$.
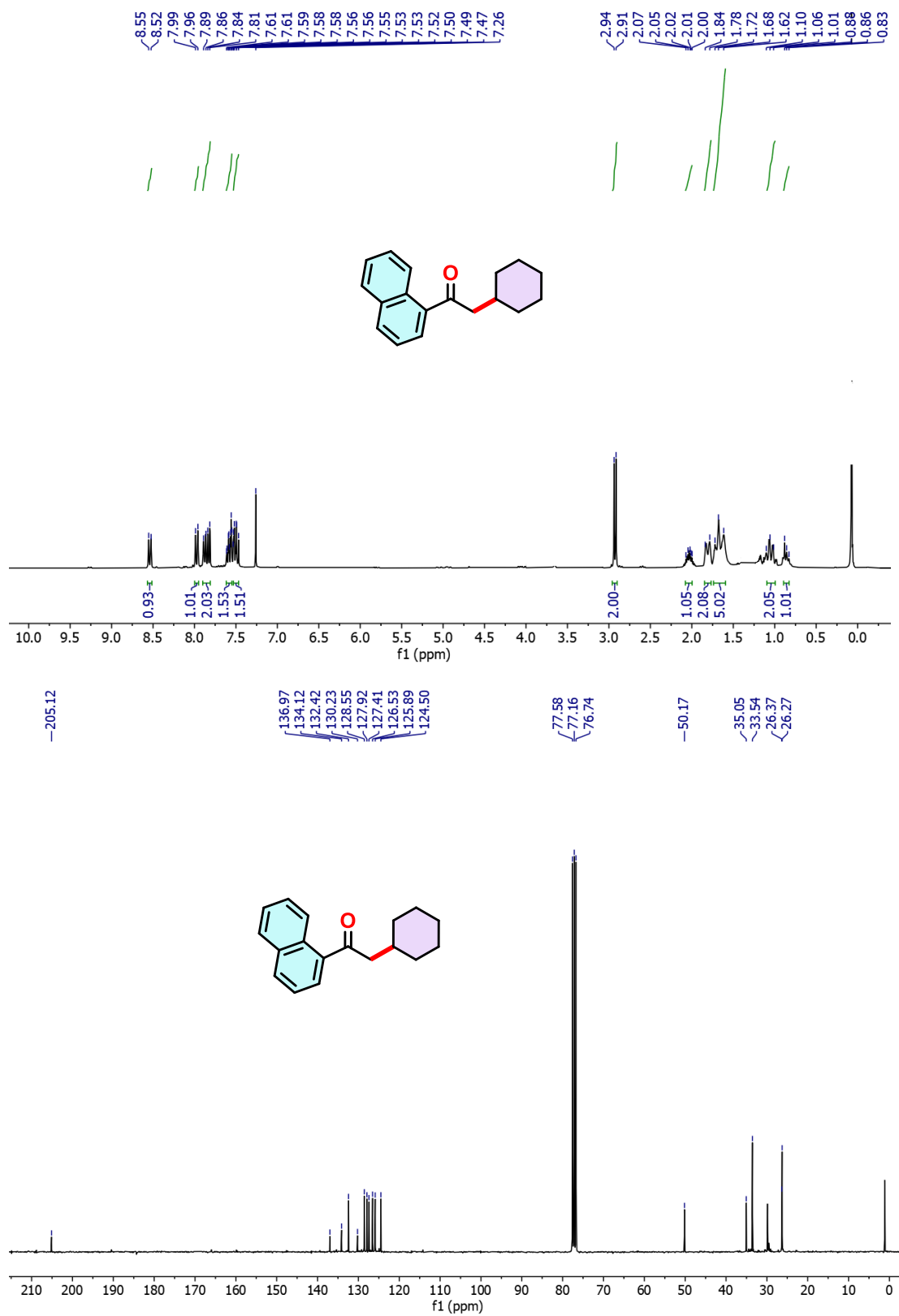
Figure 4.26. ^{1}H NMR (300 MHz) and ^{13}C NMR (75 MHz) spectra of compound **3u** in CDCl$_3$.
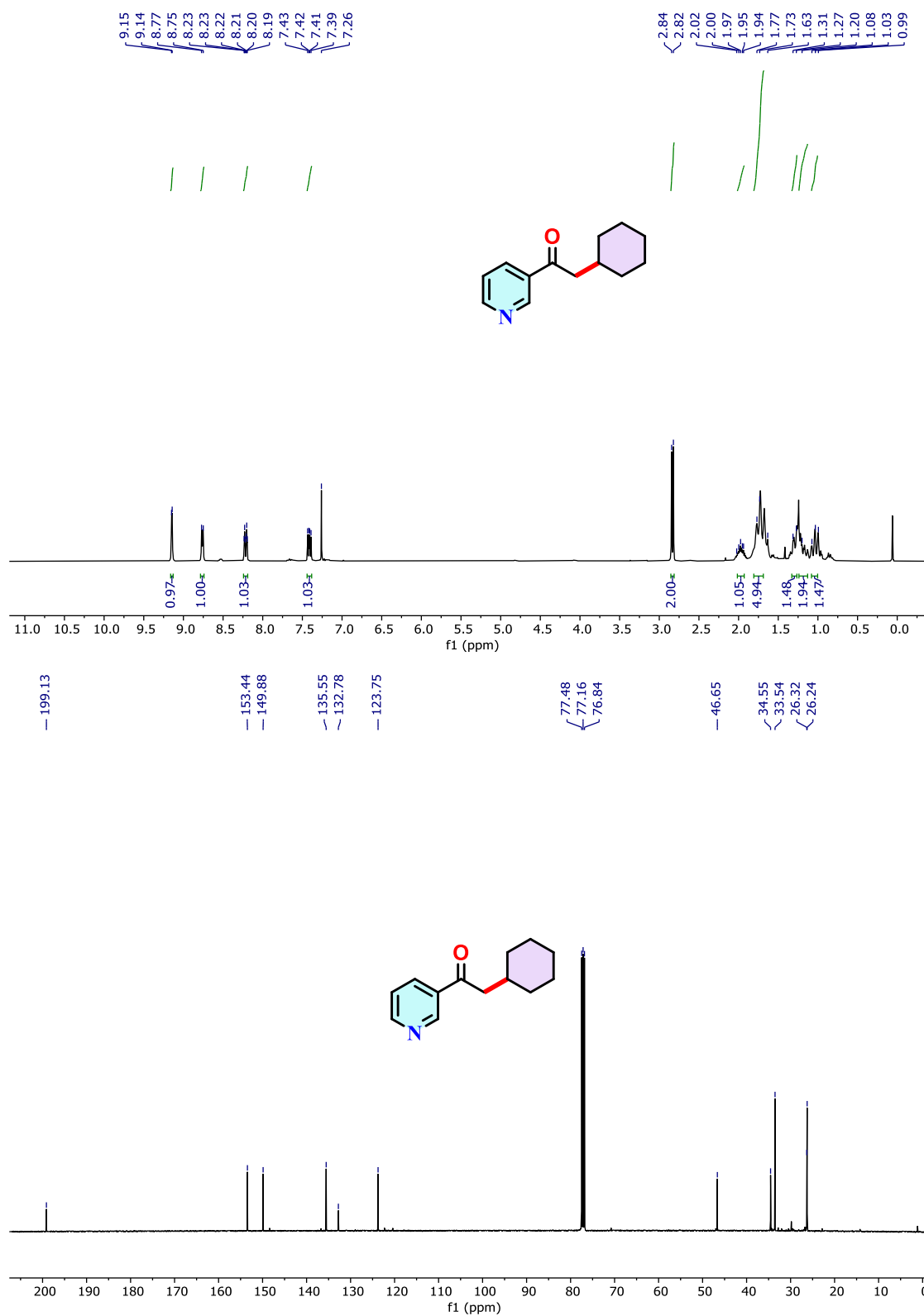
Figure 4.27. ¹H NMR (300 MHz) and ¹³C NMR (75 MHz) spectra of compound **3v** in CDCl₃.
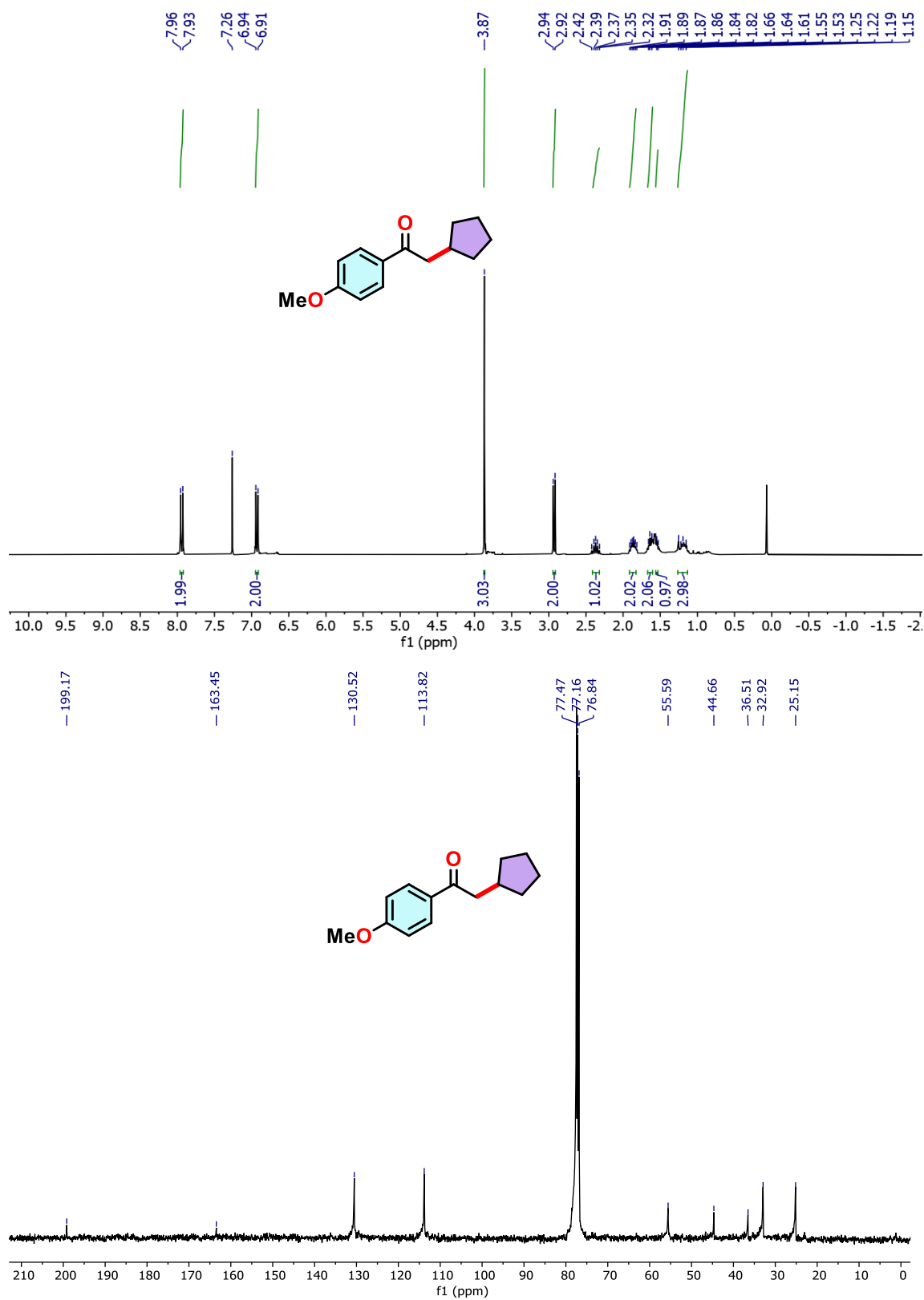
Figure 4.28. ^{1}H NMR (300 MHz) and ^{13}C NMR (75 MHz) spectra of compound **3aa** in CDCl$_3$.
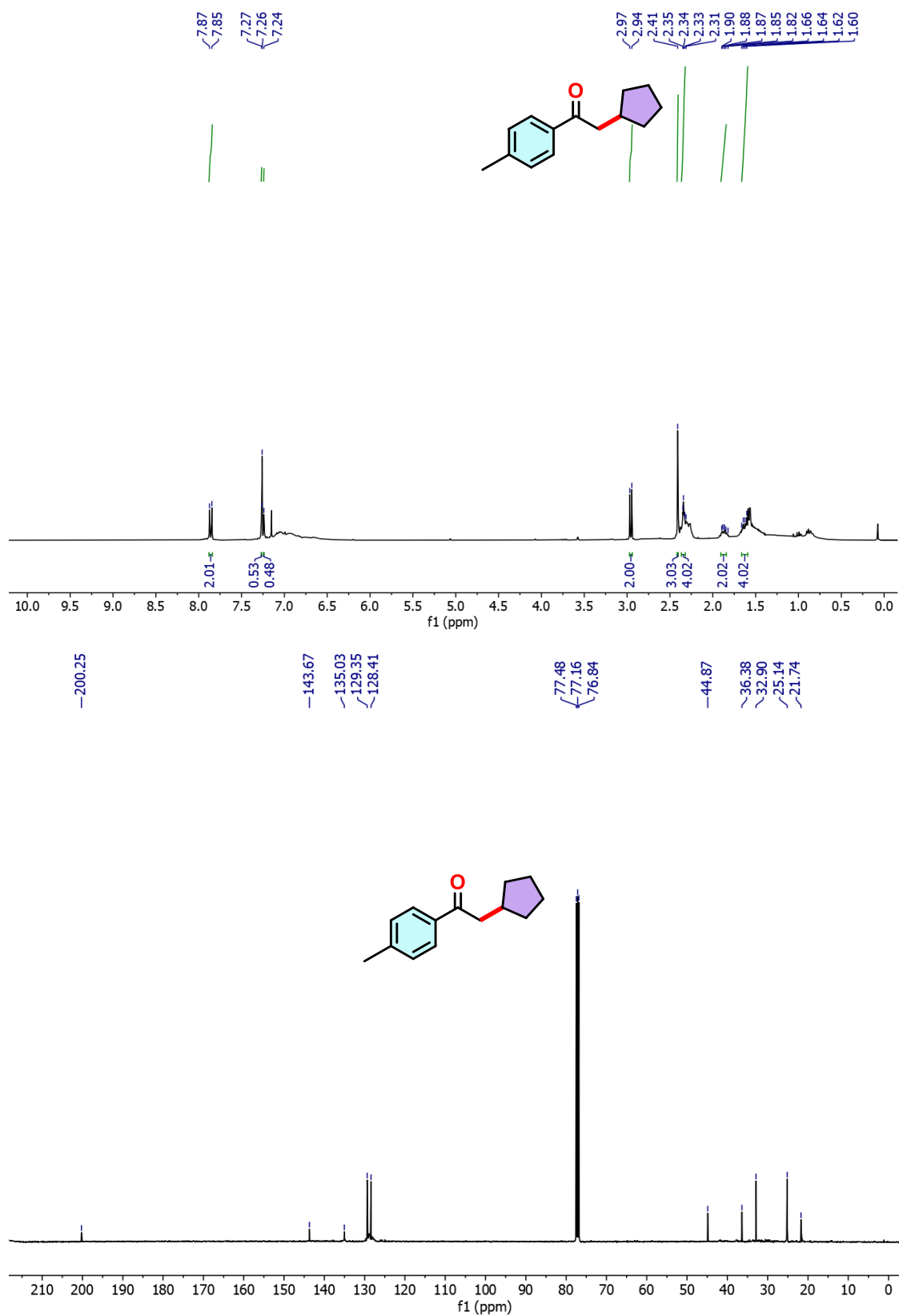
Figure 4.29. ^{1}H NMR (300 MHz) and ^{13}C NMR (75 MHz) spectra of compound **3ab** in CDCl$_3$.
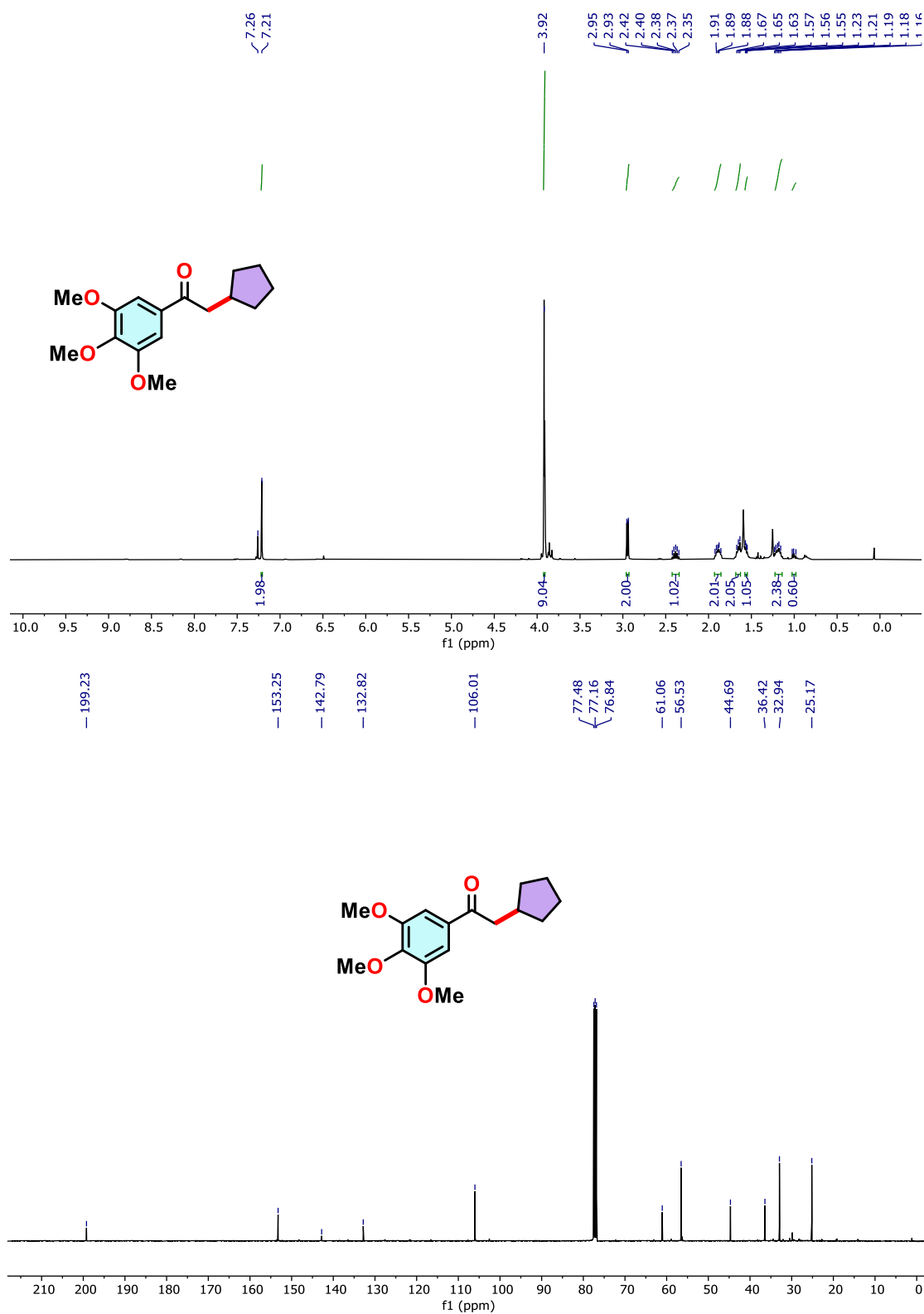
Figure 4.30. ^{1}H NMR (300 MHz) and ^{13}C NMR (75 MHz) spectra of compound **3ac** in CDCl$_3$.

Figure 4.31. HRMS of compound **3ac**.
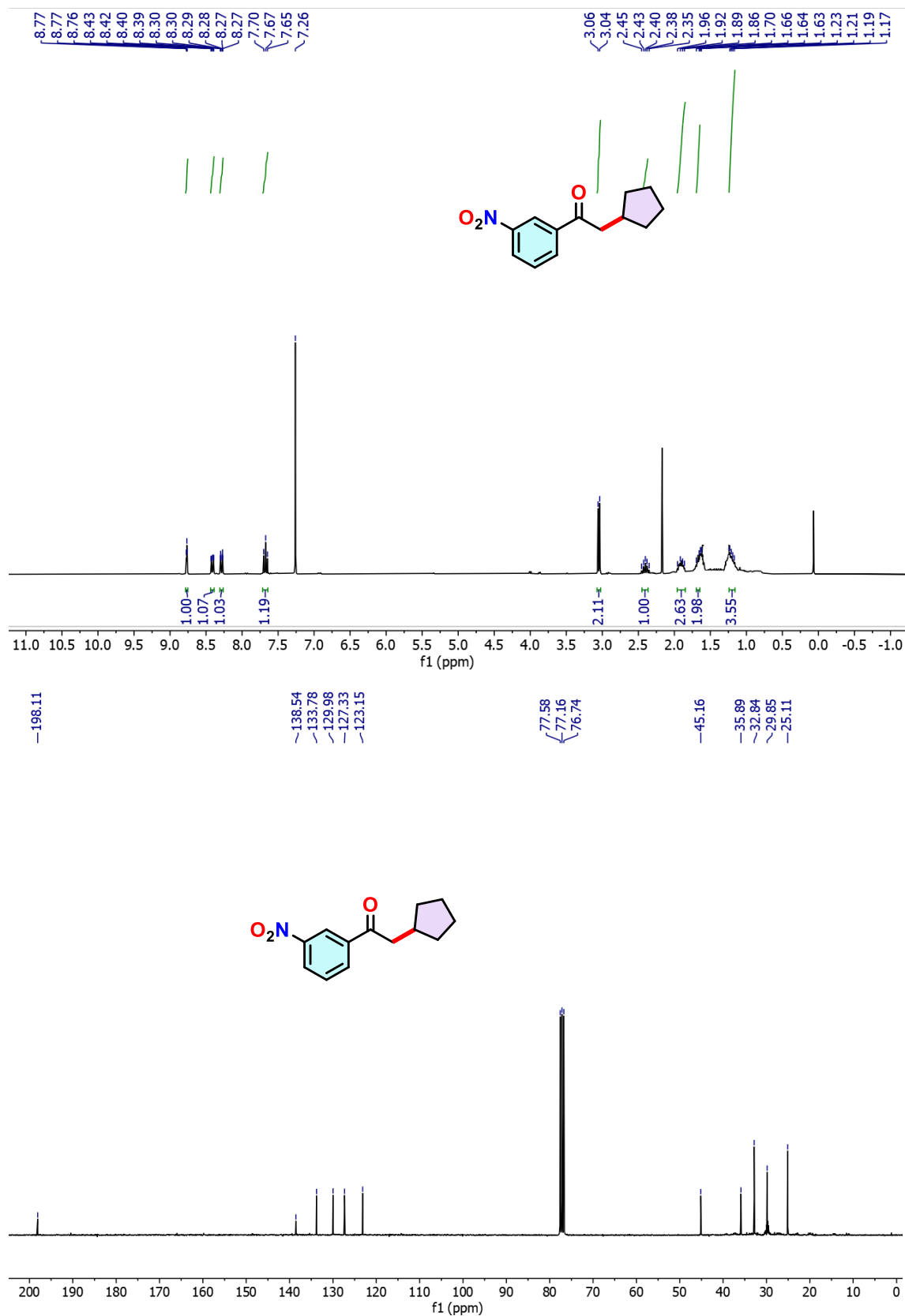
Figure 4.32. ¹H NMR (300 MHz) and ¹³C NMR (75 MHz) spectra of compound **3ad** in CDCl₃.
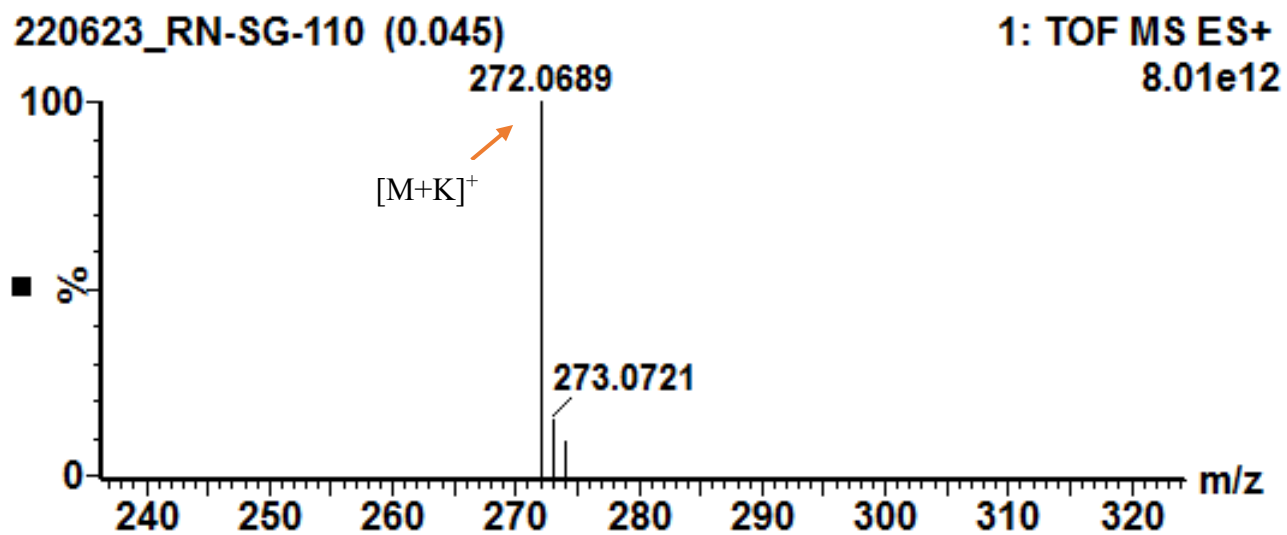
Figure 4.33. HRMS compound **3ad.**
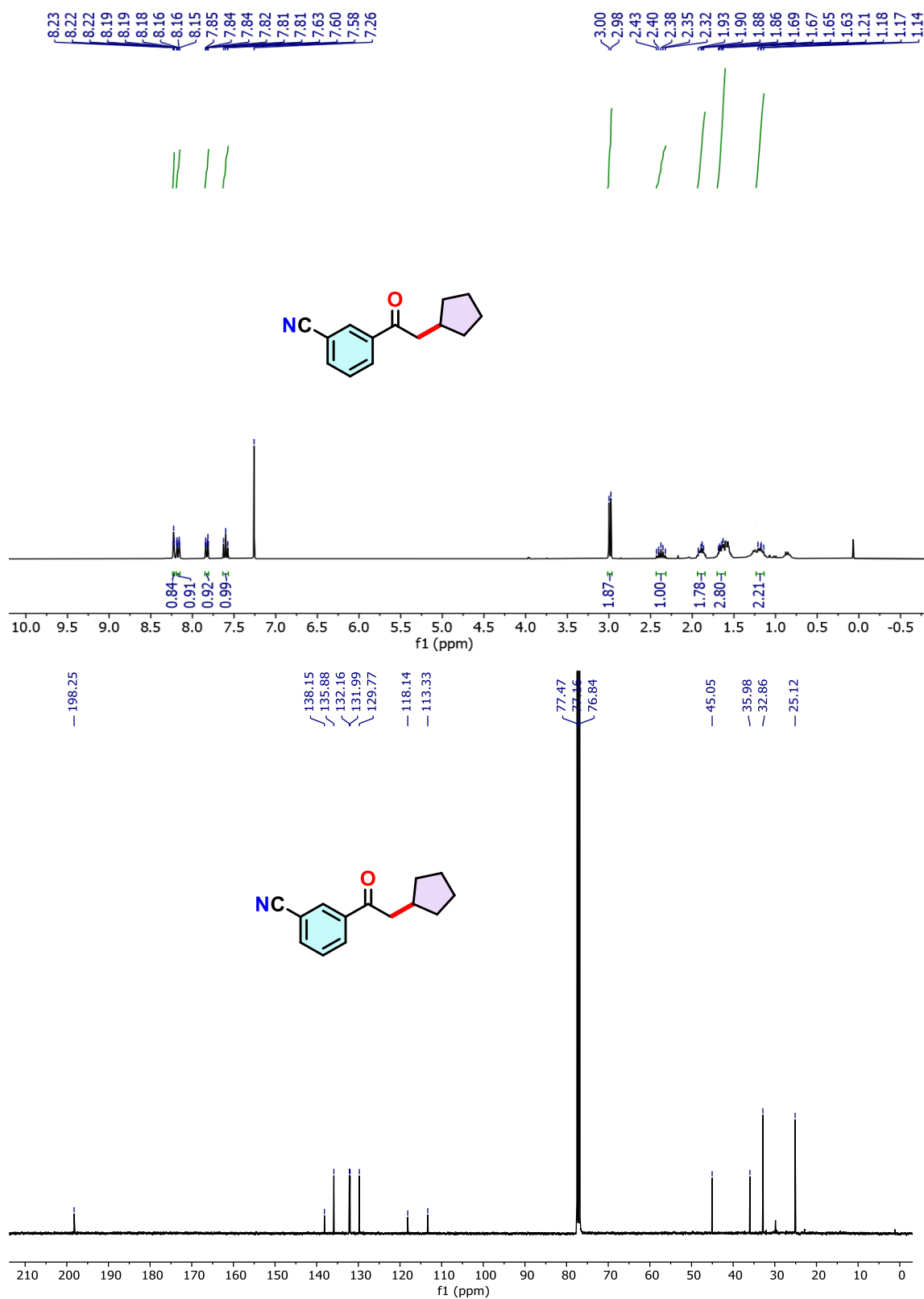
Figure 4.34. ¹H NMR (300 MHz) and ¹³C NMR (75 MHz) spectra of compound **3ae** in CDCl₃.
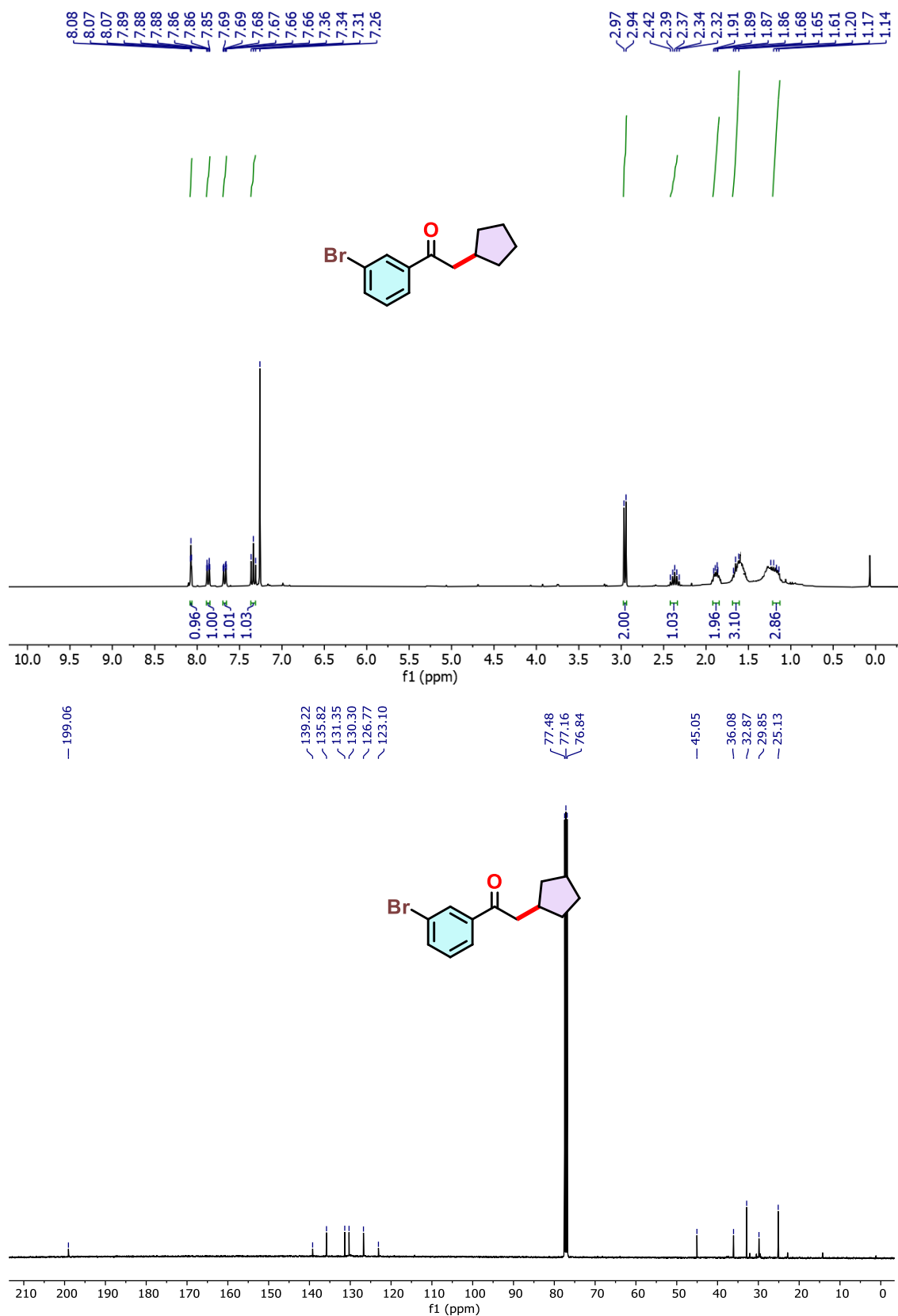
Figure 4.35. ^{1}H NMR (300 MHz) and ^{13}C NMR (75 MHz) spectra of compound **3af** in CDCl$_3$.
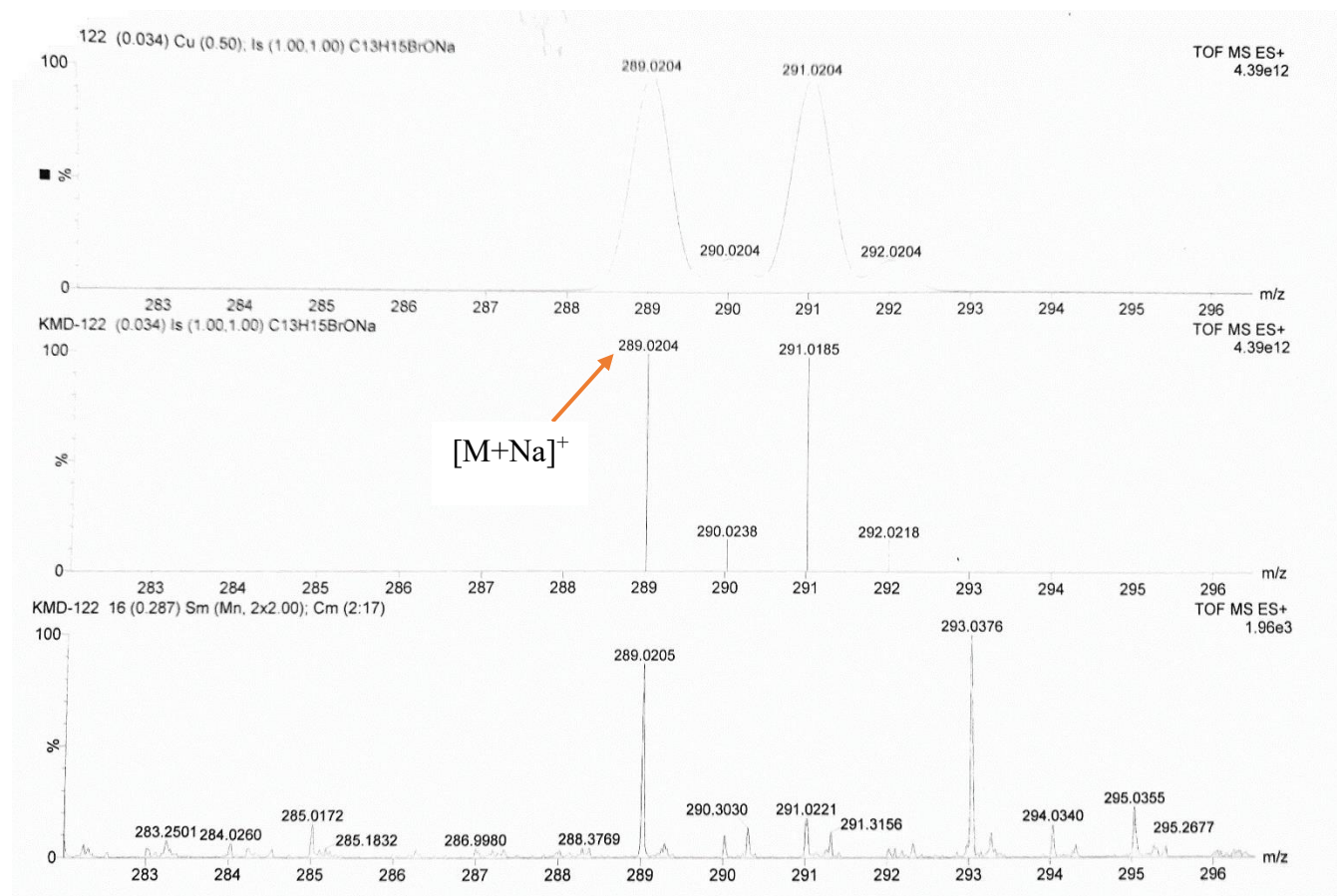
Figure 4.36. HRMS of compound **3af.**
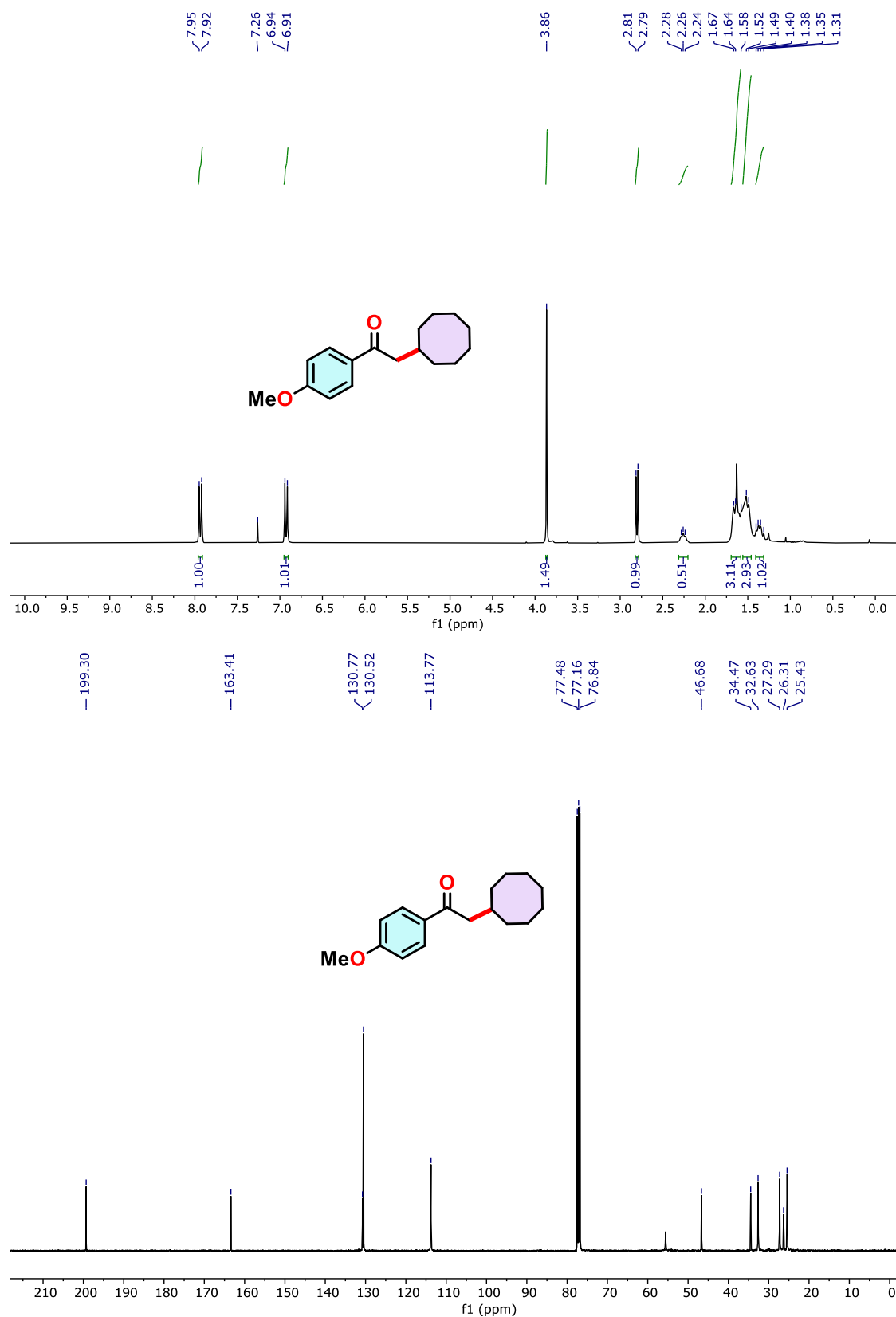
Figure 4.37. ¹H NMR (300 MHz) and ¹³C NMR (75 MHz) spectra of compound **3aa'** in CDCl₃
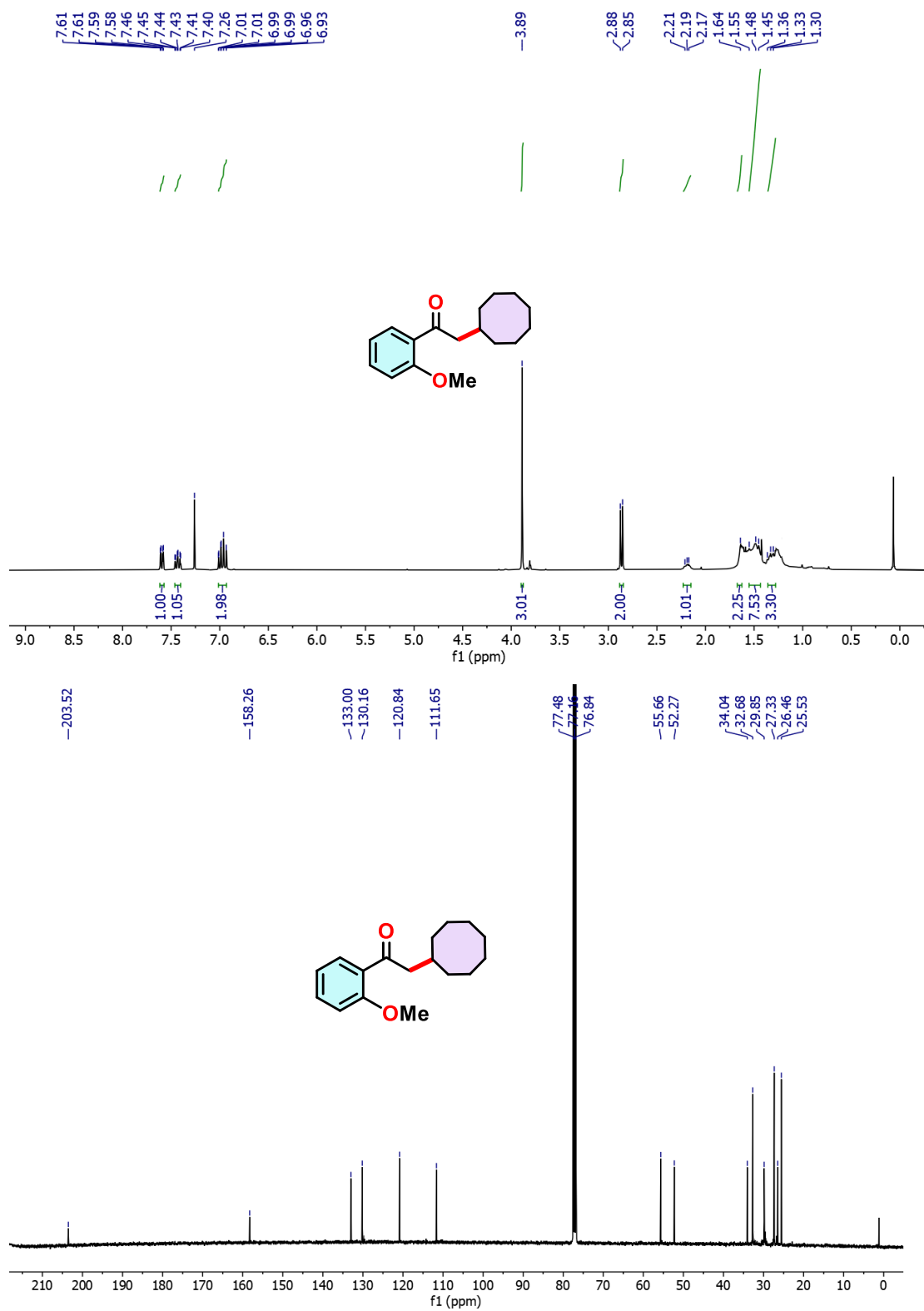
Figure 4.38. ^{1}H NMR (300 MHz) and ^{13}C NMR (75 MHz) spectra of compound **3ab'** in CDCl$_3$.
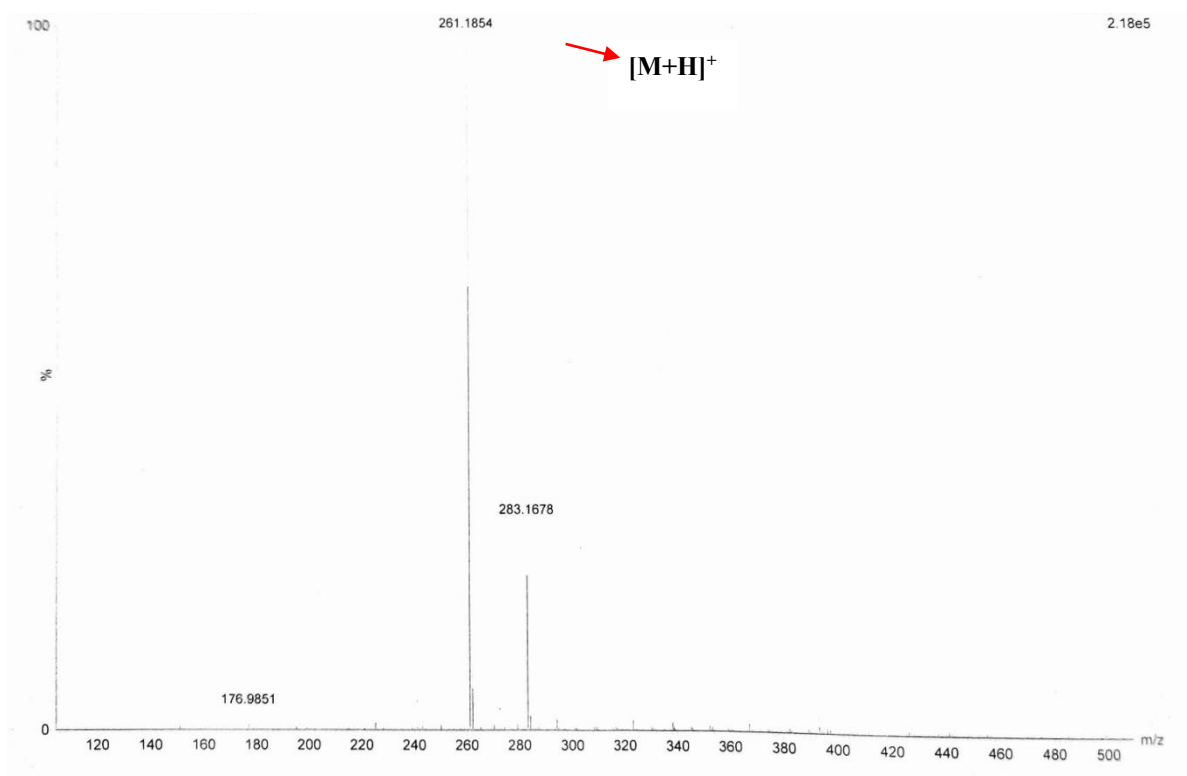
Figure 4.39. HRMS of compound **3ab'**
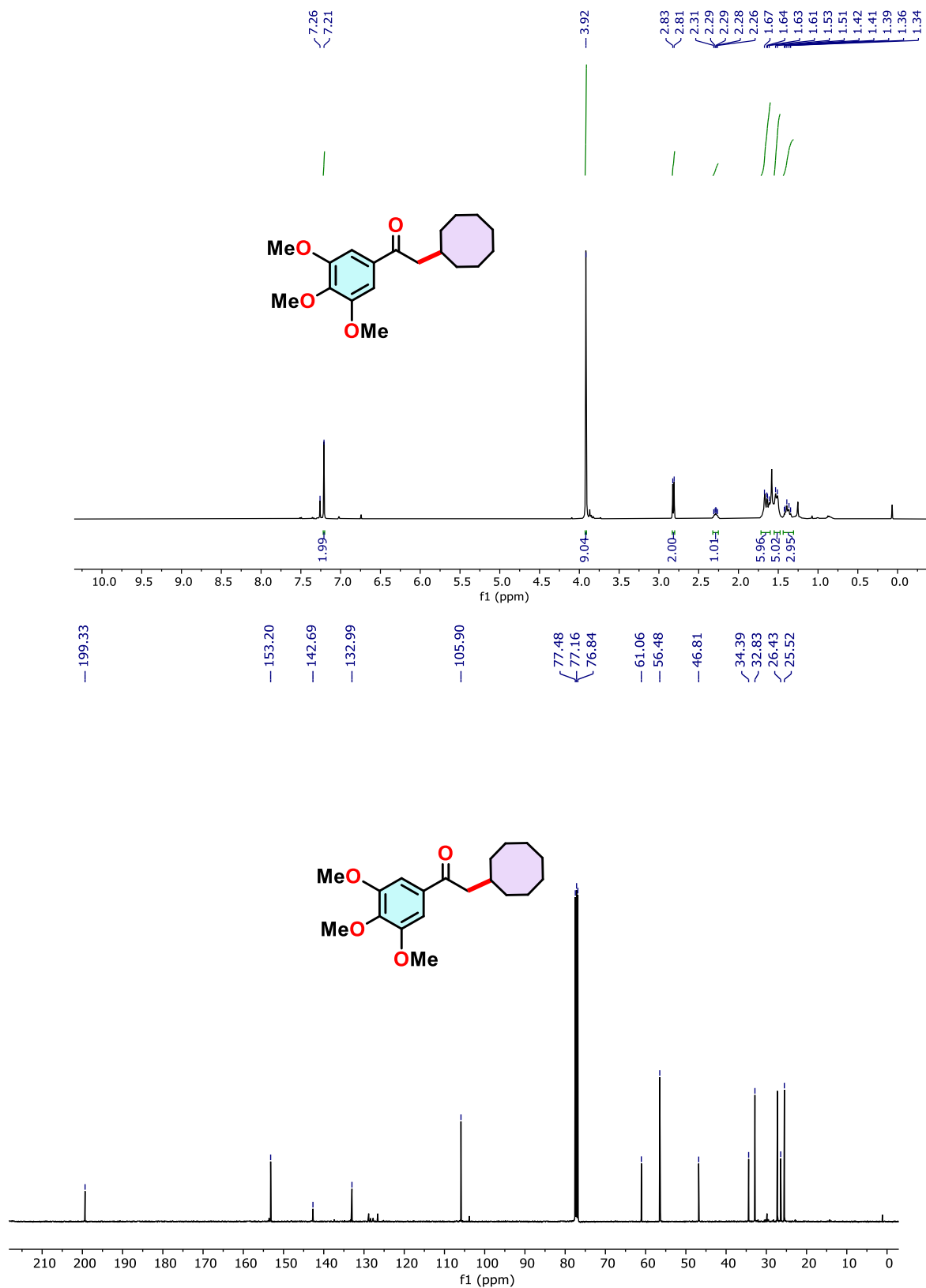
Figure 4.40. ^{1}H NMR (300 MHz) and ^{13}C NMR (75 MHz) spectra of compound **3ac'** in CDCl${}_3$.

AT-KMD-95A 1 (0.034)   343.1884   TOF MS ES+
3.59e4

[M+Na]⁺
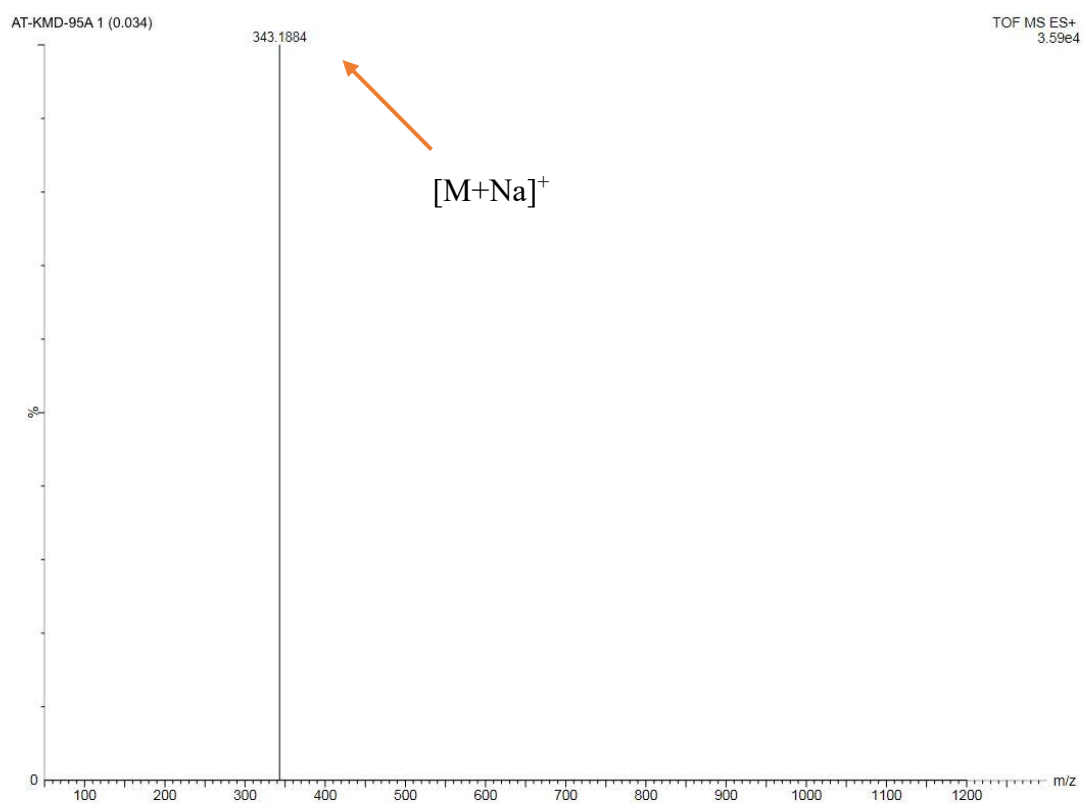
Figure 4.41. HRMS compound **3ac'**.
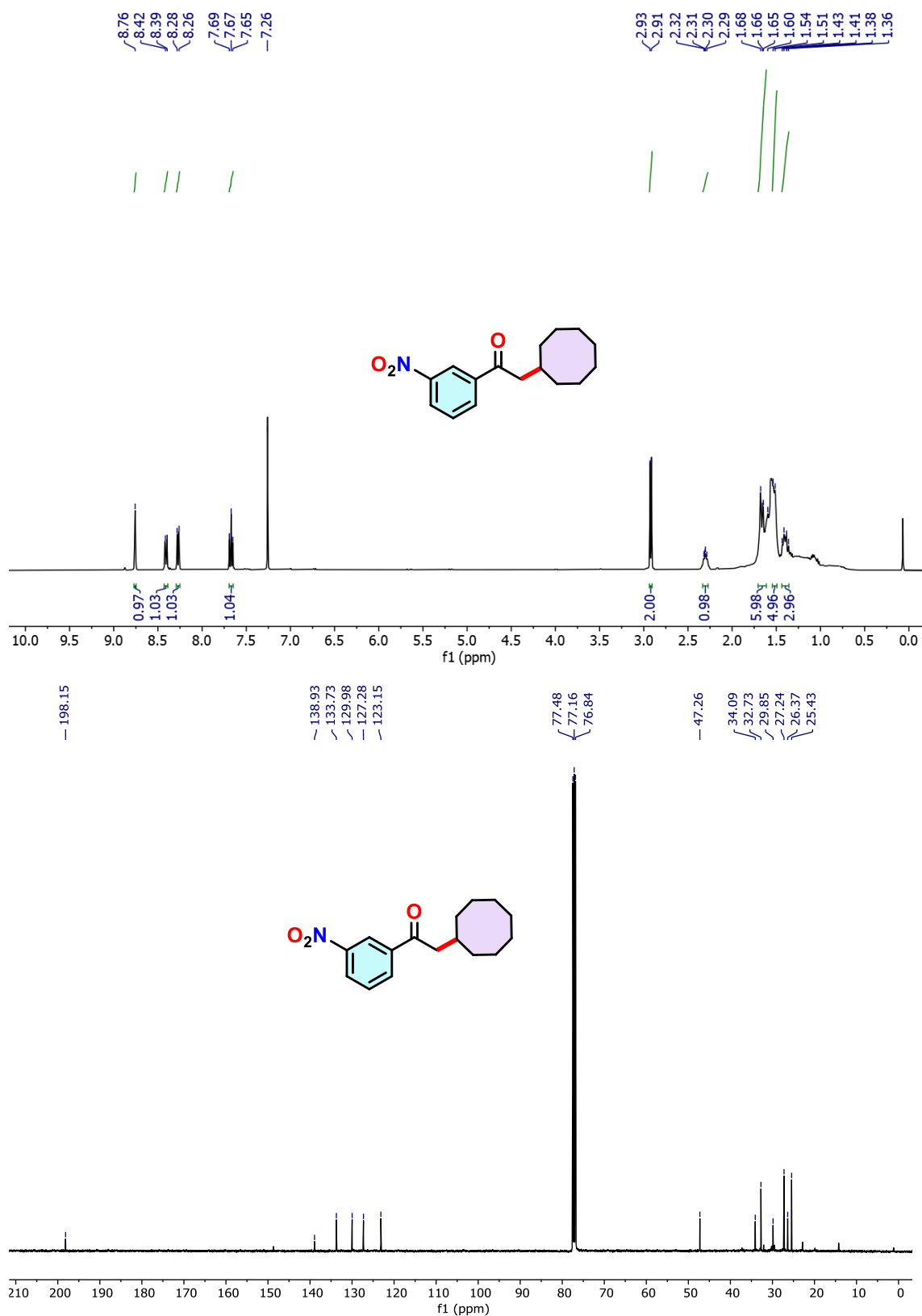
Figure 4.42. ^{1}H NMR (300 MHz) and ^{13}C NMR (75 MHz) spectra of compound **3ad'** in CDCl$_3$.
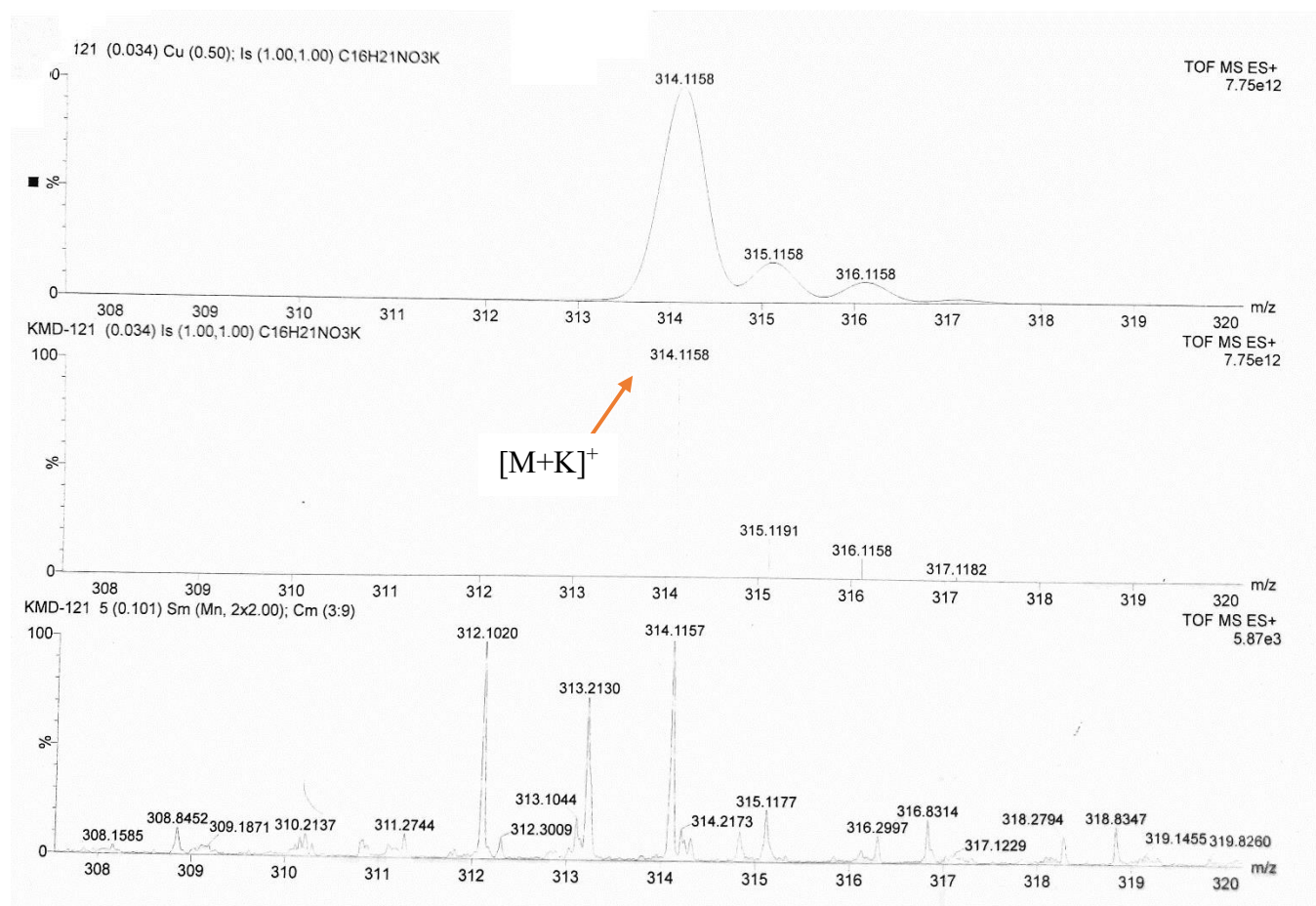
Figure 4.43. HRMS of compound **3ad'**.
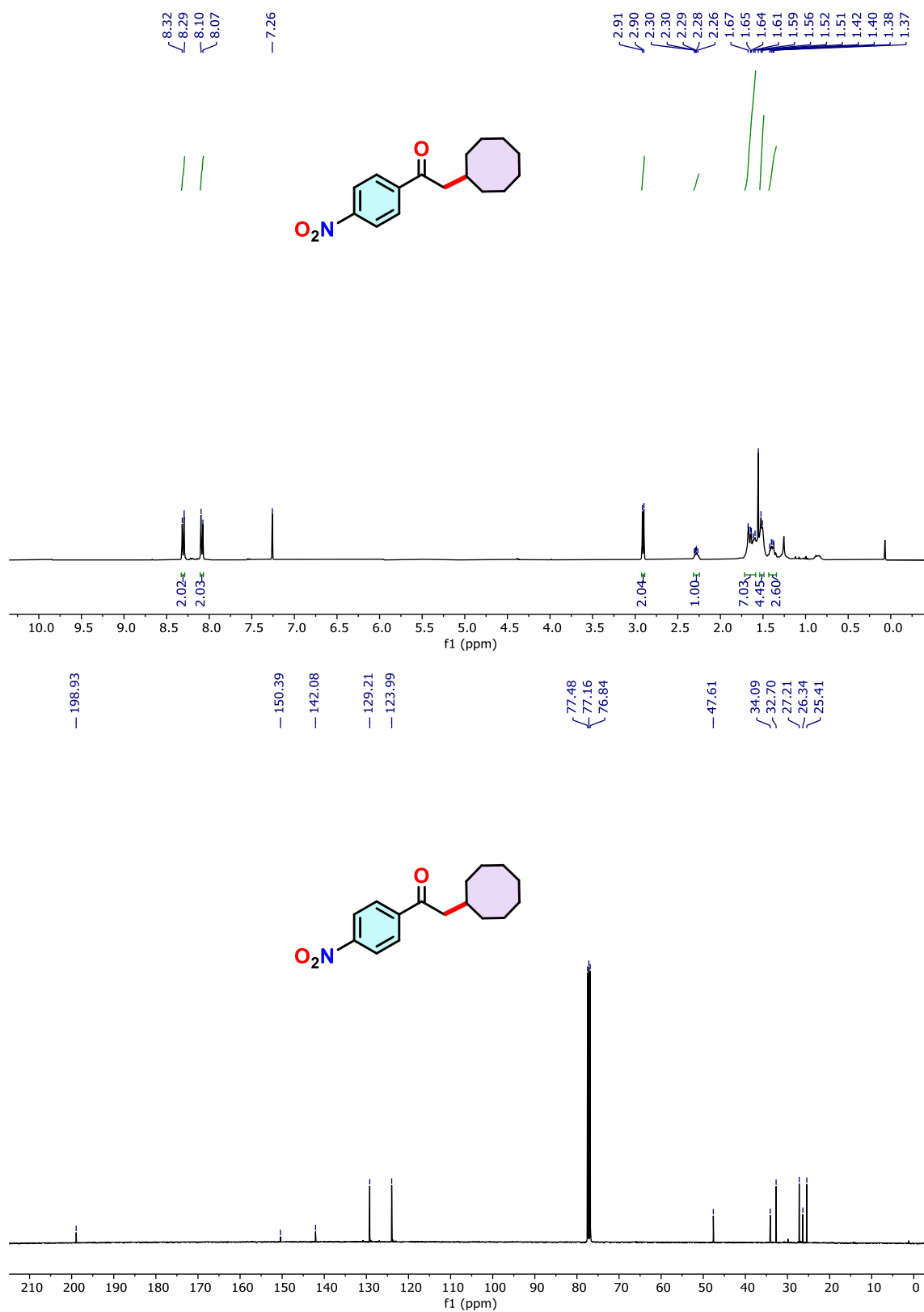
Figure 4.44. ^{1}H NMR (300 MHz) and ^{13}C NMR (75 MHz) spectra of compound **3ae'** in CDCl$_3$.
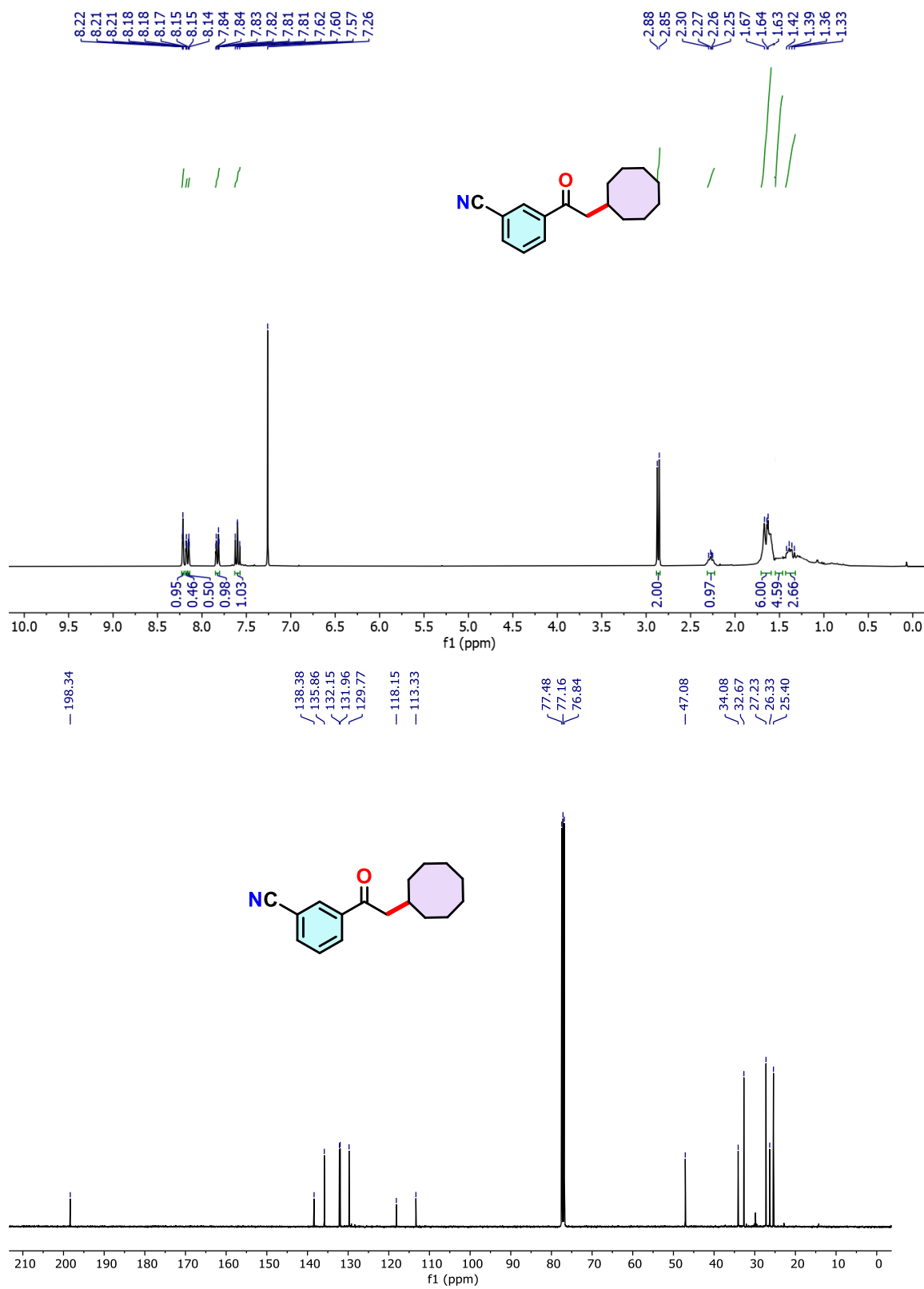
Figure 4.45. ¹H NMR (300 MHz) and ¹³C NMR (75 MHz) spectra of compound **3af'** in CDCl₃.
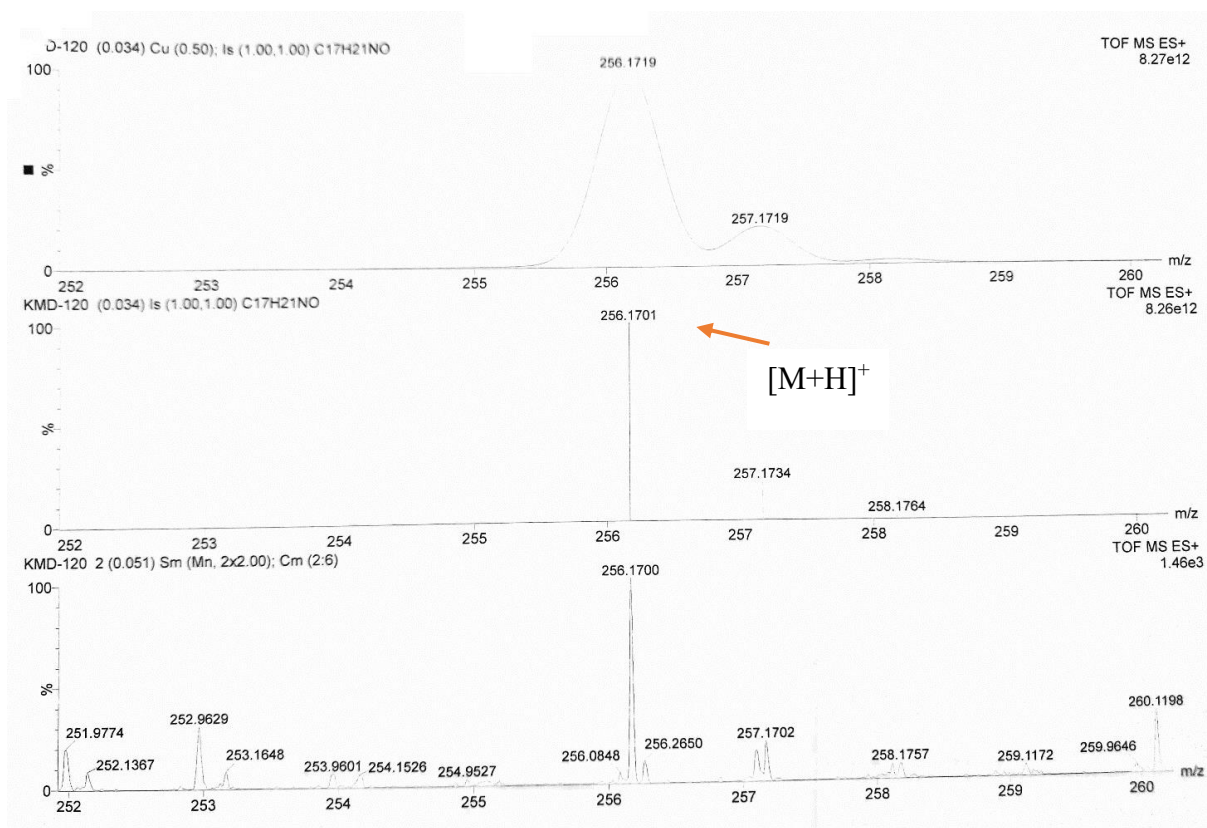
Figure 4.46. HRMS of compound **3af'**.
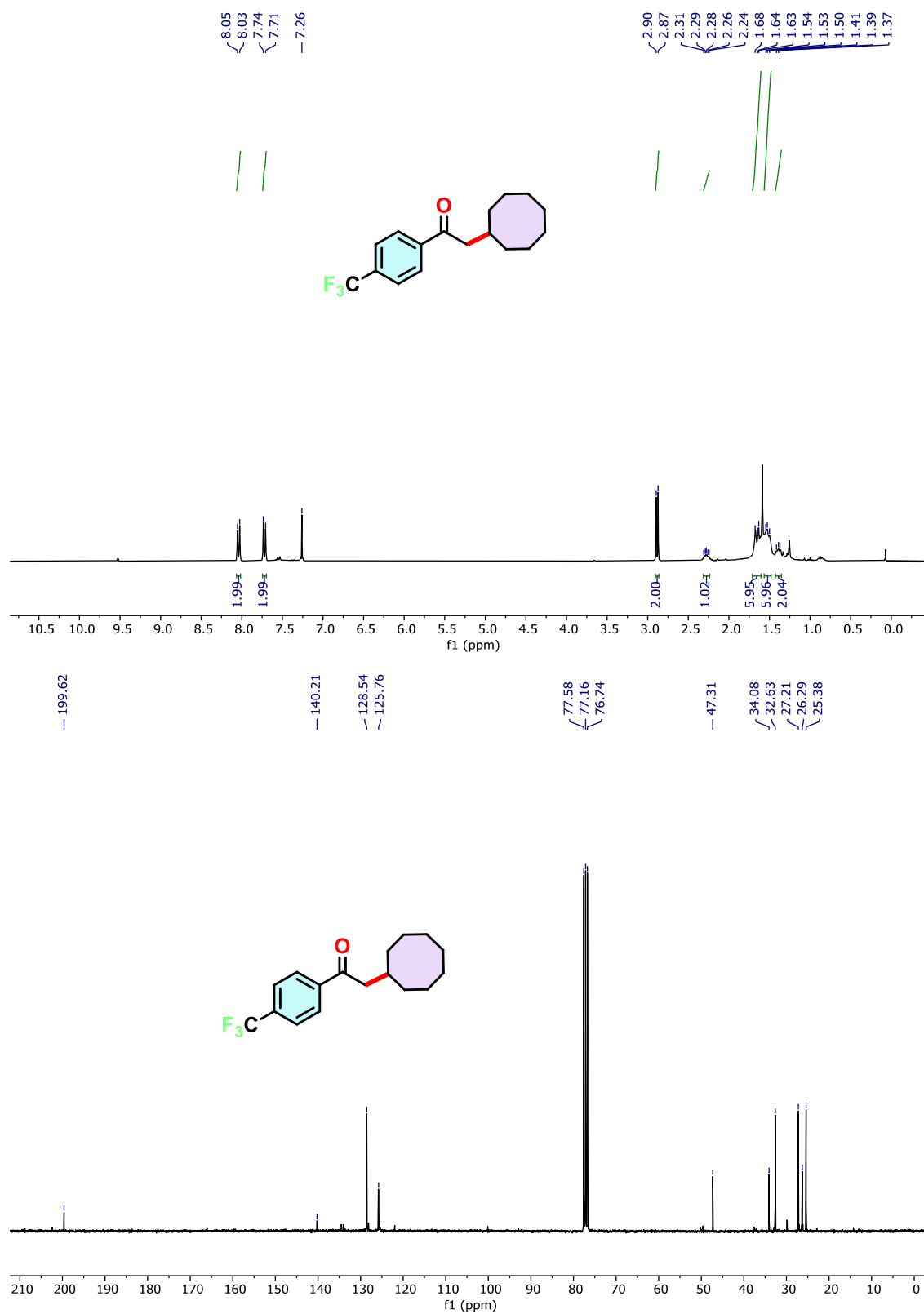
Figure 4.47. ¹H NMR (300 MHz) and ¹³C NMR (75 MHz) spectra of compound **3ag'** in CDCl₃.

220623_RN-SG-111 (0.045)   1: TOF MS ES+
337.1182   7.73e12

[M+K]$^+$

338.1216

340.1204
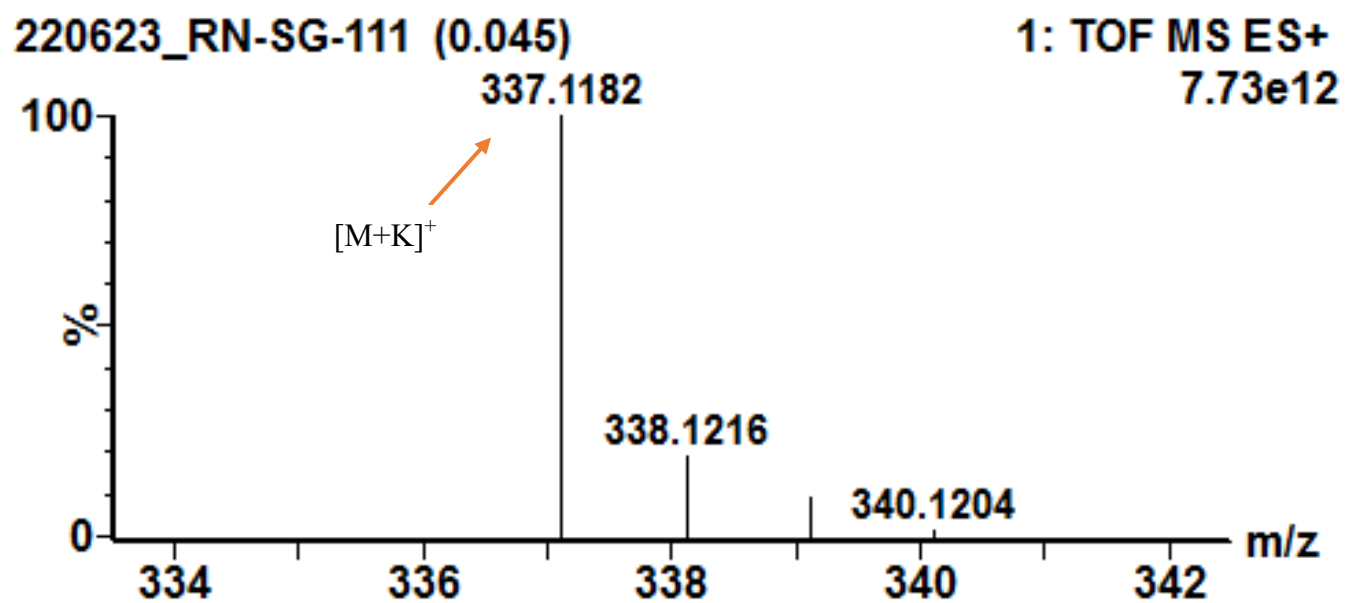
Figure 4.48. HRMS of compound **3ag'**.

7.66
7.65
7.63
7.63
7.42
7.41
7.40
7.26

2.82
2.80

1.76
1.71

1.19
1.16

9.0 8.5 8.0 7.5 7.0 6.5 6.0 5.5 5.0 4.5 4.0 3.5 3.0 2.5 2.0 1.5 1.0 0.5 0.0
f1 (ppm)

1.98
3.06

2.00

6.85

4.18

—159.09

—136.44

129.15
128.61
126.56

77.58
77.16
76.74

35.82
33.52
29.86
26.38
26.30

170 160 150 140 130 120 110 100 90 80 70 60 50 40 30 20 10 0
f1 (ppm)
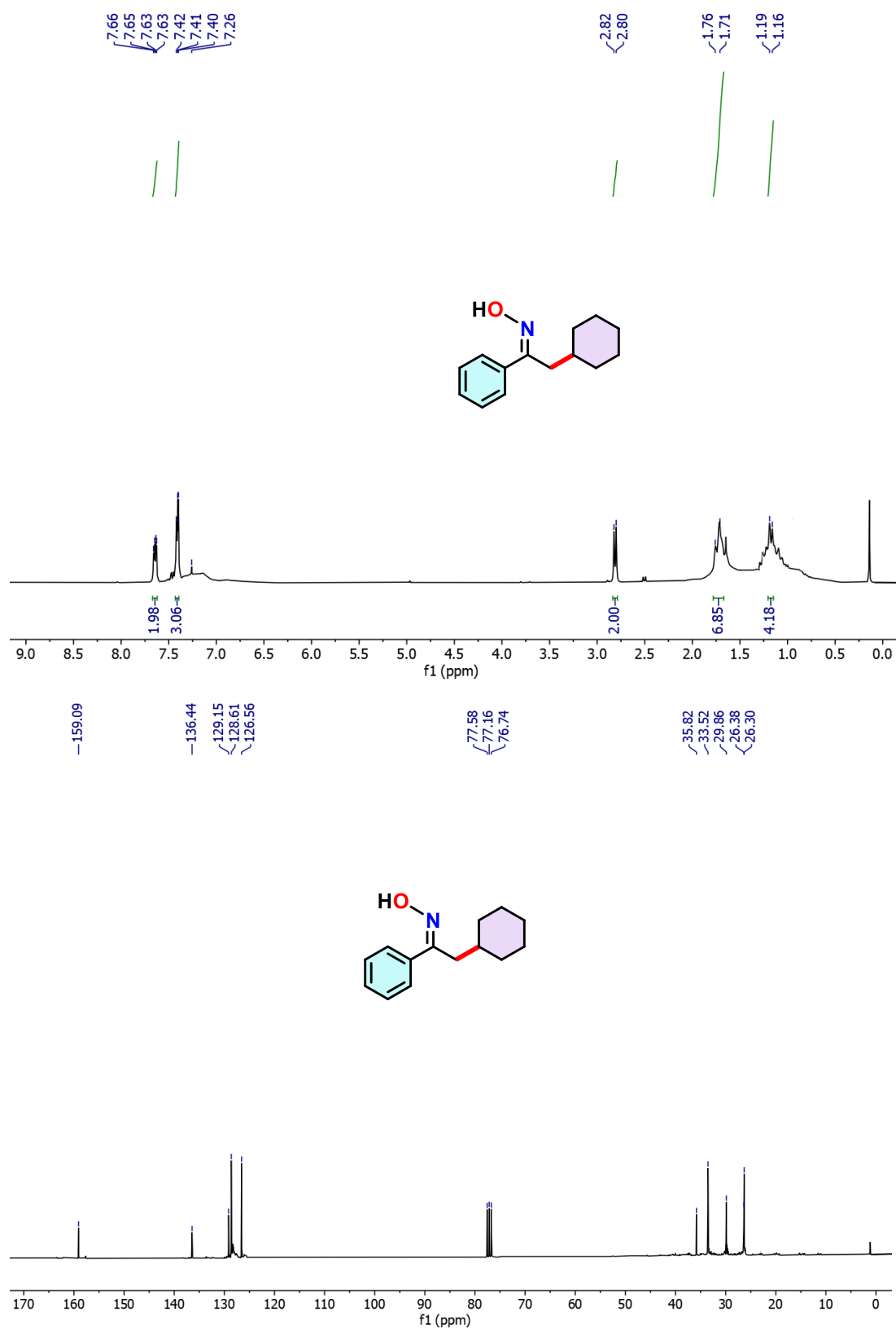
Figure 4.49. ¹H NMR (300 MHz) and ¹³C NMR (75 MHz) spectra of compound **4a** in CDCl₃.
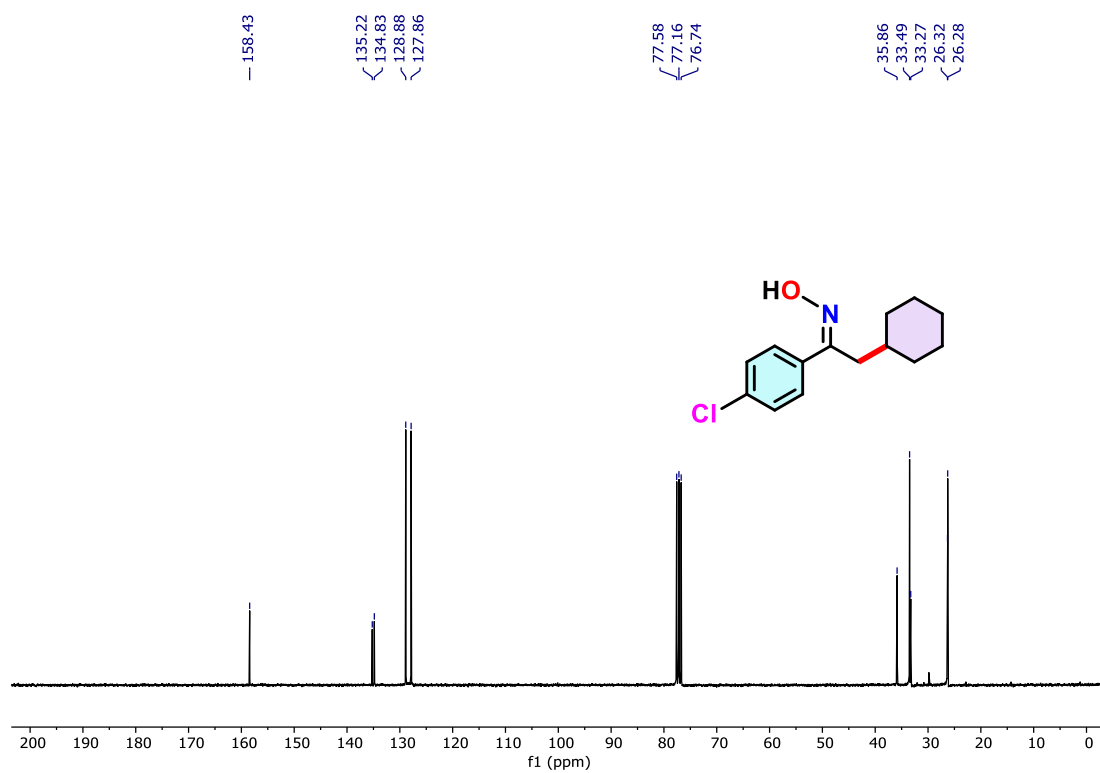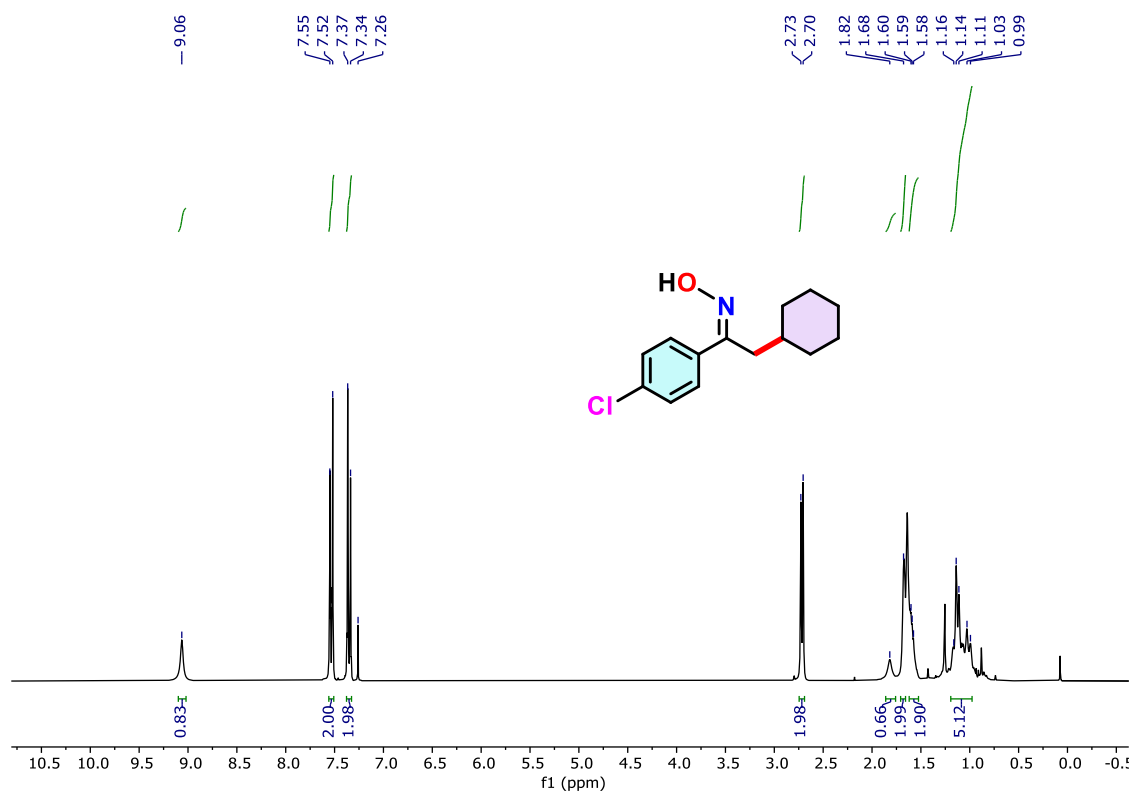
Figure 4.50. ¹H NMR (300 MHz) and ¹³C NMR (75 MHz) spectra of compound **4b** in CDCl₃.
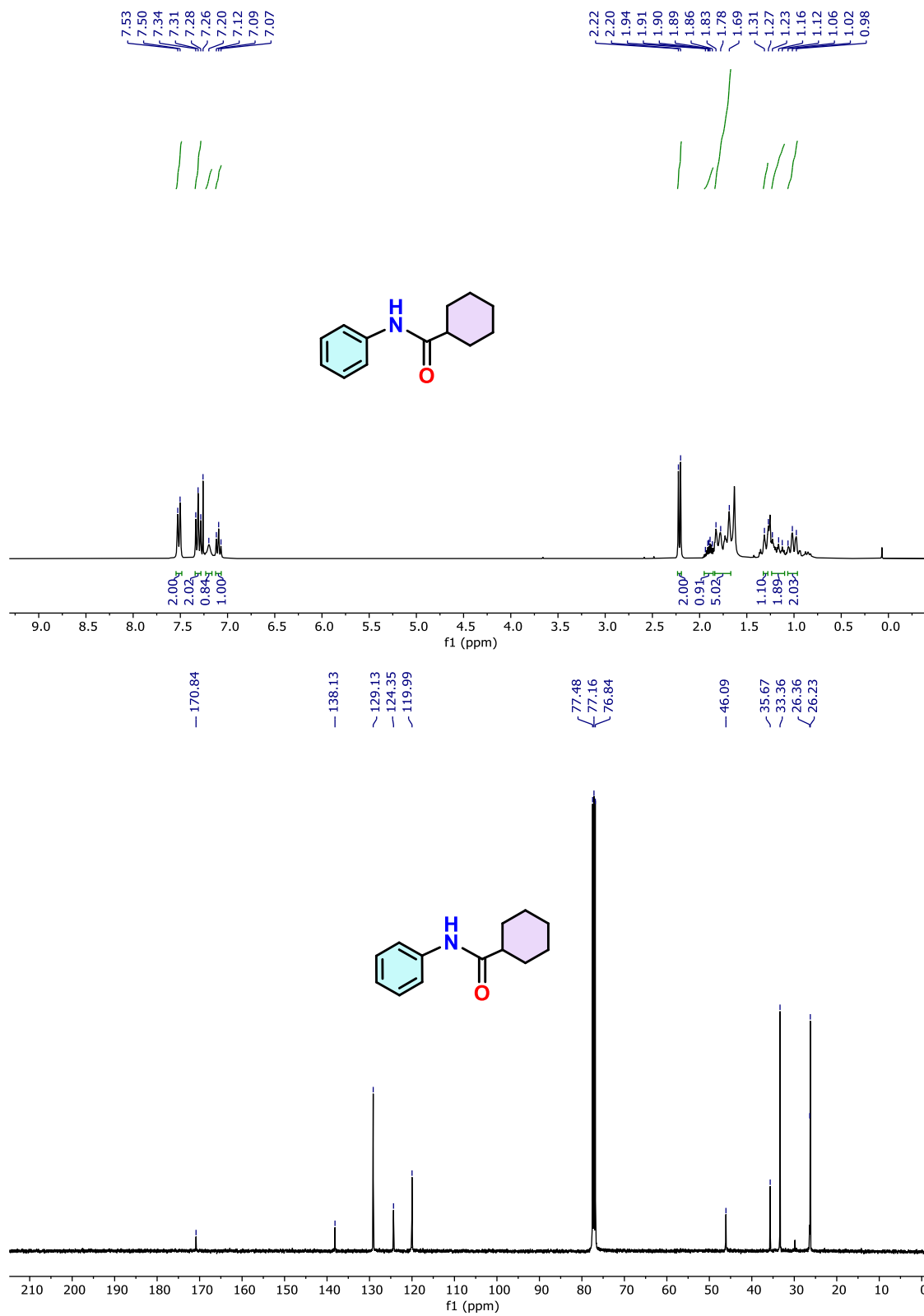
Figure 4.51. ^{1}H NMR (300 MHz) and ^{13}C NMR (75 MHz) spectra of compound **5** in CDCl$_3$.
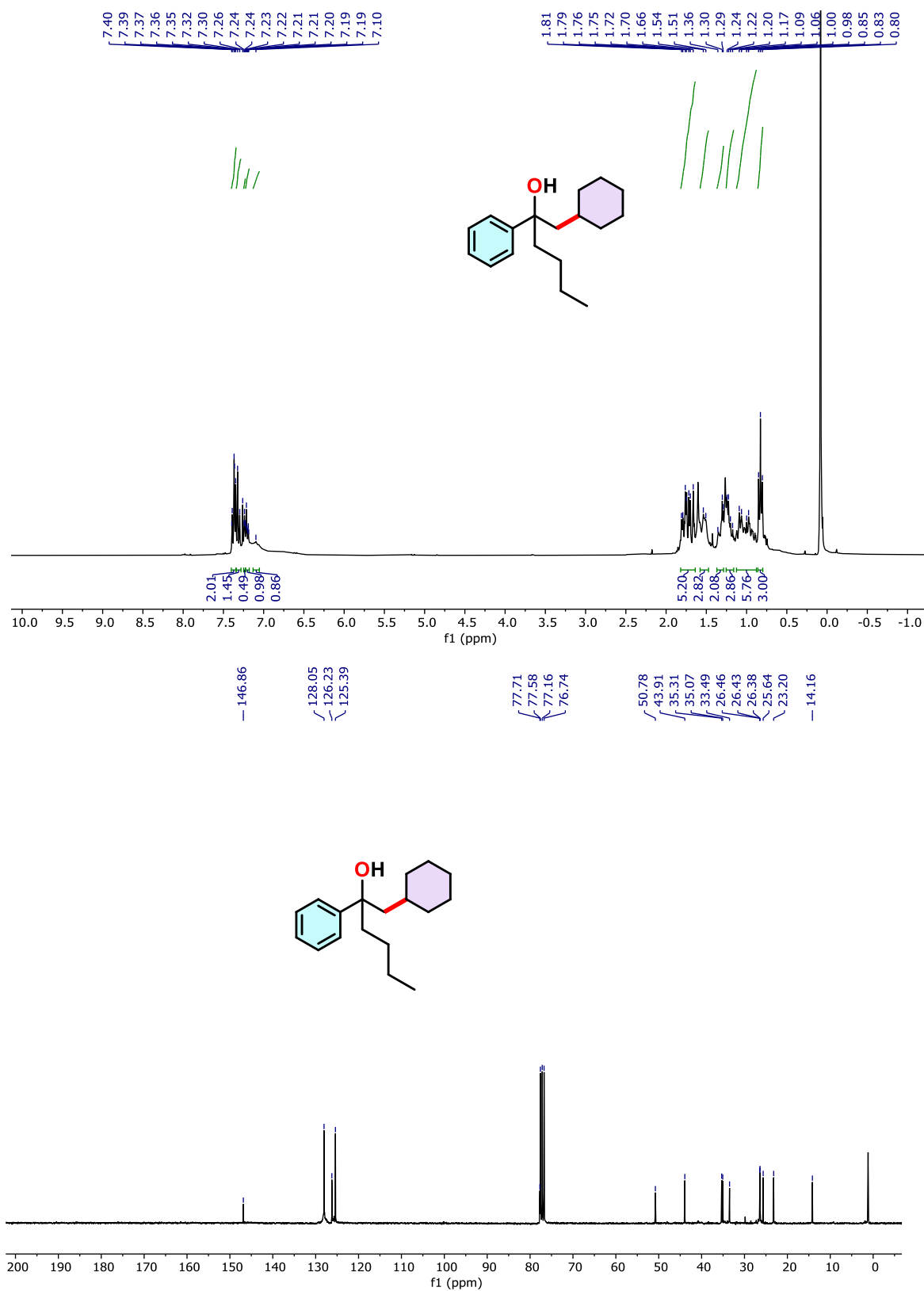
Figure 4.52. ¹H NMR (300 MHz) and ¹³C NMR (75 MHz) spectra of compound **6** in CDCl₃.
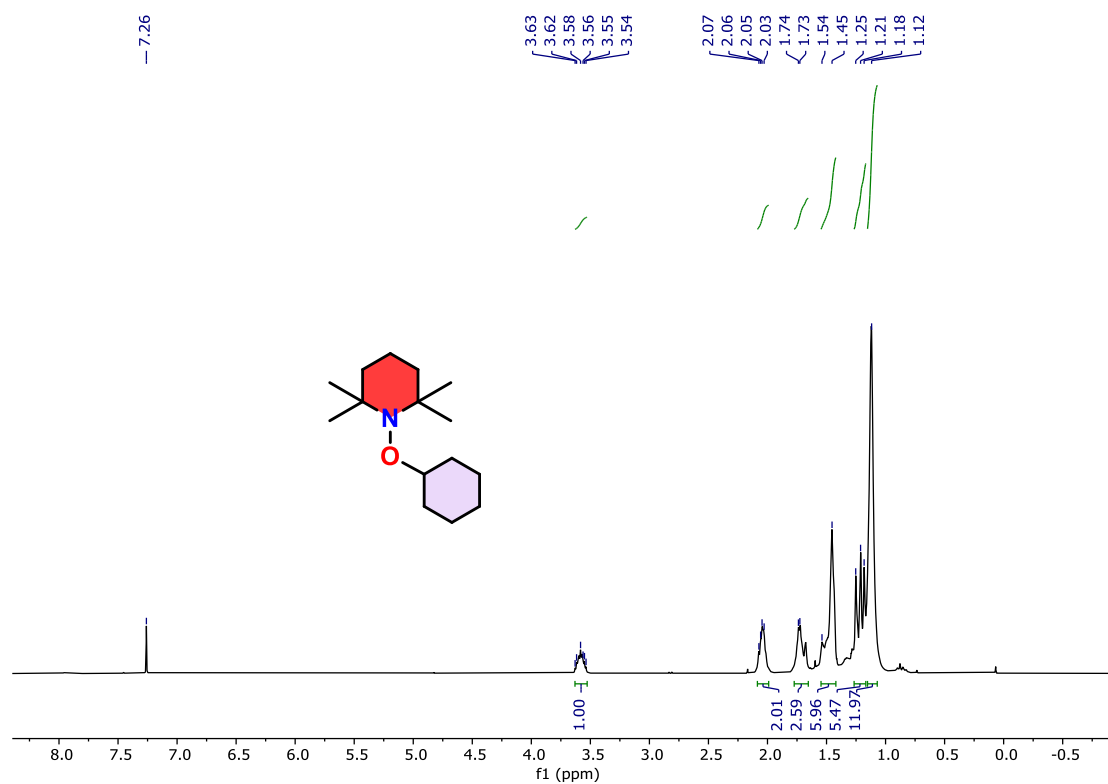
Figure 4.53. ^{1}H (300 MHz) NMR of compound **7** in CDCl$_3$.
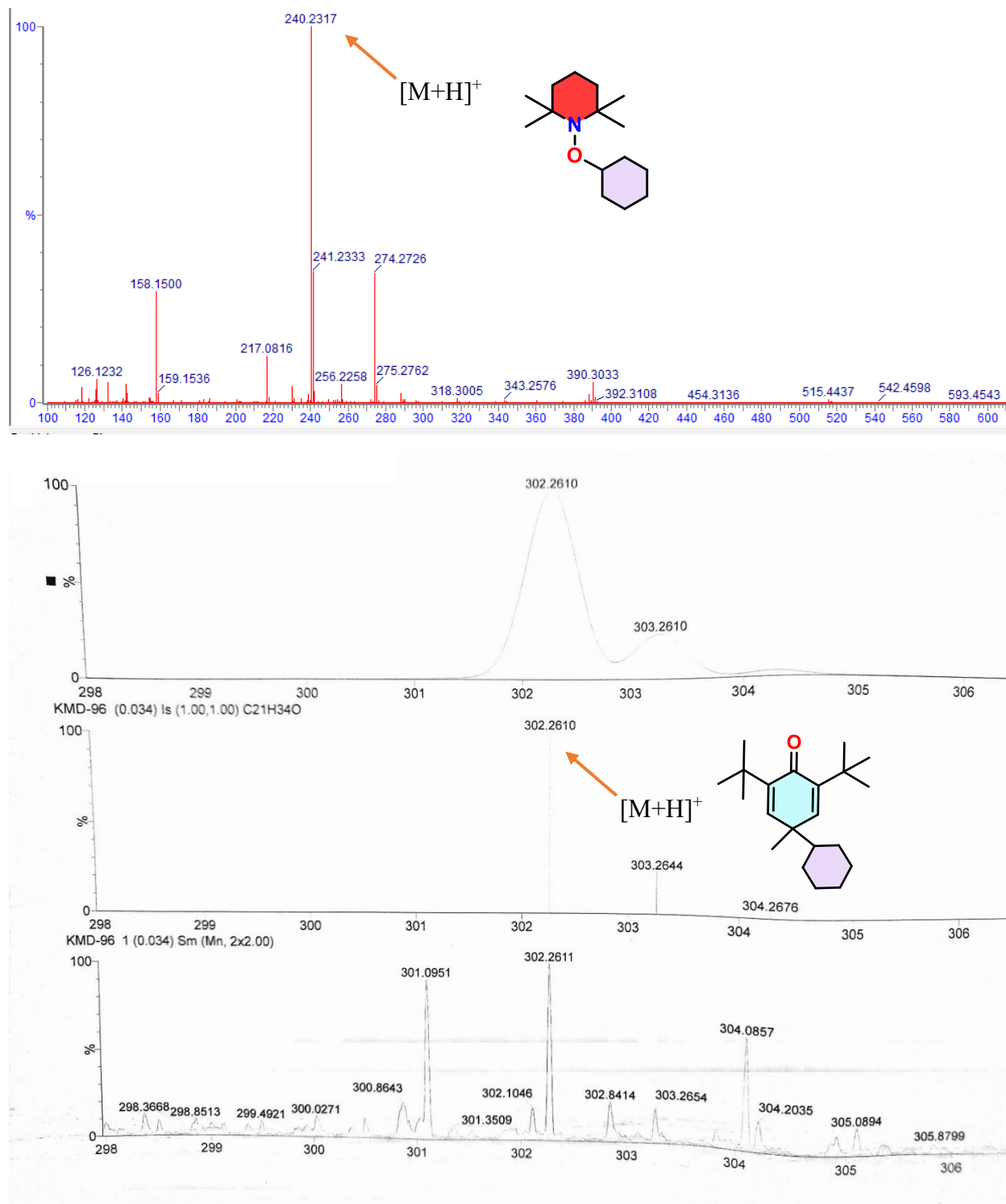
Figure 4.54. HRMS spectra of TEMPO-cyclohexyl (**7**) and BHT-cyclohexyl (**8**) radical adducts.

KIE studies:

(1) From competitive experiment:
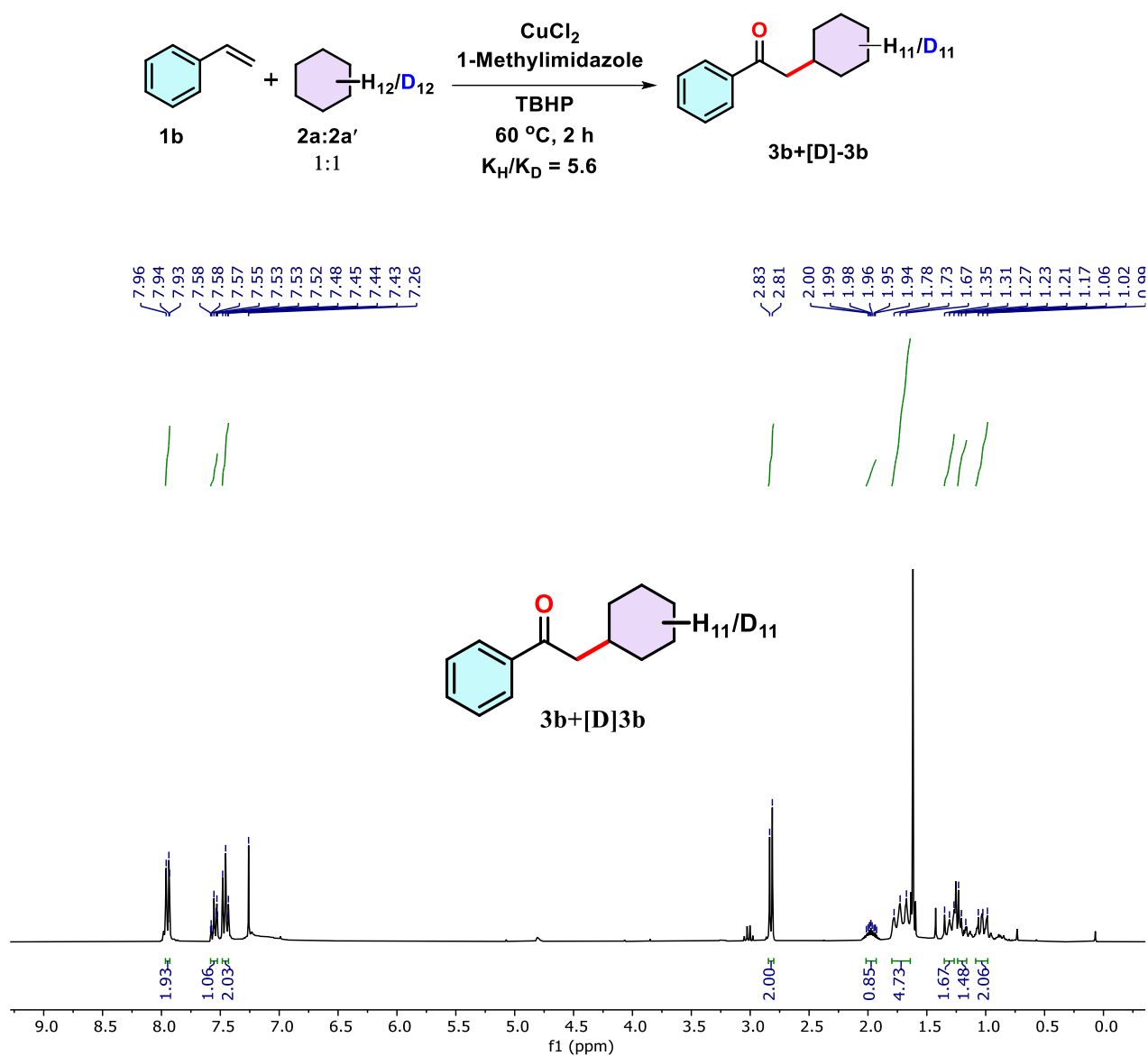
Figure 4.55. ^{1}H (300 MHz) NMR of KIE results.

(2) From parallel reaction:
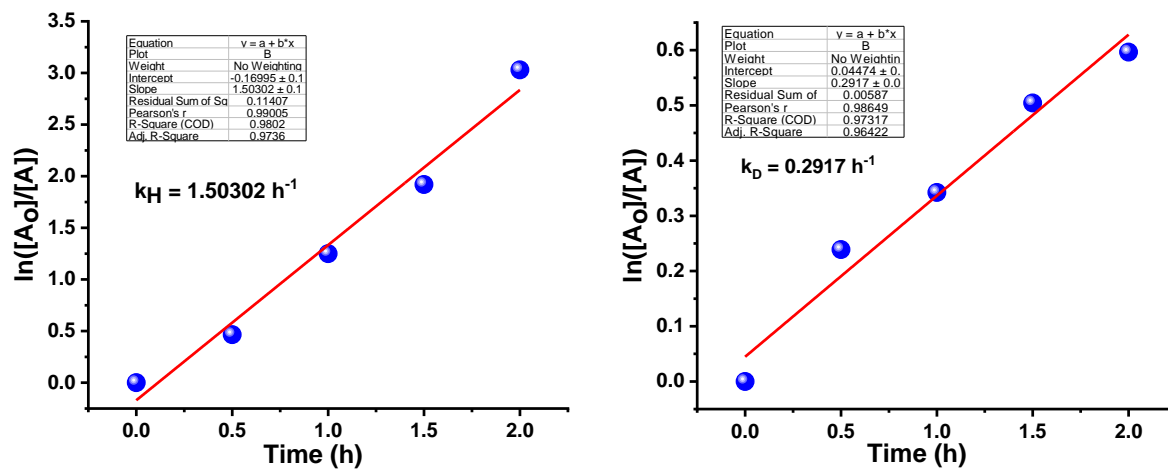
K_H/K_D value obtained from parallel reaction is 5.15

Figure 4.56. Parallel reaction for kinetic isotope effect experiment.
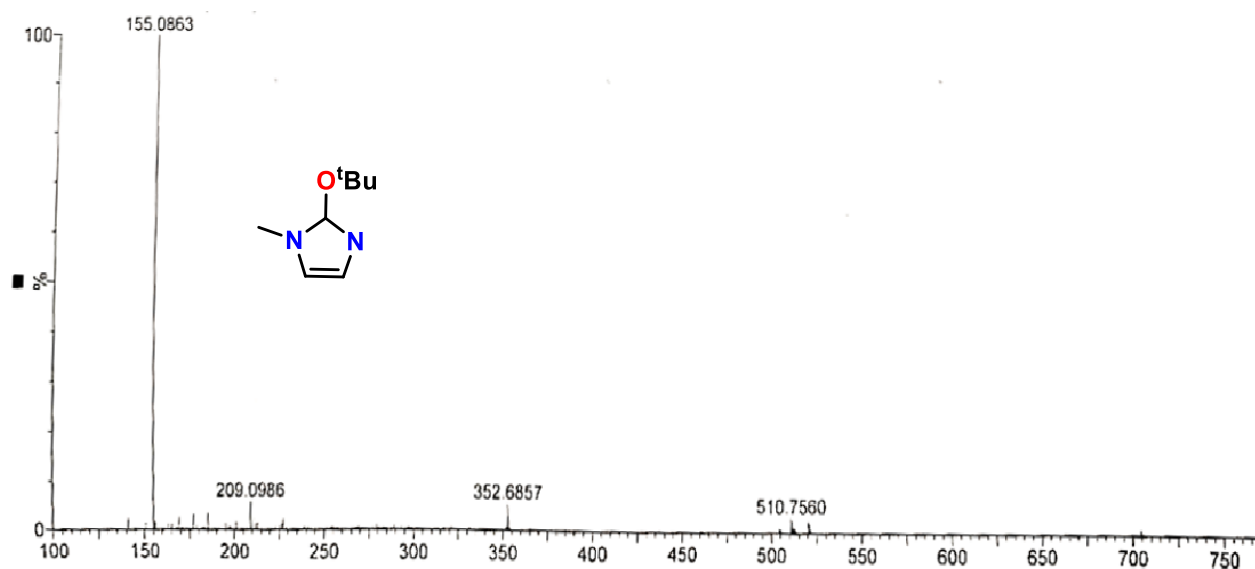
Figure 4.57. LCMS spectra of 2-(tert-butoxy)-1-methyl-2,3-dihydro-1H-imidazole compound.

| $k_X = 0.5$ | $k_H = 0.99$ | $\log(k_X/k_H) = -0.296$ |
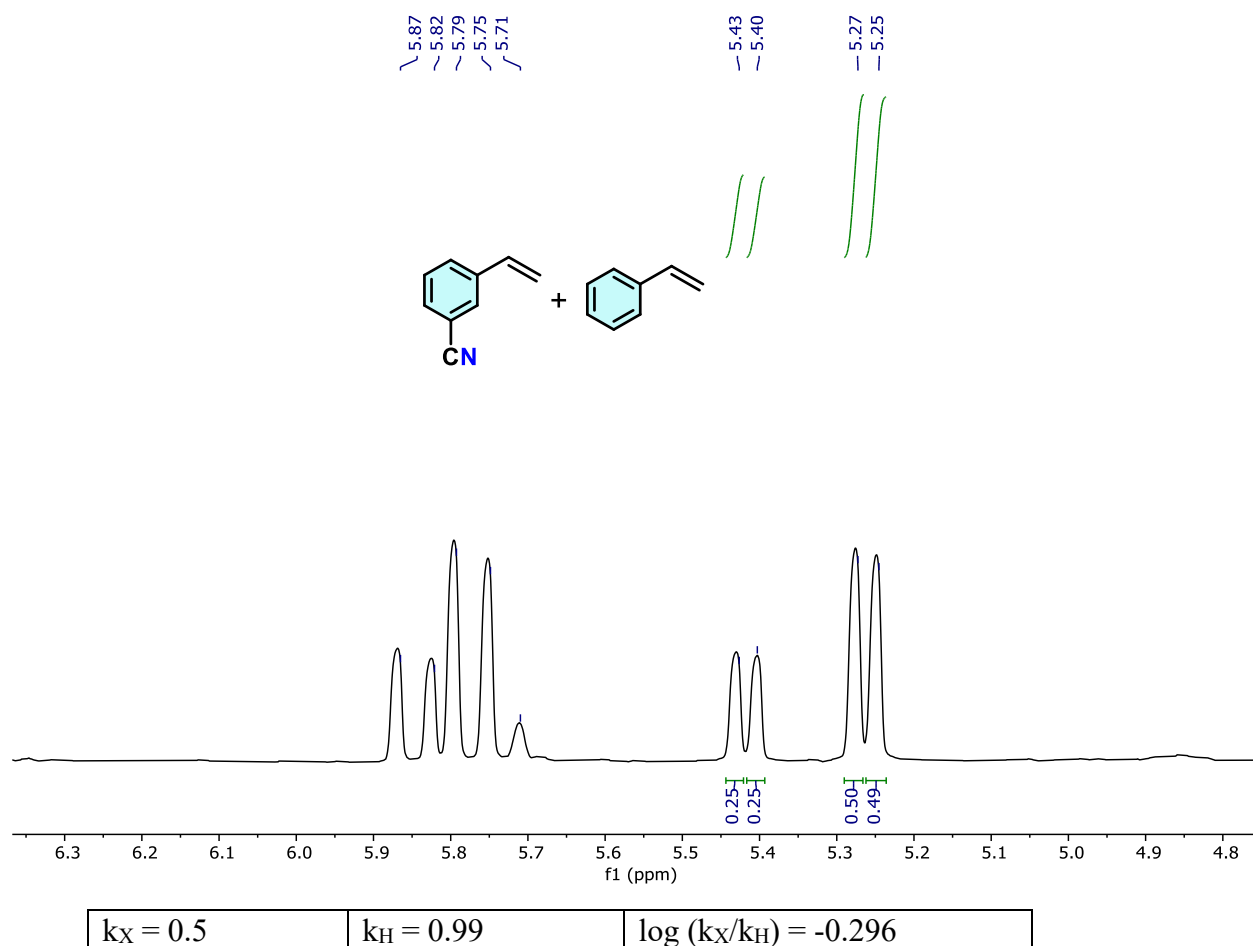
Figure 4.58. ^{1}H NMR spectra of 3-cyano styrene and styrene reaction mixture for Hammett analysis.

| $k_X = 0.41$ | $k_H = 0.99$ | $\log (k_X/k_H) = -0.383$ |
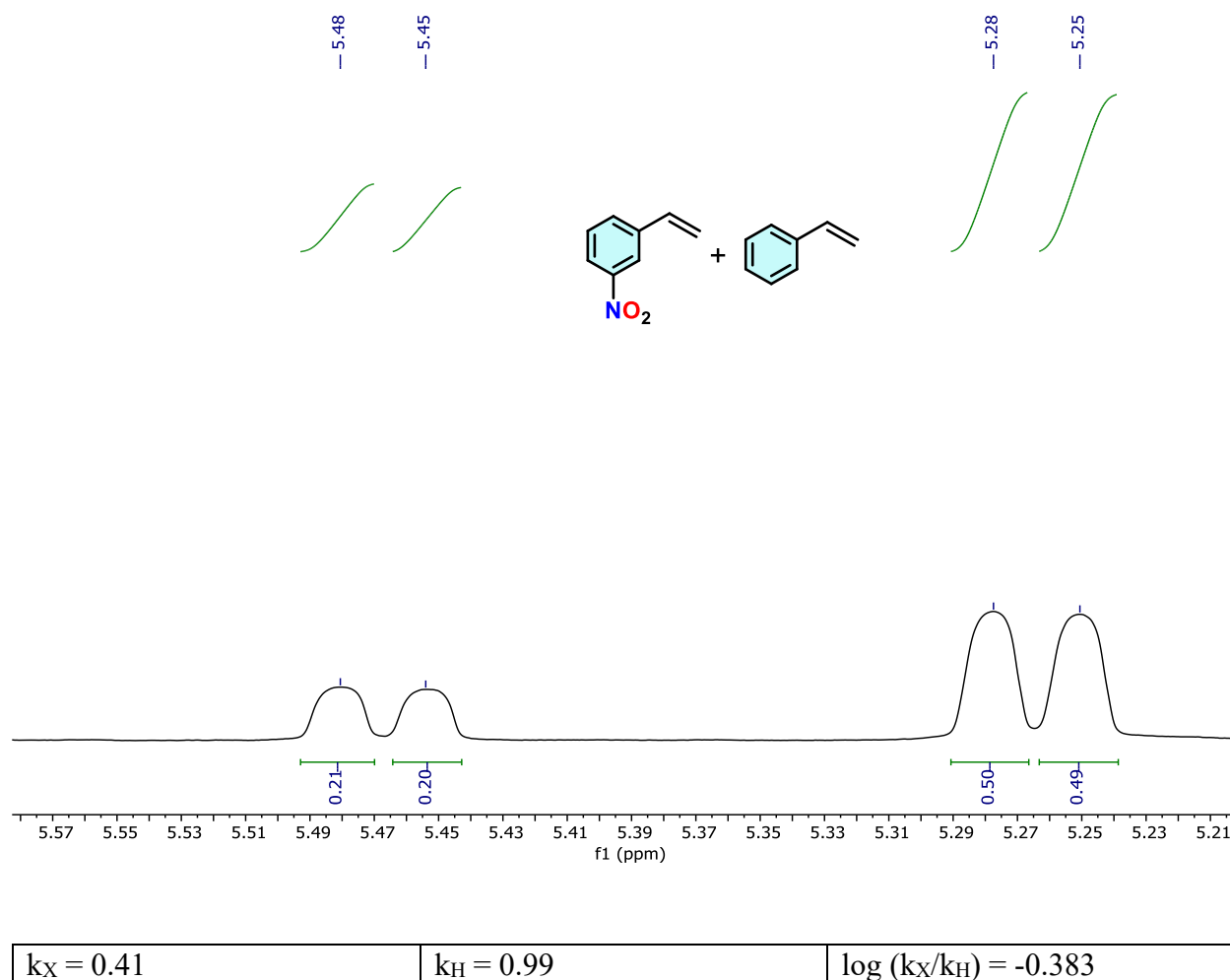
Figure 4.59. ^{1}H NMR spectra of 3-nitro styrene and styrene reaction mixture for Hammett analysis.
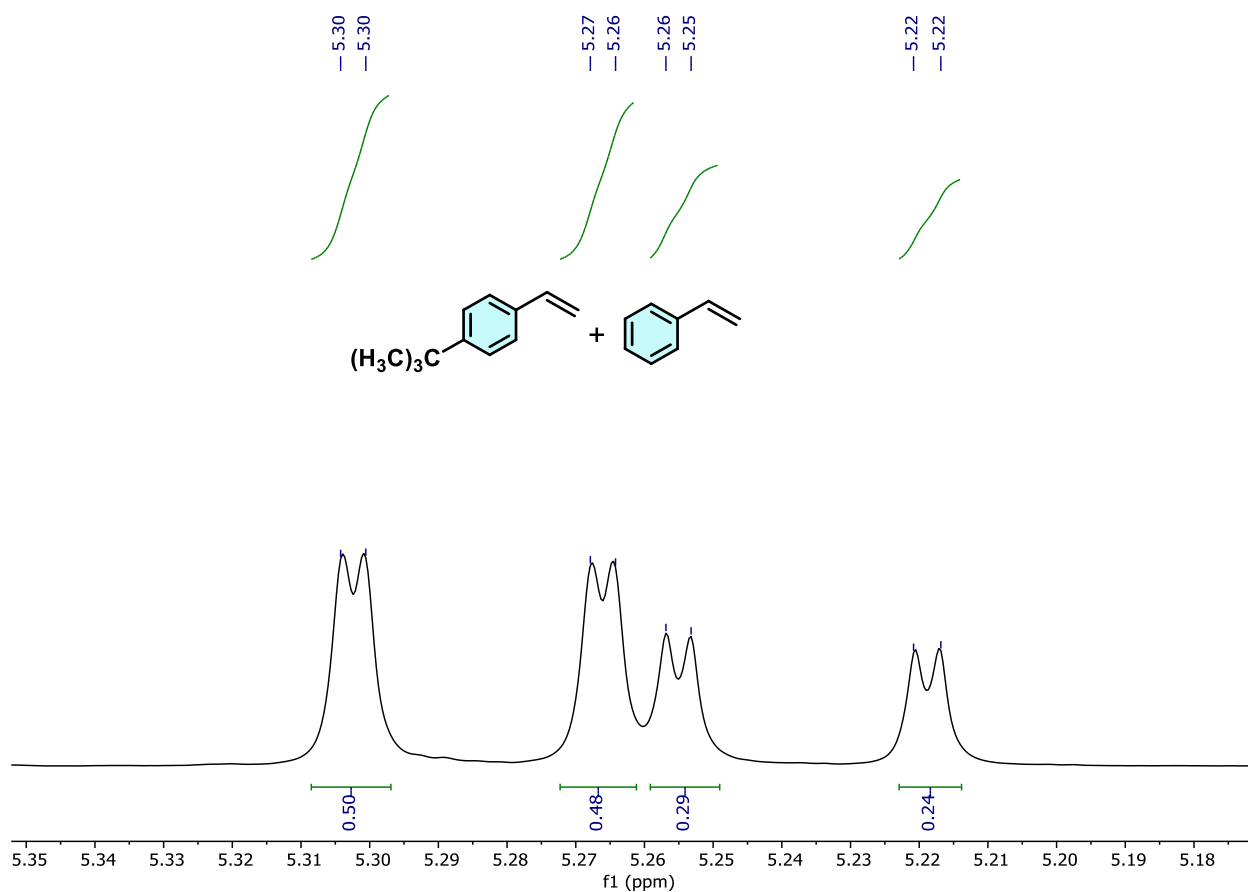
| $k_X = 0.98$ | $k_H = 0.53$ | $\log (k_X/k_H) = 0.267$ |

Figure 4.60. ^{1}H NMR spectra of 4-tert butyl styrene and styrene reaction mixture for Hammett analysis.
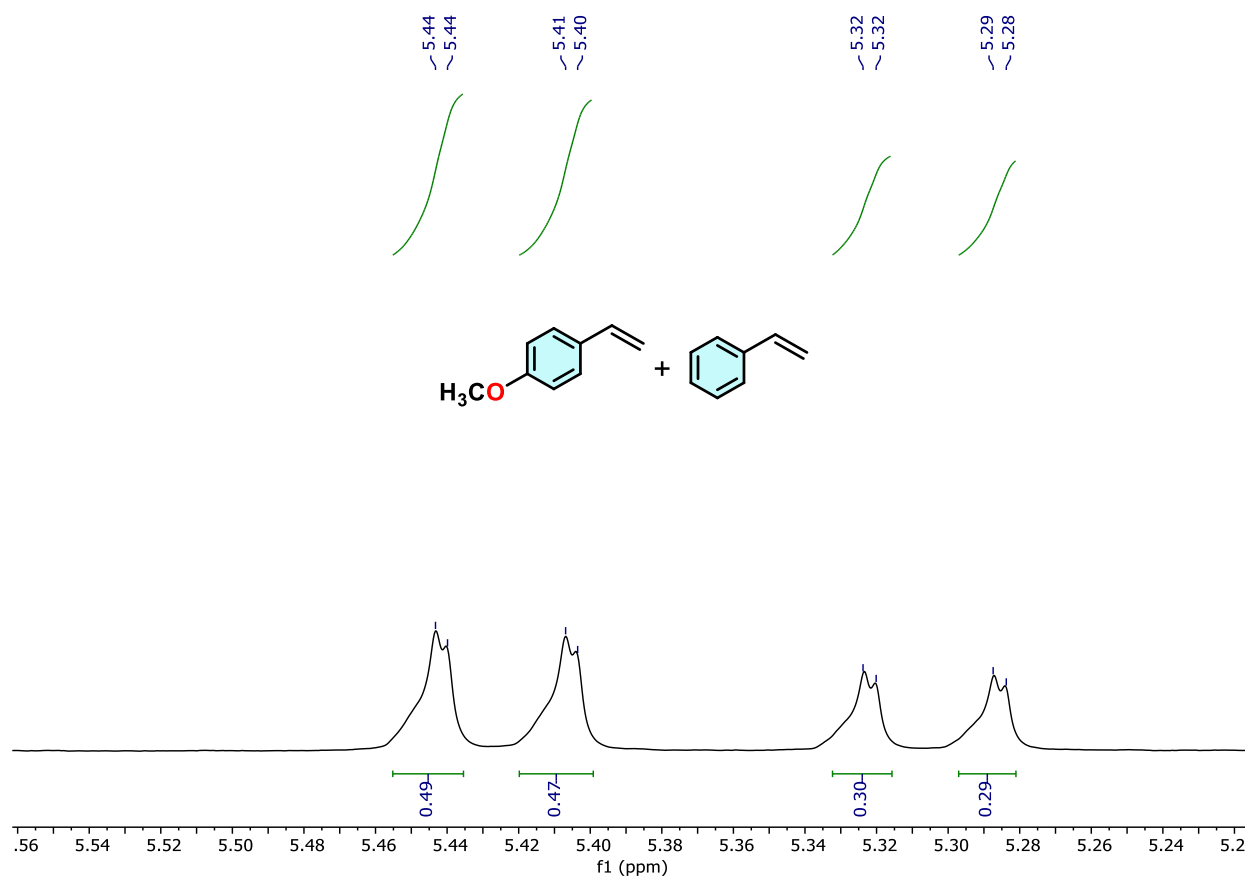
| $k_X = 0.96$ | $k_H = 0.59$ | $\log(k_X/k_H) = 0.211$ |

Figure 4.61. ^{1}H NMR spectra of 4-methoxy styrene and styrene reaction mixture for Hammett Analysis.

$k_X = 0.88$	$k_H = 0.8$	$\log (k_X/k_H) = 0.041$
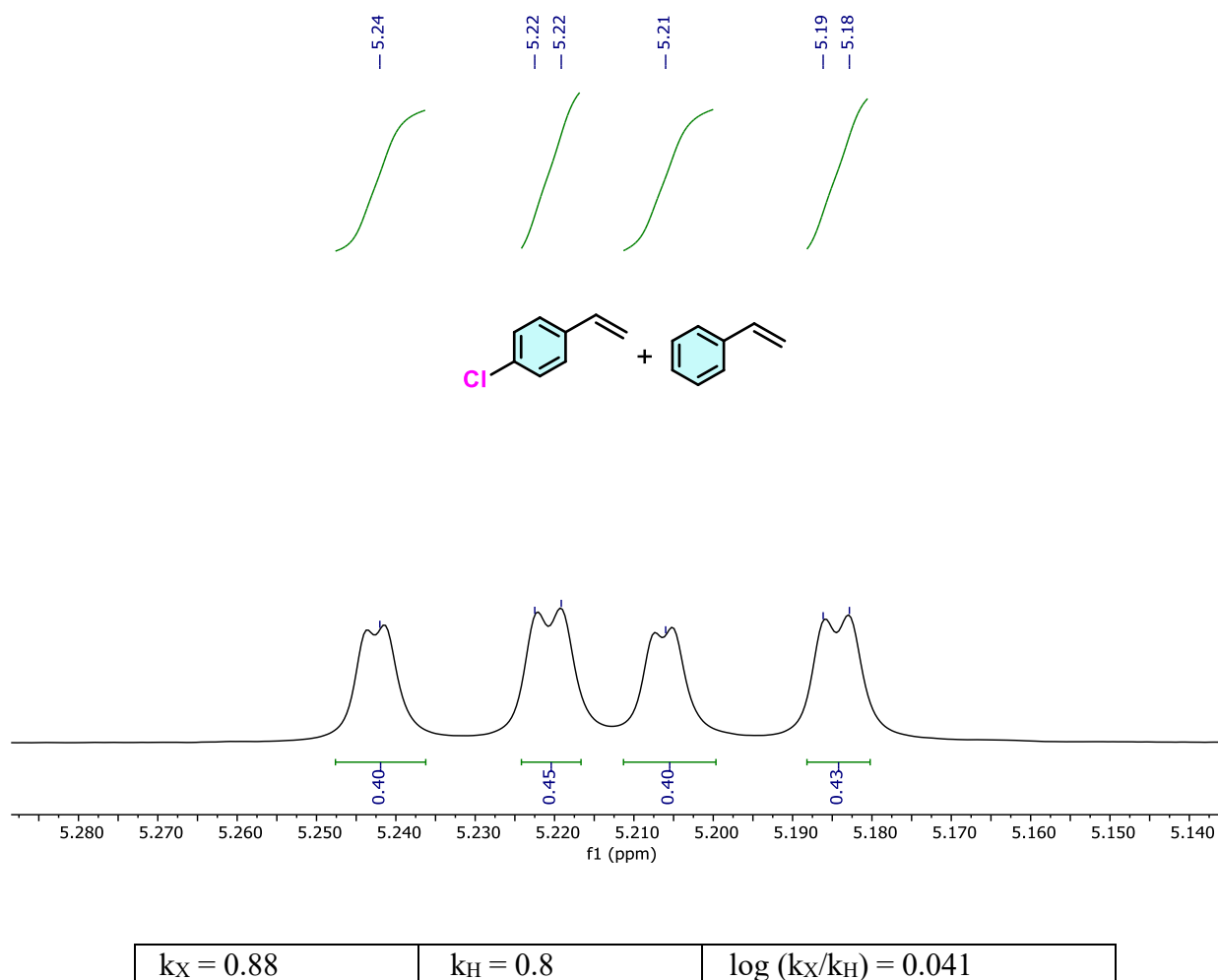
Figure 4.62. ^{1}H NMR spectra of 4-chloro styrene and styrene reaction mixture for Hammett Analysis.

Computational details:

Table 4.5. Relative Gibbs free energies for proton transfer TS3 (PT) with different bases

Base	$\Delta G^{\ddagger}$ (kcal/mol)
Imidazole	26.7
1,2-dimethylimidazole	24.6
Oxazole	31.3
Benzoxazole	29.5

Table 4.6. Relative Gibbs free energies for hydrogen atom transfer TS3 (HAT) with different bases

Base	$\Delta G^{\ddagger}$ (kcal/mol)
Imidazole	**16.9**
1,2-dimethylimidazole	**14.5**
Oxazole	**21.5**
Benzoxazole	**Not found**

Cartesian Coordinates

2a

C	0.000000000	0.000000000	-1.484745000
C	0.225382000	1.295538000	-0.689386000
C	-0.450765000	1.235324000	0.689386000
C	0.000000000	0.000000000	1.484745000
C	-0.225382000	-1.295538000	0.689386000
C	0.450765000	-1.235324000	-0.689386000
H	0.527625000	0.046988000	-2.445101000
H	-1.069540000	-0.095246000	-1.721723000
H	-0.143909000	2.158682000	-1.256383000
H	1.305449000	1.451294000	-0.553954000
H	-0.239808000	2.150141000	1.256383000
H	-1.541358000	1.197776000	0.553955000
H	-0.527625000	-0.046988000	2.445101000
H	1.069540000	0.095246000	1.721723000
H	0.143909000	-2.158682000	1.256383000
H	-1.305449000	-1.451294000	0.553954000
H	0.239808000	-2.150141000	-1.256383000
H	1.541358000	-1.197776000	-0.553955000

TBHP

C	0.306895000	-1.169588000	1.023379000
H	0.277622000	-2.123631000	0.486471000
H	1.178385000	-1.177010000	1.685391000

H	-0.589110000	-1.087464000	1.644018000
C	0.386743000	0.000163000	0.035780000
C	0.405358000	1.352170000	0.756104000
H	0.454953000	2.168230000	0.029232000
H	-0.499562000	1.478691000	1.354520000
H	1.273681000	1.423269000	1.419295000
C	1.587448000	-0.147015000	-0.906395000
H	1.549052000	-1.101342000	-1.439743000
H	1.597974000	0.661447000	-1.642645000
H	2.518296000	-0.107038000	-0.332995000
O	-0.723051000	-0.051641000	-0.894241000
O	-1.970420000	0.106584000	-0.156870000
H	-2.332179000	-0.789068000	-0.247855000

TS1

C	-1.301764000	-0.414353000	1.058545000
C	-1.596259000	1.069857000	0.982469000
C	-2.251174000	1.467673000	-0.352130000
C	-3.454541000	0.571416000	-0.682469000
C	-3.053991000	-0.911715000	-0.705503000
C	-2.421189000	-1.341209000	0.629896000
H	-0.774843000	-0.727916000	1.964682000
H	-0.677348000	1.645424000	1.143522000
H	-2.274631000	1.331293000	1.814215000
H	-2.554989000	2.520468000	-0.316923000
H	-1.503559000	1.377678000	-1.149427000

H	-3.885186000	0.860435000	-1.648542000
H	-4.243127000	0.724299000	0.069160000
H	-3.923517000	-1.542151000	-0.925517000
H	-2.328357000	-1.075467000	-1.512248000
H	-2.063109000	-2.376476000	0.576014000
H	-3.197623000	-1.330247000	1.415570000
H	-0.308993000	-0.583669000	0.107507000
O	0.466026000	-0.687561000	-0.752691000
O	1.316588000	0.434434000	-0.599599000
C	2.600095000	0.032031000	-0.037439000
C	3.354993000	1.363406000	0.022594000
H	4.366042000	1.204755000	0.409488000
H	3.430910000	1.807008000	-0.974220000
H	2.840600000	2.072322000	0.678224000
C	3.279985000	-0.957699000	-0.988593000
H	4.268346000	-1.239436000	-0.611009000
H	2.674117000	-1.860888000	-1.090227000
H	3.400996000	-0.510097000	-1.979519000
C	2.409693000	-0.566453000	1.359188000
H	1.914289000	0.149575000	2.022720000
H	1.805094000	-1.474934000	1.307743000
H	3.378886000	-0.824689000	1.797760000

2a•

C	-0.539155000	1.372160000	0.000000000
C	-0.050006000	0.792284000	1.290409000
C	-0.050006000	-0.751576000	1.268191000
C	0.626166000	-1.293797000	0.000000000
C	-0.050006000	-0.751576000	-1.268191000
C	-0.050006000	0.792284000	-1.290409000
H	-1.024701000	2.344632000	0.000000000
H	-0.642642000	1.163907000	2.134947000
H	0.987522000	1.130080000	1.482710000

H	0.448322000	-1.138973000	2.164915000
H	-1.087579000	-1.109972000	1.301465000
H	0.604503000	-2.390399000	0.000000000
H	1.687032000	-1.002987000	0.000000000
H	0.448322000	-1.138973000	-2.164915000
H	-1.087579000	-1.109972000	-1.301465000
H	-0.642642000	1.163907000	-2.134947000
H	0.987522000	1.130080000	-1.482710000

1b

C	2.265115000	0.262083000	0.000231000
C	1.361805000	1.329849000	-0.000080000
C	1.781005000	-1.046141000	0.000224000
H	1.730065000	2.352033000	-0.000171000
H	2.472344000	-1.884172000	0.000413000
C	-0.009383000	1.092589000	-0.000330000
C	0.406541000	-1.281836000	-0.000059000
H	-0.694420000	1.934956000	-0.000656000
H	0.035176000	-2.303829000	-0.000050000
C	-0.515166000	-0.220781000	-0.000278000
H	3.334718000	0.450858000	0.000460000
C	-1.954847000	-0.529669000	-0.000340000
H	-2.186931000	-1.594506000	-0.000874000
C	-2.976703000	0.335304000	0.000493000
H	-4.003247000	-0.016205000	0.000506000
H	-2.837912000	1.412470000	0.001196000

TS2

C	-3.891156000	-1.173457000	0.023846000
C	-2.803999000	-1.416478000	-0.822129000
C	-3.949793000	0.028205000	0.733425000
H	-2.753402000	-2.343581000	-1.386787000
H	-4.790886000	0.232293000	1.390419000

C	-1.787401000	-0.476026000	-0.954909000
C	-2.931858000	0.969264000	0.602698000
H	-0.963671000	-0.677677000	-1.632816000
H	-2.984808000	1.901435000	1.160085000
C	-1.821612000	0.740101000	-0.237412000
H	-4.683801000	-1.909252000	0.122855000
C	-0.784517000	1.761231000	-0.340767000
H	-1.002114000	2.690276000	0.185181000
C	0.425984000	1.653150000	-0.961561000
H	0.672529000	0.802241000	-1.587457000
H	1.040942000	2.534120000	-1.104660000
C	1.566923000	-0.151764000	1.427271000
C	2.095842000	1.034890000	0.672325000
C	3.372720000	0.873129000	-0.107588000
C	3.460103000	-0.467205000	-0.859656000
C	3.098753000	-1.647943000	0.053240000
C	1.694874000	-1.474376000	0.650845000
H	0.524558000	0.021594000	1.720726000
H	2.132361000	-0.247421000	2.373876000
H	1.958623000	1.999347000	1.158338000
H	3.514716000	1.713890000	-0.799322000
H	4.224809000	0.928794000	0.596790000
H	4.467107000	-0.594513000	-1.274288000
H	2.771723000	-0.453049000	-1.715420000
H	3.160836000	-2.590271000	-0.504395000
H	3.836220000	-1.717975000	0.866425000
H	1.451755000	-2.315447000	1.310609000
H	0.953323000	-1.491128000	-0.157924000

ᵗBuOO˙

C	0.305313000	-1.268493000	0.895623000
H	0.323586000	-2.159940000	0.261608000
H	1.164603000	-1.307857000	1.571866000

H	-0.610678000	-1.280422000	1.490224000
C	0.364831000	0.000058000	0.047743000
C	0.307019000	1.271484000	0.891403000
H	0.328568000	2.161017000	0.254855000
H	-0.609972000	1.287197000	1.484432000
H	1.165091000	1.310983000	1.569271000
C	1.534641000	-0.002468000	-0.932633000
H	1.507873000	-0.891553000	-1.569292000
H	1.507992000	0.883612000	-1.573499000
H	2.480520000	-0.001182000	-0.383081000
O	-0.823806000	-0.000413000	-0.861603000
O	-1.967244000	-0.000255000	-0.203297000

B

C	-4.501177000	-1.079125000	0.658524000
C	-4.015340000	-1.562343000	-0.717035000
C	-3.272952000	-0.448406000	-1.474784000
C	-2.101412000	0.162308000	-0.669273000
C	-2.618576000	0.623398000	0.712310000
C	-3.348435000	-0.487243000	1.485261000
H	-4.981909000	-1.900617000	1.203870000
H	-5.271486000	-0.307213000	0.515895000
H	-4.863940000	-1.915811000	-1.315533000
H	-3.354545000	-2.429675000	-0.584731000
H	-3.988535000	0.353475000	-1.705030000
H	-1.748872000	1.049365000	-1.205982000
H	-1.798844000	1.037502000	1.308621000
H	-3.320124000	1.454264000	0.551584000
H	-3.728344000	-0.092107000	2.435525000
H	-2.643715000	-1.288233000	1.748231000
C	-0.911730000	-0.820195000	-0.598529000
H	-0.662757000	-1.142957000	-1.617805000
H	-1.193059000	-1.731632000	-0.056500000

H	-2.909816000	-0.824088000	-2.440041000	C	-2.810964000	4.035738000	0.916420000
C	0.387877000	-0.302027000	0.045130000	C	-3.496996000	2.663223000	1.008516000
H	0.201198000	0.042138000	1.067754000	C	-2.684096000	1.523612000	0.349421000
C	1.457888000	-1.379014000	0.074209000	C	-2.334080000	1.917054000	-1.104412000
C	2.158174000	-1.726088000	-1.090183000	C	-1.661170000	3.295327000	-1.217722000
C	1.744531000	-2.059593000	1.263251000	H	-1.967993000	5.358974000	-0.593837000
C	3.124737000	-2.731138000	-1.061100000	H	-3.435891000	4.525833000	-1.092747000
C	2.703781000	-3.073750000	1.290911000	H	-3.450654000	4.804117000	1.368231000
C	3.397875000	-3.410986000	0.128306000	H	-1.880807000	4.029134000	1.501595000
H	1.952347000	-1.196421000	-2.015258000	H	-4.470472000	2.728825000	0.501425000
H	1.212182000	-1.795135000	2.173806000	H	-3.329246000	0.641978000	0.310078000
H	3.664735000	-2.985537000	-1.968922000	H	-1.698664000	1.153545000	-1.560259000
H	2.912413000	-3.593982000	2.221601000	H	-3.267279000	1.935639000	-1.685944000
H	4.148279000	-4.196161000	0.148563000	H	-1.495378000	3.538502000	-2.274583000
O	0.961725000	0.795311000	-0.693151000	H	-0.665654000	3.260724000	-0.756572000
O	0.285822000	2.023654000	-0.273254000	C	-1.458063000	1.139915000	1.208002000
C	1.297477000	2.991385000	0.101510000	H	-1.767070000	1.178085000	2.265756000
C	2.097996000	2.494660000	1.310425000	H	-0.675519000	1.899935000	1.100822000
H	2.625133000	1.569400000	1.066793000	H	-3.711776000	2.414064000	2.055622000
H	2.838246000	3.242735000	1.612070000	C	-0.827763000	-0.240240000	0.963418000
H	1.435003000	2.307967000	2.161370000	C	0.218170000	-0.675355000	1.924149000
C	0.442248000	4.212083000	0.462791000	C	0.624189000	-2.029128000	1.980808000
H	-0.233604000	3.981411000	1.291415000	C	0.876521000	0.234732000	2.779862000
H	1.088863000	5.041498000	0.764321000	C	1.636626000	-2.443553000	2.839275000
H	-0.156211000	4.531964000	-0.394824000	C	1.894717000	-0.186791000	3.637247000
C	2.206850000	3.287465000	-1.096671000	C	2.283608000	-1.526298000	3.675203000
H	2.923349000	4.076644000	-0.846461000	H	0.134340000	-2.746611000	1.333325000
H	2.763662000	2.393834000	-1.386474000	H	0.586174000	1.279114000	2.788077000
H	1.611088000	3.617298000	-1.952953000	H	1.923997000	-3.491686000	2.859209000
				H	2.377428000	0.538659000	4.286902000
TS3(HAT)				H	3.072317000	-1.852678000	4.346705000
C	-2.492359000	4.396561000	-0.542329000	O	-1.744065000	-1.286562000	0.822458000

O	-2.235465000	-1.331943000	-0.599971000
C	-3.090791000	-2.484777000	-0.715098000
C	-2.301167000	-3.772231000	-0.441635000
H	-2.002248000	-3.829159000	0.607131000
H	-2.911442000	-4.651708000	-0.672624000
H	-1.400333000	-3.799875000	-1.062135000
C	-3.526589000	-2.412766000	-2.185947000
H	-2.668276000	-2.523553000	-2.854916000
H	-4.235134000	-3.218695000	-2.400642000
H	-4.014101000	-1.456957000	-2.397680000
C	-4.302724000	-2.357900000	0.218345000
H	-4.967026000	-3.220486000	0.100071000
H	-3.981931000	-2.308409000	1.260750000
H	-4.871831000	-1.451939000	-0.011533000
N	0.702949000	-0.122916000	-1.274645000
C	2.095169000	-0.428395000	-0.906609000
C	0.361008000	-1.037141000	-2.249193000
C	1.351687000	-1.963265000	-2.426538000
N	2.358392000	-1.732226000	-1.514993000
H	2.210230000	-0.464619000	0.181008000
H	1.414319000	-2.772762000	-3.140933000
H	-0.595781000	-0.989091000	-2.745952000
C	3.703291000	-2.255068000	-1.615722000
H	4.159462000	-2.290599000	-0.621555000
H	3.663572000	-3.276671000	-2.003962000
H	4.341124000	-1.645534000	-2.268381000
O	3.009541000	0.487996000	-1.485845000
C	3.511241000	1.610840000	-0.716559000
C	2.365786000	2.504300000	-0.223464000
H	1.718051000	2.783626000	-1.057848000
H	1.757211000	1.995374000	0.528452000
H	2.767055000	3.415457000	0.233435000

C	4.371939000	2.365344000	-1.735815000
H	5.170066000	1.719517000	-2.114126000
H	3.760350000	2.685251000	-2.584065000
H	4.827159000	3.249339000	-1.278430000
C	4.380244000	1.123031000	0.454126000
H	3.796625000	0.592766000	1.212472000
H	5.169436000	0.457638000	0.090306000
H	4.855802000	1.975811000	0.950079000
H	-0.034305000	-0.121436000	-0.310883000

Me-Imd

N	1.477542000	-0.769102000	0.000005000
C	0.200204000	-1.084996000	-0.000018000
C	1.501991000	0.607114000	-0.000014000
C	0.226087000	1.115652000	0.000044000
N	-0.611252000	0.017008000	-0.000003000
H	-0.206318000	-2.088189000	0.000041000
H	-0.158654000	2.124478000	-0.000128000
H	2.434410000	1.155055000	0.000015000
C	-2.062995000	0.029430000	0.000003000
H	-2.449592000	0.534760000	0.890544000
H	-2.449560000	0.535498000	-0.890129000
H	-2.426039000	-1.000144000	-0.000440000

ᵗBuO•

C	-0.000500000	1.387668000	-0.580764000
H	0.889155000	1.948880000	-0.286248000
H	-0.000458000	1.259042000	-1.667671000
H	-0.890556000	1.948243000	-0.286249000
C	0.000008000	-0.026339000	0.081702000
C	-1.277402000	-0.793633000	-0.314432000
H	-1.304418000	-1.763807000	0.191286000
H	-2.164957000	-0.228457000	-0.017168000

H	-1.314971000	-0.970926000	-1.394410000
C	1.277919000	-0.792769000	-0.314513000
H	2.165121000	-0.227047000	-0.017241000
H	1.305562000	-1.762951000	0.191153000
H	1.315559000	-0.969978000	-1.394502000
O	-0.000023000	0.264679000	1.431137000

3a

C	4.005106000	0.773692000	0.894292000
C	3.487852000	1.366336000	-0.425667000
C	2.972043000	0.265510000	-1.367528000
C	1.891245000	-0.628603000	-0.720912000
C	2.412395000	-1.191343000	0.621957000
C	2.938312000	-0.101496000	1.571097000
H	4.330364000	1.573643000	1.570625000
H	4.893975000	0.160430000	0.686829000
H	4.280844000	1.938886000	-0.921978000
H	2.682868000	2.083221000	-0.210967000
H	3.819492000	-0.372104000	-1.655470000
H	1.703276000	-1.479835000	-1.384800000
H	1.628572000	-1.782797000	1.104929000
H	3.232927000	-1.888328000	0.402173000
H	3.347953000	-0.566924000	2.475754000
H	2.109893000	0.536023000	1.910728000
C	0.550341000	0.113343000	-0.574982000
H	0.343208000	0.694651000	-1.485804000
H	0.582083000	0.852722000	0.234630000
C	-0.648566000	-0.803411000	-0.345610000
H	2.590108000	0.707435000	-2.297111000
C	-1.997670000	-0.181290000	-0.116467000
C	-3.087052000	-1.038355000	0.108447000
C	-2.212343000	1.205669000	-0.122032000
C	-4.360680000	-0.521930000	0.325898000

C	-3.489664000	1.723176000	0.093911000
C	-4.564640000	0.861371000	0.319072000
H	-2.903359000	-2.107531000	0.107027000
H	-1.387721000	1.888730000	-0.296831000
H	-5.196069000	-1.193853000	0.500564000
H	-3.645455000	2.798036000	0.086468000
H	-5.558589000	1.265925000	0.488312000
O	-0.529305000	-2.020543000	-0.360492000

C

N	-1.243704000	-1.508800000	-0.427567000
C	-0.625492000	-0.187938000	-0.537768000
C	-2.428493000	-1.335187000	0.345331000
C	-2.725852000	-0.031441000	0.398894000
N	-1.751732000	0.702921000	-0.318131000
H	-3.598342000	0.463060000	0.800198000
H	-2.995493000	-2.187290000	0.688529000
C	-1.484779000	2.092199000	0.005662000
H	-2.434820000	2.633986000	0.038258000
H	-0.965176000	2.227177000	0.964166000
H	-0.874187000	2.543517000	-0.783128000
O	0.389255000	0.016040000	0.460415000
C	1.784020000	-0.028001000	0.077990000
C	2.141354000	-1.379046000	-0.565833000
H	1.600661000	-1.542083000	-1.503817000
H	3.211858000	-1.424908000	-0.791530000
H	1.906480000	-2.202453000	0.117044000
C	2.140367000	1.137516000	-0.861262000
H	1.847186000	2.089273000	-0.408620000
H	3.219846000	1.162388000	-1.044044000
H	1.647338000	1.052318000	-1.834448000
C	2.523531000	0.131901000	1.410766000
H	2.248914000	-0.675764000	2.095213000

H	3.607867000	0.111789000	1.261185000
H	2.253622000	1.081795000	1.881197000
H	-0.179727000	-0.028313000	-1.526008000
H	-0.589956000	-2.191675000	-0.060306000

Bases (HAT)

Imidazole

C	-0.673513000	4.892592000	0.392448000
C	-2.070501000	4.323793000	0.685577000
C	-2.442925000	3.222649000	-0.321548000
C	-1.408227000	2.076474000	-0.382806000
C	-0.005201000	2.668701000	-0.649529000
C	0.383861000	3.778546000	0.342652000
H	-0.401706000	5.646971000	1.141230000
H	-0.694769000	5.409420000	-0.578047000
H	-2.819526000	5.124918000	0.657970000
H	-2.092665000	3.919430000	1.707130000
H	-2.517850000	3.676380000	-1.320115000
H	-1.671204000	1.438525000	-1.231605000
H	0.751221000	1.878287000	-0.669052000
H	-0.006775000	3.097140000	-1.661810000
H	1.360138000	4.196304000	0.066240000
H	0.509874000	3.360685000	1.351827000
C	-1.472632000	1.187382000	0.887091000
H	-2.519549000	1.108371000	1.207582000
H	-0.951218000	1.682098000	1.710944000
H	-3.437233000	2.818431000	-0.090480000
C	-0.965135000	-0.256346000	0.757386000
C	-0.100064000	-0.835464000	1.813901000
C	-0.073840000	-2.229935000	2.050729000
C	0.793044000	-0.035722000	2.561069000
C	0.785093000	-2.784148000	2.996252000

C	1.652068000	-0.598113000	3.504277000
C	1.654315000	-1.975811000	3.733656000
H	-0.738276000	-2.871269000	1.484855000
H	0.823974000	1.036675000	2.401857000
H	0.772726000	-3.858643000	3.160685000
H	2.321199000	0.048660000	4.065614000
H	2.320446000	-2.410838000	4.472862000
O	-1.997753000	-1.185907000	0.502651000
O	-2.618829000	-0.838672000	-0.792837000
C	-3.951128000	-1.400895000	-0.802908000
C	-3.885966000	-2.926198000	-0.650538000
H	-3.502343000	-3.202976000	0.333750000
H	-4.883549000	-3.362275000	-0.765830000
H	-3.229766000	-3.358502000	-1.411797000
C	-4.447532000	-1.006607000	-2.200082000
H	-3.820952000	-1.451631000	-2.978355000
H	-5.473755000	-1.359559000	-2.339391000
H	-4.435380000	0.079901000	-2.323576000
C	-4.816278000	-0.762737000	0.290322000
H	-5.835504000	-1.160651000	0.249528000
H	-4.402665000	-0.973139000	1.278791000
H	-4.865183000	0.322092000	0.156675000
N	0.575723000	-0.717865000	-1.363720000
C	1.966414000	-0.972455000	-0.986206000
C	0.116073000	-1.847173000	-1.997653000
C	1.090810000	-2.795276000	-2.104176000
N	2.272157000	-2.300954000	-1.554734000
H	2.085858000	-0.987811000	0.106214000
H	1.065097000	-3.749153000	-2.613857000
H	-0.896296000	-1.880009000	-2.372904000
O	2.748479000	0.055074000	-1.551930000
C	4.050522000	0.353144000	-0.989335000

C	3.896598000	1.077091000	0.357720000	H	-2.923847000	-0.524536000	-1.667302000
H	3.296861000	1.983445000	0.233699000	H	-1.262880000	-0.754319000	-2.169375000
H	3.412619000	0.446713000	1.109861000	H	-3.842254000	-2.633168000	-1.349579000
H	4.878097000	1.364160000	0.750522000	C	-1.505153000	0.527057000	-0.459822000
C	4.669319000	1.292500000	-2.030270000	C	-1.483100000	1.839227000	-1.157182000
H	4.776088000	0.778224000	-2.989516000	C	-1.481044000	3.042700000	-0.414810000
H	4.024271000	2.162544000	-2.180583000	C	-1.423950000	1.950545000	-2.564179000
H	5.655170000	1.638996000	-1.704176000	C	-1.410581000	4.282628000	-1.044389000
C	4.921182000	-0.905394000	-0.835636000	C	-1.352211000	3.194364000	-3.189403000
H	4.549979000	-1.565223000	-0.043251000	C	-1.342510000	4.370876000	-2.436907000
H	4.954644000	-1.466603000	-1.772999000	H	-1.555655000	2.989016000	0.664228000
H	5.942519000	-0.620866000	-0.562199000	H	-1.442086000	1.058940000	-3.180502000
H	-0.126442000	-0.365662000	-0.414200000	H	-1.414607000	5.187818000	-0.442370000
H	2.833354000	-2.929366000	-0.992337000	H	-1.312953000	3.242863000	-4.274620000

1,2dimethylimidazole

				H	-1.291141000	5.338588000	-2.927473000
C	-0.928606000	-4.220870000	-2.425296000	O	-2.260827000	0.679480000	0.712934000
C	-2.326519000	-3.601452000	-2.576110000	O	-1.579380000	-0.022847000	1.866065000
C	-2.847359000	-3.079930000	-1.227156000	C	-2.477216000	0.043489000	2.990220000
C	-1.891979000	-2.066600000	-0.555043000	C	-2.742456000	1.503461000	3.385590000
C	-0.480107000	-2.687150000	-0.442560000	H	-3.260861000	2.033604000	2.584169000
C	0.052493000	-3.229887000	-1.780413000	H	-3.361503000	1.549481000	4.287673000
H	-0.550192000	-4.556377000	-3.399048000	H	-1.800542000	2.021675000	3.593585000
H	-1.001513000	-5.118283000	-1.793444000	C	-1.674240000	-0.681526000	4.080155000
H	-3.026816000	-4.338464000	-2.988574000	H	-0.729657000	-0.166099000	4.276209000
H	-2.284110000	-2.778656000	-3.303424000	H	-2.253067000	-0.710484000	5.008663000
H	-2.973940000	-3.937470000	-0.550620000	H	-1.451849000	-1.708508000	3.777406000
H	-2.257329000	-1.888763000	0.459230000	C	-3.788334000	-0.696910000	2.692337000
H	0.221776000	-1.961051000	-0.022522000	H	-4.448928000	-0.668351000	3.565284000
H	-0.529999000	-3.520637000	0.273330000	H	-4.306387000	-0.234982000	1.849618000
H	1.028790000	-3.704412000	-1.625569000	H	-3.591726000	-1.744624000	2.446076000
H	0.231603000	-2.400609000	-2.478763000	N	1.024903000	0.492091000	0.510474000
C	-1.905572000	-0.702978000	-1.284312000	C	2.211988000	0.485449000	-0.365973000

C	1.110082000	1.586469000	1.323636000
C	2.281927000	2.265961000	1.121507000
N	3.028212000	1.612326000	0.162874000
H	2.677513000	3.123106000	1.649953000
H	0.343660000	1.776372000	2.060550000
C	4.018474000	2.293033000	-0.651830000
H	3.573700000	2.938654000	-1.422457000
H	4.644652000	2.913502000	-0.003824000
H	4.661669000	1.555742000	-1.137290000
O	2.893232000	-0.754118000	-0.363493000
C	3.610986000	-1.337783000	0.765529000
C	5.040950000	-0.774775000	0.808730000
H	5.514519000	-0.867755000	-0.173770000
H	5.044193000	0.276516000	1.103825000
H	5.646564000	-1.332038000	1.531865000
C	3.653055000	-2.826446000	0.393060000
H	2.642172000	-3.242259000	0.369231000
H	4.101562000	-2.958973000	-0.595908000
H	4.245428000	-3.389069000	1.121800000
C	2.919353000	-1.161662000	2.122745000
H	2.907374000	-0.118554000	2.445043000
H	1.890225000	-1.523718000	2.093201000
H	3.472307000	-1.736979000	2.873839000
H	-0.082822000	0.374530000	0.012076000
C	1.839830000	0.686913000	-1.838687000
H	1.189553000	-0.131263000	-2.152535000
H	1.315619000	1.633427000	-1.983305000
H	2.738580000	0.660302000	-2.458668000

Oxazole

C	-2.805665000	-4.108261000	-0.901922000
C	-3.715360000	-2.979019000	-1.409670000
C	-3.820031000	-1.843998000	-0.377678000

C	-2.447851000	-1.274114000	0.048737000
C	-1.534192000	-2.426509000	0.521908000
C	-1.423135000	-3.573745000	-0.495947000
H	-2.704999000	-4.891279000	-1.664078000
H	-3.279330000	-4.582330000	-0.029620000
H	-4.714870000	-3.369726000	-1.638000000
H	-3.316602000	-2.589069000	-2.356582000
H	-4.323490000	-2.235296000	0.517907000
H	-2.610980000	-0.599894000	0.893995000
H	-0.542499000	-2.037196000	0.770948000
H	-1.953850000	-2.827652000	1.456107000
H	-0.815472000	-4.384834000	-0.074390000
H	-0.885289000	-3.224728000	-1.386358000
C	-1.838366000	-0.398174000	-1.062989000
H	-2.615798000	0.295949000	-1.411203000
H	-1.552338000	-0.999002000	-1.934814000
H	-4.458836000	-1.038196000	-0.761347000
C	-0.645777000	0.473715000	-0.621791000
H	0.354810000	-0.404316000	-0.788319000
C	-0.193842000	1.549730000	-1.576803000
C	0.699743000	2.532614000	-1.118362000
C	-0.598798000	1.590007000	-2.921540000
C	1.154594000	3.535584000	-1.969526000
C	-0.142721000	2.597075000	-3.774957000
C	0.733921000	3.574079000	-3.302611000
H	1.019503000	2.493728000	-0.083669000
H	-1.290483000	0.846904000	-3.304898000
H	1.838481000	4.292146000	-1.594234000
H	-0.479059000	2.619549000	-4.808020000
H	1.087074000	4.358732000	-3.965887000
O	-0.528636000	0.732827000	0.659194000
O	-1.926724000	1.888151000	1.079072000

C	-1.751105000	2.325661000	2.399955000
C	-0.441593000	3.117991000	2.562578000
H	-0.400181000	3.926290000	1.826232000
H	-0.361395000	3.553654000	3.564921000
H	0.416712000	2.461529000	2.400191000
C	-1.820971000	1.155627000	3.397294000
H	-1.019674000	0.441872000	3.191459000
H	-1.722355000	1.506089000	4.430941000
H	-2.776512000	0.630996000	3.299262000
C	-2.964856000	3.267613000	2.603924000
H	-2.949009000	3.676994000	3.619941000
H	-2.930888000	4.095076000	1.890081000
H	-3.900607000	2.720688000	2.459861000
C	3.128896000	-0.616632000	-2.356331000
C	1.788626000	-0.846120000	-2.464254000
N	1.261443000	-1.267496000	-1.266376000
O	3.582222000	-0.863183000	-1.110768000
C	2.404985000	-1.375304000	-0.361506000
H	2.634747000	-2.435200000	-0.183653000
O	2.206288000	-0.669054000	0.787134000
C	2.889020000	-1.088014000	2.017152000
C	2.561878000	0.046610000	2.988727000
H	1.479751000	0.162193000	3.084646000
H	2.984636000	-0.163494000	3.975782000
H	2.976547000	0.990822000	2.624967000
C	4.402853000	-1.192543000	1.794329000
H	4.900971000	-1.392875000	2.748193000
H	4.663251000	-2.001810000	1.105959000
H	4.795346000	-0.259088000	1.383635000
C	2.294387000	-2.412428000	2.511966000
H	2.498490000	-3.239825000	1.824854000
H	2.732699000	-2.679584000	3.478738000

H	1.211755000	-2.323573000	2.635102000
H	3.853922000	-0.300678000	-3.093317000
H	1.172679000	-0.719686000	-3.341867000

Benzoxazole

C	0.640337000	4.502242000	-0.786558000
C	0.730240000	4.015008000	-2.241184000
C	1.889330000	3.021213000	-2.430067000
C	1.827002000	1.819952000	-1.457748000
C	1.716509000	2.337609000	-0.006710000
C	0.552502000	3.321983000	0.194702000
H	-0.218497000	5.173411000	-0.660682000
H	1.536464000	5.094791000	-0.551741000
H	0.857602000	4.868154000	-2.919001000
H	-0.219299000	3.540084000	-2.524081000
H	2.835015000	3.554144000	-2.257545000
H	2.770095000	1.268340000	-1.536789000
H	1.657425000	1.490275000	0.681965000
H	2.652599000	2.861282000	0.235796000
H	0.549945000	3.690710000	1.228506000
H	-0.408793000	2.808510000	0.051336000
C	0.714468000	0.833322000	-1.862502000
H	0.827856000	0.624417000	-2.936780000
H	-0.275152000	1.298140000	-1.759090000
H	1.919592000	2.668148000	-3.468895000
C	0.732799000	-0.533468000	-1.126135000
H	-0.115783000	-0.302492000	-0.089789000
C	-0.136957000	-1.640551000	-1.684453000
C	-0.015054000	-2.939481000	-1.161275000
C	-1.107649000	-1.407924000	-2.674604000
C	-0.823776000	-3.973246000	-1.625602000
C	-1.914273000	-2.450154000	-3.141759000
C	-1.778316000	-3.736327000	-2.620184000

H	0.724147000	-3.115560000	-0.387795000
H	-1.220239000	-0.418805000	-3.107482000
H	-0.709339000	-4.971565000	-1.211174000
H	-2.644720000	-2.252961000	-3.922342000
H	-2.405889000	-4.545116000	-2.983401000
O	1.869097000	-0.913642000	-0.612034000
O	1.875402000	-0.872633000	1.301758000
C	3.120640000	-1.383475000	1.698565000
C	3.280715000	-2.850648000	1.251163000
H	3.248422000	-2.915286000	0.161679000
H	4.229526000	-3.275676000	1.598510000
H	2.463806000	-3.457355000	1.657095000
C	3.112368000	-1.315376000	3.245078000
H	2.281470000	-1.903174000	3.648946000
H	4.047322000	-1.714582000	3.655264000
H	3.006100000	-0.278659000	3.581616000
C	4.279320000	-0.523159000	1.155575000
H	5.248716000	-0.889185000	1.513433000
H	4.282597000	-0.540372000	0.064004000
H	4.160822000	0.515386000	1.481058000
C	-2.680706000	0.484141000	2.255833000
C	-3.962623000	0.799769000	2.678243000
C	-2.351546000	0.181369000	0.930826000
H	-4.187123000	1.031366000	3.712899000
C	-4.939025000	0.795597000	1.680194000
C	-3.333740000	0.166898000	-0.060658000
H	-5.964133000	1.034562000	1.944675000
H	-3.094200000	-0.098724000	-1.084096000
C	-4.630301000	0.482839000	0.342659000
H	-5.427288000	0.482998000	-0.394037000
N	-0.977100000	-0.079977000	0.915614000
O	-1.522571000	0.400051000	3.008693000

C	-0.558336000	0.061617000	2.135773000
H	0.471641000	-0.094079000	2.446251000

Hammett

TS3(HAT) (R=p-OMe)

C	-5.573730000	1.796258000	-1.752796000
C	-4.919339000	2.024353000	-0.382036000
C	-4.234583000	0.750140000	0.142070000
C	-3.221020000	0.143492000	-0.857886000
C	-3.905154000	-0.048425000	-2.231056000
C	-4.562969000	1.234732000	-2.763989000
H	-6.012779000	2.729079000	-2.127388000
H	-6.403424000	1.082683000	-1.642337000
H	-5.667039000	2.365684000	0.344426000
H	-4.184681000	2.836919000	-0.464714000
H	-5.010244000	-0.002563000	0.345097000
H	-2.941709000	-0.848188000	-0.485729000
H	-3.181876000	-0.435039000	-2.960997000
H	-4.682692000	-0.818943000	-2.126853000
H	-5.055739000	1.031344000	-3.722660000
H	-3.793015000	1.991471000	-2.968163000
C	-1.919841000	0.973019000	-0.972680000
H	-2.147583000	2.047769000	-0.951830000
H	-1.472771000	0.790247000	-1.960103000
H	-3.736942000	0.952744000	1.095186000
C	-0.833444000	0.665236000	0.071687000
C	0.280993000	1.638475000	0.185193000
C	0.936491000	1.869324000	1.408275000
C	0.750374000	2.353566000	-0.940487000
C	1.996004000	2.770540000	1.517417000
C	1.804678000	3.251318000	-0.843385000
C	2.438640000	3.470573000	0.388131000

H	0.606420000	1.328663000	2.286470000
H	0.278795000	2.212839000	-1.907508000
H	2.462053000	2.921569000	2.484508000
H	2.154051000	3.801654000	-1.711239000
O	-1.390423000	0.257333000	1.277600000
O	-0.492081000	-0.800651000	1.885469000
C	-1.207610000	-1.410532000	2.975750000
C	-1.555473000	-0.369219000	4.048006000
H	-2.225394000	0.393407000	3.645653000
H	-2.049311000	-0.848965000	4.899639000
H	-0.648796000	0.124736000	4.411308000
C	-0.171515000	-2.414544000	3.503993000
H	0.731764000	-1.896622000	3.839648000
H	-0.590299000	-2.965591000	4.351834000
H	0.102461000	-3.123717000	2.718917000
C	-2.457823000	-2.137591000	2.463821000
H	-2.919046000	-2.717857000	3.270129000
H	-3.196269000	-1.426794000	2.088035000
H	-2.187966000	-2.819146000	1.652001000
N	0.238634000	-1.430002000	-1.206955000
C	1.367299000	-2.015683000	-0.470631000
C	-0.647930000	-2.471637000	-1.419886000
C	-0.252571000	-3.598541000	-0.757947000
N	0.882750000	-3.325642000	-0.019624000
H	1.645035000	-1.380461000	0.374951000
H	-0.694534000	-4.585882000	-0.761523000
H	-1.525089000	-2.347251000	-2.039669000
C	1.813942000	-4.343517000	0.427068000
H	2.429776000	-3.945365000	1.238817000
H	1.251398000	-5.196504000	0.818171000
H	2.479462000	-4.686443000	-0.374447000
O	2.485023000	-2.286156000	-1.298832000

C	3.415574000	-1.241760000	-1.689519000
C	2.820458000	-0.405395000	-2.831224000
H	2.508682000	-1.060316000	-3.649975000
H	1.947912000	0.155651000	-2.494871000
H	3.565609000	0.301490000	-3.213328000
C	4.626363000	-2.038529000	-2.192022000
H	5.055672000	-2.637174000	-1.38265300
H	4.324236000	-2.716426000	-2.995706000
H	5.399792000	-1.366375000	-2.576600000
C	3.824760000	-0.356693000	-0.503431000
H	3.009781000	0.280485000	-0.151592000
H	4.180847000	-0.969526000	0.331958000
H	4.642520000	0.304194000	-0.808055000
H	-0.232707000	-0.483849000	-0.586411000
O	3.463784000	4.375485000	0.380442000
C	4.129429000	4.640352000	1.603092000
H	3.445916000	5.050888000	2.358028000
H	4.608062000	3.739475000	2.009484000
H	4.897548000	5.381545000	1.375569000

TS3 (HAT) (R= p-Cl)

C	-5.555374000	1.870088000	-1.693805000
C	-4.905465000	2.039417000	-0.312391000
C	-4.226145000	0.742449000	0.160802000
C	-3.210136000	0.174566000	-0.859303000
C	-3.889029000	0.042504000	-2.242084000
C	-4.542481000	1.347992000	-2.723769000
H	-5.990328000	2.818765000	-2.031217000
H	-6.387307000	1.154955000	-1.615796000
H	-5.654865000	2.351865000	0.425052000
H	-4.168954000	2.853205000	-0.358384000

H	-5.004644000	-0.015681000	0.329244000	C	-2.538649000	-2.272282000	2.351390000
H	-2.934840000	-0.832505000	-0.527321000	H	-3.000578000	-2.879426000	3.137127000
H	-3.164212000	-0.313854000	-2.986021000	H	-3.248025000	-1.496512000	2.056570000
H	-4.667801000	-0.730608000	-2.173358000	H	-2.345057000	-2.911728000	1.485183000
H	-5.032598000	1.184847000	-3.691394000	N	0.300881000	-1.309591000	-1.292318000
H	-3.770194000	2.110551000	-2.895088000	C	1.384096000	-1.989839000	-0.567113000
C	-1.906750000	1.004121000	-0.931689000	C	-0.585067000	-2.300437000	-1.662359000
H	-2.134945000	2.077644000	-0.879765000	C	-0.237655000	-3.503905000	-1.109805000
H	-1.446713000	0.854357000	-1.919715000	N	0.862338000	-3.336357000	-0.300843000
H	-3.732302000	0.903321000	1.123891000	H	1.613003000	-1.460432000	0.361531000
C	-0.841412000	0.661529000	0.124849000	H	-0.694717000	-4.475134000	-1.243426000
C	0.250543000	1.640291000	0.329855000	H	-1.431618000	-2.092548000	-2.301807000
C	0.903892000	1.753548000	1.575516000	C	1.748212000	-4.409521000	0.106021000
C	0.702386000	2.468650000	-0.719558000	H	2.287501000	-4.116660000	1.011586000
C	1.947965000	2.652950000	1.768998000	H	1.152710000	-5.296734000	0.338793000
C	1.748700000	3.371008000	-0.537208000	H	2.482472000	-4.658516000	-0.669153000
C	2.366697000	3.458802000	0.708897000	O	2.541588000	-2.180502000	-1.355959000
H	0.579274000	1.122851000	2.393573000	C	3.522597000	-1.122910000	-1.541812000
H	0.228590000	2.417437000	-1.694078000	C	3.014807000	-0.110127000	-2.576859000
H	2.433335000	2.734703000	2.735902000	H	2.732700000	-0.626972000	-3.498614000
H	2.078651000	4.004289000	-1.353726000	H	2.141056000	0.428121000	-2.207289000
O	-1.396620000	0.150317000	1.284883000	H	3.799071000	0.618511000	-2.810103000
O	-0.526404000	-1.008124000	1.774735000	C	4.736673000	-1.881682000	-2.092168000
C	-1.226938000	-1.653901000	2.852777000	H	5.103598000	-2.606082000	-1.358504000
C	-1.468488000	-0.676912000	4.011554000	H	4.462771000	-2.423570000	-3.002060000
H	-2.107054000	0.150009000	3.694947000	H	5.548079000	-1.187485000	-2.331548000
H	-1.955224000	-1.190212000	4.847443000	C	3.887860000	-0.435657000	-0.218569000
H	-0.520065000	-0.264385000	4.369708000	H	3.076377000	0.181762000	0.174950000
C	-0.231309000	-2.749704000	3.265396000	H	4.167345000	-1.176448000	0.538418000
H	0.716690000	-2.308817000	3.587579000	H	4.746611000	0.224269000	-0.375494000
H	-0.644189000	-3.327928000	4.097953000	H	-0.184354000	-0.420924000	-0.618067000
H	-0.036939000	-3.424681000	2.428099000	Cl	3.689379000	4.596955000	0.948344000

Chapter-5

Strategic Design of a 2,6-disubstituted Pyridine-Based Probe Having Hard-Soft Centers: Responsive Divergence from One Core
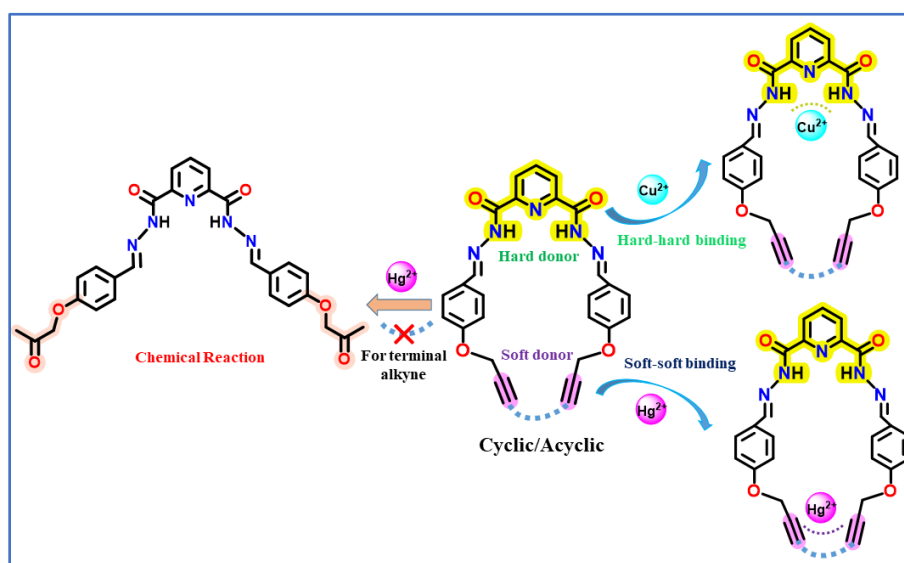
5.1 Introduction

This chapter of my thesis describes synthesis of biologically active organic compounds in presence of copper catalyst and its application to metal ion sensing. Copper-catalyzed reactions are widely used in organic synthesis due to the versatility of copper as a catalyst and its ability to facilitate various transformations efficiently. Compared to other transition metals like Pd, Rh, Ir, and Ru, copper is very cheap, easy to handle and found in large stock in the earth's crust. In this content, we have designed chemosensor molecules that are synthesized by Glaser-Hay coupling between two terminal alkynes in presence of copper catalyst. This chapter deals with the synthesis of biologically active organic molecules using copper catalyst and its further application to detect biologically relevant metal ions.

The field of supramolecular chemistry using macrocyclic hosts is a widely applied field and a rapidly growing study in the fields of chemistry, material science and biology. Since non-covalent interactions like hydrogen bonding, hydrophobic interaction etc. are used to build these host-guest based supramolecular assemblies, they are extremely dynamic and easily tunable through their responses to a wide range of external stimuli, such as biologically active multiple metal ions. Apart from that, the host molecule possesses a "signalling unit" such as a chromophore or fluorophore which has a binding site and it helps Interaction between the host and guest and physiologically significant metal ions (Scheme 5.1). Therefore, applications for differential detection using molecular sensors emerged as the most promising ones of this kind of host-guest recognition. To comprehend the binding phenomena through various channels we have designed a well-organized system consisting of a fluorophore moiety to detect biologically active metal ions (Hg^{2+}/Cu^{2+}).
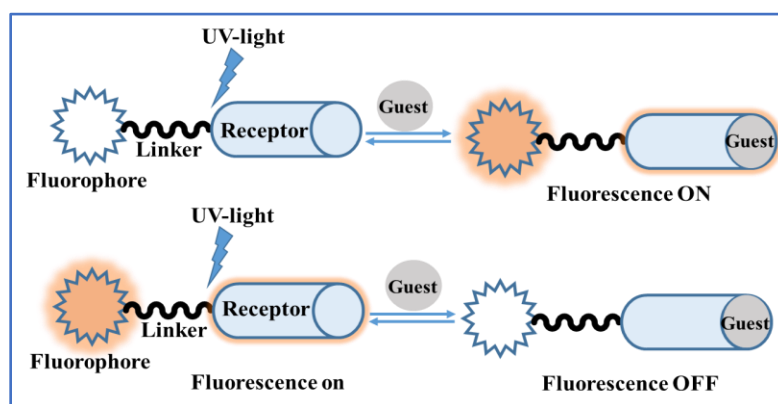
Scheme 5.1. Schematic representation of host-guest interaction.

Geometry of molecules plays pivotal role in regulating the gross properties exhibited by them. In the broad area of molecular recognition, it is known that a particular geometry (size or shape) of host can encapsulate a particular guest depending upon various factors like shape and size, ionic potential, soft/hard centres (HSAB principle), relative acidity and basicity of host and guest, pH etc.[1-6] Utilizing this concept (HSAB), we have designed two ligand systems, **5** and **7**, based on pyridine scaffold, both of which contain a hard donor centre (constituted by N atoms) and a soft donor centre (constituted by C≡C). The only structural dissimilarity between them is in the position or nature of the soft centres. In case of **5** (acyclic), the soft centre is terminal alkyne, and in case of **7** (cyclic), it is internally conjugated 1,3-dialkyne unit. Owing to presence of both hard and soft binding centres within each of the two molecules, two analytical aspects can be focussed on: 1) the selective recognition of hard and soft metal ions by binding to the respective hard and soft binding sites of each ligand and 2) the comparative study of the cyclic and acyclic ligand systems by their difference in interacting ability with a particular analyte. Among various hard metal ions, Cu^{2+} has a strong tendency of binding with the tridentate N-chelating centre.[7-9] On the other hand, a comparatively soft metal ion like Hg^{2+} can interact with soft centres (π-cloud of the alkyne units) preferably over hard tridentate N-chelating centre. Such interactions, although are feasible according to HSAB principle, but literature reports are rather rare.[10-12] Hg^{2+} ion is known to have a high affinity towards the alkyne functionality, and therefore it is anticipated to serve as a potential interactive unit towards any kind of alkyne, but the nature of such interactions in different alkynes with similar surroundings of probes has not been explored yet. Hg^{2+} ion is also well-known to bind with hard donors like N, O atoms,[13-17] however, any insight about the nature of interaction of Hg^{2+} in presence of both hard and soft centres, simultaneously in a probe, is rather very rare.[18] This apparent non-transparency in the subject have motivated us to design our molecules in order to have both the hard and soft interacting units. In case of dual metal ion sensing, many multichannel probes are reported that can interact *via* the same binding site and mechanism,[19] however, a probe capable of detecting dual metal ions *via* different binding sites and different mechanisms is rarely found.[20] The inclusion of both hard and soft centres can enable our designed probes to detect dual metal ions with different mechanisms. Our aim here, however, is not to establish our designed probes as superior sensors, compared to those reported in literatures, but to investigate the differences in the sensitive responses of the cyclic and acyclic structures towards Hg^{2+} ion, which remain virtually unexplored so far.

For the design of our coveted probes, pyridine-2,6-dicarbohydrazide based imine derivatives have been chosen owing to the geometry of 2,6-disubstituted pyridine derivatives in forming a proper bite angle in metal ion chelation. Furthermore, pyridine serves as a good fluorophore such that the detection of the analyte can be made feasible fluorometrically.[9,21-23] To the best of our knowledge, this is the first report of pyridine-2,6-dicarbohydrazide based system for the detection of Cu^{2+} and Hg^{2+} ions *via* different binding sites and dissimilar mechanism and a detailed comparative response of the acyclic and cyclic architectures of same molecular unit towards metal ion recognition was demonstrated. A series of experimental and theoretical (DFT) studies unravel the binding modes and mechanistic details and the comparative divergent interaction modes of the present probes with selective metal ions.

5.2 Results and Discussion

5.2.1 Synthesis and characterization

With an aim to determine the different response patterns of acyclic and cyclic alkynes towards soft metal ion binding and to investigate site selectivity of metal ions according to HSAB principle, we have synthesized two pyridine-2,6-dicarbohydrazide based ligands, **5** and **7**. Starting with commercially available pyridine-2,6-dicarboxylic acid (**1**), the methyl ester (**2**) was prepared, which was subjected to react with hydrazine monohydrate, giving corresponding acyl hydrazide derivative (**3**). The free amine group of the acyl hydrazide **3** was further reacted with 4-(prop-2-yn-1-yloxy)benzaldehyde (**4**), giving imine bonds in the C_2-symmetric open-chain molecule **5** as white crystalline solid in 95% yield (Scheme 5.2).
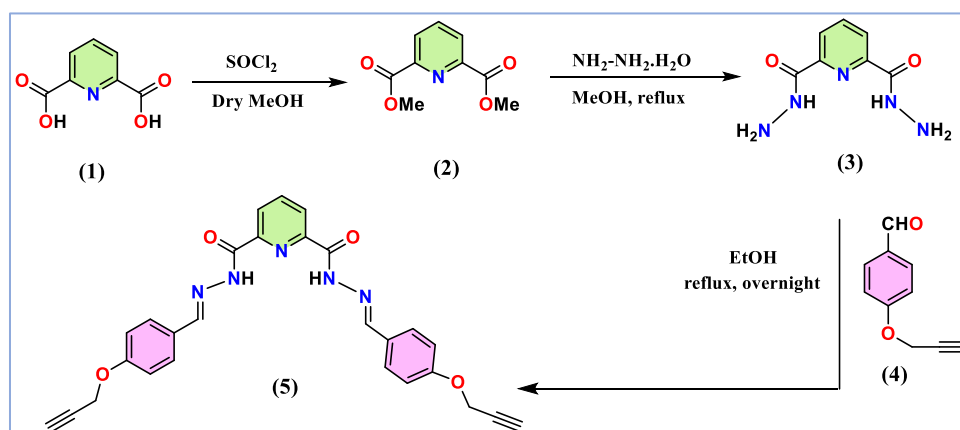
Scheme 5.2: Synthetic route for preparation of compound **5** starting from compound **1**.

Direct synthesis of cyclic 1,3-dialkyne unit containing molecule **7** by the C-C coupling reaction of terminal alkynes of **5** was not very successful by either of conventional or modified Glaser-Hay reaction.[24] Hence to obtain **7** in good yield, we have changed the course of reaction, as shown in Scheme 5.3. Starting with compound **4**, the alkyne-alkyne coupling reaction was performed first by using $Cu(OAc)_2.H_2O$ as the catalyst and piperidine as base to obtain the conjugated 1,3-dialkyne product **6** in 90% yield. Finally, Schiff base condensation reaction between **6** and **3** resulted in formation of **7** in 64% yield. All the synthesized compounds are characterized by ^1H and ^{13}C NMR, IR spectroscopy and elemental analysis and additionally compound **5** was characterized by single crystal X-ray diffraction studies.
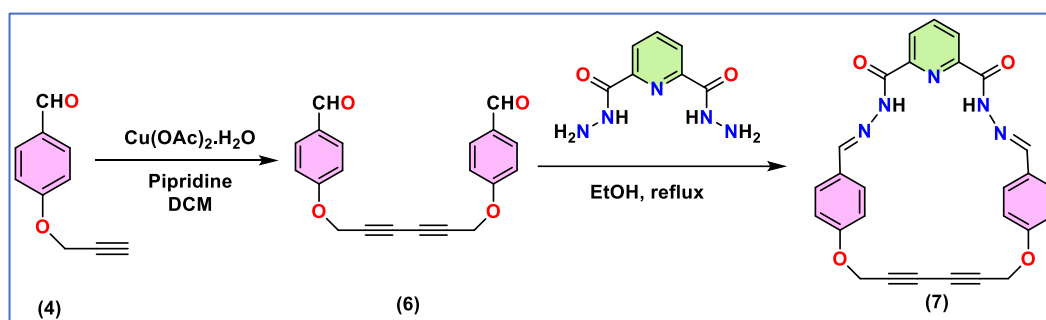
Scheme 5.3: Synthetic route of compound **7** starting from compound **4**.

The single crystal X-ray diffraction analysis of **5** showed that it crystallized in the monoclinic non-centrosymmetric system with C2/c space group with a half molecule in the asymmetric unit. The 2-fold crystallographic axis is passing through the plane of the central aromatic ring. The ligand exhibits a non-planar conformation in which the aromatic rings showed a torsion angle of 16.28–28.89°. The amide functionality of **5** showed non-classical hydrogen bonding interaction with alkyne moiety [C–H···O = 3.392(3) Å, ∠ C–H···O = 161°] lead to the formation of 1D zig zag chains. Moreover, such chains are further stabilized by C–H···π interactions [3.603 Å] involving C–H of aromatic ring and alkyne functionality. Interestingly these chains are further packed in a parallel fashion along crystallographic axis "c" supported by C–H···π interactions [3.479 Å] between the alkyne moieties resulted in a 2D sheet structure. Such sheets are further packed on top of each other supported by various supramolecular interactions (Figure 5.1).
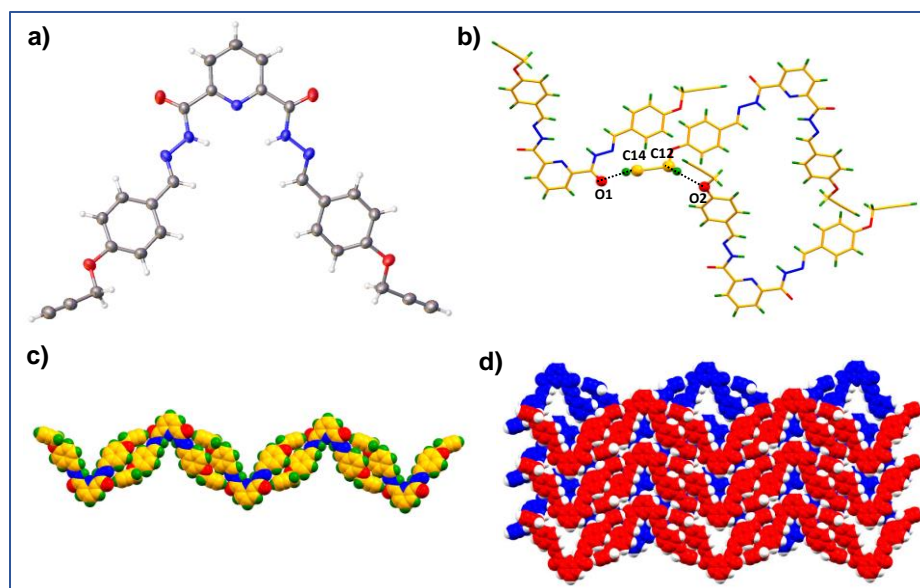
Figure 5.1 Crystal structure illustration of **5** – a) ORTEP diagram (50% probability) of compound **5** (color code – C – grey, N – blue, O – red, H – white), b) hydrogen bonding interaction in **5**, c) 1D zig zag chain, d) offset packing of 2D sheets (adjacent sheets are shown in red and blue color). Color code in 1(b) and 1(c) – C – orange, H – green, O – red, N – blue).

5.2.2 UV-vis absorption studies

UV-vis absorption spectral patterns are unique inherent characteristics of any molecule and the study of them can help in assessing any mechanistic change associated when analytes are employed externally. The absorbance of compounds **5** and **7** in DMSO:H_2O (7:3, *v/v*) at 22 °C showed a broad absorption band at λ_{max}~ 320 nm ($\varepsilon = 39354$ M^{-1} cm^{-1} for **5**; 36774 M^{-1} cm^{-1} for **7**) due to π–π* transition from the conjugated system of the ligand[25] and a small absorption band at λ_{max}~ 262 nm ($\varepsilon = 1548$ M^{-1} cm^{-1}) for **5** (Figure 5.2). For the study of metal ion detection, perchlorate salts of Na^+, K^+, Ag^+, Mg^{2+}, Ca^{2+}, Mn^{2+}, Fe^{2+}, Co^{2+}, Cu^{2+}, Zn^{2+}, Hg^{2+}, Pb^{2+}, Al^{3+}, Cr^{3+}, Fe^{3+} were individually mixed with the DMSO solution of the ligands **5** and **7** (3.1×10^{-5} M). None of the metal ions produced a pronounced effect except Cu^{2+} and Hg^{2+} ions (Figure 5.2c and e). With stepwise addition of Cu^{2+} and Hg^{2+} ions into **5** and **7**, the absorption intensities changed differently for the different ligand systems. When Cu^{2+} ion was added to the DMSO solution of ligands, **5** and **7** separately, both of them displayed decrease in absorption band intensity along with appearance of isosbestic points at $\lambda_{max} = 358$ nm (**5**) and 364 nm (**7**) (Figure 5.2a and c). Saturation of the absorption intensities could be obtained after addition of around 1 equiv of Cu^{2+}

ion in both cases. The three N atoms from pyridine and amide linkages in its vicinity are known to interact with Cu^{2+} ion,[25] hence, there is a probability to form a chelate complex of Cu^{2+} ion with the tridentate site. On the other hand, for Hg^{2+} ion, the absorption intensities of both **5** and **7** got diminished with gradual addition of the metal ion, however, the decrement is not harmonious with respect to each other. In **5**, the gradual addition of Hg^{2+} up to 2 equiv decreased the pre-existing peak of free ligand (Figure 5.2b), whereas, in **7**, it got diminished and attained saturation with 1 equiv Hg^{2+} only, without any isosbestic point (Figure 5.2e), indicating the absence of any well-defined reaction equilibrium. It can be perceived from this observation that the complexation between Hg^{2+} and ligands **5/7** is not assisted by strong chemical interactions, rather weak interactions. The saturation of **5** with 2 equiv of analyte, presumably indicates a 1:2 (host:guest) ratio, which is validated by fitting the UV-vis titration data into the UV 1:2 *Bindfit* model[26] (Figure 5.32). However, to address our quest about whether there is only interaction or reaction of the terminal alkyne units of **5** in presence of Hg^{2+} ion, the complexed solution was left undisturbed for 2 h, anticipating the slow reaction of alkyne moiety of our synthesized molecule and water molecules in presence of Hg^{2+} ion. The absorption intensity for the metal-complexed solution of **5** decreased to a large extent (Figure 5.2b). Repeating the same experiment with **7** yielded a constant intensity of the complexed species with lapse of time (Figure 5.2d). This suggests an apparent variation in the kind of interactions between **5** and **7** with Hg^{2+} ion. Job's plot analysis from the absorption data, using the literature reported procedure [26, 27] with different sets of host/guest concentrations (Figure 5.33, 5.34) suggested a 1:1 (**5**:Cu^{2+}/**7**:Cu^{2+}/**7**:Hg^{2+}) binding pattern (Inset: Figure 5.2a,c,d). The stoichiometries were also validated by fitting the absorbance titration data into 1:1 binding model using the *Bindfit* software.[26] The Job's plot method is not accurate enough to validate the 1:2 ratio,[26] hence, the stoichiometry determination by Job's plot was not conducted for compound **5** with Hg^{2+}. The association constants, obtained from the fitting of absorbance data in *Bindfit*, were found to be 2.11×10^6 M^{-1} (**5**·Cu^{2+}), 1.51×10^6 M^{-1} (**7**·Cu^{2+}) and 1×10^4 M^{-1} (**7**·Hg^{2+}) (Figure 5.35 to 5.37). The absorption intensity with each aliquot of analyte addition was noted along with the corresponding host concentration and guest concentration and those three sets of data were fitted in the corresponding model of the *Bindfit* software,[26] wherefrom the fitting curves were obtained.
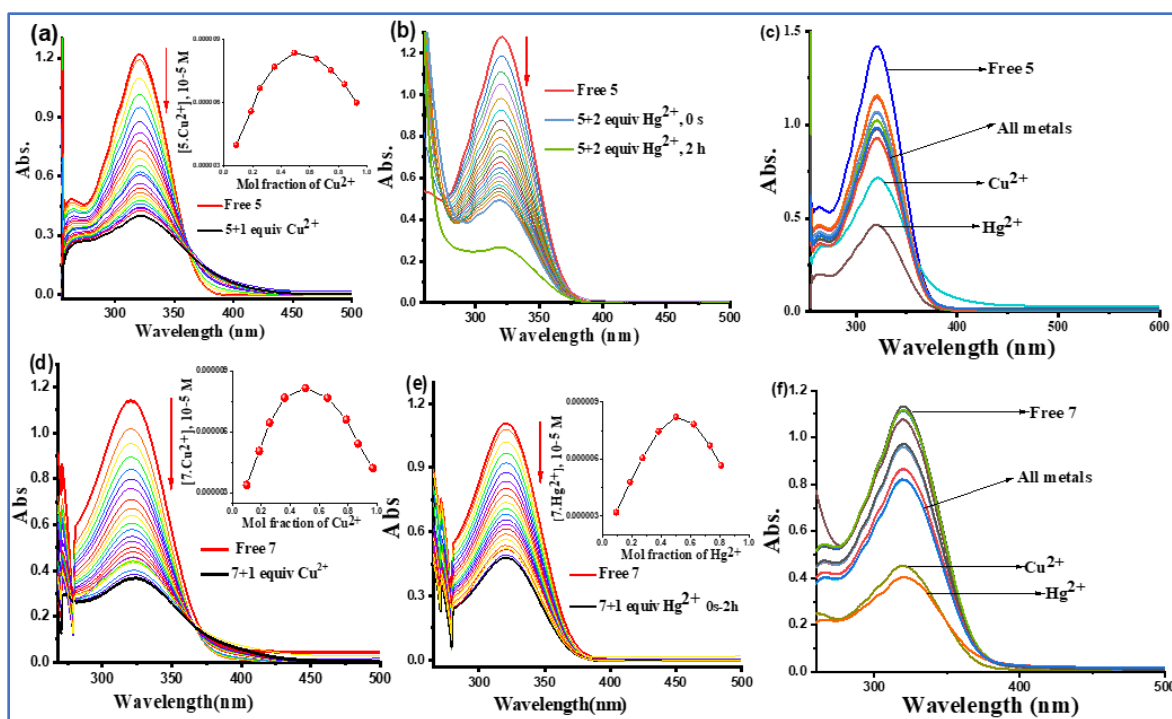
Figure 5.2 Absorption spectra of compound **5** (3.1×10^{-5} M) upon addition of up to (a) 1 equiv Cu^{2+} and (b) 2 equiv Hg^{2+} (c) with all metals and compound **7** upon addition of up to (d) 1 equiv Cu^{2+} and (e) 1 equiv Hg^{2+} in (f) with all metals in DMSO:H_2O (7:3, *v/v*) solvent at 22 ˚C (inset: Jobs plot of the corresponding interactions using 3.1×10^{-5} M concentration).

5.2.3 Fluorescence studies

       Fluorescence spectra is a kind of emission spectral study that plays an instrumental role in determining the nature of interaction with analyte owing to its accurate results. Both compounds **5** and **7** displayed two emission bands at 464 and 357 nm, when excited at λ_{exc}= 320 nm in DMSO:H_2O (7:3, *v/v*) at 22 ˚C. The emission band corresponding to 464 nm is the principal emission band for both the ligand systems, whereas the 357 nm peak corresponds to the solvent system. In order to investigate the metal ion-induced fluorescence signalling responses of probes **5** and **7**, the aforementioned set of metal ions in DMSO (7.8×10^{-6} M), were added into the DMSO:H_2O (7:3, *v/v*) solutions of **5** and **7** (7.8×10^{-6} M) separately. No significant change was observed in the emission spectra of compounds **5** and **7** after the addition of metal ions except for Cu^{2+} and Hg^{2+} ions (Figures 5.4c,f). To study in detail, titrations of the ligands with the two metal ions were conducted with the addition of small aliquots of metal ion solution. As shown in Figs. 3a and c, the gradual addition of Cu^{2+} ion up to 1 equiv into DMSO solutions of compounds **5** and

7 showed similar patterns of change in the fluorescence intensity. The emission peaks of **5** and **7** gradually shifted from 464 nm (Free **5/7**) to 435 nm ($[5 \cdot Cu^{2+}]/[7 \cdot Cu^{2+}]$) displaying a hypsochromic shift of 29 nm with a decrement in the emission intensity. Noteworthy, to check the solvent effect (residual water in DMSO), we have performed titration by addition of small aliquots of water, which shows no shift in the spectral pattern of the free ligands. Hence, the blue shift observed after metal ion addition is solely due to their interaction. Addition of Hg^{2+} ion up to 1 equiv into **5** gradually decreased the fluorescence intensity of the 464 nm peak but no saturation was obtained thereafter. Continuing with the addition of Hg^{2+} ion up to 2 equiv saturated the spectral pattern with an overall 29 nm hypsochromic shift (Figure 5.3b). From the fluorescence pattern, a simple complexation, most probably at the alkyne centres, can be suggested. To keep our experimentation in line with the UV-vis spectral studies, the fluorescence spectrum of the Hg^{2+}-mixed solution of **5** was recorded after 2 h. A fluorescence spectral pattern, completely different from the complexed species and similar to the free probe was obtained, with the emission being shifted to 463 nm (Figure 5.3b). From this observation and UV-vis spectral studies, it can be suggested that for probe **5**, simple interaction was followed by a chemical reaction with Hg^{2+} ion, which is most probable to occur at the terminal alkyne centres. For compound **7**, saturation of the spectral pattern after gradual fluorescence quenching (hypsochromic shift of 20 nm) can be observed with 1 equiv Hg^{2+} ion, which remains almost unchanged even after a long-time interval. Thus, Hg^{2+} produces a clear distinction between the acyclic and 1,3 conjugated cyclic alkyne-containing probes, which may indicate a difference in the mechanism of interaction.
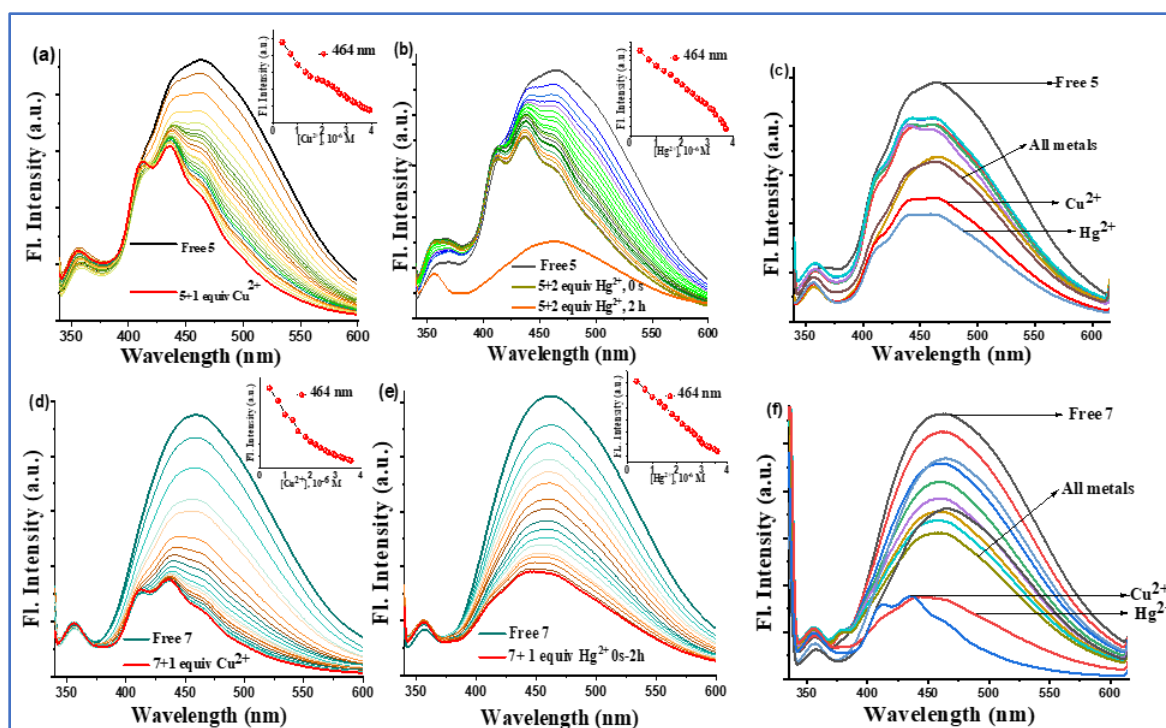
Figure 5.3 Emission spectra of compound **5** (7.8×10^{-6} M) upon addition of up to (a) 1 equiv of Cu^{2+} and (b) 2 equiv of Hg^{2+} ion and **7** (7.8×10^{-6} M) upon addition of up to (c) 1 equiv of Cu^{2+} and (d) 1 equiv of Hg^{2+} ion in $DMSO:H_2O$ (7:3, *v/v*) solvent at 22 ˚C, when excited at 320 nm (inset: variation of fluorescence intensity of 464 nm peak with increasing concentration of the corresponding analytes).

Changes in fluorescence lifetimes of **5** and **7** with the addition of the respective analytes have been examined in $DMSO:H_2O$ (7:3, *v/v*) at 22 ˚C. The lifetime of free **5** was found to be 0.432 ns which changed to 0.705 ns after interaction with 1 equiv Cu^{2+} (Figure 5.5a) and to 0.846 ns after interaction with 2 equiv Hg^{2+} (Figure 5.5b). On the other hand, in **7**, the lifetime changes to 0.433 ns from 0.205 ns, upon interaction with the Cu^{2+} ion (Figure 5.5c). For Hg^{2+} ion also, the lifetime of **7** changed from 0.205 to 0.512 ns (Figure 5.5d) suggesting that in all the cases, the fluorescence quenching mechanism does not follow a purely static mechanism,[28,29] rather it follows a dynamic quenching mechanism.[30,31] However, when considering only the dynamic collisional quenching, the bimolecular quenching constant k_q (**5**+Cu^{2+}: 5.9×10^{14} $M^{-1}s^{-1}$, **7**+Cu^{2+}: 3.8×10^{15} $M^{-1}s^{-1}$, **7**+Hg^{2+}: 2.1×10^{15} $M^{-1}s^{-1}$) becomes greater than the diffusional limit of oxygen in water (1×10^{10} $M^{-1}s^{-1}$). This indicates the presence of static mechanism along with dynamic process.
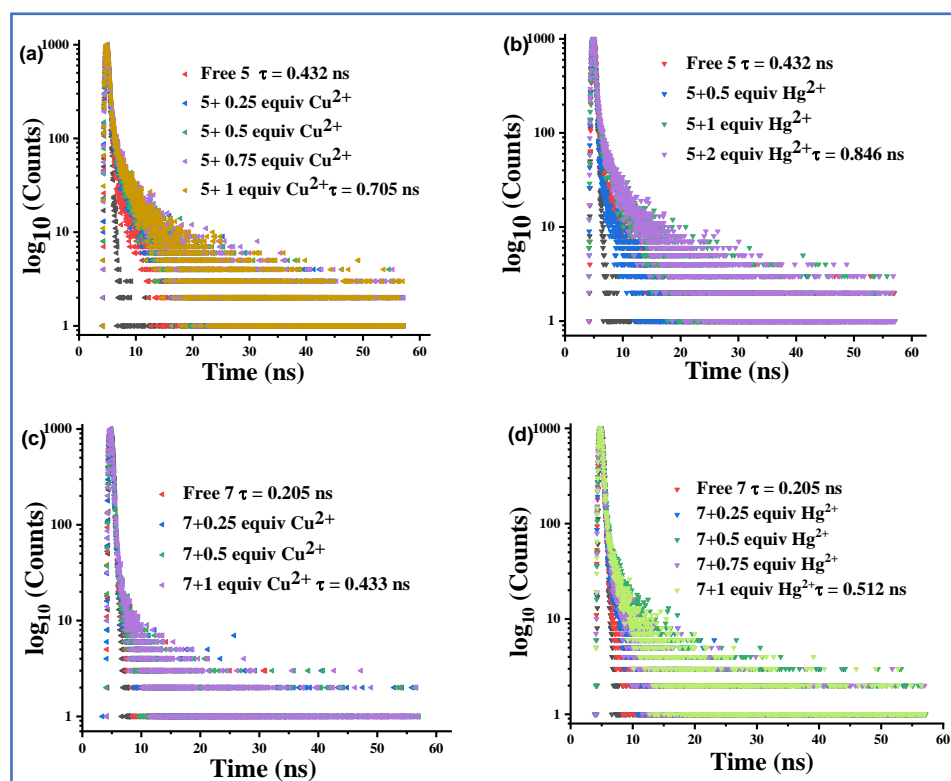
Figure 5.4 Fluorescence lifetime of **5** (7.8×10^{-6} M) upon titration with (a) Cu^{2+} ion (7.8×10^{-6} M) (b) Hg^{2+} ion (7.8×10^{-6} M) and **7** (7.8×10^{-6} M) upon titration with (c) Cu^{2+} ion (7.8×10^{-6} M) and (d) Hg^{2+} ion (7.8×10^{-6} M) in DMSO-H_2O (7:3, *v/v*) at 22 ˚C.

The presence of such a mixed static-dynamic mechanism has been further verified by the non-linear plot of I_0/I vs [Q] (Figure S18-S20) following the Stern-Volmer equation $I_0/I = 1 + K_{app}[Q]$, I_0 is the initial fluorescence intensity, I is the intensity with each addition of quencher concentration [Q] and K_{app} is the apparent quenching constant for both static and dynamic mechanisms occurring simultaneously.[32] The quenching of fluorescence intensity upon analyte addition is usually associated with the decrease in fluorescence lifetimes as well, however, the increase in lifetimes can also be observed in many cases.[33,34] In our case, the pulse width of the Instrument Response Function (IRF) used for these studies is 0.9 nm, and with this pulse width the changes in the fluorescence lifetimes may be considered insignificant.

The LOD obtained from fluorescence titration data by $3\sigma/s$ method ("σ" = standard deviation of the blank; "s" = slope of the calibration curve) for **5** are 5.5×10^{-7} M (Cu^{2+}) and that for **7** are 5.2×10^{-7} M (Cu^{2+}) and 4.4×10^{-7} M (Hg^{2+}) (Figure 5.5). The binding constant values are obtained from the Benesi-Hildebrand equation considering the ground-state 1:1 complexation

between the host and guest species (inset, Figure 5.2 and 5.3). It is assumed that at the end of titration, the complex is fully formed, which is responsible for the change in fluorescence intensity. The equation henceforth used is $1/\Delta I = 1/\Delta I_{max} + (1/K[Q])(1/\Delta I_{max})$, where $\Delta I = I_0-I$ and $\Delta I_{max} = I_0 - I_{max}$, in which I, I_{max}, and I_0 are the emission intensities of the molecules at an intermediate analyte concentration, at a concentration of complete interaction, and in the absence of analyte respectively, K is the binding constant, and [Q] is the analyte concentration. The plot of $1/\Delta I$ vs $1/[Q]$ gave the corresponding slope and intercept, from which, intercept/slope gave the corresponding K value.[35] The values thus obtained are $1.02\times10^5\,M^{-1}$ (**5**-Cu^{2+}), $3.9\times10^5\,M^{-1}$ (**7**-Cu^{2+}) and $7.4\times10^4\,M^{-1}$ (**7**-Hg^{2+}) (Figure 5.6). The moderate binding constant of Hg^{2+}, as obtained from UV-vis and fluorescence titrations, indicate towards a weaker interaction in
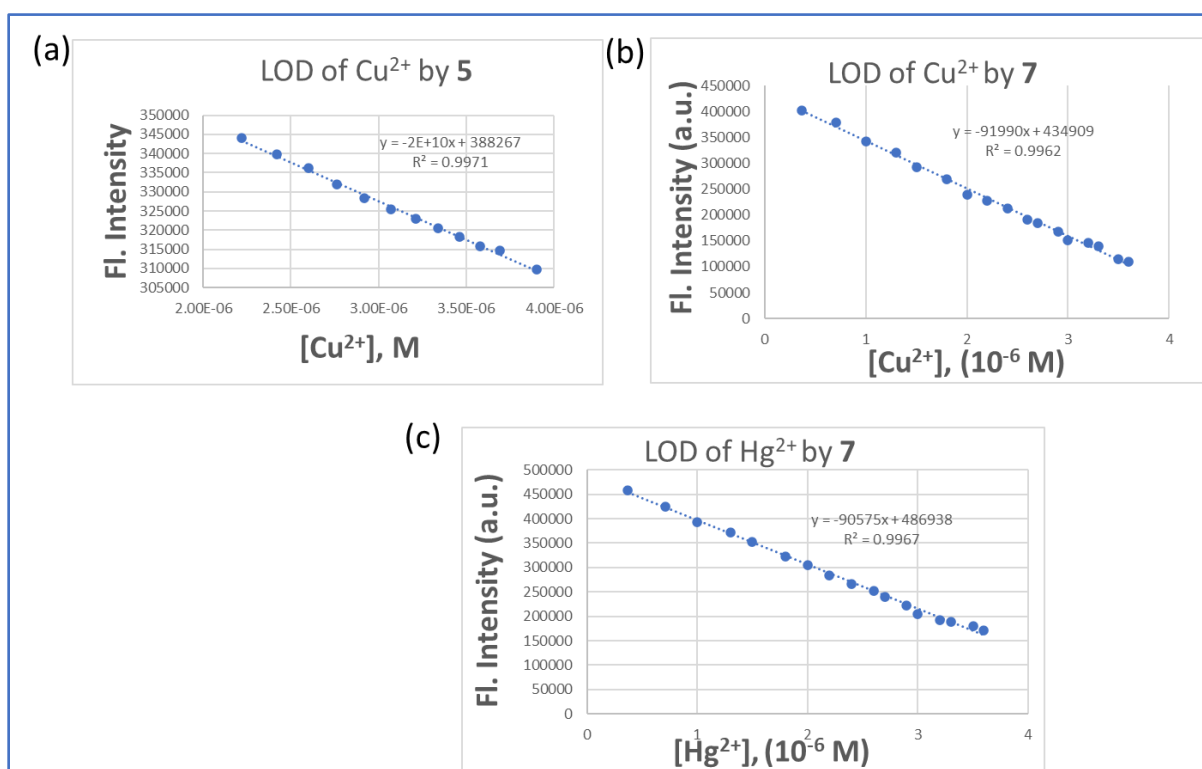
Figure 5.5 Limit of detection (LOD) of compound (a) **5**+Cu^{2+}, (b) **7**+Cu^{2+} and (c) **7**+Hg^{2+} from fluorescence spectra by $3\sigma/s$ method.
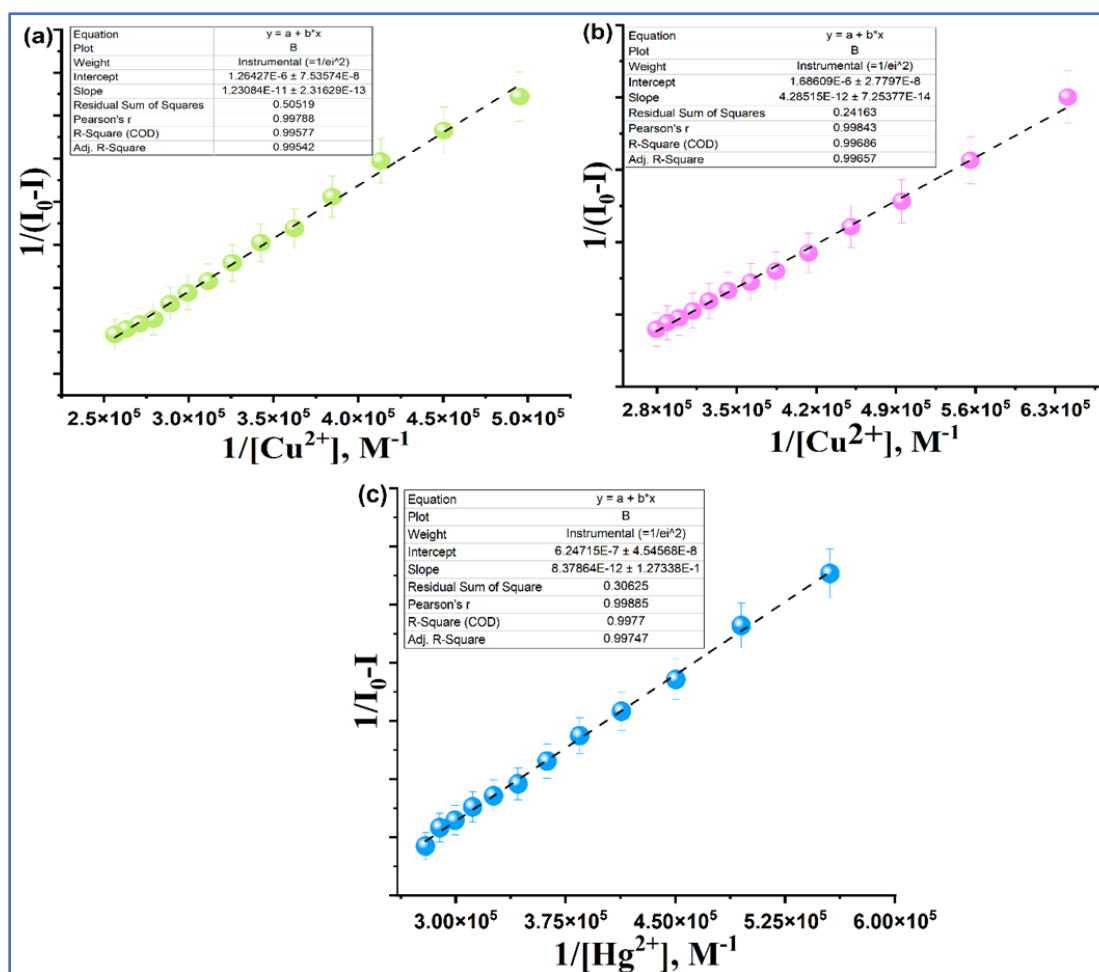
Figure 5.6 Association constant of compound (a) **5**+Cu^{2+}, (b) **7**+ Cu^{2+} and (c) **7**+Hg^{2+} from Benesi-Hildebrand plot. Error bars represent standard deviation.

comparison to those for Cu^{2+} ion. These values are comparable with the literature reported values for such binding of Cu^{2+} with similar tripodal N-binding centres.[8,25,36,37] Moreover, as long as soft centre as a binding unit for Hg^{2+} ion is concerned, our probe has comparable LOD.[38-41] The Cu^{2+} complexes with both **5** and **7** are formed by hard-hard binding, hence are expected to be stronger than the soft-soft complexation formed by Hg^{2+} ion with **7**. The stability and sensitivity of **5** and **7** towards Cu^{2+} ion are almost similar or comparable as per their stability constants and LOD values. For the sake of legibility, a comparison with other literature-reported probes is incorporated in a tabular form (Table 5.1).

Table 5.1 Comparison table for LOD and association constant

Entry	Molecular formula	LOD	Association constant	Ref
1	$C_{31}H_{37}N_5O_3$	(a) 3.5×10^{-6} M for Cu^{2+} (b) 6.11×10^{-8} M for Hg^{2+}	(a) 3.51×10^6 M^{-1} for Cu^{2+} (b) 6.06×10^6 M^{-1} for Hg^{2+}	42
2	$C_{15}H_{12}N_6O$	(a) 50×10^{-9} M for Cu^{2+} (b) 0.8×10^{-8} M for Hg^{2+}	(a) 1.3×10^5 M^{-1} for Cu^{2+} (b) 0.05×10^5 M^{-1} for Hg^{2+}	43
3	$C_{47}H_{48}N_4OS_2$	(a) 97×10^{-9} M for Cu^{2+} (b) 80×10^{-8} M for Hg^{2+}	3.5×10^6 M^{-1} for Cu^{2+}	44
4	$C_{47}H_{48}N_4O$	(a) 2.1×10^{-8} M for Cu^{2+} (b) 1.8×10^{-8} M for Hg^{2+}	1.6×10^7 M^{-1} for Cu^{2+}	45
5	$C_{260}H_{491}N_5O_{117}S$	(a) 5.92×10^{-7} M for Cu^{2+} (b) 2.85×10^{-6} M for Hg^{2+}	(a) 5.38×10^4 M^{-1} for Cu^{2+} (b) 1.63×10^5 M^{-1} for Hg^{2+}	46
6	$C_{32}H_{33}FeN_3O_2S_2$	(a) 6.17×10^{-7} M for Cu^{2+} (b) 7.94×10^{-7} M for Hg^{2+}	(a) 9.06×10^4 M^{-1} for Cu^{2+} (b) 3.01×10^4 M^{-1} for Hg^{2+}	47
7	$C_{24}H_{22}N_2O_5S$	(a) 2.02×10^{-6} M for Cu^{2+} (b) 1.24×10^{-6} M for Hg^{2+}	(a) 2.4×10^5 M^{-1} for Cu^{2+} (b) 7.46×10^5 M^{-1} for Hg^{2+}	48
8	$C_{23}H_{20}N_2O$	(a) 7.74×10^{-6} M for Cu^{2+} (b) 7.67×10^{-6} M for Hg^{2+}	(a) log β=5.23 M^{-1} for Cu^{2+} (b) logβ=5.49 M^{-1} for Hg^{2+}	49
9	$C_{22}H_{20}FeS$ and $C_{22}H_{20}FeO_2S$	(a) 5.22×10^{-7} M for Cu^{2+} (b) 6.93×10^{-7} M for Hg^{2+}	(a) 5.74×10^4 M^{-1} for Cu^{2+} (b) 5×10^4 M^{-1} for Hg^{2+}	50
10	$C_{20}H_{13}NS_3$	(a) 7.06×10^{-8} M for Cu^{2+} (b) 1.16×10^{-7} M for Hg^{2+}	(a) 9.4×10^4 M^{-1} for Cu^{2+} (b) 8.69×10^4 M^{-1} for Hg^{2+}	51
11	$C_{56}H_{67}N_6O_2$	(a) 1.3×10^{-6} M for Cu^{2+} (b) 1.45×10^{-6} M for Hg^{2+}	(a) 3.25×10^7 M^{-1} for Cu^{2+} (b) 6.88×10^6 M^{-2} for Hg^{2+}	52
12	$C_{21}H_{22}N_3O_2S$	(a) 2.9×10^{-6} M for Cu^{2+} (b) 2×10^{-9} M for Hg^{2+}	(a) 5.69×10^5 M^{-1} for Cu^{2+} (b) 1.85×10^4 M^{-2} for Hg^{2+}	53
13	$C_{27}H_{21}N_5O_4$ (**5**) and $C_{27}H_{19}N_5O_4$ (**7**)	(a) 5.5×10^{-7} M (**5**-$Cu^{2+)}$ and 5.2×10^{-7} M (**7**-Cu^{2+}) (b) 4.4×10^{-7} M (**7**-Hg^{2+})	(a) 1.02×10^5 M^{-1} (**5**-Cu^{2+}) and 3.9×10^5 M^{-1} (**7**-Cu^{2+}) (b) 7.4×10^4 M^{-1} (**7**-Hg^{2+})	This work

To determine the reversibility of the binding phenomenon by the probes **5** and **7**, test with Cu^{2+} and Hg^{2+} ions were conducted in DMSO-H_2O (7:3, *v/v*) (7.8×10^{-6} M) using aqueous solution of Na_2EDTA (7.8×10^{-6} M). Probe **5** was found to be reversible towards Cu^{2+} ion effectively for 2 cycles of alternate additions of analyte and Na_2EDTA, whereas, towards Hg^{2+} ion, the interaction is completely irreversible. This may signify a permanent transformation in the structure of probe **5** upon Hg^{2+} addition, which cannot be reversed back. Probe **5** therefore, is not a sensor, although

it has a specific response for Hg^{2+} ion and hence can be considered as chemodosimeter. Probe **7**, on the other hand, was found to have reversible interaction with both the metal ions (Figure 5.7).
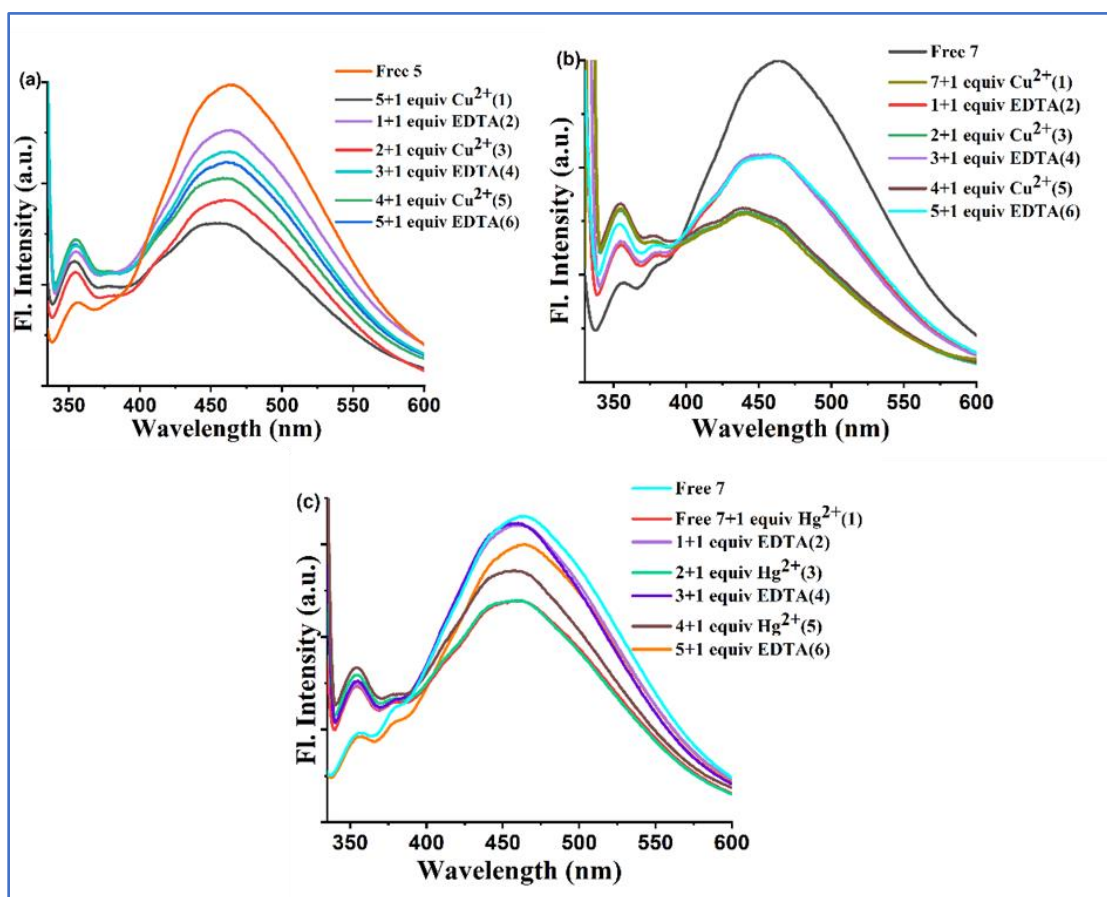
Figure 5.7 Reversibility test of compound (a) **5**+ Cu^{2+}, (b) **7**+ Cu^{2+} and (c) **7**+ Hg^{2+} (7.8×10^{-6} M) in presence of EDTA in DMSO:H_2O (7:3, v/v) solvent at 22 ˚C.

5.2.4 Construction of Molecular Logic Gate

The fluorescence responses of probes **5** and **7** towards Cu^{2+} and Hg^{2+} ions can be converged together to form a molecular logic operation, wherefrom, the OR logic gate can be constructed for each ligand system. Each of the two metal ions is taken as an input and the respective relative fluorescence response is taken as the output. For input, the binary numbers 1 and 0 represent the respective presence and absence of the metal ion and for output, they represent the relative fluorescence intensity ($1-I/I_0$) above and below the threshold value 0.18 (for **5**) and 0.25 (for **7**), respectively. The threshold values have been selected by considering the responding fluorescent intensity after analyte addition, which is vividly different from that of the free ligand. For example,

the I_0 for **5** is 2.5×10^5, whereas I is taken as 2.05×10^5, giving the value of $1-I/I_0$ as 0.18.[54] The bar diagrams depicted in Figure 5.8a and d show the output signals for each of the inputs. From these input and output, OR logic operation (Figure 5.8c) can be constructed according to the truth tables described in Figure 5.8b and e. When both the inputs are absent, the $1-I/I_0$ becomes nearly zero, which is less than the threshold values 0.18 or 0.25, hence the output is 0, whereas when either or both of Cu^{2+}/Hg^{2+} ion is present $1-I/I_0$ becomes greater than the respective threshold value, hence the response is 1.

Figure 5.8 (a) Bar diagram, (b) truth table for probe **5**, (c) circuit of the OR logic gate, (d) bar diagram, (e) truth table for probe **7**, taking the fluorescence response for Cu^{2+} and Hg^{2+} at 464 nm as the two inputs.

5.2.5 ^{1}H and ^{13}C NMR studies

^{1}H and ^{13}C NMR titration studies are powerful methods towards unambiguous assignment of binding site, as speculated previously by absorption and emission spectral studies. As shown in Figure 5.9a, the ^{1}H NMR spectral pattern of free ligand **5** does not suffer any shift of the existing peaks upon treatment with 2 equiv of Hg^{2+} ion except the peak for alkyne H at $\delta = 3.64$ ppm, which disappears with the generation of a new peak at $\delta = 2.19$ ppm. This new peak can only arise if the

terminal alkynes undergo chemical reaction with H_2O in presence of Hg^{2+}, giving ketomethyl functional group. This chemical transformation can also be evidenced from ^{13}C titration, where two new peaks at 26.6 ppm (CH_3) and 204.2 ppm (C=O) appears and the alkyne peaks at 79.4 and 79.0 ppm disappear after treatment with DMSO solution of Hg^{2+} salt (Figure 5.9b).

On the other hand, the ^1H NMR titration of probe **5** with Cu^{2+} gave absolutely contrasting results from that with Hg^{2+} ion. Here, only binding of the analyte took place, which is evident from the upfield shifts of the amide hydrogen, imine hydrogen and OCH_2 by about 0.03 ppm (Figure 5.41). This indicates the symmetrical binding of Cu^{2+} by the tripodal pyridine core.
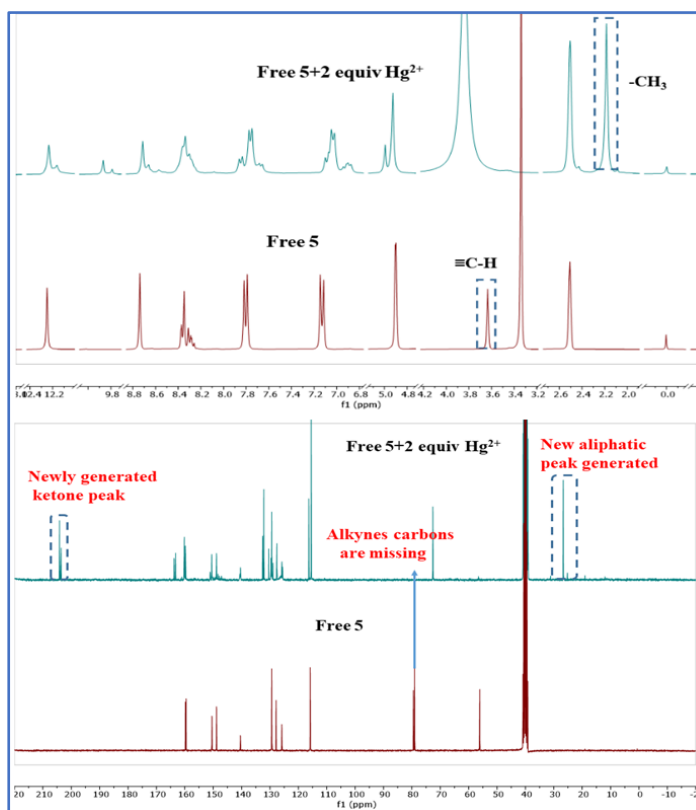
Figure 5.9 (a) ^1H NMR and (b) ^{13}C NMR of ligand **5** before and after addition of 2 equiv of Hg^{2+} ion in DMSO-d_6 medium.

The ^1H NMR titration of compound **7** with Cu^{2+} ion displayed more visible results as the upfield shift gradually decreased from the amide H ($\Delta\delta = 0.04$ ppm) through the adjacent imine H ($\Delta\delta = 0.03$ ppm) to the OCH_2 ($\Delta\delta = 0.025$ ppm) (Figure 5.10), as should be realized if the Cu^{2+} binds to the tridentate cage consisting of the amide N's and the pyridine N. On the other hand, for Hg^{2+} ion complexation with **7**, the only visible chemical shifts in the peaks are for the OCH_2 peaks by 0.05 ppm (Figure 5.42), so as to conclude no binding with the heteroatoms. This only leaves

the possibility of interaction of the Hg^{2+} ion with the soft internally conjugated alkyne centres, which is in concurrence with our theoretically optimized geometry (*vide infra*).
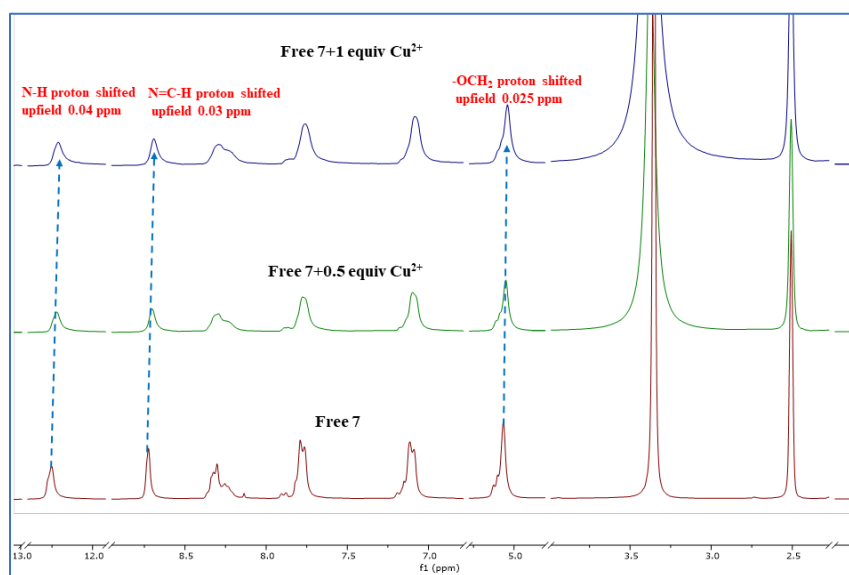
Figure 5.10 ^{1}H NMR titration of ligand **7** with addition of up to 1 equiv of Cu^{2+} ion in DMSO-d_6 medium.

5.2.6 IR titration

To further verify the binding modes of probes **5** and **7**, the IR titration was performed, taking all the samples in solid form. As shown in Figure 5.11, the free probe **5** displayed the characteristic peaks of amide N-H stretching at 3291 cm^{-1}, $\equiv$C-H at 3244 cm^{-1}, C$\equiv$C at 2126 cm^{-1}, C=O at 1687 cm^{-1} and C=N stretching at 1606 cm^{-1}. Upon addition of 1 equiv of Cu^{2+} ion in probe **5**, significant changes in the amide N–H and C=O stretching could be found (Figure 5.11a), whereas the C$\equiv$C stretching stays intact. This supports the fact that the amide functionalities are involved actively in the Cu^{2+}-binding phenomenon. However, with Hg^{2+} ion, the scenario is different such that the N-H bond, amide bond and C=N remains unperturbed, whereas the $\equiv$C–H stretching at 3244 cm^{-1} and C$\equiv$C stretching at 2126 cm^{-1} got disappeared (Figure 5.11b). This validates the participation of the terminal alkyne units of **5** in interaction with Hg^{2+} and H_2O. Carrying out similar experiments with Cu^{2+} for compound **7**, the amide C=O stretching of the free probe at 1608 cm^{-1} was found to get shifted to 1659 cm^{-1} and the C=N stretching frequency shifted slightly from 1597 to 1606 cm^{-1} (Figure 5.11c). Furthermore, the peak at 3273 cm^{-1} corresponding to the N-H stretching shifted to 3255 cm^{-1} after treatment with Cu^{2+}. This clearly indicates the involvement of

the amide N atoms in Cu^{2+} binding, similar to that in **5**. But for Hg^{2+} ion, the amide and rest of the peaks corresponding to the C=N and N-H stretching frequencies, were unperturbed (Figure 5.11d). This indicates that the heteroatoms do not participate in Hg^{2+} binding, rather, it can be bound by the soft internally conjugated alkynes. Moreover, in all the spectra, the Cl-O stretching frequency can be prominently observed at around 1079 cm^{-1},[55,56] demonstrating the incorporation of the perchlorate anion into the metal-complexed system.
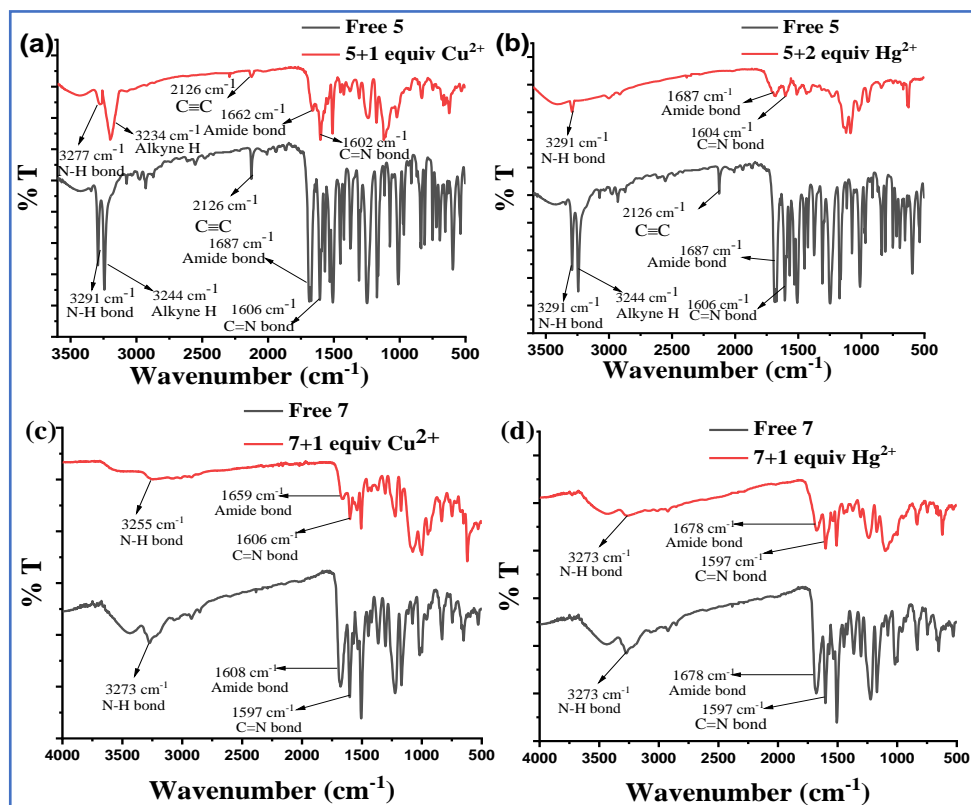
Figure 5.11 IR titration spectra of compound **5** with (a) 1 equiv of Cu^{2+} ion and (b) 2 equiv of Hg^{2+} ion and **7** upon addition of up to (c) 1 equiv of Cu^{2+} and (d) 1 equiv of Hg^{2+} ion in solid state at 22 ˚C.

5.2.7 Electron Paramagnetic Resonance (EPR) studies

To investigate about the binding centre of Cu and its oxidation state, EPR spectra have been recorded for both the copper complexes with **5** and **7**. It is well-established that different coordination modes can give rise to different EPR patterns like normal, inverse or intermediate spectra.[57] EPR spectra have been taken for both **5** and **7** in presence of Cu^{2+} ion in DMF solution at low temperature (100K) to investigate more into the binding pattern of both the ligands. The

EPR spectra for both the host-guest complexes have shown similar hyperfine splitting pattern with $g\perp = 2.08$, which gives evidence for the presence of Cu-N bond.[58] The spectrum is significantly broadened owing to the underlying ^{14}N superhyperfine couplings from the pyridine ligand, Also, here, the $g\parallel > g\perp$, as can be seen from the spectral pattern, which indicates the presence of Cu(II) in the system (Figure 5.12).
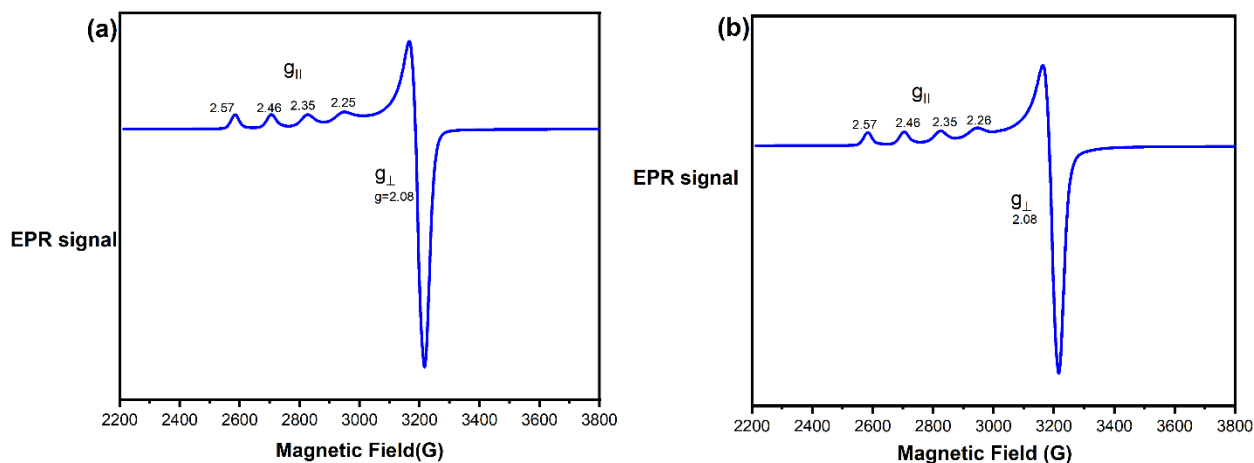
Figure 5.12 EPR spectra of (a) **5** and (b) **7** in upon interaction with Cu^{2+} ion in DMF at 100 K.

The overall interaction patterns, as evidenced from all the above studies with the two probes can be schematically represented as indicated in Scheme 5.4
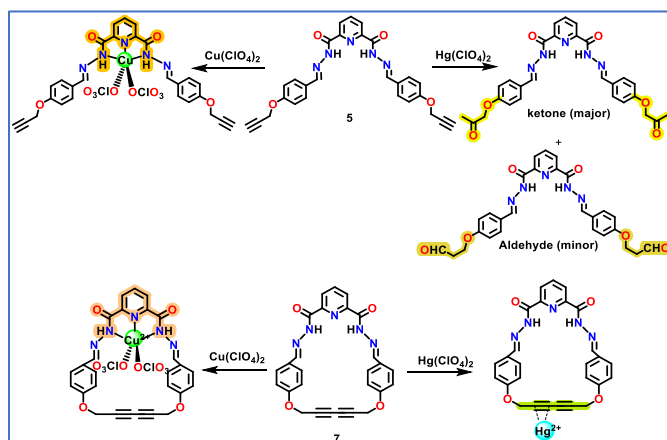
Scheme 5.4 Schematic representation of the binding and reaction phenomenon of probes **5** and **7** with Cu^{2+} and Hg^{2+} ions.

5.2.8 Naked eye detection

A sensor having the visual color changing property upon interaction with analytes makes its practical application easier. Upon addition of DMSO solutions (1×10^{-5} M) of different metal ions in their perchlorate salts, significant color changes from colorless to yellow of the DMSO solutions (1×10^{-3} M) of compounds **5** and **7** were observed for Cu^{2+} and Hg^{2+} ions only. For rest
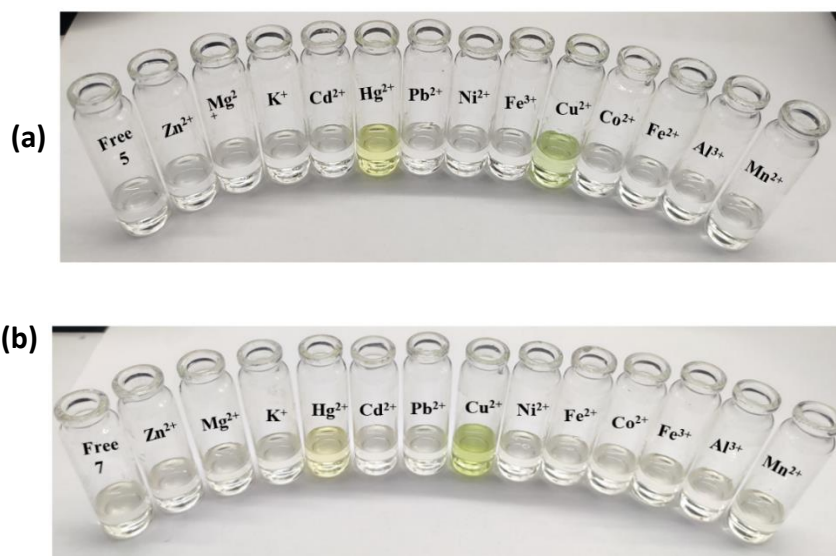
Figure 5.13 Naked eye detection of Hg^{2+} and Cu^{2+} among all other metal ions (1×10^{-5} M) by compounds (a) **5** and (b) **7** (1×10^{-3} M) in DMSO solvent.

of the metal ions, as shown in Figure 5.13, no-change in color of the DMSO solutions was observed.

5.2.9 pH, Temperature and Response Time studies

Environmental factors like pH, temperature play significant roles in the binding process and stability of a probe, hence their influence needs to be assessed properly to determine the optimum working conditions. To evaluate such factors, fluorescence intensity with varying pH of the medium, temperature and response time of the probes as well as the complexes have been examined for each set of analyte and probe in DMSO at 22 °C. From the complete set of pH study of the free ligand along with its corresponding metal-complex (Figure 5.14a and b), the pH range

of 5-7 was found to be optimum for the free probes. On the other hand, the metal complexes were found to be stable only around the physiological range (~pH 7).
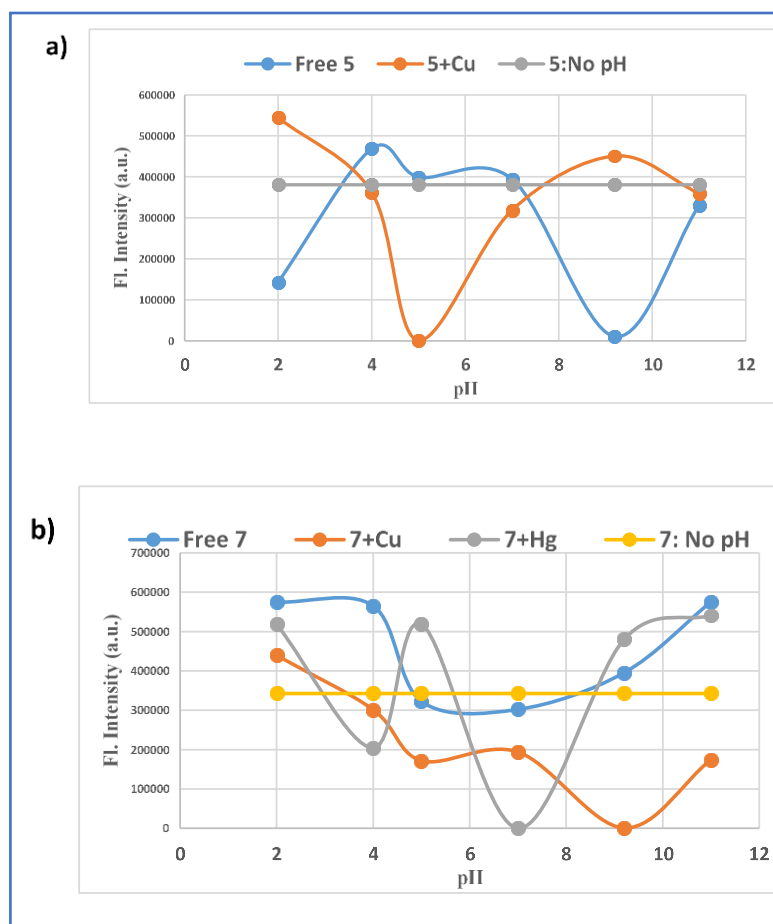
Figure 5.14 Variation of fluorescence intensity with pH in (a) Free **5** and **5**+Cu^{2+}, (b) Free **7**, **7**+Cu^{2+} and **7**+Hg^{2+} in DMSO solvent at 22 ˚C.

Thermal stability of any probe is a necessary and essential feature to be examined carefully before subjecting the probe into any practical use. This is because if the probe itself gets damaged during the course of experimentation, the results obtained in the laboratory cannot be reproduced in the practical field. Both the free probes and their complexes are found to be stable up to a temperature of 80 ˚C (Figure 5.15a-c) in DMSO. Apart from these environmental factors, the response time of a probe plays a significant role in its real time sensing. Lower the response time better is the sensor. Here in both the probes, the time taken by them to give a substantial response in presence of analytes is rather low (30 s), which is an advantage in the course of practical on-field usability of the probes (Figure 5.15d-f). Both the cyclic and acyclic probes responded within

the first minute of the analyte addition by the change of the fluorescence intensity, which stayed almost constant with passage of time up to 8 minutes.
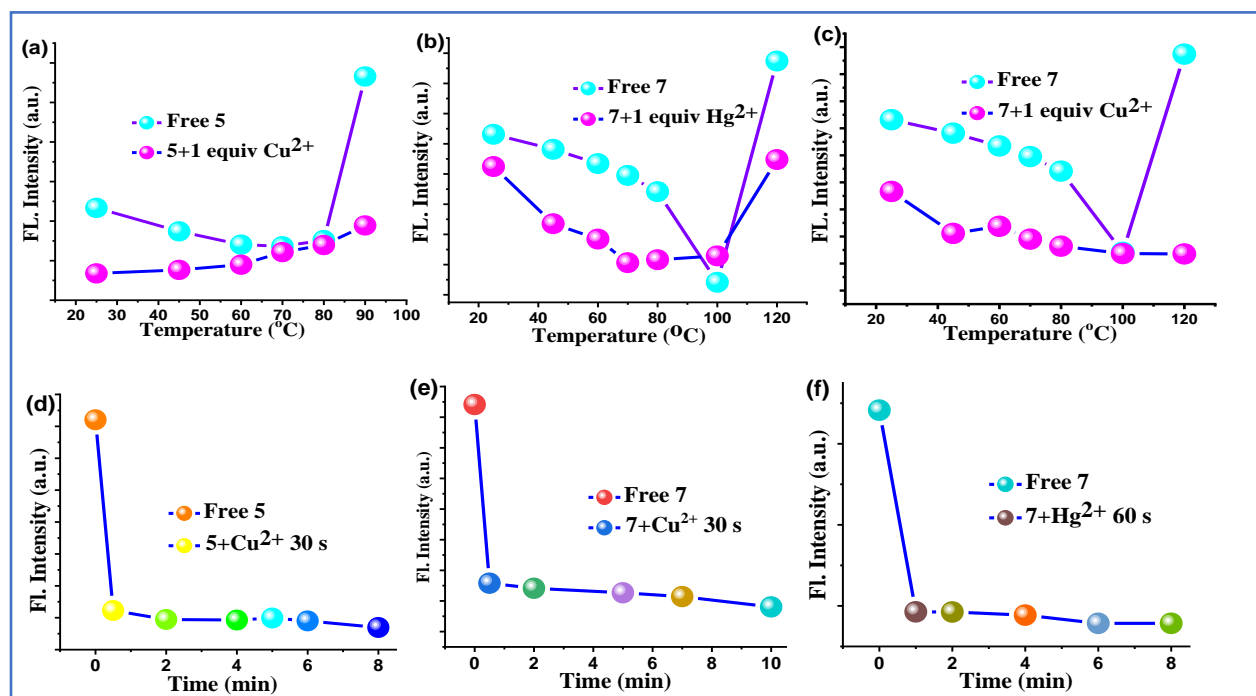
Figure 5.15 Variation of fluorescence intensity with temperature in (a) Free **5** and **5**+Cu^{2+}, (b) Free **7** and **7**+Hg^{2+} in DMSO solvent at 22 ˚C and (c) Free **7** and **7**+Cu^{2+} and variation of fluorescence intensity with response time of (d) **5** for Cu^{2+}, (e) **7** for Cu^{2+} and (f) **7** for Hg^{2+} in DMSO solvent at 22 ˚C.

5.2.10 Real Sample Analysis

Real sample analysis deals with analysing real water samples for the detection of specific analyte in it by the respective probe. These studies are important basically for the immensely hazardous substances like Hg^{2+} ion in water, however, among the two probes developed by us, the acyclic one undergoes chemical reaction in presence of Hg^{2+} ion. This leaves only the cyclic probe, **7** to be used for real sample analysis. Tap water from Jadavpur University campus were collected and filtered. The pH of the tap water was maintained around 7. The variation in fluorescence intensity with different concentrations of Hg^{2+} ion was found to be linear, with the equation y = 6E+10x + 516350. Using this equation as standard for this particular probe for detection of Hg^{2+},

the recovered analyte concentrations were calculated, the average of which is provided in Table 5.2 as below:

Table 5.2: Real sample analysis for Hg^{2+} ion by probe **7**.

Sample	Added conc of analyte (M)	Recovered conc of analyte (M)	% Recovery
Tap water sample-I	0.394×10^{-6}	0.550×10^{-6}	106
Tap water sample-II	0.4102×10^{-6}	0.438×10^{-6}	107

5.3 Theoretical Calculations

To explore the electronic structure and bonding scenario of the receptors **5** and **7** and their binding affinity to Cu^{2+} and Hg^{2+}, quantum chemical calculations were performed using density functional theory (DFT) methodology (*cf. below*, Experimental Section). First, receptor **5** has been optimized, taking coordinates from the crystal data. The acyclic receptor adopted a geometry where both the arms around the pyridine show an eclipsed conformation, creating a vacant site for metal atoms through three planar nitrogen atoms. The calculated structural parameter is well corroborated with the crystal structure data, which can be visualized in the overlay of X-ray structure and DFT optimized structure of receptor **5** (Figure 5.46). For receptor **7**, geometry optimization was performed on several starting geometries to confirm that optimized structures correspond to global minima. The cyclic receptor resulted in a slightly distorted structure, keeping the three-nitrogen center almost planar to bind various metal atoms. The optimized geometries of the receptors at singlet ground electronic states are shown in Figure 5.16. Selected bond distances and their corresponding FMO's are shown in Table 5.3 and Figures 5.17 and 5.18, respectively.
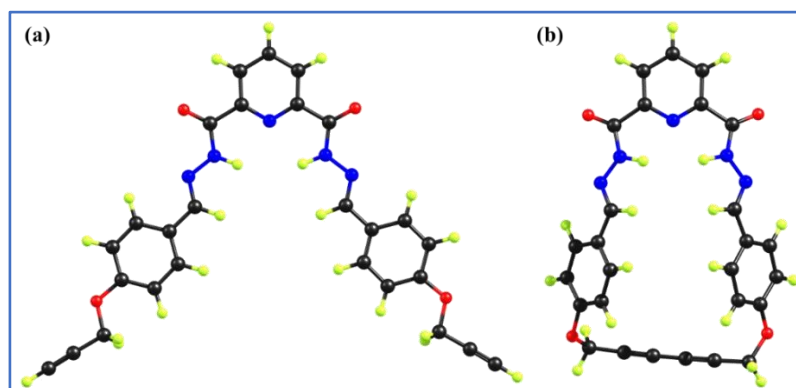
Figure 5.16 Optimized structures of the (a) receptor **5** and (b) receptor **7**

Table 5.3. The selected distances (Å) of receptors **5** and **7** calculated at B3LYP/6 311g(d)/cpcm (acetonitrile) level (The labeled primary binding core of both receptors **5** (left) and **7** (right) are shown above the table).
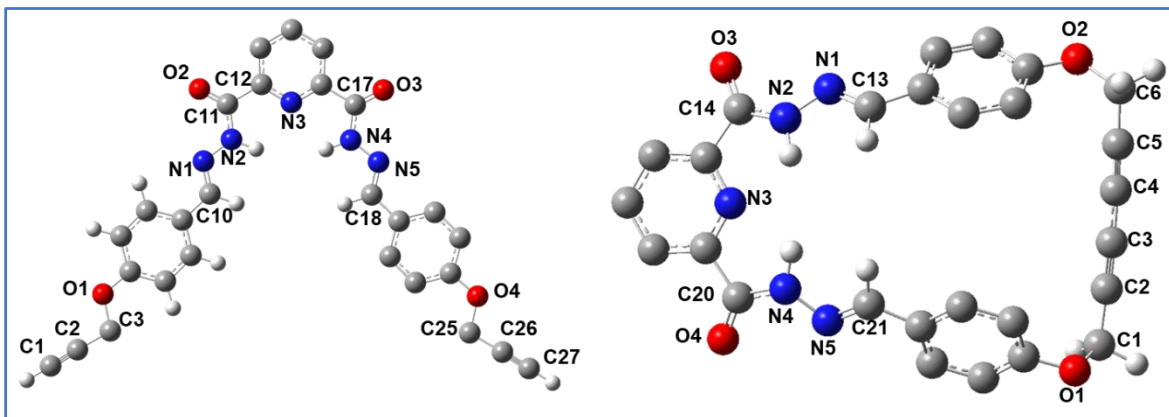
	contact	Distance (Å)			contact	Distance (Å)
	C1-C2	1.20120			O1-C1	1.44165
	C2-C3	1.45721			C1-C2	1.46116
	C3-O1	1.43501			C2-C3	1.21151
	C10-N1	1.28331			C3-C4	1.36336
Receptor [5]	N1-N2	1.36129		Receptor [7]	C4-C5	1.21123
	N2-C11	1.36383			C5-C6	1.46086
	C12-N3	1.33802			C6-O2	1.43574
	C11-O2	1.22191			C13-N1	1.28535
	C17-N4	1.36383			N1-N2	1.37255
	C17-O3	1.22191			N2-C14	1.36563

N4-N5	1.36129		C14-O3	1.22013
N5-C18	1.28331		C20-N4	1.36600
O4-C25	1.43501		C20-O4	1.21987
C25-C26	1.45721		N4-N5	1.36923
C26-C27	1.20120		N5-C21	1.28452
N2-N4	**4.58178**		**N2-N4**	**4.36916**
N2H-N4H	**2.68537**		**N2H-N4H**	**2.47027**
N2-N3	**2.70241**		**N2-N3**	**2.64242**
N3-N4	**2.70241**		**N3-N4**	**2.63921**
N1-N5	**6.72499**		**N1-N5**	**5.93003**
C10-C18	**6.21463**		**C21-C13**	**5.05133**
C10H-C18H	**4.15275**		**C10H-C18H**	**3.31883**

HOMO (**- 6.07 eV**)	HOMO-1 (**-6.08 eV**)

HOMO-2 (**-7.39** eV)	LUMO (**-2.16** eV)
LUMO+1 (**-2.12** eV)	LUMO+2 (**-1.39** eV)
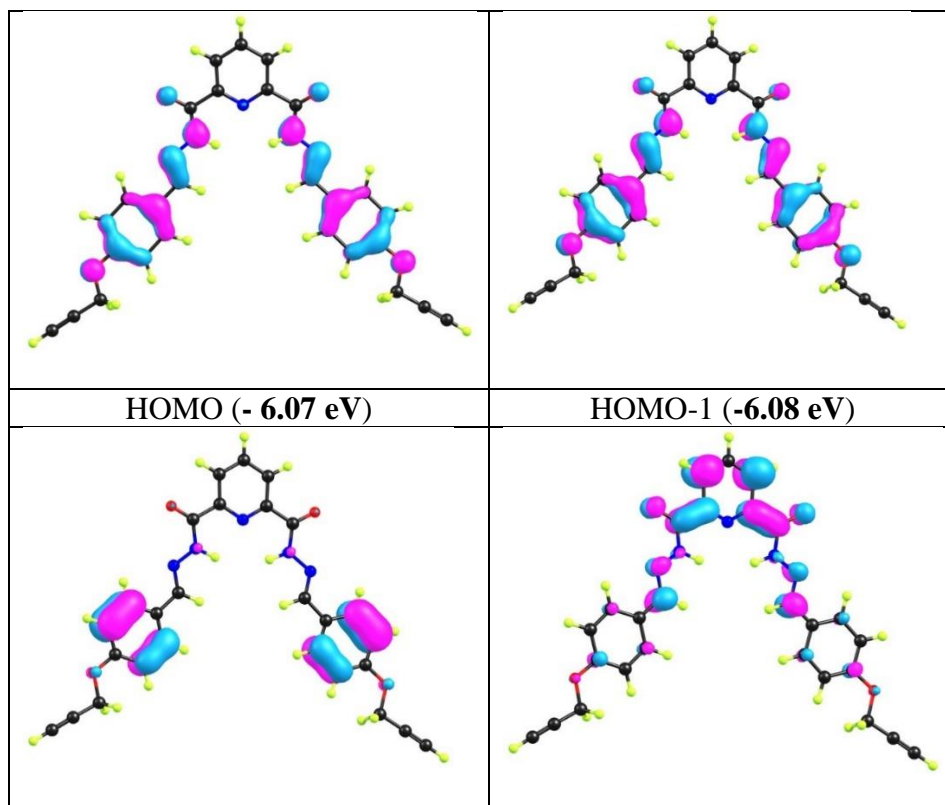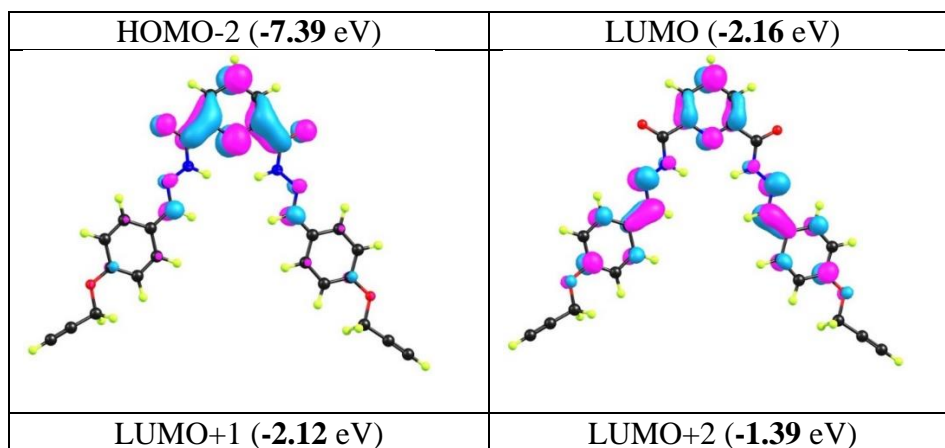
Figure 5.17 Frontiers MOs of the acyclic receptor **5** with corresponding energy values in parenthesis. (iso surface value= 0.04)

HOMO (**-6.12 eV**)	HOMO-1 (**-6.37 eV**)
HOMO-2 (**-7.21** eV)	LUMO (**-2.22 eV**)

| LUMO+1 (**-2.13 eV**) | LUMO+2 (**-1.56** eV) |
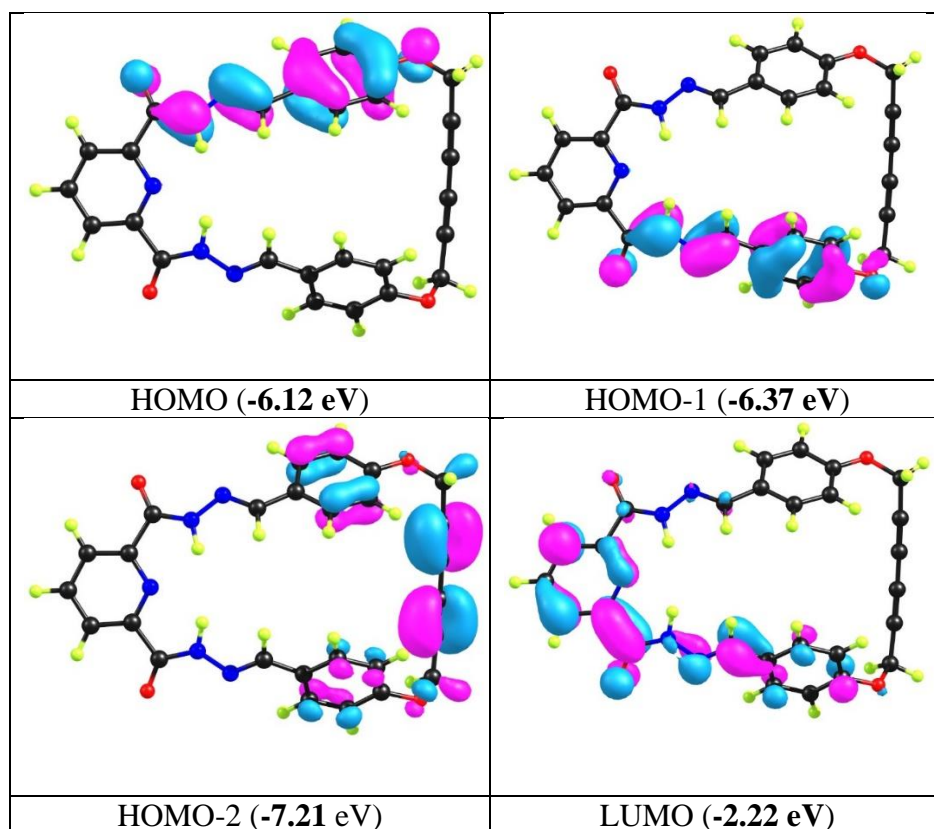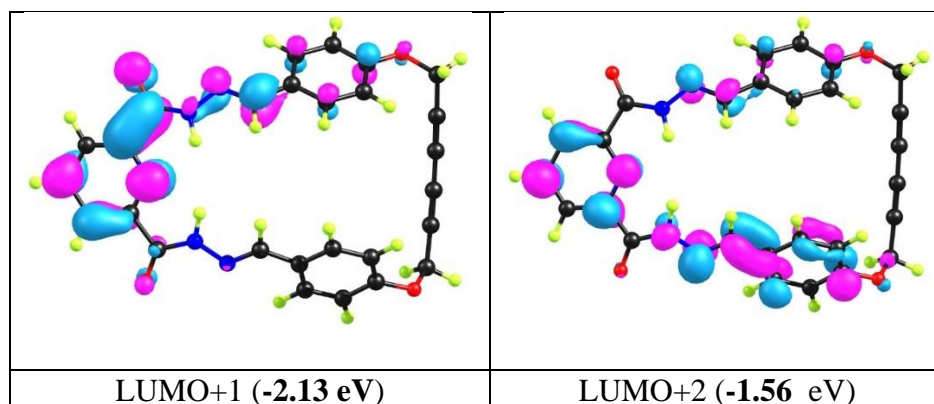
Figure 5.18 Frontiers MOs of the cyclic receptor **7** with corresponding energy values in parenthesis. (iso surface value = 0.04).

Based on the experimental observations from absorption and emission spectra, we have found that the ligand: metal (Cu) binding ratio for both the receptor **5** and **7** is 1:1. Thus, first, both [**5**·Cu(ClO$_4$)$_2$] and [**7**·Cu(ClO$_4$)$_2$] were modeled using DFT calculations at the B3LYP level (*cf. below*, Experimental Section) (Figure 5.19a). After complete geometry optimization, we have found that in the case of acyclic receptor **5**, it gives a distorted trigonal bipyramidal geometry. The free ligand, **5** binds the Cu^{2+} ion through three nitrogen centers and other coordination sites are occupied by two perchlorate ions. Surprisingly, even after several trials, the optimized geometry for [**7**·Cu(ClO$_4$)$_2$] could not be obtained may be due to higher strain in the ligand structure. From the interatomic distances of the two molecules [N2-N4: 4.58 Å (5), 4.36 Å (7); N2-N3: 2.70 Å (5), 2.64 Å (7); N1-N5: 6.72 Å (5), 5.93 Å (7)] (Table 5.3), it can be perceived that the cyclic molecule **7** exists in a more compact form, as compared to **5**. However, there is enough experimental evidence to prove the binding of Cu^{2+} by the N-containing tridentate core of the cyclic probe **7**. For the binding of Hg^{2+} ion with the cyclic receptor **7**, optimization from several starting geometries concluded that Hg^{2+} preferred to bind either one of the alkyne units of the 1,3-dialkyne system of **7** (Figure 5.19b,c). However, when we tried to model the endocyclic binding mode of Hg^{2+} ion with receptor **7**, it finally converged to an optimized geometry where Hg^{2+} cation did not bind any alkyne unit specifically rather, it preferred to stay in between two alkyne units (Figure 5.50). However, when the same binding model was conducted with exocyclic binding of Hg^{2+} ion, the energy minimized structures could be obtained, as shown in Figure 5.19b and c. Both binding modes are almost equal in energy, such that Hg^{2+} ion exhibits a sweeping motion between the two

alkyne units by dynamic binding to each alkyne at an instant. Hence, the most plausible binding mode of Hg^{2+} cation can be *via* the exocyclic linkage with compound **7**.
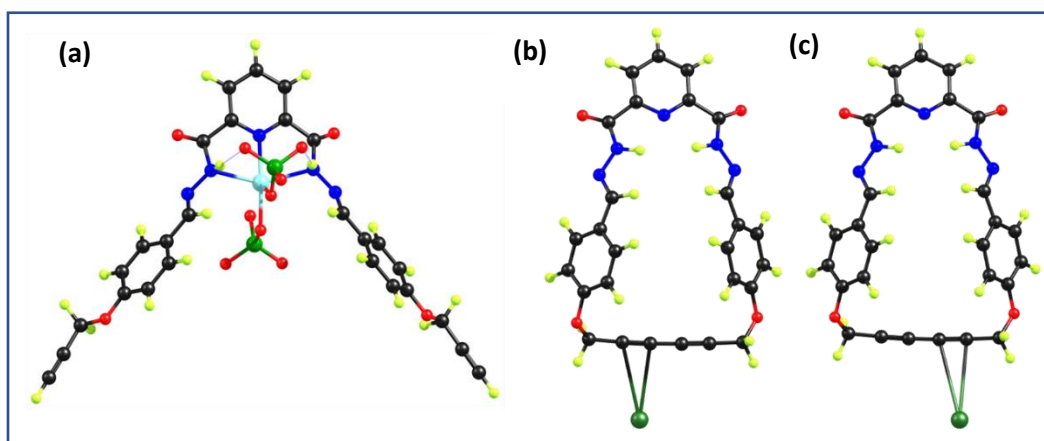
Figure 5.19 Optimized structure of the complexes (a) [**5**·Cu(ClO$_4$)$_2$], (b) [**7**·Hg^{2+}] (left sided alkyne unit), and (c) [**7**·Hg^{2+}] (right sided alkyne unit).

Additionally, the space-filling model (Figure 5.20) of the optimized geometries of compound **7**, suggested that the two aromatic rings attached to the –O–CH$_2$–alkyne units are in close proximity, with distance between their centroids being 6.750 Å. The C-C distances of two close carbon atoms of the aromatic rings from the front face are 4.958 Å and 5.597 Å respectively. This can point to the steric crowding as the most probable reason of Hg^{2+} not getting attached to any particular alkyne unit endocyclically.
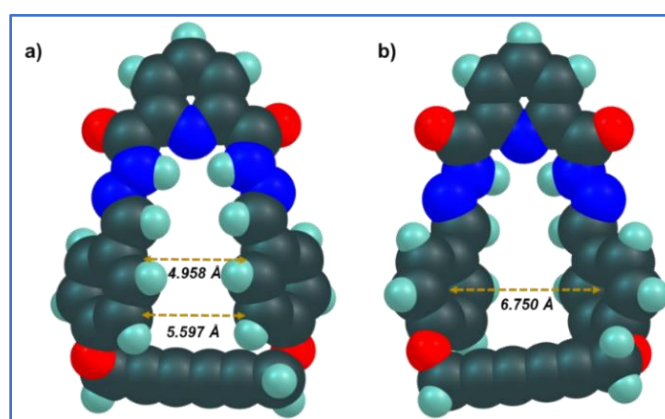
Figure 5.20 Space filling model of the compound/host **7**: a) from the front side, b) from the backside.

Furthermore, time-dependent DFT (TDDFT) calculations were performed to understand the detailed information on electron transition associated with the receptors. TD-DFT calculation on receptor **5** resulted in a strong transition at 293.7 nm (Oscillator strength=1.7195) and a weak transition at 235.6 nm (Oscillator strength=0.1162), which nicely matches with the experimental values (320 and 262 nm) (Figure 5.21a and Table 5.4). Strong electronic transition results from HOMO (benzene π-orbitals) to LUMO (localized on pyridine moiety with a slight delocalization from amide nitrogen atom) transition. Similarly, TD-DFT calculation on receptor **7** resulted in a strong transition at 289.4 nm (Oscillator strength=1.769), for which the experimental value is 320 nm (Figure 5.21b and Table 5.5). This electronic transition mainly corresponds to HOMO-1 (localized on benzene π-orbitals with a small contribution from nearby imine nitrogen atom) to LUMO (localized on pyridine moiety with a slight delocalization toward amide nitrogen atom) transition.
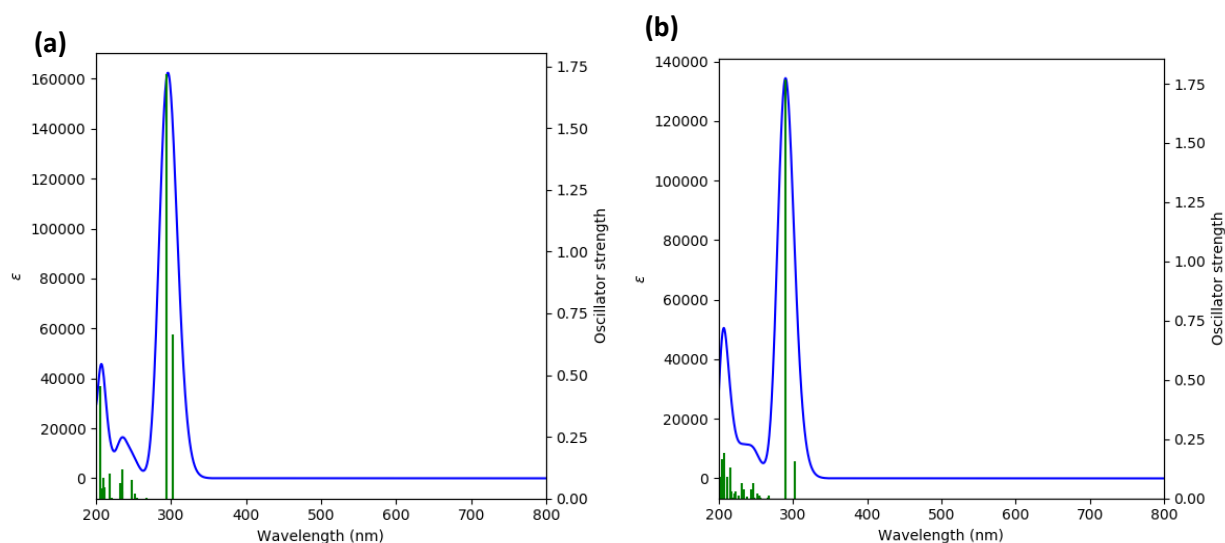
Figure 5.21 (a) Calculated absorption spectrum of the acyclic receptor **5** and (b) cyclic receptor **7**.

Table 5.4 Major excited state transitions of the acyclic receptor **5** with Osc. Strength and λ_{ex}.

λ_{ex} (nm) (Exp.)[a]	λ_{ex} (nm) (Calc.)[b]	Oscillator Strength (f)	Major Transitions[c]
321	293.7	1.7195	H-1 → L+1 (35%), H → L (45%)

| 263 | 235.6 | 0.1162 | H-1→ L (12%), H-1 → L+3 (31%), H → L+2 (36%) |

Table 5.5 Major excited state transitions of the cyclic receptor **7** with Osc. Strength and λ_{ex}.

λ_{ex} (nm) (Exp.)[a]	λ_{ex} (nm) (Calc.)[b]	Oscillator Strength (f)	Major Transitions[c]
321	289.4	1.769	H-1 → L (53%), H-1 → L+1 (9%), H → L+1 (17%)

[a]Experimental wavelength in DMSO. [b]TD-DFT calculated wavelength of acyclic receptor **5** in DMSO. [c]Transitions with greater than 10% contribution are represented.

Notably, TD-DFT calculations on [**5**·Cu(ClO₄)₂] predict a strong HOMO (benzene π-orbitals) to LUMO+2 (localized on pyridine) transition at 305.9 nm (oscillator strength f = 0.3656), with validating the experimental UV−vis results (Figure 5.22 and Table 5.6). Similarly, TD-DFT calculations on [**7**·Hg²⁺] showed a strong HOMO−1 (localized on benzene with a delocalization to imine center) to LUMO+1 (localized on pyridine with a delocalization to imine center) transition at 289.1 nm (oscillator strength f = 1.7992) (Figure 5.23 and Table 5.7 and 5.8).
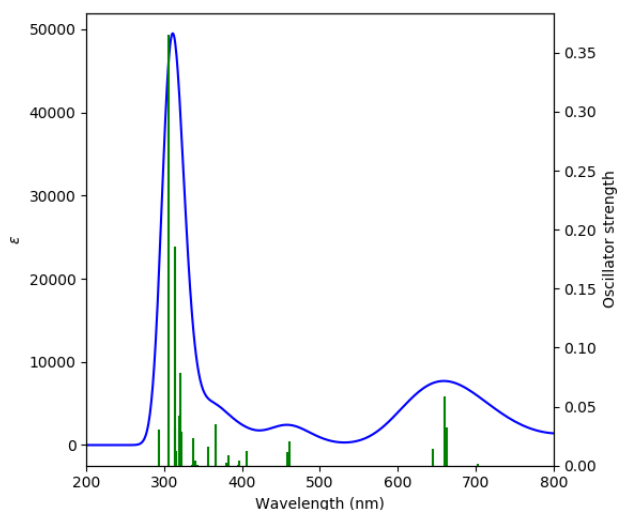
Figure 5.22 Calculated absorption spectrum of the complex [**5**·Cu(ClO₄)₂].

Table 5.6 Major excited state transitions of the complex [**5**·Cu(ClO₄)₂] with Osc. Strength and λ_{ex}.

λex (nm) (Exp.)[a]	λex (nm) (Calc.)[b]	Oscillator Strength (f)	Major Transitions[c]
321	305.9	0.3656	H-1(B)->L+1(B) (23%), HOMO(B)->L+2(B) (42%)

[a]Experimental wavelength in DMSO. [b]TD-DFT calculated wavelength of complex [**5**·Cu(ClO$_4$)$_2$] in DMSO. [c]Transitions with greater than 10% contribution are represented.
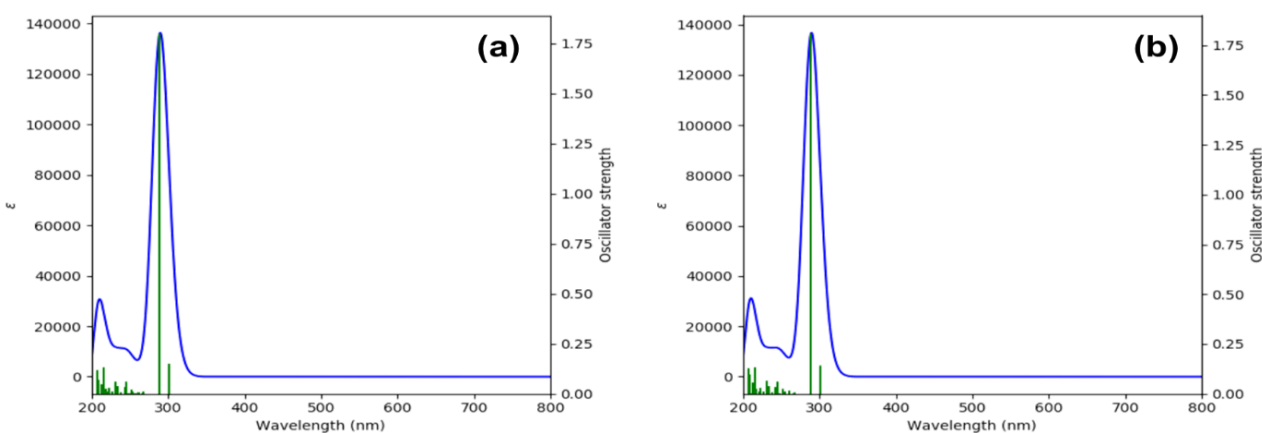
Figure 5.23 Calculated absorption spectrum of the complex (a): [**7**·Hg^{2+}] (left side); (b): [**7**·Hg^{2+}] (right side).

Table 5.7 Major excited state transitions of the complex [**7**·Hg^{2+}] (involving left-sided alkyne as a binding unit) with Osc. Strength and λex.

λex (nm) (Exp.)[a]	λex (nm) (Calc.)[b]	Oscillator Strength (f)	Major Transitions[c]
321	289.1	1.7992	H-1->L+1 (53%), HOMO->L+2 (18%)

Table 5.8 Major excited state transitions of the complex [**7**·Hg^{2+}] (involving right-sided alkyne as a binding unit) with Osc. Strength and λex.

λ_{ex} (nm) (Exp.)[a]	λ_{ex} (nm) (Calc.)[b]	Oscillator Strength (f)	Major Transitions[c]
321	289.08	1.8078	H-1->L+1 (51%), HOMO->L+2 (19%)

[a]Experimental wavelength in DMSO. [b]TD-DFT calculated wavelength of complex **7**·Hg^{2+} in DMSO. [c]Transitions with greater than 10% contribution are represented.

To understand the fluorescence quenching mechanism upon Cu^{2+} binding with receptor **5**, TDDFT calculations were performed at same level of theory. For [**5**·Cu(ClO$_4$)$_2$], the LUMO of the copper centre with energy −5.20 eV lies between the benzene fluorophore orbitals, HOMO (−6.34 eV) and pyridine orbitals, LUMO+2 (−2.090 eV), as shown in Figure 5.24a. Thus, this type of arrangements in [**5**·Cu(ClO$_4$)$_2$] favours the electron transfer from the pyridine centred orbitals to copper centred orbitals in the excited molecule. Therefore, the fluorescence of the complex was efficiently quenched upon metal binding. The reduction in the energy difference between the transition orbitals from 3.91 eV to 3.39 eV accounts for the blue shift in fluorescence spectra of **5** upon Cu^{2+} binding. For [**7**·Hg^{2+}], TD-DFT calculations at the same level of theory revealed that the mercury centered empty orbital, LUMO (-3.44/-3.45 eV) lies between the pyridine orbitals, LUMO+1 (-2.30/-2.29 eV) and benzene orbitals, HOMO-1 (-6.46/-6.45 eV) (Figure 5.24b,c). So, the excited electrons of the pyridine-centered orbital (LUMO+1) favor to transfer into the low-lying LUMO (mercury-centered empty orbital) instead of HOMO−1 state. This type of orbital orientation causes the fluorescence quenching of receptor **7** in the presence of Hg^{2+} ion.
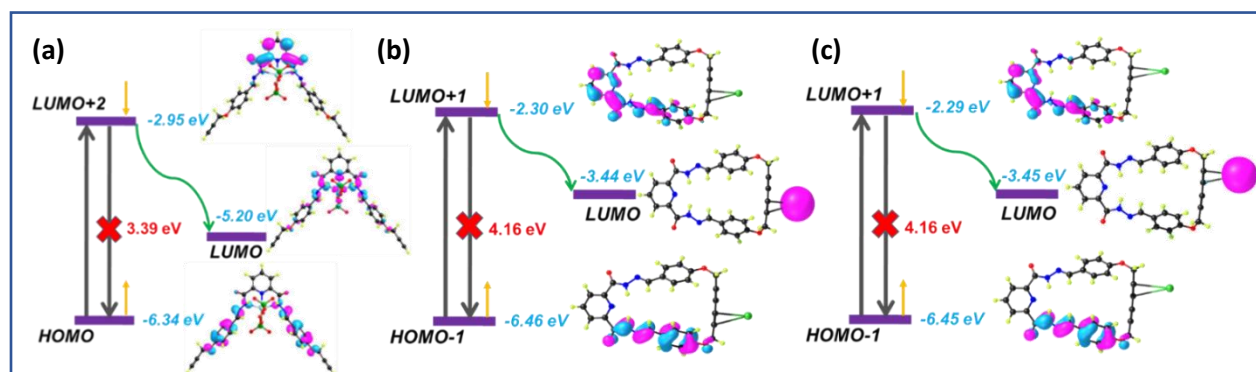
Figure 5.24 Schematic representation of fluorescence quenching of (a) **5** due to $Cu(ClO_4)_2$ binding, and of **7** due to Hg^{2+} ion binding to the (b) left sided alkyne and (c) right sided alkyne of the 1,3-dialkyne unit of the cyclic receptor.

5.4 Conclusion

       We have developed a concept of designing a unique probe capable of detecting dual metal ions *via* different binding site and different mechanism within a single molecular scaffold with a vision to study the different interactive behaviour of the metal ions in varying chemical environments. The thermally stable and fast-responding pyridine-containing ligand systems were found to recognize Cu^{2+} and Hg^{2+} ions. Cu^{2+} ion binding is feasible in the tripodal centre formed by the hard (N) atoms, whereas, Hg^{2+} interacts with the soft π-cloud of alkyne. In **5**, with terminal alkyne, Hg^{2+} induces the functional group transformation of alkyne to ketone, whereas in **7**, Hg^{2+} gets bounded to the probe by the π-cloud of the conjugated dialkyne unit. The differential modes of interaction of the alkynes with Hg^{2+} ion have established the superiority of internal alkynes over terminal alkynes, in terms of use as binding probe, such that compound **7** was successfully employed for detection of Hg^{2+} ion in water samples. From the present study, it is evident that terminal alkynes cannot serve as a good sensor for Hg^{2+} ion, keeping its functional integrity, since they are more prone to functional group transformation. However, the same functional group when placed internally in conjugation with another alkyne, can serve as efficient probe for soft metal ions like Hg^{2+}. Such differential interacting ability of alkynes can be harnessed in potential exploration of sensing. The divergent behaviour of alkynes is expected to accelerate the exploration of the functionality in differentiating between analogous structures. Interestingly, the fluorescence responses given by the two analytes (Cu^{2+} and Hg^{2+} ions) has been used to generate a molecular system exhibiting the OR logic operation.

5.5 Experimental Section

5.5.1 Materials and reagents

       Among the metal ions used $NaClO_4 \cdot H_2O$ (99%), $KClO_4 \cdot xH_2O$ (99%), $Fe(ClO_4)_2 \cdot xH_2O$ (98%), $Fe(ClO_4)_3 \cdot xH_2O$ (99.9%), $Al(ClO_4)_3 \cdot 9H_2O$ (98%), $Mg(ClO_4)_2 \cdot 6H_2O$ (99%), $Pb(ClO_4)_2 \cdot xH_2O$ (98%), $Cu(ClO_4)_2 \cdot 6H_2O$ (98%) and $Hg(ClO_4)_2 \cdot 3H_2O$ (99.9%) were purchased from Sigma Aldrich and $AgClO_4 \cdot xH_2O$ (99.9%), $Ca(ClO_4)_2 \cdot 4H_2O$ (98%), $Mn(ClO_4)_2 \cdot 6H_2O$

(98%), Zn(ClO$_4$)$_2$·6H$_2$O (99.9%), Co(ClO$_4$)$_2$·6H$_2$O (99.9%) were purchased from Alfa Aesar, as their respective perchlorate salts and used directly without further purification. Thionyl chloride, hydrazine monohydrate, copper acetate monohydrate, piperidine and ethanol were purchased from local brand. Pyridine-2,6-dicarbohydrazide was synthesized by literature reported procedure.[59] Chromatography was carried out using 60-120 mesh silica gel in a column of 2.5 cm diameter. DMSO AR grade was purchased from Merck and was used directly for experiments to prepare metal salt solutions. All the necessary solvents, used for the synthesis, were dried by conventional methods and distilled under N$_2$ atmosphere. The UV-vis spectra were carried out in DMSO-H$_2$O (7:3, *v/v*) as a solvent at c = 10^{-5} M and fluorescence spectra also were carried out in DMSO-H$_2$O (7:3, *v/v*) solvent as it is stated in the corresponding Figure captions. All the experiments were carried out at 22 ˚C without addition of any buffer, unless mentioned otherwise. pH tablets of pH 7, 4, 9.2 and pH solutions of pH 2, 5 and 11 were purchased from LOBA Chemie. The solutions were directly used for preparing ligand and complex solutions at pH 2, 5, 11. Each pH tablet was dissolved in 100 ml of water in a volumetric flask (as per standard instructed procedure) and this solution was used for preparing ligand and complex solutions at pH 7, 4 and 9.2.

5.5.1.1 Preparation of solutions at different pH

A stock solution of 1×10^{-3} M in DMSO was prepared for each probe and analyte. The stock solution was diluted to 7.8×10^{-6} M DMSO solution. For pH study of the free probe, 0.5 ml of each buffer solution (pH 2, 4, 5, 7, 9.2 and 11) was added separately to 2 ml 7.8×10^{-6} M DMSO solution of the free probe. pH of resulting solution was verified by testing with pH meter and the fluorescence intensity recorded. For 1:1 host-guest complex, 1 ml 7.8×10^{-6} M DMSO solution of metal ion was mixed well with 1 ml 7.8×10^{-6} M DMSO solution of ligand. 0.5 ml of each of each buffer solution was added separately to 2 ml DMSO solution of complexed species. pH of resulting solution was verified by testing with pH meter and the fluorescence change at 464 nm with pH variation was monitored at 22 ˚C. The resultant DMSO:H$_2$O ratio in each of the solutions is 4:1.

5.5.1.2 Preparation of solid samples for IR, EPR and CHN analysis

The free ligands were taken directly in the solid form for the IR spectra and CHN analysis. For the metal complexed/reacted species, the acyclic and cyclic compounds **5** and **7** were dissolved in minimum amount of DMSO. 2 equiv and 1 equiv of Hg(ClO$_4$)$_2$ in DMSO were mixed with **5**

and **7** respectively, whereas, 1 equiv Cu(ClO$_4$)$_2$ in DMSO was mixed with both of them separately. The four solutions were subjected to evaporation under reduced pressure. The resulting solid complexes were washed several times with H$_2$O to remove any extra perchlorate anion, followed by filtration by suction. Finally, they were dried under vacuum for several hours. The resulting dry solid powder were used directly for IR and elemental analysis, and their DMF solution were used for EPR analysis. Elemental analysis: Anal. Calcd for C$_{27}$H$_{21}$N$_5$O$_{12}$Cl$_2$Cu [**5**·Cu(ClO$_4$)$_2$]: C, 43.71; H, 2.85; N, 9.44. Found: C, 43.66; H, 2.71; N, 9.52; for C$_{27}$H$_{19}$N$_5$O$_{12}$Cl$_2$Cu [**7**·Cu(ClO$_4$)$_2$]: C, 43.83; H, 2.59; N, 9.47. Found: C, 43.69; H, 2.71; N, 9.60 and for C$_{27}$H$_{19}$N$_5$O$_4$Hg [**7**·Hg^{2+}]: C, 47.82; H, 2.82; N, 10.33. Found: C, 48.01; H, 2.71; N, 10.73.

5.5.1.3 Titration Procedure

The path length of the cell used for UV-Vis or fluorescence titration is 1 cm. Fluorescence titration was done using 10 nm×10 nm slit width. For UV-vis or fluorescence titration, stock solution of $1×10^{-3}$ M in DMSO-H$_2$O (7:3, *v/v*) was prepared for each probe and analyte. The stock solution of each probe and analyte was diluted to $3.1×10^{-5}$ M DMSO-H$_2$O (7:3, *v/v*) solution (for UV-Vis titration) and $7.8×10^{-6}$ M DMSO-H$_2$O (7:3, *v/v*) solution (for fluorescence titration). 2 ml of each ligand was given 0.1 ml aliquots of analyte solution gradually up to corresponding equivalences, and the signals were recorded after each addition. This is a continuous process.

5.5.1.4 Determination of stoichiometry by Job's plot

$1.25×10^{-4}$ M, $6.25×10^{-5}$ M and $3.1×10^{-5}$ M solutions of both host and guest were prepared. For each concentration, the host and guest were mixed in the volume ratio of 1.8:0.2, 1.6:0.4, 1.4:0.6, 1.2:0.8, 1.0:1.0, 0.8:1.2, 0.6:1.4, 0.4:1.6 and 0.2:1.8 to prepare solutions with mole fraction of the guest 1, 2, 3, 4, 5, 6, 7, 8 and 9 respectively. For all the solutions, the total volume was maintained at 2 ml. Absorbance of each solution along with absorbance of free ligand and metal were recorded. The absorbance data for each mole fraction of guest was processed according to literature reported equation[27] to get the equilibrium concentration of the complex. The plot of

equilibrium concentration of the complex, versus mole fraction of guest gave the obtained Job's plot. The temperature was maintained at 22 ˚C during the whole experiment.

5.5.1.5 Calculation of LOD and binding constant

LOD was calculated by the formula $3\sigma/s$, where "σ" is standard deviation of the blank and "s" is slope of the calibration curve. They can be obtained by plotting the fluorescence intensity vs concentration of the analyte.

Equal concentrations of host and guest were used for the titration to extract the binding constant. The temperature has been kept constant at 22 ˚C during the whole titration for obtaining binding constant. The host concentration was kept constant changing the guest concentration, *i.e.,* dilution method was used as the titration procedure.[60] Each titration was repeated 3 times and the data points were used for determining binding constants. The guest was assumed (and found) to be "silent" i.e., non-absorbing and non-fluorescing. Binding constant from UV-vis absorption spectral titration was obtained by fitting the titration data in the form of excel sheet containing host concentration, guest concentration, and the corresponding absorption intensity with each aliquot of analyte addition, into the free online software *Bindfit*. Selection of the proper stoichiometric model (UV 1:1 and UV 1:2 in our case) for the fitting of the data gave the fitting along with the association constant with corresponding error percentage of the fitting. Binding constant from fluorescence titration was determined according to the modified Benesi-Hildebrand equation by division of intercept by slope obtained when $1/\Delta I$ was plotted against $1/[Q]$. Each data point represents the average of three individual data obtained from three separate experiments, with error bars representing the standard deviation.

5.5.2 Instrumentation

^{1}H and ^{13}C NMR spectra were obtained with BRUKER 300 MHz FT-NMR spectrometers and the chemical shifts are reported in ppm, using tetramethylsilane as an internal standard and were referenced to the residual solvent as follows: $CDCl_3$ = 7.26 (^{1}H), 77.16 (^{13}C) ppm, DMSO = 2.50 (^{1}H), 39.52 (^{13}C) at 22 ˚C. For ^{1}H NMR, coupling constants *J* are given in Hz and the resonance multiplicity is described as s (singlet), d (doublet), t (triplet), m (multiplet). The fluorescence lifetime experiments were performed on a Horiba Jobin-Yvon IR spectral studies

were done on Perkin Elmer LX-1 FTIR spectrophotometer. The absorption spectra were recorded with a SHIMADZU-2450 UV-vis spectrophotometer at 22 ˚C. Fluorescence was recorded with SHIMADZU RF-5301pc spectrophotometer.

Caution! Metal perchlorate salts are potentially explosive in certain conditions. All due precautions should be taken while handling perchlorate salts!

5.5.3 Synthesis of compounds 2 -7

5.5.3.1 Synthesis of compound 2: 2,6-pyridine di carboxylic (500 mg, 2.99 mmol) acid was dissolved in dry MeOH (10 mL) solvent in a 100 mL schlenk flask at inert condition (N_2 atmosphere). $SOCl_2$ (5.98 mmol, 0.43 mL) was slowly added dropwise to a suspension of acid solution at ice cold condition. The colourless precipitate was came within one hour which was collected by filtration and dried in vacuum giving 2,6-pyridine dimethyl ester (380 mg, yield 66%).

5.5.3.2 Synthesis of compound 3: Pyridine 2,6-di methyl ester (250 mg, 1.28 mmol) and hydrazine mono hydrate (10.24 mmol, 0.49 mL) were heated at reflux in MeOH (10 mL) overnight. The resulting precipitate was isolated by suction filtration and washed with cold MeOH to give a white solid product (230 mg, yield 90%).

5.5.3.3 Synthesis of compound 5: 4-(prop-2-yn-1-yloxy) benzaldehyde (540.95 mg, 3.38 mmol) and 1 equiv of pyridine-2,6-dicarbohydrazide (320 mg, 1.648 mmol) were taken in a 100 mL round bottom flask and dissolved in EtOH. The reaction mixture was allowed to stir overnight at reflux condition. The resulting precipitate was isolated by filtration and washed with cold EtOH to give compound **5** as a white solid (750 mg, 1.56 mmol, yield 95%). ^{1}H NMR (d$_6$-DMSO, 300 MHz) δ = 12.25 (s, 1H, $H_{N=CH}$), 8.74 (s, 1H, $H_{aromatic}$), 8.38-8.26 (m, 1.5H, $H_{pyridine}$), 7.81 (d, 2H, J = 7.8 Hz, $H_{aromatic}$), 7.13 (d, 2H, J = 8.1 Hz, $H_{aromatic}$), 4.90 (s, 2H, OCH_2), 3.64 (s, 1H, H_{alkyne}). ^{13}C NMR (d$_6$-DMSO, 75 MHz) δ = 159.8, 159.5, 150.4, 148.8, 140.4, 129.3, 127.8, 125.8, 115.8, 79.4, 79.0, 56.0. Anal. Calcd for $C_{27}H_{21}N_5O_4$ (**5**): C, 67.63; H, 4.41; N, 14.61. Found: C, 67.29; H, 4.15; N, 14.39.

5.5.3.4 Synthesis of compound 6: 4-(prop-2-yn-1-yloxy) benzaldehyde (500 mg, 3.12 mmol) was taken in a 100 mL round bottom flask and dissolved in dichloromethane. Then Cu (OAc)$_2$.H$_2$O (1

equiv) and piperidine (1 equiv) were added to the reaction mixture. After that reaction mixture was allowed to stir overnight at 22 ˚C. Reaction mixture was diluted with dichloromethane and washed with distilled water. Organic phase was separated, dried using sodium sulphate and solvent was removed under reduced pressure. Then the crude product was purified by silica gel column chromatography by using 40% EtOAc/Hexane gives yellow coloured solid compound **6** (300 mg, yield 30%). ^{1}H NMR (CDCl$_3$, 300 MHz) δ = 9.91 (s, 1H, C*H*O), 7.86 (d, 2H, J = 8.7, $H_{aromatic}$), 7.06 (d, 2H, J = 8.7, $H_{aromatic}$), 4.84 (s, 2H, OC*H*$_2$). ^{13}C NMR (CDCl$_3$, 75 MHz) δ = 190.8, 162.2, 132.4, 131.2, 115.6, 74.1, 71.6, 56.4. Anal. Calcd for C$_{20}$H$_{14}$O$_4$ (**6**): C, 75.46; H, 4.43. Found: C, 75.28; H, 4.25.

5.5.3.5 Synthesis of compound 7: 4,4'-(hexa-2,4-diyne-1,6-diylbis(oxy)dibenzaldehyde (54 mg, 0.169 mmol) and 1 equiv of pyridine-2,6-di carbohydrazide (32.8 mg, 0.169 mmol) were taken in a 100 mL round bottom flask and dissolved in EtOH. Reaction mixture was allowed to stir overnight at reflux condition. The resulting precipitate was collected by filtration and washed with cold EtOH give compound **7** as a yellow solid (52 mg, yield 64%). ^{1}H NMR (d$_6$-DMSO, 300 MHz) δ = 12.24 (s, 1H, H_{NH}), 8.71 (s, 1H, $H_{N=CH}$), 8.33-8.24 (m, 1.5H, $H_{pyridine}$), 7.76 (d, 2H, J = 7.5 Hz, $H_{aromatic}$), 7.09 (d, 2H, J = 7.5 Hz, $H_{aromatic}$), 5.05 (s, 2H, OC*H*$_2$). ^{13}C NMR (d$_6$-DMSO, 75 MHz) δ = 159.3, 158.7, 149.8, 148.3, 131.7, 128.9, 127.6, 125.3 115.3, 75.9, 70.1, 56.1. Anal. Calcd for C$_{27}$H$_{19}$N$_5$O$_4$ (**7**): C, 67.92; H, 4.01; N, 14.67. Found: C, 67.53; H, 4.15; N, 14.38.

5.5.4 Single Crystal X-ray Diffraction

X-ray-quality crystal of **5** was grown by slow diffusion of DMF solution at 22 ˚C. Single crystal X-ray data of Compound **5** was collected at 140 K with a Microfocal D8 venture Bruker APEX 3 using Mo Kα (λ = 0.71069 Å) radiation. The single crystal was selected from the mother solution, mounted in inert oil, and transferred to the cold gas stream for flash cooling. The unit cell parameters were refined using all the collected spots after the integration process. Data collection, data reduction, structure solution/refinement was carried out using the software package of Bruker APEX 3. The crystal structure was solved by direct method and refined by full-matrix least-squares on F^2 using SHELXL97.[61] X-band EPR spectra were recorded on a Broker Biospin EMX^micro spectrometer. All non-hydrogen atoms were treated anisotropically and the hydrogen atoms were geometrically fixed. CCDC 2068242 contains the supplementary crystallographic data for this paper. These data can be obtained free of charge *via* www.ccdc.cam.ac.uk/data_request/cif, or by

e-mailing data_request@ccdc.cam.ac.uk, or by contacting The Cambridge Crystallographic Data Centre, 12 Union Road, Cambridge CB2 1EZ, U.K.; fax: +44 1223 336033.

5.5.4.1 Crystallographic data for 5

Empirical Formula $C_{27}H_{21}N_5O_4$, crystal system, monolinic; space group, $C2/c$; unit cell dimensions, $a = 26.676(2)$Å, $b = 11.1232(8)$Å, $c = 8.111(6)$ Å, $\beta = 103.747(4)°$,; $V = 2337.9(3)$ Å^3; $Z = 4$; $\rho = 1.362$ g cm^{-3}, T (K) 140 (2), θmin/max: 1.992/ 27.113, reflections: 2588 collected, Goodness-of-Fit (GOF) on F^2 1.126, $R_{int} = 0.0316$, $R_1(all) = 0.0762$, $wR_2(all) = 0.1316$. Final R indices [I>2σ(I)]: $R_1 = 0.0570$, $wR_2 = 0.1222$.

5.6 Computational details

Theoretical calculations were performed using the density functional theory (DFT) method implemented in the Gaussian 16 program package.[62] The ground state geometries were optimized with B3LYP (Becke, three-parameter, Lee−Yang−Parr) functional[63-64] in combination with the LANL2DZ basis set[65,66] for the metal (Cu and Hg) and 6-311g(d) basis set[67,68] for the non-metallic atoms (C, H, N, O, Cl). The geometries were optimized without any symmetry constraints. The vibrational frequencies were computed at the optimized geometries to confirm that the optimized geometries represent the local minima and obtain only positive eigen values. TDDFT calculation on the optimized structures was carried out using the Coulomb—attenuated functional CAM-B3LYP[69] at the aforementioned level of theory incorporating the solvent effect using DMSO as a solvent through the conductor-like polarizable continuum model[70,71] (CPCM). The 3D images of the optimized geometries were visualized, and canonical orbitals were rendered in the Chemcraft[72,73] visualization software.

5.7 References

1   D. J. Cram and M. J. Cram, *Science,* 1974, **183**, 803-809.

2   A. Pal, S. R. Bhatta and A. Thakur, *Coord. Chem. Rev.,* 2021, **431**, 213685.

3   Jr. J. Rebek, *Chem. Commun.,* 2000, 637-643.

4   J. Teyssandier, S. D. Feyter and K. S. Mali, *Chem. Commun.,* 2016, **52**, 11465-11487.

5   T. L. Ho, *Chem. Rev.,* 1975, **75**, 1-20.

6 P. K. Chattaraj, H. Lee and R. G. Parr, *J. Am. Chem. Soc.,* 1991, **113***, 1856-1857.

7 J. Wu, L. Zhao, M. Guo and J. Tang, *Chem. Commun.,* 2015, **51**, 17317-17320.

8 R. Kumar, H. Jain, P. Gahlyan, A. Joshi and C. N. Ramachandran, *New J. Chem.,* 2018, **42**, 8567-8576.

9 N. Hussain and V. K. Bhardwaj, *Dalton Trans.,* 2016**, 45**, 7697-7707.

10 M. Tian, L. Liu; Y. Li, R. Hu, T. Liu, H. Liu, S. Wang and Y. Li, *Chem. Commun.,* 2014, **50**, 2055−2057.

11 A. Pal, K. M. Das, B. Goswami and A. Thakur, *Inorg. Chem.*, 2020, **59**, 10099−10112.

12 A. Pal, B. Goswami and A. Thakur, *New J. Chem.*, 2022, **46**, 2989–3005.

13 S. R. Bhatta, M. Karmakar and A. Thakur, *J. Organomet. Chem.,* 2021, **949**, 121958-121968.

14 S. R. Bhatta, B. Mondal, S. Lima and A. Thakur, *Dalton Trans.,* 2019, **48**, 8209-8220.

15 S. R. Bhatta, B. Mondal, G. Vijaykumar and A. Thakur, *Inorg. Chem.,* 2017, **56**, 11577-11590.

16 M. Alfonso, A. Tárraga, and P. Molina, *Org. Lett.,* 2011, **13**, 6432–6435.

17 S. R. Bhatta, A. Pal, U. K. Sarangi and A. Thakur, *Inorg. Chim. Acta*, 2019, **498**, 119097-119107.

18 Y. Huang, J. Lin, W. Zhang, B. Zhang and Q. Sun*, Inorg. Chem. Commun.*, 2019, **105**, 129–134.

19 V. S. Elanchezhian and M. Kandaswamy, *Inorg. Chem. Commun.*, 2010, **13**, 1109-1113.

20 N. Kaur, P. Kaur and K. Singh, *Sens. Actuators B,* 2016, **229**, 499-505.

21 K. Santhiya, S. K. Sen, R. Natarajan, R. Shankar and B. Murugesapandian, *J. Org. Chem.,* 2018, **83**, 10770-10775.

22 S. H. Jung, T. K. Hyun, J. Y. Kim and J. H. Jung, *RSC Adv.* 2015, **5**, 26662-26665.

23 N. Yadav and A. K. Singh, *New J. Chem.,* 2018, **42**, 6023-6033.

24 A. K. Pati, M. Mohapatra, P. Ghosh, S. J. Gharpure and A. K. Mishra, *J. Phys. Chem. A,* 2013, **117**, 6548−6560.

25 C. Liao, J. Shi, M. Zhang, R. Dalapati, Q. Tian, S. Chen, C. Wang and L. Zang, *Mater. Adv.,* 2021, **2**, 6213-6245.

26 D. B. Hibberta and P. Thordarson, *Chem. Commun.,* 2016, **52**, 12792—12805.

27 S. A. Kadam, K. Haav, L. Toom, A. Pung, C. Mayeux, I. Leito, *Eur. J. Org. Chem.*, 2017, 1396-1406.

28 P. Yu, X. Wen, Y. -R. Toh, Y. -C. Lee, K. -Y. Huang, S. Huang, S. Shrestha, G. Conibeer and J. Tang, *J. Mater. Chem. C*, 2014, **2**, 2894–2901.

29 S. S. Bag, S. Talukdar, K. Matsumoto, and R. Kundu, *J. Org. Chem.,* 2013, **78**, 2, 278–291.

30 H. Yu, Q. Liu, J. Li, Z. -M. Su, X. Li, X. Wang, J. Sun, C. Zhou and X. Hu, *J. Mater. Chem. C*, 2021, **9**, 562—568

31 J. Maillard, K. Klehs, C. Rumble, E. Vauthey, M. Heilemann and A. Fürstenberg, *Chem. Sci.,* 2021, **12**, 1352–1362.

32 J. R. Lackowicz, Principles of Fluorescence Spectroscopy, 3rd Ed., Springer, Page-282, ISBN 978-0-387-46312-4.

33 C. Freymüller, S. Kalinina, A. Rück, R. Sroka and A. Rühm, *J. Biophotonics*, 2021, **14**, e202100024.

34 R. Sinha, A. Chatterjee, and P. Purkayastha, *J. Phys. Chem. B*, 2022, **126**, 1232−1241.

35 H. A. Benesi and J. H. Hildebrand, *J. Am. Chem. Soc.*, 1949, **71**, 2703−2707.

36 K. Rezaeian, H. Khanmohammadi and A. Talebbaigy, *Anal. Methods*, 2020, **12**, 1759-1766.

37 A. Bhattacharyya, S. Ghosh and N. Guchhait, *RSC Adv.*, 2016, **6**, 28194-28199.

38 H. Jeon, W. Suh and D.-Y. Noh, *Inorg. Chem. Commun.*, 2012, **24**, 181–185.

39 Q. Teng, Y. Liu, J. Hu, H. Chai, K. Li and H. Zhang, *Tetrahedron*, 2016, **72**, 3890–3897.

40 J. -Z. Ge, Y. Zou, Y. -H. Yan, S. Lin, X. -F. Zhao and Q. -Y. Cao, *J. Photochem. Photobiol. A: Chem.,* 2016, **315**, 67–75.

41 A. Sola, F. Otón, A. Espinosa, A. Tárraga and P. Molina, *Dalton Trans.,* 2011, **40**, 12548–12559.

42 C.-B. Huang, H.-R. Li, Y. Luo and L. Xu, *Dalton Trans*., 2014, **43**, 8102–8108.

43 A. Mondal, A. Roy Chowdhury, S. Bhuyan, S. K. Mukhopadhyaye and P. Banerjee, *Dalton Trans*., 2019, **48**, 4375–4386.

44 M. Kaur, M. J. Cho and D. H. Choi, *Dyes and Pigments*, 2016, **125**, 1-7.

45 M. Kaur, Y. H. Ahn, K. Choi, M. J. Cho and D. H. Choi, *Org. Biomol. Chem*., 2015, **13**, 7149–7153.

46 G. Li, L. Bai, F. Tao, A. Deng and L. Wang, *Analyst*, 2018, **143**, 5395–5403.

47 J. Dong, J. Hu, H. Baigudea and H. Zhang, *Dalton Trans*., 2018, **47**, 314–322

48 S. Lal, K. Prakash, N. Khera, Drashya , S. Singh, A. Singh, S. Hooda and R. Chandra, *J. Mol. Str.,* 2020, **1211**, 128091.

49 P. Kaur, S. Kaura and K. Singh, *Org. Biomol. Chem*., 2012, **10**, 1497–1501.

50 Y. Liu, J. Hua, Q. Tenga and H. Zhang, *Sensors and Actuators B*, 2017, **238**, 166–174.

51 S. Zhang, Q. Niu, L. Lan and T. Li, *Sensors and Actuators B*, 2017, **240**, 793–800.

52 C. S. M. Park, M. H. Kim, J. I. Choe, K. T. No and S.K. Chang, *J. Org. Chem*. 2007, **72**, 3550-3553.

53 Y. W. Sie, C. F. Wan and A. T. Wu, *RSC Adv*., 2017, **7**, 2460–2465.

54 D. C. Magri, M. C. Fava and C, J. Mallia, *Chem. Commun.,* 2014, **50**, 1009-1011.

55 Y. Chen, Y. -H. Zhang and L. -J. Zhao, *Phys. Chem. Chem. Phys.*, 2004, **6**, 53 –542.

56 A. E. Wickenden and R. A. Krause, *Inorg. Chem.*, 1965, **4**, 404-407.

57   E. Garribba and G. Micera, *J. Chem. Educ.* 2006, **83**, 8, 1229.

58   A. J. Hallett, T. M. O'Brien, E. Carter, B. M. Kariuki, D. M. Murphy and B. D.Ward, *Inorg. Chim. Acta*, 2016, **441**, 86–94.

59   R. M. Duke, T. McCabe, W. Schmitt and T. Gunnlaugsson, *J. Org. Chem.*, 2012, **77,** 3115-3126.

60   P. Thordarson, *Chem. Soc. Rev.,* 2011, **40**, 1305–1323.

61   G. M. Sheldrick, *Acta. Crystallogr.*, 2008, **A64**, 112-122.

62   M. J. Frisch, G. W. Trucks, H. B. Schlegel, G. E. Scuseria, M. A. Robb, J. R. Cheeseman, G. Scalmani, V. Barone, G. A. Petersson, H. Nakatsuji, X. Li, M. Caricato, A. V. Marenich, J. Bloino, B. G. Janesko, R. Gomperts, B. Mennucci, H. P. Hratchian, J. V. Ortiz, A. F. Izmaylov, J. L. Sonnenberg, D. Williams-Young, F. D. Lipparini, F. Egidi, J. Goings, B. Peng, A. Petrone, T. Henderson, D. Ranasinghe, V. G. Zakrzewski, J. Gao, N. , Rega, G. Zheng, W. Liang, M. Hada, M. Ehara, K. Toyota, R. Fukuda, J. Hasegawa, M. Ishida, T. Nakajima, Y. Honda, O. Kitao, H. Nakai, T. Vreven, K. Throssell, J. A.; Peralta, J. E. Montgomery Jr., F. Ogliaro, M. J. Bearpark, J. J. Heyd, E. N. Brothers, K. N. Kudin, V. N. Staroverov, T. A. Keith, R. Kobayashi, J. Normand, K. Raghavachari, A. P. Rendell, J. C. Burant, S. S. Iyengar, J. Tomasi, M. Cossi, J. M. Millam, M. Klene, C. Adamo, R. Cammi, J. W. Ochterski, R. L. Martin, K. Morokuma, O. Farkas, J. B. Foresman and D. J. Fox, *Gaussian 16*, Revision B.01; Gaussian, Inc.: Wallingford, CT, 2016.

63   D. Becke, *J. Chem. Phys.,* 1993, **98**, 5648-5652.

64   C. Lee, W. Yang and R. G. Parr, *Phys. Rev. B: Condens. Matter Mater. Phys.,* 1988, **37,** 785-789.

65   A. D. Becke, *Phys. Rev. A: At., Mol., Opt. Phys.,* 1988, **38,** 3098-3100.

66   W. R. Wadt and P. J. Hay, *J. Chem. Phys.,* 1985, **82,** 284-298

67   P. J. Hay and W. R. Wadt, *J. Chem. Phys.,* 1985, **82,** 299-310.

68   G. A. Petersson and M. A. Al-Laham, *J. Chem. Phys.*, 1991, **94,** 6081-6090.

69   G. F. Weigend and R. Ahlrichs, *Phys. Chem. Chem. Phys.,* 2005**, 7**, 3297-3305.

70   T. Yanai, D. P. Tew and N. C. Handy, *Chem. Phys. Lett.,* 2004, **393**, 51-57.

71   A. Klamt and G. Schüürmann, *J. Chem. Soc., Perkin Trans.,* 1993, **2**, 799−805.

72   V. Barone and M. Cossi, *J. Phys. Chem. A,* 1998, **102**, 1995−2001.

73   G. A. Andrienko, http://www.chemcraftprog.com.

Spectroscopic

and

Computational Details
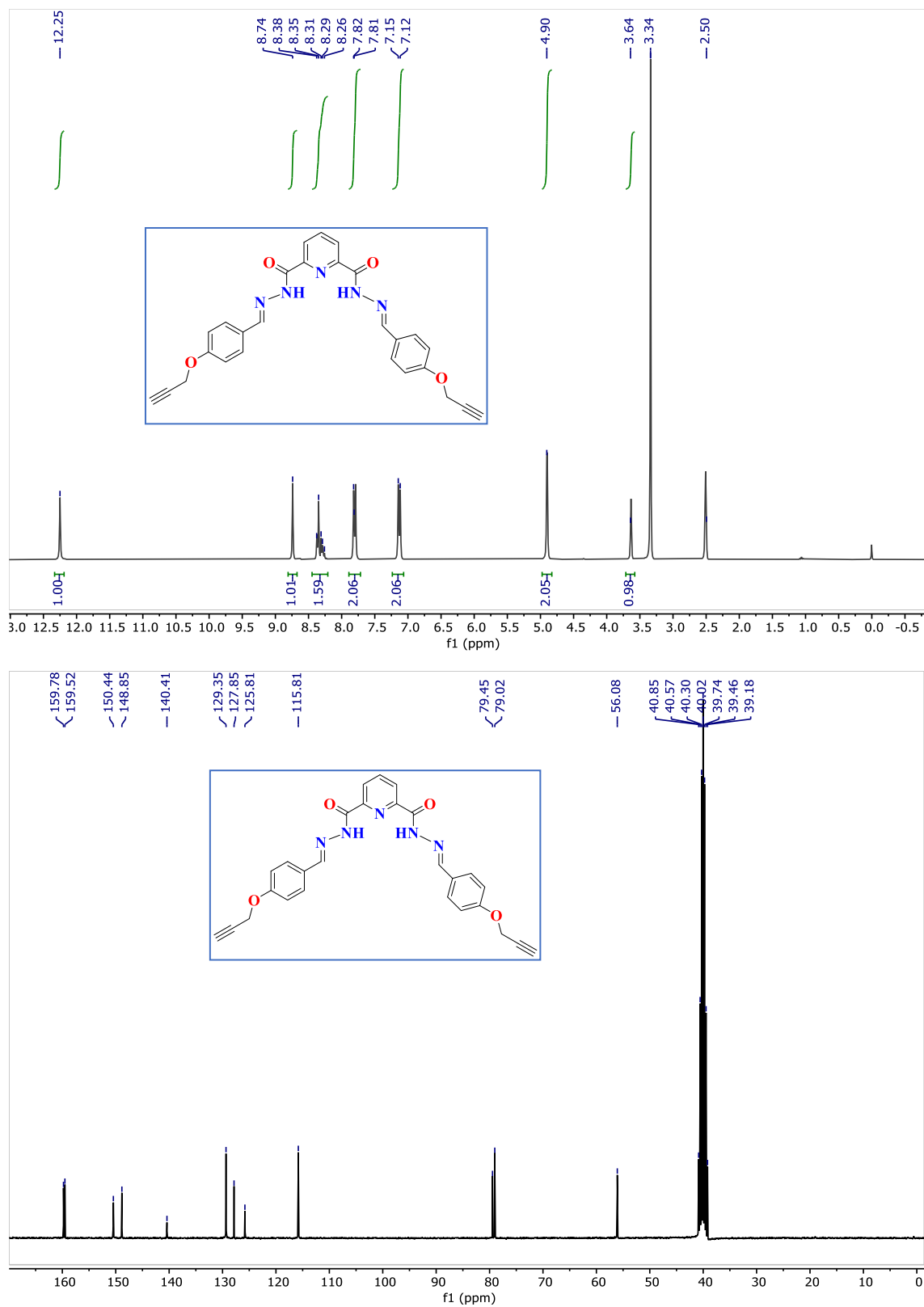
Figure 5.25 ¹H and ¹³C NMR spectra of compound **5** in DMSO-d₆ as a solvent.
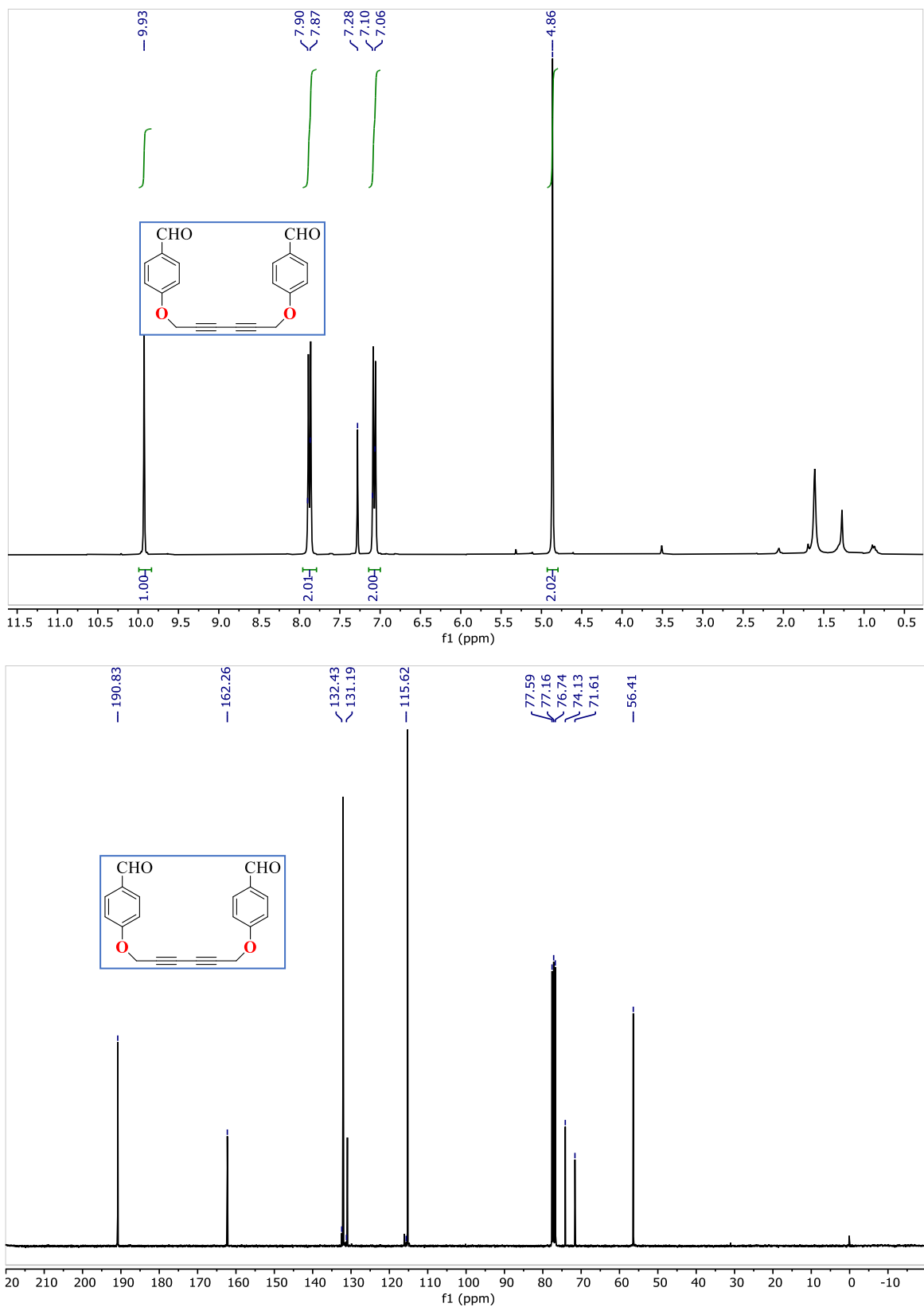
Figure 5.26 ^{1}H and ^{13}C NMR spectra of compound **6** in CDCl$_3$ as a solvent.
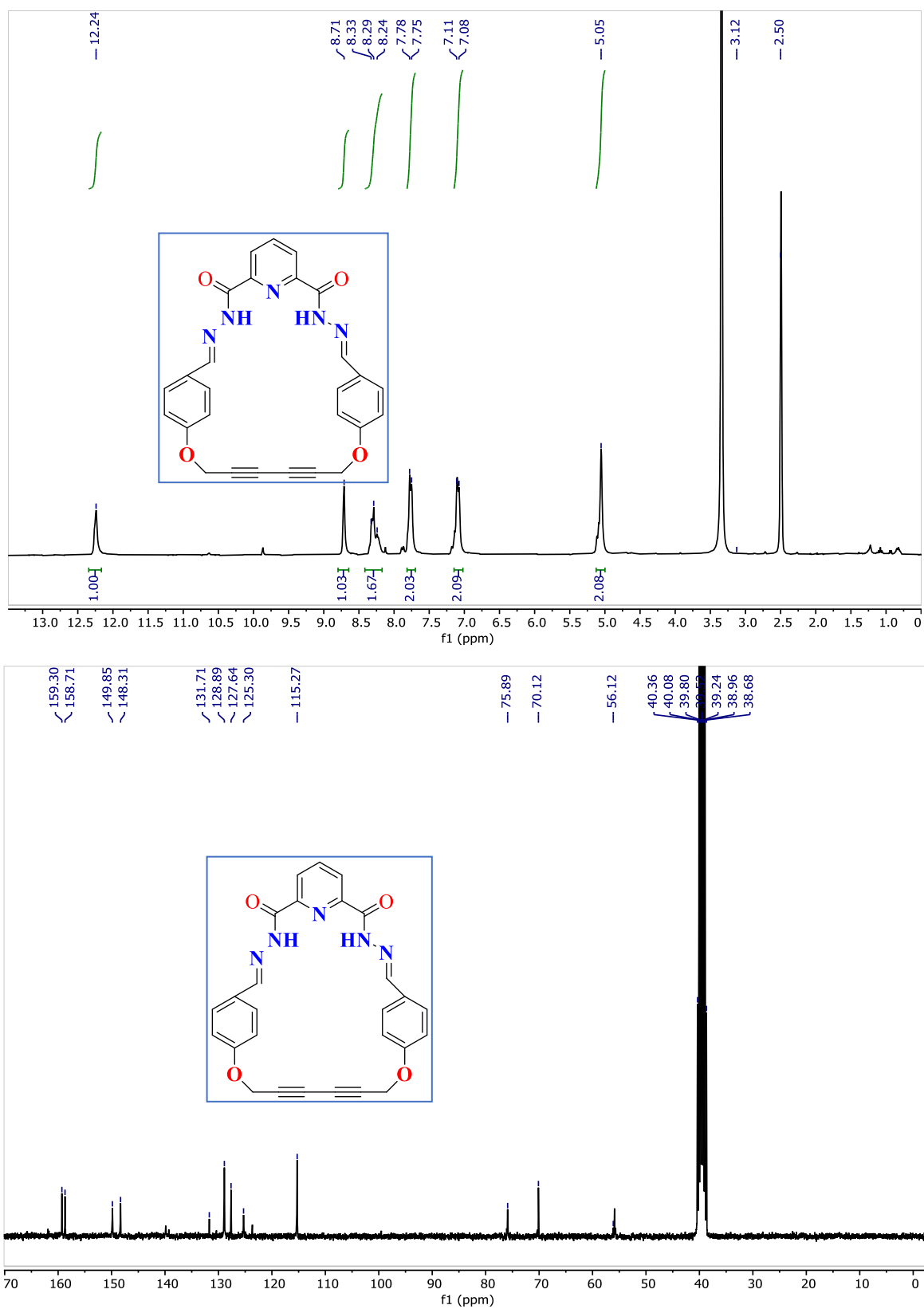
Figure 5.27 ^{1}H and ^{13}C NMR spectra of compound **7** in DMSO-d$_6$ as a solvent.
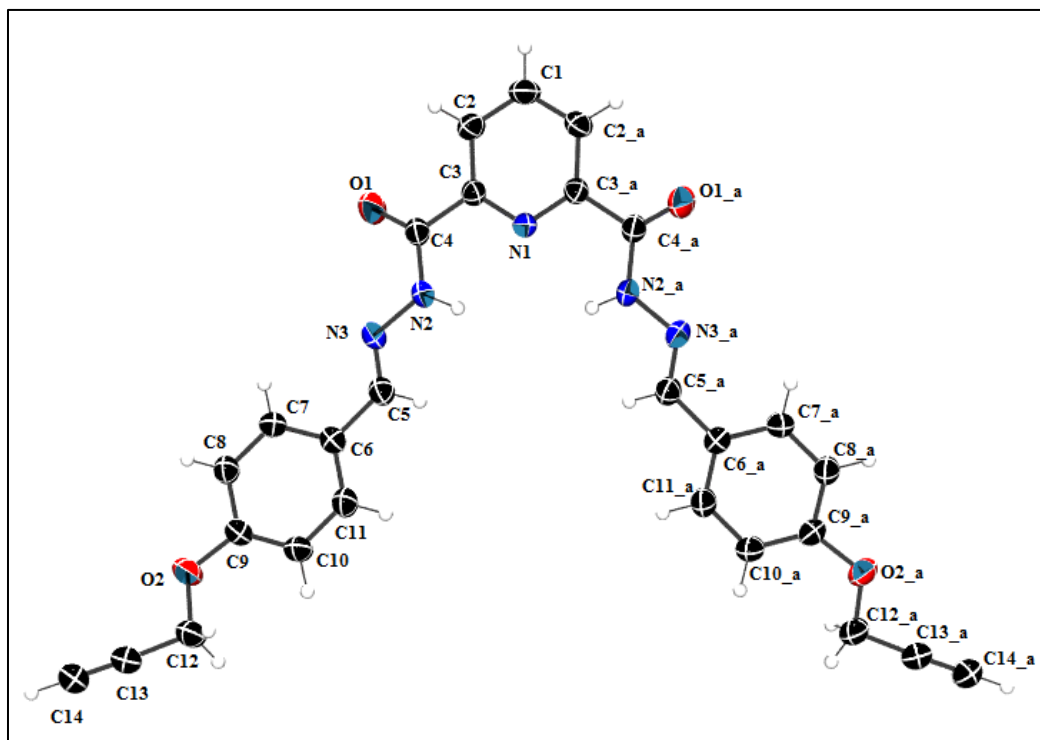
Figure 5.28 ORTEP representation of the molecular structure of **5** with thermal ellipsoids drawn at the 50% probability level. Selected bond lengths (Å) and angles (deg) for 5: C3-N1 1.337(2), C4-O1 1.220(2), C4-N2 1.348(2), N2-N3 1.381(2), N3-C5 1.227(3), C5-C6 1.459(3), C9-O2 1.366(2), C13-C14 1.171(3); N1-C3-C4 116.74(17), N1-C3-C2 123.06(18), O1-C4-N2 124.74(18), C4-N2-N3 121.29(16), C5-N3-N2 114.71(16), N3-C5-C6 121.77(18), C9-O2-C12 118.93(16), O2-C9-C10 125.50(18).
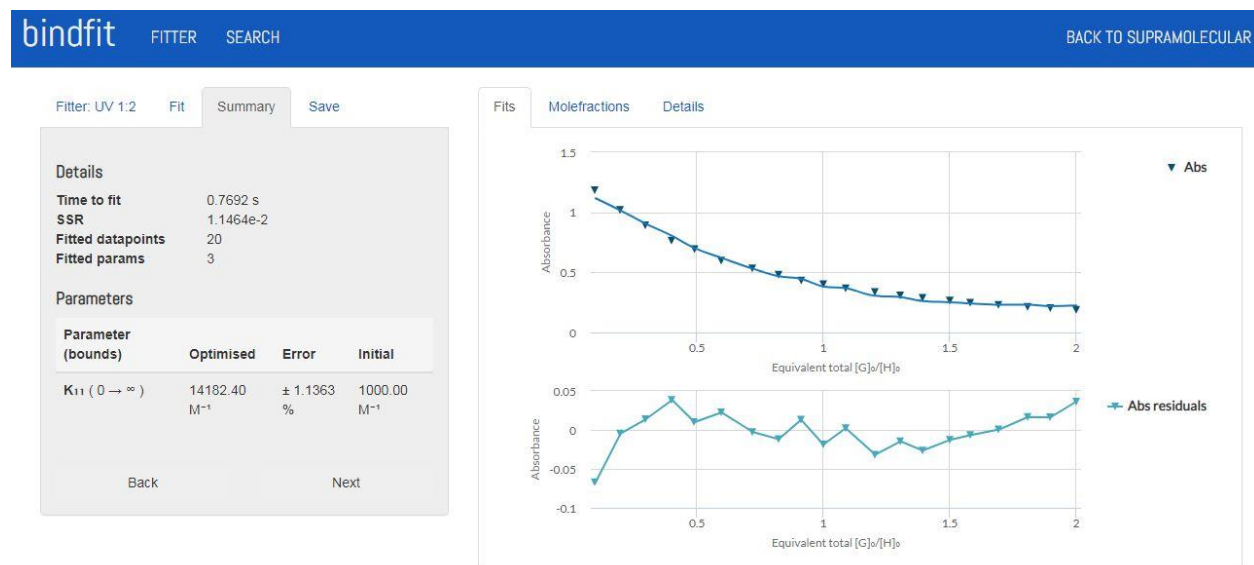
Figure 5.29 Fitting of absorption titration data of compound **5** with Hg^{2+} ion into 1:2 Nelder-Mead model in Bindfit software. Screenshots taken from the website supramolecular.org. This fitting for 1:2 fitter with a minimum error of ±1.1363 % justifies the 1:2 binding of **5** with Hg^{2+} ion with an association constant of 14182.40 M^{-1}. 20 data points have been used as input in this fitting with 3 factors viz., host concentration, guest concentration and the change in fluorescence intensity. The optimised value is the actual binding constant obtained.
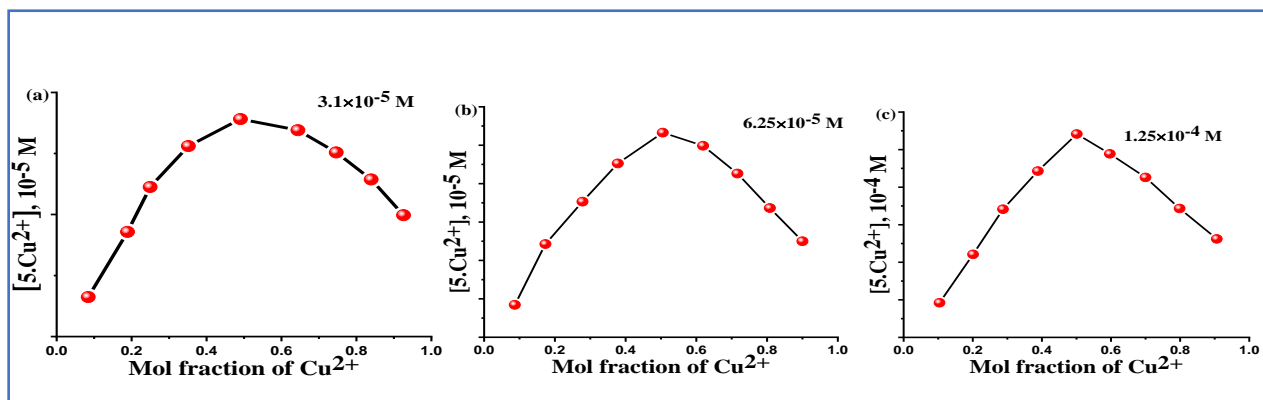
Figure 5.30 Jobs plot of compound **5** with Cu^{2+} metal ion at various concentration.
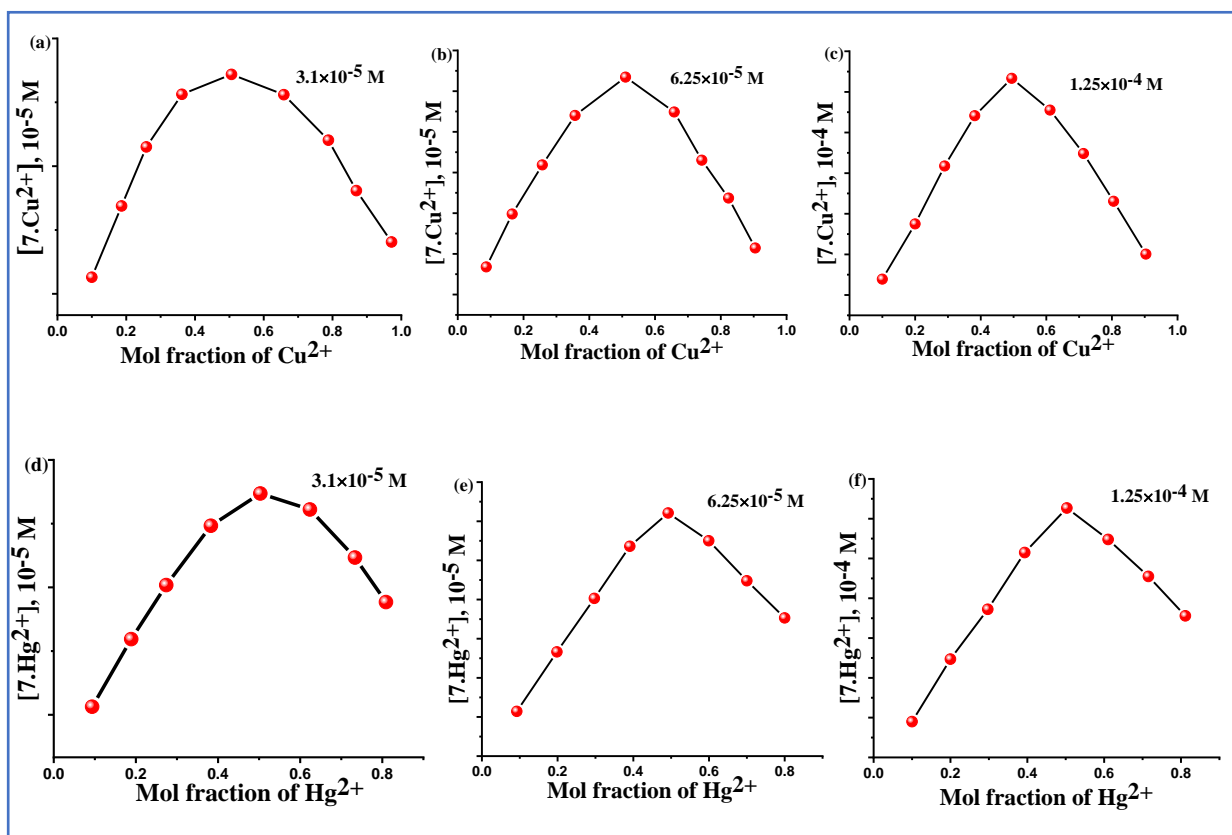
Figure 5.31 Jobs plot of compound **7** with (a)-(c) Cu^{2+} and (d)-(f) Hg^{2+} metal ions at various concentration.
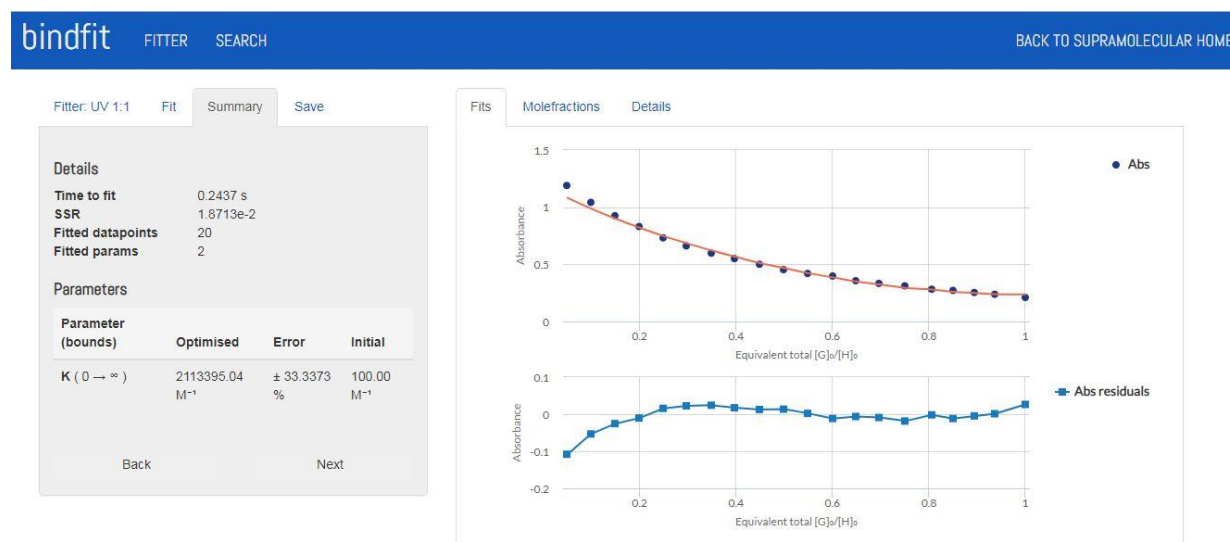
Figure 5.32 Association constant of compound **5** with Cu^{2+} ion obtained from fitting the UV-vis absorbance titration data into 1:1 Nelder-Mead model in Bindfit software. Screenshots taken from the website supramolecular.org. This fitting for 1:1 fitter with an error of ±33.3373 % (< 40 %) justifies the 1:1 binding of **5** with Cu^{2+} ion with an association constant of 2113395.04 M^{-1}. 20 data points have been used as input in this fitting with 3 factors viz., host concentration, guest concentration and the change in fluorescence intensity. The optimised value is the actual binding constant obtained.
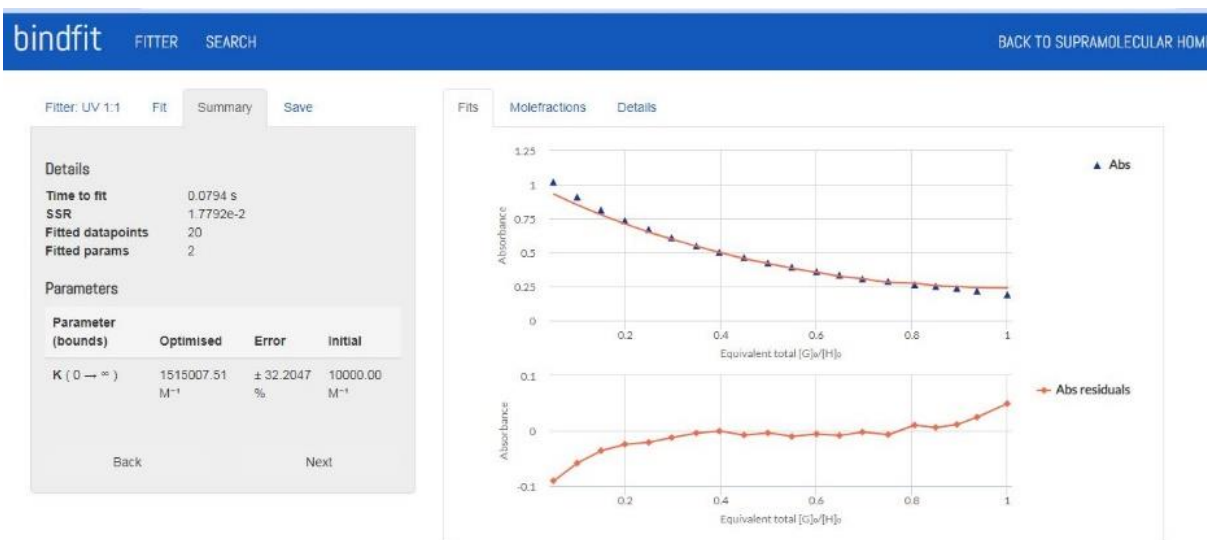
Figure 5.33 Association constant of compound **7** with Cu^{2+} ion obtained from fitting the UV-vis absorbance titration data into 1:1 L-BFGS-B model in Bindfit software. Screenshots taken from the website supramolecular.org. This fitting for 1:1 fitter with an error of ±32.2047 % (< 40 %) justifies the 1:1 binding of **7** with Cu^{2+} ion with an association constant of 1515007.51 M^{-1}. 20 data points have been used as input in this fitting with 3 factors viz., host concentration, guest concentration and the change in fluorescence intensity. The optimised value is the actual binding constant obtained.
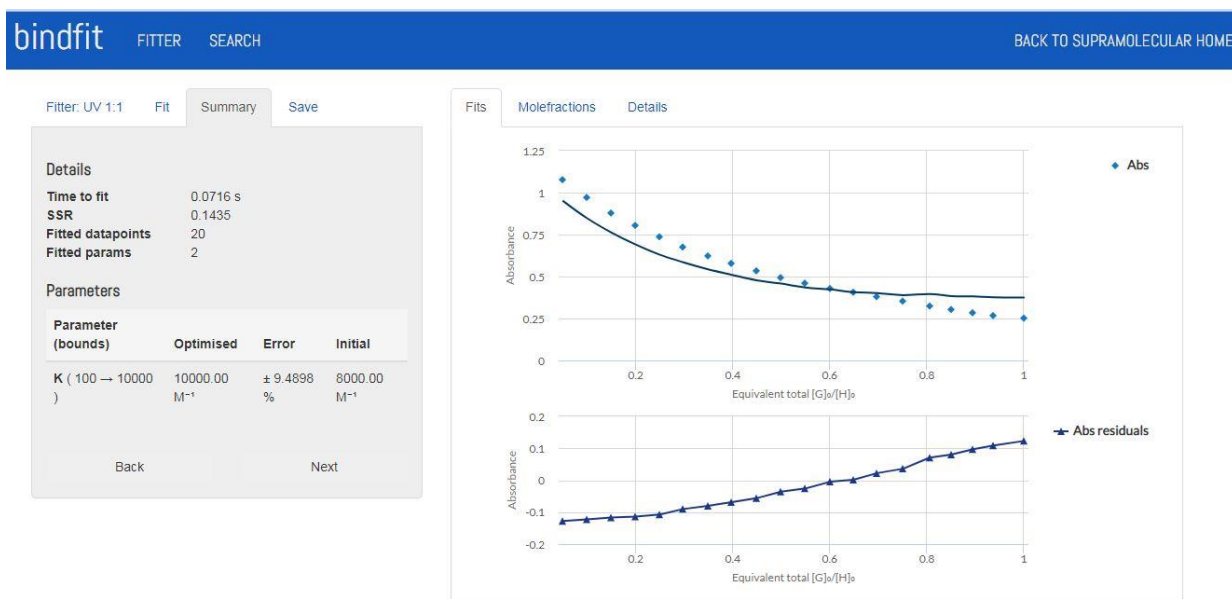
Figure 5.34 Association constant of compound **7** with Hg^{2+} ion obtained from fitting the UV-vis absorbance titration data into 1:1 L-BFGS-B model in Bindfit software. Screenshots taken from the website supramolecular.org. This fitting for 1:1 fitter with an error of ±9.4898 % (< 40 %) justifies the 1:1 binding of **7** with Hg^{2+} ion with an association constant of 10000 M^{-1}. 20 data points have been used as input in this fitting with 3 factors viz., host concentration, guest concentration and the change in fluorescence intensity. The optimised value is the actual binding constant obtained.
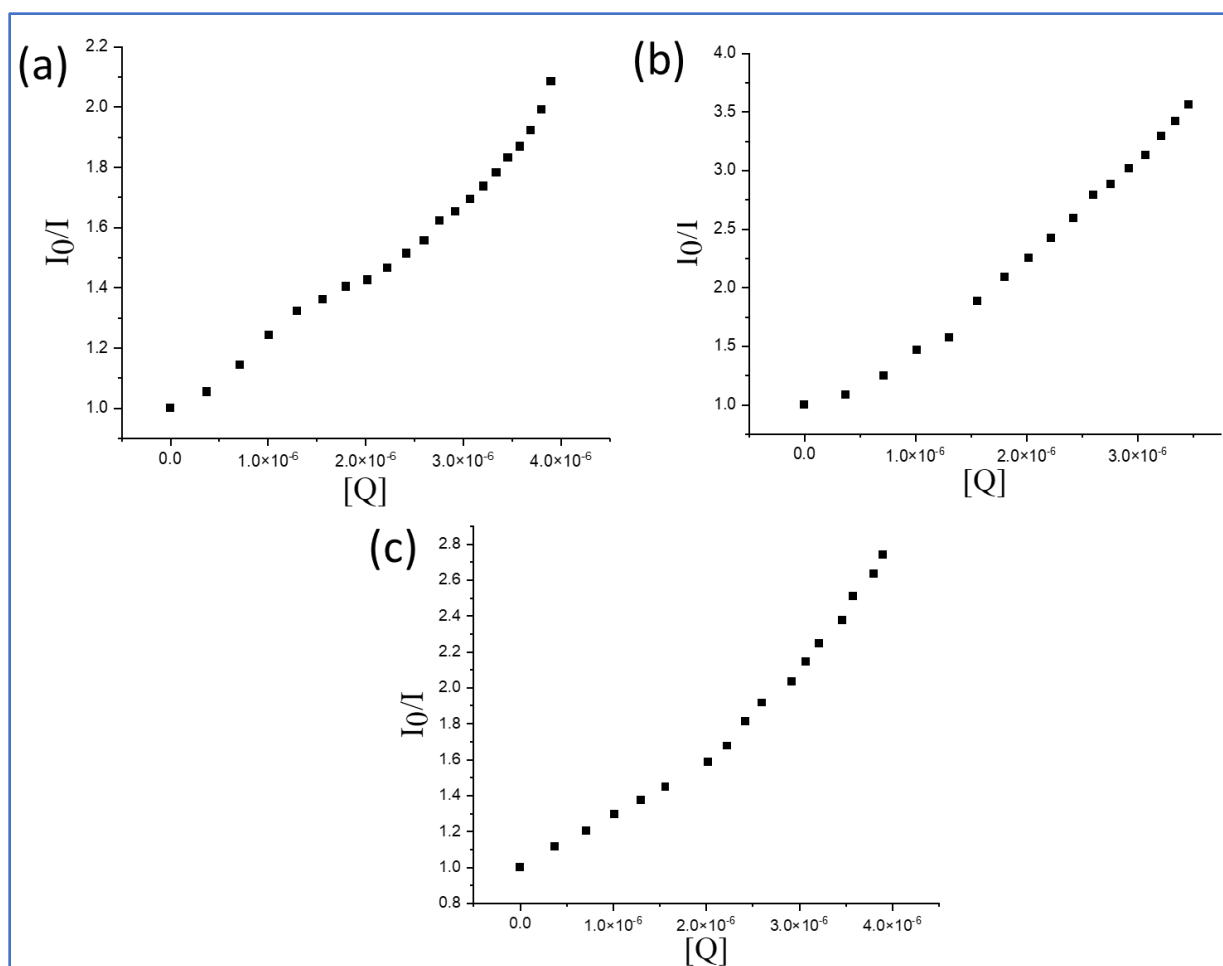
Figure 5.35 Stern-Volmer plot of (a) **5**+Cu^{2+}, (b) **7**+Cu^{2+} and (c) **7**+ Hg^{2+}.
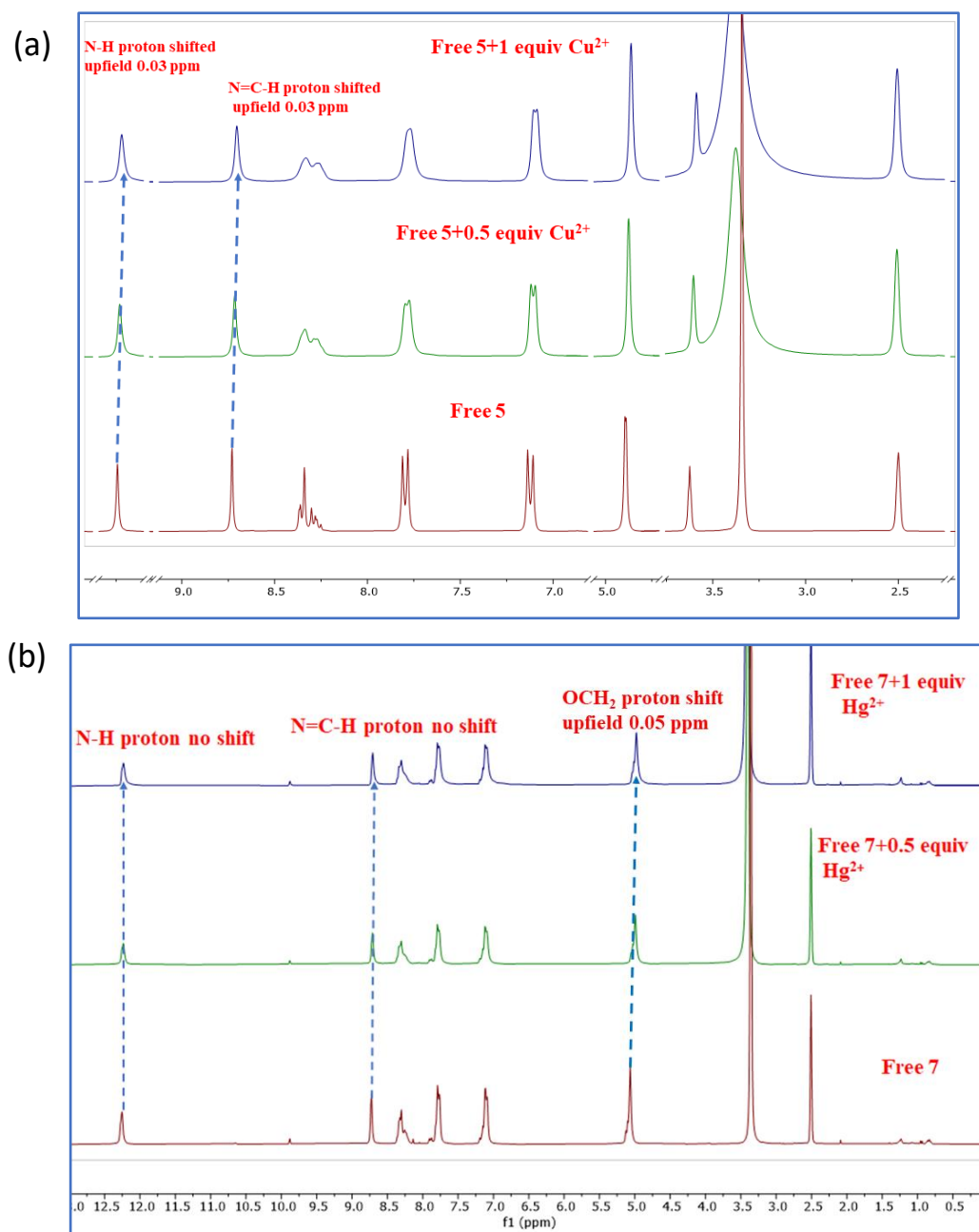
Figure 5.36 ^{1}H NMR titration of (a) ligand **5** with addition of up to 1 equiv of Cu^{2+} ion and (b) ligand **7** with addition of up to 1 equiv of Hg^{2+} ion in DMSO-d_6.
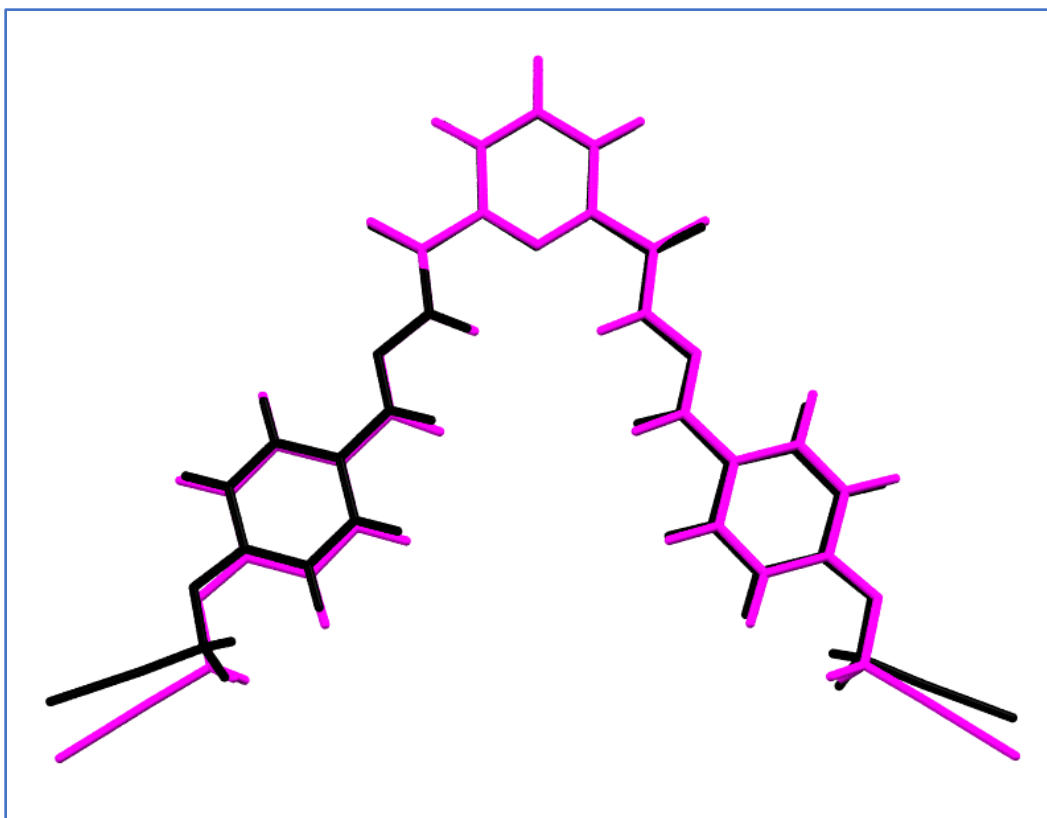
Figure 5.37 Overlay of X-ray crystal structure and DFT optimized structure of receptor **5**. (Crystal structure obtained from XRD is shown in black color, and DFT optimized structure is shown in magenta color.

Table 5.9 The selected distances (Å) of complex [**5**·Cu(ClO₄)₂] calculated at B3LYP/6-311g(d)/lanl2dz(Cu)/cpcm(acetonitrile) level (The labeled primary binding core of complex [**5**·Cu(ClO₄)₂] is shown at the left side of the table).
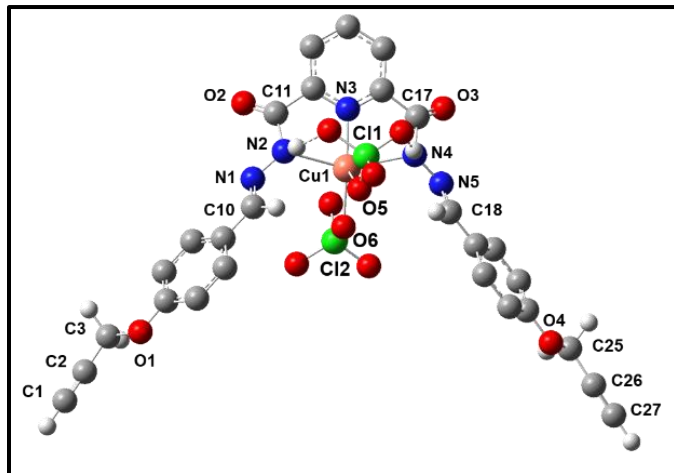
	contact	Distance (Å)
Complex [5.1Cu²⁺·(ClO₄)₂]	C1-C2	1.20100
	C2-C3	1.45611
	C3-O1	1.43968
	C10-N1	1.28805
	N1-N2	1.38611
	N2-C11	1.43524
	C11-O2	1.19948
	C17-N4	1.43518
	C17-O3	1.19949
	N4-N5	1.38611
	N5-C18	1.28804
	O4-C25	1.43967
	C25-C26	1.45611
	C26-C27	1.20100
	N2-Cu1	2.29963
	N3-Cu1	1.98024
	N4-Cu1	2.30009
	O5-Cu1	2.36077
	O6-Cu1	1.97125

α-HOMO **(-6.50 eV)**	α-HOMO-1 **(-6.54 eV)**	α-HOMO-2 **(-7.64 eV)**
α-LUMO **(-3.20 eV)**	α-LUMO+1 **(-2.98 eV)**	α-LUMO+2 **(-1.97 eV)**
β-HOMO **(-6.34 eV)**	β-HOMO-1 **(-6.71 eV)**	β-HOMO-2 **(-7.62 eV)**
β-LUMO **(-5.20 eV)**	β-LUMO+1 **(-3.12 eV)**	β-LUMO+2 **(-2.95 eV)**
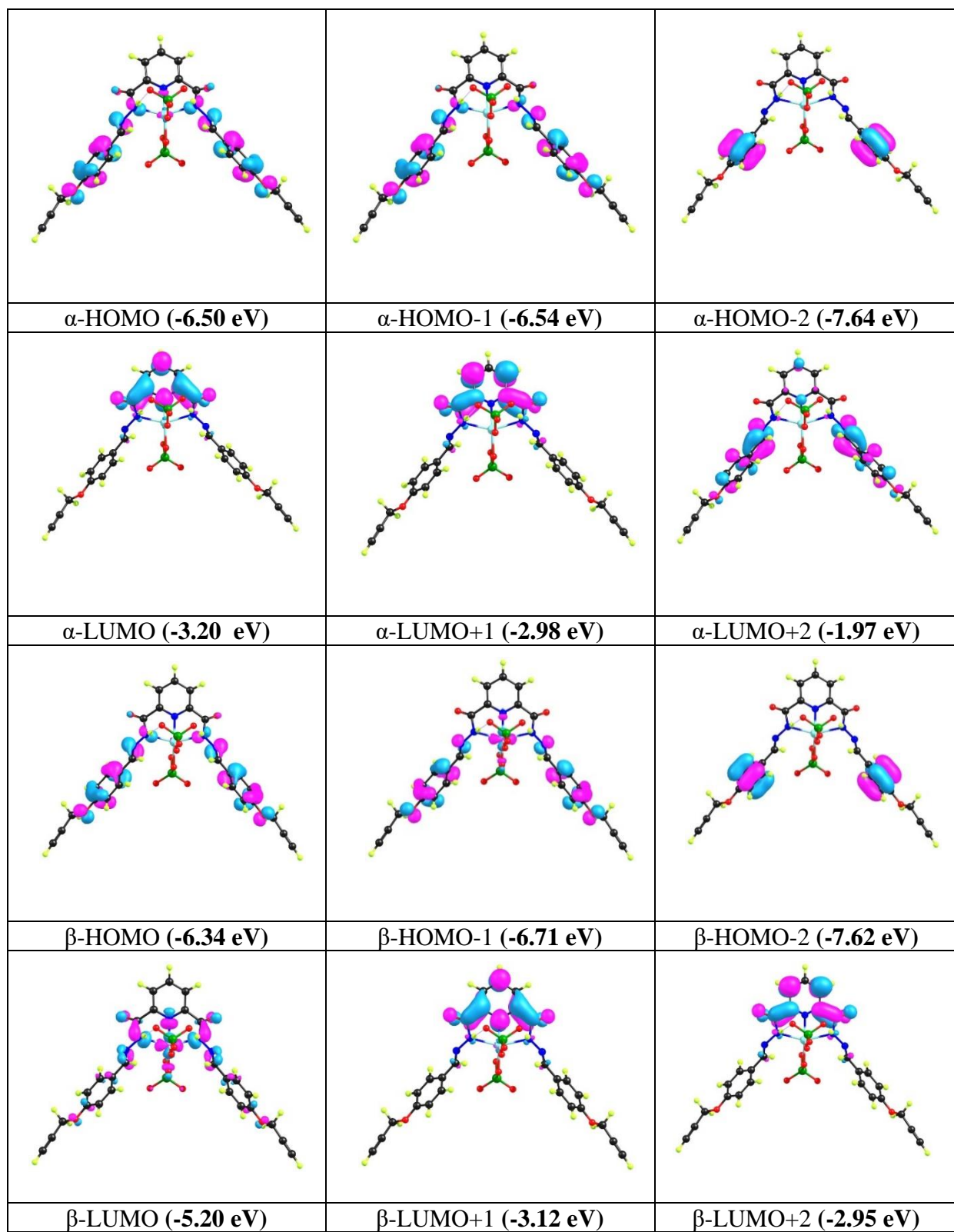
Figure 5.38 Frontiers MOs of the complex [**5**·Cu(ClO$_4$)$_2$] with corresponding energy values in parenthesis. (isosurface value= 0.04).

Table 5.10 The selected distances (Å) of complexes [**7**·Hg^{2+}] (left sided alkyne unit) and [**7**·Hg^{2+}] (left sided alkyne unit) calculated at B3LYP/6-311g(d)/lanl2dz(Hg)/cpcm (acetonitrile) level (The zoomed portions of the primary binding core of [**7**·Hg^{2+}] (left) and [**7**·Hg^{2+}] (right) with atom labeling are shown above the table).
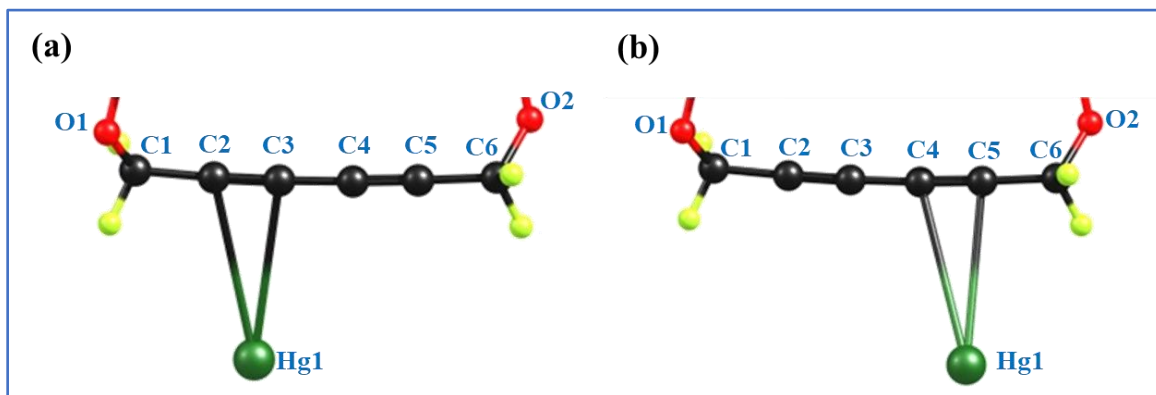
Receptor [**7**·Hg^{2+}]		
contact	**Left side alkyne unit**	**Right side alkyne unit**
	distance(Å)	**distance(Å)**
C1-O1	1.43988	1.44038
C1-C2	1.46266	1.46169
C2-C3	1.21292	1.21154
C3-C4	1.36375	1.36346
C4-C5	1.21126	1.21245
C5-C6	1.46148	1.46242
C6-O2	1.43431	1.43355
C2-Hg1	3.67708	------
C3-Hg1	3.60429	------
C4-Hg1	------	3.73262
C5-Hg1	------	3.61795

HOMO (**-6.21 eV**)	HOMO-1 (**-6.46 eV**)	HOMO-2 (**-7.385 eV**)
LUMO (**-3.44 eV**)	LUMO+1 (**-2.295 eV**)	LUMO+2 (**-2.202 eV**)
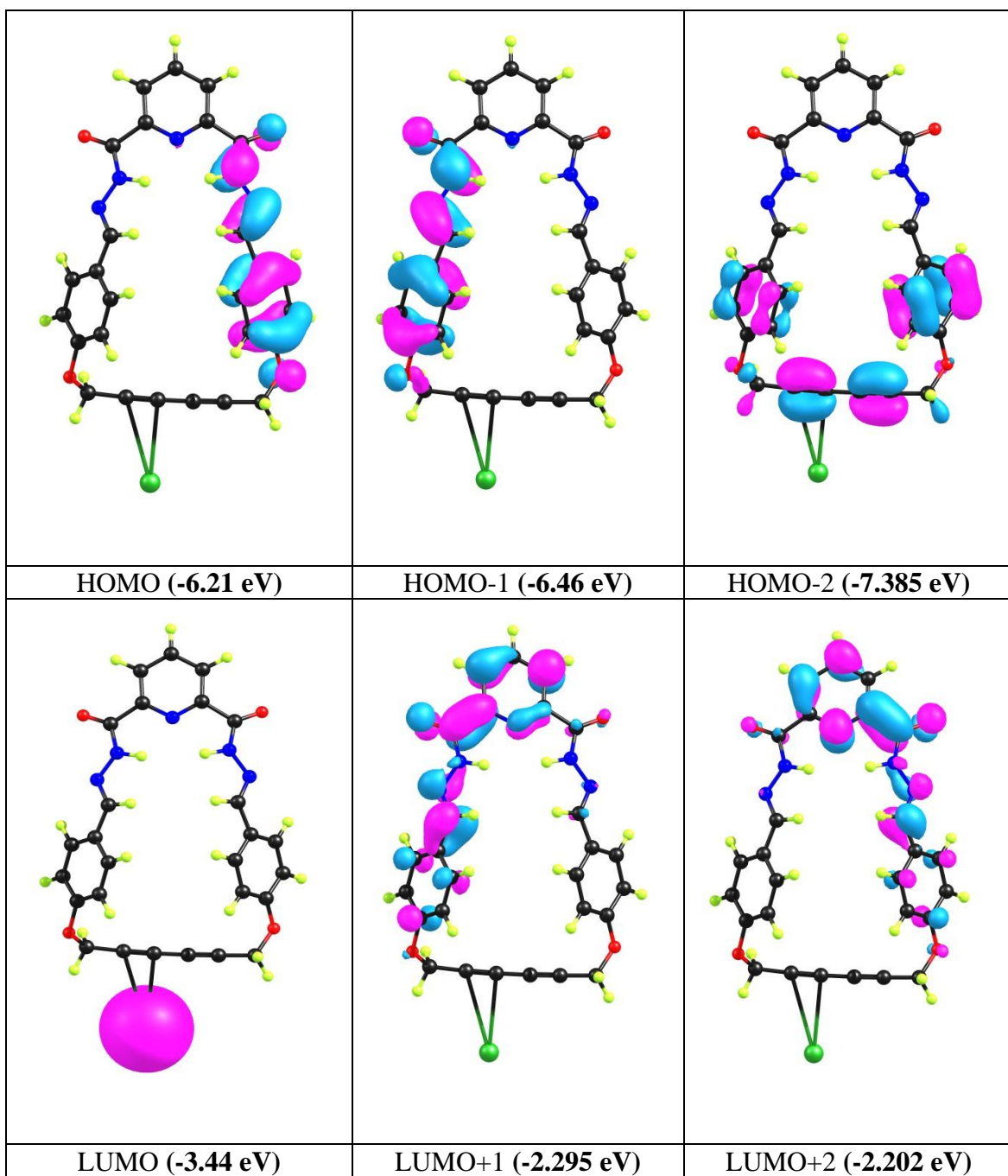
Figure 5.39 Frontiers MOs of the complex [**7**·Hg^{2+}] (left sided alkyne unit) with corresponding energy values in parenthesis (isosurface value= 0.04)

| HOMO (**-6.22 eV**) | HOMO-1 (**-6.45 eV**) | HOMO-2 (**-7.384 eV**) |
| LUMO (**-3.45 eV**) | LUMO+1 (**-2.290 eV**) | LUMO+2 (**-2.204 eV**) |
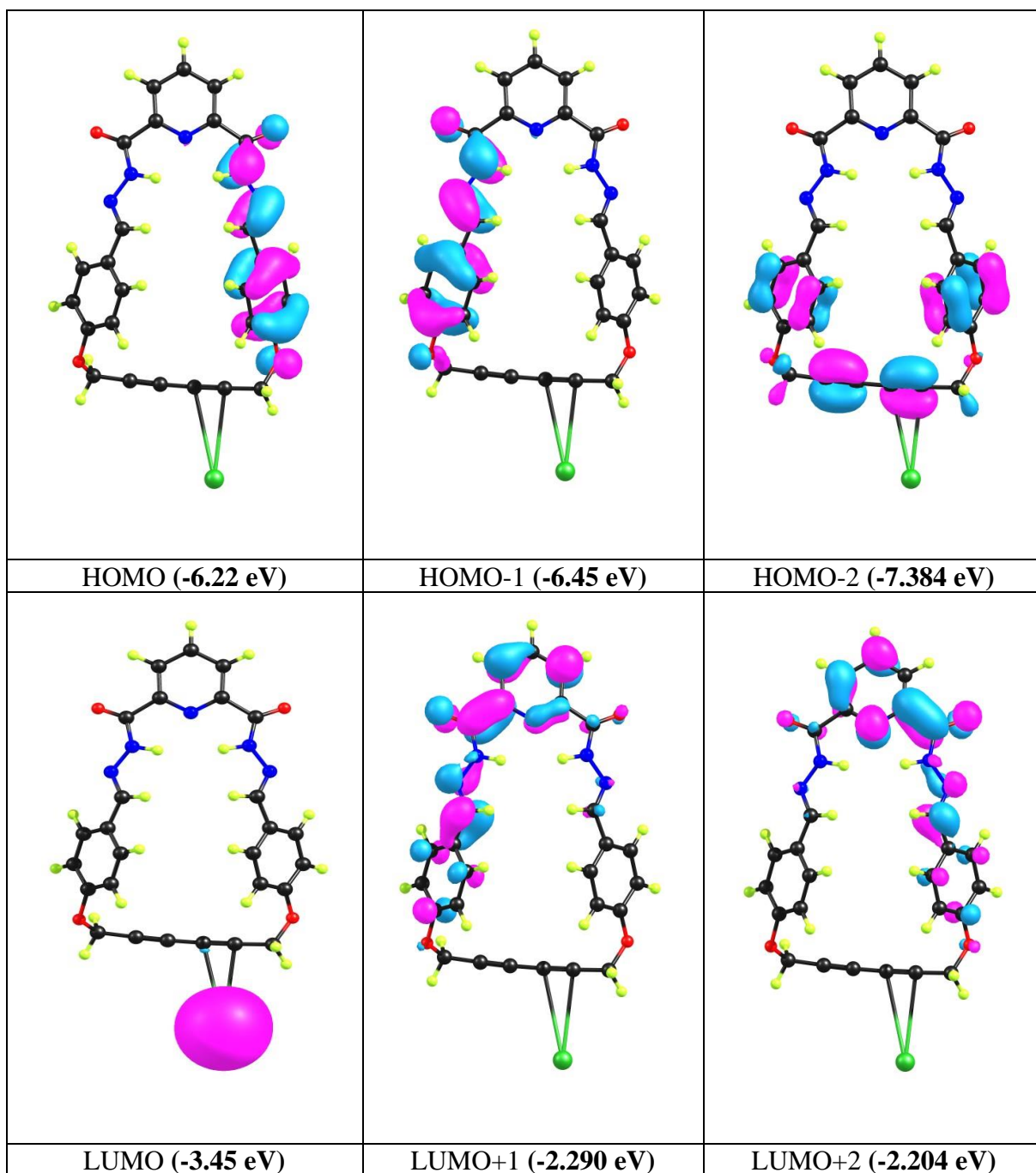
Figure 5.40 Frontiers MOs of the complex [**7**·Hg^{2+}] (right sided alkyne unit) with corresponding energy values in parenthesis (isosurface value= 0.04)
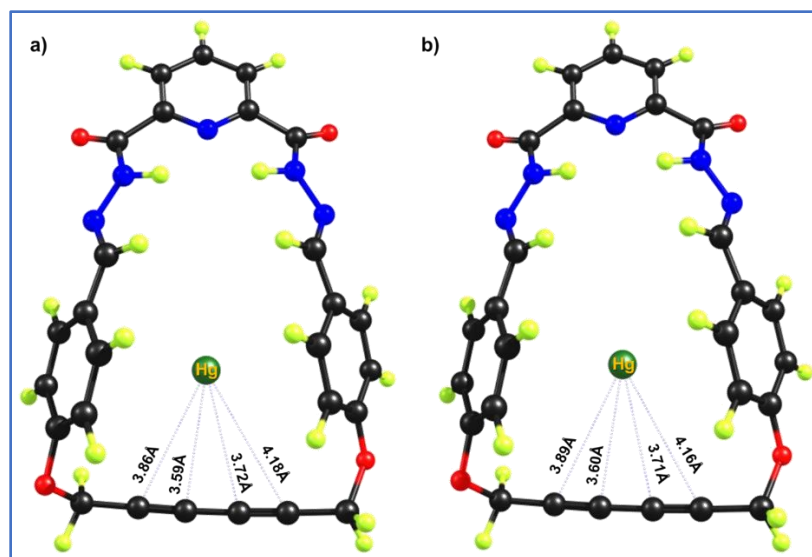
Figure 5.41 Optimized structure of the complexes considering endocyclic binding mode: **a)** [7·Hg^{2+}] (left sided alkyne unit), and **b)** [7·Hg^{2+}] (right sided alkyne unit).

Table 5.11 DFT Optimized coordinates of all the compounds

		Receptor **5** (Acyclic)				
C	-0.000014000	6.788843000	-0.000029000	C	8.163609000	-5.534801000	0.000159000
H	-0.000017000	7.872722000	-0.000045000	C	9.188389000	-6.161457000	0.000553000
C	1.197266000	6.082655000	0.000194000	H	10.099137000	-6.714842000	0.000885000
H	2.158046000	6.579698000	0.000353000	C	-1.197290000	6.082649000	-0.000231000
C	1.149371000	4.687792000	0.000205000	H	-2.158073000	6.579686000	-0.000404000
N	-0.000007000	4.002783000	0.000012000	C	-1.149388000	4.687786000	-0.000200000
C	2.452542000	3.923529000	0.000457000	C	-2.452555000	3.923516000	-0.000425000
O	3.531826000	4.496426000	0.001071000	O	-3.531842000	4.496407000	-0.001092000
N	2.290885000	2.569317000	-0.000136000	N	-2.290891000	2.569305000	0.000174000
H	1.342681000	2.204501000	-0.000630000	H	-1.342685000	2.204494000	0.000682000
N	3.362494000	1.729821000	0.000014000	N	-3.362496000	1.729803000	0.000006000
C	3.107319000	0.472134000	-0.000481000	C	-3.107314000	0.472118000	0.000508000
H	2.076380000	0.101232000	-0.001007000	H	-2.076373000	0.101221000	0.001052000
C	4.165342000	-0.532594000	-0.000408000	C	-4.165332000	-0.532616000	0.000423000
C	5.531404000	-0.186645000	0.000084000	C	-5.531396000	-0.186674000	-0.000092000
H	5.812796000	0.859852000	0.000409000	H	-5.812793000	0.859821000	-0.000426000
C	6.507199000	-1.162959000	0.000172000	C	-6.507186000	-1.162993000	-0.000191000
H	7.559683000	-0.902606000	0.000564000	H	-7.559671000	-0.902646000	-0.000600000
C	6.151638000	-2.523064000	-0.000228000	C	-6.151617000	-2.523096000	0.000220000
C	4.802129000	-2.885547000	-0.000739000	C	-4.802107000	-2.885572000	0.000753000
H	4.494441000	-3.922954000	-0.001097000	H	-4.494413000	-3.922977000	0.001119000
C	3.826519000	-1.889890000	-0.000827000	C	-3.826502000	-1.889910000	0.000852000
H	2.781184000	-2.182721000	-0.001208000	H	-2.781165000	-2.182736000	0.001250000
O	7.195340000	-3.398110000	-0.000079000	O	-7.195314000	-3.398149000	0.000059000
C	6.903412000	-4.803110000	-0.000293000	C	-6.903382000	-4.803150000	0.000289000
H	6.315562000	-5.065323000	-0.886770000	H	-6.315543000	-5.065353000	0.886777000
H	6.314874000	-5.065449000	0.885688000	H	-6.314831000	-5.065495000	-0.885681000

C	-8.163566000	-5.534862000	-0.000173000	H	-10.099545000	-6.714161000	-0.000917000
C	-9.188434000	-6.161375000	-0.000576000				

<div align="center">

· ·
Receptor 7 (Cyclic)
· ·

</div>

C	-6.407551000	1.058947000	-0.552625000	C	0.968940000	-3.911931000	-0.295084000
C	-5.068345000	1.066929000	-0.163472000	O	4.333622000	4.018714000	-0.551044000
N	-4.387264000	-0.060488000	0.059310000	C	5.470193000	3.323403000	-0.016159000
C	-4.977274000	-1.241518000	-0.143718000	C	5.487845000	1.896432000	-0.328480000
C	-6.312918000	-1.346284000	-0.530172000	O	4.640924000	-3.941491000	-0.043234000
C	-7.039140000	-0.171858000	-0.715318000	C	5.226722000	-3.270966000	-1.177069000
C	-4.272126000	2.356813000	-0.112885000	C	5.355954000	-1.827787000	-0.988582000
O	-4.671760000	3.391924000	-0.620386000	C	5.479601000	0.709243000	-0.568440000
N	-3.068400000	2.184737000	0.508712000	C	5.433306000	-0.634117000	-0.796437000
C	-4.087601000	-2.466883000	-0.064293000	H	-6.922664000	1.993310000	-0.734856000
O	-4.427515000	-3.552060000	-0.505799000	H	-6.752672000	-2.321619000	-0.693958000
N	-2.880051000	-2.180363000	0.506395000	H	-8.081737000	-0.215707000	-1.008221000
N	-1.757261000	-2.944155000	0.331026000	H	-2.900705000	1.247010000	0.858666000
N	-1.975979000	2.981558000	0.272966000	H	-2.762611000	-1.218915000	0.809827000
C	-0.905282000	2.574649000	0.856189000	H	-0.944128000	1.724920000	1.547093000
C	-0.711868000	-2.472696000	0.909709000	H	-0.788489000	-1.590256000	1.554115000
C	0.429644000	3.091458000	0.586601000	H	-0.104461000	4.467156000	-0.989319000
C	0.641986000	-2.978574000	0.703522000	H	2.243776000	5.013312000	-1.572662000
C	0.711776000	4.020193000	-0.433374000	H	3.621616000	2.359068000	1.520162000
C	2.019118000	4.325402000	-0.765365000	H	1.312616000	1.817213000	2.082402000
C	3.086186000	3.710468000	-0.088985000	H	1.438943000	-1.702162000	2.249482000
C	2.823599000	2.835204000	0.966988000	H	3.804245000	-2.313229000	1.812995000
C	1.504985000	2.530819000	1.287511000	H	2.549441000	-4.946902000	-1.326967000
C	1.675701000	-2.421207000	1.471793000	H	0.178763000	-4.351529000	-0.892815000
C	3.003166000	-2.752269000	1.230361000	H	4.643830000	-3.476423000	-2.081589000
C	3.313639000	-3.641442000	0.204206000	H	6.209906000	-3.727411000	-1.302314000
C	2.294748000	-4.238995000	-0.545659000	H	5.535363000	3.475916000	1.066499000

H	6.329460000	3.819924000	-0.468276000			

••

Complex **5·Cu(ClO₄)₂**

••

C	1.204020000	-5.489535000	-1.089960000	O	6.948249000	4.043597000	0.532210000
C	1.163520000	-4.125902000	-0.822595000	C	7.812132000	4.298787000	-0.590848000
N	0.000062000	-3.479105000	-0.667773000	C	8.614886000	5.476376000	-0.292303000
C	-1.163421000	-4.125979000	-0.822045000	O	-6.948758000	4.043251000	0.532335000
C	-1.203918000	-5.489623000	-1.089389000	C	-7.813772000	4.297315000	-0.590098000
C	0.000049000	-6.181051000	-1.199987000	C	-8.616206000	5.475221000	-0.291934000
C	2.392448000	-3.264002000	-0.827669000	C	9.291433000	6.444437000	-0.074249000
O	3.378194000	-3.529996000	-1.457187000	C	-9.292508000	6.443522000	-0.074183000
N	2.211544000	-2.053392000	-0.078255000	H	2.158360000	-5.982707000	-1.219203000
C	-2.392499000	-3.264265000	-0.826740000	H	-2.158277000	-5.982870000	-1.218200000
O	-3.378341000	-3.530583000	-1.456003000	H	0.000039000	-7.245697000	-1.397440000
N	-2.211666000	-2.053543000	-0.077609000	H	1.985945000	-2.262148000	0.907877000
N	-3.190462000	-1.093777000	-0.282780000	H	-1.985216000	-2.262014000	0.908323000
N	3.189884000	-1.093236000	-0.283792000	H	2.716453000	-0.278345000	1.567867000
C	3.324715000	-0.228675000	0.661424000	H	-2.714535000	-0.276567000	1.567233000
C	-3.324154000	-0.228183000	0.661632000	H	5.014701000	0.372946000	-1.391298000
C	4.277743000	0.859097000	0.573908000	H	6.611294000	2.223220000	-1.492780000
C	-4.277616000	0.859255000	0.574181000	H	5.387823000	3.499541000	2.435910000
C	5.095856000	1.054237000	-0.552985000	H	3.772064000	1.624722000	2.532510000
C	5.999207000	2.102392000	-0.608976000	H	-3.769677000	1.627091000	2.531330000
C	6.103532000	2.987991000	0.477636000	H	-5.385925000	3.501478000	2.434707000
C	5.292339000	2.805072000	1.609666000	H	-6.613951000	2.220725000	-1.491112000
C	4.394472000	1.756861000	1.653596000	H	-5.016925000	0.370832000	-1.389570000
C	-4.393190000	1.758153000	1.653037000	H	7.212258000	4.467071000	-1.490898000
C	-5.291326000	2.806142000	1.609090000	H	8.459135000	3.433496000	-0.766966000
C	-6.103925000	2.987709000	0.477860000	H	-8.460983000	3.431871000	-0.764704000
C	-6.000776000	2.100959000	-0.607916000	H	-7.214804000	4.464682000	-1.490925000
C	-5.097168000	1.053015000	-0.551894000	H	9.889583000	7.304053000	0.123441000

H	-9.890431000	7.303359000	0.123232000	O	-1.221206000	1.836626000	-2.198928000
Cu	0.000112000	-1.515923000	-0.408380000	Cl	0.000945000	-2.161453000	2.876123000
O	0.000218000	0.446496000	-0.594764000	O	-0.000799000	-0.999622000	1.895239000
Cl	-0.000307000	1.023975000	-2.049354000	O	-0.001210000	-1.658248000	4.257743000
O	-0.000979000	-0.142521000	-2.971629000	O	1.228907000	-2.973589000	2.598443000
O	1.220817000	1.836080000	-2.200028000	O	-1.222816000	-2.979045000	2.596384000

....

Complex **7·Hg²⁺** (left sided alkyne)

....

C	-6.411018000	1.058991000	-0.600764000	C	1.660885000	-2.398683000	1.503360000
C	-5.075605000	1.070102000	-0.198915000	C	2.989471000	-2.734446000	1.273962000
N	-4.396116000	-0.055525000	0.037300000	C	3.304491000	-3.635164000	0.259644000
C	-4.983317000	-1.238139000	-0.164554000	C	2.289946000	-4.238499000	-0.491130000
C	-6.315238000	-1.346107000	-0.562751000	C	0.963181000	-3.906217000	-0.252744000
C	-7.040399000	-0.173216000	-0.761599000	O	4.333937000	3.993995000	-0.522949000
C	-4.279191000	2.359873000	-0.149754000	C	5.462704000	3.302041000	0.028700000
O	-4.670497000	3.390413000	-0.672243000	C	5.487110000	1.874390000	-0.282977000
N	-3.083327000	2.192166000	0.488985000	O	4.633761000	-3.942616000	0.026333000
C	-4.092497000	-2.461558000	-0.071139000	C	5.228564000	-3.297231000	-1.115135000
O	-4.425556000	-3.549338000	-0.510835000	C	5.375520000	-1.852043000	-0.944190000
N	-2.890309000	-2.170108000	0.509563000	C	5.485911000	0.687413000	-0.524281000
N	-1.764917000	-2.931732000	0.346299000	C	5.447963000	-0.656399000	-0.753497000
N	-1.985630000	2.981789000	0.255415000	H	-6.925008000	1.991818000	-0.793754000
C	-0.921813000	2.575914000	0.851488000	H	-6.753076000	-2.322577000	-0.724878000
C	-0.723959000	-2.454885000	0.928321000	H	-8.080216000	-0.219494000	-1.063795000
C	0.417436000	3.085347000	0.588327000	H	-2.922384000	1.257700000	0.850639000
C	0.631325000	-2.962381000	0.734309000				
C	0.710763000	4.007452000	-0.434424000				
C	2.021779000	4.306323000	-0.757889000				
C	3.080851000	3.691243000	-0.069735000				
C	2.807338000	2.821791000	0.987921000				
C	1.485067000	2.524148000	1.300203000				

H	-2.777729000	-1.207272000	0.810481000	H	3.787308000	-2.291740000	1.858355000
H	-0.969824000	1.732378000	1.549345000	H	2.547926000	-4.956081000	-1.262476000
H	-0.805302000	-1.567997000	1.565893000	H	0.176045000	-4.351143000	-0.850482000
H	-0.099569000	4.454880000	-0.998522000	H	5.513341000	3.454109000	1.112173000
H	2.255094000	4.989957000	-1.566353000	H	6.328462000	3.798388000	-0.411207000
H	3.599090000	2.345984000	1.550397000	H	4.644255000	-3.505373000	-2.018125000
H	1.283889000	1.815862000	2.097629000	H	6.205404000	-3.768433000	-1.233621000
H	1.420346000	-1.671899000	2.272604000	Hg	8.595388000	-0.964937000	-2.482498000

Complex **7·Hg²⁺** (right sided alkyne)

C	-6.426141000	1.054363000	-0.560272000
C	-5.087574000	1.064437000	-0.169086000
N	-4.404661000	-0.061840000	0.053724000
C	-4.991769000	-1.243846000	-0.151799000
C	-6.326647000	-1.350816000	-0.540271000
C	-7.055033000	-0.177581000	-0.724925000
C	-4.292156000	2.354594000	-0.117785000
O	-4.688089000	3.387983000	-0.630889000
N	-3.091032000	2.184313000	0.510895000
C	-4.098801000	-2.466934000	-0.073103000
O	-4.434701000	-3.552502000	-0.516178000
N	-2.892446000	-2.177330000	0.499362000
N	-1.767413000	-2.937582000	0.325787000
N	-1.995608000	2.974457000	0.269275000
C	-0.925377000	2.566476000	0.852081000
C	-0.724428000	-2.463830000	0.906802000
C	0.410303000	3.078093000	0.574788000
C	0.631006000	-2.967494000	0.704227000
C	0.689808000	4.001544000	-0.450590000
C	1.996259000	4.304263000	-0.788212000
C	3.064271000	3.692070000	-0.111641000
C	2.805099000	2.820389000	0.947642000
C	1.487010000	2.518633000	1.274020000
C	1.661490000	-2.409540000	1.476331000
C	2.990072000	-2.740443000	1.240359000
C	3.304725000	-3.630136000	0.216111000
C	2.289278000	-4.227867000	-0.538055000
C	0.962372000	-3.900754000	-0.292994000
O	4.311434000	4.000321000	-0.578124000

C	5.451104000	3.329627000	-0.024613000
C	5.497173000	1.899405000	-0.326299000
O	4.633817000	-3.931960000	-0.023617000
C	5.224924000	-3.270716000	-1.158533000
C	5.368033000	-1.827989000	-0.972515000
C	5.503214000	0.709738000	-0.560168000
C	5.455048000	-0.634534000	-0.782988000
H	-6.942952000	1.987810000	-0.742465000
H	-6.764377000	-2.326740000	-0.705938000
H	-8.097158000	-0.223196000	-1.019164000
H	-2.926486000	1.247849000	0.865695000
H	-2.778649000	-1.215929000	0.804341000
H	-0.964995000	1.720460000	1.547419000
H	-0.804419000	-1.581741000	1.551248000
H	-0.127967000	4.447174000	-1.005243000
H	2.218891000	4.989247000	-1.598532000
H	3.604237000	2.345460000	1.500398000
H	1.296500000	1.808586000	2.072495000
H	1.421348000	-1.691006000	2.253437000
H	3.788539000	-2.302048000	1.827125000
H	2.546815000	-4.936735000	-1.317544000
H	0.174719000	-4.341130000	-0.893447000
H	5.500883000	3.489984000	1.057798000
H	6.307310000	3.837244000	-0.469961000
H	4.640193000	-3.470777000	-2.063049000
H	6.203954000	-3.735932000	-1.284356000
Hg	9.095788000	1.608142000	-0.092458000

Summary and Future Scope:

The entire PhD works are described and summarized within the five chapters in this dissertation. The introductory chapter of the thesis presents an overview on different aspects of C–H functionalization processes: advantages, challenges and solutions of them. All the other chapters emphasize on C–C and C–O bond forming reactions *via* copper catalyzed C–H functionalizations using strategies like cross dehydrogenative coupling directed C–H bond functionalization. The main aim of this thesis is the C-H bond activation of various organic derivatives using copper catalyst under an oxidative environment by CDC mechanism to construct complex organic molecules and their applications in various fields.

Chapter 1 is the general introduction which provides a comprehensive literature survey on C-C and C-O bond formation reaction using transition metal catalyst by C-H activation process. This chapter highlights the advantage of using a low cost and earth abundant metal catalyst for C-H functionalization over comparatively expensive and low abundant 4d transition metal like (Pd, Ru, Rh and Au). As a result, a remarkable quantity of organic transformations including oxidative cross-coupling, addition, and radical reactions have been documented for the formation of C–C and C–heteroatom bonds in presence of copper catalyst. At the end of this chapter, copper catalyzed 1,3-diyne synthesis *via* Glaser-Hay coupling are summarized and their applications in metal ion sensing have been surveyed briefly.

In **Chapter 2**, we have developed the quinoline-based NNN-pincer Cu(II) complex acts as an air stable superior catalyst for the oxidative cross-coupling of the allyl $C(sp^3)$–H bond with an acid derivatives for the construction of C-O bond at ambient temperature in a homogeneous system report for the first time. The synthesized catalyst showed excellent catalytic activity for the oxidative esterification of allylic $C(sp^3)$–H bonds. This reaction is completed within 1 h, using only 1 mol% of the catalyst at 40 °C. A wide variety of aromatic allylic esters were synthesized in moderate to good yields, which could be extended to aliphatic allyl esters as well.

Chapter 3 describes novel benzothiazole appended 2,6-di picolinamide-based Cu(II) complex as a catalyst for the formation of carbamates *via* the cross-coupling reaction of various 2-carbonyl substituted phenolic derivatives or 1,3-diketo derivatives with N,N-disubstituted formamides. A wide range of aromatic carbamates was synthesized using copper complex in good to excellent yield with broad functional group tolerance under mild conditions. Control experiments suggest that the reaction proceeds *via* the radical mechanism, and the formation of

radical-mediated intermediates was confirmed by the gas chromatography (GC), GCMS and HRMS. The use of low cost and environmentally benign catalysts in mild conditions along with the tolerance of a wide range of functional groups makes this an easy synthetic approach for the development of carbamates.

In **Chapter 4**, we report the synthesis of β-disubstituted ketones from vinyl arenes *via* oxo-alkylation with unactivated cycloalkanes as the alkylating agent in presence of Cu(II) catalyst. Here *tert*-butylhydroperoxide (TBHP) and 1-methylimidazole acts as oxidant and base respectively. β-disubstituted ketones are known to be synthesized by using either expensive metal catalyst (Ru/Ir) or low-cost metal complexes (Fe/Mn) with activated species like aldehyde, acid, alcohol, or phthalimide derivatives as the alkylating agent. However, use of unactivated cycloalkanes directly as the alkylating agent remains unexplored. A wide range of aliphatic cycloalkanes as well as various olefinic arenes and heteroarene are well-tolerated in this method. Furthermore, various controlled experiments such as kinetic isotope effect study, Hammett analysis and theoretical calculations (DFT) enable us to gain deeper insight of mechanistic intricacies of this new simple and atom-economic methodology.

The work in **Chapter 5** does not include any catalysis work rather, in this work we have developed a unique probe *via* Cu(II) catalyzed Glaser-Hay coupling. The designed probe is capable of detecting dual metal ions *via* different binding sites and different mechanisms within a single molecular scaffold. Two pyridine-derived scaffolds, **5** and **7**, containing identical molecular cores but different appendages, *viz*., terminal alkyne (**5**) and internally 1,3-conjugated alkyne units (**7**), are successfully synthesized. Both compounds are subjected to metal ion sensing at the molecular level and are found to bind Cu^{2+} and Hg^{2+} ions with different functionalities. Compounds **5** and **7** interact with Cu^{2+} by the pyridine N and the two adjacent amide N's in a tripodal fashion, whereas they interact with Hg^{2+} by their respective open-end and closed-end alkyne units. Both experimental studies and theoretical (DFT) calculations have converged on the result that terminal alkynes cannot function as a chemosensor for Hg^{2+} ions, although they can respond by functional group transformation, whereas cyclic internally conjugated alkynes can perform as potential Hg2+ sensors. The combination of Cu^{2+} and Hg^{2+} ions has been used to generate a molecular system exhibiting the OR logic operation.

Following the entire study in the present thesis and developing a route map for future scope, it will be interesting to synthesize various heterocyclic derivatives using copper catalyst that described in chapter 2 and chapter 3 or using any commercially available copper salt. Transition metals like Pd, Ru and Rh, are well-known catalysts widely used for synthesizing various heterocyclic compounds *via* the different C-H (sp, sp^2 and sp^3) bond activation. In this respect, copper catalyzed ring closing reactions for the formation of heterocyclic compounds *via* C-H bond activation are less explored. Various heterocyclic compounds including N-heterocycles, N,O-heterocycles, O-heterocycles, and N,S-heterocycles can be synthesized using our synthesized copper complex as catalyst *via* the C-H activation process (Proposed Scheme). The proposed Scheme demonstrates the formation of five membered heterocyclic compounds like imidazole and pyrazole derivatives *via* the activation of C(sp)-H bond. Since copper can coordinate with alkyne unit present in a molecule through the formation of Cu-acetylide complex, these following transformation can be achieved using our designed copper complex which is described in chapter 2 and chapter 3 instead of precious 4d transition metals like Pd, Rh or Ru. Other N,O and N,S heterocyclic derivatives such as pyrrole, furan, oxazole, thiazoles, and benzimidazole derivatives or six membered heterocyclic compounds like pyrazines, pyrimidines and pyridazines, benzoxazines, sultams and coumarins can be synthesized *via* $C(sp^2)$-H and $C(sp^3)$-H bond activation. We reported that our designed copper catalyst can activate both the $C(sp^2)$-H and $C(sp^3)$-H for the functionalization of C-H bond. These heterocyclic compounds can be synthesized using our reported copper complex. Also we demonstrated that anhyd.$CuCl_2$ can also activate $C(sp^3)$-H bond in chapter 4, these structurally important building block can also be synthesized in presence of anhyd.$CuCl_2$ through the $C(sp^3)$-H bond activation. As the heterocyclic compounds play a significant role in drug discovery, this proposed Scheme could lead towards synthesizing various heterocyclic compounds using earth-abundant cheap transition metal catalysts.
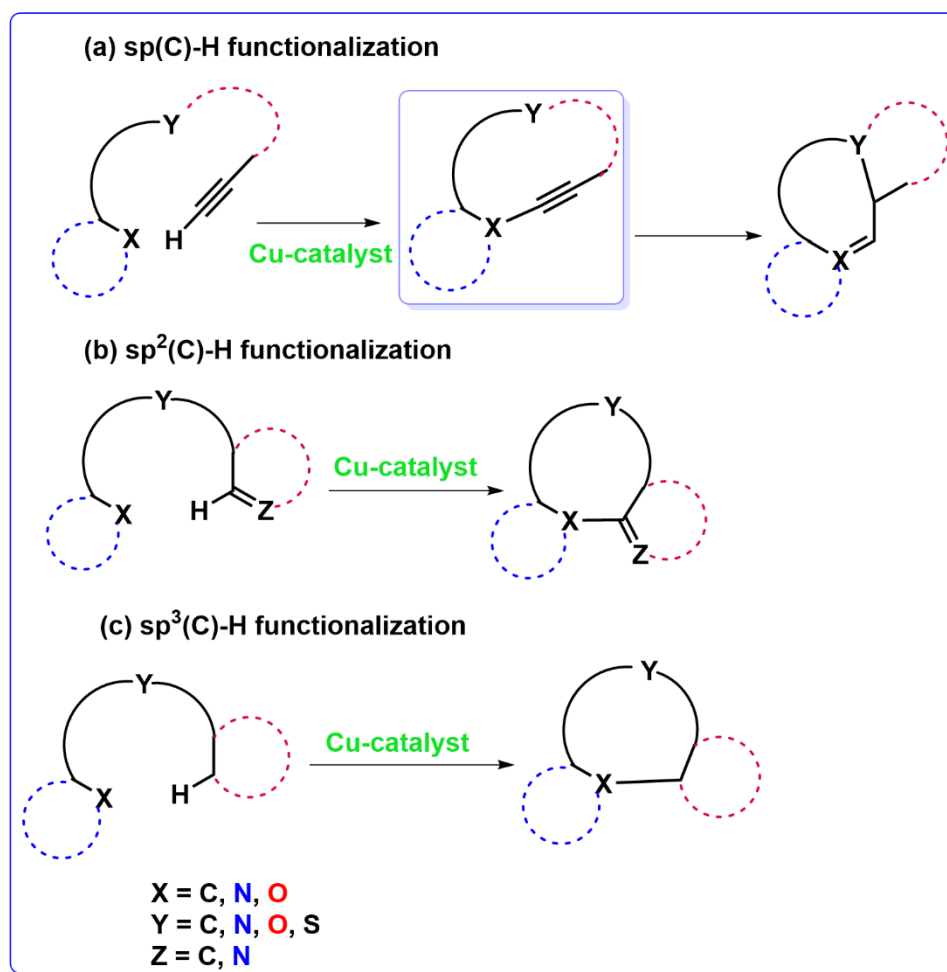
Proposed Scheme. Synthesis of heterocyclic compounds in presence of copper catalyst.

List of publications

1. **Das, K. M.**; Pal, A.; Thakur, A. A Novel quinoline-based NNN-pincer Cu(II) complex as a superior catalyst for oxidative esterification of allylic C(sp^3)-H bonds. ***Org. Biomol. Chem***. 2022, *20*, 3540-3549.

2. **Das, K. M.**; Pal, A.; Goswami, B.; Thakur, A. Strategic design of a 2,6-disubstituted pyridine-based Probe having Hard-Soft centers: Responsive divergence from one core. ***New J. Chem***. 2022, *46*, 12103-12119.

3. **Das, K. M**.; Thakur, A. Oxidative cross dehydrogenative coupling directed carbamates synthesis using Cu(II) pincer complex as active catalyst under mild reaction condition. ***J. Het. Chem***. 2023, *60*, 1165-1178.

4. **Das, K. M**.; Pal, A.; Surya. T, L.; Roy, L.; Thakur, A. Cu(II) promoted C(sp^3)-H activation in unactivated cycloalkanes: Oxo-alkylation of styrenes to synthesize *β*-disubstituted ketones. ***Chem. Eur. J***. 2024, *30*, e202303776.

5. Pal, A.; **Das, K. M**.; Goswami, B.; Thakur, A. Microwave-assisted neat synthesis of a ferrocene appended phenolphthalein diyne: A designed synthetic scaffold for Hg^{2+} ion. ***Inorg. Chem***. 2020, *59*, 10099–10112.

6. Pal, A.; **Das, K. M**.; Thakur, A. Microwave-assisted synthesis of E-aldimines, N-heterocycles, and H2 by dehydrogenative coupling of benzyl alcohol and aniline derivatives using CoCl$_2$ as a catalyst. ***J. Org. Chem***. 2023, *88*, 8955−8968.

7. Pal, A.; **Das, K. M**.; Sau. S.; Thakur, A. Co(II) acetate assisted direct synthesis of acyl hydrazones from acyl hydrazides under mild condition. ***Chem. Asian J***. 2023, *22*, e202300755

8. Sau, S.; **Das, K. M**.; Thakur, A. Cobalt (II) catalyzed synthesis of γ-diketones from aryl-alkenes and its utilization in synthesis of various heterocyclic compounds. ***J. Org. Chem***. 2024, accepted (doi:10.1021/acs.joc.4c00487).

List of scientific conference attended and poster presentations

1. National Seminar on Chemical Sciences: Today and Tomorrow (CSTT-2019), 14th March **2019**, Department of Chemistry, Jadavpur University, Kolkata, India.

2. National Seminar on Celebration of the International Year of the Periodic Table (CIYPT), Department of Chemistry Jadavpur University, Kolkata, India, Date: 13 & 14th August **2019**.

3. 2nd International Conference on Main Group Molecules to Materials (MMM-II), NISER Bhubaneswar, India, Date: 13th to 15th December, **2021**.

4. 28th CRSI National Symposium in Chemistry, Indian Association for the Cultivation of Science. Date: 4th June, **2022**.

5. 2nd International Conference on Emerging Trends in Chemical Science (IC-ETCS-2024), 7th March to 9th March **2024**, Department of Chemistry, IIT Kharagpur, India (**Received best poster award**).